

**International Association of Hydrogeologists**

**Eugene S. Simpson  
and  
John M. Sharp, Jr.  
(Editors)**

**Selected Papers  
on  
Hydrogeology**

**Volume 1  
1990**

**Volume 1  
1990**

**from the  
28th International Geological  
Congress  
Washington, D.C., U.S.A.  
July 9-19, 1989**



**Volume 1, 1990  
Hydrogeology, Selected Papers**





# International Association of Hydrogeologists

**Eugene S. Simpson**

Department of Hydrology and Water Resources  
The University of Arizona  
Tucson, Arizona

and

**John M. Sharp, Jr.**

Department of Geological Sciences  
The University of Texas-Austin  
Austin, Texas

(Editors)

## **Selected Papers on Hydrogeology**

**from the  
28th International Geological Congress  
Washington, D.C., U.S.A.  
July 9-19, 1989**



Volume 1, 1990  
Hydrogeology, Selected Papers

**Verlag Heinz Heise**

CIP-Titelaufnahme der Deutschen Bibliothek

**International Geological Congress**

**<28, 1989, Washington, DC>:**

Selected papers on hydrogeology from the 28th International Geological Congress: Washington, DC, USA, July 9-19, 1989 / Internat. Assoc. of Hydrogeologists.

Eugene S. Simpson and John M. Sharp, Jr. (ed). –

Hannover: Heise, 1990

(Hydrogeology; Vol. 1)

ISBN 3-922705-60-X

NE: Simpson, Eugene S. [Hrsg.]; International Association of Hydrogeologists; HST; GT

Volume 1, 1990

Hydrogeology, Selected Papers

E. S. Simpson, J. M. Sharp, Jr. (Editors)

ISSN 0938-6378

ISBN 3-922705-60-X

Printed by R. van Acken GmbH, Josefstraße 35, D-4450 Lingen (Ems), West Germany

Copyright by Verlag Heinz Heise GmbH & Co KG.

P.O.B. 61 04 07, D-3000 Hannover 61, West Germany



# TABLE OF CONTENTS

|  | <u>Page</u> |
|--|-------------|
| PREFACE  | v           |
| ACKNOWLEDGMENTS  | vi          |
| SECTION 1: <u>AVANT-PROPOS</u>   | 1           |
| <i>Current and Future Difficulties in the Practice of Engineering Geology</i> , by James E. Slosson, John W. Williams, and Vincent E. Cronin   | 3           |
| SECTION 2: <u>CARBONATE SYSTEMS</u>  | 15          |
| <i>The Transport of Chemical Contaminants in Karst Terranes: An Outline and Summary</i> , by Malcolm S. Field  | 17          |
| <i>Groundwater Recharge in an Arid Karst Area in Saudi Arabia</i> , by A.K. Al-Saafin, T.A. Bader, W. Shehata, H. Hoetzl, S. Wohnlich, and J.G. Zoetl  | 29          |
| <i>Surface Subsidences and Sinkhole Formation Due to the Partial Recharge of a Dewatered Area on the Far West Rand, Republic of South Africa</i> , by J.H.T. Beukes and A. du Plessis                          | 43          |
| <i>Karst and Urbanization: Investigation and Monitoring in Cajamar, Sao Paulo State, Brazil</i> , by Fernando L. Prandini, Valdir A. Nakazawa, Ana Maria de Azevedo Dantas, and Thomas L. Holzer               | 53          |
| <i>Stratigraphic, Geomorphic, and Structural Controls on the Edwards Aquifer, Texas, USA</i> , by John M. Sharp, Jr.   | 67          |
| <i>Interpreting Calcite, Dolomite, and Gypsum Saturation Conditions in the Edwards Aquifer, Texas</i> , by Albert E. Odgen and Paul D. Collar  | 83          |
| <i>Dolomite Dissolution Rates and Possible Holocene Dedolomitization of Water-Bearing Units in the Edwards Aquifer, Southcentral, Texas--A Summary</i> , by Ruth G. Deike                                      | 97          |
| <i>Hurricane Gilbert: Its Effects on the Aquifer in Northern Yucatan, Mexico</i> , by L.E. Marin, E.C. Perry, K.O. Pope, C.E. Duller, C.J. Booth, and M. Villasuso   | 111         |
| <i>High Frequency Sea Level Cyclicity, Karstification, and a Carbonate-Siliciclastic Transition: Geologic Controls on the Development of the Floridan Aquifer System, Southwest Florida</i> , by Mark W. Evans | 129         |

## TABLE OF CONTENTS--Continued

|   | <u>Page</u> |
|---|-------------|
| <i>Geochemical Reactions in Carbonate Coastal Aquifers, Catalonia, Spain, by Xavier Bosch, Emilio Custodio, and Manel Pascual</i>   | 147         |
| <br>SECTION 3: <u>GEOCHEMISTRY AND ISOTOPE HYDROLOGY</u>  | <br>161     |
| <i>Ultrabasic Groundwaters of the Zlatibor Ultramafic Massif, by Petar Papic and Neven Kresic</i>   | 163         |
| <i>The Retention of Cd, Pb, and Zn by Fractured Shale Units: Simulation of Reactivity in the Unconsolidated Zone, by Ernest E. Angino and Cindy K. Wilbur</i>                                 | 169         |
| <i>Long-Term Observation of a Low Temperature Hydrothermal System (Campiglia, Central Italy), by S. Grassi, R. Celati, L. Bolognesi, C. Calore, F.D'Amore, P. Squarci, and L. Taffi</i>       | 181         |
| <i>Studies of Surdulica Geothermal Water Dynamics With Environmental Isotopes, by B. Milovanovic, R. Gonfiantini, M. Hadzisehovic, N. Miljevic, V. Sipka, M. Zupancic, and D. Golobocanin</i> | 199         |
| <i>Coupled Geochemical Speciation and Groundwater Transport Modeling in Sedimentary Basins, by Anne Coudrain-Ribstein, Ghislain de Marsily, and Patrick Goblet</i>                            | 211         |
| <i>Ground-Water Geochemistry and Information Transfer in Alluvial Basins in Arizona, by Frederick M. Robertson</i>  | 223         |
| <br>SECTION 4: <u>WETLANDS</u>  | <br>237     |
| <i>Hydrologic and Water-Quality Characteristics of a Wetland Receiving Wastewater Effluent in St. Joseph, Minnesota, by Rob G. Brown and James R. Stark</i>                                   | 239         |
| <i>Groundwater Systems Analysis of the Naardermeer Wetland, The Netherlands, by P.P. Schot</i>  | 257         |
| <i>Wetland Hydrologic System With Special Reference to the Gurinai Wetland Within the Gobi Desert, by Gu Weizu</i>  | 271         |
| <i>Numerical Modelling of the Groundwater Contribution to the Hydrological Budget of Lakes, by A.S. Crowe</i>   | 283         |

## TABLE OF CONTENTS--Continued

|  | <u>Page</u> |
|--|-------------|
| <i>Groundwater Indicator Plants in the Tertiary Aquifers of Central Spain</i> , by F.G. Bernaldez, J.M. Rey Benayas, B. Peco, and C. Levassor                                      | 301         |
| <br>SECTION 5: <u>FRACTURED ROCK</u>   | <br>313     |
| <i>Morphological Analysis of a Natural Fracture</i> , by Silvie Gentier  | 315         |
| <i>Hydromechanical Behavior of a Single Natural Fracture Under Normal Stress</i> , by Silvie Gentier   | 327         |
| <i>Hydraulic Impedence Technique for Unsaturated Rock Characterization</i> , by Daniel D. Evans and Todd C. Rasmussen  | 339         |
| <i>Evaluation of Aquifer Parameters and Well Characteristics in Fractured Rock Formations of Karnataka, India</i> , by B.B.S. Singhal and D.C. Singhal                             | 351         |
| <br>SECTION 6: <u>WATER MANAGEMENT</u>   | <br>363     |
| <i>Dynamic Management of Surface and Groundwater Hydrologic Systems</i> , by Nathan Buras  | 365         |
| <i>Well Head Protection Areas for Preserving Natural Drinking Water Quality--Experiences and New Developments in the Federal Republic of Germany</i> , by R. Schleyer and G. Milde | 379         |
| <i>A Variable Scale Approach for the Delineation of Ground-water Protection Zones Using Field and Numerical Modelling Techniques</i> , by Georg Teutsch                            | 393         |
| <i>Wellhead Protection: Assessing the Potential for Microbial Contamination of Drinking Water</i> , by Marylynn V. Yates   | 405         |
| <i>Compact Expert Systems for Water Resources Assessment in Africa</i> , by Patrice Poyet and Michel Detay   | 417         |
| <br>SECTION 7: <u>MISCELLANEOUS</u>  | <br>431     |
| <i>Assessment of Predictive Accuracy of a Model of Artificial Recharge Effects in the Upper Coachella Valley, California</i> , by Leonard F. Konikow and Lindsay A. Swain          | 433         |

# TABLE OF CONTENTS--Continued

|   | <u>Page</u> |
|---|-------------|
| <i>Overflow Thermal Springs in Tuscany and Northern Latium Regions, Italy</i> , by R. Celati, S. Grassi, and C. Calore  | 451         |
| <i>Influence of the Development of the Saprolite Reservoir and of Its State of Saturation on the Hydrodynamic Characteristics of Drillings in the Crystalline Basement</i> , by Michael Detay and Patrice Poyet | 463         |
| <i>Conventional Method and Digitally Enhanced Landsat Imagery for Groundwater Exploration in the Main Rift Valley of Ethiopia</i> , by Tilahun Aberra and Heikki Wihuri   | 473         |
| <i>Water Prospecting Using Surface SP (Spontaneous Potential): Reconnaissance and Detailed Studies</i> , by John A. Randall Roberts   | 489         |
| <i>Modern Problems of Regional Hydrogeodynamics</i> , by G.S. Vartanyan and L.V. Borevsky   | 501         |

## PREFACE

This volume contains a selection of papers in hydrogeology presented at the 28<sup>th</sup> International Geological Congress (IGC) held July 9-19, 1989, in Washington, D.C., U.S.A. It is made part of a series issued occasionally by the International Association of Hydrogeologists (IAH) under the general title "Selected Papers".

The 28<sup>th</sup> IGC drew hydrogeologists from many countries to present research results and perspectives to their colleagues. More than 200 papers relating to hydrogeology were presented in the various sessions of the Congress. After an initial screening of abstracts and oral presentations, we invited about 100 authors to submit formal papers for possible publication. Fifty-four papers were submitted but, because of space limitations, only 37 manuscripts could be published. The task of final selection was difficult, as all papers were worthy of publication. We rejected some because of their length, editorial problems, or late submission. We are especially pleased to be able to publish several papers by authors who submitted abstracts but, for various reasons, had been unable to attend the IGC to present their papers.

The papers describe research results from 17 different countries and cover a wide range of subdisciplines. They are grouped in seven sections: (1) Avant propos; (2) Carbonate systems; (3) Geochemistry and isotope hydrology; (4) Wetlands; (5) Fractured rock; (6) Water management, and (7) Miscellaneous. The avant propos paper sounds a warning concerning education in hydrogeology that deserves to be heard. Section 2 contains an overview paper followed by papers covering a variety of hydrogeologic settings. Three of these deal with the Edwards aquifer of Texas with some diverging viewpoints. Analysis of metamorphic rock, fractured shale systems, and studies on a wide range of aquifer scale are included in Section 3. Section 4 examines groundwater interactions with wetlands from modeling, water balance, geochemical, and geobotanical standpoints. The relatively short Section 5 includes two papers on evaluation techniques and two papers that analyze single-fracture characteristics. Section 6 includes an overview paper, several studies involving well-head protection strategies, and a paper on compact expert systems. Finally, Section 7 examines geophysical techniques, an assessment of a model of artificial recharge, landsat imagery, thermal springs, and regional hydrogeodynamics.

We think that the breadth of topics, both theoretical and applied, speaks well for the international state of health of the science of hydrogeology, and we are grateful to the IAH for publishing this volume.

E.S. Simpson and J.M Sharp, Jr.

## ACKNOWLEDGMENTS

The editors wish to acknowledge, with thanks, the support and assistance offered by the staff in the Department of Hydrology and Water Resources of the University of Arizona and by the staff in the Department of Geological Sciences of the University of Texas at Austin. In addition, we wish to thank Ms. Corla Thies, University of Arizona, for her patient and accurate typing of many of the manuscripts.

SECTION 1: AVANT-PROPOS





CURRENT AND FUTURE DIFFICULTIES IN  
THE PRACTICE OF ENGINEERING GEOLOGY

SLOSSON, JAMES E., Slosson and Associates, 14046 Oxnard  
Street, Van Nuys, California 91401

WILLIAMS, JOHN W., Department of Geology, San Jose State  
University, San Jose, California 95192-0102

CRONIN, VINCENT S., Department of Geosciences, University  
of Wisconsin - Milwaukee, P.O. Box 413, Milwaukee,  
Wisconsin 53201

Introduction

The next five to ten years will be critical to the survival of engineering geology as a profession. A crisis currently exists in the quality of work being done in many sectors of engineering geology. If the professional geologic community does not accept the challenge to improve its overall performance record, the contributions that the engineering geologist can make will not be sought or valued by society. The opportunity to appropriately include geology in construction and land-use decisions will become more limited to non-existent if the work now assigned to the engineering geologist is relinquished to the geotechnical and civil engineering community.

In this paper, the term "engineering geology" is used in the broadest of senses--that is, the application of the understanding of geologic principles and processes to human activities. Specifically, this includes the traditionally more narrowly defined fields of engineering geology, environmental geology and hydrogeology. As an example, in the field of engineering geology, the following items are subjects of concern:

- \* Landslide recognition and mitigation
- \* Recognition and mitigation of earthquake hazards
- \* Flood hazards as affected by geologic environs
- \* Origin of mudflow/debris flow
- \* Causes, effects of slope instability in relationship to timber harvest
- \* Coastal erosion/marine geology
- \* Siting and operation of critical facilities and life lines
- \* Siting of critical facilities offshore
- \* Ground water/hydrogeology
- \* Toxic waste recognition, containment, reclamation
- \* Reclamation of mined land
- \* Location, extraction, use of non-metallic minerals and rocks
- \* Land-use planning
- \* Planning, construction, maintenance of dams, highways, aqueducts, etc.

The geologic community is defined to mean that part of the greater community of geologists who provide geologic information and services to members of the general public. There are many who may elect to substitute the term "applied"

geology for the word "engineering" geology. The choice of wording is relatively unimportant for the purpose of this paper.

The reasons for the rather bleak outlook for engineering geology result from trends that are varied and complex. The outlook will continue to be bleak unless the current state of affairs is altered in such a way as to improve both the performance and the public perception of engineering geology. In all probability, no single factor is responsible for the current situation, but several factors have come together at this time to create the crisis. "Crisis" is not too strong a word, for the field of engineering geology will be changed or eliminated if action is not taken now.

As an example to illustrate a common problem that is currently prevalent in engineering geology, the quality of geological reports for Class I Waste Disposal Sites submitted to the Regional Water Quality Control Boards of California can be cited. It has been estimated by the geologists who review geologic reports for the RWQC Board that most of the reports have to be returned for additional work, including correction of errors and submission of additional data to support the conclusions which have been presented. A recent survey of practicing engineering geologists who review professional geological reports in central California indicates that three major problems were encountered in a significant percentage of those reports in which professionals were involved. These are: erroneous information, incomplete or omitted data, and conclusions which are not supported by the data which have been presented. Some reviewers of geological reports in southern California indicate that often the most important data are lacking and thus erroneous conclusions are often presented. One reviewer recently referred to the prevailing practice as "synthetic geology" which tends to "make the facts fit the model"--a practice which, indeed, can result in disastrous conditions. These are rather damning commentaries on the current state of practice.

The current inability to produce quality studies is the result of many related factors including:

- \* lack of adequate academic preparation,
- \* inexperience in the application of investigation and analytical techniques,
- \* lack of motivation or incentive to do the best work,
- \* lack of competent and timely supervision,
- \* marketing prevailing over professionalism, and
- \* use of subjective "judgement" factors rather than scientific concepts

#### Educational Deficiencies

During the past twenty years, many universities and colleges have dropped field techniques, field geology, engineering geology, hydrogeology, and geomorphology from their schedules of regularly offered courses. These are among the courses considered essential elements in the academic preparation of engineering geologists (Higgins and Williams, in press; Slosson, 1987). These reductions in offerings have been prompted by several factors including the precipitous

decline in enrollments in geology departments, shifts in areas of perceived academic importance, and inability to attract and retain qualified faculty.

The number of schools which offer engineering geology and hydrogeology is small. Currently, in the United States, there are only five major schools which offer a program in engineering geology that leads to a PhD degree. The number of schools which offer PhD programs in hydrogeology is somewhat larger, but the projected rate of growth in this area is not great enough to meet the projected demand for individuals educated at the graduate-school level. It is both interesting and disturbing to note that not only are schools in the United States suffering from declines in numbers of students and numbers of course offerings, but the number of schools in Great Britain which are limiting their programs increases each year as a result of many of the same problems which exist in the United States.

The number of schools that offer programs in engineering geology through the PhD level is critical because these schools are the sources of future faculty. The great majority of colleges and universities will not accept or award tenure to an individual who does not have the PhD, except under very unusual circumstances. In addition, many of the more prestigious schools regard engineering geology (as well as applied geology) as a second-class science and not one as worthy as other areas of geology. This "anti-applied geologist attitude" essentially guarantees that qualified faculty will not be hired and retained in a department which considers their work to be of second-class stature. Under these circumstances, relatively few graduate students in these schools are able to pursue the PhD degree or even the MS degree in engineering geology. The pool of future faculty is thereby further reduced.

Tenure committees and deans are typically more interested in promoting faculty who conduct research that is perceived to be on the cutting edge of science, rather than faculty who are involved in applied science. In many academic/scientific environments, a person who is interested in the practical application of the geosciences may be labeled a technician, rather than respected as a scientist. Funding agencies like the National Science Foundation tend to award grants for studies perceived to advance pure science (i.e., the understanding of general processes) rather than for studies that develop the practical application of science. Applied geoscience is often viewed as being too local in scope to be supported by national funding agencies. Few state or local agencies can afford to support university research in engineering geoscience, particularly with overhead costs that vary from 35% to over 100% of the study cost. Prestigious geoscience publications, like the Geological Society of America Bulletin, the Journal of Geology and the Journal of Geophysical Research, typically do not publish applied-geoscience papers. Journals that do publish such papers are considered by some to be technical (i.e. not scientific) journals, and are therefore less prestigious. Even technical journals prefer to publish papers describing technological advances rather than papers on case studies, even though case studies describe the experience upon which advances in technology are based. If young engineering geology faculty often do not command peer respect among science faculty because of the applied nature of their work or the status of the journals in which their work is published, and cannot secure grants that are lucrative for the university, then they are at a great

disadvantage in competitive tenure processes.

Complicating the problem is the fact that there are various "circles" in which faculty tend to exchange among schools. Traditionally, the graduate students from the prestigious schools go on to become faculty at other prestigious schools; it is uncommon that graduate students from less-known graduate schools move into the faculty ranks of the prestigious schools. Graduate students from the prestigious school can join the faculty at the less-known schools; however, because of the limited number of students in graduate programs in engineering geology, a serious shortfall in qualified faculty and potential faculty exists. The outlook is not very encouraging inasmuch as very limited numbers of graduate students are being educated to become instructors of engineering geology (or applied geology).

Declines in oil company hiring have directly led to declines in geoscience student enrollment at both the graduate and undergraduate levels, even though the demand for engineering geoscientists has increased. University students were attracted to the geosciences during the boom days of the oil business because of the large number of jobs available, the lack of specific academic requirements other than degrees in the geosciences, the high rate of pay, the generous benefit packages, and the promise of working on interesting exploration projects in some rather exotic locations. Engineering geology has not been able to generate the same sort of student interest, even though employment opportunities in engineering geology are relatively abundant. Lower salaries, poorer benefits, greater exposure to lawsuits, job instability, the need to pass an exam to become certified, and the perception that many companies and individuals in engineering geology work at (or below) a bare minimum level of competency -- indicating a lack of personal and professional ethics --are all factors that make engineering geology less attractive than other options available to current university students.

Some geology departments are producing graduates who excel in computer science but who do not have the ability to identify, collect, or evaluate the geologic data they place into the computer. These graduates are essentially computer technicians, rather than geoscientists. It has been noted (Slosson and Petak, 1989) that ninety to ninety-five percent of the recent graduates in geology have not had the fundamental academic courses to prepare them to work effectively in the fields of hydrogeology, engineering geology, or hazardous waste management.

The total number of students in the geology major has declined dramatically since it peaked in 1983, at which time there were approximately 35,000 undergraduate majors in all fields of geology. In 1987, there were only about 15,000 majors, indicating a decline in majors of more than 60 percent. One area of geological instruction which has been most significantly impacted has been field geology, which is considered by most practicing engineering geologists to be the backbone of the geological sciences. A chief cause for this unusually large decline is that current field camp operations are expensive. With declining enrollments, school administrators are looking much more critically at the numbers of students electing to take summer field programs. Currently, it is estimated that only about 25 to 40 percent of the available capacity of established

field camps is being utilized. This means that the cost per student, which is already high in comparison to the cost per student for on-campus instruction, is even higher given that many of the costs associated with established summer camps are relatively fixed and independent of student enrollments. In some cases, the rapid rise in the cost of liability insurance has financially crippled field programs. This creates a situation in which field camps are particularly vulnerable targets for budget-conscious departments and universities. Would it not be wise if schools pooled their resources to continue one of the most important components of a geological education? A few of the well-established field camps draw from many universities, usually with one or more universities acting as a lead or coordinator.

Sophisticated (and expensive) research laboratories with related courses are perceived by many individuals and funding agencies as having greater prestige and value than field-oriented programs. The result of this preferential funding and support is that these laboratory-based programs are able to grow and to produce more individuals educated to PhD level, many of whom seek faculty teaching and research positions at other academic institutions throughout the United States. They carry with them the attitudes, including their feelings about applied geology, which have been developed at the schools from which they received their degrees.

Currently, few professors are teaching the basic concepts of courses in geomorphology, engineering geology, and hydrogeology. The latest statistics of the American Geological Institute indicate that only about 3 percent of the faculty members teaching and doing research at American colleges and universities consider or declare themselves to be engineering geologists or hydrogeologists. Compare that statistic with the fact that 30 percent of the new jobs in geology last year were in the field of engineering geology with the majority of these in consulting. In 1987 and 1988, the growth in the consulting sector of employment increased by approximately 30 percent compared to an average 2 to 7 percent growth in other sectors of geological employment. It becomes apparent that a good portion of the 30% of the students who have been able to find employment were not able to take the classes necessary to prepare them adequately for their professional careers. Practicing hydrogeologists and engineering geologists have no manuals available for most of the problems that they encounter. There are relatively few standard text book solutions to many of the engineering geology problems encountered, simply because of the complexity of the geological environment. In fact, it has only been during the past five years that more than one or two textbooks have become available in this field. For more than 25 years, a single textbook was really the only one available. To further complicate the problem, the evolution of the practice of engineering geology and hydrogeology is so rapid that material currently in textbooks becomes outdated quickly. Even materials presented in the professional journals may have a short shelf life because of the rate at which research and case experience are able to improve our understanding. The practicing professional geologists must bring all the elements of their background to bear on a geological problem. The broader and the more field-oriented the academic background, the better able the geologists are to recognize, acquire, and analyze the evidence that can be observed, and to appreciate and describe the implications of that evidence. Why should we expect that a correct analysis and solution will be made if the abil-

ity to detect and analyze evidence has not been developed and the geologist lacks peripheral vision?

### State of the art - State of practice

Research engineering geologists are making great strides in many of the technical aspects of the science. Computers can process large volumes of data using complex numerical and analytical models to help in solving the complex problems of engineering geology. However, an analysis of these advances in technology and hardware, in comparison with the results of the current practice of engineering geology, is distressing. Final solutions to investigations appear to rely increasingly on sophisticated and less realistic geological models which are often inappropriate for the problem. There are large and increasing numbers of records, and an embarrassing lack of geological understanding. The variation in resulting interpretations from the same data set among individuals with differing levels of academic training and professional experience is often so great that the results could not be considered usable (Williams, in press). Comparison of the computer-generated results with the results from interpretation developed by the geologist indicated that although the results from the computer may be more repeatable, there is little if any indication that many of the results are geologically realistic.

Computer models of geological processes are generally first-order approximations, based upon a series of assumptions and input parameters, regarding the variation in the physical and chemical characteristics of a rock mass and its interstitial fluids through time. What is a first-order model, as contrasted with higher-order models? Imagine an equation of the following form:

accurate answer =  $a + b + c + \dots + n$ .

The model equation

answer =  $a$

is the first-order model; however, the value of 'answer' is only  $x\%$  of the 'accurate answer'. The model equation

second answer =  $a + b$

is the second-order model, and 'second answer' is  $y\%$  of 'accurate answer', where  $y$  is greater than  $x$ . As we continue to add terms to the model equation, we have ever higher-order models that are more accurate than the lower-order models. A good first-order model is expandable to higher-order modeling when additional data is available. A first-order model may provide 95% of the accurate answer for a given problem, or it may supply only 5% of the accurate answer. The test of a model lies in the comparison between predictions made by the model and the observed phenomena. Anyone who uses the results of a computer model uncritically, without thoroughly evaluating those results in comparison with observational data, is guilty of having misused the model. Such results are not scientifically valid.

Computer modeling can only be as accurate as (1) the knowledge of the physical processes involved, as reflected in the model equations governing the rheology, constitutive properties, boundary conditions, temperature, chemistry, etc., and (2) the input values derived from observational data. Reproducibility (precision) is not an indicator of accuracy (correspondence with reality). For example, a factor-of-safety calculation can be made using software written with

the tacit assumption that an isotropic, homogeneous, linear-elastic mass is at rest on a cylindrical, spherical or planar frictional surface. If the mass is actually a collage of various non-linear rheologies in a discontinuous, anisotropic, inhomogeneous mass, then a simple first-order model of slope stability will not be able to provide accurate stability assessments. Higher-order modeling will be required; that is, geoscientists who can recognize that the software is inappropriate for use in this case and who can perform the required higher-order modeling are required if accurate stability assessments are to be made.

If better scientific models and analytical methods exist, why are the results of investigations not improving and, in fact, appear to be regressing (Slosson and Petak, 1989)? Even with advanced technology and models, people who are unable to use the state-of-the-art knowledge effectively will not produce quality results and may produce erroneous results (see Fig. 1).

#### Problems in Meeting Employment Demands

Shortages of well-educated and experienced individuals in engineering and applied geology have been documented. The shortages result from insufficient courses and programs in engineering geology (including hydrogeology) and in the sparsity of adequately prepared faculty members to present those courses and programs. In addition to the shortages in the academic sector, shortages of qualified management and supervisory personnel exist in the consulting firms and government agencies. There is an inadequate supply of middle-management professionals who are adequately trained to supervise entry-level geologists. The growth in many companies, particularly those associated with the hazardous waste field, has been so rapid that many entry-level geologists have risen to levels of management within a few years or less but have had little opportunity to develop the expertise and experience necessary to be able to supervise others effectively. Thus, most of the recently hired are not receiving on-the-job training or supervision necessary during the first two or three critical learning years simply because the supervisors are not adequately prepared to do their job or are so impacted by their own responsibilities that they are unable or unwilling to devote the appropriate time to training the entry-level geologists. The result of the above factors leads to frequently occurring errors such as:

- \* Inadequate subsurface analysis
  - poorly located
  - insufficient depth
- \* Misinterpretation or non-use of aerial photos
- \* Failure to conduct thorough overview
- \* Failure to look at adjacent properties and geology
- \* Failure to think in three (let alone four) dimensions

Some of the necessary capable professionals are even involved in marketing management and not applied geology.

The problem of limited management experience is not restricted to the private sector but impacts the governmental regulatory sector as well. Many government agencies are finding it increasingly difficult, if not impossible, to

attract and retain experienced individuals. Public agencies have become training grounds for geologists prior to their entry into private sector practice and much of this background experience is, again, without professional supervision. Part of the inability of government agencies to retain experienced staff results from comparatively low pay and limited opportunities for advancement.

The academic preparation and professional experience of many field investigators must be evaluated. Generally, the principal of a company does not collect the basic information to determine the final solutions to a problem. The individual collecting the data is often one of the least experienced of the firm's geological employees. Although these data are reviewed by more experienced people, they can only review the data they receive and cannot comment upon what has not been noted or reported by those who conducted the investigation. If the original observer did not appreciate the significance of, or understand what was present, critical information was not recorded and thus inappropriate interpretations and conclusions are likely to be made.

### Synthetic Geology

Decisions are frequently based on subjective or "judgement" factors rather than on prudent scientific concepts and good engineering practices. The practitioner who attempts to please the client and/or politicians may filter, deliberately or subconsciously, the observed data set to develop conclusions that are compatible with the "expected" or desired results. A client will occasionally make specific suggestions about the results that are expected to be obtained and reported by an engineering geologist. Such suggestions may not be subtle, particularly during discussions of payments and contracts, when the question may be asked "This fee is for a report that will give us a clean bill of health on the site and will satisfy government so that we can get a permit, isn't it?"

The concept that *the level of professional standards of work will drop to the lowest level allowed by government* is a characterization of a serious problem. For financial reason, many clients request that the work of the consultant not exceed the minimum required by government---in fact, this may be the most important contributing factor to lowering of the Standard of Practice. Thus, the professionals are coerced to reduce the thoroughness of the work effort. Cases have been reported from southern California where, because the governmental requirements as to the level of study vary from jurisdiction to jurisdiction, companies have been tailoring their studies to meet the minimum requirements of the area in which the site being evaluated is located. This practice creates a ready market for the less-competent consultants---those limited in knowledge, training, and professional skills and perhaps, professional ethics.

### Outlook

The outlook is not encouraging. The decline in enrollments in the nation's geology departments indicates that there are fewer students preparing themselves to enter the profession of geology. Employment trends show that demand for well-educated and well-trained individuals will triple or quadruple during the next decade. Turner (in press) clearly indicates that the demand for engineering geologist, primarily in work in the clean-up of hazardous-waste sites, will



increase by more than 600 percent in the next decade. There is reason to believe that the demand will continue to grow following that period. It is important to note that, in addition to the number of individuals that are in demand, the targeted individual from the employer's perspective is one with a Master's degree or equivalent level of graduate training. The Master's degree is becoming the entry-level degree for work in the hazardous-waste field, just as it had become the entry-level degree for work in the petroleum industry prior to the collapse of hiring in that sector. This demand places additional stress on academic programs already under-prepared to educate students to adequately perform in engineering geology.

One indication that efforts are underway to attempt to improve upon the quality of work being done is the increase in the number of states in which professional registration (or licensing in some form) for engineering geologists is in place or being considered by the respective legislatures. One of the principal justifications for registration is protection of the public---that is, members of the public are provided some governmental assurance that the level of geological work being done meets at least minimum standards. The growth in number of states with registration is a reflection of an underlying feeling that steps must be taken to improve the current practice. Simple projection of the data about the number of states with registration and the decade in which that registration was enacted indicate that by the mid-1990's the majority of states will have some form of professional registration for geologists. In some states, in addition to implementing registration, active consideration is being given to requirements that continuing education be demonstrated in order to maintain registration.

Despite the increase in professional registration requirements, indications are that the current trend is not going to change. Investigations will continue to be hastily made by unprepared and inexperienced individuals and will be reviewed by those not qualified to conduct the reviews or those who are so badly overworked that the quality of their reviews suffers. Even if they are qualified and have time to conduct reviews, they cannot compensate for errors and omissions in the investigation. If the geologic community fails to accept its responsibility, the engineering profession will eagerly step in and usurp the work, and the critical role that geology should play will be eliminated.

It is clear that the engineering community stands ready and willing to take over the responsibilities of the engineering geologists. The logical consequences are that, before long, geology will no longer be considered in most land-use and construction decisions. It is imperative that we in the profession reassess the educational backgrounds, current practices, and resulting performances of engineering geologists and take steps promptly to remedy deficiencies, starting with curricula, teaching staff, and attitudes about the ethics and values of engineering geology.

#### References

American Geological Institute, 1988, Directory of Geoscience Departments, United States and Canada, 27th Edition, p. 243.

Higgins, D. and W. Williams (eds.), in press, Academic preparation for careers in engineering geology and geological engineering: American Geological Institute, Special Publication.

Legget, R. F., 1939, Geology and engineering: McGraw-Hill Book Co., Inc., 650 pp.

Paige, S., 1950, Applications of geology to engineering practice: Geological Society of America Berkey Volume, 327 pp.

Slosson, J. E., 1987, Challenging academia to return to basics, in Geotimes, V. 32, N. 11, p. 4.

Slosson, J. E. and W. J. Petak, 1989, Why is the gap between "standard practice" and "state-of-the-art" widening?, in Association of Engineering Geology News, V. 32, N. 2, pp. 18-19.

Turner, A. Keith, in press, Technical personnel requirements to support the national clean-up of hazardous waste sites, in Higgins, J. and Williams, J. W. (editors), Academic preparation for careers in engineering geology and geological engineering: American Geological Institute, Special Publication.

Williams, J. W., in press, Is interpretation of subsurface geological data from an alluvium filled basin geological art or science?: (abstract) 1989 Annual Meeting of Association of Engineering Geologists.

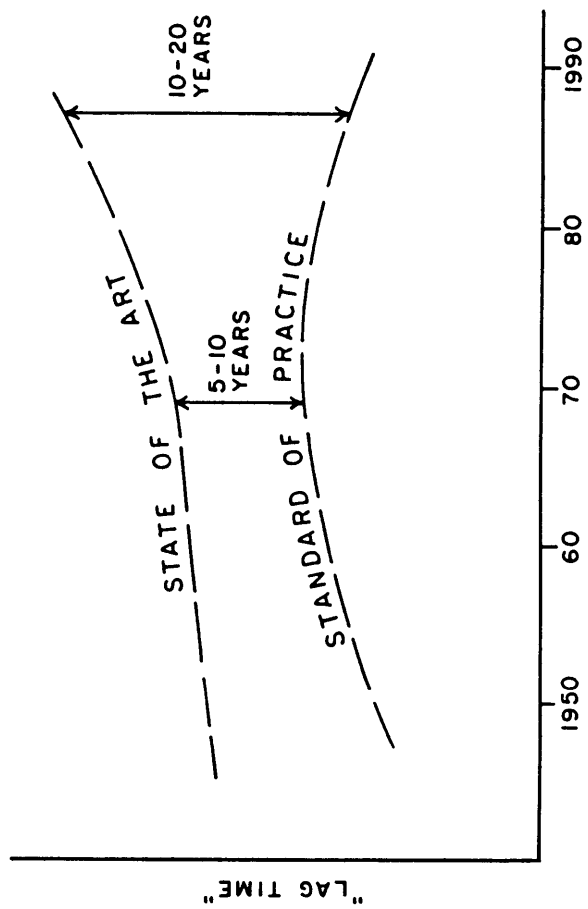


Figure 1. Estimated differential between standard of practice and state of the art.



## SECTION 2: CARBONATE SYSTEMS



## TRANSPORT OF CHEMICAL CONTAMINANTS IN KARST TERRANES: OUTLINE AND SUMMARY

Malcolm S. Field  
Exposure Assessment Group (RD-689)  
Office of Health and Environmental Assessment  
U.S. Environmental Protection Agency  
401 M St. SW  
Washington, DC 20460

Disclaimer: The views expressed in this paper are solely those of the author and do not necessarily reflect the views or policies of the U.S. Environmental Protection Agency.

### Abstract

Chemical spills that reach an aquifer in karst terranes do not behave like those in granular or highly fractured aquifers. Spills reaching diffuse-flow aquifers display relatively slow transport, are radially dispersive, and can be tracked through the use of monitoring wells. Spills in most karst terranes, however, are stored and transported in both the vadose and phreatic zones and do not exhibit radial dispersion. Actual contaminant transport in the phreatic zone of a karst aquifer may be extremely rapid to and highly concentrated at eventual discharge points, but the pollutant(s) cannot be tracked by any methods currently known. Contaminant attenuation is greatly limited in karst terranes. The unusual storage and transport characteristics responsible for the rapid transport and poor attenuation of contaminants in karst aquifers are a consequence of the unique properties of their flow system. Sinkhole development, the absence of surface water drainage, solutional enlargement of vertical fractures in the unsaturated zone, and the development of subsurface conduits (caves) are some of the properties of karst terranes that have substantial effects on the storage and transport of chemical contaminants.

### Introduction

Great progress has been made during the past 15 years in the field of contaminant hydrogeology. The primary emphasis has been directed towards studies of: (1) development of better contaminant investigation methods, (2) a better understanding of contaminant behavior in the subsurface, (3) the development of better computer models for the accurate prediction of contaminant migration, and (4) the development of more effective aquifer remediation techniques. Nevertheless, most researchers in each of these four interrelated areas would agree that the state-of-the-art for these topics leaves much to be desired. Contaminant hydrogeology is still in its infancy and poorly understood. Many of the theories developed for contaminant behavior in the subsurface have had to be repeatedly revised when they have been compared with field data.

Contaminant behavior in the subsurface must be understood better than current knowledge allows if detection and remediation techniques are ever to be really effective. New and useful research on the subject of subsurface contaminant behavior continues to be published, either building on, or refuting

past work. Good general discussions on the behavior of organic contaminants in the subsurface can be found in the works of Mackay et al. (1985) and Mackay and Cherry (1989). In these two papers, the fate and transport basics in relation to granular and fractured media are presented, but the authors are very careful not to go beyond the current level of understanding. The most commonly discussed aspects regarding subsurface contaminant behavior, advection, dispersion, sorption and retardation, and chemical and biological transformations are well reviewed in these papers. For any location with organic chemical contamination of the subsurface, each of the above physical, chemical, and biological factors must be carefully evaluated along with the geology and hydrology of the site.

Karst aquifers present a uniquely different situation. The basic hydrogeological assumptions normally made when attempting to understand their subsurface flow regime are not valid when applied to karst terranes. Groundwater flow in most karst terranes is turbulent, convergent in the upper drainage reaches, and dispersive in the lower reaches. Flow commonly occurs in large passages at very high velocities with nearly insignificant hydraulic gradients (Field, 1989; Quinlan and Ewers, 1985). The complexities of groundwater flow in karst terranes have been discussed in many recent publications. The interested reader is referred to Milanović (1981), Quinlan and Ewers (1985), White (1988), Ford and Williams (1989), Quinlan (1989), and Field (1989) as good sources of information.

In this paper, I shall attempt to combine the physicochemical characteristics of organic chemical contamination of a karst aquifer with the complex hydrogeological characteristics that typically exist in karst terranes. Other authors have attempted this in the past. Memon and Prohic (1989) tried to define contaminant transport in karst terranes utilizing conventional groundwater flow and transport equations originally developed for flow and transport in porous media. Their attempts failed because of their lack of recognition of the hydrogeologic complexity associated with karst terranes and because most karst aquifers are unlike those they purportedly described. Contrary to what might be expected, it is possible to develop an understanding of contaminant behavior in a karst terrane, but only after the dominant factors that control karst groundwater circulation and contaminant transport are recognized.

#### Contaminant Infiltration

Chemical releases in karst terranes do not behave in a manner similar to those in terranes underlain by granular or highly fractured aquifers. Contaminants reaching diffuse-flow aquifers generally move slower than those in conduit-flow aquifers. Their movement is radially dispersive, and can be tracked with monitoring wells (Quinlan and Ewers, 1985; Quinlan, 1989). Releases in most karst terranes are stored and transported in both the vadose and the phreatic zones. Transport in the vadose and phreatic zones may be turbulent and cover hundreds of meters in only a few days. Actual contaminant transport in the phreatic zone can be expected to be extremely rapid to and highly concentrated at eventual discharge points, but cannot be tracked by methods currently used successfully in other aquifers. It should be noted that karst aquifers dominated by "diffuse-flow" may be significantly different from granular aquifers. Karst aquifers dominated by diffuse-flow are not always characterized by the slow-moving laminar flow that is described by Darcy's law, but is often a fast-moving



turbulent flow that violates Darcy's law. It can be envisioned as a giant sponge with water flowing uniformly through it. Thus, most karst aquifers dominated by diffuse-flow and all those dominated by conduit-flow cannot be described by the basic flow and transport equations normally employed in contaminant studies.

The unusual behavior of chemical contaminants in karst aquifers begins when a release actually occurs. Initially, the contaminant infiltrates through the soil zone, flows overland to run down a sinkhole (doline), or flows into a nearby sinking stream. When released onto or within a soil-covered area, the downward migration of the contaminants is likely to be retarded as a result of either the degree of heterogeneity of the soil zone, or as a result of specific physicochemical properties of the contaminant, or as some combination of the two. None of these retardation factors are expected to prevent a chemical release from reaching the water table, however, unless the release is of a "very" small volume. Rate of movement through the soil may be greatly enhanced by flow through soil macropores; over 90% of total water flow in saturated soil may occur in soil macropores (Dragun, 1988, p. 24).

Much of the vertical migration through the soil zone occurs through soil macropores which may be considered to be controlling factors on the rate and direction of contaminant infiltration. Macropores are cracks and fissures that may be formed by the shrinkage of clay-rich soils during dry periods, tubes that may be formed by rotting of roots or by burrows, differential chemical weathering of bedrock material, freeze-thaw cycles, and cultivation techniques. It is important to recognize that water and chemicals percolating through soil macropores have minimal reaction with the soil because macropores tend to channel chemicals away from soil water (Dragun, 1988, p. 29).

Sorption of chemical constituents to microparticles cannot be expected to prevent the downward (or lateral) migration of contaminants because the microparticles are themselves readily transported through the soil zone (Lyman and Loreti, 1987, p. 87), either by eluviation or through macropores. They report that highly sorbing chemical constituents (PCB's may be a good example) may actually be very mobile because of the natural mobility of soil particles. Eluviation is an important process by which contaminants may pass through the soil zone.

Flow into a sinkhole or through the bed of a sinking stream (the stream may either slowly leak water through its bed or it may actually flow into a discrete opening) can result in extremely rapid transport of contaminants into an aquifer by way of subcutaneous drains (Smart and Hobbs, 1986) which allow for almost unimpeded vertical transport in the subsurface (Figure 1, Flow Type 5, and Figure 2). Subcutaneous drains are the main discharge points for flow within the epikarstic zone.

#### Behavior in the Epikarstic Zone

Directly beneath the soil zone is the top of the epikarstic (subcutaneous) zone (Williams, 1985). This zone consists of the uppermost portion of the unsaturated rock where significant fracturing, solutional enlargement, and storage may occur (Figure 2). It is approximately 3 to 10 meters thick and is separated from the water table by a relatively unfractured, unweathered, waterless zone of rock that is sporadically breached by subcutaneous drains and

vadose shafts (Quinlan, 1986, 1989). Vadose shafts are solutionally produced vertical tubes ranging in size from a few centimeters to several meters across. They often occur in complexes, and contain a drain hole at their bottom (Figure 1, Flow Type 4).

The myriad of minute fractures in the epikarstic zone are capable of retaining large quantities of chemical contaminants after a release because of electromolecular forces that exist between soil particles, water, and contaminants. Soil particles washed down from the overlying soil zone may be able to adsorb some of the contaminants while infiltrating through the soil zone, but these soil particles are themselves readily stored and transported through the epikarstic zone.

Contaminants will be subjected to the flow and storage characteristics of the epikarstic zone. If these contaminants have not entered directly into a subcutaneous drain, they are likely to flow both vertically and laterally through this zone, always taking the easiest, most direct path downward. Substantial storage within this zone can be expected, thus allowing for the slow release of chemical constituents to the underlying aquifer for many years (Even et al., 1986).

Release of contaminants from the epikarstic zone occurs primarily during large storm events that tend to flush out the chemicals and temporarily perch local water tables. Such perching occurs as the volume of water entering the epikarstic zone begins to exceed the drainage capacity of the zone; this leads to the development of a hydraulic gradient that commonly has the form of an elongated cone of depression (Field, 1989; Williams, 1985) with a subcutaneous drain acting as the lowest point of hydraulic head, similar to a pumping well (Figure 2). Lateral flow and transport to subcutaneous drains may exceed several hundred meters and allow for very rapid flow rates.

### Contaminant Transport

As noted previously, contaminants entering the subsurface of a karst terrane often do so in a relatively unrestricted manner, initially as point sources. Flow in the vadose zone of the bedrock occurs along major vertical joints, faults, and bedding plane partings. Divergent flow readily occurs in the vadose zone, as shown by the large number of diversion passages for vadose cave streams (Palmer, 1986). Water and contaminants are always moving progressively downward to lower-flow routes where they may feed larger conduits extending over long distances.

Although groundwater flow in karst aquifers can be envisioned as ranging between conduit and diffuse flow end-members, most flow is mixed, with one of the flow-types predominating over the other (Quinlan and Ewers, 1985). Their characteristics are reviewed by White (1988) and Ford and Williams (1989). Conduit flow occurs in large passages with relatively high flow velocities that result in turbulent flow conditions and may have an almost insignificant hydraulic gradient.

Between the epikarstic zone and the water table, subsurface water and contaminants percolate downwards, generally via vadose shafts. Often, however, flow occurs in vadose conduits which are typically oriented down the dip of the

rock (Figure 1, Flow Type 7). A series of vadose conduits tend to form different cave levels that may be a reflection of the geomorphic history of a region. Flow and transport are primarily in the vertical direction, but vadose conduits can intercept this vertical flow in lateral directions that may exceed several kilometers.

Upon reaching the phreatic zone, flow and transport will be in response to the hydraulic gradient in the direction of the nearest phreatic conduit, usually along the strike of the bedrock (Palmer, 1986). Intergranular flow and flow through micro- fractures in the phreatic zone will comprise a diffuse-flow component that leads to the phreatic conduit. This flow will most often be laminar and obey Darcy's law although the strong anisotropy may invalidate the assumption that flow lines are normal to equipotential lines (Palmer, 1986). Significant amounts of storage may occur within the microfractures in this zone. Evidence for this storage is seen in the high concentrations of contaminants that appear at springs during high flow. During storm events, chemical constituents stored in the rock matrix are flushed out at springs (Figure 1, Flow Types 9 and 10).

Actual flow and solute transport within a conduit will emulate turbulent flow in a sewer line with velocities on the order of meters/day to several thousand meters/day. A phreatic conduit, unlike a sewer line, will be very rough, contain many more sharp bends and turns, and may be subject to numerous blockages, either temporary or permanent. Vertical flow upwards along passages can be expected. On a flow net of a groundwater basin, the phreatic conduits are the true flow lines of the aquifer.

The floor of a conduit is often lined with a bed of insoluble sediment over which contaminants may travel. If clays are present in these sediments, sorption of the contaminants to them is likely to occur. Backwater zones in a cave tend to store and concentrate contaminants. Collapse of a cave roof to form breakdown may also result in the temporary storage and concentration of contaminants. Storm events tend to flush contaminants through or around the breakdown.

Storm events do not flush out all residual contaminants. In fact, storms tend to create a type of bank storage in which water and contaminants are driven up into older, higher cave levels and also into the rock matrix. Once in the cave matrix, drainage and chemical reactions may occur slowly. Thus, chemical contaminants reaching phreatic conduits are not necessarily flushed out freely. Rather, they may be retained for very long periods.

Another important factor to consider is the potential relationship between a sinkhole and a phreatic conduit. If there is a direct connection between the two, storm events may greatly affect contaminant migration. Flow into a sinkhole may be so rapid that the tremendous influx of water causes very rapid and extreme rises in the water table. In this instance, two problems may occur. First, the inflowing water may act as a hydraulic dam, causing water and contaminants to back up against the greater pressure head created by the inflowing water. Second, the inflowing water may be under enough pressure to actually drive phreatic water and contaminants back upgradient of the sinkhole. This backflowing of contaminants has been observed in dye tracing experiments where the dye, acting as a surrogate for a pollutant, was driven up the regional gradient over 300 meters to an upgradient sampling location (Ewers et al., 1989).

### Contaminant Discharge

Conduits are rarely intercepted by wells. If they are, however, obviously the wells could be monitoring points for water-borne contaminants. Natural discharge occurs in the form of springs, and seeps. Commonly, the convergent nature of conduit-flow that occurs in the upper reaches of a karst groundwater system gives way to a divergent system at the lower reaches (Quinlan and Ewers, 1985). This is evident from the number of adjacent springs shown by dye tracing studies and similarity in water chemistry to be connected to the same cave system.

If springs are the discharge points for conduits, then they may be releasing very large quantities of contaminants because of the large volumes of water discharged. Most commonly, contaminant concentrations at springs tend to rise during storm events when the system is being flushed out (Quinlan and Alexander, 1987). A similar situation occurs at springs at the bottom of sinkholes which are just windows to a flow line. At such a spring, a stream of water enters at one end of the bottom of the sinkhole and disappears at the opposite end. Seeps will not have large flows and will not show such large variations in water quality because most are more of a result of a diffuse flow component in a karst system (Figure 1, Flow Type 10).

Contamination may actually be temporarily stored in portions of a conduit until a water level rise in the system allows the contaminant to be drawn out of the system. Estavelles (reversing springs) may be important influences on the transport and discharge of contaminants. [An estavelle is a type of sinkhole that is directly connected to a subsurface conduit (Milanović, 1981, pp. 102-105; Smart, 1988)]. Initially during low flow events, a contaminant is likely to be transported along the subsurface conduit. However, during a large storm event, an increase in hydraulic head may be so great that the piezometric surface will actually rise above the land surface. When this happens, water is forced out of the ground. Contaminants will be: (1) forced into the surrounding rock matrix, (2) forced back up the subsurface conduit, and (3) discharged from the estavelle. Thus, estavelles may either dilute or discharge contaminants.

### Immiscible Contaminants

Special consideration must be given towards the behavior of immiscible liquids. Most contaminant hydrogeologists are aware of the fact that light nonaqueous phase liquids (LNAPLs) tend to float and dense nonaqueous phase liquids (DNAPLs) tend to sink. Neither LNAPLs nor DNAPLs are readily miscible with water. Most of these types of chemicals slowly "bleed" into the water over an extended period of time, however.

LNAPLs released in karst terranes are not easily affected by dispersion caused by the bifurcation of vadose water along the various routes of flow. This results in the contaminants becoming concentrated in major active conduits (Palmer, 1986). Large storms tend to flood karst groundwater systems. If LNAPLs are present in a karst system, the sudden flooding of the system may cause localized decreases in flow velocity (Palmer, 1986) and force globules of organic chemicals to be driven into the rock matrix and up into older, higher levels. These globules may be held onto the cave walls or in the tight fractures for long periods. Light volatile contaminants tend to rise up and flow through cave

passages in gaseous form. These can then rise into basements creating hazards in the form of toxic vapors that may also be explosive.

DNAPLs tend to sink rapidly to the bottom of an aquifer where they will form sludges in deep pools (Palmer, 1986) and adsorb to microparticles. These sludges will not respond to the hydraulics of flowing groundwater in most instances, but will instead flow as a bulk density phase. An exception where flow hydraulics may be important could be groundwater flow in a conduit system where very high velocities may be able to influence transport of the bulk mass. If low flow conditions persist for long periods and allow the water table to drop below the level of the sludge pool, a sudden influx of water during a storm event may possess sufficient force to rip out and entrain much of this sludge along the conduit. Throughout the retention of this sludge, small portions of this contaminant slowly become miscible with the water and are advected through the system, thus providing a continuous source of contamination to discharge points (Mackay and Cherry, 1989, Figure 3).

#### Contaminant Attenuation

As described above, karst aquifers are excellent transporters of contaminants. Unfortunately, karst aquifers are not very effective at attenuating subsurface contaminants because they lack the self-treatment capacity found in other aquifer types (Ford and Williams, 1989, p. 518).

According to Ford and Williams (1989, p. 519), the natural attenuation of contaminants in karst aquifers is limited because of the (1) significant lack of available surface area for adsorption, for ion exchange, or for colonization by microorganisms, (2) rapid infiltration of water and contaminants restricts the ability of highly volatile chemicals to evaporate, (3) typically thin soil cover and the relatively large secondary voids allow for rapid transport of contaminants, (4) turbulent flow regimes associated with the high flow rates enhances contaminant transport, and (5) lack of sufficient time for time-dependent elimination mechanisms (e.g., bioremediation) to act on contaminants because of the rapid flow-through. These five limiters of attenuation greatly affect the transport and discharge of contaminants.

#### Summary

Contaminants released in a karst terrane may be expected to travel very rapidly from the site of a spill to discharge locations several kilometers away. Significant amounts of storage may occur within the system. Once contaminants are released into the subsurface, there is very little that can be done to track or remove the contaminants from the subsurface. The natural system can do minimal self-treatment. The problems associated with transport, storage, and attenuation of contaminants in a karst aquifer are a consequence of specific attributes characteristic of it.

#### References

Dragun, J., 1988, The Soil Chemistry of Hazardous Materials, Hazardous Materials Control Research Institute, Silver Spring, MD, 458 pp.

- Even, H., I. Carmi, M. Magaritz, and R. Gerson, 1986, Timing the transport of water through the upper vadose zone in a karstic system above a cave in Israel, Earth Surf. Processes and Landforms, 11, 181-191.
- Ewers, R. O., D. Keagy, J. F. Quinlan, and M. S. Field, 1989, Discussion of "'Testing' a limestone aquifer using water-table response to storm water discharged into sinkholes," by A. Michalski and J. Torlucci, Jr., Ground Water, 27, 715-716.
- Field, M. S., 1989, The vulnerability of karst aquifers to chemical contamination, Proc. of the 3rd Inter. Conf. on Advances in Ground-Water Hydrology, (Tampa, FL), edited by, J. E. Moore, A. A. Zaporozec, S. C. Csallany, and T. C. Varney, American Institute of Hydrology, Gurr & Associates, Inc., Lakeland, FL, 130-142.
- Ford, D. C., and P. W. Williams, 1989, Karst Geomorphology and Hydrology, Unwin Hyman Inc., Winchester, MA, 601 pp.
- Lyman, W. J., and C. P. Loreti, 1987, Prediction of soil and sediment sorption for organic compounds, Contract No. 68-01-6951, Task 15, U. S. Environmental Protection Agency, Office of Water Regulations and Standards, Washington, D. C., 99 pp.
- Mackay, D. M., P. V. Roberts, and J. A. Cherry, 1985, Transport of organic contaminants in groundwater: Distribution and fate of chemicals in sand and gravel aquifers, Envir. Sci. and Tech., 19, 384-392.
- Mackay, D. M., and J. A. Cherry, 1989, Groundwater contamination: Pump-and-treat remediation, Envir. Sci. and Tech., 23, 630-636.
- Memon, B. A., and E. Prohic, 1989, Movement of contaminants in karstified carbonate rocks, Envir. Geol. and Water Sci., 13, 3-13.
- Milanović, P. T., 1981, Karst Hydrogeology, Water Resources, Publications, Littleton, CO., 434 pp.
- Palmer, A. N., 1986, Prediction of contaminant paths in karst aquifers, Proc. of the 1st Conf. on Envir. Prob. in Karst Terranes and Their Solutions, (Bowling Green, KY), National Water Well Association, Dublin, OH, 32-53.
- Quinlan, J. F., 1986, Recommended procedure for evaluating the effects of spills of hazardous materials on ground water quality in karst terranes, Proc. of the 1st Conf. on Envir. Prob. in Karst Terranes and Their Solutions, (Bowling Green, KY), National Water Well Association, Dublin, OH, 183-196.
- Quinlan, J. F., 1989, Ground-water monitoring in karst terranes: Recommended protocols, regulatory problems, and implicit assumption, Report in press, U.S. Environmental Protection Agency, E. N. Koglin, Project Officer, Environmental Monitoring Systems Laboratory, Las Vegas, NV, 79 pp.
- Quinlan, J. F., and Alexander, E. C., Jr., 1987, How often should samples be taken at relevant locations for reliable monitoring of pollutants from an agricultural, waste disposal, or spill site in a karst terrane? A first approximation, Proc. of the 2nd Multidisc. Conf. on Sinkholes and the

- Envir. Impacts of Karst, edited by B. F. Beck and W. L. Wilson, Balkema, Rotterdam, 277-286.
- Quinlan, J. F., and R. O. Ewers, 1985, Ground water flow in limestone terranes: Strategy rationale and procedure for reliable, efficient monitoring of ground water quality in karst areas, Proc. of the 5th Nat. Symp. and Expo. on Aquifer Restor. and Ground Water Monitor., (Columbus, OH), National Water Well Association, Worthington, OH, 197-234.
- Smart, C. C., 1988, Artificial tracer techniques for the determination of the structure of conduit aquifers, Ground Water, 26, 445-453.
- Smart, P. L., and S. L. Hobbs, 1986, Characterisation of carbonate aquifers: A conceptual base, Proc. of the 1st Conf. on Envir. Prob. in Karst Terranes and Their Solutions, (Bowling Green, KY), National Water Well Association, Dublin, OH, 1-14.
- White, W. B., 1988, Geomorphology and hydrology of karst terrains, Oxford University Press, New York, NY, 464 pp.
- Williams, P. W., 1985, Subcutaneous hydrology and the development of doline and cockpit karst, Zeit. fur Geomorph., 29, 463-482.

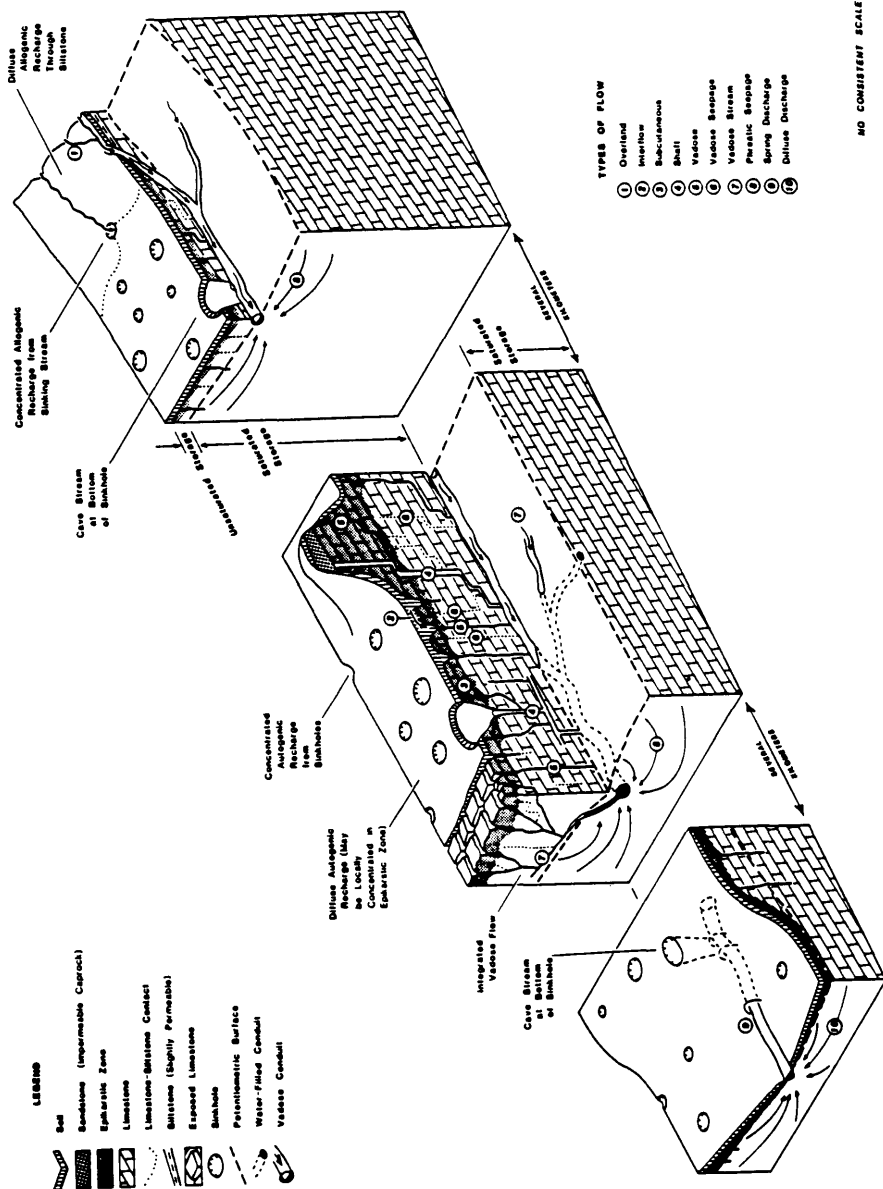


Figure 1. Block diagram of a maturely karsted terrane in gently dipping rocks of a low-relief landscape. Groundwater flow occurs through the inflow from (1) sinking streams, (2) vertically percolating water infiltrating through soils and sinkholes, (3) tributary cave streams, and (4) seepage through conduit walls. Contaminants will enter the aquifer through the same mechanisms that control water inflow (after Quinlan, 1989).



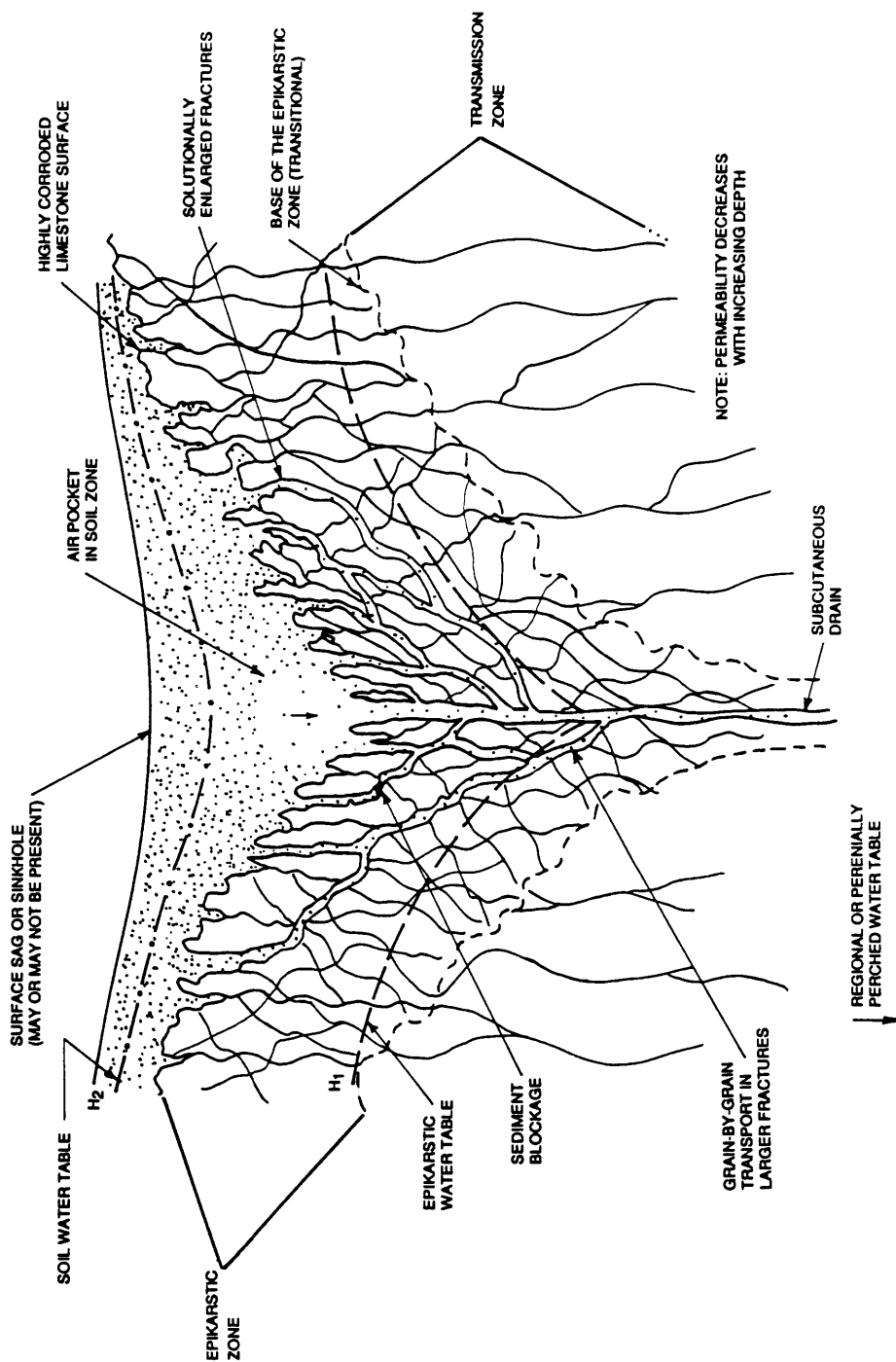


Figure 2. The epikarstic (subcutaneous) zone during a period of substantial recharge. Perching may occur in both the epikarstic zone ( $H_1$ ) and in the soil zone ( $H_2$ ), but flow is always directed towards a subcutaneous drain.



# GROUNDWATER RECHARGE IN AN ARID KARST AREA IN SAUDI ARABIA

AL-SAAFIN, A.K., BADER, T.A., SHEHATA, W.  
King Fahd University of Petroleum and Minerals  
Research Institute,  
Dhahran 31261, Saudi Arabia

HOETZL, H., WOHNLICH, S.  
University of Karlsruhe  
Dept. of Applied Geology  
D-7500 Karlsruhe, Germany

ZOETL, J.G.  
Forschungszentrum Joanneum  
Institut f. Geothermie und Hydrogeologie  
A-8010 Graz, Austria

## Abstract

Groundwater recharge in arid areas suffers generally under the unfavourable climatic conditions and requires high permeability of the surface. The efficiency of such conditions was investigated in the eastern Saudi Arabian desert, where the karstified Umm Er Radhuma formation, the most prolific aquifer of the Gulf region, is outcropping. Numerous catchment areas there are directly connected to open karst shafts. Meteorological and hydrologic events were monitored in selected small watersheds. The precipitation rate of the episodic rainfalls averages 140 mm/a. Depending on the infiltration capacity of different soil types surface runoff into cave shafts takes place if precipitation exceeds 4.5 mm per half an hour. The total discharge to the shafts was calculated with 45 percent of the yearly rainfall. This confirms that even under arid conditions a considerable amount of recharge can be expected in open karst areas.

## Introduction

In arid land hydraulic water resources management the question of groundwater recharge to deep aquifers is one of the most controversially discussed issues. Because of evapotranspiration rates, which by far exceed the annual precipitation, a percolation of infiltrating water down to the groundwater is indeed questionable. Nevertheless the question of present time groundwater recharge into deep aquifers has vital influence on future groundwater resources management. No recharge would mean, that all presently used aquifers will progressively show head loss and increasing salinity. Later on they can even fall dry.

Dramatically dropping groundwater levels in most arid land aquifers prove, that due to advanced technical possibilities in the last 30 years, the existing resources have been exaggerated. Most of the investigations on groundwater recharge of deep aquifers were done in the discharge areas, which usually are far apart from possible recharge areas. They were done by interpreting mostly incomplete water level data or by investigations on hydrochemical and isotopic data. But due to uncontrolled withdrawals from the aquifer and/or unknown infiltration areas the question kept to be open, if there is a considerable amount of recharge to deep aquifers at certain areas or if there is only fossil ground water.

The investigation presented here were conducted within the possible infiltration area of the most important fresh water aquifer of Eastern Saudi Arabia, the Umm Er Radhuma (UER) aquifer. The study area (figure 1) lies next to the village of Ma'aqala in north-central Saudi Arabia.

The objective of the research was to evaluate the actual amount of groundwater recharge which takes place in the karstified outcrop area of the UER aquifer. The major field work was done in two field campaigns in 1986 and 1987 and several inspection tours. The following field program was performed:

- Geological, geomorphological and hydrological mapping of the outcrop area
- Selection of small test water sheds and their equipment with hydrological instruments
- Monitoring of meteorological and hydrologic events

Measurements were taken during the winter seasons of 1987, 1988 and partially 1989.

### **Hydrogeological overview**

#### **Sediment sequence and structure**

The hydrogeological situation of Eastern Saudi Arabia is characterized by the flat eastward dipping of the Mesozoic and Cenozoic sediment sequence of the Arabian Shelf Platform towards the subduction zone in front of the Zagros Mountain chains. Cretaceous sediments outcropping east of Riyadh, about 400 km from the Gulf and at an altitude of 600 m, occur in a depth of more than 500 m below sea level along the Gulf coast. Tertiary sediments like the Paleocene-Eocene Umm Er Radhuma formation dip down about 600 m of over a distance of 300 km (AL-SAYARI & ZOETL; 1978). This flat asymmetric monocline has its recent expression in the small basin of the Arabian Gulf.

#### **Aquifers**

The change of pervious and impervious formations created several ground water storeys which are outcropping in the west and dipping to the east according the tectonic structure. The most important aquifers there is the Umm Er Radhuma formation, a sequence of mainly limestones and dolomites. The aquifer is alimenting most of the natural artesian groundwater outflows in the eastern provinces including some submarine springs. The total natural discharge is estimated of more than 100 m<sup>3</sup>/s. An increased pumping rate by hundreds of wells has depleted significantly the pressure head, therefore there is the danger to reverse the hydraulic gradient and to initiate sea ingression in coastal areas.

### **Karstification**

The UER formation outcrops in a 50 to 70 km wide strip extending in North-South direction over nearly 1000 km. Salinity isopaches of the aquifer reveals preferential underground discharge areas linking strongly karstified catchment zones with the main discharge areas near the coast (NAIMI, 1965).

The karstification of the UER proved to be an old and multiple reactivated process. First the solution weathering occurred after the deposition of the limestone in Mid Tertiary (Eocene), when the sea regressed and this area became land surface nearly 20 million years ago. Afterwards the landscape was covered by clastic sedimentation of the Neogene. Several cycles of accumulation and erosion with further karstification occurred. Last time during the more humid phases of Pleistocene when discharge to the Gulf was favoured by the depleted sea level. Even under the recent arid climate karst phenomena are still dominant features of the UER outcrop area. To be mentioned are dolines, collapse structures and small poljes. Shafts and horizontal caves, partly covered with speleothem emphasize the strong influence of solution processes for the development of the underground water paths.

## Field investigations

### Hydrogeologic features of the investigated area

The karstic outcrop area of the UER-formation in the area around Ma'aqala is characterized by a large number of caves and shafts, which serve as a connection between the surface drainage system and the groundwater. The surface drainage pattern is closely connected to the shafts. Due to the distribution of the karst openings, different sizes of watersheds have developed. In most cases only very small catchment areas of much less than one square kilometer are found around each opening. The subsurface drainage prevented the development of a wadi system. In general three major groups of drainage systems can be subdivided (see figure 2):

### Open karst systems

In open karst areas the surface water is drained towards one or several caves entrances, which usually is situated in the middle of the catchment area. Typically a ditch like channel system carved into the outcropping rock only in the next vicinity of the shafts. We have subdivided the open karst group into three types. The subdivision was done according to their stage of development and geologic setting.

### Closed basins

Especially in the northern and eastern part of the Ma'aqala area fewer caves are known. In this region flat depressions have developed. The pan floor is covered by carbonatic, silty material. With few exceptions these pans are barely vegetated. Some of the depressions have sinkholes at their center or at the margins which were partly clogged with sediment when we examined them.

### Sand dune areas

In the southeastern and northwestern part of the Ma'aqala area the Tertiary formations are covered by sand dunes. They belong to the Ad Dadna sand belt. The sand dunes cover the Quaternary morphology as well as the cave systems.

The groundwater level in the UER formation in this area is found at a depth of 130 m to 265 m below the surface. No continuous water table observations are available, but the few measurements which were taken during the field trips indicate, that a fast response of the water level to rainstorms can be assumed.

Figure 3 shows the results of the analysis of groundwater samples from 7 wells in the surrounding of the studied area. Though no regular observation rhythm could be maintained, these values indicate fluctuations of the water chemistry, which may be due to recharge events correlated with rainstorms. The range of the total dissolved content varies from 1200 to 1900 mg/l. The dominant ions are calcium and sodium as well as sulfate and chlorine with changing shares between the wells.

The stable isotopes show values, which are close to a reference line given as  $D = 8 \cdot ^{18}\text{O} + 10$ , which is indicated in figure 4. Compared with the springs of the coastal area they are not so strongly enriched on heavy isotopes but have clearly higher values than the flat Wadi groundwater from Wadi Hanifah further to the West. Only in one sample tritium values were higher than 1 TU could be found. The tritium values of recent rain water samples were determined with 8 to 10 TU.

## Test areas

Several small watersheds were selected in the area for detailed studies of the amount of recharge which takes place through direct streamflow into caves. These test areas should provide data for modelling the whole UER outcrop area. As an example test area 5 shall be described in detail:

#### Test area 5

Test area 5 is situated in the center of the UER outcrop area around Ma'aqala. Its drainage pattern belongs to the open karst group. Figure 5 shows the hydrological units mapped during the second field campaign in 1987. In the central part of this catchment area a vertical shaft serves as final drainage point. Most of the area is covered by the outcrop of UER highly weathered limestone, which is covered by a thin gravel/sand layer. This material is washed out in the flow channels.

The central flat area of the test field is formed by sandy silts. Their thickness varies from few cm to more than 40 cm in the central part. Since there is an UER outcrop ridge between this flat and the cave, it can be assumed that the flat was formed above a second shaft, which was clogged.

Towards the central cave entrance, which is too small to be entered by a man, a small canyon system was cut into the UER outcrop. This canyon was used to install a V-notch weir. The V-notch weir is connected to a water level recorder, which was in operation during the winter seasons of 1986 and 1987. In addition a meteorological station was working during the same period.

Intensive infiltration tests were performed in all of the test areas, covering all major hydrologic units. These infiltration tests were also done in the whole Ma'aqala area.

### **Results of the field investigations**

During the observation period several rainstorm events occurred. Unfortunately not all the installed recorders gave satisfactory readings of the components. Here are several examples of readings:

#### Precipitation:

Desert precipitation may be characterized with a single descriptive phrase: "highly variable in both time and space" (FOGEL: in EVANS & THAMES, 1981). In the Arabian desert precipitation usually occurs in the winter season, in connection with short-duration and local thunderstorms. The precipitation for individual events have to be collected within the watershed which is under investigation. An example of the variation is given in figure 6, which shows the variation of three events recorded during the 1986 field campaign.

For larger areas single station recordings cannot be used for individual events. This limitation is principally the result of the small sample size due to the relatively infrequent occurrence of the precipitation events. As an example at least thirty years of data are required to obtain stable frequency hydrologic distributions in arid lands (FOGEL: in EVANS & THAMES, 1981).

For the area under investigation only a 16 year observation period is available, which gives a mean annual precipitation of 143.1 mm/a with a variation of 196 to 26.6 mm.

#### Infiltration:

During most of the year desert soils are generally dry. Only after rainfall events water is stored and a small portion may seep deeper to recharge the groundwater. If the precipitation exceeds the infiltration capacity, surface runoff is caused.

The table 1 lists the results of the infiltration tests done in the Test Field 5:

Table 1: Infiltration rates and hydraulic conductivities for the hydrological units in test area 5.

| Unit          | Infiltration rate<br>(mm/min) | K<br>(m/s)          |
|---------------|-------------------------------|---------------------|
| UER duricrust | 0.11                          | $3.3 \cdot 10^{-8}$ |
| UER leached   | 0.15                          | $4.3 \cdot 10^{-7}$ |
| silty flats   | 0.15                          | $8.9 \cdot 10^{-8}$ |
| sand sheets   | 0.14                          | $4.2 \cdot 10^{-6}$ |
| hillwash      | 0.08                          |                     |

It can be shown that the infiltration rate is not directly dependent on the hydraulic conductivity of the soil derived from soil samples in the laboratory. Only minor changes in the infiltration rate correspond to changes in the k-value by several orders of magnitude. This is caused by surface crusting, which is typical for arid soils.

#### Runoff:

Runoff is closely related to high-intensity and short duration thunderstorms. Figure 7 shows the diagram of a runoff event which occurred in Test Area 5. This curve followed a rainfall event of 5mm, which fell within 30 minutes, with a maximum between 5 and 15 minutes. The maximum of the surface runoff was delayed by 40 minutes compared to the rain maximum. The long tailing of the runoff curve is caused by the central flat area in Test Area 5, which was first ponded and later on discharged slowly into the cave.

The total precipitation of 5 mm only slightly exceeded the infiltration capacity of the soils, therefore only about 1% of the total precipitation were discharged into the karst system.

### **Groundwater recharge to karst aquifers**

For recharge measurements long term observations are necessary in order to be able to give confidential values on the water balance in arid regions. The data collected up to now cover only three winter seasons and cannot be used for calculations of the average groundwater recharge.

But, on the base of the existing data, it is possible to predict the recharge into the open karst system for individual events.

#### Unit hydrograph method

One approach was to use physiographic variables namely topographic characteristics, soil and rock characteristics and vegetation characteristics for the synthesis of unit hydrographs, using the method of SEYHAN (1977). A unit hydrograph is defined as the hydrograph of a storm runoff, at a given site, created by a unit event of effective rainfall occurring within a unit of time and spread in an average pattern over the contributing watershed area. A unit hydrograph for Test Area 4 is shown in figure 8. The actual amount of runoff will be calculated after several years of record of rainfall is obtained.

#### Water balance method

A second approach calculates the amount of total runoff per unit rainfall event by using a waterbalance approach:

$$R = P - ET - F - G - T$$

where :

|    |                                 |
|----|---------------------------------|
| R  | = runoff = discharge into caves |
| P  | = precipitation                 |
| ET | = evapotranspiration            |
| F  | = infiltration                  |
| G  | = amount of surface pondage     |
| T  | = transmission loss             |

The infiltration rate (F) is calculated from the results of the infiltration test. The infiltration rate was determined for all major soil and morphological units in the test areas (Tab. 1) and consequently averaged over the test area. Fig. 9 illustrates this mean infiltration rate by the horizontal line. The infiltration rate is assumed to be constant over the duration of short term thunderstorms. For short term events in this hilly area evapotranspiration (ET) and surface pondage (G) can be neglected. The excess of rainfall than is equal to the amount of the lateral inflow of runoff which is transferred to the flow channels. Along the flow channels and in the flat areas of the test area a transmission loss (T) occurs. It is calculated from the United States Soil Conservation Service (SCS) runoff equation (LANE, 1985) in dependency of the runoff curves (Fig.6) measured in the test area 5. For this purpose the test area was subdivided into a northern area with direct runoff and a southern area with delayed runoff (compare Fig. 5).

As a result it can be said, that groundwater recharge from discharge of surface runoff into caves takes place only if the precipitation rate exceeds 4.5 mm per half an hour. Such events occur regularly within the area. On the basis of the available data, an average of 4 events per year exceeded this value, with a mean of 12.55 mm per thunderstorm (maximum 27.2 mm).

Table 2 summarizes for the existing rainfall data (1981-1983) the actual amount of runoff which flew into the caves of test area 5.

Table 2: Groundwater recharge in Test Area 5 for the years 1981, 1982 and 1983, calculated from the precipitation data of the Ma'aqala weather station.

| year | rainfall<br>(mm) | runoff<br>(mm) | precipitation<br>(%) |
|------|------------------|----------------|----------------------|
| 1981 | 26.8             | 0              | 0                    |
| 1982 | 196.1            | 81.8           | 47.7                 |
| 1983 | 62.0             | 27.0           | 43.0                 |

These values show, that quite a considerable amount of recharge can be expected in open karst areas.

For water resources management decisions the long term average infiltration rate for the UER-outcrop area has to be determined. In Saudi Arabia only very limited data exist over such a period and none exist for the UER outcrop area. This value needs to be calculated for a at least thirty years period. Therefore further measurements need to be done in this respect.

Moreover the value of the groundwater recharge is subject to regional as well as global changes. The effects of these changes, especially for arid areas have not been investigated up to now.



## Acknowledgments

This paper presents the results of a joint research project between the King Fahd University of Petroleum and Minerals in Dhahran, Saudi Arabia, the Austrian Academy of Science and the University of Karlsruhe. The results presented were achieved in an interdisciplinary working group, which included Geologists, Hydrogeologists, Hydrochemists, Speleologists, Geomorphologists and Engineers, and involved more than those named as authors. Our special thanks and acknowledgments may be expressed here to the sponsoring institutions with special reference to A.E. Dabbagh and to our colleagues W. Ahmed, R. Benischke, H.K. Barth, H.S. Edgell, G. Fuchs, O. Irtam, R.L. deJong, A. Khan, Z. Kidwai, F. Quilel, M. Ukayli and V. Weissensteiner.

## References

- Al-Sayari, S.S. & Zoetl, J.G. (Editors) (1978): Quaternary Period in Saudi Arabia. 1: Sedimentological, Hydrogeological, Hydrochemical, Geomorphological and Climatological Investigations in Central and Eastern Saudi Arabia. XI, 335 p., Vienna, New York (Springer).
- Evans, D.D. & Thames, J.L. (Editors) (1981): Water in Desert Ecosystems. - 280 p.; Stroudsburg (Dowden).
- Lane, J.L. (1985): Estimating Transmission Losses.- Proceedings "Development and Management Aspects of Irrigation and Drainage Systems" IR Div., ASCE/San Antonio, TX, July 1985.
- Naimi, A.I. (1965): The ground water of Northeastern Saudi Arabia. Fifth Arab. Petroleum Congress: 16-23, Cairo.
- Seyhan, E. (1977): Regression of morphometrical variables with synthetic hydrograph parameters. Publ. Geogr. Inst. Rijksuni. Utrecht, Ser. B, 65, 18 p., Utrecht.

## Figures

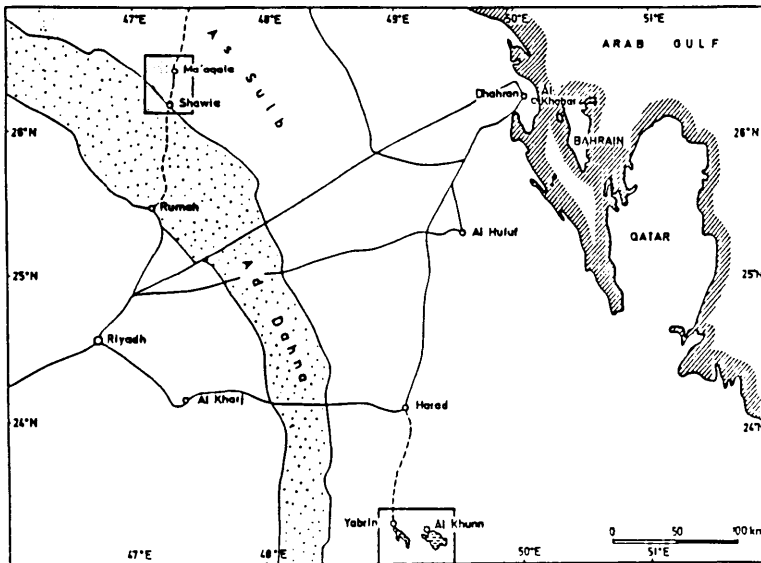
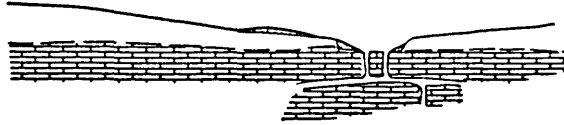


Fig.1: Location map of the Ma'aqala area

## I Open Karst Systems

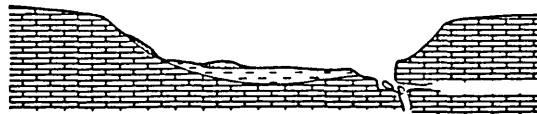
### Ia Tsm - covered type



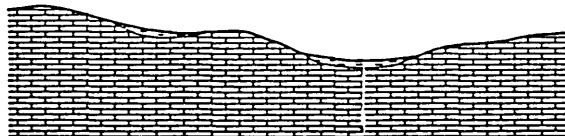
### Ib Tu - hill type



### Ic Tu - polje type



## II Closed Basins (confluence into pans without karstic openings visible)



## III Sand Dunes



### Explanations :





-  Qes (eolian sand)
-  Qs (silt)
-  Tsm (sandstone, limestone)
-  Tu (limestone, marl)

Fig.2: Subdivision of Karst systems in the UER outcrop area.

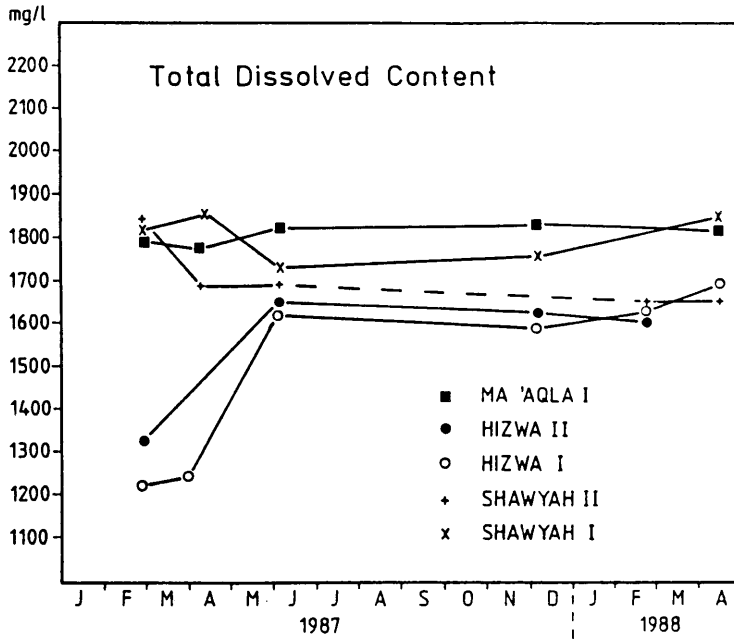


Fig.3: Total dissolved contents in water samples from the wells of the Ma'aqala area.

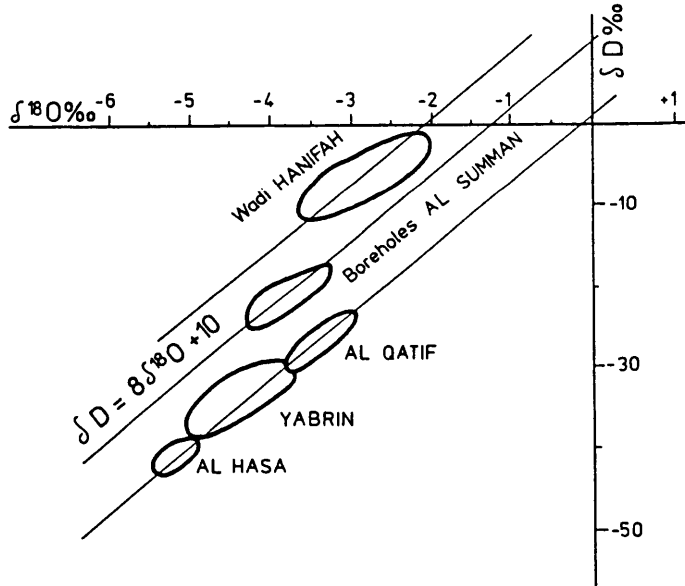


Fig.4: Isotopical ratio of Oxygen-18 and Deuterium of UER-groundwater from the Ma'aqala area (Al Summan plateau) in comparison to groundwater from a shallow wadi aquifer ( Wadi Hanifah, south of Riyadh) and to the confined UER-groundwater from the Gulf coast area (Al Quatif, Yabrin, Al Hasa).

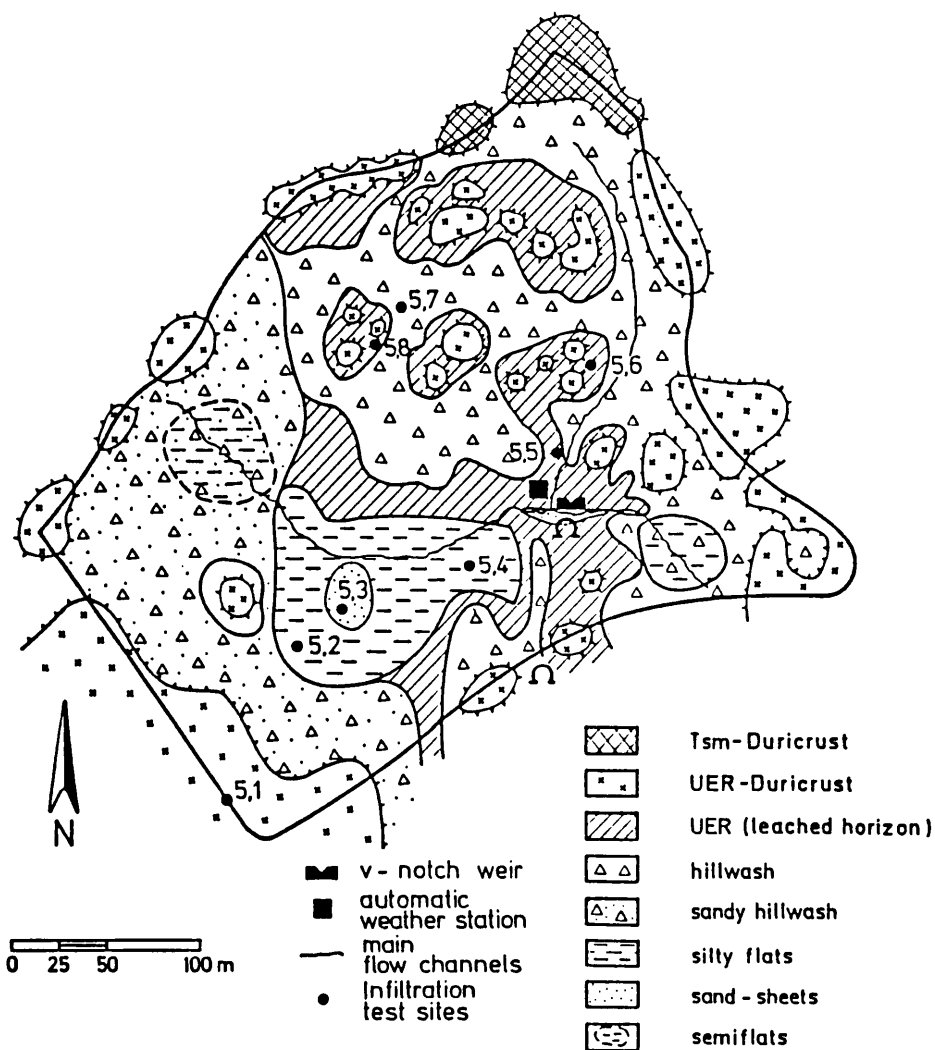


Fig.5: Hydrological units in test area 5

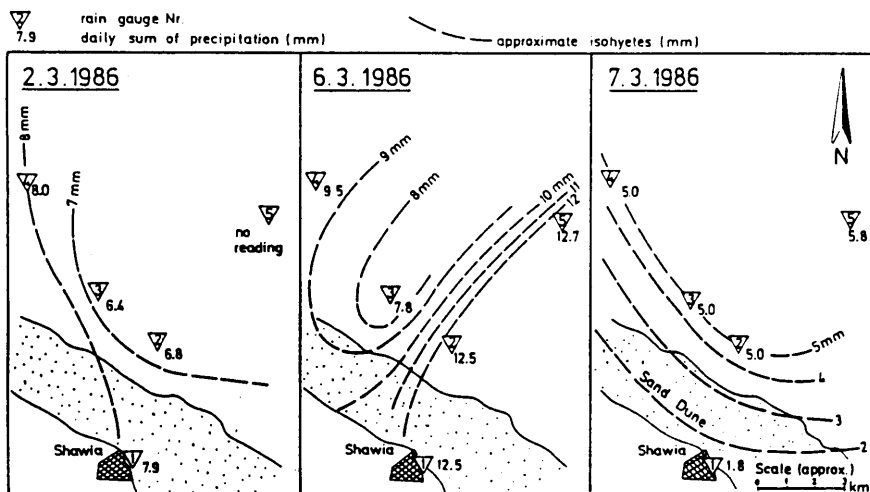


Fig.6: Distribution of precipitation in the studied area between Ma'aqala and Shawia after three rain fall events in March 1986.

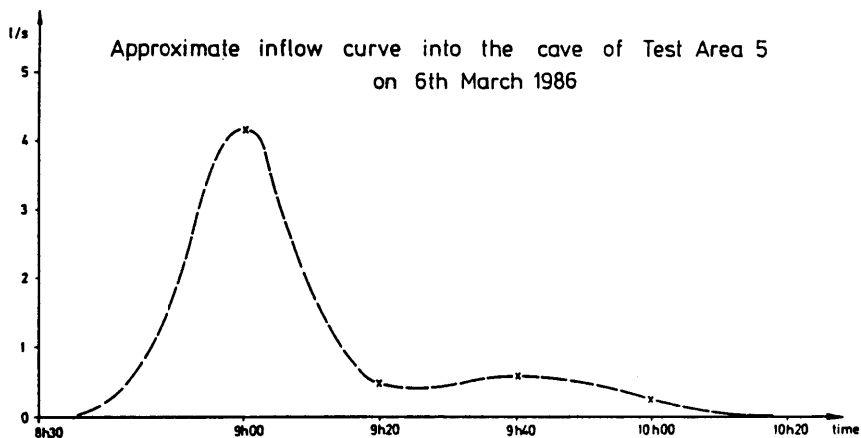


Fig.7: Surface runoff in test area 5 on the March 6, 1986.

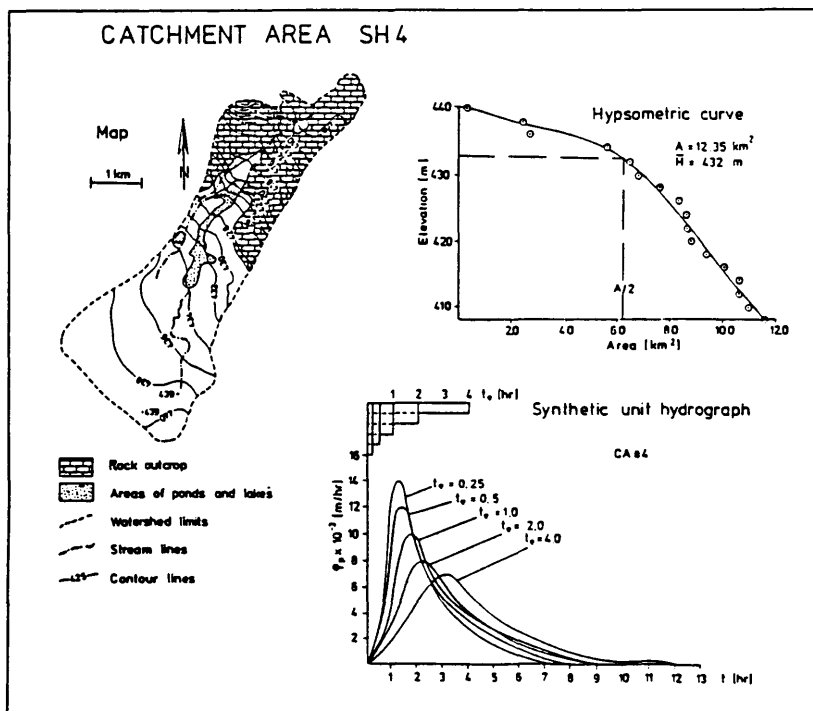


Figure 8. Synthetic unit hydrographs for test area SH4. The map and the hypsometric curve show the topographic situation.

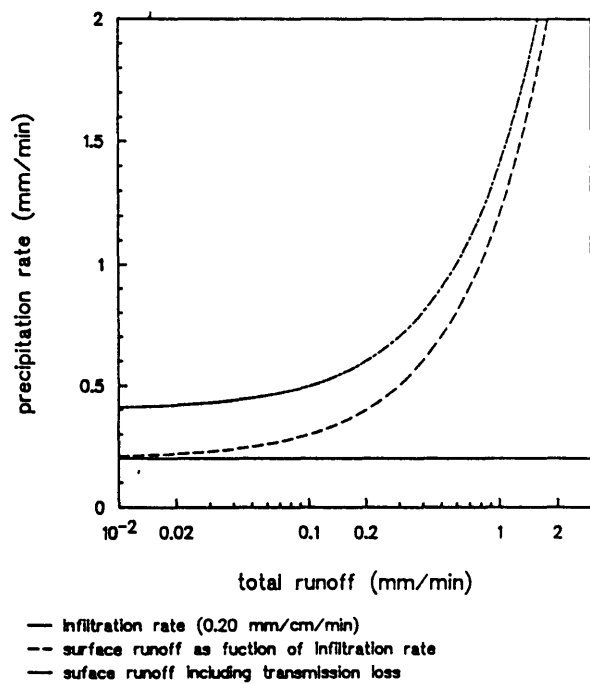


Figure 9. Weighted standard runoff curve for test area 5.





SURFACE SUBSIDENCES AND SINKHOLE FORMATION DUE TO THE PARTIAL  
RECHARGE OF A DEWATERED AREA ON THE FAR WEST RAND,  
REPUBLIC OF SOUTH AFRICA

J.H.T. Beukes and A. du Plessis  
Geological Survey, Private Bag X112, Pretoria, Republic of South Africa

ABSTRACT

It is well known that slow ground subsidences occur and sinkholes form when a dolomitic area is dewatered and that some time after dewatering relative stability returns. There has always been speculation as to what effect recharge of a dolomitic terrain will have on the stability of the surface. When the dewatered Venterspost dolomitic ground-water compartment, situated approximately 50 km south/southwest of Johannesburg was partially recharged by abnormally high rainfall in the period 1975 to 1978, a renewed but smaller cycle of instability which included both the formation of sinkholes and accelerated slow ground movement occurred in certain areas. Therefore, the apparent stability that sets in over a dewatered dolomitic area is a meta-stable condition only.

Introduction

The Far West Rand is situated approximately 50 km south-southwest of Johannesburg (Republic of South Africa). There are 15 gold mines in the area which extract ore from various reefs in the Archaean Witwatersrand and Ventersdorp Supergroups. Overlying these latter rocks are the formations of the Transvaal Supergroup which has near its base a 1 500 m thick sequence of dolomitic limestone in the Chuniespoort Group. The dolomite is a major aquifer where ground-water is contained in a vast network of inter-connected joints, fault planes, cavities, solution channels in the solid rock and also in the overlying dolomitic residuum. Many fractures and fault planes extend into the underlying Witwatersrand rocks and thus intersect the gold bearing reefs. Many of the features, particularly the tension faults, form conduits which, when exposed in the gold mines discharge water under great pressure.

In 1960 it became obvious that for economic and safety reasons the only solution to the problem of vast amounts of water entering some of the mines was to dewater the above lying dolomites. The following fortuitous phenomenon made dewatering a practical possibility. The east-west striking dolomitic limestones are cut by a number of vertical, generally north-south striking syenitic dykes (Fig. 1). These intrusions which are 6 to 60 m thick, are impervious to water migration. They cut through the entire geological column and thereby effectively divide the dolomite into a number of separate subsurface reservoirs or compartments. The overflow from one compartment to the next occurs at the lowest point of the relevant dyke where water emerges as a spring. Therefore, dolomitic compartments can be selectively dewatered leaving adjacent compartments undewatered.

From the early 1960's onwards a number of compartments were dewatered. In all cases this action gave rise to surface subsidences and the formation of sinkholes. Generally, the first signs of slow ground subsidences occurred soon after dewatering was initiated and sinkholes formed mostly in the low lying areas of the compartment where the water-table was originally close to

the surface.

Intensive research was initiated to locate areas more vulnerable for sinkhole formation or slow ground subsidences (Kleywegt and Enslin, 1973). No direct solution to the problem was found but a method was developed to evaluate the relative safety of a terrain using all available geological, geophysical and geohydrological information.

Following the instability described above, relative stability returned to all compartments after a number of years. However since the lowering of the water-level was a temporary condition it was a matter of concern as to what effect the return of the water-table into weathered and compactible material would have on surface stability. In the period 1975 to 1978 the dewatered Venterspost Compartment was partially recharged and this paper describes the effect it had on surface stability.

#### Partial Recharge of the Venterspost Compartment

On the Far West Rand the Chuniespoort Group strikes east-west and the dolomitic outcrop and its residuum is situated in a fairly flat lying valley bounded in the south by a series of hills formed by chert layers and to the north by quartzites and granites. In Figure 1 it is seen that the syenitic dykes have created a number of compartments; from west to east in sequence the Boskop-Turffontein, Oberholzer, Bank, Venterspost, Gembokfontein and Suurbekom Compartments. In 1975 the Boskop-Turffontein Compartment in the west and the Gembokfontein and Suurbekom Compartments in the east were intact but the adjacent Oberholzer, Bank and Venterspost Compartments had been dewatered. Levelling surveys and visual inspections which had been conducted continuously since the mid 1960's showed that from early 1970 relative stability prevailed in the small Venterspost Compartment. The only ground movement occurring was at locations where water flow was unnaturally concentrated by e.g. leaking pipes or badly designed storm water drainage systems. During the period 1975-1978 however, due to an abnormal high rainfall in the area, vast amounts of surface water, mainly from the adjacent Gembokfontein Compartment flowed into the Venterspost Compartment. It was estimated that at one stage after a heavy thunder storm more than 3 500 Ml of water per day flowed over the dyke at the Gembokfontein eye. A number of existing sinkholes in the low lying area facilitated the infiltration and virtually no water flowed over the Venterspost Compartment into the Bank Compartment.

Major variations in the water-level started to occur. In Figure 2 the water-level in borehole W4 near the inflow point is shown. Annual water-table fluctuations in the order of 50 m are seen from the dry to the rainy season in the years 1975, 1976, and 1977. A cumulative rise in the water-level of approximately 100 m occurred from early 1976 to 1978 (from 1 452 m to 1 540 m above sea-level). In a topographically higher lying area further from the inflow point a rise of 42 m was registered in borehole G1411 over the same period. There, a more continuous rise with less pronounced seasonal fluctuations was observed. In many places in the Compartment the water-table returned into more unconsolidated compactible material above the solid bedrock interface.

The partial recharge of the compartment gave rise to mainly two problems.

1. Mines operating in the Compartment experienced an increase in the quantity of water entering their underground workings and were thereby forced to increase pumping rates. In Figure 3 it is seen that in the Venterspost Mine the pumping rate of 900 Ml per month in 1973 had to be increased to 1 500 Ml per month in 1978. Subsequent to 1978 it took ten years to regain the water-level of 1973 and during that period 50 000 Ml more than "normal" had to be pumped to achieve the result.
2. The most important consequence of the recharge was a renewed cycle of ground instability. Four expressions of ground instability could be defined:
  - (a) Three sinkholes which had formed in the early 1960's and had been filled at that time, became active again (Fig. 4). This may have been due to compaction of the filling material or a further collapse of the retaining arch in depth.
  - (b) Nine new sinkholes formed in areas where no movement had previously occurred (Fig. 4).
  - (c) Four of the known 13 palaeosinkholes in Westonaria showed accelerated subsidence though no collapse during the period of recharge. Figure 5 shows a typical cross section through a palaeosinkhole as derived from borehole information. It is seen that dolomite, dolomitic residuum and Karoo shales are down warped towards the centre of the structure which had an open throat prior to being filled with red coloured Quaternary sands. The water-level over the structure was stable for many years prior to 1975 and no appreciable ground movement occurred. In January 1975 the water-level started to rise and from that date to March 1976 rose 9 m still without ground movement registered at surface. From March 1976 onwards the water-level rose another 33 m to peak, in February 1978, at 42 m above its former low level. During the latter period the ground subsided 60 mm. From February 1978 onwards the water-level started to subside and ground movement over the structure ceased.
  - (d) In certain areas where the dolomitic limestone was leached to depths below the original water-table, renewed subsidences were observed. In Figure 6 it is seen that, as in the case of the palaeosinkhole, accelerated subsidence did not occur immediately after the water-level started to rise; it occurred after the water rose above the level of the solid dolomite. A surface subsidence of 100 mm was registered during the period June 1976 to February 1979. Again the ground subsidence ceased virtually immediately the water-level had peaked and started to recede. The borehole shown in Figure 6 is situated next to a motor repair shop which was slightly damaged during the initial dewatering. During the recharge period the structure was damaged to such an extent that demolition was at one stage considered.

Over the years 412 levelling points were monitored in the town of Westonaria of which 68 (11,5%) showed signs of movement during dewatering. During the recharge period 30% of these unstable points again registered subsidence. It is speculated that in areas where the original water-level was nearer to surface more dramatic movement must have taken place when the compartment was recharged. Unfortunately, because these areas were evacuated soon after dewatering started, no data on ground movement are available.

### Conclusions

Observations in the Venterspost Compartment have shown that a sudden inrush of water into a dewatered area should be prevented by whatever means possible as the apparent stability that sets in over a dewatered dolomitic area is a meta-stable condition only. With a recharge of a dewatered area sinkholes may form, old sinkholes and palaeosinkholes may be reactivated and accelerated differential slow ground subsidence may again occur. Furthermore an area found to be unstable during dewatering remains unstable and should not later on again be considered for development. The position of filled sinkholes should be clearly identified and fenced to avoid any land use over them.

The possibility of using dewatered dolomitic compartments as underground water reservoirs has been investigated. The advantage would be a saving in water through a deduction in evaporation. This line of thinking needs reconsideration as it will result in periodic changes in water-levels with all the attended ill effects that have been pointed out.

### Reference

- Bezuidenhout, C.A. and J.F. Enslin, 1969, Surface subsidences and sinkholes in the dolomitic area of the Far West Rand, Transvaal, Republic of South Africa, Proc. IAHS Symp. on Land Subsidence, Tokyo, V.2 IAHS-UNESCO, 1976.
- Kleywegt, R.J. and J.F. Enslin, 1973, The application of the gravity method to the problem of ground settlement and sinkhole formation in dolomite on the Far West Rand South Africa, Proc IAEG Symp. Sinkholes and subsidences engineering, Hannover, 1.3, 1-15.
- Kleywegt, R.J. and D.R. Pike, 1982, Surface subsidence and sinkholes caused by lowering of the dolomitic water-table on the Far West Rand Gold Fields of South Africa, Ann. Geol. Surv. South Africa, 16(1982), 77-105.

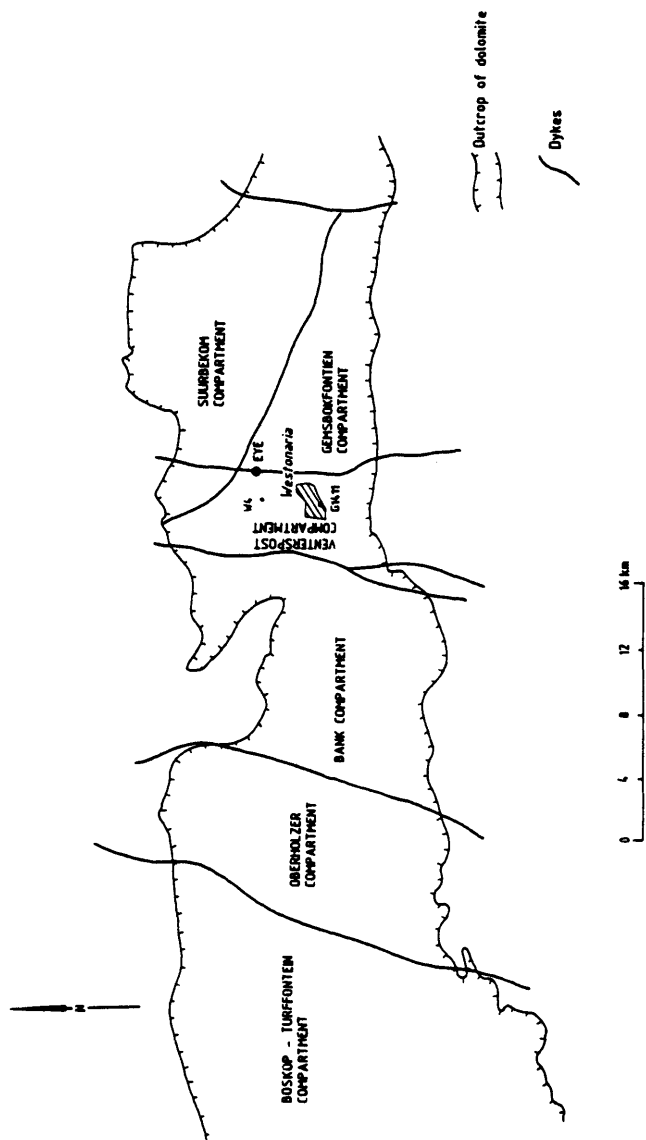


Figure 1. Dolomite area--Far West Rand.

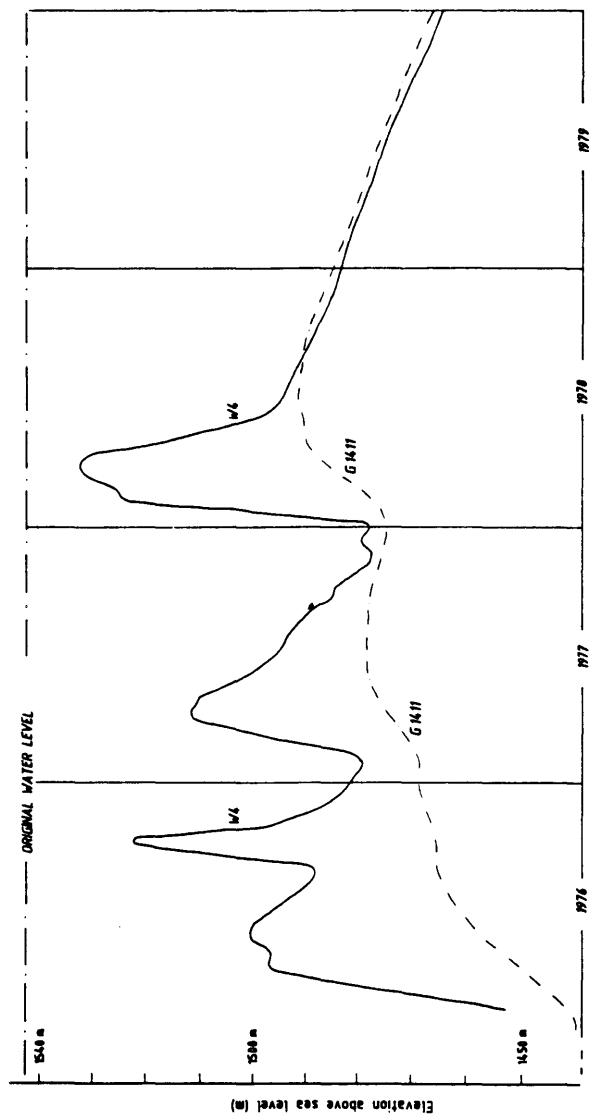


Figure 2. Water level in boreholes W4 and G1411 in the Venterspost compartment.

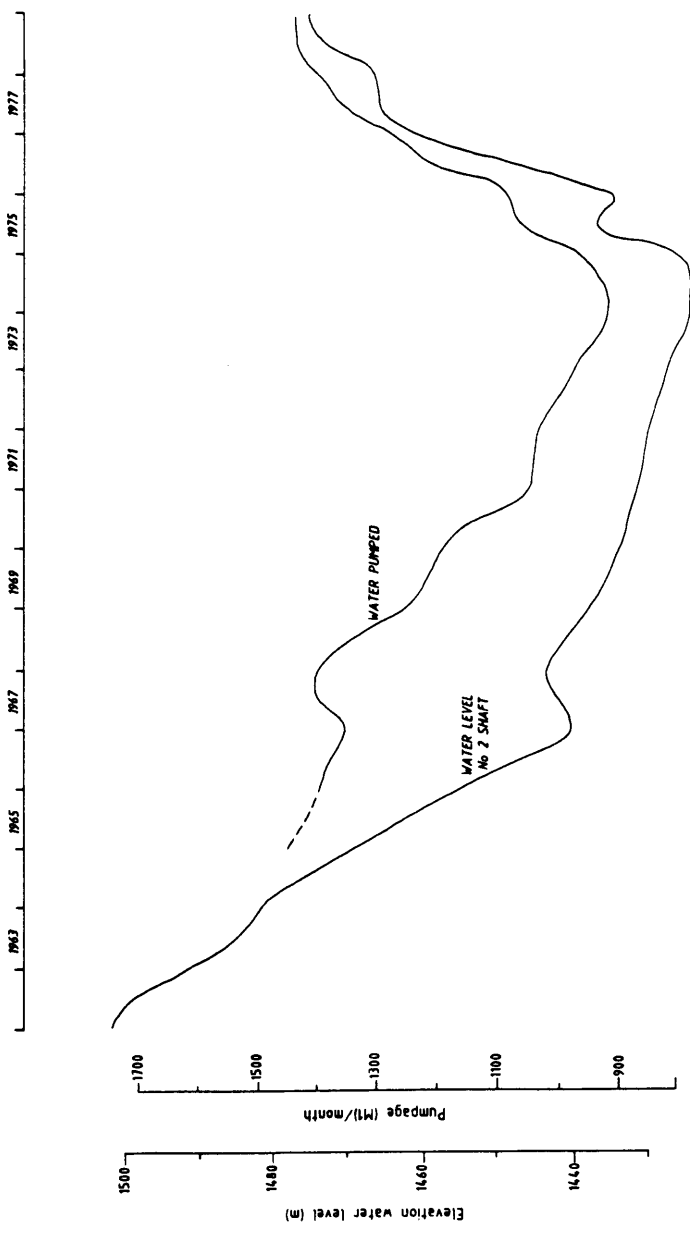


Figure 3. Water level in shaft and amount of water pumped by the mine in the Venterspost Compartment.

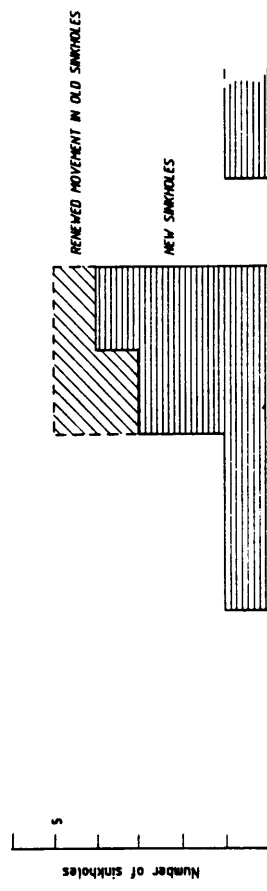


Figure 4. Number of new sinkholes and old sinkholes showing renewed movement in the Ventspost Compartment.



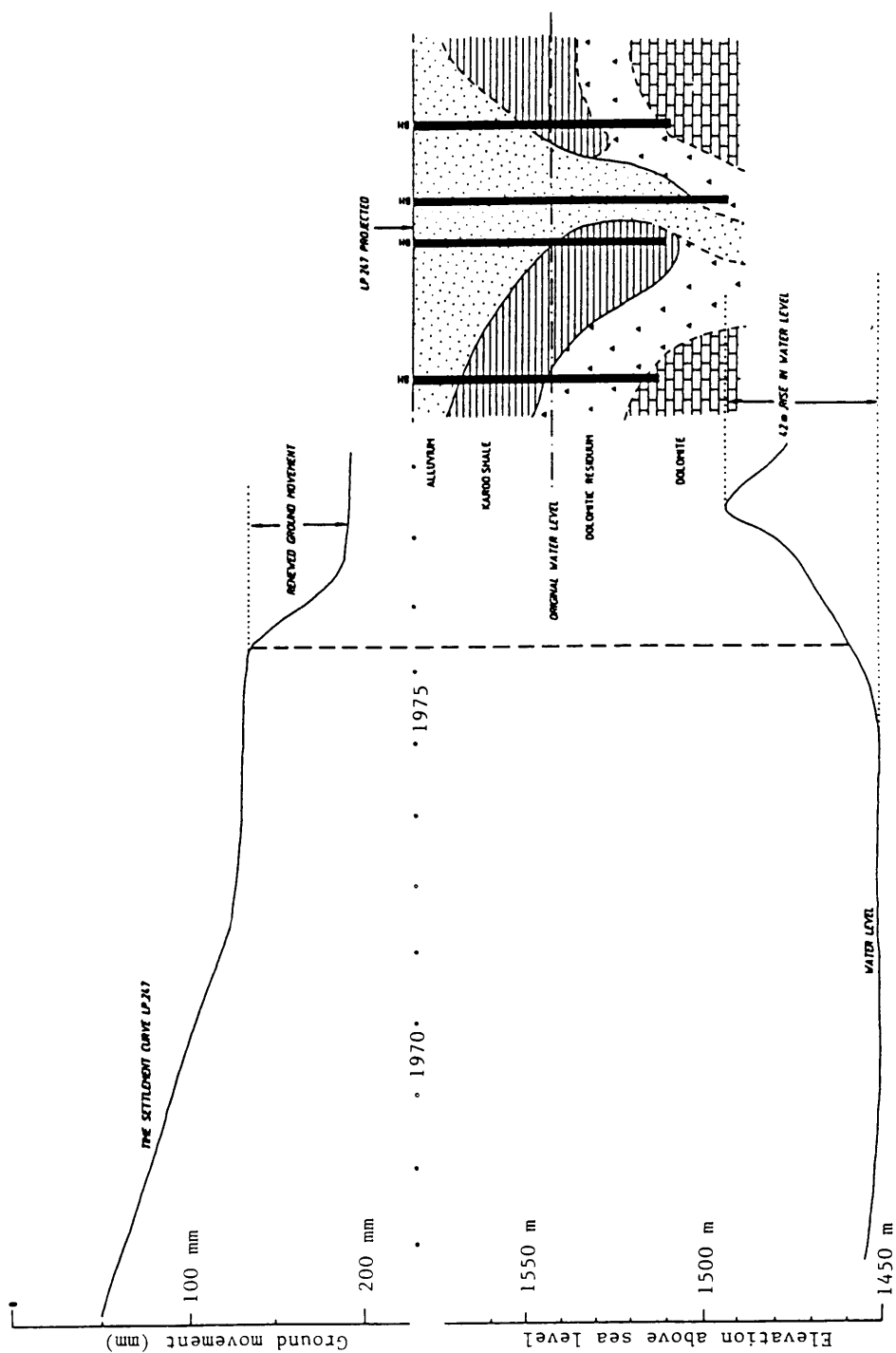


Figure 5. Water level and renewed ground movement over a palaeo sinkhole in Westonario, Venterspost Compartment.

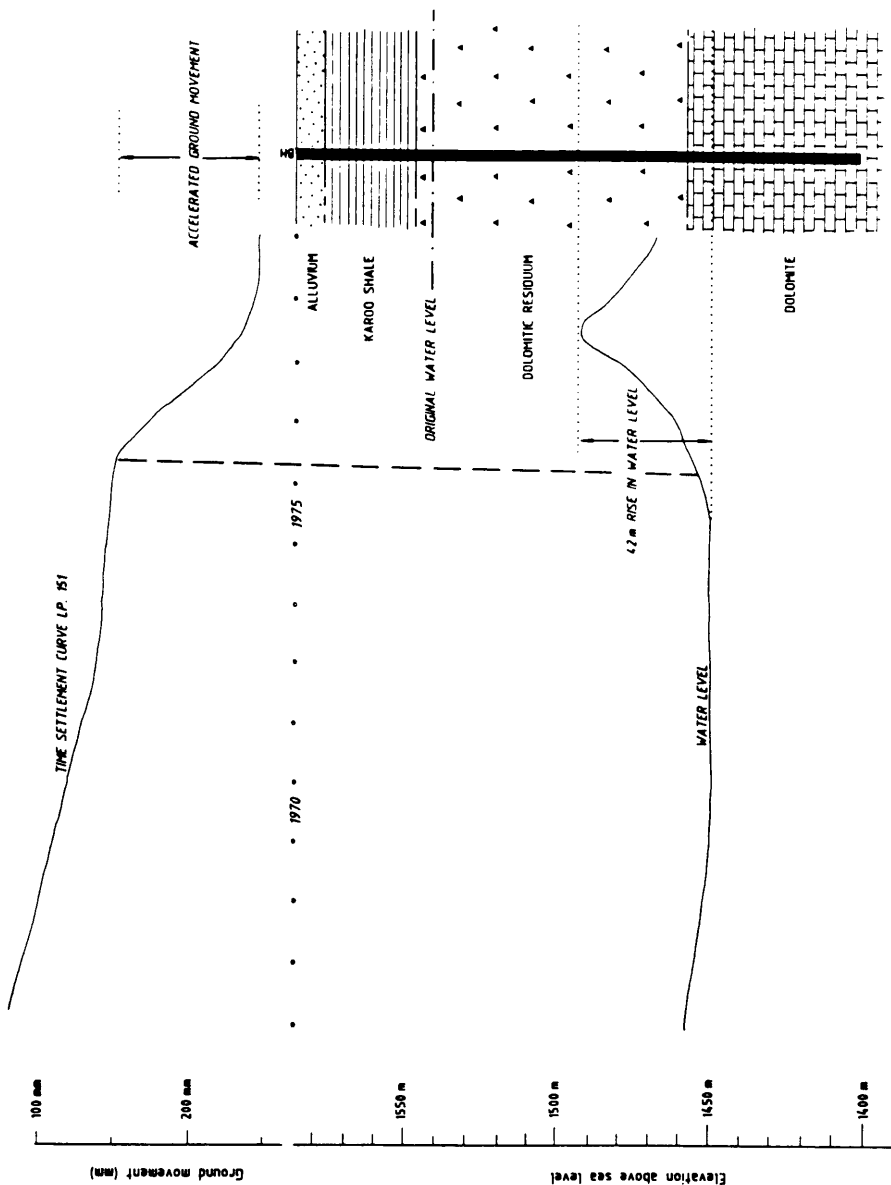


Figure 6. Water level and renewed ground movement in an area where dolomitic limestone is weathered below the original water level.

KARST AND URBANIZATION: INVESTIGATION AND  
MONITORING IN CAJAMAR, SAO PAULO STATE, BRAZIL

Fernando Luiz Prandini  
Valdir Akihiko Nakazawa  
Ana Maria de Azevedo Dantas  
IPT-Sao Paulo State Technological Research Institute  
Cidade Universitaria-Butanta-C.P. 7141  
CEP 01051-Sao Paulo (SP)-Brazil

Thomas L. Holzer  
United States Geological Survey  
345 Middlefield Road  
Menlo Park, California 94025

Abstract. The investigation and follow-up of the subsidence and collapse that took place in the urban area of Cajamar-SP, beginning on August 12, 1986, was aimed at ascertaining the extent, conditions, and dynamics involved in the development of the Cajamar covered karst and, as soon as possible, assess the risks imposed on the population and establish measures to solve the problem. The purpose of this paper is to give an overview of the investigations carried out and to briefly present the most important results.

Introduction

On August 12, 1986, a soil collapse occurred in the urban area of Cajamar, a small town of approximately 500 houses. Before dawn and early in the morning of that day, noises similar to those of thunderstorms and explosions were heard in the vicinity of the collapse, which took place around 9:00 a.m. Late in the afternoon, the crater was about 10 meters wide by 10 meters deep. Houses with recent cracks were observed more than 400 meters away from the collapse site. Due to these facts, IPT researchers began work on diagnosing the problem and indicating the measures to tackle the problem.

Initial Evidence

The evidence collected from the moment of the event indicated that the evolution of subsoil cavities originating under karstic conditions was the most likely hypothesis to explain the collapse and also the subsidence on several acres of urban settlement. In brief, the evidence considered was as follows:

- (1) fast initial evolution of the collapse;
- (2) Beginning a few months before the collapse, there were occurrences such as thunderlike noises, deformation of floors, cracks in the houses, high incidence of breakage in water-supply networks, drying out of perennial springs;
- (3) after the collapse, there continued an evolution of cracks in houses and breakage of water-supply pipes;

- (4) involvement of large volumes of soil, both in the collapse site itself and in the areas affected by lesser movements;
- (5) data for a local water-supply well that indicated the presence of limestone with deep cavities, and the specific capacity of the well was high (20.2 m<sup>3</sup>/h/m);
- (6) presence of limestone outcrops, a little over 1 km from the affected area, showing dissolution cavities and cavities filled with soil. In the surrounding area, sinkholes are common features;
- (7) crater caused by the collapse, shaped as a frustum of an inverted cone in its upper portion and extending downward as a cylinder; and
- (8) morphology of the topographical depression where the urban area is located, which suggests a unit of relief, the model of which is corroborated by such phenomena as sinking and accumulation of detrital materials.

All of this suggests a situation known as "covered karst". This hypothesis implies two possible variants in the development of the phenomenon, each with different consequences in terms of risk to the local population: (1) Collapse of the limestone cave roof, and (2) migration of soil downwards to the interior of cavities in the limestone (Prandini et al., 1987a).

If confirmed, the collapse of a rocky roof of a cave inside the limestone would lend the August 12<sup>th</sup> collapse a punctual character, with damage confined to its immediate surroundings. On the other hand, if the collapse resulted from the migration of soils into limestone cavities, it would be but one episode within a sequence of events and, hence, much more serious.

An antecedent to the collapse and subsidence was a significant increase of underground water exploitation of two deep wells for local water supply, since 1984 and 1986, respectively. Both wells exploited underground water from cavities in the limestone. In addition, a limestone quarry, about 1.5 km from the collapse site, had its pit emptied of water between April and August 1986. This pit had previously accumulated a 7-meter-high water head during the previous three years in which mineral extraction was halted. These changes took place at the end of an abnormally dry period that extended from 1984 to August 1986. It is evident that the role played by groundwater was important and must be understood.

#### Research and Site Investigation

The initial research consisted of the assessment of the phenomenon history, rainfall analysis, collection of data about underground water exploitation, and the observation and follow-up of the phenomena, the most important results of which have already been presented in the preceding section.

Site investigation consisted of geological and geomorphological mapping, geophysical prospecting, direct subsoil investigations, hydrogeological studies,

seismological survey, soil movement measurements, and follow-up of the collapse evolution.

The geological mapping was made on a 1:10,000 scale for a regional approach and 1:2,000 for a local approach, with the purpose of describing the rocks that crop out, their stratigraphy and structural pattern, with a detailed study of the horizon of carbonate rocks occurring south of the affected area and, in subsurface location, under the same area.

The geomorphological mapping of the affected area was carried out to identify possible evidence of subsidence and other surface evidence of dissolution and filling, both in the urban area and in its surroundings.

Geophysical prospecting was used to locate the cavities in the subsurface and to guide the drillings; several methods were utilized: The electromagnetic method did not give adequate resolution due to the noise level typical of the urban area; seismic reflection and seismic refraction methods also did not provide satisfactory results due to the low energy of the mechanical source utilized (use of explosives was not possible), which was absorbed by the thick layer of soils; the gravimetric method, although indicating an abnormality in the collapse area, did not give sufficiently detailed results. Only the electric method profiling technique, with a dipole-dipole array and a theoretical depth of 40 to 120 m determined by a 40-m electrode spacing, by showing conductive anomalies, proved effective in indicating the probable location of saturated cavities in soil and rock. Eight lines of electrical profiling were carried out, totaling 6,480 meters.

Direct subsoil investigations consisted of rotary and percussion drillings to characterize, both geologically and geotechnically, the materials upon which the urban area is located, to enable the installation of piezometers, and, above all, to determine the extension of the area affected by the subsidence and collapse phenomena.

Guided by the geophysical results, 32 percussion drillings were performed, totaling 1,568 m; in addition, 20 rotary drillings were performed, totaling 204 m of rock and 369 m with soil sampling.

Hydrogeological studies were undertaken to characterize the massifs of soil and rock under the urbanized area, and to understand the role of groundwater in the development of the subsidence and collapse phenomena. They consisted of monitoring the piezometric network (43 single, double, and triple piezometers), infiltration tests, and pumping tests.

The follow-up of the subsidence and collapse phenomena was made through seismological surveys, mapping of cracks, accurate topographical mapping, measurement of subsidence and deformations in houses, and direct observation of the evolution of the collapse itself.

The seismological survey was carried out through three seismological stations, two installed within the urban area and one on an abandoned quarry located 1 km from the affected area. This type of control sought to confirm the information from the local dwellers that noises similar to those of thunder and explosions had been heard prior to the collapse and up to two weeks after, probably corresponding to microseisms produced by the rupture and fall of soil materials in cavities in the subsurface. The control was carried out in a 30-day period between October and November.

Measurements of subsidence and deformation in houses were carried out to determine the amplitudes and velocity of soil movements and, mainly, the area affected by them. Subsidence was measured by periodical topographical leveling of 174 surface benchmarks installed throughout the area, using an optical level with micrometer and invar sight with a maximum deviation of 3 mm in the measurements obtained. The intensive follow-up period went from early September 1986 to February 1987. Deformation in houses was monitored through instruments placed in ten houses, with clinometers to measure rotation and mechanical extensometers to measure the evolution of wall cracks. Systematic measurements were carried out between September and December 1986.

### Summary of Results

**Geology:** In regional terms, five Pre-Cambrian lithological units of the Sao Roque Group crop out in the area, with recognition, on the base, of a detrital metasedimentary sequence, with prevailing metapelites (mica-schists, sometimes porphyroblastic, to phyllites). Between phyllites, there occur bodies of metabasitic amphibolites. There are chemical and chemical-detrital metasediments (metamorphic limestones and dolomites and calcium-silicated rocks) interbedded with phyllites. Crowning the Sao Roque Group column in this region are impure metapsammites interbedded with phyllites.

The second folding phase of the Sao Roque Group (folds which affect schistosity or slate cleavage) is well marked in the area surveyed, constituting mainly antiforms and synforms, the mapping of which permitted the reconstitution of the stratigraphy of the sequence. The orientation of such structures is northeast. Small faults crack the rocks, some being transcurrent, others being normal.

The detailed geological mapping indicated an antiformal structure of slightly metamorphized limestones (metacalcarenites, metadolomites, brecciated dolomitic metaconglomerates) that occur in the subsurface of the urban area.

On top of these limestones there occurs, in practically all the urban area, thick soils of detrital materials, and soils from the weathering of low-grade metamorphic rocks that are interbedded with the limestones.

**Geomorphology:** The township of Cajamar is located in a portion of the Atlantic Plateau called Serrania de Sao Roque, characterized by rounded-top hills and straight-profile slopes, sometimes steep, within which small ranges stand out; drainage presents a high-density, pine-like dendritic pattern, narrow valleys and restricted inner alluvial plains (Ponciano et al., 1981). The urban area is located on one of such alluvial plains in the form of a hollow, the bottom of which presents maximum gradients of 10%, as opposed to the high hills and steep slopes around it.

This relief is a result of erosion on the ancient Japi surface; consequently, the more outstanding reliefs can be considered as inselbergs related to it. This is the case of the small elongated ranges in the vicinity of the urban area, the altitude of which exceeds 920 m, being supported by meta-arenites. Finer-grained metamorphites (phyllites and schists) and carbonate rocks support progressively lower reliefs.

In its turn, the hollow on which the area is located, the lower portions of which barely exceed 720 m of altitude, could be correlated to similar features typical of the Atlantic Plateau, that have been attributed to the widening of valleys upstream of lithological sills, produced by erosion processes related to quaternary climatic fluctuations (Ab'Saber, 1969; Melo and Poncano, 1983). Nevertheless, the occurrence of a collapse in its interior, associated with observations made in the vicinity, especially at a limestone quarry, leads us to consider that the hollow (and, therefore, comparable features in other areas with carbonate substratum) must be regarded as a form resulting from the association of surface erosion processes and chemical dissolution and its consequences.

In the environs of the urban area, there are various limestone lenticular bodies that have been exploited, the inspection of which revealed the following major points:

- (1) subsidence features, ranging from one to ten meters in diameter, occur in the soils covering the limestone rocks;
- (2) the limestone exposed in these subsidence areas usually presents itself in the form of slabs with rounded edges, without any feature of carbonate reprecipitation. This characteristic is an indication of dissolution under soil coverage (Back, 1986, personal communication);
- (3) the smaller cavities seem to be controlled by fracturing planes; their walls in all the cases observed are shown to be devoid of reprecipitation features;
- (4) the cuts in the quarries show that the cavities near the surface of the terrain behave as soil-filled pockets; and
- (5) important dissolution features are observed in the contact between the phyllites and limestone lenses; phyllite remnants, as if they were the counter molds of dissolved limestones, are also found in the quarry areas.

Therefore, one can observe that, although the Cajamar karstification does not present conditions of significant occurrence in the area, which are normally given by limestone massifs with horizontalized banks, it possesses other predisposing factors that the literature (Therond, 1973) shows to be very important, namely, the limestone fracturing and its interbedding with insoluble rocks, that create favorable conditions for the concentration of water flows and, therefore, for the formation of cavities by limestone dissolution.

The observation of cavities in the limestones forming the bedrock of the affected area, in its turn, leads to the differentiation of two phases in the karstification process: an initial one, which formed the voids, and the current second one, characterized by widening of previous cavities, formation of new cavities, downwards migration of soils of the most varied types toward the interior of the cavities, favorable conditions for water circulation, and soil coverage unfavorable for the reprecipitation of carbonates.

Such considerations ascribe originality to the Cajamar karstification and differentiate it from that which, until then, was the only region with karstic features in the State of Sao Paulo, namely the Ribeira River Valley. The

characteristics of karst in evolution under soil coverage extend the possibility of this type of occurrence to all crystalline regions of the State with limestone substratum in a way that such processes may be recognized as regionally important, although discontinuous.

Finally, some observations about the hollow are necessary: This feature presents irregular, terraced level sections, shown by several declivity ruptures; these forms once more stress the possibility of genesis by combined fluvial, mass movement, and subsidence processes. Due to the impossibility of direct observation because of the urbanization, inferences shall be made from the drillings and, in the future, by analogy with other areas. On the other hand, the only perennial drainage of the site is that of Lavras Creek, the course of which (even part of associated alluvia) has been modified by goldmining activities developed there by religious orders in the 18<sup>th</sup> Century. Although the slopes bordering the hollow are cut by small valleys with steep slopes, there are no other water courses besides the above-mentioned Lavras Creek.

We may say that the karst investigation in the Cajamar region is a problem of applied geomorphology and engineering geology (Holzer, 1984). However, given its complexity, the various features mentioned and others will be examined in accord with the technical areas and methods of investigation employed in this case.

Geophysical Prospecting: The electrical profiling indicated strips with conductive anomalies in the subsoil in roughly all the area of the district. The investigation, carried out in five levels (40, 60, 80, 100, and 120 m of theoretical depth) shows a tendency of interconnection of conductive strips in depth.

Subsoil Investigations: Overlying the limestone which makes up most of the bedrock of the urban area, drillings identified a soil with an average thickness between 40 to 50 m, reaching up to 100 m. This soil is formed by a superficial layer of red clayey soil, clearly of colluvial nature, with small alluvial bodies located near Lavras Creek. In many places, it contains a horizon of centimetric fragments of quartz and quartzite in its base. Its thickness reaches up to 20 m in the central portion of the affected area, thinning out toward the edges of the hollow.

Underlying this layer, there are two types of soils: the first one is of an essentially silty texture, variegated color and containing many millimetric to centimetric fragments of phyllite, quartz, and quartzite chaotically oriented in the silty matrix; the second one is also of silty texture and variegated color but with conspicuous foliation and generally with strong inclination. Whereas the latter type corresponds to soils of alteration of phyllites and other low-grade metamorphic rocks interbedded with the limestones, the former type may relate to materials of two distinctive origins: as detrital materials or as soils of alteration of weak metamorphic grade conglomerates. From about 20 meters above the top of the limestone, these soils are dark brown, the texture remaining essentially silty, which gives them a "coffee-powder" aspect. Besides the color, this soil is characterized by low resistance to penetration (SPT), which, from a few meters above the top of the limestone, presents null values and even free falls from the perforation composition, always with total loss of circulation water. They constitute soft soil pockets with heights up to 10 m, always located next to the top of the limestone, probably representing residues from limestone dissolution. Its dark brown color is due to manganese, the presence of which was verified by chemical analysis, with contents around one percent.



In addition, in contact with this soil and the limestone, we identified cavities up to 4 meters high without any filling except water and, on the bottom of the cavity, granular material similar to fluvial sands made up of predominantly quartz, angled, and well-selected grains.

The limestones are of a massive nature, gray color, and low metamorphic grade and, at the top, are made up of metacalcarenites, metadolorudites, and dolomitic metaconglomerates of a predominantly pinkish color. They contain dissolution cavities with typical dimensions around one meter high, occurring as far down as 100 m below the phreatic surface, corresponding to fractures and/or faults enlarged by dissolution. The most significant cavity directly detected in the limestones is that present in well number 1, 9 meters high, between 60 and 69 meters of depth, exactly in the water extraction interval.

Hydrogeologic Studies: The local aquifer system consists of two units with rather complex constitution and spatial conformation. The upper one, of the free type, with poor hydraulic characteristics, very low permeability and drainage capacity, is made up of predominantly clayey silt, colluvial soils. This unit has transmissivities nearly 5,000 times smaller than those of the lower unit and behaves as an aquitard. The lower aquifer, of the confined to locally semiconfined type, heterogeneous and with marked hydraulic anisotropy, consists of the karstified limestones and the "brown silty soils" ("coffee-powder") from the base of the soil. Its constitution and the spatial relationships with the upper unit which confines it are rather complex, particularly because of the differences in the hydraulic characteristics of both units.

On the right bank of Lavras Creek, the upper and lower aquifers are readily differentiated, and the hydraulic head difference between them, from the creek margin, varies from 2 to 20 m. On the left bank, the two aquifers are not readily differentiated, and the locality is believed to be a recharge area for the lower aquifer.

It is from the lower aquifer, in cavities existing in the karstified massif, that the groundwater for public and industrial use is extracted. The hydraulic response to the lowering induced by such pumping is nearly instantaneous and is transmitted to practically all the area. Another important fact is that, in well number 1, the depth of static and dynamic levels underwent a significant lowering, going from 2.41 m and 9.54 m at the time of its installation to 8.32 m and 20.2 m by the end of 1986, together with a reduction from 150 to 80 m<sup>3</sup>/h in flow rate.

Figure 1 shows two geological sections with the position of the potentiometric level and the phreatic level in December 1986. At the collapse site, the phreatic surface descended to the potentiometric surface from August to November 1986.

Seismological Survey: Eleven seismic events were recorded at the three seismological stations in a period of less than 30 days, probably due to collapse in subsoil cavities. An accurate location of these events was not possible due to the impossibility of a more suitable arrangement of the three stations.

Mapping of Cracks: Mapping identified a crack system of circular pattern affecting both the soil and the houses, with a diameter of approximately 150 meters and with the collapse located eccentrically to this circle. However, the area where houses showed cracks was larger than this circle, extending more than 400 m

away from the collapse of August 12. The great majority of the cracks occurred up to a few weeks after said collapse.

Measurement of Movements: The most marked settling occurred in the area between the collapse of August 12 and Lavras Creek. In a few months, many areas showed settling of more than 3 cm and others more than 5 cm. These settlings are high, both in comparison to other similar subsidence cases and in respect to the stability of the houses. The movements, measured until the end of field work (January 1987) in nearly 70 points, had maximum velocities of around 1 cm/month, indicating the high subsidence activity in the area. A house approximately 200 m away from the collapse showed a continuous opening of a crack at least until December, when systematic measurements were discontinued.

Follow-up of Collapse Evolution: The collapse, which by the end of August 12 was 10 m wide by 10 m deep, progressed rapidly in the first month, reaching 25 m in diameter and 13 m in depth. From there on, the progression was much slower, reaching its present configuration early in December, being 32 m wide and still 13 m deep and having totally destroyed four adjacent houses. Underground water appeared at the bottom of the crater in mid-November, rising up to 7 m of depth by February 1987.

Diagnosis and Summary: The investigation showed the presence of limestones under a large portion of the urban area, said limestones with dissolution features, producing cavities with metric dimensions, and probably related to the system of fractures, faults, and bedding. On top of the limestones, at the base of the thick soil, we detected pockets containing loose earthy materials (up to 10 m high) and cavities empty except for water (up to 4 m deep).

These pockets and cavities in the soil, the origin of which would be related to the dissolution of portions of the limestone top, naturally tend to evolve toward the surface, conditioned by hydraulic processes and by the action of gravity, with materials being carried to the interior of the cavities in the limestone. The cavities and pockets of soft soil, initially developed by the dissolution of the portions close to the limestone top, are filled with water or loose earthy materials, with hydraulic and mechanic behavior different from the soils which surround them. The variations of hydrostatic pressure which follow the oscillations of the potentiometric surface, especially those produced by cyclic pumping operations, act on the walls and ceiling of the soil-filled cavities and pockets.

Forces are created that act from the soil toward the interior of the cavities, which either by themselves or by flow induction (percolating friction) may remove the soil particles from the interface into the cavities. During cycles of recovery, when forces are reversed, even assuming an inflow of particles in the opposite direction, the sum of the movements will result in a descending displacement toward the cavities in the limestone.

Through this mechanism, the cavities develop up to the water table, where they are subject to the action of water infiltration and more susceptible to the weight of the overlying layer. However, the action of gravity may, by itself, induce ruptures in the soils of the ceilings of the cavities located below the water level, thus helping the evolution of the cavities toward the surface. Vibrations induced by explosions in nearby quarries may act as an auxiliary factor by rupturing the soil, thereby facilitating its removal to the interior of the cavities. Figure 2 presents a schematic drawing of the development of the

subsidence and collapse phenomena according to an interpretive model resulting from the investigations.

As a consequence of these factors, in particular the erratic behavior of the soft soil cavities and pockets, their different evolution stages and the time unpredictability of their consequences on the surface, all the area with limestone in the subsoil (18 ha, equivalent to 86 percent of the urbanized area) was considered unsuitable for urban use and virtually condemned for housing purposes (Figure 3).

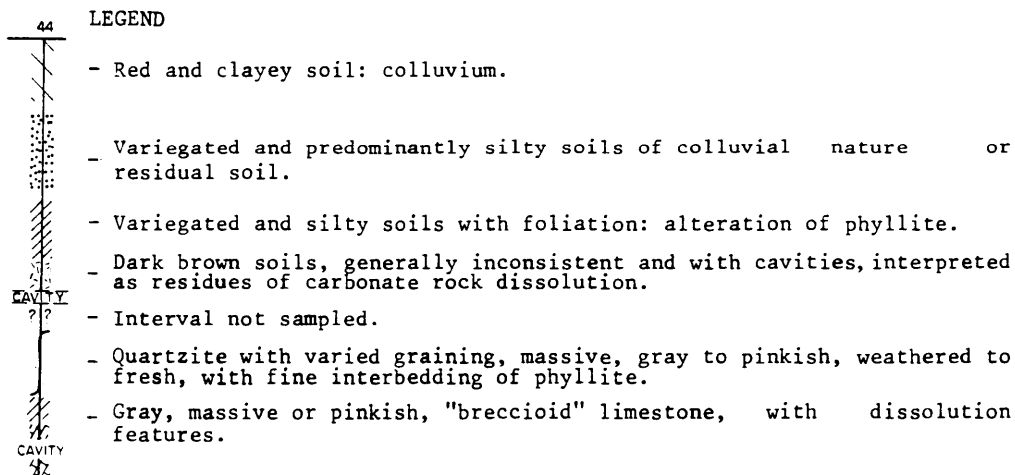
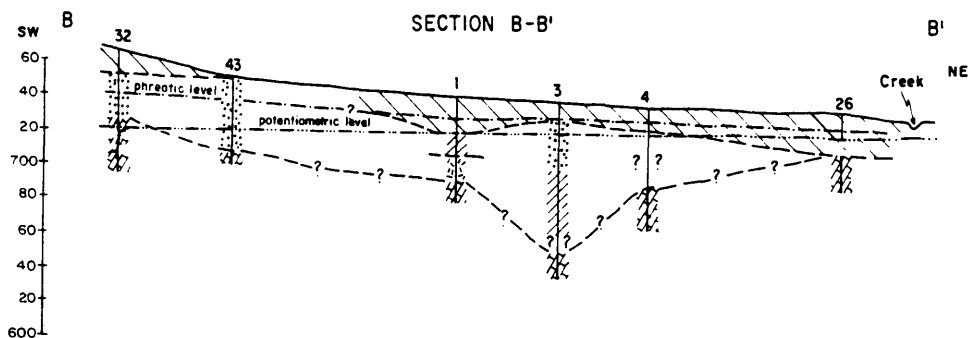
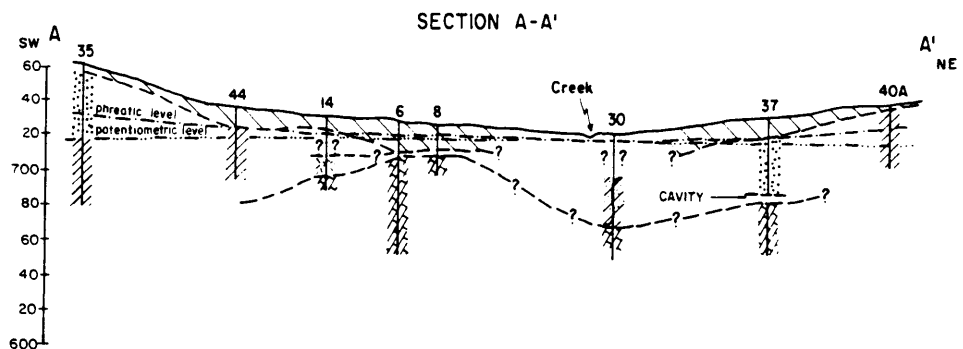
A portion of this area (3.8 ha or 18 percent of the urbanized area) had cracks in the soil and houses, marked subsidence, and a subsidence velocity of up to 1 cm/month, in full activity at least until February 1987, thus indicating a continued evolution of the processes in the subsoil. Such facts led to the immediate and definitive condemnation of this area for housing purposes. The considerations as to risk and utilization recommendations were presented in detail by Prandini et al. (1987b).

#### Final Considerations

Of the two variants previously mentioned for explaining the subsidence and collapse, this investigation confirms the second hypothesis, namely, a migration of soil into the interconnected cavities in the interior of the limestone. However, the ultimate objective of the work in Cajamar is that of determining, as soon as possible, measures to eliminate the risks imposed upon the population. This requires future research and investigation.

### References

- Ab'Saber, A.N., 1969, Uma revisao do Quaternario Paulista: do presente para o passado, *Rev. Bras. Geogr.*, Rio de Janeiro, 31(4), 1-51.
- Holzer, T.L., (Ed.), 1984, Man-induced land subsidence, Boulder, The Geological Society of America, 221 p. il. (*Reviews in Engineering Geology*, Vol. 7).
- Melo, M.S. de, and W.L. Poncano, 1983, Genese, distribuicao e estratigrafia dos depositos cenozoicos no Estado de Sao Paulo, (IPT, Publicacao 1 364, Monografias 6).
- Poncano, W.L., C.D.R. Carneiro, C.A. Bistrichi, F.F.M. de Almeida, and F.L. Prandini, 1981, Mapa geomorfologico do Estado de Sao Paulo, 1:1,000,000 scale, Sao Paulo, 2 vols. (IPT, Publicacao 1 183, Monografias 5).
- Prandini, F.L., W.L. Poncano, A.M. de A. Dantas, and M.C. Jacinto, 1987a, Caja mar-carst e urbanizacao: a experiencia internacional (sintese bibliografica), Paper presented at the 5<sup>th</sup> Brazilian Congress on Engineering Geology, Sao Paulo.
- Prandini, F.L., V.A. Nakazawa, I.G. de Avila, A.M. dos S. Oliveria, and A.R. dos Santos, 1987b, Cajamar-carst e urbanizacao: zoneamento de risco, Paper presented at the 5<sup>th</sup> Brazilian Congress on Engineering Geology, Sao Paulo.
- Therond, R., 1973, Recherche sur l'etancheite des lacs de barrage en pays karstique, Paris, Eyrolles, 444 p. il. (Collection du Centre de Recherches et D'essais du Chatou).



OBS.: The geotechnical sections location is shown on Figure 3.

Figure 1 - Geological sections.

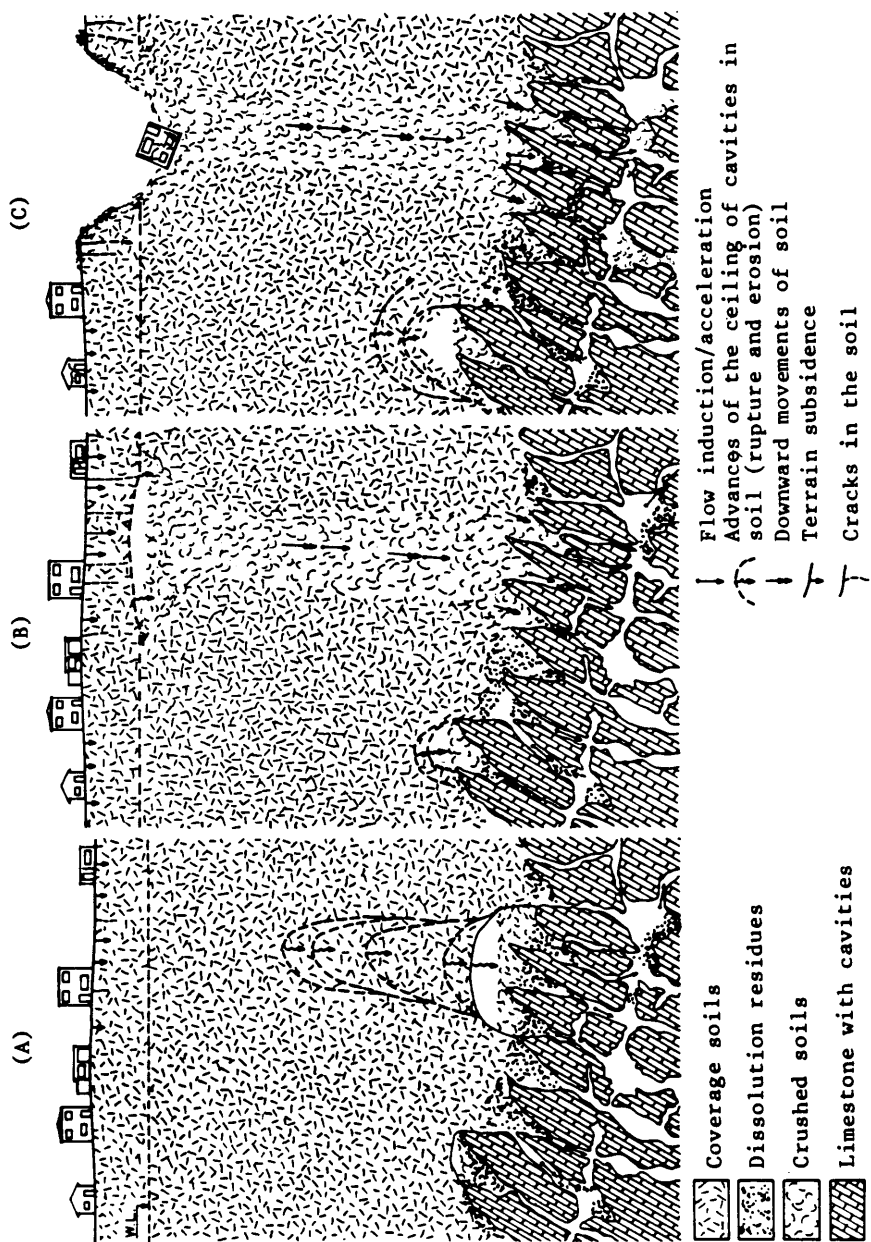


Figure 2 - Interpretative model of Cajamar phenomena.

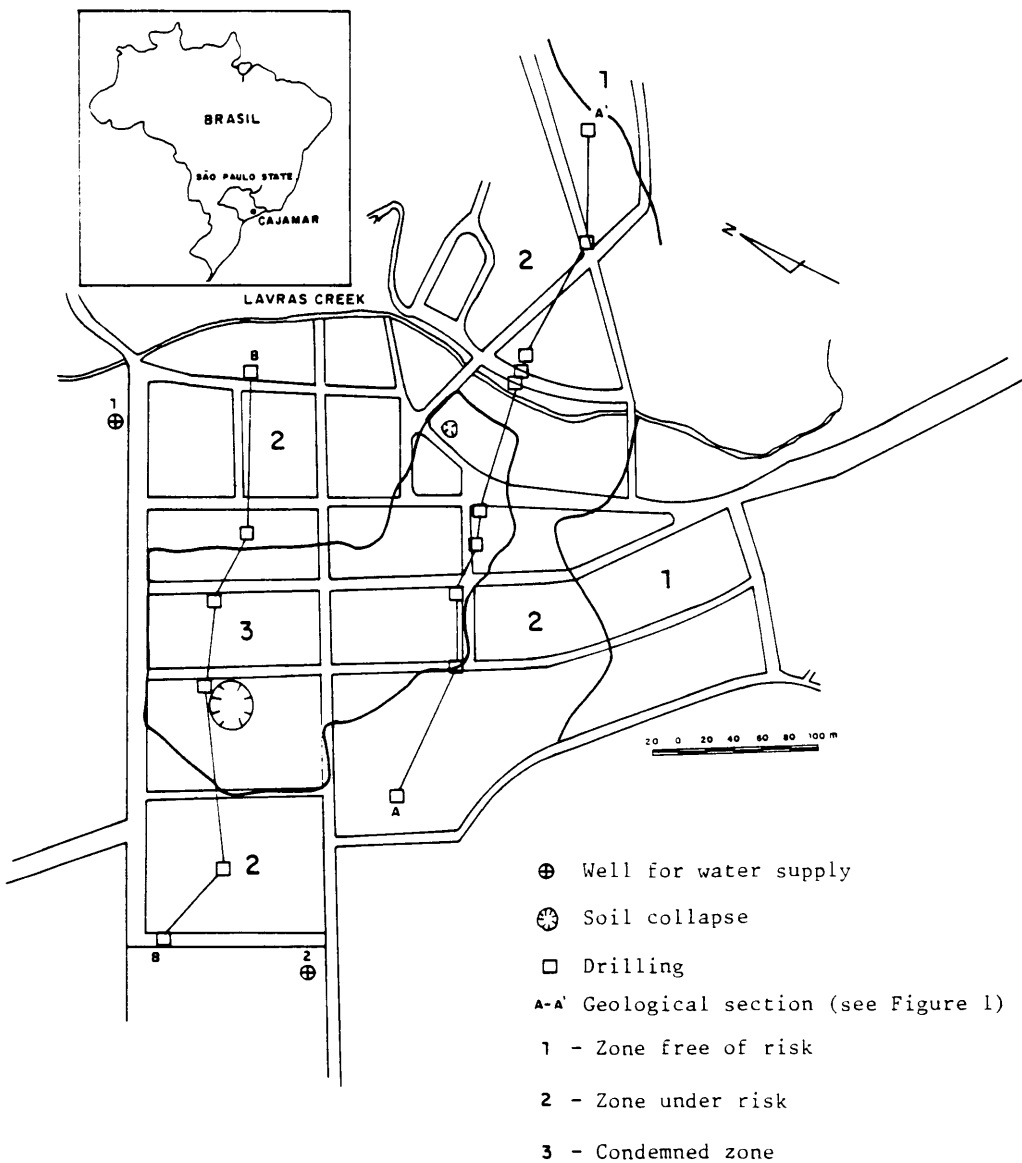


Figure 3 - Risk zoning map of Cajamar.





# STRATIGRAPHIC, GEOMORPHIC, AND STRUCTURAL CONTROLS ON THE EDWARDS AQUIFER, TEXAS, USA

by

John M. Sharp, Jr.

Department of Geological Sciences  
The University of Texas  
Austin TX 78713-7909, USA

**ABSTRACT:** The Edwards aquifer is a narrow band of Cretaceous carbonate rocks on the periphery of the Gulf Coastal Plain. The aquifer's great productivity is caused by early Cretaceous and late Cenozoic karstification, enhanced along fractures and Miocene-age faults. Primary flow is subparallel to strike for the most part, but is directed subparallel to dip at the aquifer's western and northern extremities. Recharge is predominantly by losing streams and natural discharge is primarily to springs along incised major streams. Water quality is controlled by aquifer stratigraphy, structure, and lithology, and by a variety of hydrogeochemical processes: cross-formational flow, mixing with saline formation waters, and rock-water interactions within the aquifer. The aquifer is both confined and unconfined. Proper development and utilization of this important aquifer requires an understanding of the aquifer's structural, geomorphic, geochemical, and stratigraphic evolution.

## Introduction

The Edwards aquifer of Texas is the principal source of water for almost 2 million people and provides a superlative example of how various geologic processes control the evolution of an aquifer, including its present areal extent, water quality, and hydraulic properties. The important processes include deposition in a variable sedimentary environment, early diagenesis, tectonic activity, the geomorphic processes of karstification and fluvial erosion, late diagenesis, and modern geologic processes both within the aquifer and in the adjoining Gulf of Mexico Basin. Finally, the effects of man on the present system should also be considered, at least from an economic standpoint.

The Edwards aquifer is most commonly defined as the narrow (less than 64 km) belt along the Balcones Fault Zone, which stretches some 400 km from a ground-water divide near the Rio Grande to the northeast near Salado, Texas. Equivalent carbonate rocks, however, form an important aquifer throughout the Edwards-Trinity Plateau and locally to the north in the Washita Prairie (Figure 1). Edwards-equivalent rocks also form important petroleum reservoirs downdip in the Gulf of Mexico Basin. Consequently, our understanding of the Edwards aquifer(s) requires a broader regional perspective, even though research and economic studies tend to concentrate on the Balcones Fault Zone portion of the system. The term "Edwards aquifer" in this paper will refer to the Balcones Fault Zone aquifer. For more detailed discussions of the Washita Prairie and Edwards Plateau aquifers, see Yelderman and others (1987) and Hammond (1984), respectively. The U.S. Geological Survey is also preparing a regional aquifer study of the Edwards-Trinity Plateau.

Also depicted on Figure 1 are oil fields in downdip portions of rocks equivalent to the Edwards aquifer. Oil seeps are found in aquifer outcrops along the Balcones Fault Zone (K. P. Young, pers. comm.); the hydrocarbons and associated oil-field brines do influence water chemistry along the bad-water line, especially in the central portion of the Edwards aquifer.

The Edwards aquifer is bounded by the edge of the outcrop on the northern and western boundary (Figure 2) except on its westernmost part where it is continuous with the Edwards Plateau. The southern and eastern boundary is somewhat arbitrarily defined as the "bad-water" line, with total dissolved solids of greater than 1000 mg/l. A ground-water divide is present in the west in Kinney County. West of this divide, flow is generally south towards the Maverick Basin; east of the divide, flow is generally subparallel to regional strike and discharge is to major springs. This is true in both the confined and unconfined portions of the aquifer. Equipotentials in the unconfined portion are generally subparallel to strike, but the aquifer is extremely anisotropic. Equipotentials tend to be subparallel to regional dip in the confined portion of the aquifer. Natural discharge is to springs, especially in Bexar, Comal, Hays and Travis Counties, where streams have incised into the aquifer. Continuing to the northeast, another ground-water divide is present in Hays County, which divided flow to the south (San Marcos Springs) from flow to the north to major springs, which discharges via Barton Springs into the Colorado River in Travis County. A final ground-water divide is present in northern Travis County, which separates the Colorado River ground-water drainage from the northern portion of the Edwards aquifer. In the northernmost section, flow is more downdip, similar to the situation in the Maverick Basin. Natural discharge is to springs and, probably in the past prior to aquifer development, by diffuse cross-formational flow.

Typical recharge/discharge relationships are demonstrated in cross-section (Figure 3). Streams flowing from the Edwards Plateau towards the Gulf of Mexico generally cross the aquifer nearly perpendicular to strike. Most of the recharge (85% in the Central Texas area) is by streamflow infiltration and most of the remainder by precipitation on the outcrop. The outcrop has extensive secondary porosity features. Cross-formational flow also recharges the aquifer; this contribution, although not a high percentage of total recharge, has an important effect on water chemistry. Proceeding downdip, the overlying Del Rio Clay becomes present and effective recharge by precipitation ceases. Therefore, the Edwards aquifer has both unconfined and confined bands of varying widths subparallel to strike. The faulting, discussed below, creates extremely anisotropic conditions. Flow is often channeled along fractures, and faulting may juxtapose permeable beds or where the throw is significant enough to create permeability barriers across fault blocks. The permeability of the rocks is so great, however, that the system has been successfully simulated as an isotropic and homogeneous medium (Maclay and Small, 1984; Slade and others, 1985).

The bad-water line separates the fresh-water zone (the Edwards aquifer) from the bad-water zone. In the fresh-water zone, water is a  $\text{Ca-HCO}_3$  or  $\text{Ca-Mg-HCO}_3$  facies with less than 1000 mg/l total dissolved minerals. The transition to the bad-water zone is often very abrupt. The origin of the bad-water zone has been debated for a number of years. Clement and Sharp (1987; 1988) and Sharp and Clement (1988) documented four distinct hydrochemical facies along the bad-water line (Figure 4). The westernmost facies (I) is  $\text{Ca-SO}_4$ . Proceeding to east of the Kinney County divide, the facies changes to a  $\text{Ca-Mg-SO}_4$  facies (II) with high Na and Cl; near San Antonio the facies (III) changes to  $\text{Na-Cl}$ ; and north of the upper divide shown in Figure 2, the bad-water changes abruptly to an  $\text{Na-Cl-SO}_4\text{-HCO}_3$  facies (IV). The freshwater facies throughout the aquifer is generally  $\text{Ca-HCO}_3$  or  $\text{Ca-Mg-HCO}_3$ . Both the aquifer's water chemistry and hydraulic properties are controlled by the stratigraphic, geomorphological, and structural evolution of the Edwards aquifer.

### Stratigraphic Controls

The formations comprising the Edwards aquifers were deposited in an extensive, shallow-water marine platform which was bounded by deeper basins (Fig. 5). Stratigraphic sections for representative areas are shown in Fig. 6. Fisher and Rodda (1969), Rose (1972), Maclay and Small (1983), Young (1986), and Pavlicek and others (1987), among others, provide more detailed stratigraphic reports.

The lower confining unit is the Glen Rose Formation of the Upper Trinity Group. The areally extensive Glen Rose consists of alternating layers of limestone and marl. The upper confining unit, the Del Rio Clay, was equally extensive but is eroded in portions of the Edwards-Trinity Plateau and in the Edwards aquifer recharge zones. The Del Rio is a selenitic, calcareous, pyritic, and fossiliferous clay. Kaolinite and illite are the major clay minerals; the illite weathers near the surface to smectite. Near-surface exposures of the Del Rio are very plastic and very low in permeability.

The intervening Edwards-aquifer carbonate rocks were deposited on the stable San Marcos and Central Texas Platforms fringed by the Maverick Basin, the North Texas-Tyler Basin, and the ancestral Gulf of Mexico Basin which was bordered by the Stuart City Reef trend. The Devils River Reef trend and the Central Texas Reef trend bordered, respectively, the Maverick and North Texas-Tyler Basins. The Maverick Basin is of particular interest. The carbonates deposited therein have a higher mud content and typically a higher content of evaporitic minerals.

The West Nueces Formation consists of shell-fragment wackestones and grainstones (classification of Dunham, 1962) and is generally low in permeability. The overlying McKnight Formation grades from thinly bedded carbonate mudstones to petroliferous shales and evaporites to grain-stones. The overlying Salmon Peak is a deep-water carbonate mudstone. The total stratigraphic section is approximately 200 m thick. The bordering Devils River Reef portion of the aquifer consists of approximately 140 m of reefal and interreefal deposits. Especially permeable are the reefal grainstones and breccias in the middle portion of the aquifer.

Gypsum is widely disseminated throughout Edwards aquifer rocks and was also concentrated in laterally extensive evaporite-rich layers. The McKnight Formation and the Kirschberg Member of the Fort Terret and Kainer Formations were formed in evaporitic lagoons (see Fig. 5). Leaching of the evaporite minerals and selective leaching along the rudistal reef trends and local bioherms surrounding the lagoons created beds of high permeability.

Along the San Marcos Platform (section 4 of Figure 6), the Kainer Formation (~75 m thick) consists of four members (Rose, 1976). The lowest is the Basal Nodular Member, a marine deposit of massive, nodular limestones that grade into the overlying Dolomitic Member. Early diagenesis along the Platform was extensive. The Dolomitic Member consists of burrowed intertidal and tidal wackestones. The Kirschberg Evaporite Member is formed from supratidal, evaporitic deposits. The Grainstone Member represents a transgression and is a well-cemented grainstone with intercalated mudstones. In some cases, the underlying Walnut Formation is considered the basal portion of the Edwards aquifer, but it is generally relatively low in permeability. Commonly overlying the Kirschberg and Grainstone Evaporite Members is the Regional Dense Member (RDM) of the Person Formation. This carbonate mudstone is easily identifiable in well logs and serves in some places as a confining bed within the aquifer. The Personal Formation (~55 m thick) is subdivided into five members (Rose, 1972) and is generally more permeable in its upper sections because of Cretaceous and subsequent karstification. Above the RDM are the Collapsed and Leached Members of supratidal/intertidal origin. These members contain collapsed breccias and burrowed and dolomitized wackestones. They are highly permeable. Above are the Marine (permeable rudistid-reef wackestones, packstones, and shell-fragment grainstones) and the Cyclic Members. Along the San Marcos Platform (section 4 on Figure 6), an erosional episode stripped off approximately 30 m of Edwards limestones. Overlying the unconformity is the Georgetown Formation, which consists of relatively low-permeability carbonate mudstones 6-12 m thick.

In the northern portions of the Edwards aquifer (sections 5 and 6 of Figure 6), the aquifer is thinner. The rocks are equally variable, but no formal members have been proposed.

The entire section is also less permeable, except for scattered bioherms. The lower-permeability Comanche Peak and Walnut Formations are proportionately thicker and the Kiamichi Shale divides the Georgetown and Edwards Formations into separate hydrostratigraphic units. In all portions of the Edwards and Edwards Plateau aquifer (Figure 1), karstification may provide extensive horizontal and vertical zones of high permeability.

Early diagenesis of these rocks leached evaporite minerals and reefal deposits, creating collapsed zones and layers of high permeability. Dolomitization was extensive along the San Marcos Platform and peripheral to the Kirschberg Lagoon. Both the reflux theory and freshwater/saltwater mixing may explain the localization of early dolomitization. Because recent freshwater diagenesis has not significantly altered Edwards rocks in the bad-water zone, the depositional provinces control the proportion of limestone and dolomite in the aquifer rocks, the preservation of gypsum and anhydrite, and the distribution of fossiliferous and porous beds. These facies have profound effects on the distribution of aquifer hydraulic properties and its water quality.

### Structural and Tectonic Controls

There are two types of structural/tectonic features which affect the Edwards aquifer-- faulting and Cretaceous volcanic plugs. The faults, as illustrated in Fig. 3, are the most important feature. They cross-cut the aquifer and control the areal distribution of confined and unconfined portions of the aquifer. The strike of the faults in the Balcones Fault Zone corresponds closely to the buried Ouachita fold belt trend (Caran and others, 1981). Both the number of faults and the amount of throw are greatest along the San Marcos Arch, decreasing both to the west and to the northeast. Faulting may juxtapose permeable beds to permit flow across faulted blocks. In other cases, less permeable zones are brought into juxtaposition with permeable beds to create barriers to flow across the faults. In some cases near the crest of the San Marcos Arch, the throw is sufficient to completely offset the aquifer and some faulted blocks become hydrologically isolated (Maclay and Small, 1983). These features can be set into the more general structural setting (Fig. 7).

Several gentle fold patterns cross the strike of the Edwards aquifer. The most important is the San Marcos Arch, which corresponds to the crest of the San Marcos Platform. This trend has been a zone of persistent relative stability since the late Paleozoic Ouachita orogeny. The present location of the Edwards aquifer (Balcones Fault Zone) corresponds to the trend of buried Ouachita belt, which separates the stable Texas Craton from the subsiding Gulf of Mexico Basin (Clark, 1982). North of the San Marcos Arch are the Round Rock Syncline and the Belton High. These broad structural trends correlate with changes in the badwater hydrochemical facies. The Na-Cl facies is found in the zone of the San Marcos Arch and the Round Rock Syncline. The Na-Cl-SO<sub>4</sub>-HCO<sub>3</sub> facies is found in and north of the Belton High.

Cretaceous igneous rocks are exposed or have been found by drilling in over 200 locations. Most of them are concentrated in the Travis and Uvalde volcanic fields (Fig. 7). These have created a variety of hydrocarbon traps (Ewing and Caran, 1982). They are also associated with anomalous water chemistry in the Edwards aquifer. The volcanic plugs (Barker and Young, 1979) and the adjacent, permeable deposits form avenues for vertical fluid migration; hydrochemical reactions with volcanic rocks (nephelite basalts) may account for anomalous Na-HCO<sub>3</sub> waters in the aquifer (Clement, 1989).

### Geomorphic Controls

Uplift and erosion, faulting, stream incision, and stream piracy control the extent of the Edwards outcrop. The Central Texas region has a long history of solution and collapse

(Kastning, 1987), but the key periods of karstification occurred in the early Cretaceous when extensive areas along the stable San Marcos and Central Texas Platforms were exposed and in the late Tertiary-Quaternary. Figure 8 depicts the generalized geomorphic evolution of the Edwards aquifer in the San Antonio-Austin area along the San Marcos Arch (Fig. 7).

In the early Cretaceous, the Edwards Group rocks were karstified with the most intense solutioning in the uppermost Person Formation, with the erosion of over 30 meters of section. In some cases, however, karst solution/collapse features penetrated throughout the entire aquifer sequence. This has been thoroughly documented in outcrops in the Edwards Plateau. The Cretaceous karstification was widespread along the San Marcos Arch, even well downdip from the aquifer, as indicated by petroleum production in the downdip Edwards Formation, where the best reservoirs occur in elevated fault blocks with solution features. Dolomitization along the Arch occurred at this time. The Person erosional surface again submerged in the shallow Cretaceous sea. The overlying Georgetown and confining Del Rio Clay were then deposited with a thick sequence of overlying Cretaceous and probably lower Tertiary units.

Continued Cenozoic deposition in the Gulf of Mexico Basin ("forebulging"), probably coupled with tectonics in the southern Rockies, created uplift and erosion by the beginning of the Miocene and faulting during the Miocene. Erosion separated the Balcones Fault zone from the Edwards-Trinity Plateau except in the southwest. The increased relief created by the faulting caused rapid headward erosion by consequent streams and stream piracy, which occurred when the previously eastward-flowing streams were captured by the newly incising streams (Woodruff, 1977; Woodruff and Abbott, 1979). The deep incision of resistant carbonate rocks along the fault zone created points for concentrated discharge from the aquifer. The modern flow pattern in the aquifer was probably established at this time.

Since the Miocene, continued downcutting and, in some cases, stream piracy has left some cave and collapse systems above the water table. Continued solutioning (Miocene to present) along fractures and conduits has enhanced permeability, especially in the unsaturated zone.

The more intense karstification, however, is in the late Cenozoic. Extensive cavern and doline development is still occurring along the Balcones Fault Zone and the periphery of the Edwards Plateau; the Devils River Uplift (in the western portion of the Edwards aquifer) underwent large-scale solution subsidence before the middle Pleistocene (Kastning, 1987). The dolines and solution-enlarged fractures provide sites for rapid infiltration of overland flow; losing streams are common in the unconfined portions of the aquifer. Cave systems are common in aquifer rocks, with a distinctive cave fauna. Longley (pers. comm., 1988) suggests that this fauna has been "in place" since the early Tertiary or, perhaps, even the late Cretaceous.

### Ground-Water Chemistry

Extensive reviews of the ground-water chemistry of the Edwards aquifer have recently been provided by Clement (1989) and, with special reference to the San Antonio area, by Groschen (written comm., 1988). Water in the fresh-water zone is, generally, Ca-HCO<sub>3</sub> or Ca-Mg-HCO<sub>3</sub> facies. The bad-water zone (south and east of the bad-water line; Figure 1) contains variable water chemistry, discussed above (Figure 4). The characteristics of rocks in the fresh-water and bad-water zones near San Antonio are summarized by Groschen (1988, written comm.). Three main theories have been advanced to explain the bad-water zone. One theory, advanced by Prezbindowski (1981), suggests that the bad-water line is created by the mixing of Edwards freshwater with saline brines being driven out of the Gulf of Mexico Basin by compaction and coupled with dedolomitization in both the aquifer and, perhaps, downdip Edwards-equivalent rocks. A second hypothesis suggests that the difference in chemistry is the result of different diagenetic histories in the fresh-water and bad-water zones, and that intensive

fresh-water diagenesis has never occurred downdip of the bad-water line. In the fresh-water zone, calcite cement has occluded much of the aquifer's primary porosity; evaporite minerals, both disseminated and in beds, leached; and the rocks dedolomitized (Longman and Mench, 1978). The rocks are light-colored and conditions are oxidizing. In contrast, bad-water-zone rocks are darker in color and conditions are reducing. Anhydrite or gypsum, celestite, pyrite, and organic matter remain preserved in the rocks. The varying hydrochemical facies might simply reflect water/rock reactions. The third theory suggests that the bad-water zone reflects fault controls of the flow system with the faults serving as permeability barriers preventing freshwater from flowing in a downdip direction. It is suggested that the bad water is a stagnant, "connate" water. Alternatively, it's been suggested that the faults serve as conduits for cross-formational flow and, in line with Prezbindowski, that the bad-water zone represents upward leakage of brines. Clement and Sharp (1988) and Clement (1989) examined bad-water zone hydrochemistry on a regional basis. They concluded that the bad-water zone resulted from a varying combination of mineral solution and mixing with waters migrating updip and across formations and that there is, therefore, some validity to each of the theories. Clement and Sharp's conclusions are summarized below.

The Ca-SO<sub>4</sub> facies in the Maverick Basin can be explained by continued dissolution of anhydrite/gypsum along flow paths. The lack of Na and Cl suggests that halite, if ever present, has long ago been flushed from aquifer rocks. This implies that the increase of Na and Cl to the east along the bad-water line is not derived chiefly from dissolution of disseminated halite. This is reinforced by the fact that the restricted environment in the Maverick Basin should have been more conducive to deposition of halite. The percent and absolute amount of dissolved Na and Cl increase along the bad-water line towards the San Marcos platform. This is coincident with the increase in faulting intensity and throw. In this area, the Prezbindowski theory makes sense. The higher Mg content of the waters is caused by dedolomitization in the San Marcos Arch. The lack of Mg in bad-water facies I is attributable to the lack of dolomite in the Maverick Basin. Clement suggests that updip and/or cross-formational flow of brines is partially responsible for water chemistry in zones II and III. This implies that the bad-water zone of facies II and III is the confluence of the rapidly flushing fresh-water system and a very slow-moving but not stagnant bad-water system.

The bad-water zone facies (IV), Na-Cl-SO<sub>4</sub>-HCO<sub>3</sub>, is very similar to waters in the underlying Hosston Formation. Clement and Sharp (1987) present detailed evidence for origin of the bad water in this case by cross-formational flow. The thinner hydrostratigraphic section apparently allows less dilution by fresh water and the flow in the northern portion of the aquifer is in a more downdip direction, similar to that of the Ca-SO<sub>4</sub> facies system.

### Discussion

In recent decades, man's effects have become important in the continued evolution of the Edwards aquifer. Nitrate contamination is not uncommon (Kreitler and Browning, 1983) and occasionally surface spills of hydrocarbons have entered the aquifer through discrete recharge features (sinkholes and fractures). The general influence of land use on water quality in the aquifer has recently been reviewed by Buszka (1987). Man's use of ground water has also altered the natural hydrologic systems. Natural discharge to the recreationally and socially important springs has been diminished and, in some cases, flow has ceased. Continued population growth along the aquifer is projected to further deplete spring flows, unless methods of recharge augmentation are developed (Slade and others, 1985). These proposals would store surface waters in updip reservoirs and release water to the streams in the recharge zone during periods of potential recharge.

### Acknowledgements

Acknowledgement is made to the donors of the Petroleum Research Fund of the American Chemical Society for partial support of this research. Manuscript preparation was funded by the Owen-Coates Fund of the Geology Foundation, the University of Texas at Austin. Jeff Horowitz prepared the figures; Rosemary Brant assisted in the editing.

### References

- Abbott, P. L., 1975, On the hydrology of the Edwards Limestone, south-central Texas, *Jour. Hydrology*, v. 24, p. 251-269.
- Barker, D. S., and Young, K. P., 1979, A marine Cretaceous nepheline basinite volcano at Austin, Texas, *Texas Jour. Science*, v. 31, p. 5-24.
- Buszka, P. M., 1987, Relation of water chemistry of the Edwards aquifer to hydrogeology and land use, San Antonio region, Texas, U.S. Geol. Survey Water-Res. Inv. 87-4116, 100 p.
- Caran, S. C., Woodruff, C. M., Jr., and Thompson, E. J., 1981, Lineament analysis and inference of geologic structure--examples of the Balcones-Ouachita trend of Texas, *Trans., Gulf Coast Assoc. Geol. Societies*, v. 31, p. 59-69.
- Clark, H. C., 1982, Ouachita orogenic complex, central Texas geophysical measurements and basement offset, *Trans., Gulf Coast Assoc. Geol. Societies*, v. 32, p. 157-163.
- Clement, T. J., 1989, Hydrochemical facies in the badwater zone of the Edwards aquifer, Central Texas, unpubl. M.A. thesis, Univ. Texas, Austin, 168 p.
- Clement, T. J., and Sharp, J. M., Jr., 1987, Hydrochemical facies of the Edwards aquifer, Williamson and Bell Counties, Texas, in *Hydrogeology of the Edwards Aquifer in the Northern Balcones and Washita Prairie Segments*, Geol. Soc. America (South-Central Sec.) Guidebook, p. 61-70. Reprinted in *Austin Geol. Soc. Guidebook No. 10*, 1987.
- Clement, T. J., and Sharp, J. M., Jr., 1988, Hydrochemical facies in the bad-water zone of the Edwards aquifer, Central Texas, *Proceedings of the Ground Water Geochemistry Conf.*, Nat. Water Well Assoc., Dublin, Ohio, p. 127-149.
- Dunham, R. J., 1962, Classification of carbonate rocks according to depositional texture, in Ham, W. E. (ed.), *Classification of Carbonate Rocks*, Am. Assoc. Petrol. Geologists Mem. 1, p. 108-121.
- Ewing, T. E., and Caran, S. C., 1982, Late Cretaceous volcanism in south and central Texas--stratigraphic, structural, and seismic models, *Trans., Gulf Coast Assoc. Geol. Societies*, v. 32, p. 137-145.
- Fisher, W. L., and Rodda, P. V., 1969, Edwards Formation (Lower Cretaceous), Texas: dolomitization in a carbonate platform system, *Am. Assoc. Petrol. Geologists Bull.*, v. 53, p. 55-72.
- Groschen, G. E., 1988, Evaluation of theories of the freshwater/salinewater interface in the Edwards aquifer, San Antonio, Texas region--with results from the 1985-1987 test-drilling and monitoring study, U.S. Geol. Survey (unpubl. report).
- Hammond, W. W., Jr., 1984, Hydrogeology of the lower Glen Rose aquifer, south-central Texas, unpub. Ph.D. diss., Univ. Texas, Austin, 243 p.
- Jacka, A. D., and Stevenson, J. C., 1977, The JFS Field, Dimmit County, Texas: some unique aspects of Edwards-McKnight diagenesis, *Trans., Gulf Coast Geol. Societies*, v. 27, p. 45-60.
- Kastning, E. H., 1987, Solution-subsidence-collapse in Central Texas: Ordovician to Quaternary, in (Beck, B. F., and Wilson, W. L., eds.) *Karst Hydrogeology: Engineering and Environmental Applications*, A. A. Balkema, Rotterdam, p. 41-45.
- Kreitler, C. W., and Browing, L. A., 1983, Nitrogen-isotope analysis of groundwater nitrate in carbonate aquifers: natural sources vs. human pollution, *Jour. Hydrology*, v. 61, p. 285-301.
- Longman, M. W., and Mench, P. A., 1978, Diagenesis of Cretaceous limestones in the Edwards aquifer system of south-central Texas: *Sed. Geology*, v. 21, p. 241-276.

- Maclay, R. W., and Small, T. A., 1983, Hydrostratigraphic subdivisions and facult barriers of the Edwards aquifer, south-central Texas, USA, *Jour. Hydrology*, v. 61, p. 127-146.
- Maclay, R. W., and Small, T. A., 1984, Carbonate geology and hydrology of the Edwards aquifer in the San Antonio area, Texas, U.S. Geol. Survey Open-File Rept., 83-537, 72 p.
- Pavlicek, D., Small, T. A., and Rettman, P. L., 1987, Hydrogeologic data from a study of the freshwater zone/saline-water zone interface in the Edwards aquifer, San Antonio region, Texas, U.S. Geol. Survey Open-File Report, 87-389, 108 p.
- Prezbindowski, D. R., 1981, Carbonate rock-water diagenesis, unpub. Ph.D. thesis, Univ. Texas, Austin, 237 p.
- Rose, P. R., 1972, Edwards Group, surface and subsurface, central Texas, Univ. Texas Bur. Econ. Geology Rept. Inv. 74, 198 p.
- Sharp, J. M., Jr., and Clement, T. J., 1988, Hydrochemical facies as hydraulic boundaries in karstic aquifers--the Edwards aquifer, U.S.A., in *Proceedings of the 21st I.A.H. Congress, Karst Hydrogeology and Karst Environment Protection*, Guilin, P.R.C., v. 2, p. 841-845.
- Slade, R. M., Jr., Ruiz, L., and Slagle, D., 1985, Simulation of the flow system of Barton Springs and associated Edwards aquifer in the Austin area, Texas, U.S. Geol. Survey Water-Res. Inv. Rept. 85-4299, 49 p.
- Woodruff, C. M., Jr., 1977, Stream piracy near the Balcones Fault Zone, Central Texas, *J. Geology*, v. 85, p. 483-490.
- Woodruff, C. M., Jr., and Abbott, P. L., 1979, Drainage-basin evolution and aquifer development in a karstic limestone terrain, South-Central Texas, *Earth Surface Processes*, v. 4, p. 319-334.
- Yelderman, J. C., Jr., Slade, R. M., Jr., Sharp, J. M., Jr., and Woodruff, C. M., Jr., 1987, Hydrogeology of the Edwards aquifer in the northern Balcones and Washita Prairie segments, Guidebook for 1987 Geol. Soc. America South-Central Mtg., Waco, Tex., 127 p. (Reprinted by the Austin Geol. Soc., Austin, Texas, as Guidebook No. 10.)
- Young, K., 1986, Cretaceous, marine inundations of the San Marcos Platform, Texas, *Cretaceous Research*, v. 7, p. 117-140.



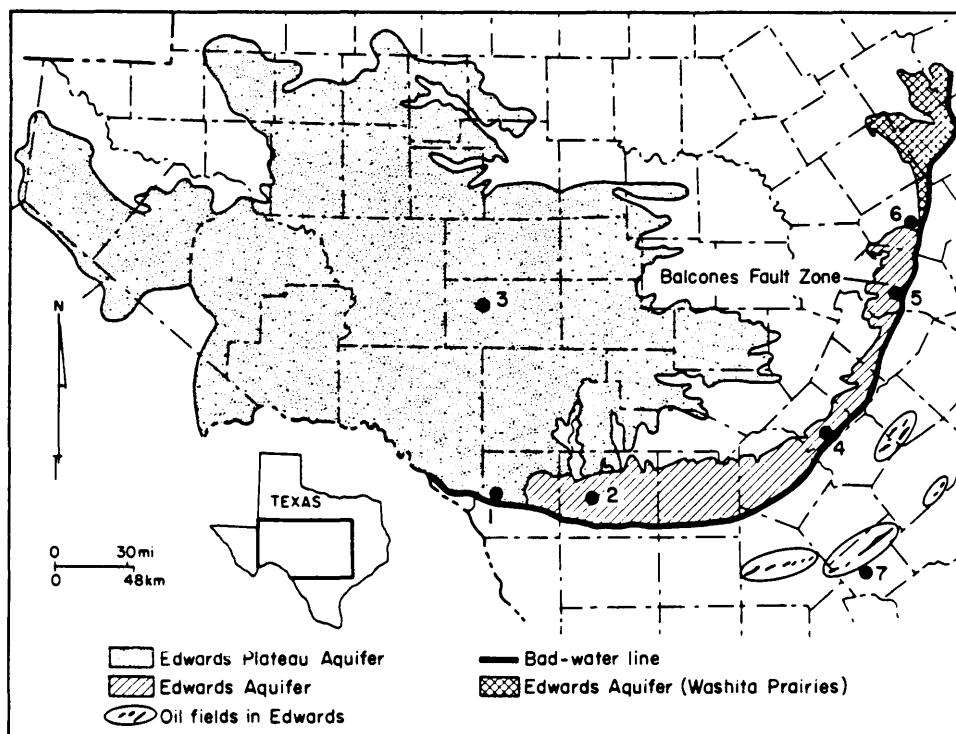


Figure 1. Edwards aquifers showing the major geographic units. Also shown are the locations of the numbered cross-sections shown in Figure 6.

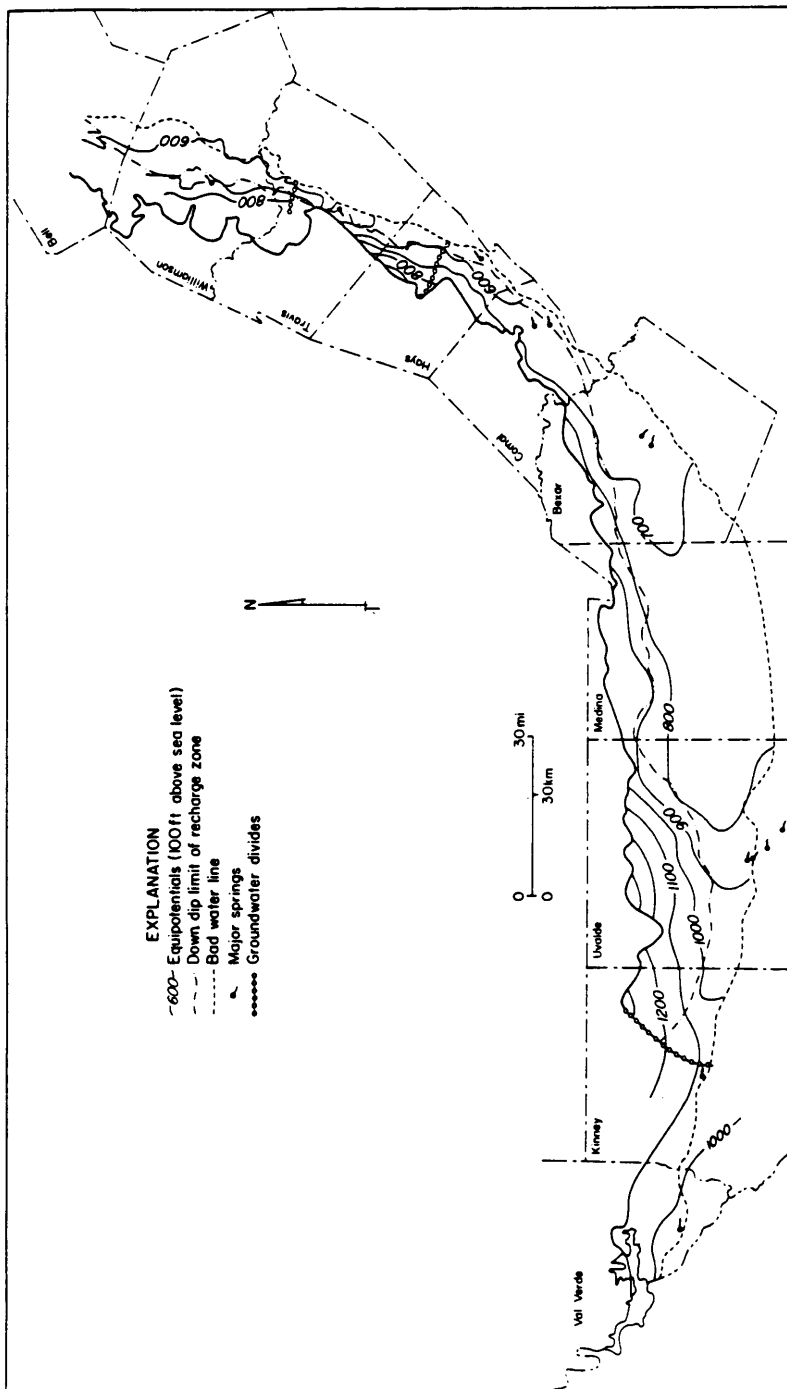


Figure 2. Potentiometric surface of the Edwards aquifer in winter, 1981 (from Clement and Sharp, 1988; reprinted courtesy of the National Water Well Association, Dublin, Ohio).

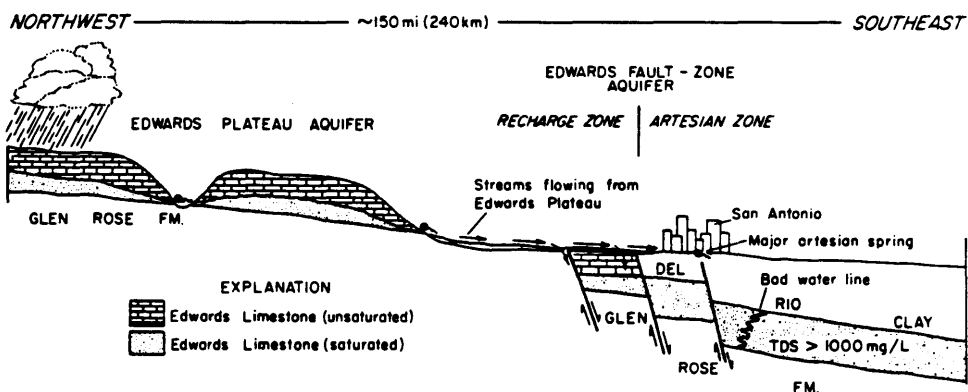


Figure 3. Generalized cross-section across the Edwards aquifer near San Antonio, showing major hydrogeologic features (from Clement and Sharp, 1988; reprinted courtesy of the National Water Well Association, Dublin, Ohio).

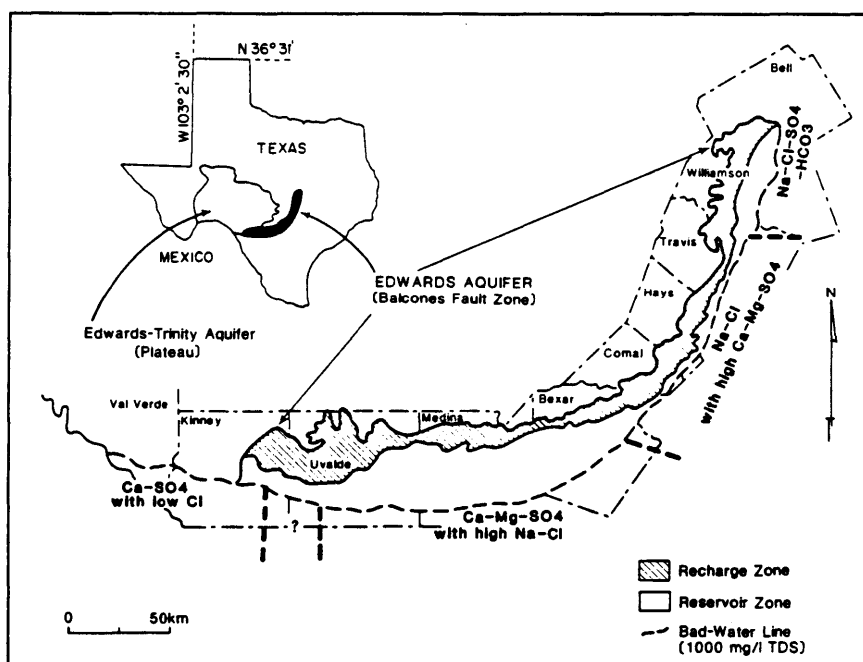


Figure 4. Bad-water zone facies in the Edwards aquifer (after Clement and Sharp, 1987; 1988; and Sharp and Clement, 1988).

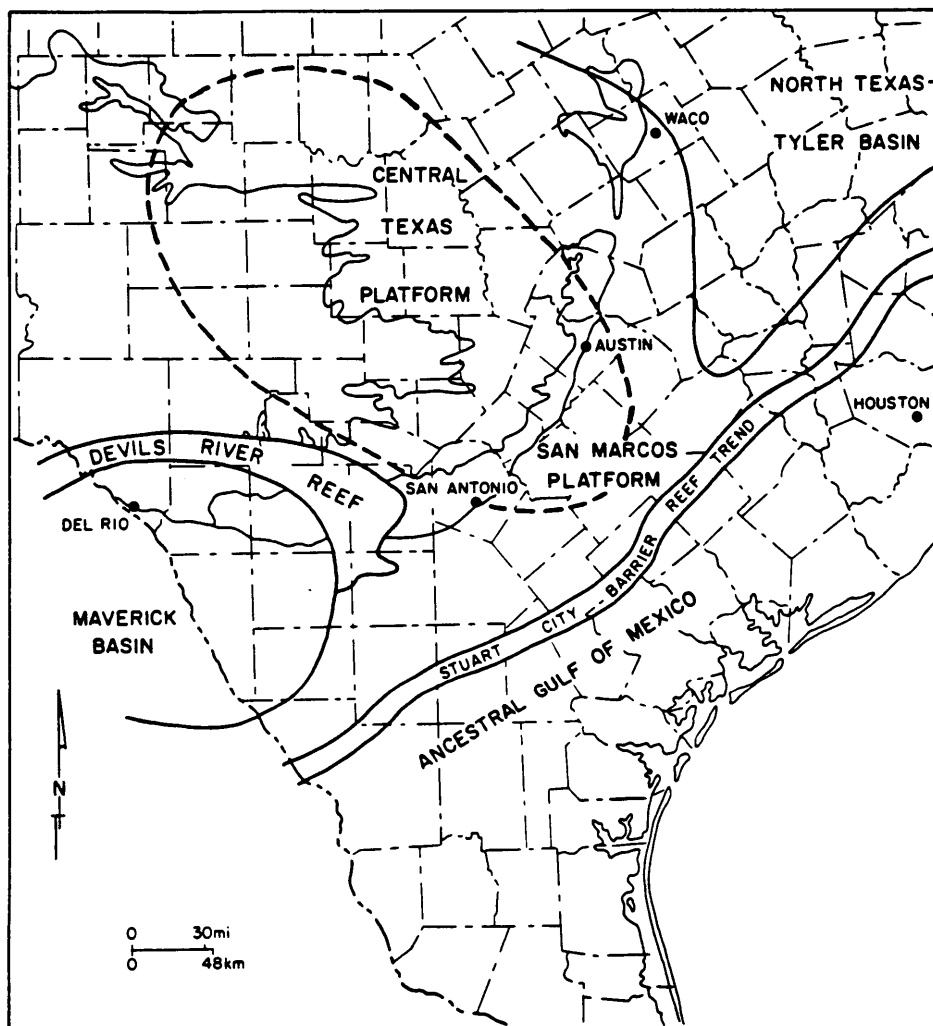


Figure 5. Depositional provinces of Edwards aquifer carbonate rocks. The Maverick Basin was, at times, an evaporative lagoon (Jacka and Stevenson, 1977; Fisher and Rodda, 1969). Dashed line indicates the approximate position of the Kirschberg evaporite lagoon.

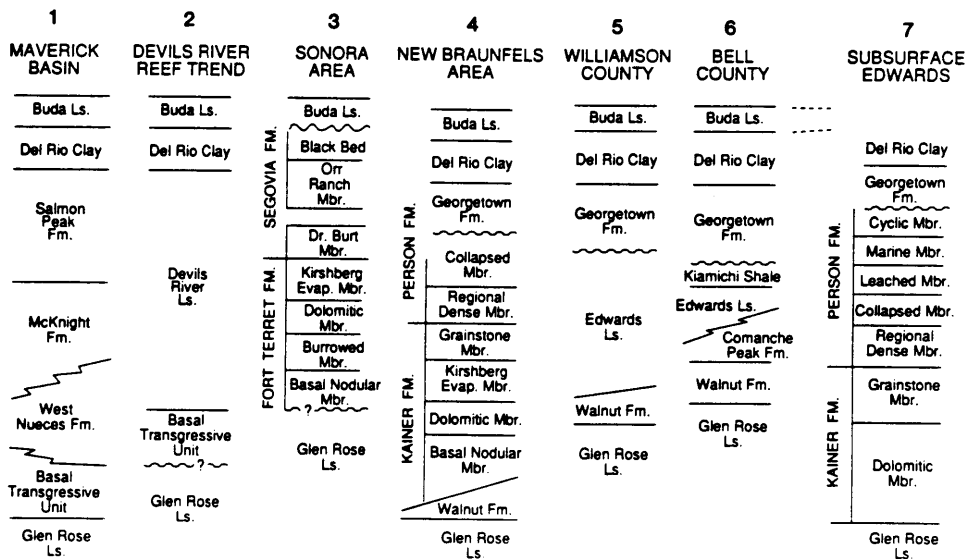


Figure 6. Stratigraphic columns (numbers refer to Figure 1 locations) of the Edwards aquifers. Units above the Glen Rose Formation and below the Del Rio Clay comprise the aquifer, except for the Kiamichi Shale (6). The subsurface Edwards (7) is identified from well cuttings and petroleum well logs (Rose, 1972).

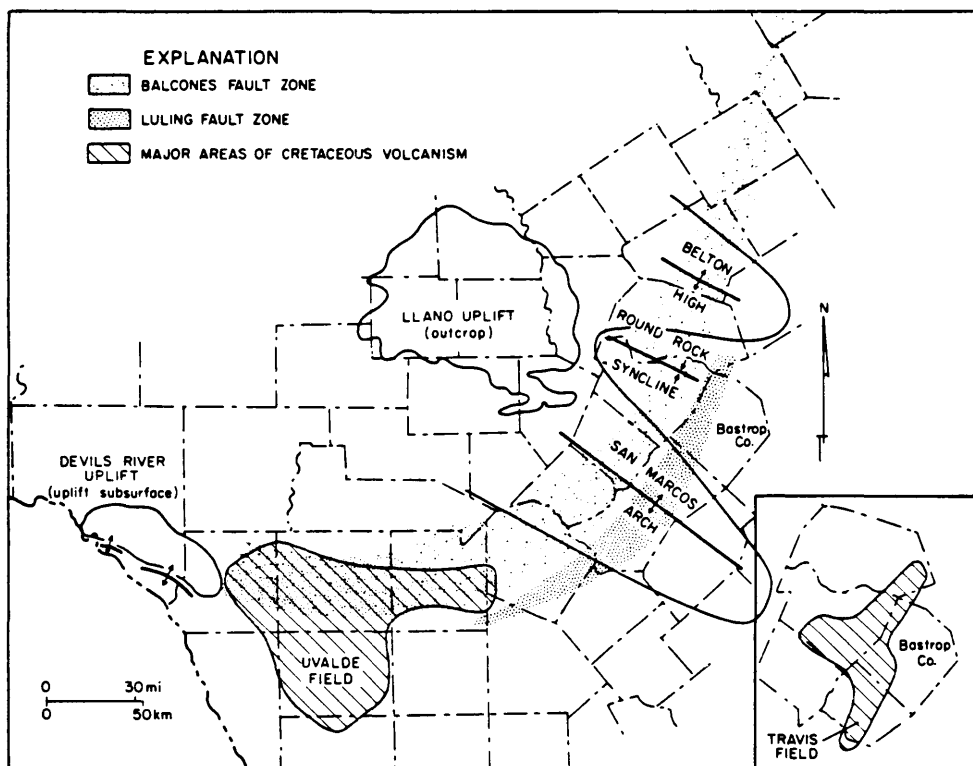
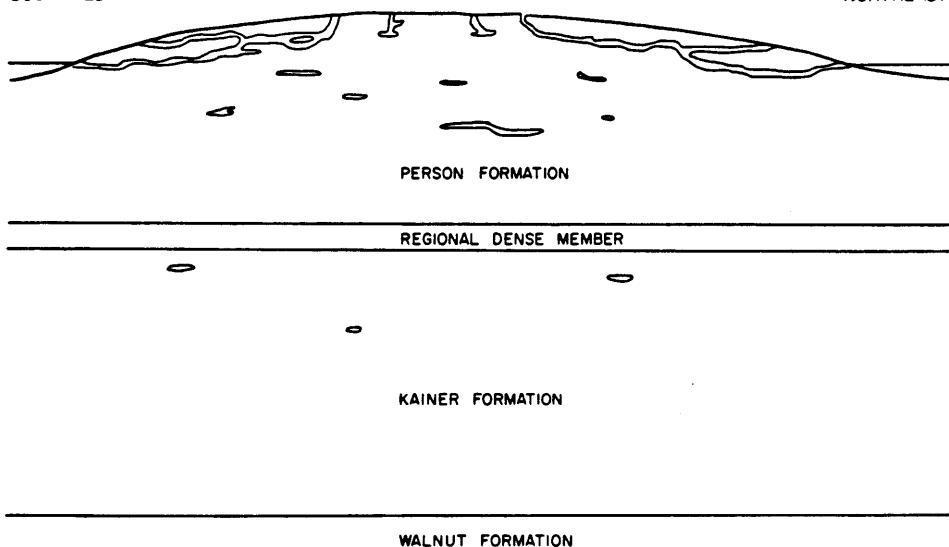


Figure 7. Structural setting of the Edwards aquifer. Faulting is most intense along the San Marcos Arch. Ground-water quality variations (Fig. 4) correspond to both structural and hydrodynamic features (from Clement and Sharp, 1988; reprinted courtesy of the National Water Well Association, Dublin, Ohio).

## A. CRETACEOUS

SOUTHWEST

NORTHEAST



## B. PALEOGENE

SOUTHWEST

NORTHEAST

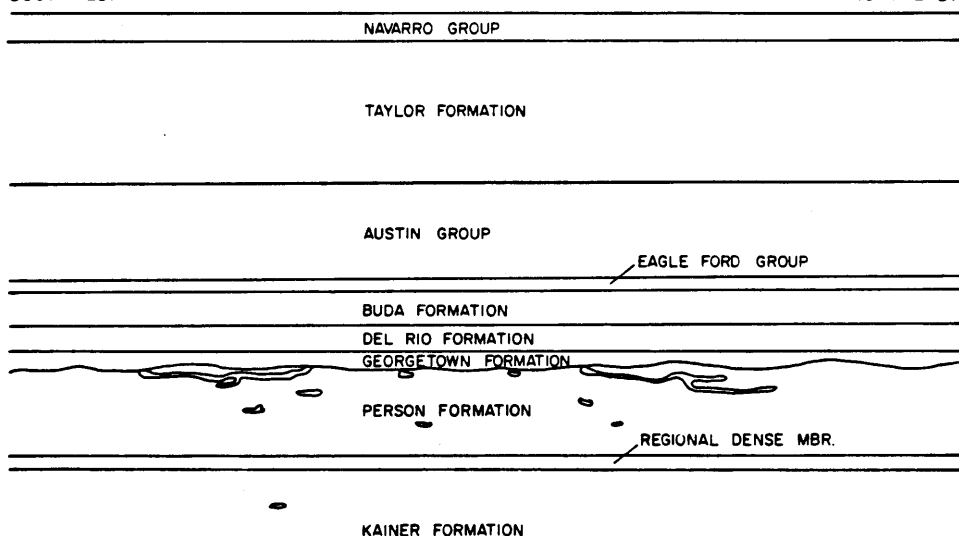
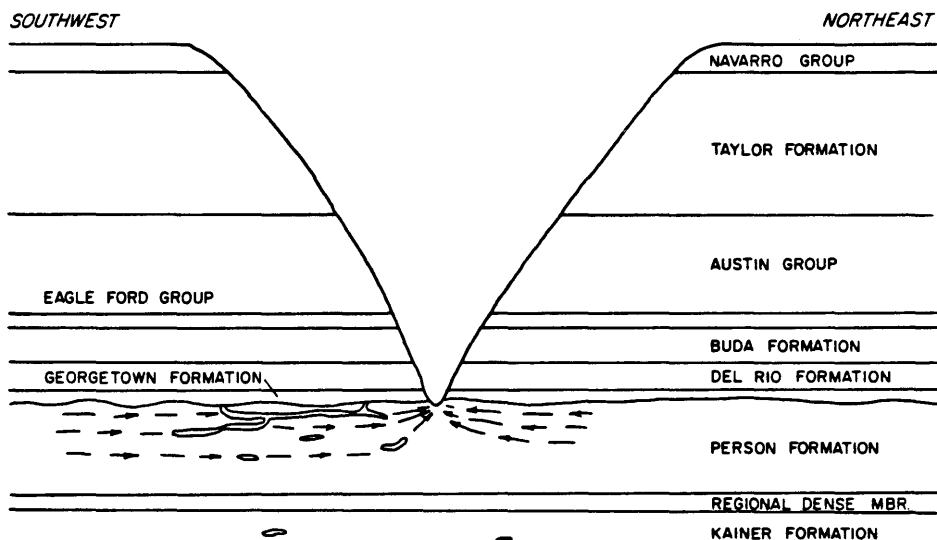


Figure 8. Geomorphic evolution of the Edwards aquifer (after Abbott, 1975). A. Cretaceous. Erosional episode strips the upper section of the Person and equivalent formations. B. Paleozoic. The overlying Georgetown Formation and confining unit, the Del Rio Clay, are deposited. Over 200 m of Upper Cretaceous rocks are deposited.

## C. MIDDLE MIOCENE



## D. RECENT

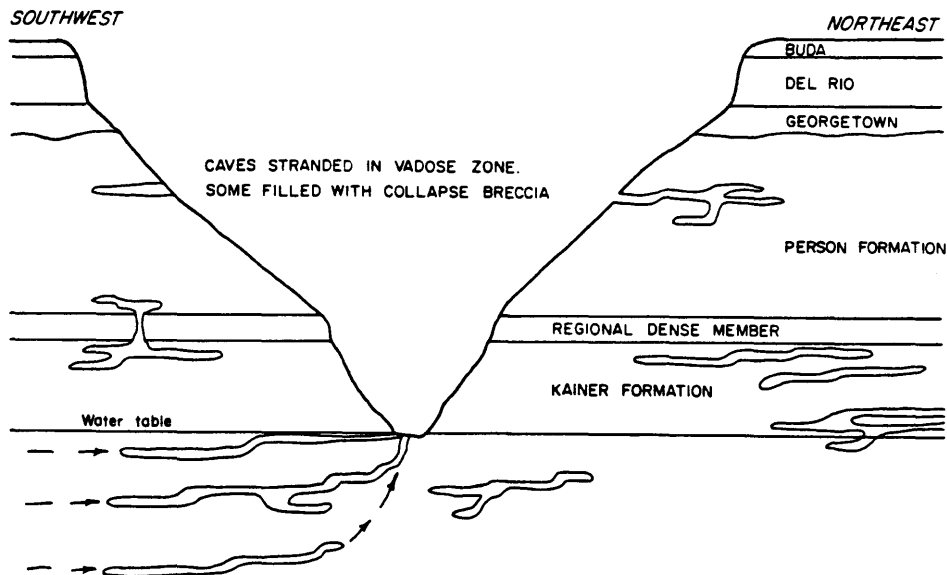


Figure 8 (continued). C. Middle Miocene. Faulting and uplift creates erosion, stream dissection, and renewed karstification. The basic flow system of the aquifer is established at this time. D. Recent. Continued downcutting and stream piracy leaves cave systems above water table. Solutioning along fractures and conduits increases permeability, particularly in the unconfined portions of the aquifer.



INTERPRETING CALCITE, DOLOMITE, AND GYPSUM SATURATION CONDITIONS  
IN THE EDWARDS AQUIFER, TEXAS

Albert E. Ogden  
Center for the Management, Utilization and  
Protection of Water Resources  
Tennessee Technological University  
Box 5082, Cookeville, Tennessee 38505  
and

Paul D. Collar  
U.S. Geological Survey - Water Resources Division  
G.P.O. Box 4424, San Juan, Puerto Rico 00936

**ABSTRACT:** Time series hydrogeochemical data from three of the largest springs in Texas showed seasonal effects on calcite, dolomite, and gypsum saturation. Saturation indices were also calculated from data for ninety wells sampled within a 130 square kilometer area around San Marcos, Texas. High calcium hardness values in ground waters within some fault blocks were thought to be related to gypsum dissolution, but the well waters were all found to be undersaturated with respect to gypsum. Gypsum saturation does increase between the recharge zone and the bad water line. No increasing trends occurred in saturation with respect to calcite and dolomite between the recharge zone and the bad water line, as anticipated. Despite long transport distances and deep circulation, Comal, San Marcos, and Hueco springs remained undersaturated except during a six-month period associated with a severe drought which produced a large decrease in spring flow. Well waters remained undersaturated throughout the year study period except during the height of the drought. The level of saturation appears to be related to a well's proximity to a fault or fracture. Faster ground water velocities within the caves and along the solution-enlarged fractures and faults cause lower levels of calcite and dolomite saturation. Undersaturation is also related to calcite deposition before reaching the springs; mixing effects of undersaturated, local recharge waters; and small water/rock contact in the aquifer's large cavities.

### Introduction

Several researchers have suggested that the nature of ground water flow in carbonate rocks can be ascertained, in part, by the waters' state of saturation with respect to dissolved carbonates (Jacobson and Langmuir, 1970; Shuster and White, 1971; Thrailkill, 1972; Hess, 1974; Ogden, 1988). Saturation indices of carbonate minerals can be useful in interpreting time of travel, distance between recharge and discharge points, and aquifer transmissivity (diffuse versus conduit flow). Theoretically, as undersaturated water moves toward a discharge point, more and more carbonate rock is dissolved until saturation occurs. In Texas, Abbott (1977) calculated the saturation indices of calcite (SIC) and dolomite (SID) for a one-time sampling of nine wells and five springs in the Edwards aquifer and concluded that the waters were generally undersaturated. For the spring waters, this is demonstrated by the lack of travertine deposits downstream from the outlets. He recommended that a detailed spatial and time-series analysis of saturation data was needed to make better conclusions about flow

conditions in the Edwards aquifer. The input data necessary for calculating saturation indices was published in reports by the Edwards Aquifer Research and Data Center for samples collected between 1981 and 1985 (Ogden et al., 1985a and 1985b). This data was utilized for the present research to test whether the ground water becomes more saturated along its pathway to the springs and the bad water zone, and to answer questions about hydrogeological factors controlling the state of saturation and the development of caverns.

### Location and Hydrogeology of the Study Area

The study area is located along the Balcones Fault Escarpment in Hays and Comal counties, Texas (Figure 1). The Edwards Limestone aquifer is composed of a group of Cretaceous carbonates that have a total thickness of approximately 137 meters in the San Marcos area. The Edwards aquifer is composed of the Comanche Peak Limestone, Edwards Limestone, and Georgetown Limestone. Rose (1972) raised the Edwards Limestone to group status in central Texas and divided it into the Kainer (lower) and Person (upper) members. The Edwards aquifer was later divided into hydrostratigraphic units by Maclay and Small (1983) through a detailed analysis of cores and geophysical logs. Lithologically, the Edwards aquifer consists of rudist limestones; burrowed tidal-flat wackestones; grainstones; dolomite; nodular chert; solution-collapse breccias; and weathered, honeycombed beds.

DeCook (1963) performed the first detailed analysis of the ground water resources of Hays County. The occurrence of ground water within the hydrostratigraphic units of the Edwards aquifer has been described by Maclay and Small (1983). The differing solubilities of the hydrostratigraphic units have had a profound effect on transmissivity and porosity.

Recharge to the aquifer occurs through losing streams located primarily to the west and south of San Marcos and New Braunfels. Surface water moves across the impermeable rocks of the Glen Rose Formation (drainage zone, Figure 1) until the Edwards aquifer is encountered at the Balcones Fault Zone. Most of this water generally moves in an east/northeast direction, where it discharges at the Comal, Hueco, and San Marcos springs. Complex "down-to-basin" faulting causes the Edwards aquifer to lie deeper and deeper below the surface as one moves in a southeast direction. The bad water line represents the eastern edge of the aquifer where poor circulation has caused the water to have a high TDS (>1000 mg/l) and to be non-potable. An analysis of the hydrochemical facies in the bad water zone has been performed by Clement and Sharp (1988).

The effects of the intense faulting on ground water movement in the Edwards aquifer was discussed by Maclay, et al. (1985). Kastning (1977) studied faults and their influence on conduit enlargement throughout the Edwards Plateau as well. He found that faults can have either positive or negative effects on water movement and cavern development. Beck (1968) also noted that faulting has an effect on cave development in Comal County, which lies just 25 kilometers south of San Marcos. A comparison of fault, joint, and photo-lineament orientations around San Marcos was made by Rothermel and Ogden (1989). A broader-scale analysis of photo-lineaments was recently made by Woodruff, et al. (1989). Many of the delineated photo-lineaments concur with mapped faults.

Significant local recharge occurs for the San Marcos Springs and Hueco Springs, but faulting has hydrologically separated local recharge points from Comal Springs (MacLay, et al., 1985; and Ogden, et al., 1986). Comal Springs (Figure 1) is the largest spring group in Texas with a mean historic flow of approximately 8.3 cms. This average has been decreasing in recent years as water-well withdrawals around San Antonio have increased. The springs are located in New Braunfels, Comal County, and issue from four major orifices above the lake surface. These orifices are located along a 372 meter stretch of the Balcones Escarpment. The spring openings are at about 190 meters above sea level. The lake is presently used for recreation and the production of hydroelectric power.

The San Marcos Springs (Figure 1) are the second largest spring group in Texas with an average historic flow of 4.5 cms. They are located in the city of San Marcos in Hays County and are owned and operated as a tourist attraction by Aquarena Springs, Inc. The spring orifices are now under as much as 12 meters of water due to a dam originally created for hydroelectric power. Water from the San Marcos Springs issues from six major orifices along the base of the Balcones Escarpment as well as from numerous smaller openings.

Hueco Springs (Figure 1) are located five kilometers north of New Braunfels and are composed of two major orifices in limestone covered by Quaternary alluvium 90 meters west of the Guadalupe River. The altitude of the springs' orifices are 200 meters above sea level. Spring flow is very variable and historically has not been measured as often as the Comal and San Marcos springs. Hueco Springs commonly cease to flow during droughts. The maximum recorded discharge was 3.7 cms in 1968 (Guyton and Assoc., 1979).

Figure 2 shows the location of the ninety wells analyzed for this study. The wells are located in both the confined and unconfined portions of the aquifer with depths ranging from 30 to 125 meters.

#### Methods

Water samples were collected generally twice a month from the Comal, Hueco, and San Marcos springs. Discharge was recorded at the time of sampling. Static water well levels and water samples were collected twice a month from August 1984 through July 1985 at ten domestic wells (Figure 2, numbered wells). Water quality tests were performed during an initial pumping (aquifer) test to determine the optimum time for obtaining a representative sample. Samples from ninety wells were collected, in addition, during a three-week period between February 21, 1985 and March 14, 1985. All samples were collected in one-liter containers from the water faucet closest to the well. Temperature, dissolved oxygen, and pH were measured in the field. Samples were then placed on ice and brought to the laboratory for further analysis. The following methods were utilized to determine the chemical concentrations: (1) barium sulfate method for sulfate (mg/l), (2) EDTA (0.02 N EDTA) titration method for calcium and total hardness (mg/l as  $\text{CaCO}_3$ ), (3) mercuric nitrate (0.0141 N) method for chloride (mg/l), (4) sulfuric acid (0.02N) titration method for alkalinity (mg/l as  $\text{CaCO}_3$ ), (5) cadmium reduction method for nitrate (mg/l), (6) ascorbic acid method for orthophosphate (mg/l), and (7) the magnesium

hardness (mg/l as  $\text{CaCO}_3$ ) was recorded as the difference between the total hardness and calcium hardness. Time series plots of these chemical parameters for the wells and springs have been published by Ogden and Lunsford (1985) and Ogden, et al. (1986).

The USGS WATEQF (Plummer, et al., 1976) program was used to calculate the saturation indices of calcite, dolomite, and gypsum. The input requires measurements for calcium, bicarbonate, pH, temperature, magnesium, and sulfate. Ionic strength was calculated by the Debye-Huckel method using the concentrations of all ions entered into the program.

### Results

Figure 3 shows a comparison of discharge of the San Marcos Springs to calcite, dolomite, and gypsum saturation levels. As discharge increased in 1983, the waters became less saturated. Then, essentially no recharge took place during a nine-month drought period in 1984. As a result, the waters became supersaturated with respect to calcite and dolomite, but gypsum saturation levels remained relatively constant. This suggests that significant amounts of local recharge must occur from the nearby Blanco River and Sinking Creek during wet times, but during the drought only old water which had moved great distances in the aquifer emerged from the springs. Also during drought conditions, the ground water moves much slower, allowing more time for dissolution to take place. This was demonstrated by two dye traces to the San Marcos Springs during different water table conditions. On April 1, 1983, a successful dye trace was performed from Ezell's Cave to the San Marcos Springs (Figure 4) during average flow conditions (3.9 cms). In eleven days the dye traveled about three kilometers to emerge at the springs, thus yielding a flow rate of about 300 m/day. On August 30, 1984, dye was placed in Rattlesnake Cave, about two kilometers from the San Marcos Springs, during low flow conditions (1.7 cms). In forty days the dye emerged from the springs yielding a flow rate of only 38 m/day. In April 1983, the water emerging from the springs was undersaturated with respect to calcite, whereas it was supersaturated during August 1984.

One factor that might cause undersaturated conditions during normal flow periods is the precipitation of calcite before reaching the springs. Water table fluctuations associated with mixing of ground waters with different  $\text{PCO}_2$  levels could cause calcite precipitation and new aggressiveness of the water (Bogli, 1964). This possibility is suggested by calcite-filled vugs seen in cores taken about three kilometers upgradient of the springs.

Gypsum saturation levels were unaffected by the reduced volume of water during the drought. The low levels of gypsum saturation and its uniformity through time suggest that gypsum beds within the aquifer have long since been removed by dissolution.

Hueco Springs is much smaller than San Marcos Springs and receives local recharge as demonstrated by turbidity after storms and a successful dye trace from a nearby sinking stream. Despite local recharge points, the spring water remained near saturation with respect to calcite and showed little variation (Figure 5). Only after a large storm event in May 1983,

did calcite saturation show a marked decrease. In contrast, dolomite saturation showed large variability corresponding to storm events. In general, saturation decreased during storms as a result of faster ground water velocities and the correspondingly reduced contact time with the rock. This effect is less pronounced for calcite, possibly due to its greater solubility. Higher gypsum saturation levels were found at Hueco Springs compared to Comal and the San Marcos Springs. This may be due to leakage across the Hueco Springs Fault from gypsum-rich beds in the Glen Rose Formation. This possibility, based on flow rates, has been speculated upon by Maclay and Small (1983).

The water issuing from Comal Springs also remained generally undersaturated with respect to calcite and dolomite during the 1983 study period (Figure 6). The water was more saturated than at Hueco Springs due to much greater transport distances and lack of nearby recharge points. Comal Springs does not become turbid even after very large storm events. Since the water emerging from Comal Springs is very old, as shown by low tritium measurements (Ogden, et al., 1986), it was anticipated that the waters would be supersaturated. Lack of saturation may be related to precipitation of calcite before the water emerges, or the influx of an unknown source of local, unsaturated recharge.

Figure 7 shows the distribution of calculated SIC, SID, and SIG values for ninety wells. There is a marked lack of uniformity of the data and no apparent evolutionary trend between the recharge zone and the bad water line. The intersecting "valley and ridge" topography of the plots are thought to reflect zones of high and low transmissivity corresponding to solutionally enlarged faults and fractures separating blocks of less fractured rock. Due to faster ground water flow along such open fractures, water would be expected to be more undersaturated than slower moving water in the unfractured rock. Some lineations of highly undersaturated waters (troughs) correlate with known faults and photo-lineaments. Higher saturation values of SID and SIG seen in the west/northwest portion of the study area may suggest leakage across faults which have juxtaposed gypsum-rich members of the Glen Rose Formation with higher quality water in the Edwards aquifer.

Three wells were chosen for time-series analysis of the saturation data (Figure 8). During the study period, water levels changed less than three meters, with most change occurring after mid-May of 1985. Water levels in the wells surprisingly did not increase with the significant increase in discharge of the San Marcos Springs that began in October 1985. The Longley well is located in the recharge zone while the Klaerner well is located in the bad water zone. The Keck well is located in the recharge zone, but is close to the artesian zone. Nearly similar levels of saturation are seen despite the different distances from the bad water zone. The water is slightly more saturated with regard to gypsum in the bad water zone. The Keck well may be less saturated with respect to calcite and dolomite than the Longley well because the former is located on a fault and also intersects a cave. The Keck well is also the most shallow, with the depth to water being only twelve meters. Several large sinkholes next to the well likely provide rapid recharge during precipitation events.

Generally, the level of ground water saturation is affected by recharge events more in the recharge zone where no confining layers exist to impede rapid recharge. Depth to the water table and a well's proximity to a discrete recharge point, such as a sinkhole, affect the amount of saturation change in response to recharge events. All of the well waters went from supersaturated to undersaturated with respect to calcite and dolomite with the onset of rains in July 1984. Over 12.7 centimeters of rain fell in October 1984, and the impact is seen in both the Keck and Klaener well waters. Once undersaturated conditions returned, subsequent storm events had much less impact.

### Conclusions

Since the ground water in the Edwards aquifer is usually undersaturated with respect to calcite and dolomite, dissolution is an active process causing enlargement of fractures and the growth of caves. Pumping test data (Ogden, et al., 1986) and well logs show that the highest transmissivity values and the most caves (intersected by wells) occur just inside the confined-unconfined boundary of the aquifer, probably due to "mixing corrosion" (Bogli, 1964). High transmissivity and sulfur values just within the bad water zone suggest that some caves are forming due to "sulfuric-acid" corrosion, similar to the theory for the origin of Carlsbad Caverns in New Mexico (Egemeier, 1987). Sulfur reducing bacteria feed on hydrocarbons found in the bad water zone and are responsible for the production of hydrogen sulfide gas. This phenomena produces aggressive water within a transition zone between the artesian and bad water zones. The process appears to cease deeper within the bad water zone since transmissivity values rapidly decrease downdip. Unfortunately, few wells occur east of the bad water line, so it is difficult to determine saturation conditions within this ground water zone.

Gypsum saturation values are particularly low except in the west/northwest portion of the study area where leakage across faults from gypsum beds in the Glen Rose Formation is believed to occur. This could also be affecting gypsum saturation levels at Hueco Springs. No evolutionary trend in saturation of well waters occurs between the recharge zone and the bad water line, as anticipated. Instead, less saturated waters generally occur along faults and fractures where the ground water moves faster, is affected more greatly by recharge events, and where there is less water/wall rock contact due to the large cavities. Finally, mixing of local recharge waters of different  $\text{PCO}_2$  concentrations and precipitation of calcite before reaching the springs are believed to contribute to the undersaturated conditions.

### References

- Abbott, P.L., 1977, On the state of saturation of ground water with respect to dissolved carbonates, Edwards artesian aquifer, south-central Texas, Texas Jour. of Sci., 29(3), 17-24.
- Beck, B.F., 1968, Speleogenesis in Comal County, Texas, Unpublished M.A. thesis, Rice Univ., 67 pp.

- Bogli, A., 1964, Mischungskorrosion - ein Beitrag zur Verkarstungs problem, Erd Kunde, 18, 83-92.
- Clement, T.J., and J.M. Sharp, Jr., 1988, Hydrochemical facies in the Bad Water Zone of the Edwards Aquifer, central Texas, Proc. Natl. Water Well Assoc. Ground Water Chemistry Conf., Dublin, Ohio, pp. 127-149.
- DeCook, K.J., 1963, Geology and ground-water resources of Hays County, Texas, U.S. Geological Survey Water-Supply Paper 1612, 72 pp.
- Egemeier, S.J., 1987, A theory for the origin at Carlsbad Caverns, Bull. Natl. Speleol. Soc., 49(2), 73-76.
- Guyton, W.F., and Associates, 1979, Geohydrology of Comal, San Marcos, and Hueco Springs, Texas Dept. of Water Resources, Rept. 234, 85 pp.
- Hess, J.W., 1974, Hydrochemical investigation of the Central Kentucky karst aquifer system, Office of the Water Research and Technology, NTIS publ. PB -238, 218 pp.
- Jacobson, R.L., and D.D. Langmuir, 1970, The chemical history of some spring waters in carbonate rocks, Groundwater, 8, 5-9.
- Kastning, E.H., 1977, Faults as positive and negative influences on groundwater flow and conduit enlargement, in Dilamarter, R.R., and Csallany, S.C. (editors), "Hydrologic Problems in Karst Regions": Western Kentucky Univ., Bowling Green, Kentucky, pp. 193-201.
- MacLay, R.W., and T.A. Small, 1983, Hydrostratigraphic subdivisions and fault barriers of the Edwards aquifer, south-central Texas, U.S.A., Jour. of Hydrology, 61, 127-146.
- MacLay, R.W., L.F. Land, and D.G. Woodward, 1985, Influence of barrier faults on ground water flow in the Edwards Aquifer, San Antonio region, Texas, Proc. of the Natl. Water Well Assoc., Southern Regional Ground Water Conf., Dublin, Ohio, pp. 1-13.
- Ogden, A.E., A.J. Spinelli, and J. Whordon, 1985a, Hydrologic and hydrochemical data for the Edwards Aquifer in Hays and Comal counties, 1981-1983, Edwards Aquifer Research and Data Report, San Marcos, TX, 83 pp.
- \_\_\_\_\_, 1985b, Hydrologic and hydrochemical data for the Edwards Aquifer in Hays and Comal counties, 1983 to 1985, Edwards Aquifer Research and Data Center Report, San Marcos, TX, 101 pp.
- Ogden, A.E., and D. Lunsford, 1985, Hydrochemistry as a means of defining flow regimes within a fractured limestone aquifer, Proc. of the Natl. Water Well Assoc., Southern Regional Ground Water Conf., Dublin, Ohio, pp. 33-49.
- Ogden, A.E., R.A. Quick, S.R. Rothermel, and D. Lunsford, 1986, Hydrogeological and hydrochemical investigation of San Marcos Springs, Contract Report to the U.S. Fish and Wildlife Service, Office of Endangered Species, Santa Fe, NM, 367 pp., 6 plates.

- Ogden, A.E., R.A. Quick, and S.R. Rothermel, 1986, Hydrochemistry of the Comal, Hueco, and San Marcos springs, Edwards Aquifer, Texas, in "The Balcones Escarpment - Geology, hydrology, ecology and social development in central Texas," L. Abbott and C.M. Woodruff, editors, GSA Field Trip Guidebook, Denver, CO, pp. 115-129.
- Ogden, A.E., 1988, Distinguishing flow regimes of springs in carbonate rock terranes, Proc. Natl. Water Well Assoc. Ground Water Chemistry Conf., Dublin, Ohio, pp. 53-73.
- Plummer, L.N., B.F. Jones, and A.H. Truesdall, 1976, WATEQF - a FORTRAN IV version of WATEQ, a computer program for calculating chemical equilibrium of natural waters, U.S. Geol. Survey, Water Res. Invest. 76-13, 61 pp.
- Rose, P.R., 1972, Edwards Group, surface and subsurface, central Texas, University of Texas, Bureau of Economic Geology, Report of Invest., No. 74, 198 pp.
- Rothermel, S.R. and A.E. Ogden, 1989, Investigation of ground water flow patterns from comparison of fault, joint, and photo-lineament trends in the Edwards Limestone, Texas, USA, Proc. 2nd Canadian/American Conf. on Ground Water Flow in Fractured Rock, Banff, Canada, (in press).
- Shuster, E.T., and W.B. White, 1972, Source areas and climatic effects in carbonate ground waters determined by saturation indices and carbon dioxide pressures, Water Res. Research, 8(4), 1067-1073.
- Smith, A.R., 1965, Caves and the Balcones Fault Zone, Texas Caver, 10, 158-160.
- Thrailkill, J.W., 1977, Relative solubilities of limestone and dolomite, in "Karst Hydrogeology," Univ. of Alabama, Huntsville Press, pp. 491-500.
- Woodruff, C.M., Jr., L.D. LaGarza, F.R. Snyder, and A.E. Ogden, 1989, Lineaments and the Edwards Aquifer--Barton Springs Segment, Travis and Hays counties, Texas, Edwards Aquifer Research and Data Rept., San Marcos, TX, R1-88, 50 pp.



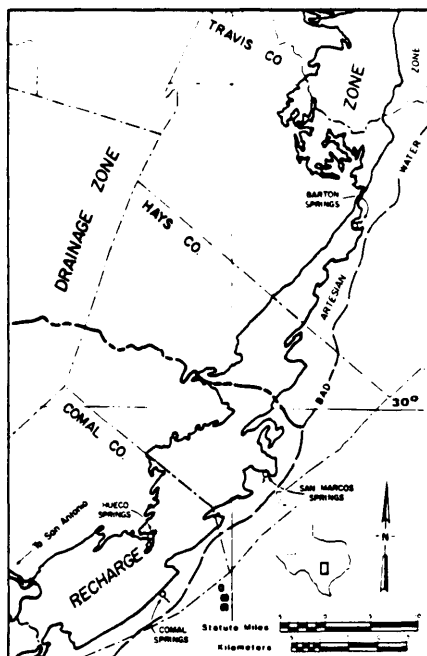


Figure 1. Location of the Study Area.

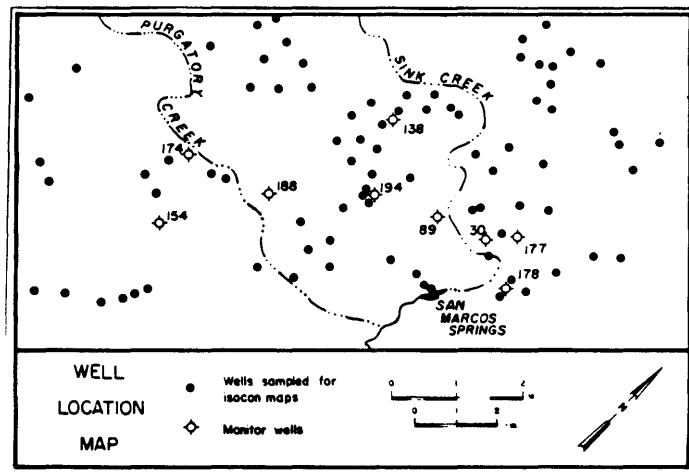


Figure 2. Location of 90 Sampled Wells.

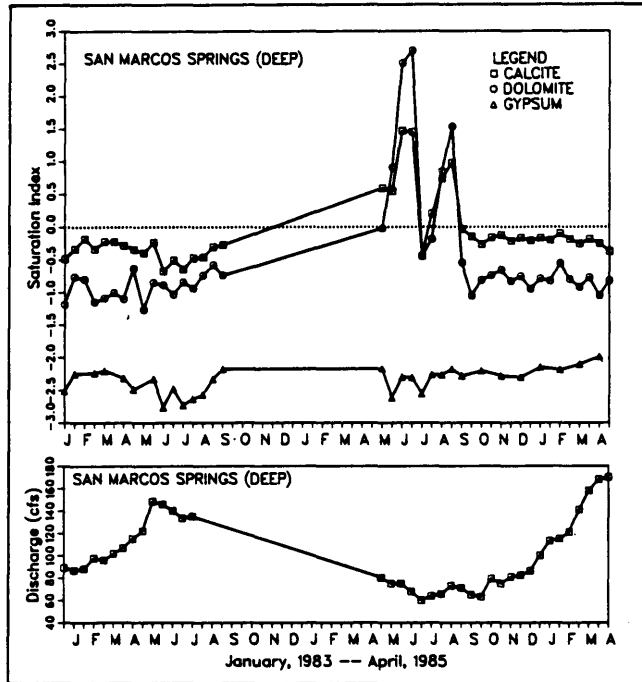


Figure 3. SIC, SID, SIG, and Discharge versus Time for the San Marcos Springs.

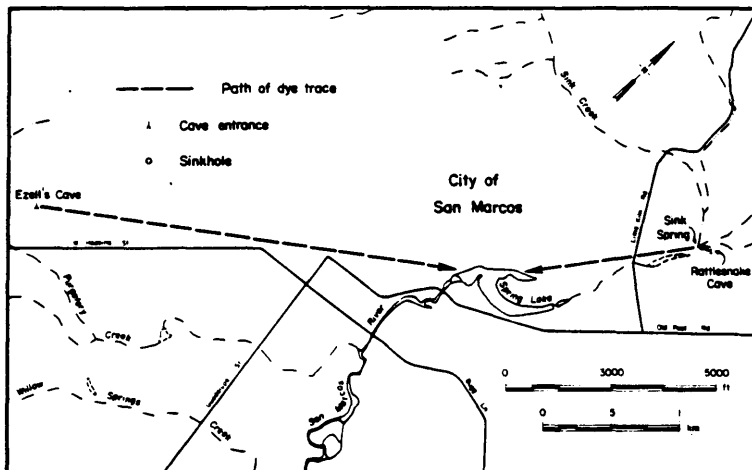


Figure 4. Dye Trace Results to the San Marcos Springs.

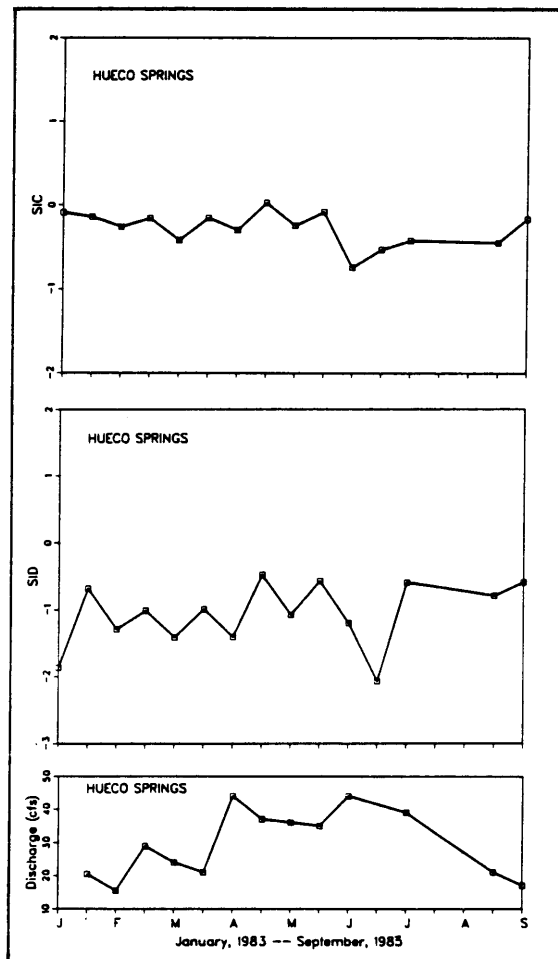


Figure 5. SIC, SID, and Discharge versus Time for Hueco Springs.

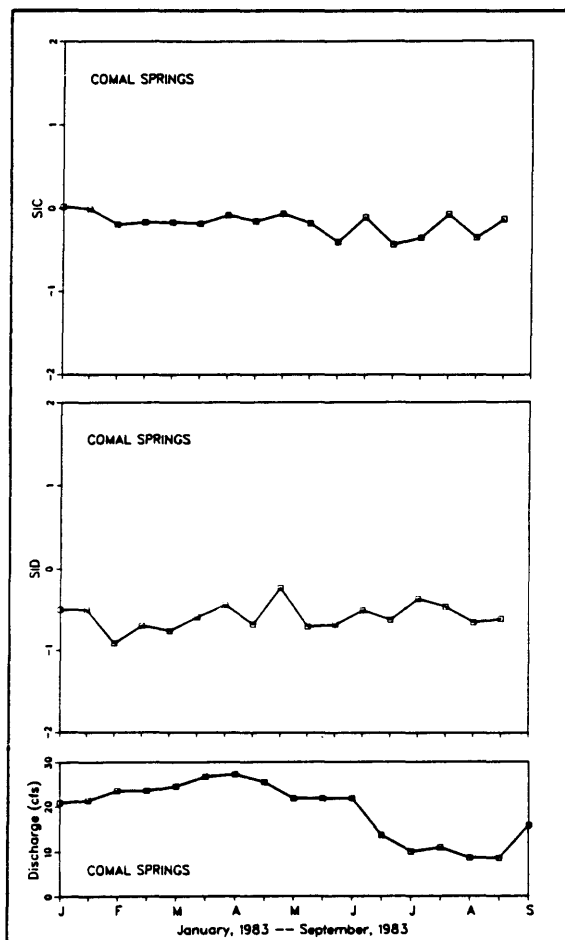


Figure 6. SIC, SID, and Discharge versus Time for One Outlet of Comal Springs.

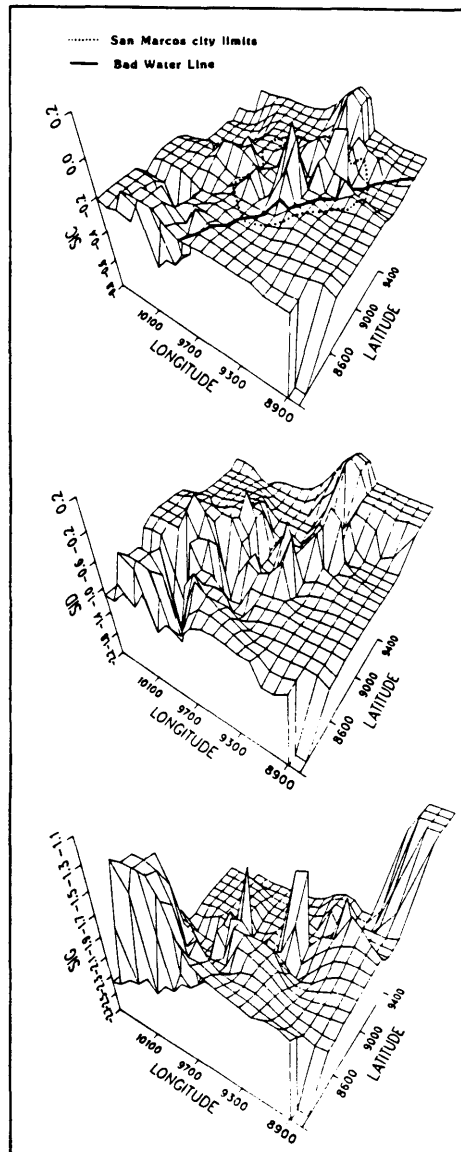


Figure 7. Distribution of SIC, SID, and SIG Values Calculated for 90 Well Sites Around San Marcos.

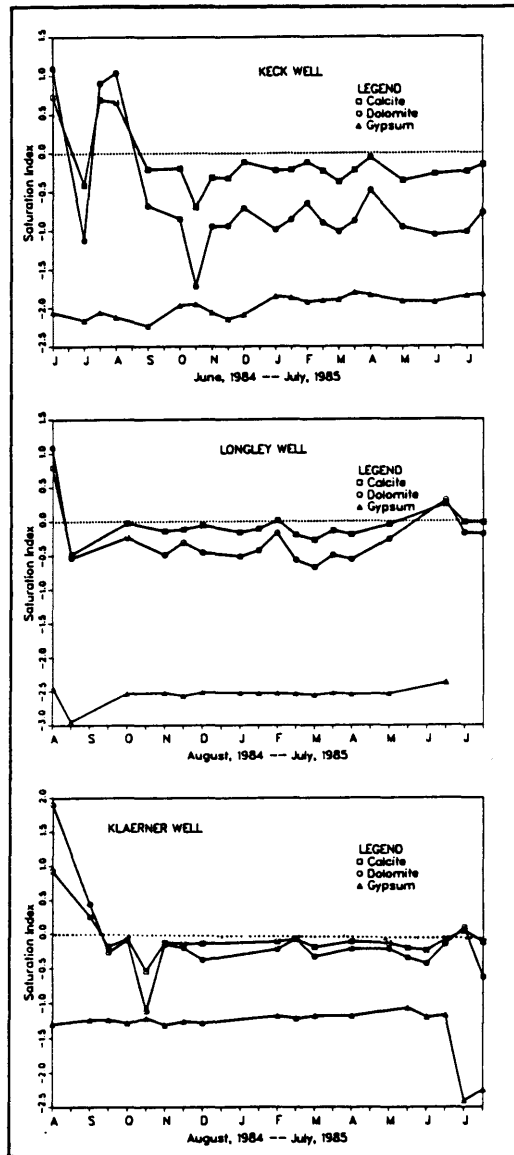


Figure 8. SIC, SID, and SIG versus Time for Three Wells Around San Marcos.

# DOLOMITE DISSOLUTION RATES AND POSSIBLE HOLOCENE DEDOLOMITIZATION OF WATER-BEARING UNITS IN THE EDWARDS AQUIFER, SOUTH-CENTRAL TEXAS--A SUMMARY

Ruth G. Deike

U.S. Geological Survey, 432 National Center, Reston, VA 22092 (U.S.A.)

## ABSTRACT

Rapid development of this major carbonate aquifer suggested by geomorphologic evidence is supported by dolomite dissolution rates. Cavernous porosity development and dolomite dissolution were synchronous because of the volume difference between calcite gained and dolomite lost during groundwater reactions. The dolomite dissolved during a period of mixing zone dedolomitization that resulted from hydrologic readjustments following low Pleistocene sea levels. Rates are based on a reaction time of 10,000 years and were determined for both observed mineral changes and for reconstructed pore fluid changes during aquifer formation. Results of the study have important applications to mixed groundwater solutions created by modern liquid waste disposal techniques.

## Introduction

A large quantity of fresh water moves annually through carbonate rock of the Edwards aquifer in south-central Texas (Maclay and Small, 1976; Maclay and Land, 1988). There is ample evidence to suggest that a geochemical reaction, referred to as dedolomitization, resulted in the cavernous porosity that allows for this water flow. This study describes that evidence and presents an argument that the cavernous porosity developed rapidly.

The aquifer is located in south-central Texas, where it extends for 320 km along the southern margin of the Edwards Plateau (Fig. 1). It is mostly contained in the Edwards Group (Rose, 1972) of rocks (Fig. 2) after which it is named. The Edwards Group is an uppermost-lower Cretaceous (Albian) backreef assemblage that includes: 1) secondarily dolomitized and hence very permeable units that ultimately became the aquifer units, and 2) locally massive gypsum, the upgradient dissolution of which was critical to later dedolomitization reactions.

During the Miocene, in response to the subsiding Gulf of Mexico, the Edwards and overlying rocks were deformed. The Edwards Plateau remained stable forcing the development of a structural hinge along its southern (gulfward) margin. The hinge consists of a band of en echelon faults that ultimately developed a cumulative relief in the subsurface of several hundred meters across an area now known as the Balcones Fault Zone.

In the fault zone, two roughly parallel, but distinctly different hydrologic systems evolved (Mench et al., 1980; Ellis, 1985). The main fresh-water system is immediately adjacent to the plateau in a zone that varies from 8 to 65 km wide and is 60 to 210 m beneath land surface. Over 692 km<sup>3</sup>/yr of dilute calcium bicarbonate water flows rapidly through the fault blocks in horizontal cavernous conduits that are vertically connected along fault planes. Bordering the fresh-water system to the south is a saline-water system that is generally hydraulically unconnected with it. The saline system is contained in fault blocks that are deeper beneath land surface effectively isolating aquifer units from fresh-water recharge. Pore fluids in the saline system are brines with total dissolved solids as high as 10,000 mg/L, a negative redox potential, and that often includes H<sub>2</sub>S (Pearson et al., 1975; Pearson and Rettman, 1976). Clement and Sharp (1988) find that major cations and anions vary along strike, but particularly to the west are dominated by Ca and SO<sub>4</sub>. Toward the central and eastern parts

of the Balcones Fault Zone these are accompanied with variable Mg, Na and Cl. The fresh-water and saline-water systems are separated by the bad water line (Fig. 1), an isochemical contour at 1,500 mg/L total dissolved solids.

Dedolomitization reactions, concentrated north of the bad water line, occurred whenever saline brines discharging from dolomitic units allowed ingress of oxidizing meteoric water. This apparently happened most recently near the Pleistocene/Holocene boundary. The discharge occurred when the early aquifer units were exposed by erosion along major river valleys that cut deeply across the fault zone in response to low Pleistocene sea levels (Woodruff and Abbott, 1979). Meteoric water originating on the plateau gained access to permeable dolomitic units along fault planes that parallel the escarpment. The fresh water mixed with the resident calcium-sulfate brine; and in equilibrating with the rock, the mixed solution dissolved dolomite and associated minerals, creating cavernous porosity that resulted in the confined fresh-water flow system (Abbott, 1975; Maclay and Small, 1976, 1984; and Ellis, 1985). Water in the modern system is meteoric, and it flows eastward under artesian head to discharge at major springs and along river valleys in and east of San Antonio, Texas. Tritium analyses (Pearson and Rettman, 1976) show that residence times are roughly from 20 to 100 years.

The mineralogic effects of dedolomitization can be studied where the fresh-water aquifer units are close to stratigraphically equivalent unaltered units in the saline system south of the bad water line (Deike, 1984, and in press (a)). Rock in the fresh-water units is composed of calcite, and there is clear petrographic and isotopic evidence for reactions involving meteoric water that resulted in dedolomite, or dolomite replacement by calcite (Abbott, 1975; Longman and Mench, 1978; Deike, 1984; Ellis, 1985). By contrast, rock in the saline zone is roughly 50 weight percent dolomite and the remainder mostly calcite, with accessory celestite ( $\text{SrSO}_4$ ), gypsum, pyrite, organic matter, quartz, and kaolinite. The dolomite is generally sucrosic with well-formed, medium-fine rhombs and up to 28% intergranular porosity. Stable carbon isotope ratios of both calcite and dolomite indicate no reaction with dilute meteoric water (Mench et al., 1980; Deike, 1984).

The details of the dedolomitization reaction have been discussed by Abbott, 1975, and Deike, in press (b).

#### Quantitative Dissolution of Dolomite and Porosity Development

The relationship between dolomite mass loss and porosity development requires a quantitative comparison of the mineral composition of representative equal volumes of rock from the modern fresh-water aquifer and from the nearby saline aquifer.

Continuous core, along with geophysical logging and sedimentary data from two uniquely positioned wells located in the eastern portion of the Balcones Fault Zone (Fig. 1), provide the necessary samples and information to construct a detailed stratigraphic correlation (Fig. 2) (Deike, 1984, and in press (a)) across the fault zone from altered to unaltered rock. These wells are the Selma well, drilled by the U.S. Army Corps of Engineers, and the Randolph well, drilled by the USGS Water Resources Division, in cooperation with the San Antonio Water Board. The method of defining a representative aquifer volume and of obtaining dolomite mass loss (Deike, in press (b)) is based on the thickness of individual aquifer units, along with analyses of samples from each unit. These analyses include average x-ray diffraction mineralogy, grain density, and porosity. The results (Tables 1 and 2) show that after dedolomitization an average volume of pre-aquifer, or precursor rock, has retained its original mass of calcite and gained an additional calcite mass, has lost all but a tiny amount of its original dolomite,



and has lost all original non-carbonate minerals except quartz. By expressing these changes as volume fractions (Table 2), we can see that the average porosity has increased from 20 to 44% and, more importantly, that the volume of unreplaced dolomite lost during the reaction can account for 75% of this porosity increase. The rest of the porosity increase is due to loss of non-carbonate minerals, primarily celestite, gypsum, and pyrite.

**TABLE 1**

Mineral mass,  $M_j$ , and differences between Randolph and Selma cores per representative 100 cm<sup>3</sup> unit of rock plus pore space. n.d. means not determined. (From Deike, 1984).

|              | Randolph core |       | Selma core |       | Differences in |        |
|--------------|---------------|-------|------------|-------|----------------|--------|
|              | grams         | moles | grams      | moles | grams          | mole   |
| Calcite      | 75            | 0.75  | 138        | 1.38  | + 63           | +0.63  |
| Dolomite     | 123           | 0.67  | 2.7        | 0.002 | -120           | - 0.67 |
| Noncarbonate | 22            | n.d.  | 12.6       | n.d.  | - 9            | n.d.   |

**TABLE 2**

Volume fractions of minerals and pore space and differences between Randolph and Selma cores per 100 cm<sup>3</sup> unit of rock plus pore space, in cm<sup>3</sup> (modified from Deike, 1984).

|               | Volume Fractions |        | Difference per 100 cm <sup>3</sup><br>(cm <sup>3</sup> ) |
|---------------|------------------|--------|--|
|               | Randolph         | Selma  |  |
| Pore space    | 0.20             | 0.44   | +24  |
| Calcite       | 0.27             | 0.51   | +24  |
| Dolomite      | 0.43             | > 0.01 | ≈ -43  |
| Non-carbonate | 0.10             | 0.05   | - 5  |

#### Rate of Dolomite Mass Loss and Porosity Development

From mineral mass changes we can calculate an average dolomite dissolution rate during development of the fresh-water aquifer. This "paleo-rate" can be compared to modern dolomite reaction rates observed in other carbonate aquifers along flow paths where dedolomitization is the controlling reaction. This is probably the first time rates determined from observed mineral changes in a field area have been compared to rates determined from down flow changes in aquifer chemistry.

## Derivation of rate function

There are several assumptions implicit in the derivation of a rate function (John D. Bredehoeft, U.S. Geological Survey, personal communication, 1988) that describes the synchronous dissolution of dolomite and increase in porosity. The derivation may be found in Deike (in press (b)), but it will be useful to summarize the assumptions here. First, we must account for the opposing effects on porosity created by the dissolution of non-carbonate minerals and by the precipitation of calcite. We can do this by expressing the rate of change of porosity in terms of the rate of change of a volume of dolomite modified to account for calcite and non-carbonate mineral volume changes. The assumption here is that all the mineral changes are going on more or less at the same time and in the same place. Petrographic evidence (Deike, 1984) supports this assumption, and in addition, suggests that the reactions were rapid.

The rate function must account for water movement, since the dissolution of dolomite is a response to changing pore fluid composition as resident brine mixes with dilute recharge water. The dilute recharge is carried to the reaction site by a rate that is equivalent to the discharge of fluid through the reaction volume. Dolomite mass loss can be related to the discharge by assuming, 1) the conservation of  $\text{MgCO}_3$  between solid and liquid portions of the rock volume, and 2) assuming that over time the amount of  $\text{MgCO}_3$  leaving the rock volume is proportional to discharge. The first assumption is valid because recharge waters are low in  $\text{Mg}^{2+}$ , hence the major source of  $\text{Mg}^{2+}$  is the reacting dolomite. The second assumption is justified since the reaction (and loss of  $\text{Mg}^{2+}$ ) would stop quickly without a replenishment of the dilute pore fluids creating the mixing zone.

With these assumptions, we can define the dolomite reaction rate as the mass dissolved per unit volume water per unit time  $\tau$ , or,

$$\bar{R} = \frac{\Delta m_{\text{MgCO}_3}}{\Delta t \bar{Q}\tau}, \quad (1)$$

where

$\bar{R}$  = average value of the reaction rate during time  $\Delta t$ ,

$\Delta m_{\text{MgCO}_3}$  = change in mass of  $\text{MgCO}_3$  within the rock volume during time  $\Delta t$ ,

$\Delta t$  = total time for the reaction, and

$\bar{Q}\tau$  = the average volume of water which passed through a volume of rock in unit time,  $\tau$ .

The rate obtained will be a "paleo-rate" consisting of the average estimated value during some time period,  $\Delta t$ , in the history of the Edwards aquifer. We can express the average reaction rate,  $R$ , in units, millimoles dolomite per kilogram water per year, in order to compare the results with dolomite reaction rates determined from the solution phase in other carbonate aquifers (Plummer, 1977; Plummer and Back, 1980; Plummer et al., in press; and Busby et al., in press) and a paleo-rate reconstructed from the modern Edwards aquifer system (this study). Because chemical analyses are reported on a per kilogram basis, we will consider a volume of Edwards aquifer rock before alteration (based on data from the Randolph well core) that contains 1 kilogram, or 1000  $\text{cm}^3$  of pore space filled with water. From Table 2, the total volume of this rock will be 5000  $\text{cm}^3$  (4000  $\text{cm}^3$  rock plus 1000  $\text{cm}^3$  pore space) and from Table 1, the total mass of dolomite to be removed,  $\Delta m_{\text{MgCO}_3}$ , will be 33,500 mmol (6.70 mmol  $\text{cm}^{-3}$  x 5000  $\text{cm}^3$ ). For  $\Delta t$  we will use the total reaction time of 10,000 years based on geomorphologic

evidence for initiation of the mixing zone. For  $Q$ , we must calculate an average discharge during aquifer formation as discussed below.

#### Estimated average annual discharge during aquifer formation

An average annual mass discharge,  $\bar{Q}$  can be approximated from estimates of the initial, or preaquifer formation discharge,  $Q_0$ ; the final, or postaquifer formation, (modern) discharge,  $Q_N$ ; and a growth function describing the change in discharge over time (Jurate M. Landwehr, U.S. Geological Survey, personal communication, 1988). Discharge through the main aquifer today is three orders of magnitude greater than through rock south of the bad water line (Maclay and Land, 1988). The rate of increase during the period of aquifer formation probably was not linear (Howard and Howard, 1967), but started slowly and gradually increased. If we assume an exponential (log-linear) growth from an initial discharge,  $Q_0$  at time 0, to a final rate  $Q_N$ , at the present time,  $N$  years later, the instantaneous discharge  $Q_t$  at time  $t$ , can be expressed as:

$$Q_t = Q_0 \left[ \frac{Q_N}{Q_0} \right]^{t/N} \quad (2)$$

In order to estimate the total mass of water that has flowed through the aquifer in  $\Delta t = N$  years, eq. 2 must be integrated from 0 to  $N$  years. The average annual mass discharge,  $\bar{Q}$ , can then be estimated as

$$\bar{Q} = \frac{Q_0}{N} \int_0^N \left[ \frac{Q_N}{Q_0} \right]^{t/N} dt, \quad (3)$$

which simplifies to

$$\bar{Q} = \frac{Q_N - Q_0}{\ln (Q_N/Q_0)} \quad (4)$$

Note that  $\bar{Q}$  can be estimated without a specific value for  $\Delta t = N$ , the total time of reaction. Only estimates of the initial and final discharge are needed.

The mass discharge at any point in an aquifer's evolution can be determined by substituting appropriate values for parameters in the Darcy relationship expressed as follows:

$$Q = \rho \frac{T}{b \hat{\epsilon}} \frac{dh}{dl} \epsilon A \quad (5)$$

where,

- $Q$  = water mass per unit time through reference volume
- $\rho$  = density of water
- $T$  = transmissivity (representative of the aquifer as a whole)
- $b$  = saturated thickness
- $\hat{\epsilon}$  = effective porosity of the whole aquifer
- $\frac{dh}{dl}$  = hydraulic gradient
- $\epsilon$  = porosity of reference volume
- $A$  = cross-section of reference volume.

$Q_0$  is defined as  $Q$  for the pre-mixing zone aquifer, and can be calculated from rock properties and hydraulic characteristics of the Edwards Group south of the bad water line (Deike, in press(b)). Likewise,  $Q_N$  is the mass discharge after completion of the process, and it may be calculated from parameters observed in the modern fresh-water aquifer. Initial and final discharge through a reference volume, along with values for all of the parameters required for the calculation, are listed in Table 3. The derivation of these values may be found in Deike (in press (b)). An average mass discharge during formation of the Edwards aquifer, assuming a reference volume of 5000 cm<sup>3</sup>, is  $1.9 \times 10^4$  kg/yr.

**TABLE 3**

Initial discharge,  $Q_0$  (beginning of dolomite dissolution) and final discharge,  $Q_N$  (dolomite gone) calculated using eq. 4, along with values for the hydraulic parameters. Initial parameters are from the Randolph well and surrounding area; final parameters are from the Selma well and Area P (Fig. 1). (Modified from Deike (in press (b)))

|  | Initial                  | Final                               |
|--|--------------------------|-------------------------------------|
| Transmissivity (Maclay and Land, 1988)                       | 20 m <sup>2</sup> /d     | $1.3 \times 10^5$ m <sup>2</sup> /d |
| Hydraulic conductivity                                       | $1.7 \times 10^{-1}$ m/d | $1.3 \times 10^3$ m/d               |
| Hydraulic gradient   | $4.9 \times 10^{-4}$     | $3.2 \times 10^{-4}$                |
| Effective porosity   | 1%                       | 3.1%                                |
| Velocity   |                          |                                     |
| Calculated from estimated early aquifer hydraulic parameters | 308 cm/yr                |                                     |
| Calculated from Area P parameters                            |                          | $4.9 \times 10^5$ cm/yr             |
| Mass Discharge per 5000 cm <sup>3</sup>                      |                          |                                     |
| Calculated from estimated early aquifer hydraulic parameters | 90.2 kg/yr               |                                     |
| Calculated from Area P parameters                            |                          | $1.43 \times 10^5$ kg/yr            |

#### The average dolomite reaction rate, $\bar{R}$

We can now solve for an average dolomite reaction rate,  $\bar{R}$ , from the relationship in eq. 1. If we accept from geomorphic evidence that  $\Delta t$  is 10,000 years, and let  $\tau$ , the unit of time of interest be 1 year, then,

$$\bar{R} = \frac{\Delta \text{mass}}{\Delta t \bar{Q} \tau} = \frac{33,500 \text{ mmol dolomite}}{(10^4 \text{ yr})(1.9 \times 10^4 \text{ kg yr}^{-1})(\text{yr})} = \boxed{1.76 \times 10^{-4} \text{ mmol dolomite per kg per year}}$$

The comparison of this dolomite reaction rate,  $\bar{R}$ , to other rates is constrained by the assumptions made during its derivation:

- (1) The controlling geochemical reaction is dedolomitization where sulfate reduction is minor, and calcium for sodium ion exchange is not significant.
- (2) The rate is an average over the duration of the reaction.
- (3) The reaction is assumed to have lasted 10,000 years.
- (4) The hydraulic parameters of the early aquifer are similar to those in the vicinity of the Randolph well.
- (5) The paleoflow path extends from Uvalde to New Braunfels.
- (6) The rate of increasing mass discharge can be described as log-linear.

#### Rate of Dolomite Dissolution from Chemical Composition of Aquifer Waters in the Mixing Zone

During formation of the Edwards aquifer, two solutions, recharge water and saline water, mixed and reacted with bedrock to produce a final solution. The rate of dolomite dissolution during this process can be approximated from the net dolomite mass transferred to the final solution (mass transfer) along with  $\Delta t$  at the end of the reaction (Plummer et al., 1983). Mass transfer of dolomite was equivalent to the net increase in  $\text{Mg}^{2+}$  in the final solution because dolomite was the sole source of  $\text{Mg}^{2+}$ . This calculation utilizes the computer program BALANCE (Parkhurst et al., 1982) and complete chemical analyses (Pearson and Rettman, 1976) of recharge water from streams and springs draining the plateau; saline water taken from south of the bad water line; and for the final solution, a transition water found locally along the border between the fresh and saline groundwater systems. For this study we will assume that the composition of the final solution is approximated by these transition waters. Location of the sampling sites, the analyses, and a complete discussion of the application of BALANCE may be found in Deike (in press, (b)).

#### **Dissolution rate from mass transfer of dolomite**

The dolomite reaction rate in the Edwards must be determined from some estimate of the total time,  $\Delta t$ , required for the mixture of two initial solutions to transfer the necessary mass in order to obtain the composition of the final solution. In the absence of a groundwater flow path along which to simultaneously monitor changes in pore fluid composition and time of travel, the total reaction time will be approximated from the hypothesized initiation of the mixing zone 10,000 years ago. The arithmetic mean mass transfer of dolomite into solution is 0.56 mmol per kilogram  $\text{H}_2\text{O}$  (Deike, in press (b)), hence the rate of dolomite dissolution would be  $0.56 \times 10^{-4} \text{ mmol per kg}_{\text{H}_2\text{O}}^{-1} \text{yr}^{-1}$ .

#### Dolomite Reaction Rates from Other Carbonate Aquifers

The dolomite reaction rates hypothesized during formation of the Edwards aquifer can be compared to reaction rates observed in the modern Floridan and Madison aquifer systems. For this comparison, we will use rates calculated along flow paths where dedolomitization is known to be the controlling reaction and total reaction time is based on the  $^{14}\text{C}$  activity of dissolved carbon between wells

along the flow path. These rates are shown in Table 4, along with references to the source of the data.

TABLE 4

Years ( $\Delta t$ ) to dissolve 33,500 mmol dolomite (see text) from 5000 cm<sup>3</sup> Randolph core and corresponding surface area rate ( $R_f$ ) of dolomite dissolution at dolomite reaction rates determined for Edwards, Madison, and Floridan aquifers.  $\Delta t$  is obtained by substitution in eq. 1. The relationship for calculating  $R_f$  is described in Deike (in press (b)).

Modified from Table VI, Deike (in press (b)).

| Aquifer               | R<br>Dolomite reaction rate  | Total years<br>to dissolve<br>33,500 mmol<br>dolomite<br>Randolph Core | R <sub>f</sub><br>Surface area rate of<br>dolomite dissolution |
|-----------------------|--|--|--|
|                       | mmol K <sub>g</sub> H <sub>2</sub> O <sup>-1</sup> yr <sup>-1</sup><br>x10 <sup>-4</sup> |  | mmol cm <sup>-2</sup> sec <sup>-1</sup><br>x10 <sup>-13</sup>  |
| Edwards               |  |  |  |
| Solution composition  | 0.56   | 31,500   | 0.56   |
| Mineral composition   | 1.76   | 10,000   | 1.8  |
| Madison <sup>1</sup>  |  |  |  |
| Flowpath #4           | 1.2  | 14,700   | 1.2  |
| Average               | 1.9  | 9,300  | 1.9  |
| Range                 |  |  |  |
| Lowest                | 0.3  | 58,800   | 0.3  |
| Highest               | 6.6  | 2,700  | 6.6  |
| Floridan <sup>2</sup> |  |  |  |
| Polk City-Fort Meade  | 0.96   | 18,400   | 0.96   |
| Fort Meade-Wauchula   | 0.6  | 29,400   | 0.6  |
| Wauchula-Arcadia      | 4.5  | 3,900  | 4.5  |
| Polk City-Arcadia     | 0.68   | 26,000   | 0.73   |

<sup>1</sup>Busby et al. (in press)

<sup>2</sup>Plummer (1977); Plummer and Back (1980)

### Results and Discussion

Assuming a 10,000 yr elapsed time from geomorphic criteria, the Edwards dolomite dissolution rate calculated from changes in the mineral composition of aquifer rock ( $1.76 \times 10^{-4}$  mmol kg<sub>H<sub>2</sub>O</sub><sup>-1</sup>yr<sup>-1</sup>) is about three times faster than the

rate determined from Edwards aquifer solution chemistry ( $0.56 \times 10^{-4}$  mmol  $\text{kg}_{\text{H}_2\text{O}}^{-1}\text{yr}^{-1}$ ). Both rates, however, fall easily within the range of rates determined from the Floridan and Madison aquifers ( $0.3$  to  $4.5 \times 10^{-4}$  mmol  $\text{kg}_{\text{H}_2\text{O}}^{-1}\text{yr}^{-1}$ ).

A range of reaction times,  $\Delta t$ , to remove dolomite from the Edwards precursor rock can be calculated from all dolomite dissolution rates observed in Madison and Floridan aquifers. The periods of time range from 2,700 to 58,800 years (Table 4) and vary directly with the rate of mass transfer of dolomite to solution. The point to be gleaned from reaction times calculated using a variety of rates is that these time spans include the Pleistocene/Holocene boundary and thus support the concept suggested by Woodruff and Abbott (1979), that the aquifer began to form rapidly at this time.

A dolomite surface area reaction rate,  $R_p$ , expressed as mmoles dolomite  $\text{cm}^{-2}\text{sec}^{-1}$  can be calculated from the above reaction times along with the petrographic fabric of dolomite missing from fresh-water Edwards aquifer rock (Deike, in press (b). These rates, listed in Table 4, are faster than rates ( $10^{-18}$  mmol  $\text{cm}^{-2}\text{sec}^{-1}$ ), measured in the pure laboratory system,  $\text{CaMg}(\text{CO}_3)_2$ - $\text{CO}_2$ - $\text{H}_2\text{O}$  (Busenberg and Plummer, 1982), but slower than rates determined in an alpine stream study ( $10^{-10}$  to  $10^{-11}$  mmol  $\text{cm}^{-2}\text{sec}^{-1}$ ) where cold glacial melt water flows over dolostone (Appelo et al., 1984). Relative differences between Edwards surface area rates and the others can be explained by differences in mineralogy, water temperature, and  $\text{CO}_2$  partial pressure. The Edwards surface area rates of reaction, therefore, also tend to support an hypothesized Holocene reaction time.

Rapid geochemical reaction is indicated as well by evidence for rapid neomorphism of calcite matrix (Deike, 1984; Longman and Mench, 1978) and by hydrologic evidence for rapid development of cavernous conduits through which recharge flowed directly to discharge sites (Abbott, 1975).

### Conclusions

Geomorphologic evidence suggesting a timeframe of  $10^4$  years for significant permeability enhancement in the Edwards Aquifer is supported by dolomite dissolution rates from both the Edwards and other aquifers. This study suggests that the mixing of two ground waters of different composition can, in a carbonate aquifer system, quickly develop cavernous, or conduit permeability. This situation can occur anthropogenically--as, for example, during the disposal of waste water of a different composition than resident water in a carbonate rock body. The factors that affect the reaction time are the mineralogy and permeability of the carbonate rocks, the degree of undersaturation created by the mixture of solutions, and the establishment of discharge points that allow the system to remove the products of dissolution and maintain hydrologic and geochemical conditions for continuing mass transfer.

### Acknowledgements

I am deeply grateful to Jurate M. Landwehr and John D. Bredehoeft for the mathematical development of functions for the average discharge and average dolomite reaction rates, respectively. Reviews by Blair F. Jones, John Busby, L. Niel Plummer, and Donald C. Thorstenson helped substantially with the application of chemical modeling to the unique problems of the Edwards system. I am especially indebted to Deborah Wells for editing and clarifying the manuscript; to Carol Lee for expert and patient typing; to Leslie Robinson for drafting illustrations; and to Eileen O'Rourke Regan, Elizabeth Phillips, and Allen Shapiro for constructive comments and encouragement.

## References

- Abbott, P.L., 1975, On the hydrology of the Edwards limestone, south-central Texas. *J. of Hydrology*, 24,3/4, 251-269.
- Appelo, C.A.J., H.E. Beekman, and A.W.A. Oosterbaan, 1984, Hydrochemistry of springs from dolomite reefs in the southern Alps. *Int. Sym. on Hydrochemical Balances of Freshwater Systems*, Stockholm/Uppsala, 10-14, September 1984.
- Back, W., B.B. Hanshaw, L.N. Plummer, P.H. Rahn, C.T. Rightmire, and M. Rubin, 1983, Process and rate of dedolomitization: Mass transfer and  $^{14}\text{C}$  dating in a regional carbonate aquifer, *Geol. Soc. of Am. Bulletin*, 94,12, 1415-1429.
- Busby, J.F., L.N. Plummer, R.W. Lee, and B.B. Hanshaw, B.B., in press, Geochemical evolution of water in the Madison aquifer in parts of Montana, South Dakota, and Wyoming, U.S. Geological Survey Prof. Paper 1273-F, 241 pp.
- Busenberg, Eurybiades and L.N. Plummer, 1982, The kinetics of dissolution of dolomite in  $\text{CO}_2\text{-H}_2\text{O}$  systems at 1.5 to 65°C and 0 to 1 atm  $\text{P}_{\text{CO}_2}$ , *Am. J. of Sci.* 282, 45-78.
- Clement, T.J. and J.M. Sharp, Jr., 1988, Hydrochemical facies in the bad-water zone of the Edwards Aquifer, Central Texas: in *Proceedings of Ground Water Geochemistry Conference*, National Water Well Association, Worthington, OH, USA, p. 127-149.
- Deike, R.G.M., 1984, The effects of dedolomitization in a portion of the Edwards aquifer, south-central Texas, unpub. Master's thesis, George Washington U., 144 pp.
- Deike, R.G., in press(a), Comparative petrology of cores from two test wells in part of the Edwards aquifer, south-central Texas, U.S. Geological Survey Water Resources Invest. Rep., 142 pp.
- Deike, R.G., in press(b), Dolomite dissolution rates and possible Holocene dedolomitization of water-bearing units in the Edwards aquifer, south-central Texas, *J. of Hydrology*, 39 pp.
- Ellis, P.M., 1985, Diagenesis of the lower Cretaceous Edwards Group in the Balcones Fault zone area, south-central Texas, Ph.D Dissertation, U. of Texas, Austin, 290 pp.
- Longman, M.W. and P.A. Mench, 1978, Diagenesis of Cretaceous limestones in the Edwards aquifer system of south-central Texas: A scanning electron microscope study, *Sedimentary Geology*, 21, 241-276.
- Maclay, R.W. and T.A. Small, 1976, Progress Report on the geology of the Edwards aquifer, San Antonio area, Texas, and preliminary interpretation of borehole geophysical and laboratory data on carbonate rocks, U.S. Geological Survey Open-File Report 76-627, 65 pp.
- Maclay, R.W. and T.A. Small, 1984, Carbonate geology and hydrology of the Edwards aquifer in the San Antonio area, Texas, U.S. Geological Survey Open-File Report 83-537, 72 pp.
- Maclay, R.W. and L.F. Land, 1988, Simulation of flow in the Edwards aquifer, San Antonio region, Texas, and refinement of storage and flow concepts, U.S. Geological Survey Water Supply Paper 2336-A, 48 pp.
- Mench, P.A., F.G. Pearson, Jr. and R.G. Deike, 1980, Stable isotope evidence for modern freshwater diagenesis of Cretaceous Edwards limestone, San Antonio area, Texas. *Book of Abstracts*, Am. Assoc. of Petroleum Geologists, Soc. of Economic Paleontologists and Mineralogists Annual Convention, Denver, Colorado, June 8-11, 90 pp.
- Parkhurst, D.L., L.N. Plummer, and D.C. Thorstenson, 1982, BALANCE--A computer program for calculating mass transfer of geochemical reactions in ground water. U.S. Geological Survey Water Resources Investigations 82-14, 29 pp.



- Pearson, F.J., Jr., P.L. Rettman, and T.A. Wyerman, 1975, Environmental tritium in the Edwards aquifer, central Texas, 1963-71, U.S. Geological Survey Open-File Report 74-362, 32 pp.
- Pearson, F.J., Jr. and P.L. Rettman, 1976, Geochemical and isotopic analyses of waters associated with the Edwards limestone aquifer, central Texas, U.S. Geological Survey Open-File Report, 35 pp.
- Plummer, L.N., 1977, Defining reactions and mass transfer as part of the Floridan aquifer, *Water Resour. Res.*, 13,5, 801-812.
- Plummer, L.N. and W. Back, 1980, The mass balance approach: Application to interpreting the chemical evolution of hydrologic systems, *Am. J. of Science*, 280, 130-142.
- Plummer, L.N., D.L. Parkhurst, and D.C. Thorstenson, 1983, Development of reaction models for ground-water systems, *Geochimica et Cosmochimica Acta*, 47, 665-686.
- Rose, P.R., 1972, Edwards Group, surface and subsurface, Central Texas, Texas Bureau of Economic Geology Report of Investigations, no. 74, 198 pp.
- Woodruff, C.M., Jr. and P.L. Abbott, 1979, Drainage-basin evolution and aquifer development in a karstic limestone terrain, south-central Texas, U.S.A., *Earth Surface Processes*, 4,4, 319-334.

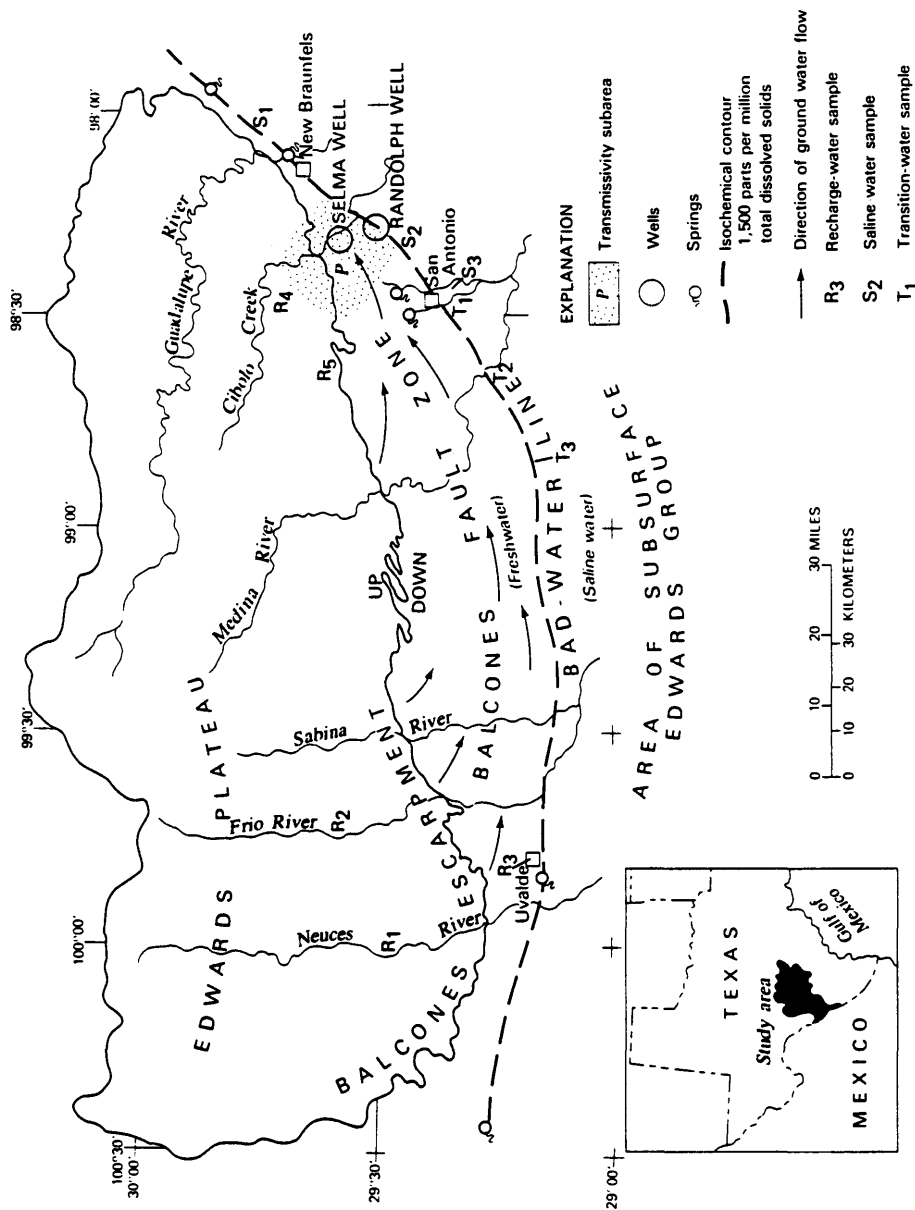


Figure 1. Map of Edwards Plateau-Balcones Fault Zone area showing locations of Selma and Randolph wells with respect to the bad water line. Springs represent the major discharge area. The main freshwater aquifer is located in the Balcones Fault Zone where recharge is along the southern margin of the plateau and groundwater flow is eastward.. Modified from Deike, in press (b).





HURRICANE GILBERT: ITS EFFECTS ON THE AQUIFER  
IN NORTHERN YUCATAN, MEXICO

L.E. Marin and E.C. Perry  
Department of Geology,  
Northern Illinois University  
DeKalb, IL 60015 USA

K.O. Pope  
Department of Applied Earth Sciences,  
Stanford University  
Stanford, CA 94305 USA

C.E. Duller  
Ecosystem Science and Technology Branch,  
NASA Ames Research Center  
Moffet Field, CA 94035 USA

C.J. Booth  
Department of Geology,  
Northern Illinois University  
DeKalb, IL 60115 USA

M. Villasuso  
Facultad de Ingenieria,  
Universidad Autonoma de Yucatan  
Merida, Yucatan, MEXICO

**ABSTRACT:** On the night of September 14-15, 1988, Hurricane Gilbert passed over the Peninsula of Yucatan, Mexico, dumping over 13 cm of precipitation. Precipitation at Merida, Yucatan, in the two weeks prior to Gilbert was in excess of 13 cm. The aquifer showed a quick response to this stress: water levels rose between 1.5-2 meters immediately after the hurricane and dropped rapidly; 11 days after the hurricane water levels were, on average, 0.90 m higher than the July, 1988 values. Coupled with the low hydraulic gradient, on the order of 0.007 m/km, this response suggests very high hydraulic conductivities. Along the coast, groundwater levels rose over three meters, probably as a result of a combination of enhanced flow within the fresh-water lens coupled with extraordinarily high tides, which also breached the coastline at several locations.

Introduction

Hurricane Gilbert, which passed over the north coast of the Yucatan Peninsula during the night of September 14-15 (Fig. 1), 1988, dumped a recorded 13.8 cm of precipitation at the meteorological station of the Merida (Yucatan) airport. Precipitation at this station in the two weeks prior to Gilbert was 13.6 cm, giving a grand total of 27.4 cm. This amount is between twenty-five percent to more than fifty percent the annual average precipitation. Presumably, a similar amount of precipitation occurred in other parts of the northern Peninsula. In addition, high seas washed over the extensive coastal dune system, inundating bench marks as high as 1.9 m above mean sea level. This damaging storm event provided an opportunity to evaluate response characteristics of the Yucatan aquifer in a network of

more than 100 wells of known elevation established during 1987-1988 in the karst plain of northwestern Yucatan (Marin, in preparation). Typical wells used for observation are hand-dug, have a diameter of approximately one meter and are finished about one meter below the water table.

#### Description of the Yucatan Aquifer System

The Yucatan aquifer system, a sole-source aquifer, consists of almost pure carbonate rock that contains a thin fresh water lens overlying a saline intrusion that penetrates more than 40 km inland (Durazo et al., 1980; Gaona et al., 1985). Along the northwest of the peninsula the aquifer is unconfined everywhere except for a narrow band parallel to the coast (Perry et al., 1989). Hydraulic gradients are very low, on the order of 0.007 m/km north to south, and 0.005 m/km east to west (Marin et al., 1987) suggesting a very high hydraulic conductivity.

Annual average precipitation on the Yucatan peninsula ranges from 500 mm/yr at Progreso (Fig. 2), to more than 1000 mm/yr at the Sierrita de Ticul, approximately 100 km south of Progreso, and 2000 mm/yr on the eastern coast (Anonymous, 1981). The spatial distribution of precipitation is reflected by the water table (Fig. 2) which is 20-40 cm higher on the eastern margin than on the western margin of the study area. Water levels in northwestern Yucatan range from less than one meter above mean sea level (MSL) near the coast to slightly over two meters (above MSL) at Sotuta 80 km inland (Fig. 2).

The Yucatan Peninsula is characterized by distinctive wet (May - October) and dry (November - April) seasons (Anonymous, 1981). Under normal conditions, maximum water level variations are on the order of 50 cm between the wet and dry period (Villasuso, 1987). The highest water levels are normally observed in September/October, the end of the wet season.

The study area contains three geomorphic surfaces that can be delineated by Landsat imagery: 1) a coastal surface composed of Quaternary beach and lagoon sediments, 2) a late Tertiary limestone surface that is nearly flat (slope ranges from 0.12-0.32 m/km) except for depressions containing cenotes (sink holes), and 3) an early Tertiary limestone surface that slopes slightly more (Fig. 3). The differences between these surfaces can be seen clearly in the Seasat altimeter data, which provide a topographic profile across the study area.

Within the study area there are two natural hydrogeologic boundaries: The Gulf of Mexico to the north and west, acting as a constant head boundary, and a "ring of cenotes" (sink holes) to the south and east, centered at Merida, acting as a no-flow boundary. The cenote ring, mapped with Landsat Thematic Mapper (TM) by C. Duller of NASA Ames Research Center, has a cenote spacing varying from approximately three cenotes per kilometer to several kilometers apart (Pope and Duller, in press). The cenote ring can also be detected in Seasat altimeter data, which show a series of depressions having the same base level, presumably the surface of the water table (Fig. 4). These Seasat water level data correlate well with measured water levels (Fig. 2).

The cenote ring marks a boundary between fractured limestone outside the ring and mostly unfractured limestone inside (Fig. 3). The ring of cenotes is bounded by the Sierrita de Ticul fault to the southwest, and the Holbox fracture zone to the east (Weidie, 1982). It is perhaps a conjugate fracture set. Whatever its origin, this aligned set of cenotes marks a zone of enhanced permeability. As we have reported (Marin et al., 1987) there is a valley-shaped low in the water table along the line of cenotes, probably indicating that groundwater flow is intercepted by, and preferentially discharged along, the cenote line. In effect, this linear low in the water table is a flow-line divide serving as a barrier to groundwater flow across the ring of cenotes. This feature has been observed continuously for some 2-1/2 years (1987-1989).

Coastal spring activity, which is greatest at the termini of the ring, provides evidence that the cenote ring is a zone of increased permeability. Landsat TM thermal infrared imagery of the northeast terminus of the cenote ring, east of Dzilam de Bravo, shows cold thermal anomalies in the coastal lagoon in the dry season (April) and in both the lagoon and off-shore during the wet season (October) (Fig. 7). Elsewhere such anomalies detected by thermal scanners have been confirmed as freshwater springs (e.g. Leveque, 1977), and we interpret the anomalies along the Yucatan coast as also coming from freshwater springs fed by flows along the cenote ring. Cold thermal anomalies are rare inside the cenote ring, west of Dzilam de Bravo, but become more abundant to the east. They are especially common near the eastern edge of the peninsula, another zone of high permeability and subsurface flows (Pope and Duller, in press). The large change in the size of the anomalies from wet season to dry season (Fig. 7) indicates that flow through the cenote ring responds to seasonal changes in rainfall.

#### Aquifer Response to Hurricane Gilbert

Heavy rainfall across northern Yucatan preceded and accompanied Hurricane Gilbert on September 14-15, 1988. The precipitation increased water levels (as measured between September 26 and October 1) by 0.35 to 1.26 meters (average 0.90 m) above the July, 1988 measurements (Fig. 2).

Water levels were recorded both before and after Hurricane Gilbert in a well in Merida. Water levels began rising slightly during early September in response to precipitation (Figs. 8 and 9). No measurements are available for the first days after hurricane but five days after the hurricane passed over the peninsula, water levels were 68 cm above the water level reading on September 13 and declined with time.

The study area north of the cenote ring has two zones, inland and coastal, which showed distinctly different aquifer response to Hurricane Gilbert. After the hurricane, the coastal zone experienced overland flow for an extended period of time.

The coastal zone is coincident with the coastal aquitard that underlies the dune ridge and lagoon and that crops out in the tzekel (a rocky band paralleling the coast that is almost bereft of soil and in which nearly impermeable calcrete covers much of the land surface) and transition zones (as defined by Perry et al. (1989)). The aquitard varies from 5 km wide (Dzilam de Bravo) to 30 km (Celestun), and embraces all of the coastal

geomorphic surfaces plus the northern-most fringe of the late Tertiary limestone surface shown in Figure 3.

The inland zone is a region of normal karst. Its northern boundary is coincident with the boundary between the coastal aquitard and normal karst, and it comprises all but the northernmost part of the Tertiary limestone aquifer (Fig. 3). In the inland zone, residents consistently reported well water elevations immediately after the hurricane that were 1.5 to 2.0 m higher than those measured in July, 1988. Water levels declined on the order of several centimeters/day. 11 days after the hurricane water levels decayed on the order of 0.7 cm per day (Fig. 10). Local, but frequent thunderstorms of up to 2 cm of precipitation during the period of observation made it difficult to determine aquifer recovery. A few wells respond differently to such local events, as evidenced by paired, closely-spaced stations that varied by as much as 11 cm (Cosgaya, Yucatan) immediately after a storm. Nevertheless, it is obvious from our data that the aquifer as a whole responds very rapidly when stressed.

The coastal zone has been shown by Perry et al. (1989) to be confined under normal circumstances. Thus, surface water in the coastal zone is in contact with the Yucatan fresh water aquifer only through springs (petenes) (Marin et al., 1988) that flow through leaks in the aquitard. Much of the surface water is normally salty due to evaporation of salt water. Two weeks after Hurricane Gilbert, we observed that much of the coastal zone remained covered by a thin, flowing sheet of fresh water that had replaced brackish water or brine isolated from the Yucatan aquifer by the coastal aquitard. One month later, in October, the coastal zone was still flooded, as indicated in satellite imagery (Fig. 11). In this zone there is a strong dependence of the aquifer water levels on tides (Perry et al., 1989; Smart and Whitaker, in press; Perry et al., in press). Our direct information about the response of this zone to the hurricane is limited because most of our observation stations in the coastal zone were accessible only on foot immediately after the hurricane. On a traverse on 27 September we found fresh-water flowing across the surface of the tzekeel as a sheet. Stations where we had previously (Reeve, in prep.) measured conductances of greater than 19,000 micromhos/cm had measured conductances of 1650-2500 micromhos/cm. Two of three piezometers that had previously been drilled through the confining layer were found on September 26 to have freely flowing water with specific conductances of 4,420 to 5,600 micromhos/cm (i.e. brackish water) into the surface fresh water sheet at high tide. The third of these piezometers could not be located beneath the fresh water sheet. We estimate the head for the confined portion of the aquifer to be about 30 cm above the July 1988 values. Flow from the coastal piezometers was greater than during any previous observation period.

It is significant that, after the hurricane, water from the confined coastal aquifer was brackish, even though surface water above the aquifer was fresh. In previous measurements all water from the aquifer measured in this zone had conductances in the range of 2500 to 7400, but it was not clear whether the salinity was derived by leakage through the aquitard from above, where extensive evaporation takes place, or whether it came from the underlying saline intrusion. The post-hurricane measurements make it clear that the increased salinity in the aquifer comes from a tidally induced mixing effect of the aquifer with the underlying saline water.



Open wells nearest to the coast were breached by hurricane waves, and thus are not useful in ascertaining aquifer responses. Residents living a few kilometers from the coast report that water in their wells rose approximately 3 m immediately after the hurricane. This rise is considerably greater than the rise reported by users of inland wells and suggests that high seas were, in part, responsible for increased aquifer water levels as much as 25 km from the coast. Again, our data indicate extremely fast aquifer response. This observation is reinforced by the recent discovery that a cenote 20 km from the coast (near Celestun) has variations in water levels on the order of 20 cm that are correlated with tides (Gamboa et al., 1989). Another consequence of the high seas accompanying Hurricane Gilbert was the repeated breaching of the coastline both in the study area and along the eastern north coast (Fig. 11).

Perhaps the impact of Hurricane Gilbert on the aquifer was enhanced because the precipitation before the hurricane saturated the ground. In the coastal zone the precipitation that fell on September 14-15 could not infiltrate the rock, resulting in overland flow. Furthermore, the rainfall associated with Gilbert occurred over a very short time interval, two days. It is likely that during this period of time, evapotranspiration was negligible.

### Conclusions

Measurements taken shortly after Hurricane Gilbert struck the Yucatan Peninsula show that: 1) the aquifer response was fast, 2) overland flow heading up in the coastal transition zone demonstrated that the edge of the coastal confining layer is coincident with the intersection of land surface with the water table, and 3) tidal pumping is responsible for a mixing effect between the fresh-water aquifer and the underlying saline intrusion. The very high hydraulic conductivity of the aquifer in Yucatan is demonstrated by the quick rise and fall in water-table elevation following the hurricane, by the tidal variation in water levels in a cenote 20 km from the coast, and by the low hydraulic gradients.

### Acknowledgements

Marin acknowledges support from the American Association of Petroleum Geologists, the Geological Society of America, Sigma-Xi, and the National Speleological Society. Perry and Marin thank the N.I.U. Graduate School for its support. Pope and Duller acknowledge support from the Ecosystem Science and Technology Branch, NASA Ames Research Center.

### References

- Anonymous, 1981, Instituto Nacional de Estadística, Geografía, e Informática, Mexico, Carta de Precipitación anual, 1:1,000,000, Merida.
- Anonymous, 1983, Secretaría de Programación y Presupuesto, Mexico, Carta Geológica, 1:1,250,000, Merida.

Anonymous, 1988, Secretaria de Agricultura y Recursos Hidraulicos, Merida, Yucatan, Mexico.

Durazo, J., S. Gaona, S. Trejo, and M. Villasuso, 1980, Observaciones sobre la interfase salina en dos cenotes del centro-noroeste de Yucatan. XXXIII Congreso Nacional de Investigacion en Fisica, Sociedad Mexicana de Fisica, Guadalajara, Jalisco, Mexico, November 24-28.

Gamboa, J., R. Gonzalez, and V. Coronado, 1989, Personal Communication.

Gaona, S., M. Villasuso, J. Pacheco, A. Cabrera, J. Trejo, T. Gordillo, C. Tamayo, V. Coronado, J. Durazo, and E. Perry, 1985, Perfiles hidrogeoquímicos del noreoeste de Yucatan, Mexico. Boletin del Instituto de Geofisica #18, UNAM, Yucatan, Mexico, D.F., Mexico.

Leveque, P. Ch., 1977, Etude du Karst, en Grece et en Crete, a l'Aide de la Teledetection et du Tritium, in Karst Hydrology, J.S. Tolson and F.L. Doyle, eds., International Association of Hydrogeologists Memoirs, vol. 12, University of Alabama, Huntsville Press, Huntsville, pp. 461-476.

Marin, L.E., E.C. Perry, and C. Booth, 1987, Abstract, EOS, Vol. 68.

Marin, L.E., A. Reeve, R. Sanborn, T. Felger, J. Gamboa, E.C. Perry, and M. Villasuso, 1988, Abstract, Petenes: A key to understanding the hydrogeology of Yucatan, Mexico, IAH's International Symposium on the hydrogeology of wetlands in arid and semi-arid areas of the world, Seville, Spain, May, 10-15.

Marin, L.E., in preparation, Ph.D. Dissertation, NIU.

Perry, E.C., J. Swift, J. Gamboa, A. Reeve, R. Sanborn, L.E. Marin, and M. Villasuso, 1989, Geologic and Environmental Aspects of Caliche Formation, North Coast, Yucatan, Mexico, Geology, Vol. 17, p. 818-821.

Perry, E.C., A. Reeve, R. Sanborn, L.E. Marin, and M. Villasuso, in press. Reply, Geologic and environmental aspects of surface cementation, north coast, Yucatan, Mexico, Geology.

Pope, K.O., and C.E. Duller, in press, Satellite observations of ancient and modern water resources in the Yucatan Peninsula, Proceedings of the Third Latin American Symposium on Remote Sensing, December, 1988, Acapulco, Gro., Mexico.

Reeve, A., in preparation, M.S. thesis, NIU.

Smart, F.L., and F.F. Whitaker, in press, Comment, Geologic and environmental aspects of surface cementation, north coast, Yucatan, Mexico, Geology.

Villasuso, M., 1987, unpublished, Precipitation over Merida, Yucatan, Mexico.

Weidie, A.E., 1982, Lineaments of the Yucatan Peninsula and fractures of the central Quintana Roo coast. Road log and supplement to 1978 Guidebook, 1982 Geol. Soc. Amer. Mtg., Field Trip no. 10 - Yucatan, p. 21-25.

1901 14SE88 19E-4ZA 00892 15581 EC1



Figure 1. Location of Yucatan showing position of Hurricane Gilbert on 14 September at 19:01 EST.

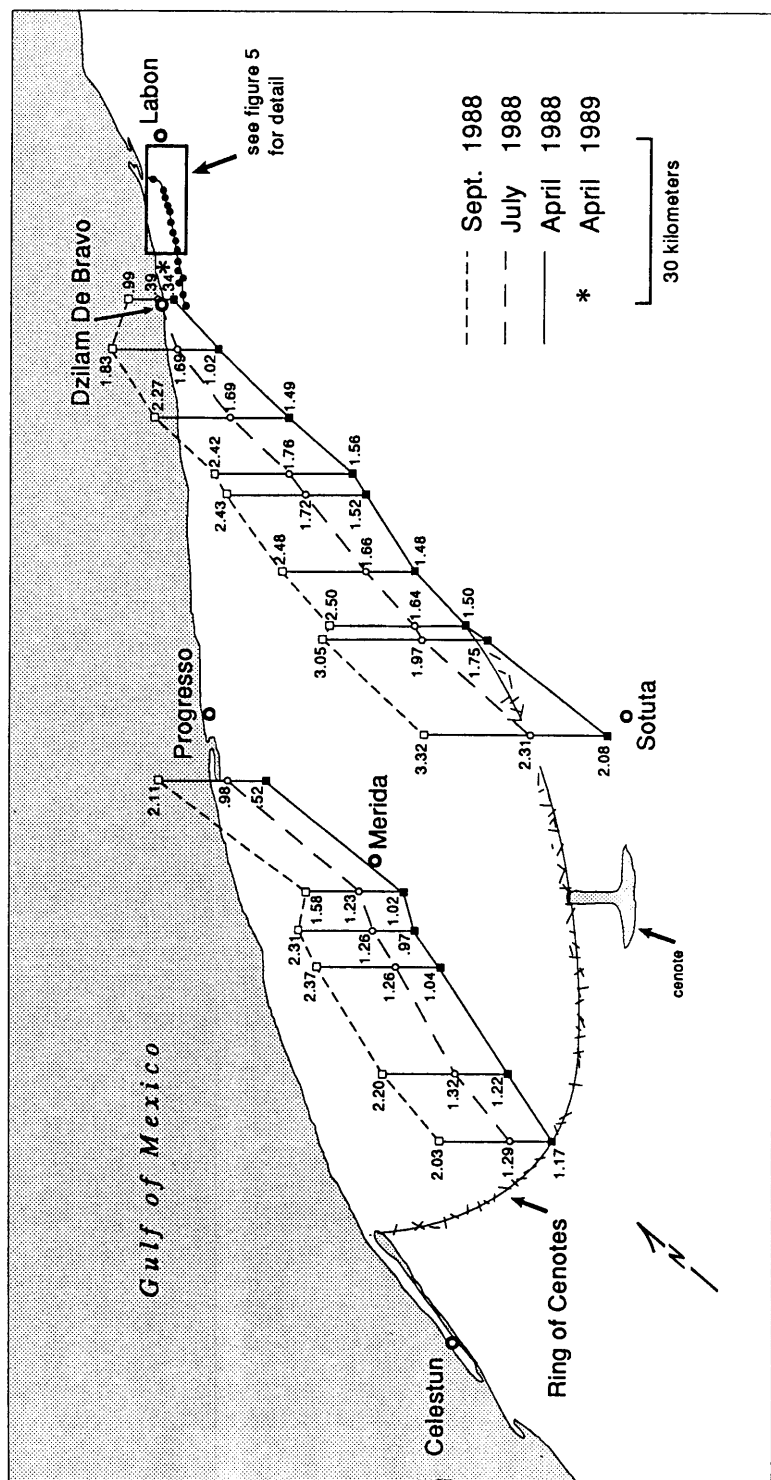


Figure 2. Water table map for northwestern Yucatan, April, 1988. Two north-south transects show water levels above MSL from the dry (April), and wet (July) seasons, plus water levels taken after Hurricane Gilbert. Note water level drops as transects cross the ring of cenotes. Lines crossing the ring of cenotes schematically indicate fractures on the ring of cenotes.

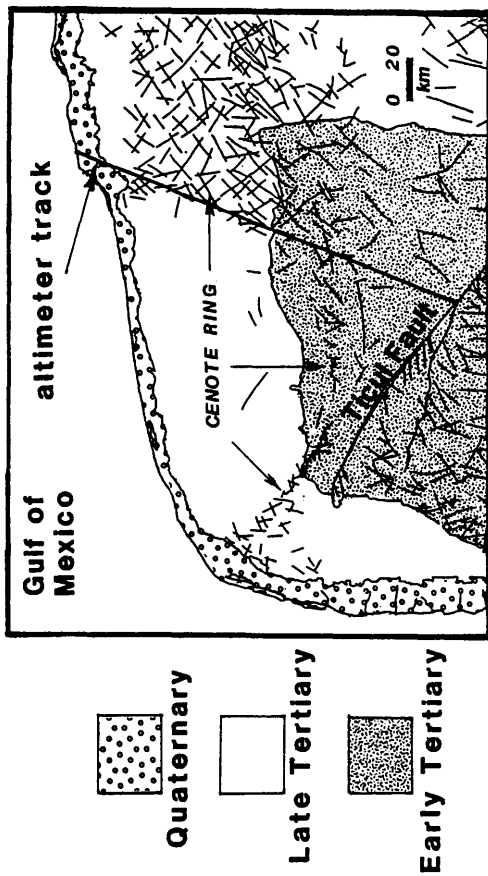


Figure 3. Geology of the northwestern Yucatan Peninsula, Mexico (Anonymous, 1983). Quaternary deposits are mostly unconsolidated beach and lacustrine sediments. A semi-circular zone of cenotes (sink holes), discovered and mapped with Landsat TM imagery, corresponds with a zone of fractures. Inside this fracture zone almost no cenotes are found. This ring of cenotes demarcates a zone of higher rates of groundwater flux and limestone dissolution.

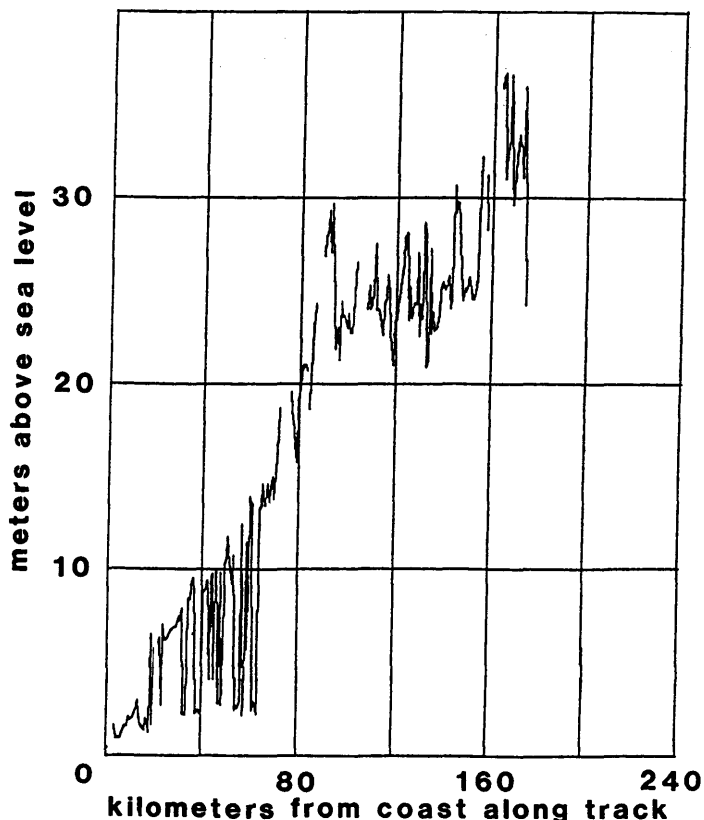


Figure 4. SeaSat altimeter track (43744). Note the change in slope and macro-scale surface roughness at the contact between the late and early Tertiary limestone platforms (approximately 90 km from the coast along track). The early Tertiary platform has a well developed rugged karst topography, whereas the younger late Tertiary platform surface is relatively smooth. Also note the horizontal base level of several karst depressions (containing cenotes) where the altimeter track crosses the cenote ring (20 to 70 km from the coast along track). This base level is controlled by the surface of the fresh water aquifer. The altimeter loses lock at the 50 m high scarp of the Ticul Fault, shown in Figure 3. Seasat altimeter data courtesy of Herbert Frey, NASA Goddard Space Flight Center.

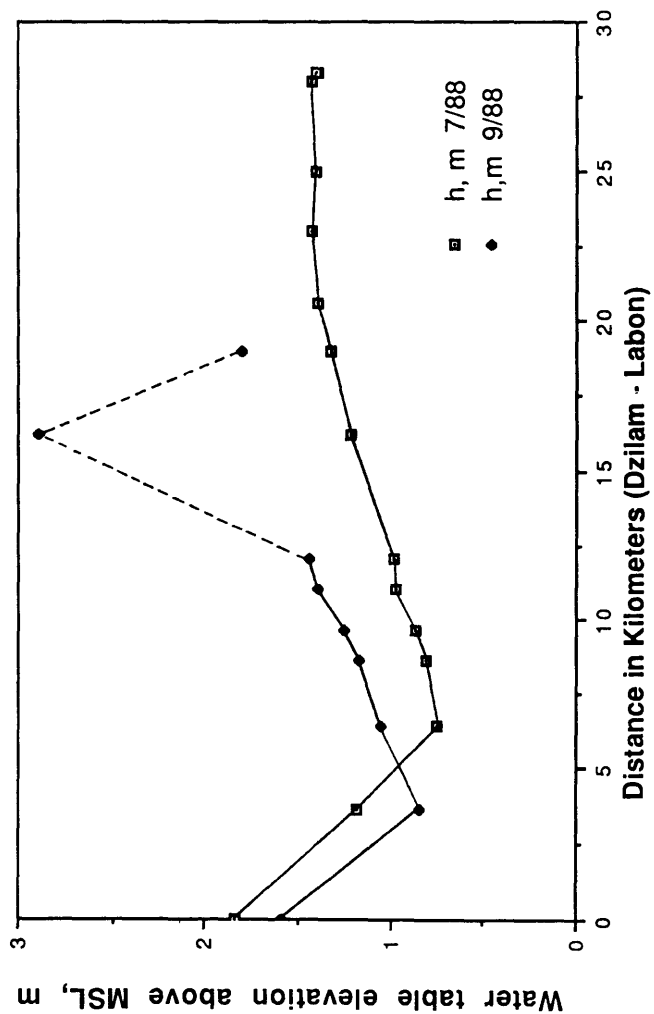


Figure 5. East-west transect across the ring of cenotes. Note the drop in the water table at the left of the diagram. The water table drops as it crosses the ring. This drop has been observed since the Summer of 1988 when the wells in this transect were surveyed. The point with an elevation of almost three meters is probably a localized, perched water table.



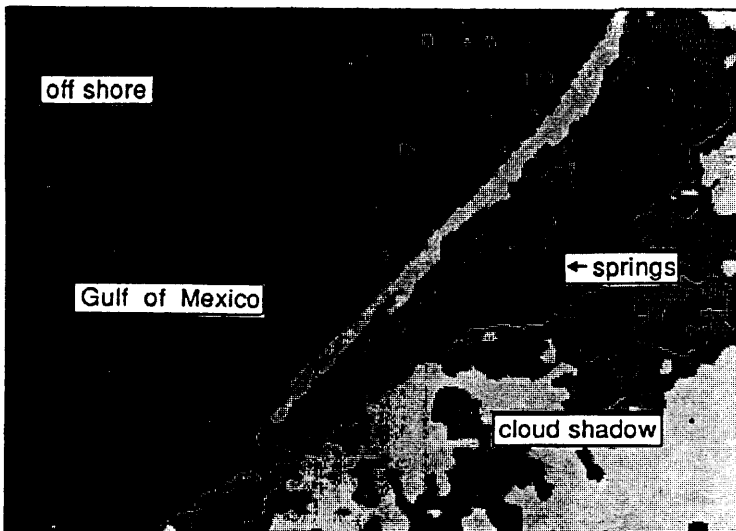
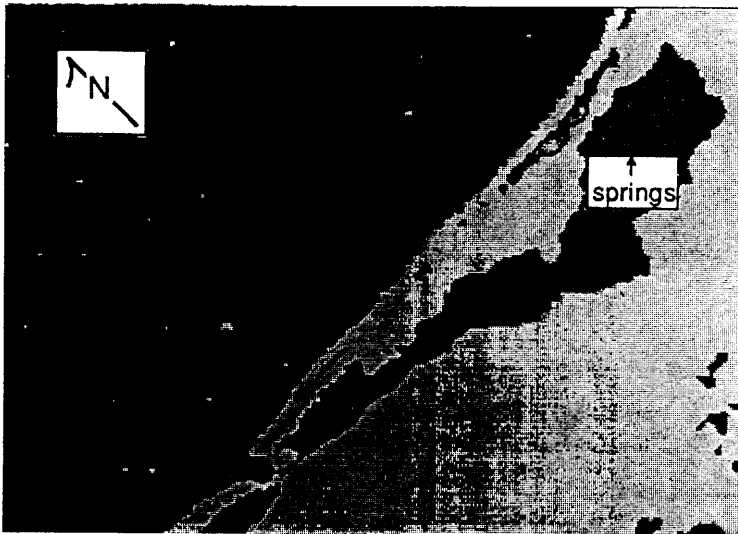


Figure 6. Landsat Thematic Mapper thermal infrared (band 6) image of the coastline and coastal lagoons at Dzilam de Bravo, Yucatan, Mexico. The upper image is from the dry season (April, 1985) and the lower one from the wet season (October 1986). Both images show cold thermal anomalies interpreted as freshwater springs color-coded black (approx. 24°C), compared with warmer lagoon and coastal waters color-coded gray (approx. 27°C). Note what appears to be a large spring along the coast in the lower left (southwest) of the wet season. Width of the scene, left to right (west to east) is about 10.5 km. Landsat data courtesy of EOSAT Co., Lanham, Maryland.

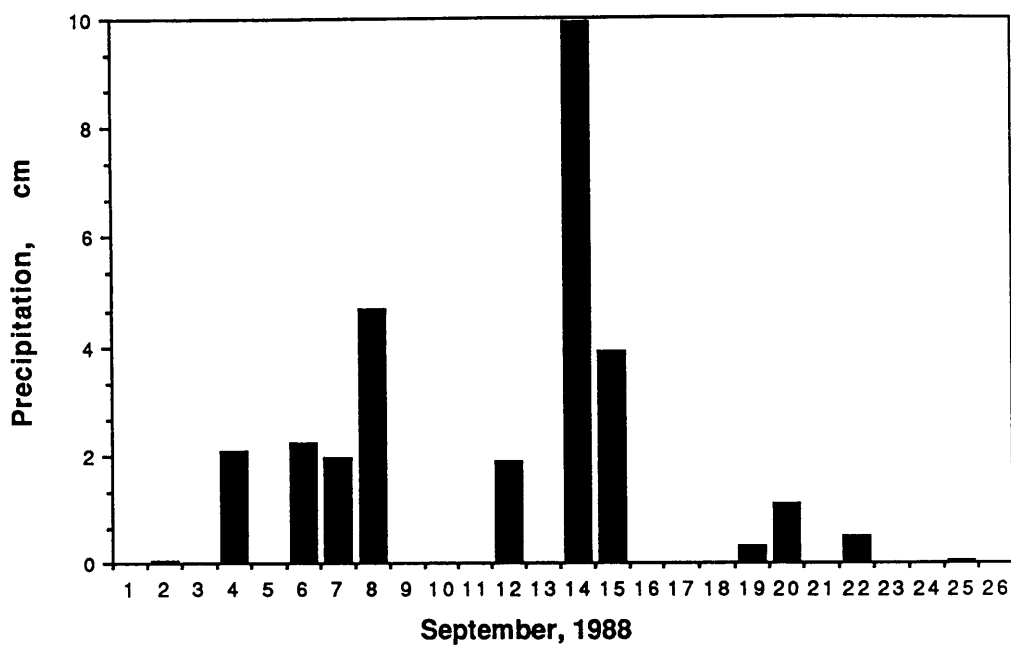


Figure 7. Histogram showing precipitation in September, 1988 at the Merida, Yucatan Airport (Anonymous, 1988).

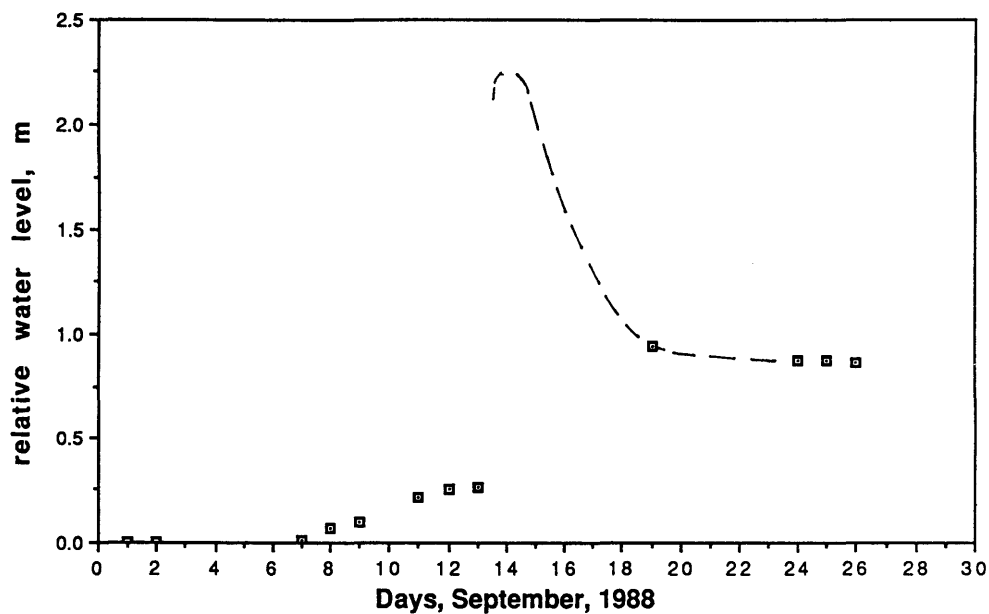


Figure 8. Scatter chart showing base water levels in an unsurveyed well in Merida. Relative changes in water levels are shown. Note increasing water table depth in early September, and the sharp rise five days after Hurricane Gilbert passed over the peninsula.

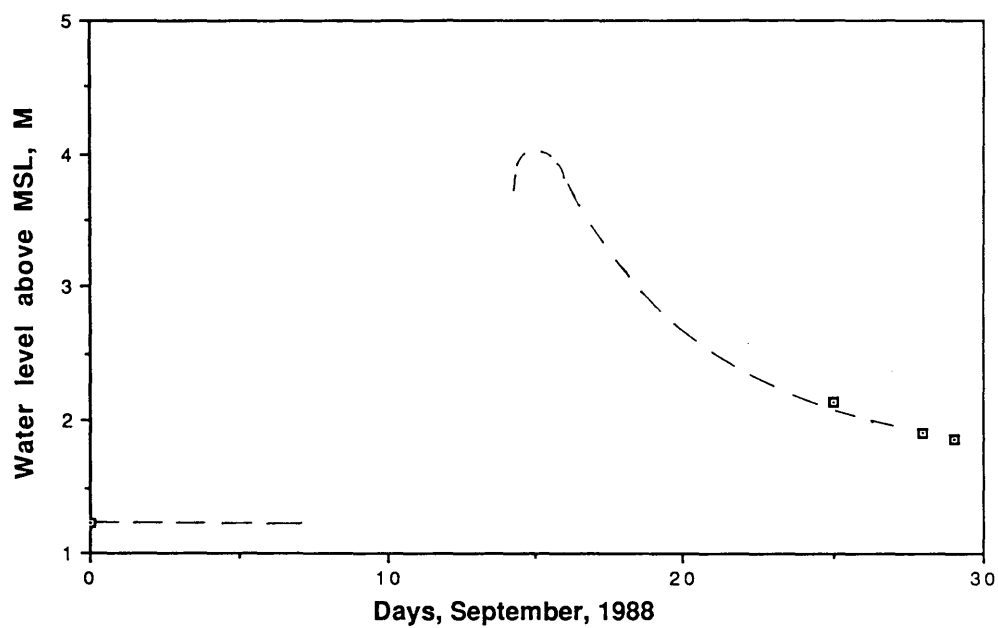


Figure 9. Generalized aquifer behavior in northwestern Yucatan. Dashed portion of the curve is synthesized from information provided by well owners. Solid portions of the curve is averaged data from our measurements 26 September - 1 October.

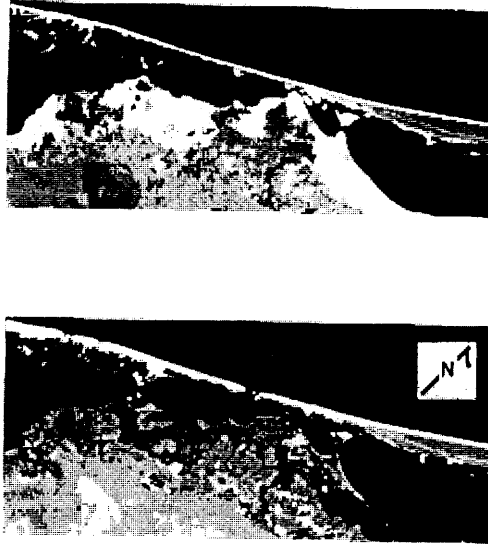


Figure 10. Landsat Thematic Mapper images, before and after Hurricane Gilbert, of coastal lagoon east of Rio Lagartos, Yucatan, Mexico (original images are false color composite of bands, 5, 4, 3). The top image was acquired before Hurricane Gilbert (April 1984) and the bottom image one month after (October 1988). The most obvious damage from the hurricane that is visible in the lower image are the several breaks in the coastal bar. The white areas along the south (bottom) shore of the lagoon are salt marshes and mudflats, which are completely dry in this dry season image. Note that this same region after Hurricane Gilbert is flooded and appears gray to black. Also note the black dots farther south from this flooded zone in the post-hurricane image. These are flooded aguadas (depressions) and flowing petenes (springs). Width of scene, left to right (west to east) is about 15 km. Landsat data courtesy of EOSAT Co., Lanham, Maryland.



HIGH FREQUENCY SEA LEVEL CYCLICITY, KARSTIFICATION, AND A  
CARBONATE-SILICICLASTIC TRANSITION: GEOLOGIC CONTROLS  
ON THE DEVELOPMENT OF THE FLORIDAN AQUIFER SYSTEM, SOUTHWEST FLORIDA

Mark W. Evans

GeoSciences Program  
Emory University  
Atlanta, Georgia 30322

Abstract

High resolution seismic profiles and subsurface borehole data have been used to evaluate the effects of sea level cyclicity, karstification and an intercalated, carbonate to siliciclastic transition on the stratigraphic development of the upper confining beds of the Floridan Aquifer System in southwest Florida. Shallow-water Eocene to middle Miocene limestones comprise the primary producing aquifers and are semi-confined by sequences of clays, quartz sands, limestones, dolomites and phosphorites that are of middle to late Miocene age.

Two regional unconformities bound six discrete depositional sequences within the late Neogene deposits. The lower regional unconformity (R-3) varies from about 20 m depth to more than 115 m. This surface is present as NW-SE and NE-SW trending troughs with sharp, irregular reflections, and isolated sinkholes indicative of subaerial exposure. The six late Neogene depositional sequences prograde to the south/southeast with a proximal-distal transition from short, steeply dipping oblique clinoforms to long, low angle clinoforms in a downdip direction. Three end-member lithologies are present: quartz/phosphate sands, a calcilutite, and poorly to well indurated, sandy, molluscan calcarenite. The depositional sequences are interpreted as a series of unconformity bounded, prograding fluvial to deltaic deposits.

The karstified antecedent topography has controlled the distribution of the Neogene depositional sequences in two ways: first, fluvial systems are localized in the antecedent lows which restricts the distribution of fluvially transported sands. Second, the relatively impermeable calcilutite deposits which occur as thin beds outside the lows, thicken to 20-40 m within the karstic depressions which limits vertical drainage and initiates the development of fluvial systems on the carbonate terrain.

## Introduction

The depositional sequences and bounding unconformities comprising the upper confining beds of the Floridan Aquifer System in southwest Florida were examined with high resolution seismic reflection profiles and borehole lithologic and geophysical data. The purpose of this study was to evaluate the effects of high frequency sea level cyclicity, karstification, and a long term, intercalated, carbonate to siliciclastic lithologic transition on the stratigraphic and hydrogeologic development of the Floridan Aquifer System.

Zones of secondary porosity within shallow-water Eocene to middle Miocene limestones comprise the primary permeable units of the FAS in southwest peninsular Florida (Johnston and Miller, 1988). These permeable limestones are overlain and semi-confined by sequences of middle to late Miocene clays, quartz sands, limestones, dolomites and phosphorites. The specific lithologies within the confining unit(s) are extremely variable in their lateral and vertical distribution (Wedderburn, *et al.*, 1982; Meyer, 1982), and collectively represent a long term, intercalated transition from the underlying carbonates to the overlying Quaternary siliciclastic deposits.

The hydrogeologic significance of this transition has been shown by Back and Hanshaw (1970) in a comparison between peninsular Florida and the Yucatan peninsula, which has not undergone a clastic transition. The Yucatan, which is composed of Cretaceous to Quaternary karstified limestones, has developed a very thin, unconfined freshwater zone over a saltwater aquifer. As a result of the deposition of relatively impermeable clays, marls, dolosilts, etc., over Paleogene karstified limestones, peninsular Florida has developed relatively higher heads, a deeper flow system, and in concert with fluctuating sea levels, widespread dolomitization (Hanshaw *et al.*, 1971). Lateral and vertical permeabilities are consequently dependent upon the depositional processes controlling the transitional units.

High frequency sea level fluctuations have been proposed as a primary depositional control for many Neogene coastal deposits (*i.e.*, Peck *et al.*, 1979; Snyder *et al.*, 1982; and, Kidwell, 1984; with reviews by Schlee, 1984, and Wilgus *et al.*, 1988). In a low lying, flat terrain such as peninsular Florida, rapid sea level fluctuations would result in: rapid facies transitions (Perkins, 1977; Evans *et al.*, 1989), frequent development of subaerial and submarine unconformities (Esteban and Klappa, 1983; Rasmussen and Neumann, 1988), and periodic carbonate dissolution (Back *et al.*, 1979). The stratigraphic result of sea level fluctuations is the development of laterally restricted, lithologically heterogeneous, unconformity-bounded depositional sequences (*e.g.* reviews by Vail *et al.*, 1977; and, Wilgus *et al.*, 1988). Definition and mapping of the resulting depositional sequences are wholly based on the distribution of unconformities (or correlative conformities) and are fundamentally different from lithology-based stratigraphic units, *i.e.*, formations (Salvador, 1987).

In light of the poor correlation between hydrostratigraphic units and lithostratigraphic units in general (Seaber, 1988) and with respect to



the Floridan Aquifer System specifically (Johnston and Miller, 1988), it may be beneficial to examine the stratigraphic arrangement and lithologic composition of unconformity-bounded sequences, and how the distribution of those sequences has controlled the hydrogeologic evolution of the aquifers in southwest Florida. Thus, within the overall goal of documenting the late Neogene sequence stratigraphy, the specific objectives of this study were: 1) to define the pattern of karst in the middle Miocene limestones, 2) to delineate the depositional sequences and distribution of permeable/impermeable facies comprising the late Miocene confining units of FAS, and 3) to examine the relationship between the resulting stratigraphic model and the hydrogeologic nomenclature.

### Methods

A network of high resolution seismic reflection profiles were obtained using an E.G. & G. "Uniboom" fired at 200 joules power setting and a 0.10 second sweep, or an O.R.E. "Geopulse" fired at 175 joules and a 0.125 second sweep. Navigational fixes were obtained at course changes and/or 5 minute intervals using LORAN C and adjusted to fixed reference points (channel markers, etc). Interpreted seismic profiles were digitized and replotted in order to standardize vertical and horizontal scales.

The seismic data were analyzed using the stratigraphic procedures of Vail, et al. (1977; 1987) and Brown and Fisher (1980). Although these procedures were developed for low frequency seismic exploration of continental shelf/slope systems, the principles are applicable to the high resolution analysis of coastal and inner shelf systems (Hine and Riggs, 1986). Sequence-bounding unconformities were identified on the basis of reflector terminations or truncations and correlated throughout the profile grid. A three-dimensional seismic model was created by constructing isopachs of the sequences and, structure contours of the intervening unconformities. Reflectors within sequences (or stratal surfaces) were evaluated with respect to continuity, shape, and frequency in order to define seismic facies.

Lithologic and geophysical logs from 22 sites around Charlotte Harbor were used to quantify the seismic model and provide substrate velocities for converting the vertical seismic time scale to measured depth. Seventeen of these sites are from existing wells drilled and logged by the U.S. Geological Survey, the Southwest Florida Water Management District and the South Florida Water Management District. Three cores drilled by the Florida Geologic Survey were re-described from the archives on the basis of color, visual grain size, and structure.

Two additional sites (drilled for this study using a 15cm rotary rig) were described during drilling and cuttings were later re-examined with a binocular microscope for color, macro-fossils, gross mineralogy (quartz sand, phosphatic sand, limestone etc.) and visual estimates of grain size. Graphic lithologic logs for all sites were redrawn from descriptive logs to ensure consistency of nomenclature and graphic symbols. Geophysical logs were evaluated at 2 foot (or half scale) intervals and replotted using Lotus 123 software to standardize horizontal and vertical scales. Natural gamma

logs were used extensively because of their value in correlating formations in cased or uncased holes and because they have been routinely collected in various monitoring and test wells. Most of the geophysical logs used in this study are uncalibrated with respect to the API standards and record counts per second (cps) vs. depth.

## Results

The locations of the seismic profiles collected and interpreted for this study are presented in Figure 1 along with the locations of all profile sections presented as raw or interpreted data in the figures. Two regional unconformities (or reflectors), which can be correlated over the entire study area, bound six depositional sequences and five intervening disconformities. The lowermost regional unconformity (R-3) represents the limit of acoustic penetration throughout most of the study area.

Figure 2 is a structure contour of the R-3 surface with depth denoted as two-way travel time (2-way TT) in milliseconds (msec). Using a velocity of 2.0 m/msec and dividing the 2-way TT by 2, for 1-way TT, the depths in 2-way TT are equal to depth in meters (i.e., 100 msec x 2.0 m/msec x 0.5 = 100 m). The depth of the R-3 unconformity varies from less than 20 msec to more than 100 msec (Figure 2). The lows in the R-3 structure contour are aligned as a broad system of NE-SW and NW-SE trending troughs. The trough system reaches its maximum depth under Pine Island Sound (115 msec 2-way TT) and continues offshore to the NW under Sanibel and Captiva Islands and extends southeasterly under southern Sanibel Island and San Carlos Bay. A north to northwest trending trough also underlies the upper and lower Harbor area with a structural high apparently separating the Pine Island Sound trough from the Harbor trough.

Six discrete depositional sequences which overlie the R-3 unconformity can be defined on the basis of reflector geometries and terminations (Figure 3). These units, and the stratal reflectors in each sequence, dip to the southeast. The distribution of the sequences is illustrated by an interpreted seismic section (Figure 4) which shows depositional thickening of up to 40 msec (m) of Sequence D within the troughs and thicknesses of <10 msec outside the antecedent lows. Elongation of sequences down the trough axes also reflects depositional control by the antecedent topography. The upper bounding disconformity of Sequence D (Figure 4) indicates that the troughs were only partially infilled with Sequence D deposition and subsequently infilled by Sequences E and F.

The sequences are composed of three lithologic end members within the study area: Quartz sand (including phosphatic sand and gravel), calcilutite, and a variably indurated, molluscan/foram rich calcarenite or dolomite. The lithologic complexity of the described formations is derived from the varying proportions of the end members, variable diagenetic alteration and induration of the carbonate components, and at least

partially, from different descriptive terminology of various geologists. The calcilutite units are primarily composed of clay- to silt-sized calcite with variable amounts of dolomite, aragonite and quartz (Peck *et al.*, 1979). These deposits have alternately been described as dolosilts (wells 2 and 8); clays (wells 5 and 13); dolomite (well 15); and commonly called dolomitic or limey marl.

The quartz sand units occur in most holes at least once and commonly as two or three discrete units, (wells 3, 11, 17 and 20). Sandy clays and sandy limestones are probably more common than the sand unit and at least partially represent sample homogenization from the rotary drilling procedure (Maher, 1964). The calcarenite units consist primarily of unconsolidated to poorly indurated, sandy, foram-rich, molluscan shell hash (sandy, skeletal grainstones) at depths of 0 to approximately 30 m. Deeper limestone units grade into poorly to moderately indurated packstones with an increased proportion of forams and lime mud and a corresponding decrease in molluscan skeletal particles.

Unconformities are common in the lithologic record and include the previously described blackened, indurated limestones and sandy, phosphate pebble lags. Chert horizons are also present as unconformities and are probably alternate descriptions for the blackened limestones. Most of the observed unconformities develop on top of the limestone units (well 13). This apparent juxtaposition of unconformities on limestone units may result from the limestones occupying a terminal position in a transgressive-regressive couplet, or because unconsolidated sands and calcilutites erode upon subaerial or submarine exposure, leaving a relatively resistant limestone.

The east-west cross section in Figure 5 integrates the borehole lithologic data with the seismic sequence model. Sequence boundaries were located on the lithologic sections using described lithologic unconformities, discrete peaks on gamma logs and the collective data comprising the sequence model. This section includes Sequences D, E, and F, with the distal portion of Sequence D pinching out to the east. Sequence D in well 20 is lithologically similar to the basal part of the overlying Sequence E, i.e., a clayey, phosphatic sand. A sequence boundary is placed within that sand unit on the basis of the seismic model and the well 20 gamma log which has large peaks at 63 m and at 58 m (Figure 5).

The correlation between seismic and lithologic sequences is indicated by the lithologic and geophysical logs for well 21 which are included in Figure 6 (well location in Figure 1). The seismic model, derived from the distribution of mappable depositional sequences, shows sequences C-D-E, with time of travel and depth conversion based on acoustic velocities of 2000 m/sec (Evans, 1989). The reflection coefficient log also shows three discrete peaks which correspond closely with the sequences (40-25 m, 25-17 m, and 17 m- with no upper boundary). The gamma log also has discrete peaks at the predicted sequence-bounding unconformities due to

concentrations of Uranium-rich phosphatic sand and gravel. The gamma, velocity and density logs have slightly offset peaks as a result of tool responses to different physical characteristics (Doveton, 1986). The offsets have a regular pattern, with corresponding gamma and density peaks followed by delayed velocity log peaks.

### Discussion

The results of this study indicate that the stratigraphic development of the units comprising the upper confining zone of the upper Floridan aquifer has occurred as a series of lithologically heterogeneous, unconformity-bounded depositional sequences. Although these Neogene sequences are poorly constrained with respect to absolute dating, they occur as morphologically distinct sequences of prograding oblique clinoforms bounded by mappable unconformity surfaces. The antecedent topography and depositional sequences described by this study have several important implications for the distribution and integrity of the regional hydrogeologic system.

The interpreted depositional sequences begin with quartz sand-dominated channel deposits overlying a basal unconformity. These deposits are conformably overlain by estuarine to prodelta carbonate muds and, in turn, by subaerial to intertidal sandy molluscan chenier ridge deposits. The calcarenite deposits may be overlain by a conformable transition to estuarine deposition, but more commonly exhibit a disconformable or unconformable contact and the initiation of another sequence. The karstified topography has controlled the sequence distribution in two ways: 1) fluvial systems are localized in antecedent lows which restricts the distribution of fluvially transported sands, and 2) relatively impermeable clay deposits, which occur as thin beds outside the lows, thicken to 20-40m within the depressions.

The relief comprising the antecedent topography of the R-3 surface is attributed to karstic dissolution of underlying late Paleogene and Neogene limestones. The enclosed basins or troughs have developed a rectilinear pattern due to fracture selective dissolution (Trudgill, 1985). Similar orientations and patterns of karst distribution have been reported by Hine et al. (1988) and Popenoe et al. (1984) in west-central and northeast Florida. Evidence of widespread subaerial or meteoric exposure necessary for carbonate dissolution is common in both the seismic and lithologic data (Figures 3,4, and 5). Vertically offset (and laterally adjacent) sinkholes also indicate that dissolution has occurred episodically and as a direct result of sea level fluctuations (Perkins, 1977; Popenoe et al., 1984; Choquette and James, 1987).

The widespread distribution of karst indicates that vertical exchange between aquifer systems is probably very common. The effect of such vertical exchange is illustrated by the presence of several saline,

geothermal springs or free-flowing wells which discharge in the area (Kohout, 1967; Figure 2). The large karst troughs are infilled with thick, relatively impermeable clay such that leakage of the saline water is apparently restricted to the margins of the troughs (Figures 1 and 2). The deposition of these clays, as well as the relatively permeable sand and calcarenite units, is controlled by the interaction of antecedent topography and sea level cyclicity.

Along most of the Florida peninsula, the hydrogeologic role of the middle to late Miocene deposits is to confine the underlying Floridan Aquifer System. In southwest Florida, these deposits are still an important aquitard, but they separate underlying upward-leaking saltwater from localized freshwater aquifers. Aquifers within the late Miocene sequences (i.e., the Sandstone aquifer, Wedderburn *et al.*, 1982) will be of limited areal extent due to their origin from laterally restricted, high frequency, sea level controlled depositional cycles over the karstified antecedent topography. Consequently, attempts to regionally correlate aquifers or aquitards developed within these sequences have been unsuccessful (Wedderburn, *et al.*, 1982; Evans, 1989). However, the discrete pattern of karstified antecedent topography and lithologically heterogeneous depositional sequences reveals the distribution of permeable and impermeable facies, and provides a means of discovering and managing water resources.

### Conclusions

The carbonate deposits which comprise the Florida platform periodically underwent subaerial and/or meteoric dissolution during sea-level low stands. In the Charlotte Harbor area, dissolution has taken the form of a rectilinear pattern of troughs trending NW-SE and NE-SW. These troughs are 50-60 km in length, 5-8 km in width, and have vertical relief of up to 60 m below adjacent topographic highs. The troughs, or uvalas of karst terminology, are coincident with the regional fracture pattern and surficial geomorphic features, such as shoreline orientations, stream beds and aligned ponds or sloughs.

Late Neogene depositional sequences, which infill and overlie the karstified antecedent topography, consist of six unconformity-bounded units which prograde south-southeast with southerly dipping internal reflectors. These seismic sequences exhibit a distinct proximal-distal facies transition, have a strong offlap relationship with basal unconformities, and have minor onlap at their updip limits. The lithologies which comprise the seismic sequences consist of three end members: 1) quartz-dominated, phosphatic, pebbly sand, 2) clay interbedded with thin sand/silt layers and containing some molluscan shells and/or molds and, 3) variably indurated quartz sandy, molluscan/foram calcarenite.

The NW-SE, NE-SW trending rectilinear troughs that underlie the study area occur in middle Miocene limestones and are infilled with late

Miocene calcareous, sandy, phosphatic clays. The hydrogeologic development of the Charlotte Harbor area is affected by episodes of both low sea levels as periods of major karstification and by transgressing sea levels which have generated discrete distributions of permeable and impermeable deposits. Sinks and springs around the margins of the troughs are evidence of lateral karst progression and suggest that vertical exchange through the aquitard is common. It is also apparent from the widespread variability of depositional and karstic processes that correlation of aquifer systems on a regional scale without continuous seismic profiles or very closely spaced borehole data will be unreliable.

### References

- Altschuler, Z.S., et al., 1964, Geology and geochemistry of the Bone Valley Formation and its phosphate deposits, west central Florida, Geological Society of America, Guidebook, Field Trip No. 6, 1964 Annual Meeting, Miami, FL, 68 pp.
- Back, W. and Hanshaw, B.B., 1970, Comparison of chemical hydrogeology of the carbonate peninsulas of Florida and Yucatan, Journal of Hydrology, 10: 330-368.
- Back, W., et al., 1986, Differential dissolution of a Pleistocene reef in the groundwater mixing zone of coastal Yucatan, Mexico, Geology, 14: 137-140.
- Brown, L.F. and Fisher, W.L., 1980, Seismic Stratigraphic Interpretation and Petroleum Exploration, American Association of Petroleum Geologists Continuing Education Course Note Series 16, Tulsa, OK, 181 pp.
- Choquette, P.W. and James, N.P., 1987, Introduction, In: James, N.P. and Choquette, P.W. (Editors), Paleokarst, Springer-Verlag, New York, pp. 1-24.
- Doveton, J.H., 1986, Log Analysis of Subsurface Geology: Concepts & Computer Methods: John Wiley and Sons, NY, 273 pp.
- Esteban, M. and Klappa, C.F., 1983, Subaerial Exposure, In: Scholle, P.A., Bebout, D.G. and Moore, C.H. (Editors), Carbonate Depositional Environments, American Association of Petroleum Geologists Memoir 33, pp. 1-54.
- Evans, M.W., 1989, Late Miocene to Quaternary Seismic and Lithologic Sequence Stratigraphy of the Charlotte Harbor Area: Southwest Florida, Unpub. Ph.D. Dissertation, Department of Marine Science, University of South Florida, St. Petersburg, FL, 336 pp.

- Evans, M.W., et al., 1989, Quaternary stratigraphy of the Charlotte Harbor estuarine/lagoon system, southwest Florida: Implications of the carbonate-siliciclastic transition, *Marine Geology*, 88: 319-348.
- Hanshaw, B.B., et al., 1971, A geochemical hypothesis for dolomitization by ground water, *Economic Geology*, 66: 710-724.
- Hine, A.C., et al., 1988, Recent geological history and modern sedimentary processes along an incipient, low-energy, epicontinental-sea coastline: Northwest Florida, *Journal of Sedimentary Petrology*, 58(4): 567-579.
- Hine, A.C. and Riggs, S.R., 1986, Geologic framework, Cenozoic history, and modern processes of sedimentation on the North Carolina continental margin, In: Textoris, D.A. (Editor), *Society Economic Mineralogist Paleontologists, 1986 Mid-Year Meeting Field Guidebook*, Raleigh, NC, pp. 129-194.
- Kidwell, S.M., 1984, Outcrop features and origin of basin margin unconformities, Miocene lower Chesapeake Group, Atlantic coastal plain, In: Schlee, J.S., (Editor), *Interregional Unconformities and Hydrocarbon Accumulation*, American Association of Petroleum Geologists Memoir 36, Tulsa, OK, pp. 37-58.
- Johnston, R.H., and Miller, J.A., 1988, Region 24, Southeastern United States, In: Back, et al., (Editors), *Hydrogeology*, Geological Society of America, Boulder, CO, *The Geology of North America*, v. O-2, p. 229-236.
- Kohout, F.A., 1967, Ground-water flow and the geothermal regime of the Floridan plateau, *Transactions of the Gulf Coast Association of Geological Societies*, XVII: 339-354.
- Maher, J.C., 1964, *Logging Drill Cuttings*, Oklahoma Geological Society, Guidebook XIV, Second Edition, Norman, OK, 49 pp.
- Matthews, R.K., 1984, Oxygen-isotope record of ice-volume history: 100 million years of glacio-eustatic sea-level fluctuation, In: Schlee, J.S. (Editor), *Interregional Unconformities and Hydrocarbon Accumulation*, American Association of Petroleum Geologists Memoir 36, Tulsa, OK, pp. 97-107.
- Meyer, F.W., 1982, Preliminary evaluation of the hydrogeology of the Floridan aquifer system, south Florida (Provisional Draft), U.S. Geological Survey, Water Resources Investigations 82-xxx, Tallahassee, FL, 77 pp.

- Peck, D.M., et al., 1979, Late Miocene glacial-eustatic lowering of sea level: Evidence from the Tamiami Formation of south Florida, *Geology*, 7: 285-288.
- Perkins, R.D., 1977, Part II: Depositional framework of Pleistocene rocks in south Florida, In: Enos, P. and Perkins, R.D., Quaternary sedimentation in south Florida, Geological Society of America, Memoir 147, Boulder, CO, pp. 131-198.
- Popenoe, P., et al., 1984, Seismic-reflection studies of sinkholes and limestone dissolution features on the northeastern Florida shelf, In: Beck, B.F. (Editor), Sinkholes: Their Geology, Engineering and Environmental Impact, A.A. Balkema, Rotterdam, pp. 43-58.
- Salvador, A., 1987, Unconformity-bounded Stratigraphic Units, *Geological Society of America Bulletin*, v.98, pp. 232-237.
- Schlee, J.S., (Editor), 1984, Interregional Unconformities and Hydrocarbon Accumulation, American Association of Petroleum Geologists Memoir 36, Tulsa, OK, 184 pp.
- Scott, T.M. and Upchurch, S.B., 1982, Introduction, Miocene of the southeastern United States, *Proceedings of a Symposium*, Tallahassee, FL, Florida Department of Natural Resources, Bureau of Geology Special Pub. 25, pp. viii-xi.
- Seaber, P.R., 1988, Hydrostratigraphic Units, In: Back, W. et al., (Editors), Hydrogeology, Geological Society of America, Boulder, CO, The Geology of North America, v. O-2, p. 9-14.
- Snyder, S.W., et al., 1982, Miocene seismic stratigraphy, structural framework and sea level cyclicity, In: Scott, T.M. and Upchurch, S.B. (Editors), Miocene of the Southeastern United States, Florida Department Natural Resources, Bureau of Geology, Special Publication No. 25, Tallahassee, FL, pp. 138-161.
- Trudgill, S. 1985, Limestone Geomorphology, Longman, New York, 196 pp.
- Vail, P.R., et al., 1977, Seismic Stratigraphy and Global Changes of Sea Level, In: Payton, C.E., (Editor), Seismic Stratigraphy- Applications to Hydrocarbon Exploration, American Association of Petroleum Geologists Memoir 26, Tulsa, OK, pp. 49-212.
- Vail, P.R., 1987, Part I: Seismic stratigraphy interpretation procedure, In: Bally, A.W. (Editor), Atlas of Seismic Stratigraphy, Volume I, American Association of Petroleum Geologists Studies in Geology No. 27, Tulsa, OK, pp. 1-11.



Wedderburn, L.A., et al., 1982, Hydrogeologic Reconnaissance of Lee County, Florida, South Florida Water Management District, West Palm Beach, FL, Technical Publication, 82-1, 193 pp.

Wilgus, C.K., et al., (Editors), 1988, Sea-Level Changes: An Integrated Approach, Society of Economic Paleontologists and Mineralogists Special Publication No. 42, Tulsa OK, 407 pp.

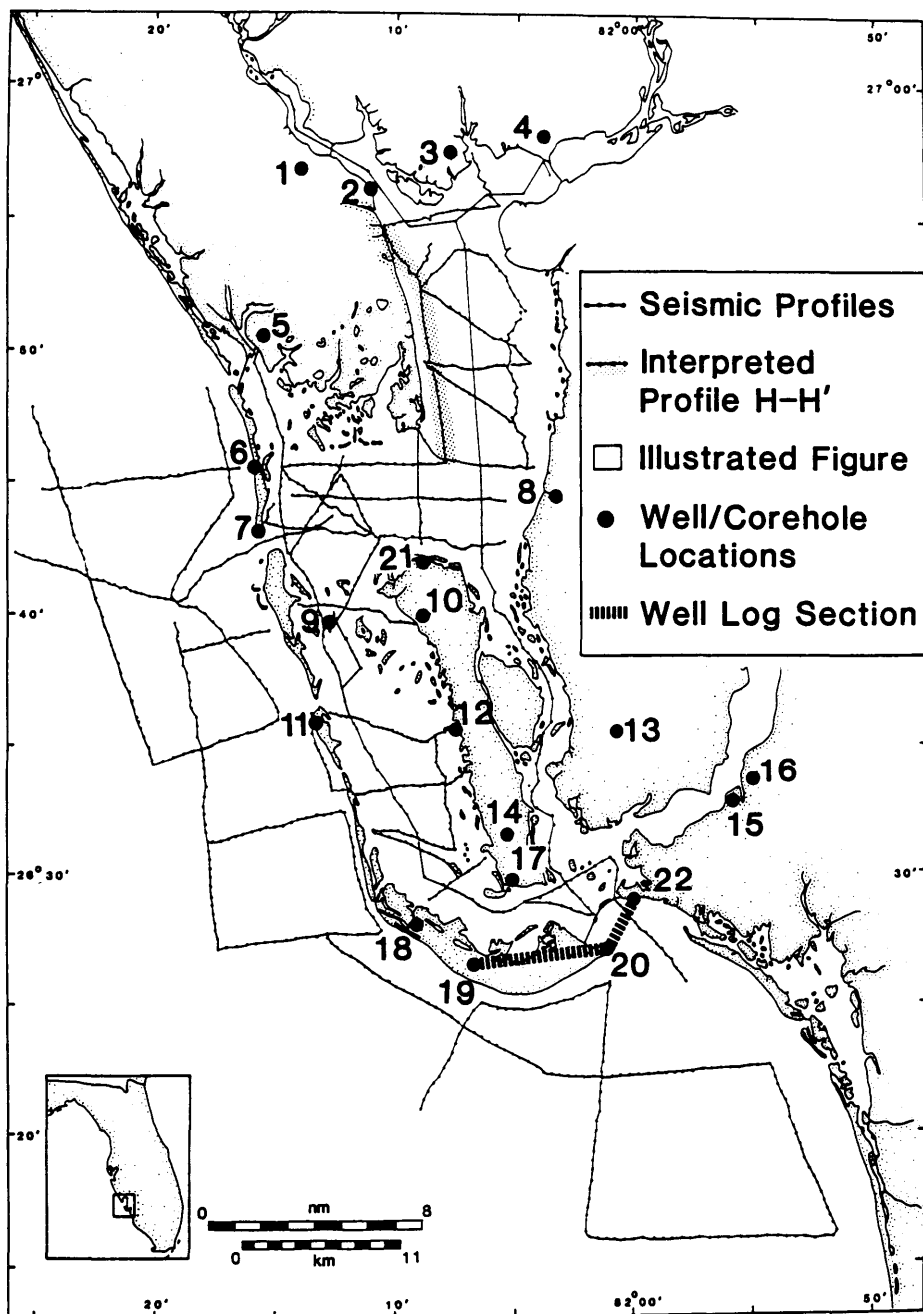


**Figure 1. Seismic and well locations,  
Charlotte Harbor area, Florida**

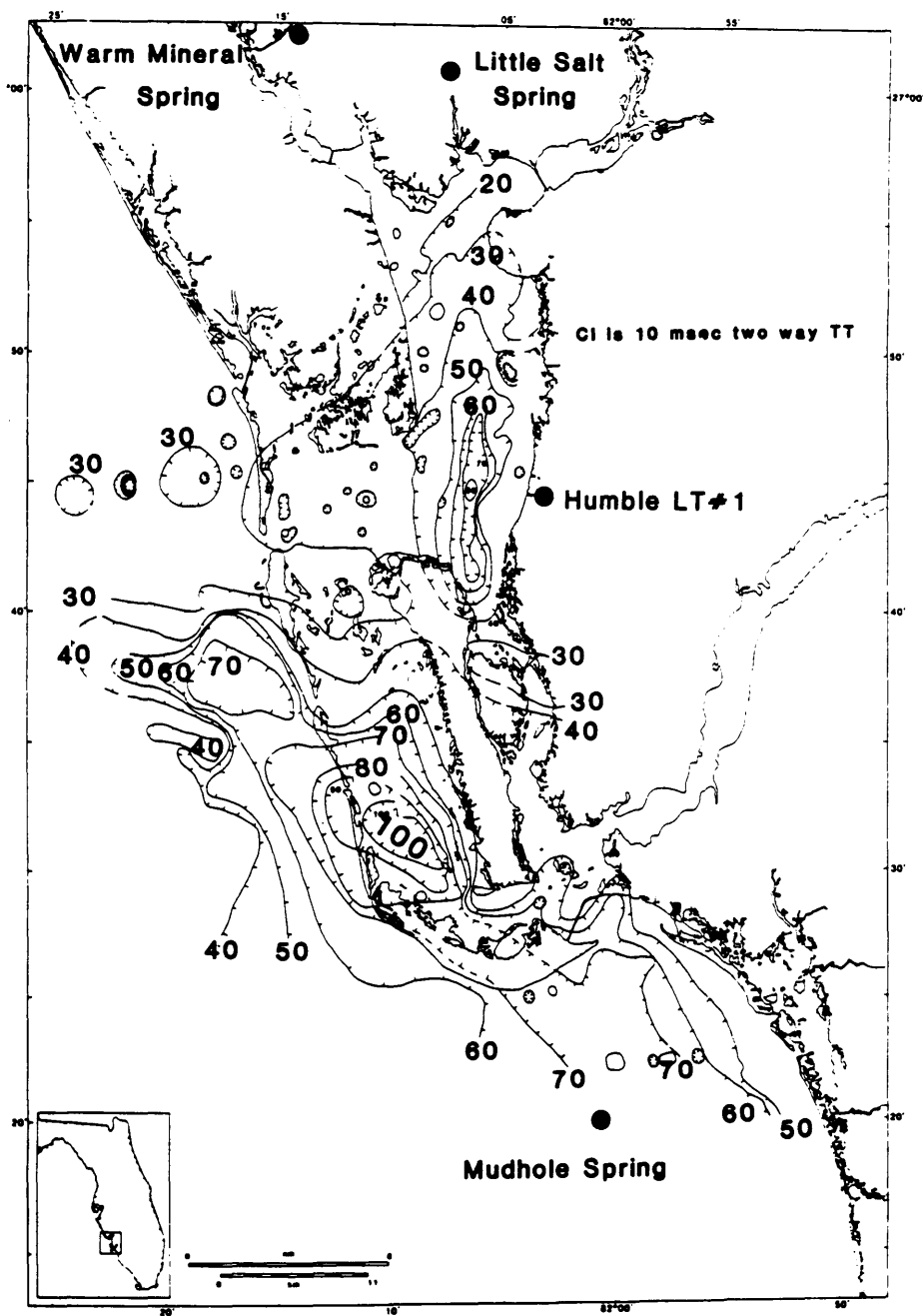


**Figure 2. R-3 unconformity structure contour map**

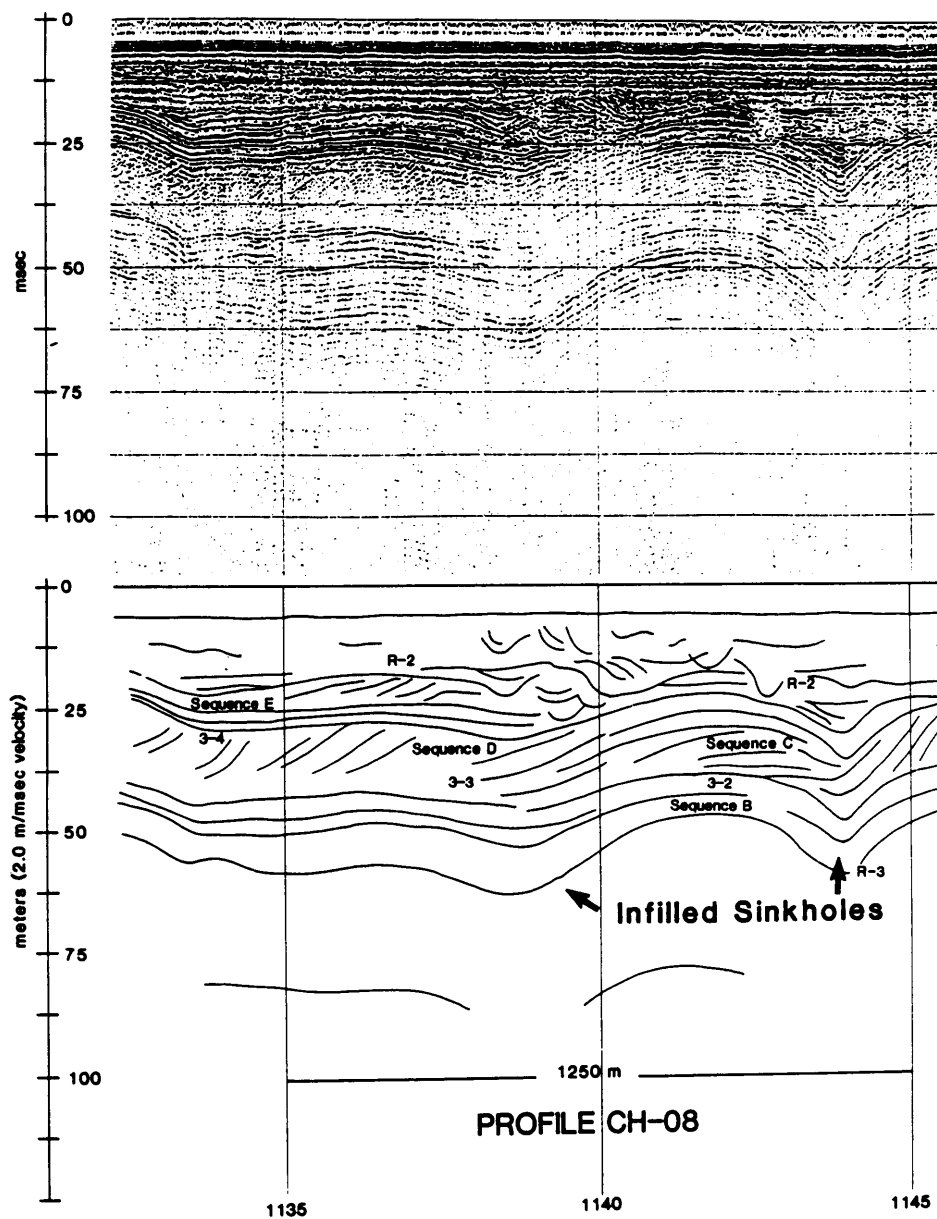


**Figure 3. Raw and interpreted seismic profiles**

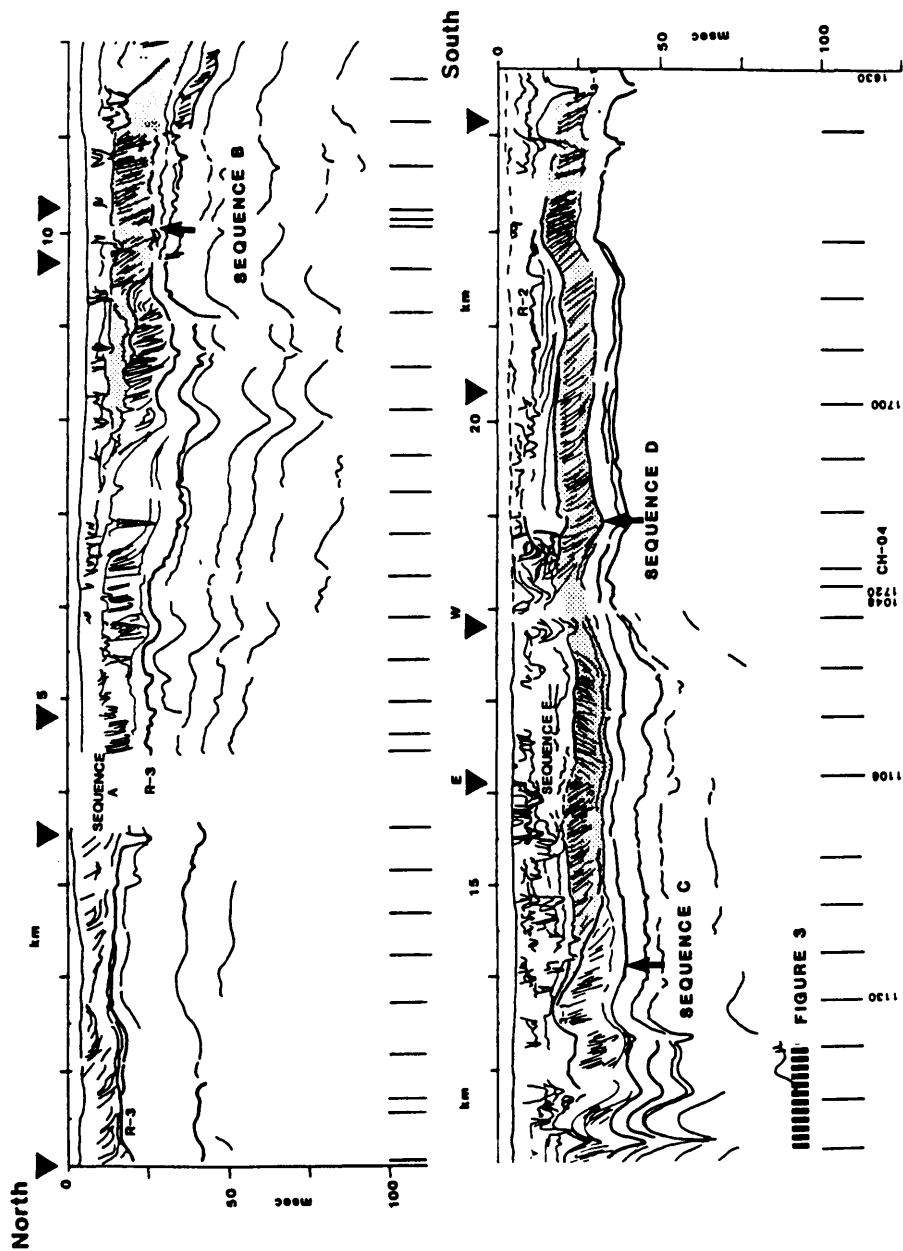


FIGURE 3

Figure 4. Interpreted seismic section H-H'

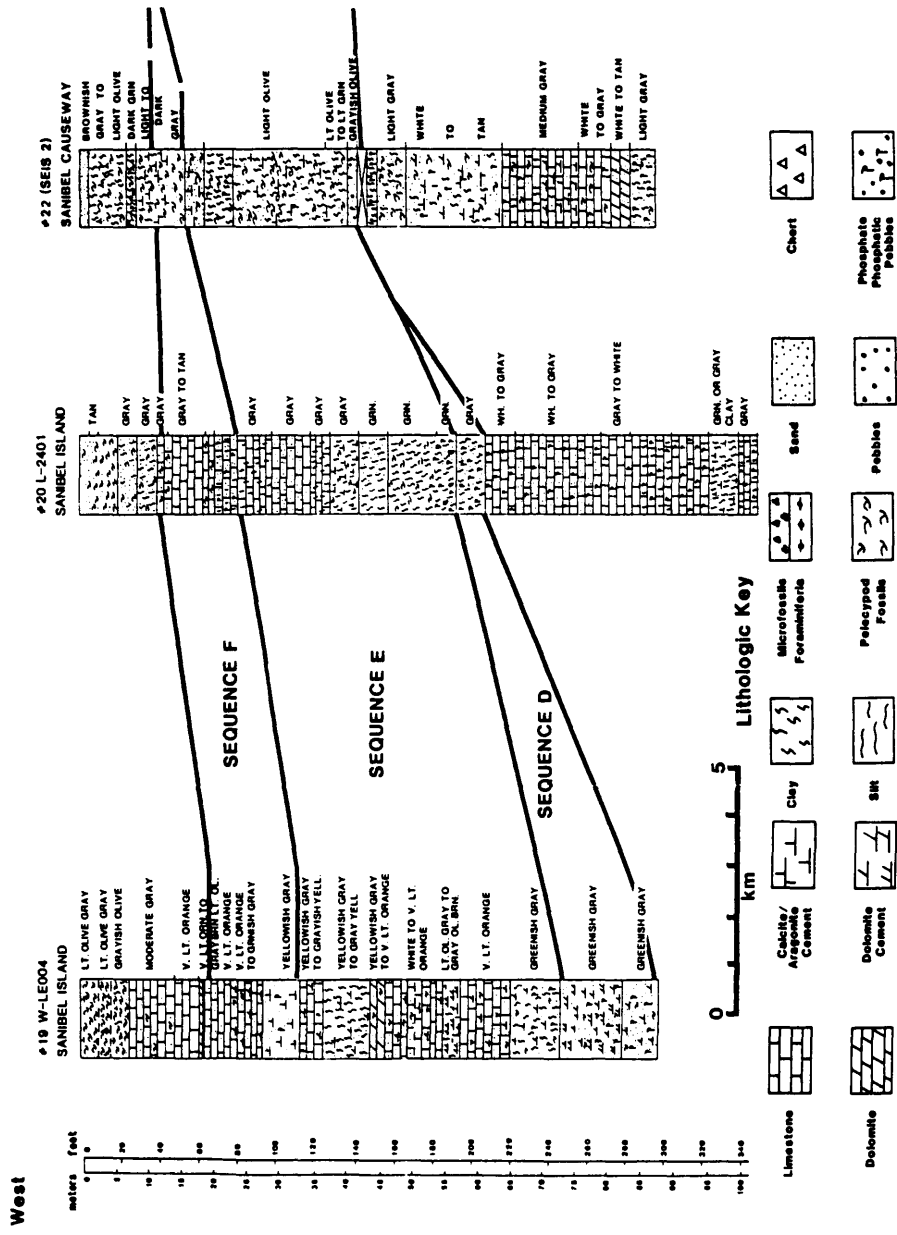
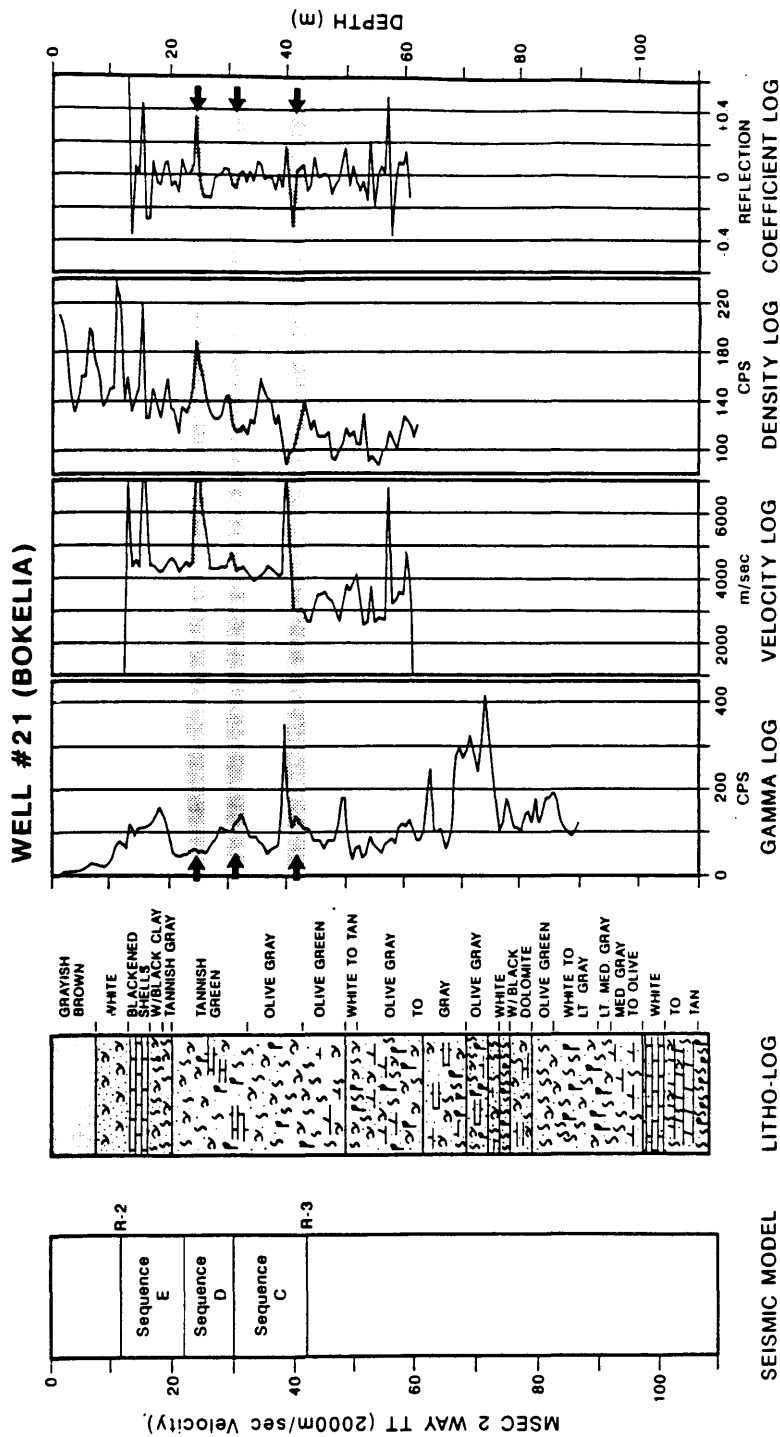


Figure 5. Lithologic cross section



**Figure 6. Seismic-lithologic sequence correlation**





## GEOCHEMICAL REACTIONS IN CARBONATE COASTAL AQUIFERS, CATALONIA, SPAIN

Xavier Bosch\*  
Emilio Custodio  
Manel Pascual\*\*

Polytechnic University of Catalonia/International Groundwater Hydrology Course,  
Barcelona, Spain

\*and Geological Service of Catalonia, Barcelona, Spain

\*\*and Water Authority of Catalonia, Lleida, Spain

### Abstract

Two well-known coastal areas in Southern Catalonia of northeast Spain have been selected for detailed studies on groundwater chemical behavior in carbonate formations. Carbonate mineral equilibrium in the freshwater-saltwater mixing zone has been studied in the Garraf and Vandellos areas, and also the water-air relationships in the thick vadose zone of Vandellos massif. Under the increasing groundwater salinity trend in the Garraf area, as a consequence of pumpage, mass balance studies show carbonate rock dissolution and a trend toward dolomitization, in spite of oversaturation periods being longer than subsaturation ones. Cation exchange plays a dominant role and fresh water chemical variations have a major influence in the results. In the Vandellos area, in carbonate sands, oxidation of organic matter, coupled with sulfate reduction control carbonate dissolution; ion exchange also has a contributing influence. In the same area, in hard carbonate formations, water infiltrating through the vadose zone is progressively enriched in dissolved inorganic carbon. This is a consequence aerobic oxidation of organic matter transported with vadose water; the subsequent decrease in oxygen has been observed.

### Introduction

Mixing of fresh water with marine salt water in coastal aquifers produces changes in carbonate mineral saturation as a consequence of the mixing itself and as a result of water-rock interactions (Plummer, 1975). Field studies in Florida and Yucatan (Back et al, 1979, 1986) and elsewhere involve limestones under given geological and climatological conditions, that led to calcite dissolution for a given interval of salinities in the mixing zone. This enhances coastal karst development. This has been modelled recently (Sanford and Konikow, 1989). In order to check if previous results can be considered common hydrogeological behavior in coastal aquifers, other areas have been studied. Some of the are in the Mediterranean Sea, such as the Greek islands, southern Turkey and Israel, in the Eastern area, Apullia (Italy) in the Central one, and Catalonia and the Balearic Islands (Mallorca island) in the Western area (Spain). Mallorca studies (Price, 1988), done under the same US-Spain Joint committee project, as the studies

presented in this paper involve Miocene calcarenites. In Catalonia, Jurassic and Cretaceous impure carbonate coastal formations, limestones and dolostones, have been selected, corresponding to the Southern Garraf and the Vandello massifs (fig. 1). Different papers (Custodio et al, 1986; Pascual and Custodio, 1987) comment on the main results obtained, which result from the doctoral dissertations of Bosch and Pascual, under the guidance of Custodio.

## Methodology

Existing or newly-drilled boreholes have been selected for repetitive sampling during a period of about two years. Water samples were obtained with either a depth sampling bottle or by suction pumping from shallow, short-screened tubes. Samples were filtered in the field, in situ measurement of pH, electrical conductivity, carbonate alkalinity temperature and in some cases, dissolved oxygen. The other major chemical constituents were determined in the laboratory in Barcelona as soon as possible by transporting the samples in tightly closed bottles in a cooled box.

Chemical equilibria with respect (to?) environmental minerals have been studied with the help of the WATEQF program (Plummer et al, 1984). Mass balance studies have been carried out with the BALANCE program (Parkhurst et al, 1982) and chemical behavior by means of the PHREEQE program (Parkhurst et al, 1980). The symbol, SI refers to saturation index for a given mineralogical species and is defined as the logarithm of the ratio of the ion activity product to the solubility product. Differences of  $\pm 0.3$  are not significant.

Actual groundwater composition is compared to the calculated results of closed-system mixing of two-end waters, fresh and marine or brackish water, referred as theoretical mixing. Proportion of mixing is deduced from chloride content, because it is assumed to be conservative.

In the vadose zone, air samples were taken with a gas pump. Oxygen and carbon dioxide percentages have been determined by gas chromatography or by using Draeger tubes. Also samples of vadose zone CO<sub>2</sub> were collected after precipitation as BaCO<sub>3</sub> for <sup>13</sup>C isotope analyses. Water and carbon isotope studies in water samples have been done, but are not considered here.

## The mixing zone in the Garraf study area

In the study area the Garraf carbonate massif is a thick sequence of limestone and dolomite formations of Cretaceous are with minor Miocene calcarenites in direct contact with the sea. Several studies provide the regional hydrogeological background (REPO, 1972; PHPO, 1985). Intensive exploitation of groundwater for urban and residential areas produces a continuously increasing salinization by sea-water intrusion. This situation differs from that of dynamic equilibrium, which is more commonly studied. Two existing PVC-cased boreholes were selected for study, one with only fresh water and the other penetrating the upper part of the mixing zone. Due to dominant landward groundwater flow at

the saline water bore, no freshwater layer is present, and the mixing zone extends to the water table. The vertical salinity gradient is maintained by local recharge. This gradient is also controlled by the distribution of heterogeneities along the bore (Custodio et al, 1988).

Systematic sampling in the brackish water borehole was done at three depths. The following comments refer to the shallowest one, 23 m deep, or about 2 m below the water table, where chemical changes over time are greatest.

Evolution of ionic strength over time is shown in figure 2. A seasonal variation of calcite and dolomite saturation indexes exists in the mixing water and in fresh water (fig. 3). Assuming a closed system with respect to  $\text{CO}_2$ , the comparison of the theoretical and actual evolution of calcite and dolomite saturation indexes shows no clear correlation. Oversaturation in winter and undersaturation during the summer, not only are explained by the variation of the activity coefficients due to the mixing of waters with different ionic strength, but also to other processes such as cation exchange. Clays from the impure carbonates provide the ion exchange capacity. The differences between theoretical and actual values of  $\log \text{PCO}_2$  and total dissolved inorganic carbon are thought to correspond with a system that is really open with respect  $\text{CO}_2$  at this shallow depth below the water table. There is an inflow of  $\text{CO}_2$  in summer, from the vadose zone, and an outflow of  $\text{CO}_2$  in winter, to the vadose zone. As a result, waters are undersaturated in summer and oversaturated in winter with respect to both calcite and dolomite.

The observed evolution of the parameters considered in the fresh water is thought to drive the evolution of the same parameters in the mixing water. A  $\text{Na}^+$  deficit is observed that does not equal the  $\text{Ca}^{++}$  excess (fig. 4). The Na deficit is greater in winter than in summer and the  $\text{Ca}^{++}$  excess does not match the winter  $\text{Na}^+$  deficit. This is thought to be due to Ca/Na exchange and to calcite precipitation during winter.

In the mixing zone, conditions are favorable for dolomitization of calcite to take place. The ratio  $\text{SI}_{\text{dol}}/\text{SI}_{\text{cal}}$ , dolomite over calcite, shows variable values in the mixing zone. In some instances it takes the right values for the formation of dolomite: calcite subsaturation and dolomite oversaturation. In fact there is always a  $\text{Mg}^{++}$  depletion in the mixing zone water.

The above mentioned processes are also supported by mass balance calculations (fig. 5). They show that calcite precipitation takes place in autumn, winter and spring, and that dissolution takes place in summer. Dolomite formation is more probably between summer and autumn. The Ca/Na ionic exchange takes place all the year round, although it is less important in summer.

Similar studies have been undertaken in more saline and deeper parts of the same water column. Contrary to what has been commented for the higher part of the mixing column, calcite dissolution and dolomite formation processes

are clearly more important than those of precipitation and dedolomitization at the 23 m depth. The results show that kinetics play an essential role because short subsaturation periods intercalated between longer oversaturation periods are enough to produce a net dissolution effect.

#### The mixing zone in the Vandellos study area

The Vandellos carbonate massif is formed by Jurassic and Cretaceous limestone and dolostone that contact the coast. Local hydrogeology is well known after studies done for the nuclear site (Bayo et al, 1976; Bosch and Custodio, 1987a). In a first stage of present studies, four steel-cased boreholes intersecting the fresh-saltwater mixing zone were selected. The vertical salinity distribution has been defined (Custodio, et al, 1988), but mineral equilibrium studies are not possible due to iron-water reactions inside these unpumped wells (Bosch and Custodio, 1987b).

To avoid these problems a small limestone sand beach at the mouth of the creek Barranco de Lleria was selected for detailed studies, because the mixing zone is shallow. Local recharge water is mainly runoff spreading on well-vegetated low lands with the upper soil layer rich in organic matter. A group of 28 mm diameter, PVC-cased wellpoints were set, each of them having the admission zone at different depths, so that when pumped they produce water with different percentages of seawater. Two sampling campaigns were performed: the first was after a heavy rainfall period (18.05.87), so that salinization was diminishing, and the second was after a long dry period (12.08.87), when salinity was increasing.

For water mixing calculations for a given sample, water samples from above and below were chosen as end members. This criterion is regarded to be more consistent with reality than selecting a relatively far freshwater spring and the sea water as end members.

Except for the two samples lowest in salinity, that are undersaturated with respect to dolomite, the rest of the samples are oversaturated with respect to the carbonate minerals. The SI increases with increasing salinity, except for low salinity samples. All the samples compared to their corresponding theoretical mixtures for any pair of end members considered show an increase of mass (fig. 6) due to mass transfer from the solid phase to the liquid phase.

All samples show a depletion of  $\text{SO}_4^{2-}$  which could be explained as a reduction of  $\text{SO}_4^{2-}$  to  $\text{H}_2\text{O}$ . This is consistent with the smell of the samples and the low dissolved oxygen, and the oxidation of organic matter. The water samples show high chemical oxygen demand (COD) - more than  $\text{H}_2\text{O}$ ,  $\text{NH}_4^+$ , and  $\text{Fe}^{2+}$  demand - thus pointing to dissolved organic matter, although no direct measurements have been attempted.

The  $\text{CO}_2$  input due to the oxidation of organic matter permits carbonate dissolution. This explains the  $\text{HCO}_3^-$  increase and some of the excess in  $\text{Ca}^{2+}$  in all the samples, and some of the excess in  $\text{Mg}^{2+}$  of the samples with low salinity. This is also consistent with the SI values.

The slight depletion of  $Mg^{++}$  versus  $Ca^{++}$  in the low salinity samples can be explained by  $Ca^{++}$  transfer from the liquid phase to the solid phase by ion exchange, so that can also explain the excess in  $Na^+$  of these samples. The more obvious depletion of  $Mg^{++}$  versus  $Ca^{++}$  in the higher salinity samples could be explained by reverse ion exchange due to the high concentration in  $Na^+$ . The depletion of  $Mg^{++}$  of the more saline samples could be explained by a dolomitization process, high dolomite SI. This would not create a depletion in  $Ca^{++}$  because of ion exchange that would supply more  $Ca^{++}$  because of ion exchange that would supply more  $Ca^{++}$  than that used in the dolomitization process.

This is consistent with the following overall process. Anoxic fresh water in equilibrium with carbonate minerals and containing organic matter mix with  $SO_4^{2-}$ -rich saline water. At the beginning of the mixing, organic matter is anaerobically oxidized by  $SO_4^{2-}$ , and  $H_2O$  and  $CO_2$  produces water become aggressive (SI<0) specially to dolomite, and  $HCO_3^-$ ,  $Mg^{++}$  and  $Ca^{++}$  increase. As water becomes more saline and the process has been going on using up all the organic matter, oversaturation (SI>0) relative to carbonates takes place, helped by ion exchange reactions.

Three groups of well points were set in the thick (30 to 100 m) vadose zone at three different sites of the Vandellos area to study the  $CO_2$  distribution in the gas phase at different depths. Four sampling campaigns were carried on. The same general trends are found in the different sampling campaigns. The percentages of  $CO_2$  (table 1) vary between 0.14 and 1.5, with a mean of 0.77. They show an increasing trend with depth; contrarily the  $O_2$  diminishes with depth. The  $\delta^{13}C$  values indicate that  $CO_2$  gets heavier with depth and  $\delta^{13}C$  also increases with increasing percentage of  $CO_2$  (fig. 7).

These results show the vadose zone to be a most active zone with respect to karstification. The high values of  $CO_2$  together with the large column of air in the vadose zone allows great volumes of percolating water to become aggressive to calcite and dolomite. The  $\delta^{13}C$  trend indicates that the origin of  $CO_2$  is the decay of organic matter; they get heavier with depth because they mix and equilibrate with heavy  $CO_2$  coming from the solid phase.

## Acknowledgements

The detailed studies have been done as project CCA 8308/007 of the US-Spain Joint Committee for Science and Technology. The cooperators are the U.S. Geological Survey, Complutense University of Madrid, and the Polytechnic University of Catalonia, jointly with the International Groundwater Hydrology Course, Barcelona. General background studies and complementary help have been provided by the Water Authority of Catalonia and the two Societies

exploiting the nuclear utilities in Vandellos. S. Balague did laboratory determinations.

**Table 1.- %CO<sub>2</sub>, %O<sub>2</sub> (volume) and  $\delta^{13}\text{C}$  in CO<sub>2</sub> from the unsaturated zone an in the Vandellós area in the three sites studied, in the four sampling campaigns.**

| SAMPLED<br>POINT | Depth<br>(m) | 1st camp. |       | 2nd camp. | 3rd camp. | 4th camp. |         | Mean<br>%CO2 |
|------------------|--------------|-----------|-------|-----------|-----------|-----------|---------|--------------|
|                  |              | % O2      | % CO2 | % CO2     | % CO2     | % CO2     | δ13-C   |              |
| T1-4             | -5.27        | 20.8      | 0.30  | 0.14      | 0.15      | 0.22      | -19.074 | 0.20         |
| T1-2             | -14.70       | 20.2      | 0.35  | 0.51      | 0.36      | 0.55      | -16.512 | 0.44         |
| T1-1             | -18.50       | 20.1      | 0.87  | 1.03      | 1.00      | 1.19      | -15.264 | 1.02         |
| T2-2             | -4.25        | 19.9      | 0.33  | 0.19      | 0.26      | 1.00      | -21.037 | 0.44         |
| T2-1             | -9.70        | 19.2      | 1.50  | 0.65      | 0.68      | 1.45      | -20.516 | 1.07         |
| T3-4             | -5.20        | 19.6      | 1.30  | 0.56      | 0.90      | 1.40      | -21.595 | 1.04         |
| T3-3             | -10.43       | 19.1      | 1.10  | 1.39      | 1.20      | 0.80      | -20.011 | 1.12         |
| T3-2             | -16.40       | 19.4      | 0.84  | 0.65      | 1.13      | 0.85      | -19.619 | 0.87         |
| T3-1             | -23.00       | 20.1      | 0.72  | 0.44      | 0.95      | 1.00      | -19.295 | 0.77         |
| Mean values:     |              | 19.82     | 0.81  | 0.62      | 0.74      | 0.94      | -19.214 | 0.77         |

## References

- Back, W., et al, 1979, Geochemical significance of groundwater discharge and carbonate solution to the formation of Caleta Xel Ha, Quintana Roo, Mexico, Water Resour. Res. 19, 1521-1535.
- Back, W., et al, 1986, Differential dissolution of a Pleistocene reef in the groundwater mixing zone of coastal Yucatan, Mexico, Geology 14., 137-40.
- Bayo, A., J., et al, 1976, Estudio geológico del macizo de Vandellos para definir sus características hidrogeológicas, Hidrogeología y Rec. Hidráulicos, I, 89-107.
- Bosch, X., E. Custodio, 1987a, Interpretación de datos de isótopos ambientales (D y O-18) de muestras de aguas subterráneas del acuífero carbonatado costero del macizo de Vandellos en las zona del Coll de Balaguer, T. M. de Vandellos (Tarragona). II Jornadas de Geoquímica, Soria, Colegio de Geólogos de España, Madrid, 67-70.
- Bosch, X., E. Custodio, 1987b, Alteración de la alcalinidad en muestras de agua procedentes de piezómetros entubados con hierro en un acuífero carbonatado afectado por intrusión marina, efecto de la corrosión del hierro sobre la concentración del ion  $\text{HCO}_3$ , Hidrogeología y Recursos Hidráulicos, XII, 197-206.
- Custodio, E., et al, 1988, Processes in the mixing zone in carbonate formations, Central and Southern Catalonia, Natuurwet. Tijchr, Ghent, 70, 263-277.
- Parkhurst, D. L., et al, 1980, PHREEQUE- a computer program for geochemical reactions, U.S. Geological Survey, Water Res. Investigations, 80-96, 210.
- Parkhurst, D. L., et al, 1982, BALANCE-a computer program for calculating mass transfer for geochemical reactions in groundwater, U.S. Geological Survey, Water Resources Investigations, 82-14, 29 pp.
- Pascual, M., E. Custodio, 1987, Procesos hidrogeoquímicos en la zona de mezcla agua dulce-agua salada en el litoral del extremo meridional del macizo carbonatado de Garraf (Tarragona), Hidrogeología y Rec. Hidráulicos, XI, 477-492.
- PHPO, 1985, Informe sobre los recursos de agua subterránea del Penedes y del macizo de Garraf, Plan Hidrológico del Pirineo Oriental, confederación Hidrográfica del Pirineo Oriental, Barcelona.

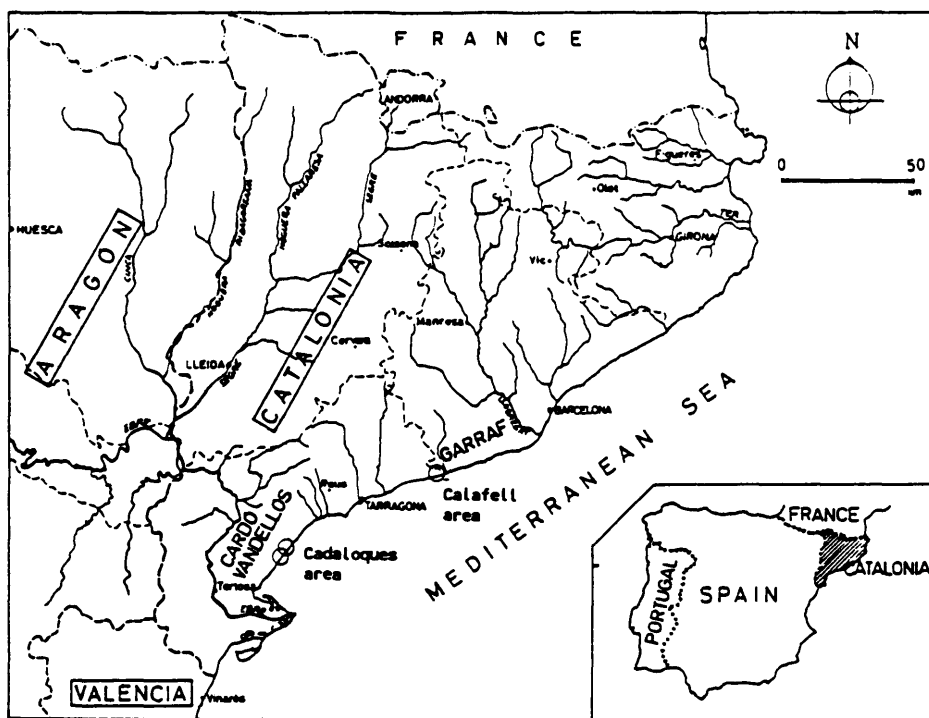


Figure 1. Location of the study sites in Catalonia (northeast Spain). The selected areas are Calafell, in southwest Garraf Massif, and Cadaloques in the Vandellos Massif, that comprise the Coll de Balaguer and Cala Jostell sites.



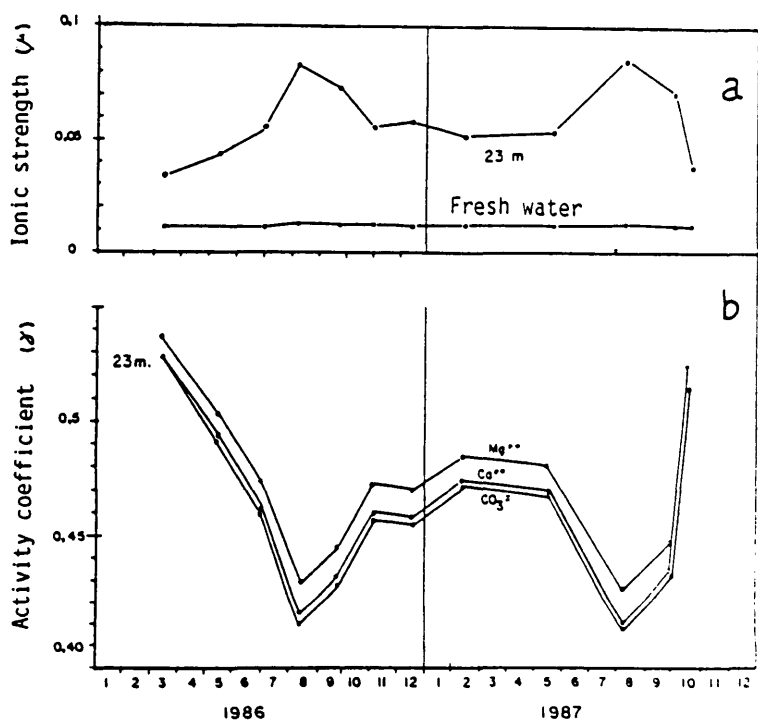


Figure 2. Evolution of chemical characteristics over time in Garraf boreholes. (a) ionic strength in the freshwater borehole and at 23 m depth in the saline water one; (b) activity coefficient of Mg, Ca, and  $CO_3$  ions at 23 m depth in the saline water borehole.

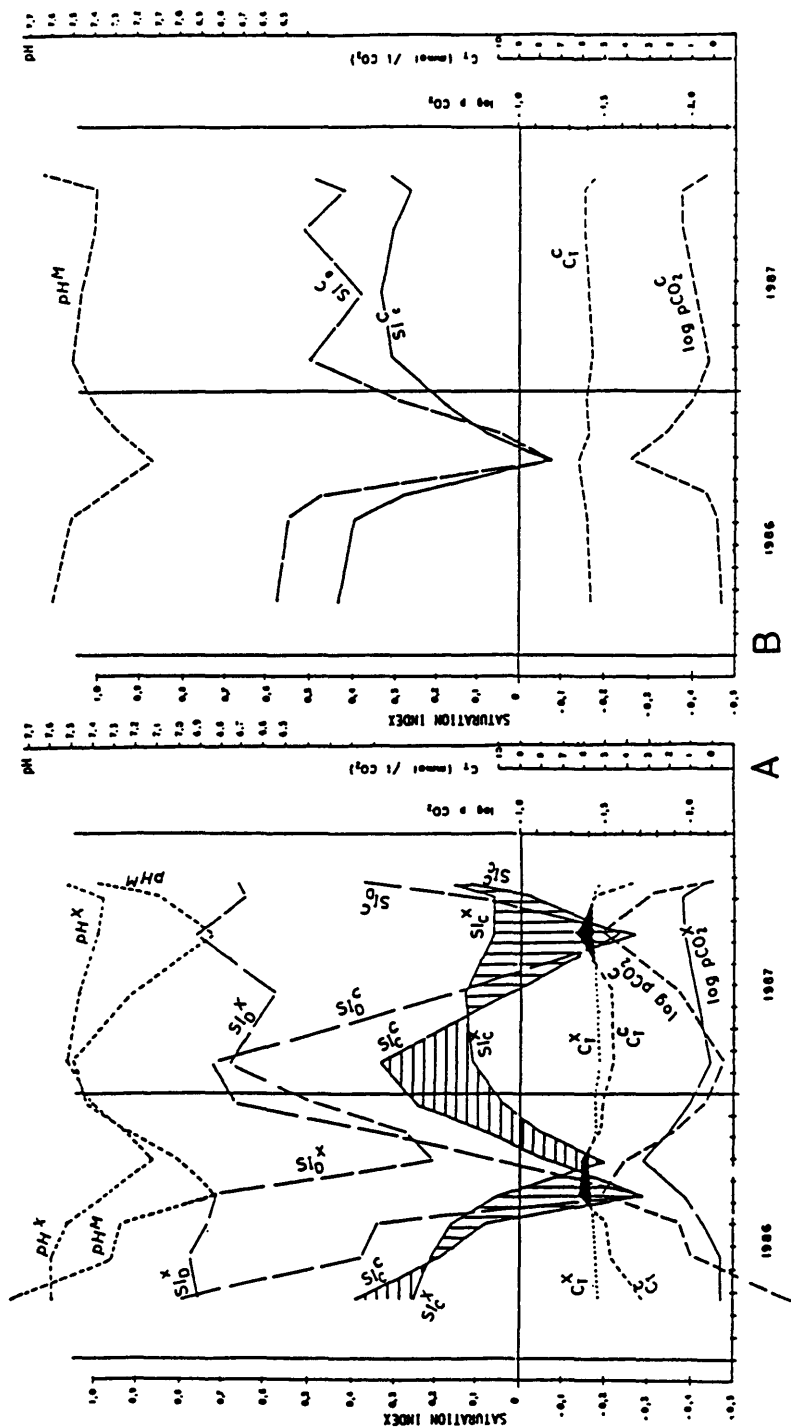


Figure 3. Evolution of calcite and dolomite saturation indexes (logarithmic),  $\log P_{CO_2}$ , total dissolved inorganic carbon and pH over time in Garraf boreholes. A. in saline water at 23 m depth; B. in the fresh-water borehole. M indicates measured; C calculated from analytical data and X the theoretical mixture of salt and freshwater according with sample  $Cl^-$  content.

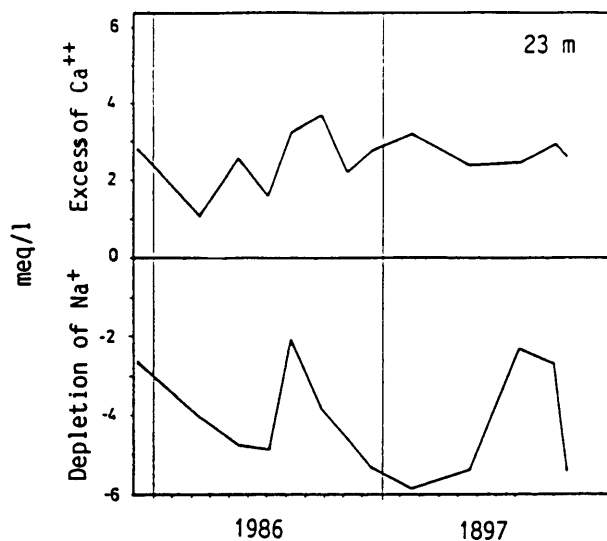


Figure 4. Evolution of  $\text{Ca}^{++}$  excess and  $\text{Na}^+$  depletion over time (actual values less theoretical values from closed system mixtures of local freshwater with local seawater) in mixed water from Garraf saline water borehole, at 23 m depth, about 2 m below the water table.

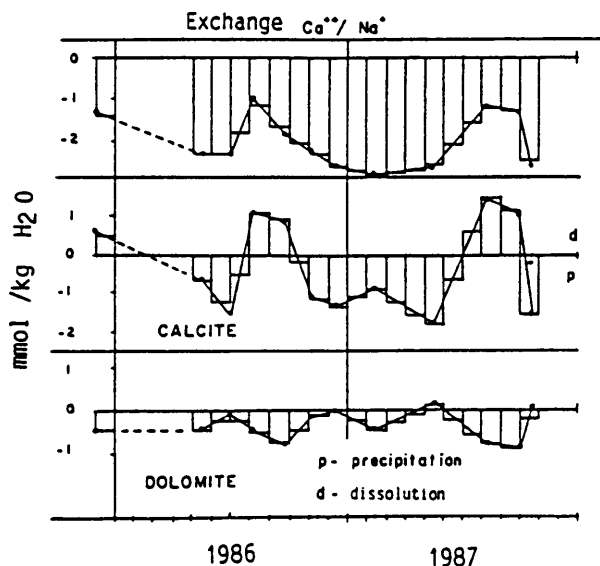


Figure 5. Evolution of mass balance over time as 23 m depth in mixed water in the Garraf saline borehole. The assumed processes are calcite and dolomite precipitation/dissolution, and Ca/Na ion exchange.

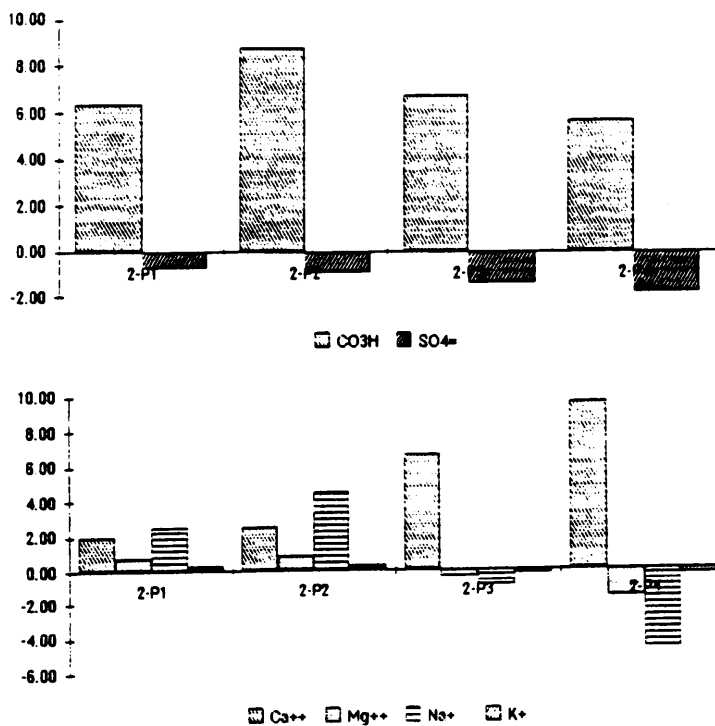


Figure 6. Difference between actual and theoretical values (in meq/l) in the point boreholes in Cala Jostell area (Vandellos Massif) using as end members the least and most saline water samples (boreholes P-1, period 1, and P-5, period 2, respectively).

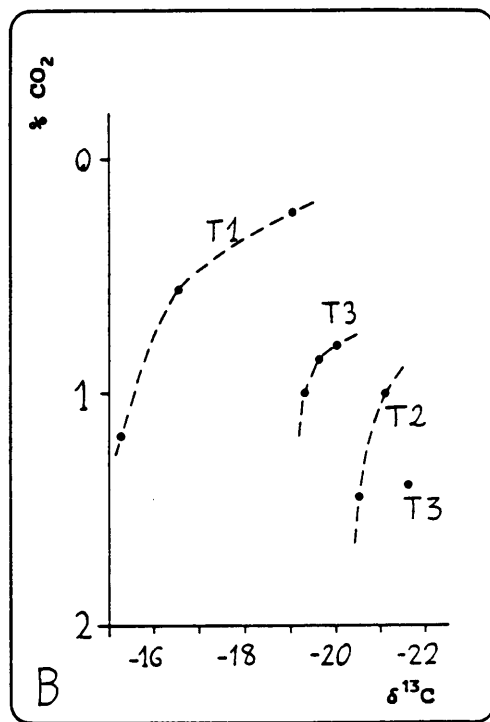
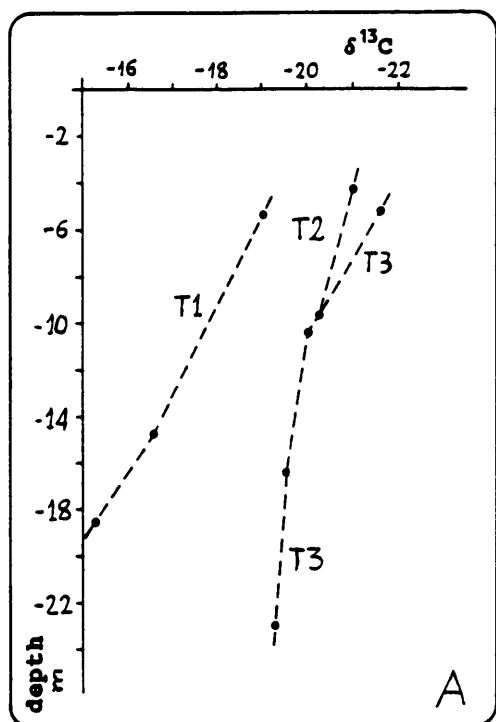


Figure 7. Results of unsaturated zone air sampling in the Vandellos area. A.  $\delta^{13}\text{C}$  profiles;  $\text{CO}_2$  becomes heavier with depth. B. Plot of  $\delta^{13}\text{C}$  versus  $\%\text{CO}_2$  (volume);  $\text{CO}_2$  increases produce a heavier  $\text{CO}_2$  gas. T1, T2, and T3 are the three sampling areas.



### SECTION 3: GEOCHEMISTRY AND ISOTOPE HYDROLOGY





## ULTRABASIC GROUNDWATERS OF THE ZLATIBOR ULTRAMAFIC MASSIF

Petar Papic and Neven Kresic

University of Belgrade  
School of Mining and Geology  
Djusina 7, 11000 Belgrade, Yugoslavia

**Abstract:** In this paper, we describe ultrabasic groundwaters of the Zlatibor ultramafic massif, the largest one in Yugoslavia, and among the largest ones in Europe. In previous scientific reports, only a few of such specific natural phenomena are described. The significance of Zlatibor ultrabasic groundwaters is mainly in their chemical composition: chemical and hydroxyl ions prevail, and the pH value reaches 11.76. The concentrations of other ions are negligible, so that these waters represent "pure" ultrabasic waters of Ca-OH type.

### Geology

The Zlatibor ultramafic massif is a Jurassic plate body divided into tectonic blocks of different thicknesses, from about 100 m to over 1000 m. The whole massif is cut by regional ruptures and systems of penetrating fractures. The Zlatibor is mainly of harzburgite composition, with appearances of lherzolite, dunite, and their serpentinites. Completely serpentinitized peridotites are rare and appear in the peripheral parts of the massif or in the tectonically disturbed zones.

The characteristic mineral composition of serpentinite in the area of Kremna, in which the first appearance of ultrabasic water was discovered, is the following: fibrous serpentine prevails, originating from olivine and rhombic pyroxenes that are completely metamorphized and transformed in bastite. The rocks are cut with little veins of secondary chlorite and calcite. The excess iron occurs as magnetite dust, dispersed in serpentine or as magnetite grain clouds.

The mineral composition of slightly serpentinitized harzburgites forming the areas of Ribnica and Crni Rzav rivers (where the most important ultrabasic groundwaters were discovered), olivine prevails completely. There are also rhombic pyroxenes, while monoclinic pyroxenes, fibrous serpentine, and bastite are rare. The rocks are intensively tectonized, as shown by warped lamellas of monoclinic pyroxenes along the slip cleavage surfaces of rhombic pyroxenes.

The chemical analyses of the rocks show typical amounts of silica and magnesium, and the iron component indicates that olivine corresponds to forsterite. The rocks contain about 0.5% of CaO by weight (Table 1).

### Hydrogeology

The Zlatibor massif, as a whole, is not a terrain rich in groundwater. The discharge of springs generally less than 1 l/s, and appear widely scattered in erosional scarps. However, in tectonically disturbed zones, exploratory drilling discovered groundwater at depths 60 m below the surface. All known springs of ultrabasic waters appear grouped along riverbeds or periodically flooded zones of

Table 1. Chemical Analyses of Rocks (in percentages)

| SiO <sub>2</sub> | Fe <sub>2</sub> O <sub>3</sub> | CaO  | MgO  |
|------------------|--------------------------------|------|------|
| <u>Kremna</u>    |                                |      |      |
| 35.85            | 8.92                           | 0.42 | 36.4 |
| <u>Ribnica</u>   |                                |      |      |
| 37.34            | 9.40                           | 0.56 | 41.6 |

deeply scarped rivers (Matijasevica River, Ribnica, and Crni Rzav rivers). The parts of valleys in which ultrabasic waters occur are associated with regional faults, clearly visible on aerial photos and scanograms. Among the fracture sets, one with a gaped slit (up to 4 cm) and crossing the streams perpendicularly, is the most important for groundwater discharge. Discharge of all ultrabasic springs is under pressure, and the water contains bubbles of nitrogen. The minimum discharge of discovered springs in the most significant zone (Ribnica River) is estimated at 2 l/s.

#### Hydrogeochemistry

As a consequence of the chemical composition of water-bearing rocks, groundwaters are mainly of the basic Mg-HCO<sub>3</sub> type (Kresic and Papic, in press). The chemical composition of ultrabasic waters near Kremna and in the Ribnica River is characterized by the domination of calcium and hydroxyl ions and by pH values over 11.5. The amounts of silica and magnesium are under 1 mg/dm<sup>3</sup>, and the sum of the ions is up to 125 mg/dm<sup>3</sup>. Specific conductivities exceed several times the results expected on the basis of ion sum (the equivalent ion conductivity of hydroxyl ions is 198 S/cm eqv. compared to 44 S/cm eqv. for hydrocarbonate ions). As can be seen by Table 2, we are describing calcium-hydroxyl ultrabasic waters without significant amounts of other constituents, such as sodium chloride in the case of ultrabasic waters described in the literature (Barnes et al., 1967, 1978).

Water aggressiveness against a given mineral is estimated by thermodynamic analysis and expressed by the index of aggressiveness A. It is defined as the logarithm of the ratio of the equilibrium constant K° and the reaction quotient Q. K° values are determined from the free energies of formation of the minerals (Helgeson et al., 1978). As the index A increases, the degree of the nonequilibrium of the given system increases, as does the water aggressiveness toward a considered mineral. The ultrabasic waters are oversaturated with respect to serpentine, forsterite, brucite, and talc and are unsaturated with respect to quartz and enstatite (Table 3).

A diagram of the stability fields of the minerals shows the position of meteoric waters, waters of Mg-HCO<sub>3</sub> composition, and ultrabasic waters (Figure 1). Meteoric waters are aggressive toward a number of minerals, basic waters of Mg-HCO<sub>3</sub> composition are in equilibrium with serpentine, and ultrabasic waters are close to equilibrium with enstatite and quartz and are oversaturated with brucite, serpentine, and forsterite.

Table 2. Chemical Analyses of Groundwaters (in mg/dm<sup>3</sup>).

|                        | mg/dm <sup>3</sup> |                               | mg/dm <sup>3</sup> |
|------------------------|--------------------|-------------------------------|--------------------|
| <u>Kremna</u>          |                    |                               |                    |
| Ca <sup>2+</sup>       | 36.00              | Na <sup>+</sup>               | 2.00               |
| Mg <sup>2+</sup>       | 0.20               | K <sup>+</sup>                | 0.25               |
| OH <sup>-</sup>        | 30.60              | Cl <sup>-</sup>               | 2.15               |
| SiO <sub>2</sub>       | 0.50               | SO <sub>4</sub> <sup>2-</sup> | 0.20               |
| pH                     | 11.50              | Sum of ions                   | 71.93              |
| t, °C                  | 12                 | Conductivity                  | 490 μS/cm          |
| <u>Ribnica</u>         |                    |                               |                    |
| <u>Ca<sup>2+</sup></u> | <u>60.80</u>       | <u>Na<sup>+</sup></u>         | <u>5.00</u>        |
| Mg <sup>2+</sup>       | 0.15               | K <sup>+</sup>                | 0.70               |
| OH <sup>-</sup>        | 54.20              | Cl <sup>-</sup>               | 3.20               |
| SiO <sub>2</sub>       | 0.65               | SO <sub>4</sub> <sup>2-</sup> | 0.20               |
| pH                     | 11.76              | Sum of ions                   | 124.90             |
| t, °C                  | 15                 | Conductivity                  | 815 μS/cm          |

Table 3. Index of Aggressiveness for Ultrabasic Water

|                 | <u>Mineral</u> |      |     |     |
|-----------------|----------------|------|-----|-----|
|                 | Se             | Fo   | Q   | En  |
| <i>AKremna</i>  | -10.5          | -1.7 | 1.1 | 1.4 |
| <i>ARibnica</i> | -12.0          | -2.6 | 1.0 | 0.4 |

Figure 2 shows a schematic view of conditions controlling the formation of ultrabasic waters. In general, these ultrabasic waters are formed by chemical interactions between deeply circulating meteoric waters and the rocks through which these waters circulate. In a first phase, meteoric waters react with serpentine or forsterite, producing basic  $\text{Mg-HCO}_3$  groundwater with a pH value of about 8.5. Deep circulation limits carbonaceous weathering, but hydrolytic processes cause pH to increase. The waters become oversaturated with respect to magnesite and then to brucite. Continuing hydrolysis removes calcium from minerals, giving rise to ultrabasic waters of  $\text{CaOH}$  type which are in an equilibrium (or close to an equilibrium) with enstatite.

The Zlatibor ultrabasic groundwaters are important because they represent "pure" ultrabasic waters of  $\text{CaOH}$  type, and especially because of their uses in balneotherapy, including external and internal uses in the treatment of kidney stones, acid gastritis, and psoriasis. There is also a possibility to bottle the water; it is chemically stable and bacteriologically sterile.

#### Acknowledgments

The authors would like to thank Dr. Vidojko Jovic, Miroslav Komljenovic, and colleagues from the Laboratory for Microbiological Chemistry from the Faculty of Sciences at Belgrade for their assistance in mineralogical, chemical, and bacteriological analyses of many rocks and water samples from Zlatibor massif.

#### References

- Barnes, I., V.C. LaMarche, Jr., and G. Himmelberg, 1967, Geochemical evidence of present-day serpentinization, *Science*, 156, pp. 830-832.
- Barnes, I., J.R. O'Neil, and J.J. Trescases, 1978, Present-day serpentinization in New Caledonia, Oman and Yugoslavia, *Geochim. Cosmochim. Acta.*, 42, pp. 144-145.
- Helgeson, H.C., J.M. Delany, H.W. Nesbitt, and D.K. Bird, 1978, Summary and critique of the thermodynamic properties of rock-forming minerals, *American Journal of Science*, 278-A, 1-229.
- Kresic, N., and P. Papic, (in press), Specific chemical composition of karst groundwaters in the Ophiolite Belt of the Yugoslav Inner Dinarides: a case of covered karst, *Environmental Geology*.

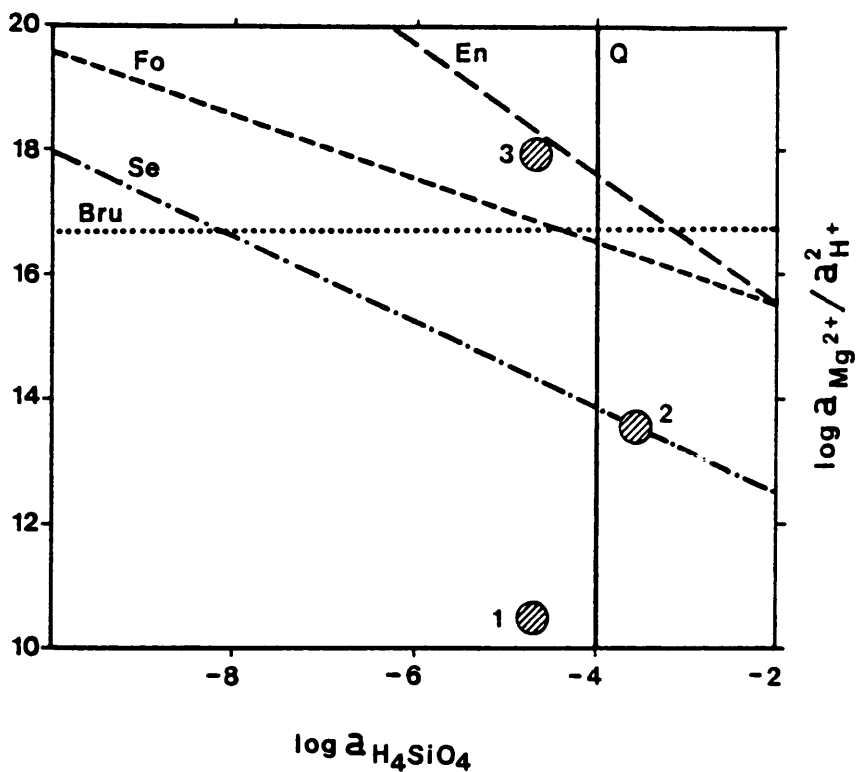


Figure 1. Stability diagram of the system  $\text{MgO-SiO}_2\text{-H}_2\text{O}$  at  $25^\circ\text{C}$ : 1. Meteoric waters, 2. Groundwaters of  $\text{Mg-HCO}_3$  type, and 3. Ultrabasic groundwaters, Q-quartz, Bru-brucite, Se-serpentine, Fo-forsterite, and En-enstatite.

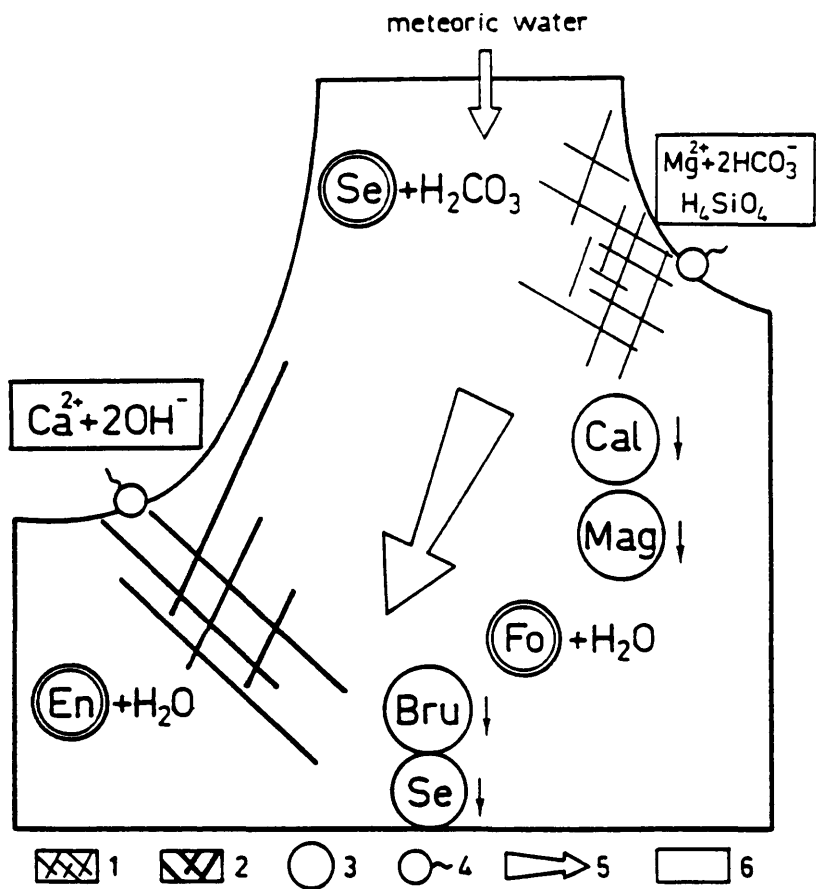


Figure 2. Schematic presentation of conditions controlling formation of ultrabasic groundwater: 1-serpentinite, 2-harzburgite, 3-mineral, 4-spring, 5-water flow direction, and 6-groundwater chemistry.

# THE RETENTION OF Cd, Pb AND Zn BY FRACTURED SHALE UNITS:

## SIMULATION OF REACTIVITY IN THE UNCONSOLIDATED ZONE.

Ernest E. Angino and Cindy K. Wilbur  
Department of Geology  
University of Kansas  
Lawrence, KS 66045

### ABSTRACT

Fractured shale units similar in composition to the Heebner and Snyderville shales commonly found in the unsaturated zone in eastern Kansas can act as effective barriers between the water table and trace amounts of  $\text{Cd}^{2+}$ ,  $\text{Pb}^{2+}$ , and  $\text{Zn}^{2+}$  leached from a concentrated metal source e.g. a sanitary landfill or fly ash pile. Packed columns of Snyderville Shale retained 100% of  $\text{Cd}^{2+}$ ,  $\text{Pb}^{2+}$ , and  $\text{Zn}^{2+}$  from simulated rainwater (pH - 5.80) that contained 0.1, 1.0, and 10 ppm of these metals. Packed columns of Heebner Shale retained between 66% and 100% of these trace metals. The amount of trace metal retained by the Heebner Shale increased with increasing initial  $\text{Cd}^{2+}$ ,  $\text{Pb}^{2+}$ , and  $\text{Zn}^{2+}$  concentration in the leaching solution. A combination of adsorption and precipitation reactions were probably responsible for the retention of  $\text{Cd}^{2+}$ ,  $\text{Pb}^{2+}$ , and  $\text{Zn}^{2+}$  by the shales.

### INTRODUCTION

A key problem related to groundwater pollution concerns the leaching and migration of trace metals from sanitary landfills or other concentrated sources to the water table. It is important to know what reactions take place as water containing these leached metals migrates downward through fractured rock units in the unsaturated zone. Much information is available on the adsorption of trace-metals by soils and clay minerals; however, little research has been done on the retention of trace-metal contaminants by rock units in the unsaturated zone. It is therefore important to determine what differences may exist between the retention of trace metals by rocks, soils, and clay minerals. Retention is used in this paper to mean a decrease in ion concentration in column effluent.

The purpose of this investigation was to examine what happens to Cd, Pb, and Zn ions in solution as they pass through shale strata in the unsaturated zone. In order to gain an understanding of what reactions might take place between the trace metals and the shale, the simultaneous leaching of  $\text{Ca}^{2+}$  and  $\text{Mg}^{2+}$  from the shales was also examined. This problem was addressed using shale-packed columns to simulate fractured shale layers in the unsaturated zone. Distilled, deionized water (pH 5.80) was used to simulate rainwater. The study was done in two parts. The first part referred to as leaching experiments, examined the leaching of  $\text{Ca}^{2+}$ ,  $\text{Mg}^{2+}$ ,  $\text{Cd}^{2+}$ ,  $\text{Pb}^{2+}$ , and  $\text{Zn}^{2+}$  from the Snyderville and the Heebner shales as a function of leaching solution pH.

The Heebner and Snyderville shales, members of the Shawnee Group of Late Pennsylvanian age, crop out in eastern Kansas and are present in the subsurface farther west (Zeller, 1983). The Heebner is a black, platy shale that contains thin phosphate-rich seams. This shale was chosen for study

because it typifies black shales found throughout the U.S. The Snyderville, a gray to green, structureless shale, was chosen because it is relatively homogeneous and has a high swelling clay content. These leaching experiments were performed to obtain background values for the amount of  $\text{Cd}^{2+}$ ,  $\text{Pb}^{2+}$ , and  $\text{Zn}^{2+}$  leached from the Snyderville and Heebner shales. The second part, referred to as trace-metal retention experiments, examined retention of  $\text{Cd}^{2+}$ ,  $\text{Pb}^{2+}$ , and  $\text{Zn}^{2+}$  ions by the Heebner and Snyderville shale as a function of trace-metal concentration of the leaching solution.

Cadmium, Pb, and Zn were chosen for study because they are common in leachate from sanitary landfills and because Pb and Cd are hazardous pollutants in the environment. Too much of these trace metals, however, can be highly toxic, and a narrow safety window exists between essential and toxic levels. A knowledge of the reactions between these trace metals and shale in the unsaturated zone is critical to ensuring the quality of groundwater supplies.

## MATERIALS AND METHODS

### Rock Sampling and Preparation

Large quantities of the Heebner and Snyderville shales were collected from the center, Sec. 35, T11S, R19E Jefferson County Kansas. Samples of Heebner Shale were collected 1 m above its base, and the Snyderville Shale was collected from the middle of the unit. After collection, bulk shale samples were mixed, passed through a jaw crusher, and sieved into four size fractions (8-4, 4-2, 2-1, and 1-1/2 mm respectively).  
Analysis of Shales.

Each size fraction of shales were examined by X-ray diffraction to determine if significant mineralogical differences existed between the size fractions of each shale. The organic and volatile content of the shales were measured using standard procedures. The major and minor elemental content of the shales was determined by XRF techniques. Results of experimental design indicated that a sample size of five was needed to determine a difference of 20 ppm  $\text{Ca}^{2+}$  in the Snyderville Shale leachate if it were to exist. Five replications were adequate to see environmentally interesting differences in leachate for other elements.

Several statistical tests (null hypothesis, T-method and Kruskal-Wallis, see Sokal and Rohlf, 1981 pp. 211, 430 and 246 respectively) were performed to determine whether pH, trace metal species, or trace-metal concentration of leaching solution caused a statistically significant difference in the leaching of Ca and Mg or in the retention of Cd, Pb, and Zn by the shales. For analytical and statistical details see Wilbur, 1987.

### Leaching Experiments

Leaching experiments were designed to examine the leaching of  $\text{Ca}^{2+}$  and  $\text{Mg}^{2+}$  and of  $\text{Cd}^{2+}$ ,  $\text{Pb}^{2+}$ , and  $\text{Zn}^{2+}$  from the Heebner and Snyderville shales as a function of leaching solution pH. Leaching was studied using packed glass columns 55 cm long and about 5 cm in dia., filled with approx. 625 g of the Snyderville Shale or 500 g of the Heebner Shale, Figure 1.



Distilled, deionized water was used as the leaching solution, and solution pH's were adjusted to 5.8, 6.5, 7.0, 7.5, or 8.5 using small amounts of  $\text{NH}_4\text{OH}$ . Leaching solution was poured into the column until the shale was saturated and the solution top was 5 cm below the top of the column. In the Snyderville Shale experiments leaching solution was allowed to flow through the column until about 7 to 45 ml of water was collected. It was not necessary to clamp the tube at the bottom of the column because swelling of the Snyderville Shale slowed the rate of water flowing through the shale. Sample-collection period varied from 5-63 days. In experiments on the Heebner Shale a clamp was placed at the top of the column tubing in order to slow the rate of flow. Five replications were made of each experiment. Leaching solution was left standing in the column for two days and was then slowly dripped through the Heebner Shale for 24 hrs.

After the leachate sample was collected, it was immediately tested for pH and then centrifuged for 20 min. The sample volume was measured and recorded, and then returned to a tightly capped collection bottle for analysis, within 48 hours. For details, refer to Wilbur and Angino, 1988.

#### Trace-metal Retention Experiments

Trace-metal retention experiments were designed to study the retention of  $\text{Cd}^{2+}$ ,  $\text{Pb}^{2+}$ , and  $\text{Zn}^{2+}$  ions by the Snyderville and Heebner shales as a function of trace-metal concentration in the leaching solution. These experiments used the same techniques as the leaching experiments. Leaching solutions were spiked with 0.1, 1.0, and 10 ppm of Cd, Pb, or Zn from stock solutions of  $\text{Cd}(\text{Cl}_2)$ ,  $\text{Zn}(\text{Cl})_2$ , and  $\text{Pb}(\text{NO}_3)_2$  (Greenberg et al., 1985, p. 157). The pH of the leaching solution was adjusted to approximately 5.8 using a small amount of  $\text{NH}_4\text{OH}$ .

#### Leaching Experiments on Shale Charges with Trace Metals

Leaching experiments on trace-metal charged shale were performed to determine how easily previously retained trace-metals could be leached from the Heebner Shale. After trace-metal-retention experiments with the Heebner Shale with leaching solutions of 0.1, 1.0, and 10 ppm  $\text{Cd}^{2+}$  and 1.0 and 10 ppm  $\text{Zn}^{2+}$  were completed, the shale was removed from the columns, dried, and replaced in the columns. The shale in the columns was then leached again with distilled, deionized water at pH 5.8, using the method described previously. The leachate was analyzed for  $\text{Cd}^{2+}$  or  $\text{Zn}^{2+}$  and  $\text{Ca}^{2+}$  and  $\text{Mg}^{2+}$  using atomic absorption spectrometry techniques and appropriate standards (Greenberg et al. 1985, p. 157).

## RESULTS AND DISCUSSION

### Results of Shale Analysis

No difference in mineralogy between the different size fractions of the Heebner and Snyderville shales were detected by X-ray diffraction. The measured organic content of the Heebner Shale was 21.1%, and that of the Snyderville shale was 3.7%.

## Results of Leaching Experiments

No Detectable Cd, Pb, or Zn was leached from the Snyderville Shale in the leaching experiments. Detection limits, respectively, were 0.002, 0.004, and 0.05 ppm. Leachate from the Snyderville Shale had an average pH of  $8.9 \pm 0.04$  regardless of the pH of the initial leaching solution or the rate of flow of the leaching solution. Initial pH of the leaching solution likely had an effect on the concentration of  $\text{Ca}^{2+}$  and  $\text{Mg}^{2+}$  leached from the Snyderville Shale despite the apparent lack of variation in the final pH of the leachate. More  $\text{Mg}^{2+}$  and  $\text{Ca}^{2+}$  were leached from shale columns that initially contained leaching solution at pH 7.0 than at pH 5.8. Less Ca and Mg were leached from pH 7.0 to pH 8.5. These were found to be significant differences. Two separate mechanisms are probably responsible for the increases and decreases. Flow rate and volume of the leachate had no apparent effect on the amount of  $\text{Ca}^{2+}$  and  $\text{Mg}^{2+}$  leached from the Snyderville Shale. The amount of Ca and Mg leached from the Heebner Shale is about 200 times that leached from the Snyderville Shale.

## Results of Trace-Metal Retention Experiments

Distilled, deionized water (pH - 5.8) spiked with 0.1, 1.0, and 10 ppm of  $\text{Cd}^{2+}$ ,  $\text{Pb}^{2+}$ , and  $\text{Zn}^{2+}$  from  $\text{Cd}(\text{Cl})_2$ ,  $\text{Zn}(\text{Cl})_2$ , or  $\text{Pb}(\text{NO}_3)_2$  solutions were independently leached through columns containing Snyderville and Heebner shales. The leachate from the Snyderville Shale contained no detectable  $\text{Cd}^{2+}$ ,  $\text{Pb}^{2+}$ , or  $\text{Zn}^{2+}$ . In general more  $\text{Pb}^{2+}$  and  $\text{Cd}^{2+}$  were retained by the Heebner Shale than  $\text{Zn}^{2+}$ . The total amount of Cd, Pb, and Zn retained by the Heebner Shale increased with increasing metal concentration in solution.

$\text{Cd}^{2+}$ ,  $\text{Pb}^{2+}$ , and  $\text{Zn}^{2+}$  were likely retained by the Snyderville and Heebner shales through a combination of precipitation reactions and adsorption. A white precipitate formed on the top of Snyderville Shale columns that contained leaching solution with 10 ppm of  $\text{Cd}^{2+}$ ,  $\text{Pb}^{2+}$ , or  $\text{Zn}^{2+}$ . The precipitate began to form immediately after the leaching solution was added to the columns. It was not possible to identify the precipitates through x-ray diffraction. Precipitation was more likely to be a mechanism for retention of Cd, Pb, and Zn ions by the Snyderville Shale than for the Heebner Shale because the leachate from the Heebner Shale had a lower final pH. The solid hydroxide and carbonate species of Cd, Pb, and Zn that may form precipitates under these experimental conditions are  $\text{Zn}(\text{OH})_2$ ,  $\text{Cd}(\text{OH})_2$ ,  $\text{ZnCO}_3$ ,  $\text{CdCO}_3$ , and  $\text{PbCO}_3$ . Solubility calculations at pH 8.9 (Snyderville leachate) and 7.9 (Heebner leachate) indicate that  $\text{Cd}(\text{OH})_2$  ( $\log K_{\text{sp}} = -14.4$ ) is not expected to precipitate under the pH and concentration conditions of this study. Solubility calculations of  $\text{Zn}(\text{OH})_2$  ( $\log K_{\text{sp}} = -15.5$ ) indicate that  $\text{Zn}(\text{OH})_2$  precipitates at pH 8.9 at concentrations of 1.0 and 10 ppm. The exact solubilities of the carbonate species were not measured but were assumed to be in equilibrium with the atmosphere ( $p\text{CO}_2 = 10^{-3.5}$ ). The amount of dissolved  $\text{CO}_2$  is important in determining the stability of solid carbonate species, because all carbonate species are more soluble in the presence of  $\text{CO}_2$  (Forstner, 1979 p. 205).

Hem (1972) calculated the solubility of  $\text{CdCO}_3$  and  $\text{ZnCO}_3$ . Using the solubility curves of Hem (1972), it was determined that solid  $\text{CdCO}_3$  and  $\text{ZnCO}_3$  would form at pH 8.9 and 7.9 in the concentration range of 0.1 to 10 ppm with the exception of  $\text{ZnCO}_3$  at 0.1 ppm at  $10^{-3}$  moles dissolved carbon dioxide

species. Under this set of conditions,  $\text{PbCO}_3$  ( $\log K_{sp} = -13.0$ ) is also expected to precipitate. Reid and McDuffie (1981) found that precipitation of  $\text{CdCO}_3$  from synthetic river water ( $\log K_{sp} = -12.0$ ) begins at pH 8.5 with Cd concentration at  $1 \times 10^{-7} \text{ M}$  (approx. 0.011 ppm). Frost and Griffin (1977) suggested precipitation as a mechanism for removal of cadmium in leachates from landfills by clay minerals. They predicted that Cd would precipitate at Cd concentrations between 3 and 29 ppm at pH 7. Griffin and Shimp (1976) determined that a crystalline form of  $\text{PbCO}_3$  ( $\log K_{sp} = -13.0$ ) would precipitate from landfill leachate at about pH 5 and 7 in the concentration range of 20 to 200 ppm.

When the pH's or concentration of the leaching solution was too low to allow precipitation of solid compounds, cation exchange and adsorption were probably the dominant mechanisms for retention of  $\text{Cd}^{2+}$ ,  $\text{Pb}^{2+}$ , and  $\text{Zn}^{2+}$  by the Heebner and Snyderville shales. The average leached concentration of  $\text{Ca}^{2+}$  and  $\text{Mg}^{2+}$  was 5.10 ppm and 9.10 ppm, respectively. Nearly three times this amount of  $\text{Ca}^{2+}$  and  $\text{Mg}^{2+}$  were leached in the presence of 10 ppm  $\text{Pb}^{2+}$  and twice as much of  $\text{Ca}^{2+}$  was leached in the presence of 10 ppm  $\text{Cd}^{2+}$ . These values were found statistically to be significantly different. This may be due in part to the higher affinity that clay minerals have for  $\text{Pb}^{2+}$  than for  $\text{Cd}^{2+}$  and  $\text{Zn}^{2+}$  respectively and partly due to the larger number of exchanged cations produced by an increase in concentration of the leaching solution (Forstner 1979, p. 210). The pH of the leachate in these experiments averaged 9.0. No significant differences were detected in final pH's of the Snyderville leachate in the trace-metal retention experiments regardless of the initial trace-metal concentration of the leaching solution.

The amount of  $\text{Ca}^{2+}$  and  $\text{Mg}^{2+}$  leached from the Heebner Shale as a function of trace-metal concentration is shown in Figure 2. The amount of  $\text{Ca}^{2+}$  and  $\text{Mg}^{2+}$  leached significantly increased in logarithmic relationship with increasing trace-metal concentration in the leaching solution. There was more  $\text{Ca}^{2+}$  and  $\text{Mg}^{2+}$  leached as the initial trace-metal concentration in the leaching solution increased but the trace metals were less efficient at causing the release of  $\text{Ca}^{2+}$  and  $\text{Mg}^{2+}$  to solution. More  $\text{Ca}^{2+}$  was leached in the presence of  $\text{Cd}^{2+}$ ,  $\text{Pb}^{2+}$ , and  $\text{Zn}^{2+}$  in that order. More  $\text{Mg}^{2+}$  was leached by the leaching solution containing  $\text{Cd}^{2+}$  and  $\text{Pb}^{2+}$  than from leaching solution containing  $\text{Zn}^{2+}$ . This is consistent with findings of Scheffer and Schachtschabel (1966) as reported by Forstner (1979). They stated that the affinity of organic and inorganic substances for trace metals (Pb, Cu, Ni, Co, Zn) is greater than for the alkaline-earth metals.

In the retention experiments using the Heebner Shale the relative amount of trace-metal retention was  $\text{Pb}^{2+} > \text{Cd}^{2+} > \text{Zn}^{2+}$ . This cannot be the result of simple ionic radii or the affinity of the organic and clay mineral fraction for these elements. Instead it is probably a combination of several factors. Scheffer and Schachtschabel (1966) as reported by Forstner 1979, proposed that a tendency to form hydroxyl species or a tendency to adopt a particular geometric relation to the crystal lattice of the exchanger play a significant role in the cation-exchange affinities of different heavy metals. It has also been suggested by Benjamin and Leckie (1981) that different heavy metals have different preferred bonding sites. All of these factors may contribute to the different concentrations of  $\text{Ca}^{2+}$  and  $\text{Mg}^{2+}$  leached from the Heebner Shale (Figure 2) and the amount of Cd, Pb, and Zn retained by the Heebner Shale. The average pH of Heebner Shale leachate in these experiments was 7.8. The pH

did not show a significant difference with increased trace-metal concentration.

Previous literature suggests that the clay minerals (kaolinite, illite, and montmorillonite), organic content, iron and manganese oxide coatings, and calcite fractions of the shales are likely to be the key factors responsible for the retention of trace metals. Much has been written on the mechanisms that control adsorption of  $\text{Cd}^{2+}$ ,  $\text{Pb}^{2+}$ , and  $\text{Zn}^{2+}$  by clay minerals, soils, and river sediments. Researchers, however, are not in agreement about the importance of the different mechanisms. Soldatini and others (1976) found that organic matter and clay were the dominant constituents contributing to adsorption of  $\text{Pb}^{2+}$  in soil. Korte and others (1976) determined that hydrous oxide content and free lime were the important factors for trace metal retention in soils. Salim and Cooksey (1980) and Salim (1983) concluded that the organic content of river mud has a higher capacity for adsorption of lead than the inorganic component. A similar conclusion was reached for  $\text{Cd}^{2+}$  adsorption by Gardiner (1974) and by Suzuki and others (1979) for  $\text{Ca}^{2+}$  adsorption by suspended river sediments. Laxen and Harrison (1981), however, found that lead is more strongly adsorbed or cation-exchanged on the inorganic solids in river sediments. This is consistent with the results of Reid and McDuffie (1981) for retention of  $\text{Cd}^{2+}$  by clay minerals and river water and of Petruzelli and others (1978) for  $\text{Cd}^{2+}$  retention by organic matter in soils. Wiley and Nelson (1984) determined that the clay and sand fraction of lake sediment absorb only negligible amounts of  $\text{Ca}^{2+}$ ; iron oxides are responsible for the majority of adsorption, and organic content and manganese oxides are responsible for the rest. McBride (1980) concluded that cation exchange of  $\text{Cd}^{2+}$  with  $\text{Ca}^{2+}$  in calcite is also a possible mechanism of cadmium retention in soils. A classical paper by Jenne (1977) suggested sorption on iron or manganese-oxide coatings as the main mechanisms for trace-metal adsorption on soils and sediments. A combination of these mechanisms was probably responsible for the retention of  $\text{Cd}^{2+}$ ,  $\text{Pb}^{2+}$ , and  $\text{Zn}^{2+}$  by Heebner and Snyderville shales.

#### Leaching Experiments Using Trace Element Charged Shale

$\text{Zn}^{2+}$  was held more tightly than  $\text{Cd}^{2+}$  when columns filled with Heebner Shale that had been flushed with 0.1, 1.0, and 10 ppm  $\text{Cd}^{2+}$  and 1.0 and 10 ppm  $\text{Zn}^{2+}$  were leached with distilled, deionized water at pH 5.8. More  $\text{Cd}^{2+}$  was released from the columns that previously contained 1.0 and 10 ppm of  $\text{Cd}^{2+}$  than from columns that previously contained 1.0 and 10 ppm of  $\text{Zn}^{2+}$  (0.09 and 0.23 ppm of  $\text{Cd}^{2+}$  as compared to 0.05 and 0.08 ppm of  $\text{Zn}^{2+}$ ). This agrees with the findings of Benjamin and Leckie (1981), who determined that the strength of the adsorptive bond increases in the order  $\text{Cd} < \text{Zn} < \text{Cu} < \text{Pb}$ . This may also be due to the fact that the  $\text{Cd}^{2+}$  that was cation exchanged for  $\text{Ca}^{2+}$  was not held as tightly as the  $\text{Zn}^{2+}$ .

The accuracy of atomic adsorption spectrophotometry for Cd, Pb, and Zn was tested using the U.S.G.S. reference water samples T3 and T93. The Cd trace-metal data were within 15% of the mean values reported for atomic adsorption absorption method for standard reference waters T3 and T93. The Zn values were within 10% of the reference waters. The accuracy of the Pb data could not be determined because the amount contained in the reference waters T3 and T93 was below the detection limit for the equipment.

## CONCLUSIONS

### Environmental Significance

The results from this study could be useful in evaluating the leaching and migration through the unsaturated zone of  $\text{Cd}^{2+}$ ,  $\text{Pb}^{2+}$ , and  $\text{Zn}^{2+}$  from sanitary landfills, fly ash piles, or other concentrated sources of these metals. It is believed that as trace amounts of these metals migrate through fractured shale units similar to those simulated in this study, they are likely to be retained by the shale. With pH and concentration conditions similar to those used in this study, a combination of precipitation reactions, cation exchange, and adsorption are all important in the retention of these metals by fractured shales. Hence, the Snyderville, Heebner, and other similar shale units in the unsaturated zone may act as important barriers between rainwater containing leached  $\text{Cd}^{2+}$ ,  $\text{Pb}^{2+}$ , and  $\text{Zn}^{2+}$  and the water table.

### Conclusions

1. The pH of the leachate from the Snyderville Shale averaged 8.9 and the pH of the leachate from the Heebner Shale averaged 7.9 regardless of the initial pH or flow rate. This indicates that the leachate from the Snyderville and Heebner shale is greatly buffered due to the dissolution of carbonate material in the shales.
2.  $\text{Cd}^{2+}$ ,  $\text{Zn}^{2+}$ , or  $\text{Pb}^{2+}$  were not detected in the Snyderville Shale leachate regardless of the initial concentration of these elements in the leaching solution. This indicates that these trace metals were completely retained by the Snyderville Shale. The amount of retention for these trace metals by the Heebner Shale was  $\text{Pb}^{2+}$  and  $\text{Cd}^{2+} > \text{Zn}^{2+}$ . Retention increased with increased metal concentrations in the leaching solutions. Thus shales could act as effective barriers between leached trace metals and the water table by retaining the trace metals through a combination of precipitation reactions, cation exchange, and adsorption reactions.
3. Zinc retained by the Heebner Shale was held more tightly than cadmium even though a smaller amount was originally retained. This probably was due to differing mechanisms responsible for adsorption of  $\text{Cd}^{2+}$  and  $\text{Zn}^{2+}$ .
4. With 10 ppm of  $\text{Cd}^{2+}$  and  $\text{Pb}^{2+}$  in the leaching solution, more calcium and magnesium were leached from the Snyderville Shale. This is probably due to the increased cation-exchange reactions that occur with increased cation concentration in the leaching solution.
5. The pH of leachate from the Snyderville and Heebner Shale did not show a significant difference with change in trace-metal concentration of the leaching solution. This indicates that pH was not responsible for the amount of  $\text{Ca}^{2+}$  and  $\text{Mg}^{2+}$  leached from the shales or the amount of  $\text{Cd}^{2+}$ ,  $\text{Pb}^{2+}$ , and  $\text{Zn}^{2+}$  retained by the shales.
6. The amount of calcium and magnesium leached from the Heebner Shale increased logarithmically with increasing concentration of  $\text{Cd}^{2+}$ ,  $\text{Pb}^{2+}$ , and  $\text{Zn}^{2+}$  in the leaching solution. The slope of the leached  $\text{Ca}^{2+}$  line for Cd was steeper than any of the others. This was not caused by direct cation exchange

of Ca for Cd. The amount of calcium leached in the presence of these trace metals was  $Cd > Pb > Zn$  and for magnesium  $Cd - Pb > Zn$ .

#### REFERENCES

- Benjamin M.M. and J. O. Leckie, 1981, Competitive adsorption of Cd, Cu, Zn and Pb on amorphous iron oxyhydroxide, *J. Colloid Interface Sci.*, 83,410-419.
- Forstner U., 1979, Metal transfer between solid and aqueous phases. In: *Metal Pollution in the Aquatic Environment*, Chap. E, 199-270. Springer-Verlag New York.
- Frost R. R., and R. A. Griffin, 1977, Effect of pH on adsorption of copper, zinc, and cadmium from landfill leachate by clay minerals, *J. Environ. Sci. Health*, 12,139-156.
- Gardiner, J., 1974, The chemistry of cadmium in natural waters-II, The adsorption of cadmium on river muds and naturally occurring solids, *Water Res.*, 8,157-164.
- Greenberg A.E. et al., 1980, *Standard Methods for the Examination of Water and Waste Water*. American Public Health Assoc., Washington D.C.
- Griffin R.A. and N. F. Shimp, 1976, Effect of pH on exchange-adsorption or precipitation of lead from landfill leachates by clay minerals, *Environ. Sci. and Tech.*, 10,1256-1261.
- Hem J.D., 1972, Chemistry and occurrence of cadmium and zinc in surface water and groundwater, *Water Resour. Res.* 8,661-679.
- Jenne E.A., 1977, Trace element sorption by sediments and soils--sites and processes. In: *Molybdenum in the Environment* (eds. W.R. Chappell and K.K. Petersen), Vol. 2, Chap. 5, pp. 425-454. Marcel Dekker Inc. New York.
- Korte, N.E. et al., 1976, Trace element movement in soils: Influence of soil physical and chemical properties. *Soil Sci.*, 122,350-359.
- Laxen D.P.H. and R. M. Harrison, 1981, The physicochemical speciation of Cd, Pb, Cu, Fe and Mn in the final effluent of sewage treatment works and its impact on speciation in the receiving river, *Water Res.*, 15,1053-1065.
- McBride M.B., 1980, Chemisorption of  $Cd^{2+}$  on calcite surfaces, *Soil Sci. Soc. Am. J.*, 44-26-28.

- Petruzzelli G. et al., 1978, Organic matter as an influencing factor on copper and cadmium adsorption by soils, *Water, Air, and Soil Poll.*, 9,263-269.
- Reid J.D. and B. McDuffie, 1981, Sorption of trace cadmium on clay minerals and river sediments: Effects of pH and Cd(II) concentrations in a synthetic river water medium, *Water, Air, and Soil Poll.*, 15,375-386.
- Salim R., 1983, Absorption of lead on the suspended particles of river water, *Water Res.*, 17,423-429.
- Salim R. and B.G. Cooksey, 1980, Kinetics of the adsorption of lead on river-mud, *Plant and Soil*, 54-399-417.
- Scheffer F. and P. Schachtschabel, 1966, *Lehrbuch der Bodenkunda*. Stuttgart, Enke.
- Sokal R.R. and J.F. Rohlf, 1981, *Biometry*. W.H. Freeman and Company, New York.
- Soldatini G.F. et al., 1976, Pb adsorption by soils, *Water, Air, and Soil Poll.*, 6,111-118.
- Suzuki M. et al., 1979, Sorption and accumulation of cadmium in the sediment of the Tuma River, *Water Res.*, 13,57-63.
- Wilbur C.E., 1987, The retention of Cd, Pb, and Zn by fractured Heebner and Snyderville Shale. unpub. M.S. Thesis, Dept. Geol. Univ. Kansas. Lawrence.
- Wilbur C.E. and E.E. Angino, 1988, Cation exchange of Pb, Cd, Zn, Mn, and Cr with unconsolidated sediments and rocks units, Contrib. No. 256, Kansas Water Resources Research Institute, Lawrence.
- Wiley J.O. and P.O. Nelson, 1984, Cadmium adsorption by aerobic lake sediments, *J. Environ. Eng.*, 110,226-243.
- Zeller D.E. (ed.), 1983, *The stratigraphic succession in Kansas*, Kansas Geological Survey Bull. 189, Lawrence.

## Leaching Apparatus

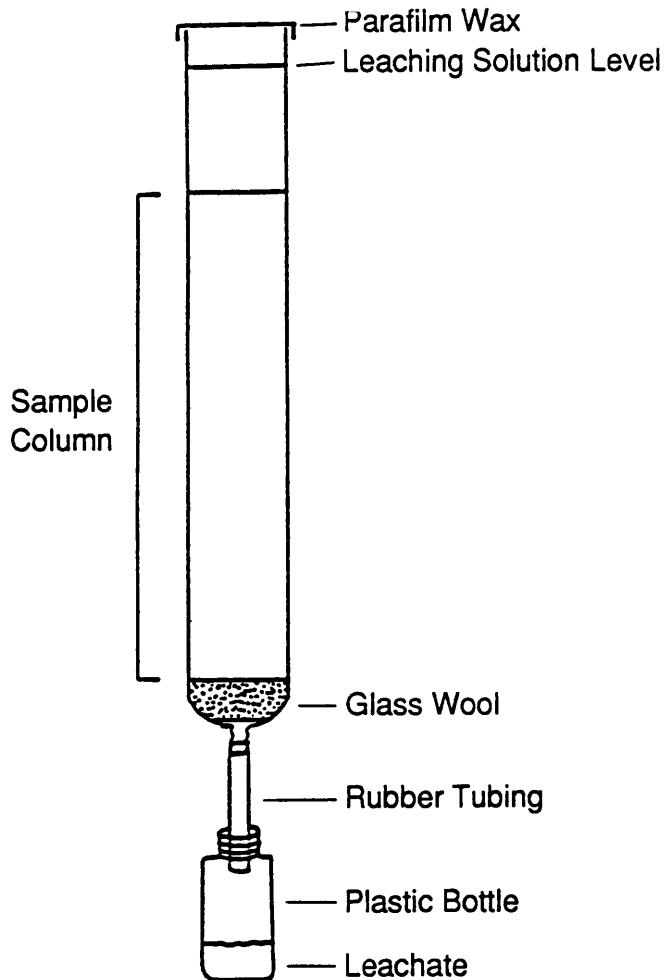


FIGURE 1 Leaching column.



**Concentration of Calcium and Magnesium Leached  
from the Heebner Shale as a Function of Original  
Concentration of Trace Metals in the Leaching Solution.**

Error Bars Represent 95% Confidence Limits.

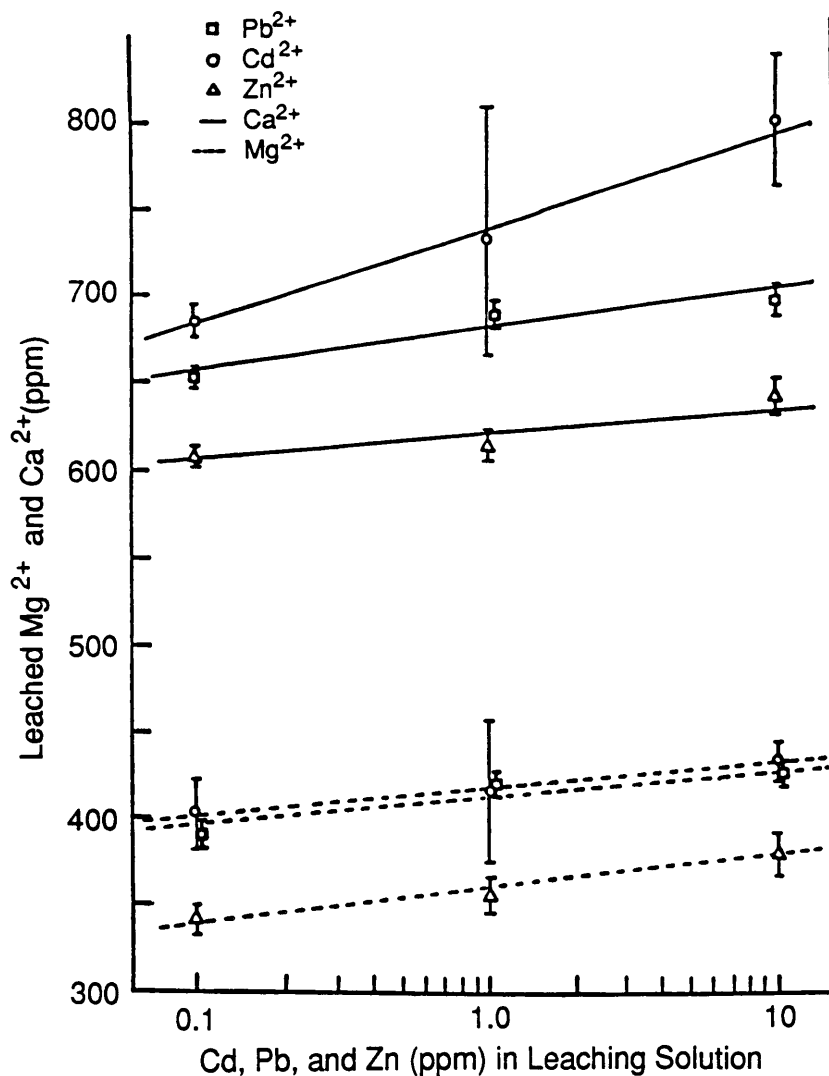


FIGURE 2 Concentration of calcium and magnesium leached from the Heebner Shale as a function of original concentration of trace metals in the leaching solution. Error bars represent 95% confidence limits.



LONG-TERM OBSERVATION OF A LOW-TEMPERATURE  
HYDROTHERMAL SYSTEM (CAMPIGLIA, CENTRAL ITALY)

S. Grassi, R. Celati, L. Bolognesi, C. Calore,  
F. D'Amore, P. Squarci, and L. Taffi

International Institute for Geothermal Research-CNR  
Piazza Solferino 2, Pisa, Italy

**Abstract:** The Campiglia low-temperature geothermal system covers an area of about 30 km<sup>2</sup> in southern Tuscany (Italy), only 20 km southwest of the Larderello geothermal field. The region is characterized by a main thermal aquifer (densely fractured carbonate-evaporitic Mesozoic formations) that is generally confined, but does crop out in some places. The thermal springs emerge on the boundaries of these outcrops. Seven water-points (springs and wells) in the geothermal system were monitored for three years. All of the springs revealed seasonal variations in flow rate, but constant chemical and isotopic composition. Two of the wells, on the contrary, revealed strong variation in water composition. On the basis of the geohydrological and geochemical data, we have identified two possible water sources for the hydrothermal system and hypothesized the flowpaths followed by the waters feeding the various water-points.

Introduction

The hydrothermal system under study is located in southwestern Tuscany, central Italy, 20 km southwest of Larderello, the most important high-temperature geothermal field in Italy. Some springs of this system, near Campiglia village, were used by the Etruscans and Romans in spas more than 2,000 years ago.

The geochemical aspects of these springs were studied by several authors (Francalanci, 1959; Bencini et al., 1977; D'Amore et al., 1979), but in a regional framework. The only detailed analysis of this system dates back to the turn of the century (Merciai, 1904).

Our study lasted about three years and included an inventory of all the springs and wells with anomalous water temperatures, a general geohydrological study of the area, and systematic physical and chemical observations on seven selected water-points (generally about eight observations per year on each water-point and continuous recording of discharge rate in the main spring). The main objectives of the study were:

- (1) to assess the areal extension of the hydrothermal system and its fluid discharge;
- (2) to define the source and flow pattern of the thermal waters;  
and
- (3) to analyze temporal variations in the main hydrological parameters of the system and in the chemical and physical characteristics of the fluid discharge.

The investigation was extended, for the first time in this type of low-temperature geothermal system, inside the potential recharge areas.

### Geological Background

The geological situation of southern Tuscany was studied in detail through drillings for geothermal and mineral research. It can be schematized, starting from the bottom, as:

- (1) a regional, mainly phyllitic, Paleozoic basement;
- (2) the Tuscan nappe, which begins with a carbonate-evaporitic complex (Trias) of alternating anhydrites and dolostones evolving upwards to massive and cherty limestones (Jurassic). The Tuscan nappe ends with mainly terrigenous formations of Cretaceous marl and Oligocene sandstone; and
- (3) the Ligurian nappe made up of three flysch tectonic units (Cretaceous-Eocene) of shales, silts with interbedded limestones, marls, and sandstones.

The overthrusting of the Tuscan and Ligurian nappes occurred in the Miocene during the Alpine orogenesis, which reached its paroxysmal phase in the Tortonian.

After the compressive phase, a tensile climax, related to the opening of the Tyrrhenian Sea, led to the formation of horst and graben and, consequently, to the deposition of mainly clayey Neogenic sediments within the subsiding basins.

### Hydrogeological and Thermal Characteristics

From the hydrogeological point of view, the main regional aquifer is represented by the carbonate-evaporitic complex of the Tuscan nappe. This aquifer, confined at the bottom by the basement and at the top by the overlying terrigenous formations, outcrops in correspondence to structural highs acting as recharge and/or discharge areas. The carbonate regional aquifer often contains warm or hot fluids, because this region is generally characterized by an anomalous heat flow.

The post-Tortonian tensional tectonics were accompanied by thinning of the crust [the Moho in southwestern Tuscany is at a depth of about 23 km (Boccaletti et al., 1985)]. The consequent rise of the mantle caused the formation of anatectic magmas (Puxeddu, 1984) which intruded the crust to the surface in some places. In the Campiglia area, there are intrusive and extrusive igneous products emplaced 5.7 and 4.7 m.y. ago, respectively (Borsi et al., 1967).

### Description of Water-Points

The Campiglia hydrothermal system was shown by our survey to be far wider than expected: apart from the well-known group of springs near Campiglia village, two wells producing warm water were discovered a few kilometers further east near Suvereto. Figure 1 shows the location of the various water-points. The Campiglia group of springs emerges from the main carbonate outcrop in the area, just on its southern boundary, where the contact between the permeable formations and the cover reaches its minimum elevation. This carbonate outcrop represents one of the main recharge areas for the hydrothermal system. The other water-points shown in Figure 1 are located either within the carbonate outcrops or close to their margins. Two

observation wells are located within the main carbonate outcrop in the Campiglia area. The main characteristics of the waters are reported in Table 1.

#### S. Caterina Well

This well was drilled for mineral research about 2 km west of Campiglia in the massive limestone outcrop and was completed by the National Research Council (CNR) for scientific observations. Figure 2 illustrates a schematic representation of well stratigraphy and completion and also shows the static temperature profile. Repeated measurements of water level in the wellbore gave useful information on seasonal pressure variations in the aquifer, as will be discussed later.

#### Temperino Mine

Temperino is a sulphide mine also located in the main local carbonate outcrop. Mineral extraction was suspended recently, but water extraction continued intermittently to supply a small industrial plant. The tapping point is a few meters below the water table, and the average pumping rate was about 2-3 l/s.

The results of chemical analyses and temperature measurements on the pumped water were rather surprising, with temperature near 30°C and the solute content of the same order as some thermal springs (Table 1). Cold, very low salinity water was expected just below the water table in an area of infiltration of meteoric water. These results led us to hypothesize a rise of deep circulating water inside this recharge area.

#### Cratere Spring

Cratere Spring, along with Canneto and Calidario, form the Campiglia group of springs. They are located a few tens of meters apart and have different chemical and physical characteristics. It is a low-discharge spring (flow rate about 1 l/s on the average) with the highest temperature (44°C) and salinity values (Table 1) of the group. Chemical and isotopic compositions are practically constant despite seasonal variations in flow rate; tritium is absent.

#### Calidario Spring

This is the main spring in the Campiglia hydrothermal system, with an average discharge rate of about 220 l/s; temperature (36°C) and salinity (Table 1) are lower than in Cratere Spring, and the tritium content is about 5 TU. The discharge rate of this spring has been continuously recorded since May 1984; it shows strong seasonal variations between 100 and 450 l/s (Figure 3). Despite these variations and the absence of tritium, water composition does not show any significant variation with time (Figure 3).

#### Canneto Spring

With an average discharge rate of 50 l/s, the characteristics of this spring are similar to Calidario Spring, except for a slightly lower temperature

Table 1. Typical chemical and isotopic composition for seven water-points in the Campiglia area. Chemical composition refers to selected dates. Isotopic values are reported as average values of all available analyses. Maximum and minimum isotopic contents are reported for Bagnarello Well. Concentrations in ppm, tritium in TU,  $\delta^{18}\text{O}$  as o/oo vs. SMOW.

| Name                  | Cratere<br>(CR) | Calidario<br>(CL) | Canneto<br>(CN) | Temperino<br>(TI) | S. Lorenzo<br>(SL) | Bagnarello<br>(B) |
|-----------------------|-----------------|-------------------|-----------------|-------------------|--------------------|-------------------|
| Date                  | 10/3/85         | 3/5/84            | 4/16/85         | 10/5/84           | 9/17/86            | 4/29/86           |
| pH                    | 6.95            | 7.05              | 6.95            | 7.5               | 6.8                | 6.85              |
| T°C                   | 43.5            | 36.0              | 32.4            | 29.0              | 46.9               | 30.5              |
| Na                    | 25.9            | 27.5              | 29.0            | 25                | 45.3               | 64.4              |
| K                     | 5.7             | 3.7               | 7.1             | 3.7               | 7.4                | 4.3               |
| Ca                    | 493             | 371               | 331             | 270               | 626                | 405               |
| Mg                    | 98              | 75                | 70              | 40                | 125                | 110               |
| HCO <sub>3</sub>      | 185             | 196               | 225             | 160               | 201                | 366               |
| SO <sub>4</sub>       | 1356            | 1028              | 920             | 652               | 1850               | 1060              |
| Cl                    | 34              | 38                | 45              | 32                | 56                 | 165               |
| SiO <sub>2</sub>      | 37              | 25                | 24              | 22                | 32                 | 22                |
| F                     | 2.4             | 1.5               | 1.2             | 1.3               | 3.0                | 1.6               |
| B                     | 0.1             | 0.7               | 0.2             | 0.3               | 10.1               | 0.4               |
| Fe                    | 0.36            | 0.02              | 0.02            | 0.5               | 1.0                | 14                |
| H <sub>2</sub> S      | 0.15            | 0.50              | 0.50            | n.d.              | 0.45               | 0.05              |
| Li                    | 0.05            | 0.03              | 0.03            | 0.03              | 0.03               | 0.05              |
| Sr                    | 10.0            | 2.9               | 6.0             | 3.5               | 10.8               | 5.2               |
| Br                    | 0.13            | 0.12              | 0.19            | 0.12              | 0.16               | 0.5               |
| TDS                   | 2248            | 1770              | 1659            | 1210              | 2968               | 2218              |
| Tritium               | 0.0             | 4.6               | 4.9             | 11.4              | 1.0                | 7.3/19.8          |
| $\delta^{18}\text{O}$ | -6.49           | -6.55             | -6.45           | -6.50             | -6.45              | -5.82/6.17        |

(32°C) and salinity values (Table 1). Water composition is constant, and tritium is about 5 TU, as at Calidario Spring.

The different characteristics of these three springs are probably the result of different flow paths of the feeding water and different residence times in the aquifer. Cratere Spring is fed either by a deep branch of the local water circulation (the one fed with water infiltrated in the local recharge area) or directly by water from the regional circulation. The lower salinity, temperature, and tritium content in Canneto and Calidario springs suggest, on the contrary, shorter, faster, and probably shallower flow paths and a substantial contribution of local recharge to spring supply.

#### S. Lorenzo Well

This old hand-dug well, together with Bagnarello Well, constitutes the Suvereto group. It has an intermittent discharge: it becomes free-flowing with discharge up to about 150 l/s during rainy periods, but water level drops below wellhead in the dry season. Temperature ranges between 37 and 47°C, depending on flow conditions, salinity (TDS = 2,968 ppm) is the highest found in the area, and the water composition is stable. Tritium is systematically detected, although the values are so low to fall within the analytical error.

#### Bagnarello Well

This well was drilled a few meters from a small carbonate outcrop (Figure 1) and taps water from a shallow clastic alluvial aquifer in contact laterally with the calcareous formation. Seasonal variations in water composition and temperature were observed (Figure 4). The relevant quantities are plotted in this figure versus time, along with the level in S. Caterina Well. In the periods when hydraulic head in the (thermal) carbonate aquifer is high,  $\text{SO}_4$ ,  $\text{Cl}$ , and temperature increase; when this head drops,  $\text{HCO}_3$  and tritium increase, while temperature,  $\text{SO}_4$ , and  $\text{Cl}$  decrease. Thus, the produced water is a mixture of thermal water from the carbonate-evaporitic aquifer, rich in  $\text{SO}_4$  and  $\text{Cl}$ , and a recent, cold water relatively rich in  $\text{HCO}_3$  and tritium. The relative fractions vary with the pressure variations in the thermal aquifer.

The thermal water supplying Bagnarello Well has a higher chloride content than the waters of the other springs and wells, probably because it derives from a deep circulation in the metamorphic complex underlying the carbonate-evaporitic series.

### General Considerations on the System

#### Geochemical Indications

All of the waters are of the calcium sulphate-calcium/magnesium bicarbonate type, with salinities from low to intermediate (Table 1). These characteristics are typical of circulation in the carbonate-evaporitic complex (Grassi et al., in press). Total salinity is almost entirely controlled by sulphate (Figure 5).

The waters can be subdivided into two classes: the Campiglia and Suvereto groups. These groups plot along separate straight lines in the Ludwig-Langelier

diagram shown in Figure 6, where three points at different salinities are reported for Bagnarello Well. The two straight lines intersect at point, in the high  $\text{SO}_4$  (and salinity) range, that could represent the most concentrated water in the system (regional water or final stage of water-rock interaction).

The salinity-tritium diagram shown in Figure 7 confirms the separation of the waters into the above two families and reveals an important difference between the two: the waters of the Suvereto group plot on a straight line that indicates a mixing without tritium decay; the waters of the Campiglia, on the other hand, plot on an upwardly concave curve which could indicate mixing with tritium decay or other processes involving long residence times in the aquifer. We formulated the following hypotheses from these observations:

*Suvereto group:* all of the waters in the group derive from mixing of the most concentrated water in the system with a low-salinity  $\text{NaHCO}_3$  type water.

*Campiglia group:* all of the waters in the group derive from:

- (1) mixing of the regional water and water from the local recharge, the mixing being accompanied by a more or less long residence in the aquifer, or
- (2) the local recharge water through water-rock interaction, without any significant contribution from the regional circulation.

With the exception of the Bagnarello well, the chloride content is low (30-60 ppm) and constant; its origin can be attributed to the presence of sea spray in the rain water because of the vicinity to the Tyrrhenian coast.

Tritium is low and constant in Calidario (Figure 3) and Canneto springs, high and variable in Temperino and Bagnarello wells (Figure 4). The former indicates that local recharge water has a major role in supplying the springs, and the latter indicates that a mixing of the thermal component with recent waters occurs just before the emergence.

The stable isotopes are nearly constant, with practically the same values in all the water-points except for the Bagnarello well, in which the higher values of  $\delta^{18}\text{O}$  can be attributed to the diluted component in the mixture (the shallow waters in the Campiglia alluvial plain have  $\delta^{18}\text{O} = -5.5$ ). We were unable to distinguish waters coming from different recharge areas from the stable isotopes as all the waters involved have very similar isotopic compositions.

### Precipitation and Spring Discharges

We also investigated the cause and mechanism of the observed variations in discharge rate. Figure 8 shows monthly precipitation in the Campiglia area (Annali Idrologici), along with the water level in S. Caterina Well and the discharge rates of Calidario, Canneto, Cratere springs, and S. Lorenzo Well, the only water-points where flow rate measurements were possible. The time lapse between a variation in precipitation and relative variation in water level can be considered normal in the hydrogeological setting of the study area.



At the end of the dry season, the first precipitations do not contribute significantly to aquifer recharge, as they are partly spent in evapotranspiration and in replenishing the water content of the soil. Even when infiltration effectively begins, the level in the aquifer continues to decrease until a balance is reached between water supply to the aquifer and water losses from it. The level will start drawdown again when this balance is reached as a consequence of the increase in spring flow rate and the reduction in infiltration. Thus, the maximum level is reached in the period of decreasing infiltration.

All of the flow rates (except perhaps that of the S. Lorenzo well where the trend is not well-defined) show an approximate phase coincidence with the level variations, as one could expect from overflow springs of this kind (Celati et al., these Proceedings).

### Sources of Water

Figure 9 illustrates the part of southern Tuscany comprising all of the recharge areas of the regional aquifer that could have some relation with the Campiglia hydrothermal system. The map also shows the potentiometric surface for the regional carbonate-evaporitic aquifer, indicating two possible primary sources of water for the Campiglia system: local recharge and the regional circulation. The latter seems to be the primary or unique source for Bagnarello and S. Lorenzo wells, but also seems to contribute to the Campiglia group of springs.

Our final observation is also supported by a mass balance consideration: infiltration in the local carbonate outcrop is estimated at about 300 l/s, which is only slightly higher than the aggregate fluid output of Calidario and Canneto springs (270 l/s). It is unlikely that such a large fraction of total infiltration is involved in the feeding of these two springs.

### Conceptual Model

Figure 10 summarizes our conceptual scheme for water circulation. The system is fed by local recharge and regional circulation. Local recharge is the main source for the Campiglia group, whereas regional circulation is the main source for the Suvereto group.

A complex circulation pattern develops in the main local recharge area, and many details of this flow pattern are unknown; the Temperino tapping point is near the merging of meteoric water infiltration and uprising thermal water; the waters feeding Calidario and Canneto springs flow at intermediate depths and their circulation is relatively fast, as indicated by the presence of tritium; Cratere Spring, on the contrary, must be supplied either by water flowing slowly at great depth or directly by the regional circulation.

In Bagnarello Well, the regional water mixes, near the bottomhole, with cold, diluted recent water from shallow aquifers. The same phenomenon seems to affect S. Lorenzo Well, although to a minimal extent.

# LIST OF REFERENCES

- Bencini, A., V. Duchi, and M. Martini, 1977. Geochemistry of thermal springs of Tuscany (Italy), *Chemical Geology*, 19, 229-252.
- Boccaletti, M., M. Coli, C. Eva, G. Ferrari, G. Giglia, A. Lazarotto, F. Merlanti, R. Nicolich, G. Papani, and D. Potspischl, 1985. Considerations on the seismotectonics of northern Appennines, *Tectonophysics*, 117, 7-38.
- Borsi, S., G. Ferrera, and E. Tongiorgi, 1967. Determinazioni con il metodo K/Ar dell'eta' delle rocce magmatiche della Toscana, *Boll. Soc. Geol. It.*, 86, 403-410.
- Celati, R., S. Grassi, and C. Calore. Overflow thermal springs, these Proceedings.
- D'Amore, F., P. Squarci, and C. Panichi, 1979. Indagine geochimica delle sorgenti termali italiane, valutazione dei serbatoi geotermici e ricostruzione geoidrologica di alcune aree preferenziali (Toscana Sud-Occidentale e Lazio Centro-Settentrionale), Report for the Commission of European Communities, Eur 6743 IT.
- Francalanci, G.P., 1959. Contributo per la conoscenza delle manifestazioni idrotermali della Toscana, *Atti Soc. Toscana Sc. Nat.*, Serie A, Fasc. II, LXV, 373-432.
- Grassi, S., R. Celati, F. D'Amore, and L. Marcolini, 1989. The low temperature hydrothermal system of Campiglia, Tuscany (Italy): a geochemical approach, in press.
- Merciai, G., 1904. Le acque termali di Caldana presso Campiglia Marittima, published by F. Mariotti, Pisa, Italy, 32 p.
- Puxeddu, M., 1984. Structure and late Cenozoic evolution of the upper lithosphere in southwest Tuscany (Italy), *Tectonophysics*, 101, 357-382.
- Annali Idrologici, 1984-86, Part 2. Publication of the Italian Ministry of Works, Hydrographic Survey.

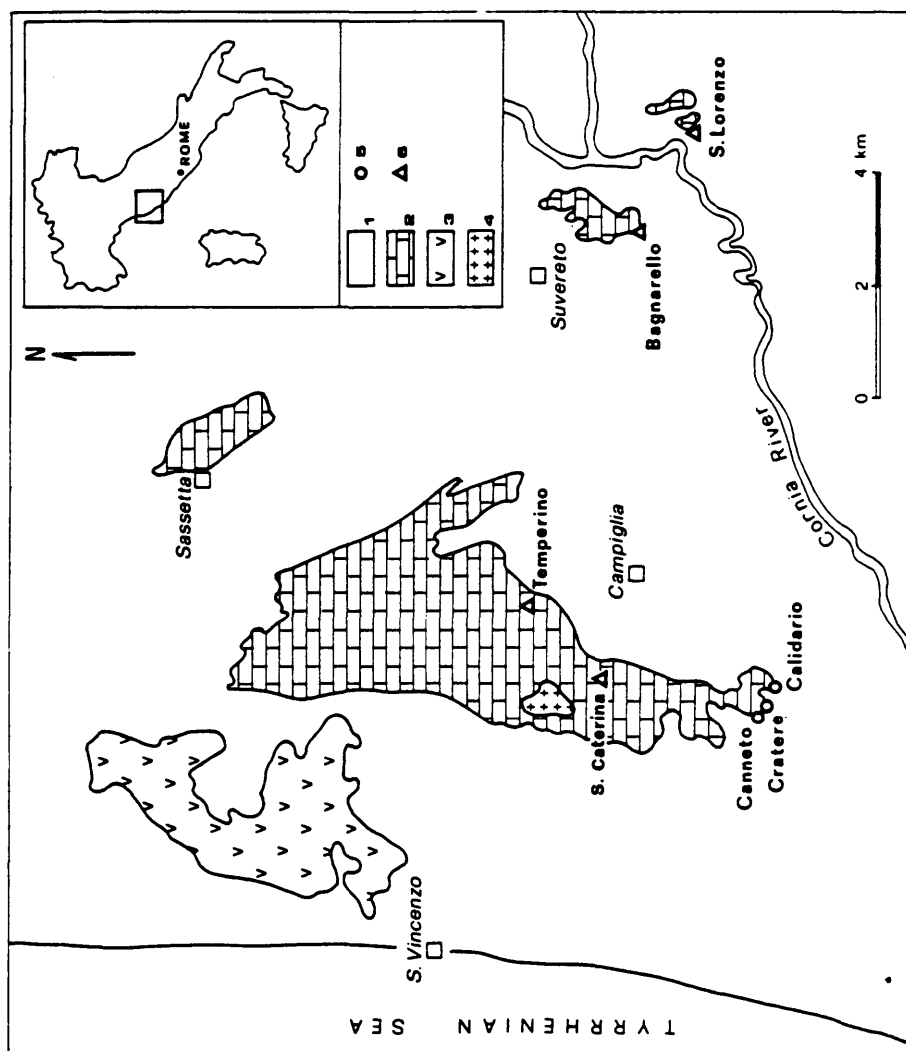


Figure 1. Location of water-points of the Campiglia hydrothermal system. (1) Cover, (2) Carbonates, (3) Volcanites, (4) Granite, (5) Spring, (6) Well.

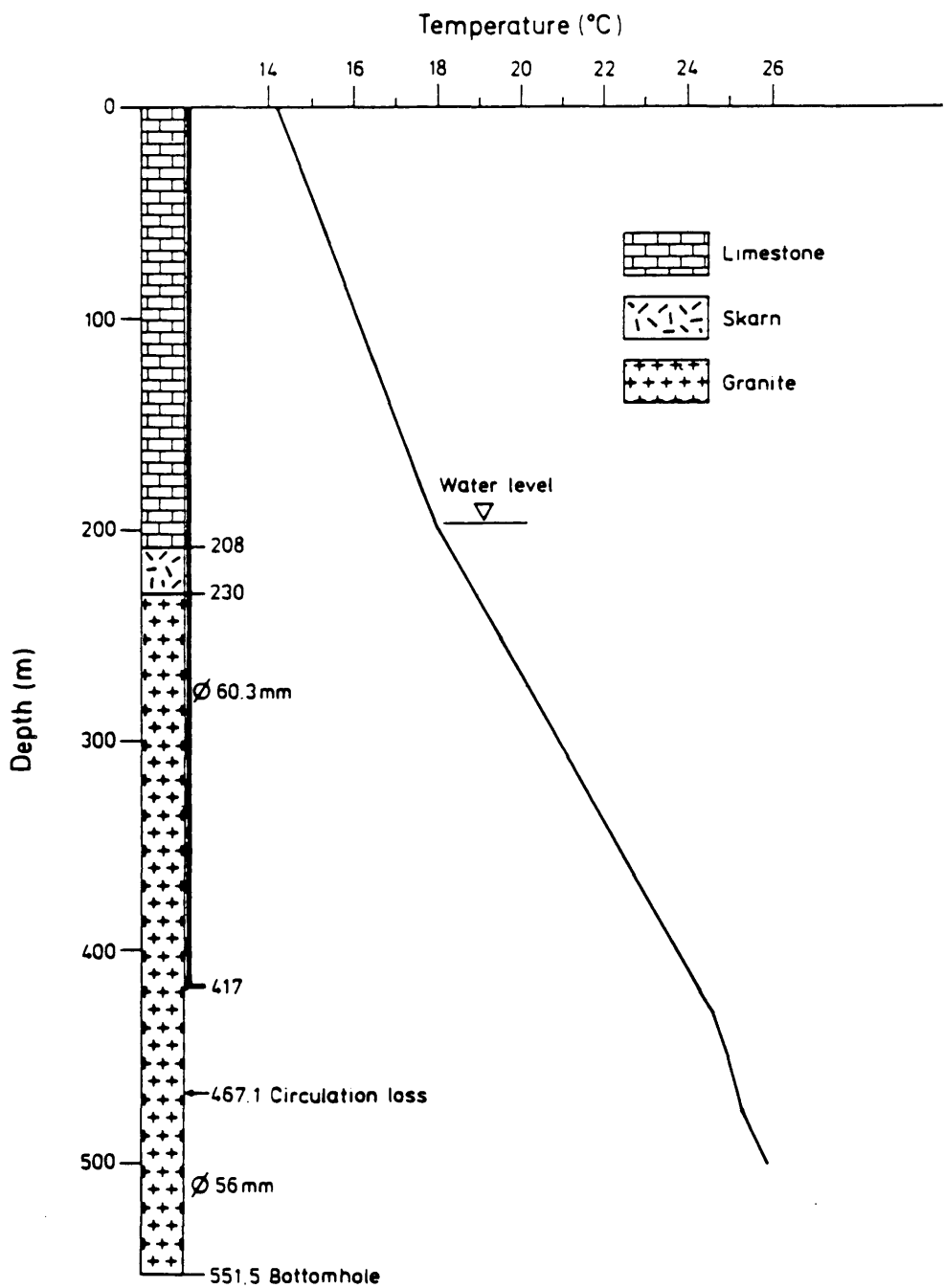
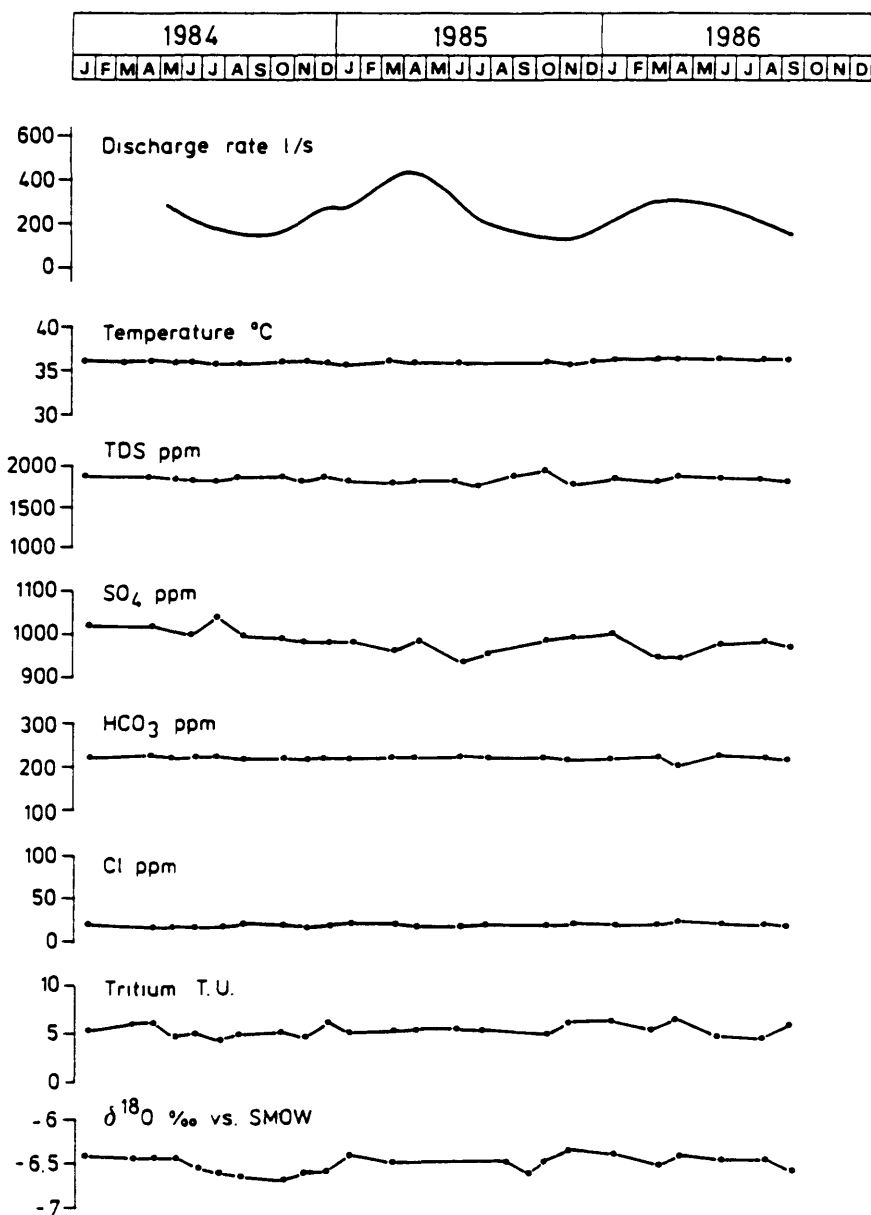


Figure 2. Characteristics of S. Caterina Well.



### CALIDARIO

Figure 3. Temporal trend of physical, chemical, and isotopic quantities in Calidario Spring.

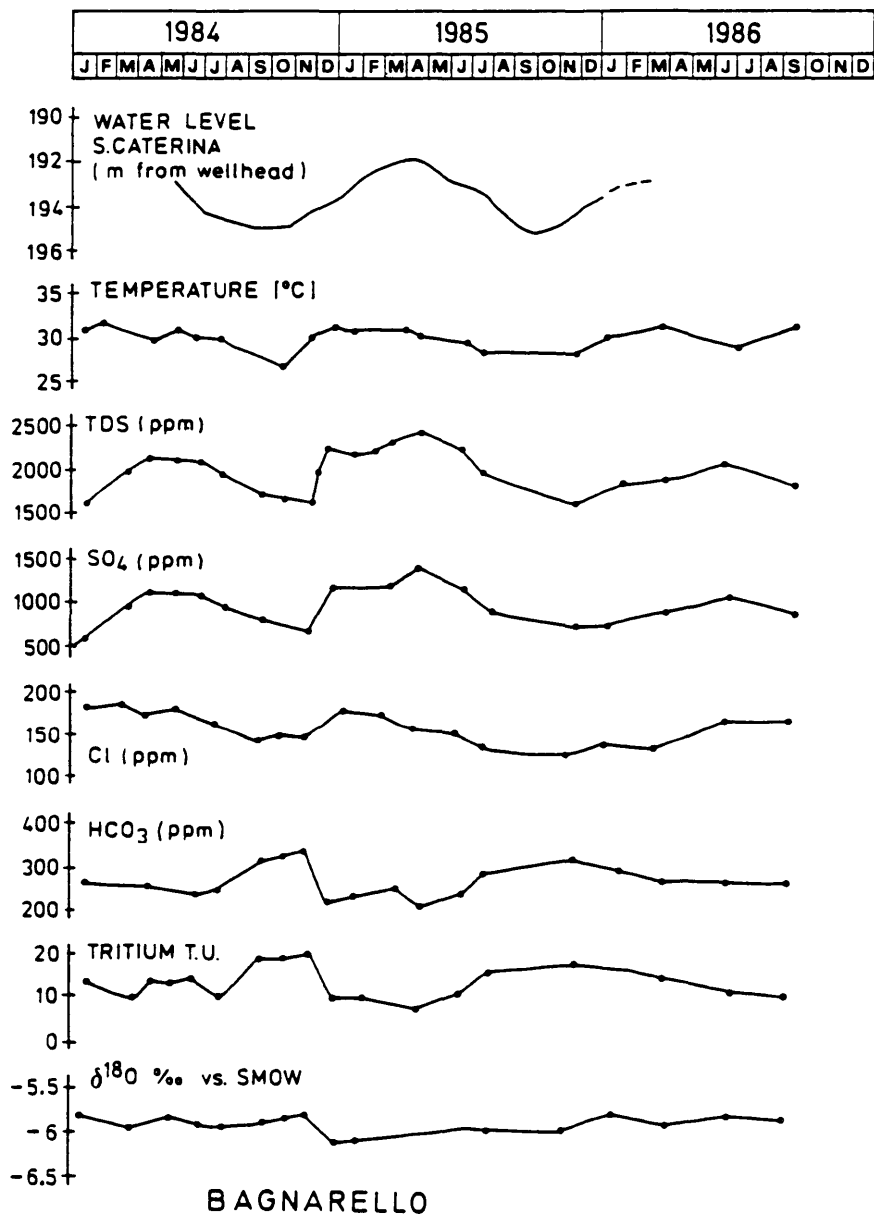


Figure 4. Temporal trend of physical, chemical, and isotopic quantities in Bagnarello Well.

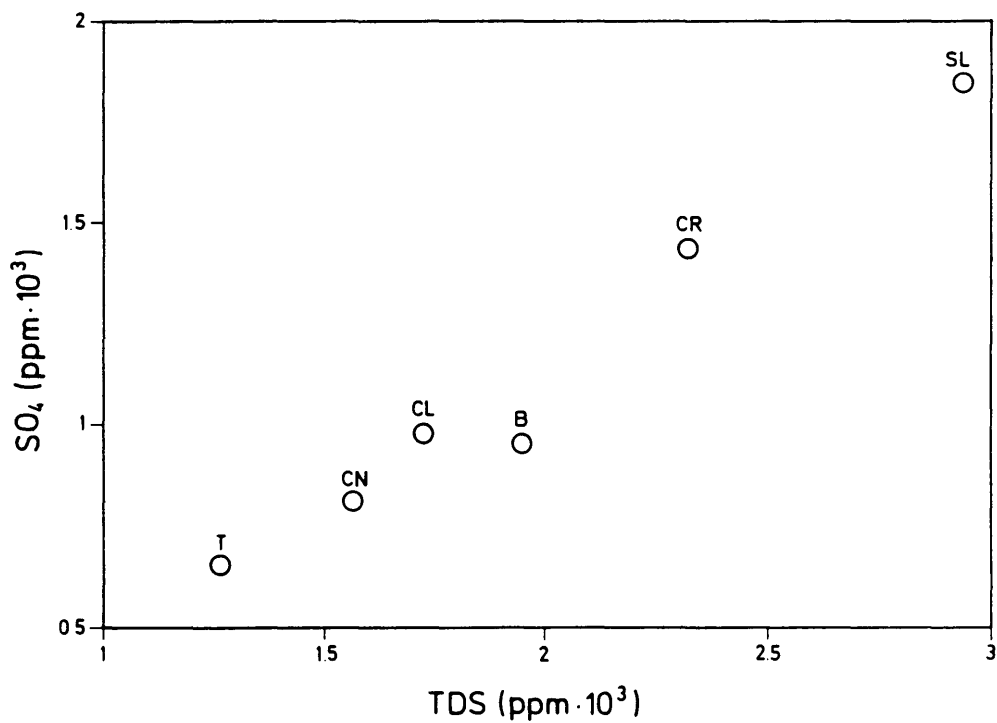


Figure 5. Sulphate/TDS relationship for the Campiglia hydrothermal system. Average values are reported.

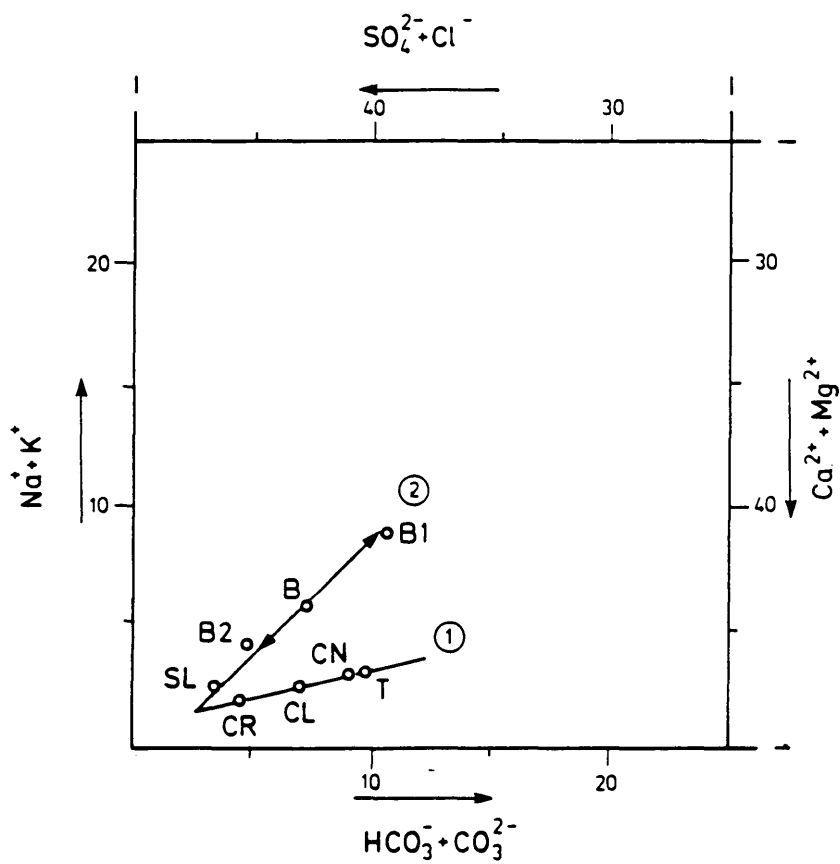


Figure 6. Magnification of the lower left-hand sector of Ludwig-Langelier diagram. (1) Campiglia group, (2) Suvereto group.



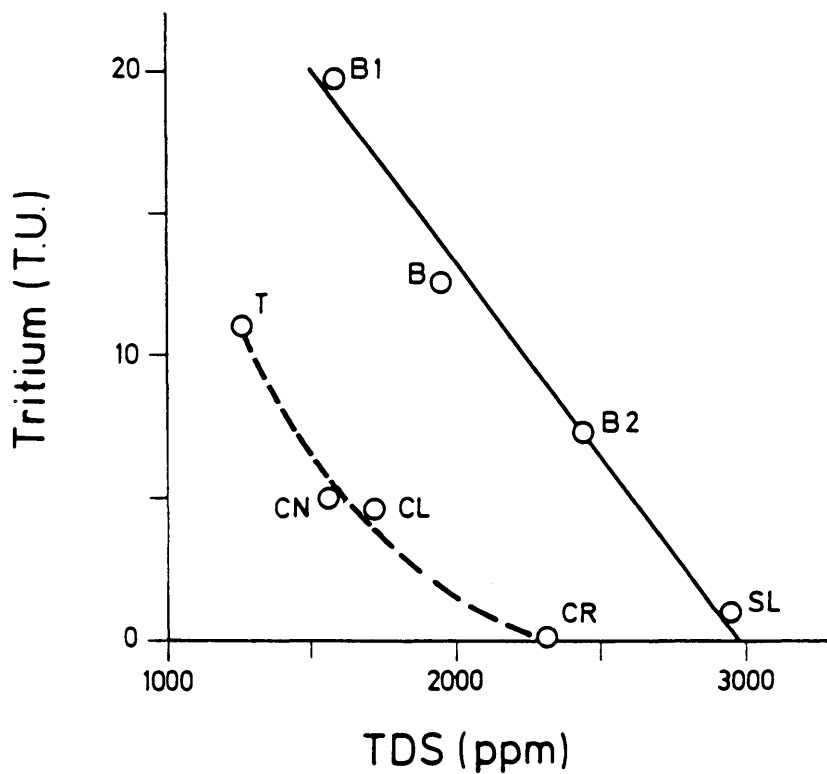


Figure 7. Tritium/TDS relationship for the Campiglia and Suvereto groups. Average values are reported.

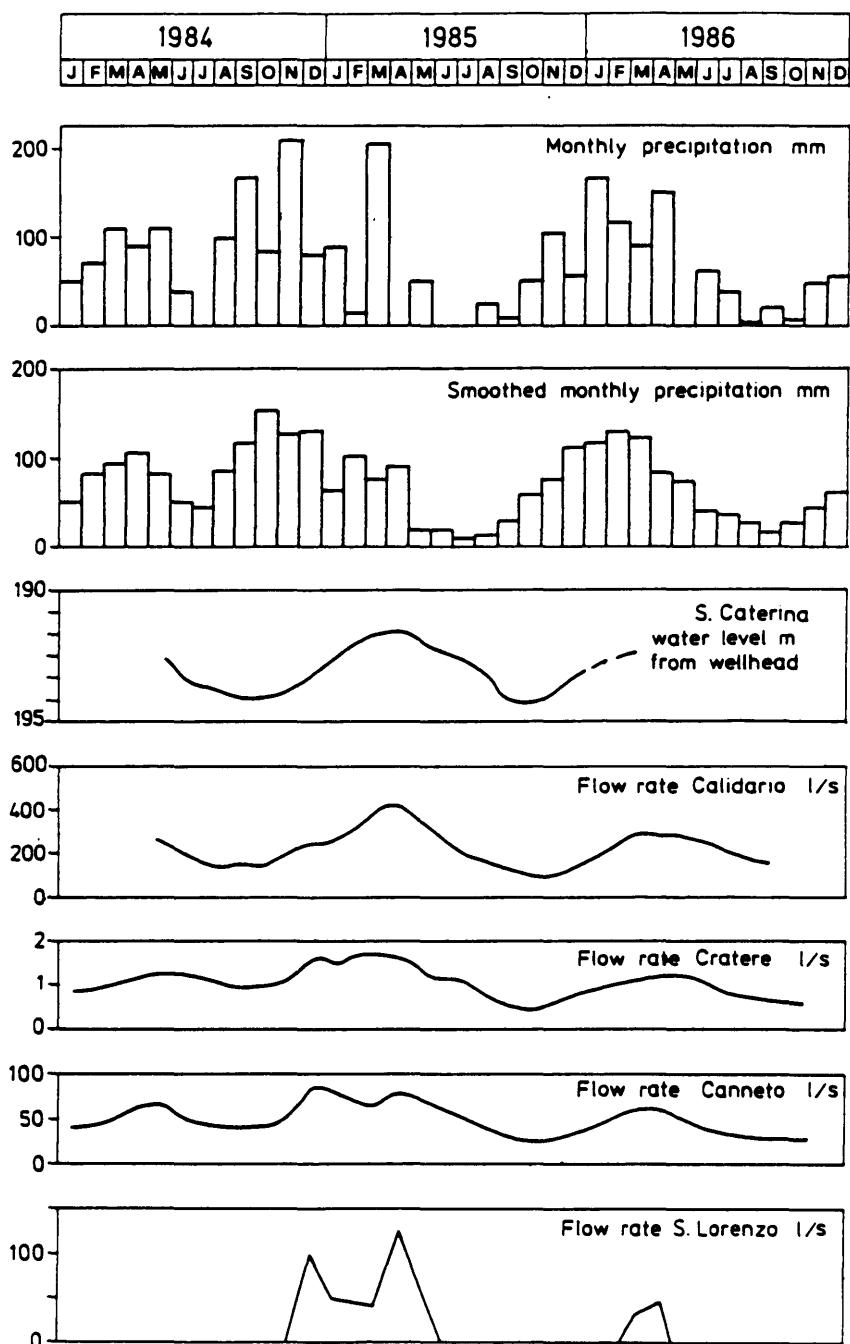


Figure 8. Precipitation in the Campiglia area and flow rates of different water-points.

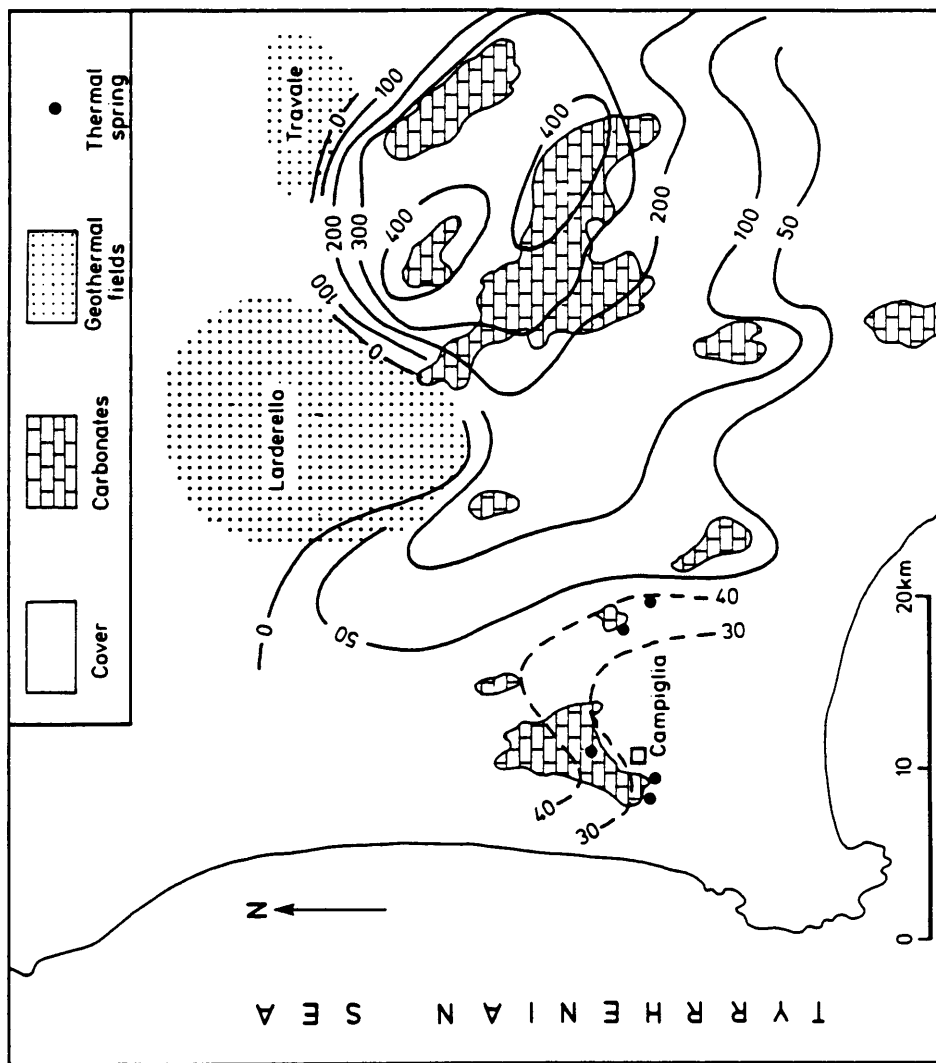
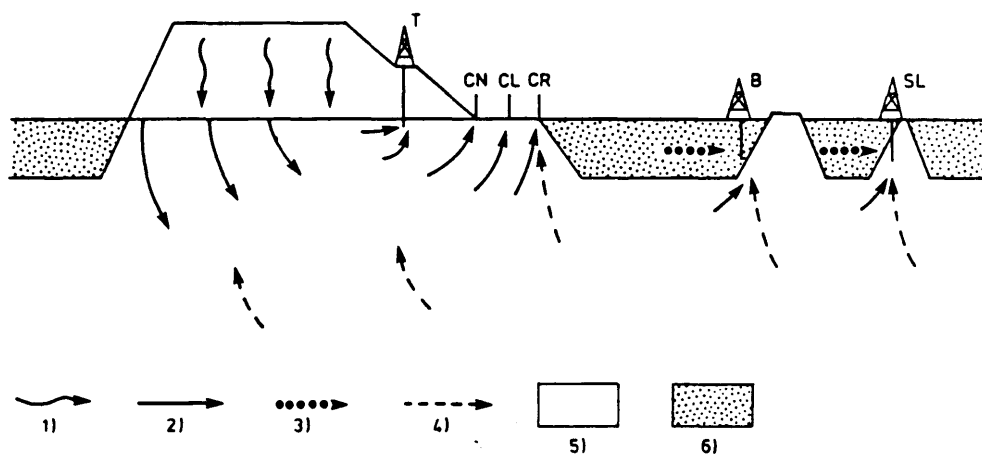


Figure 9. Piezometric sketch map of part of south Tuscany (m a.s.l.).



- 1) Infiltration    2) Local waters and mixtures    3) Shallow  $\text{NaHCO}_3$  waters  
 4) Regional waters    5) Aquifer    6) Cover

Figure 10. Circulation model of the Campiglia hydrothermal system.

STUDIES OF SURDULICA GEOTHERMAL WATER  
DYNAMICS WITH ENVIRONMENTAL ISOTOPES

B. Milovanovic  
Geozavod, Karadjordjeva 48, 11000 Belgrade

R. Gonfiantini  
IAEA, Section of Isotope Hydrology  
Wagramerstrasse 5, A-1400 Vienna

M. Hadzisehovic, N. Miljevic, V. Sipka, M. Zupancic, D. Golobocanin

Boris Kidric Institute of Nuclear Sciences, Vinca,  
P.O. Box 522, 11001 Belgrade

**Abstract:** We investigated characteristics of the Surdulica geothermal system using isotopic methods completed with chemical analyses. More than 150 samples of water, vegetation, soil, and rocks were collected in order to determine D,  $^{18}\text{O}$ ,  $^3\text{H}$ , and  $^{14}\text{C}$  content, chemical composition, and temperature. We found that D and  $^{18}\text{O}$  in precipitation collected at different altitudes varied seasonally, whereas the geothermal waters were largely homogeneous and seasonally independent. In the  $\delta\text{D}$  versus  $\delta^{18}\text{O}$  diagram, precipitation values lie on a line with slope of  $-7$  and intercept of  $-4$ , while these values for rivers and springs scatter in a broad interval from  $4$  to  $10$  for the slope and from  $-27$  to  $26\text{‰}$  for the intercept. The isotope altitude gradients from precipitation suggest that the recharge area lies above  $1,000$  m asl. On the basis of variable  $\text{HCO}_3^-$ ,  $^{14}\text{C}$ ,  $^{13}\text{C}$ , and  $^3\text{H}$  content from the top of the system downward, and the location of thermal waters appearance, the process of water transformation from precipitation to old geothermal waters is evident. Taking for the initial activity  $A_0 = 85\%$  of modern  $^{14}\text{C}$ , we estimated the age of examined thermal waters to be between  $10,000$  and  $28,000$  years. Obtained  $^{13}\text{C}$  values within  $-27.7$  and  $0.3\text{‰}$  show that apparent "age" is greater than "actual age". Silica concentrations suggest base temperature of about  $130^\circ\text{C}$  (the highest measured is  $126^\circ\text{C}$ ), which is in agreement with a predicted value of  $125^\circ\text{C}$  by Na/K/Ca corrected geothermometers.

Introduction

Granodiorite system Surdulica is the largest geothermal aquifer in Yugoslavia, situated in a southeast part (area about  $250\text{ km}^2$ ) with a large potentiality of cold and thermal waters (ca  $200\text{ l/s}$ , temperature up to  $126^\circ\text{C}$ ). The reserves are estimated to be double the current exploitation.

Because of their great interest, investigation of the system started in the last century (Zujovic, 1893). Geological formation of the Vranje Tertiary basin and its structure, tectonics, and thermal waters have been extensively surveyed (Babovic et al., 1970; Anderson, 1985). Environmental isotopic investigations began in 1986. We expect that these studies, together with chemical analyses and hydrogeological data, will provide new information to assist in thermal water evaluation.

### Hydrological Background

The Surdulica geothermal system occupies a mountain massif (maximum elevation 1,922 m asl) and belongs to the geotectonic region predominantly formed of Proterozoic crystalline schists (Figure 1). The hydrogeothermal system by itself is situated in the neogen-fissured granodiorite and granite aquifer. The outcrop of the crystalline schists (above 1,000 m asl) represent an assumed recharge area.

Geophysical measurements have shown that sedimentary layers of the Vranje Valley are very heterogeneous with large faults and decreasing porosity with depth (Figure 2). In the direction of the South Morava Valley, the steeply-sloping mountain sides of the massif are cut with deep rivers and brooks (Jelasnicka and Banjska rivers).

This region is characterized by a transitional regime between moderate continental and mediterranean climate. In addition, a watershed of the Aegean and Black seas is on the top of the system. The average precipitation is ca 600 and 1,000 mm in the valley and higher mountains, respectively. During winter (October-March), the predominant precipitation (ca 60%) is snow, which remains until May.

The system produces about 120 l/s cold and nearly 80 l/s thermal waters with temperatures in a range of 25 to 110°C. Thermal springs appear in the foothills of a schist massif at ca 400 m altitude located close to the Vranjska and the Bujanovc Spa. A few shallow (50-500 m deep, temperature 40-100°C) and three deeper boreholes (500-1,200 m deep, temperature 67-126°C) were drilled.

### Sampling and Analysis

The monthly precipitation and individual samples from rivers, cold and thermal springs, mine and boreholes were collected. At about 27 locations (Figure 1), 135 analyses of D,  $^{18}\text{O}$ , and  $^3\text{H}$  were performed as well as 40  $^{13}\text{C}$  and  $^{14}\text{C}$  analyses in carbonate species.

Geothermal and spring waters were analyzed for main cations (Na, K, Ca, Mg) and anions ( $\text{HCO}_3$ ,  $\text{SO}_4$ , Cl, F) and  $\text{SiO}_2$ . Isotopic composition of collected samples was obtained using standard methods (Milovanovic et al., 1989).

### Results

The results of this investigation are summarized in Tables 1 and 2 and in Figures 3 and 4. For isotopic measurements of precipitation, collected at elevations between 400 and 1,350 m, the values lie within -5.1 and -16.9‰ for  $\delta^{18}\text{O}$ , and from -38.5 to -114.7‰ for D, while for geothermal waters, they are between -10.1 and -11.7‰ for  $^{18}\text{O}$  and from -78 to -93‰ for D. The fluctuations for rivers and springs are within mentioned values. All examined waters, except old geothermal, contain tritium in concentrations from 11 to 75 TU. This wide interval is a result of different drainage rates through the system due to a variety of rock porosity (Figure 2). The  $^{14}\text{C}$  content ranges from 126 for vegetation (soil) samples and 1.3‰ modern for geothermal waters. The  $^{13}\text{C}$  content increases from -27.5‰ for vegetation and soil samples to a mean value of  $-29 \pm 0.7$ ‰ in geothermal waters, indicating a dilution process of  $^{14}\text{C}$  concentration in water during its passage through the system. Concentrations of  $\text{HCO}_3^-$  and  $\text{CO}_2$  dissolved

Table 1.  
Maximal variation of D,  $^{18}\text{O}$  and  $^3\text{H}$  contents

| SAMPLE                                | Map sign<br>(Fig. 1)            | $\delta^{18}\text{O}_{\text{SNOW}} \pm 0.2$<br>(%) | $\delta \text{DSNOW} \pm 1$<br>(%) | $\delta^3\text{H} \pm (10-100\%)$<br>(TU) | $\delta^{18}\text{O}_{\text{SNOW}}$<br>(%) | $\delta \text{DSNOW}$<br>(%) | $^3\text{H}$<br>(TU) |
|---------------------------------------|---------------------------------|--|------------------------------------|---|--|------------------------------|----------------------|
| PRECIPITATION<br>390 .. 1350 m asl    | 19, 20, 23                      | -5.1 to -16.9                                      | -38.5 to -114.7                    | 11 to 75                                  | -11.2<br>$\pm 1.1$                         | -75.3<br>$\pm 24.5$          | 25 $\pm 2$           |
| RIVERS<br>400-1580 m asl              | 6, 7, 13, 18                    | -8.5 to -11.1                                      | -54.6 to -84                       | 19 to 67                                  | -10.1<br>$\pm 0.7$                         | -73.6<br>$\pm 7.4$           | 32 $\pm 3$           |
| SPRINGS (MINE)<br>400 - 1525 m asl    | 5, 11, 14-17,<br>21, 22, 24, 25 | -9.2 to -12.0                                      | -68 do -88                         | 5 to 69                                   | -10.7<br>$\pm 0.6$                         | -76.0<br>$\pm 4.7$           | 34 $\pm 3$           |
| GEO THERMAL WATERS<br>400 - 425 m asl | 1-12, 26                        | -10.1 to -11.7                                     | -78 to -93                         | -3.5 to 2.7                               | -11.0<br>$\pm 0.4$                         | -81.7<br>$\pm 4.2$           | dead                 |
| BOREHOLE ROCKS<br>depth 200-1000 m    | 10, 26, 27,<br>22               | 7.0 to 16.6*<br>19.5 to 24.8**                     | (Calculated)                       |   |  |                              |                      |

\* Granodiorite

\*\* Marble from mine

Table 2. Maximal variation of carbon isotopes  $^{13}\text{C}$  and  $^{14}\text{C}$

| SAMPLE   | MAP SIGN<br>(Fig. 1)        | $^{13}\text{C}_{\text{PDB}} \pm 0.4$<br>(‰) | $^{14}\text{C} \pm (3-5)$<br>(‰ modern) | $^{13}\text{C}_{\text{PDB}}$<br>(‰) | $^{14}\text{C}$<br>(‰ modern) |
|--|-----------------------------|---|---|-------------------------------------|-------------------------------|
| VEGETATION, SOIL                                   | 5, 7, 20, 23                | -28.5 to -27.3                              | 123.9 to 126.1                          | -27.9                               | 125.0                         |
| PEAT   | 23                          | -26.7                                       | 111.4                                   |                                     |                               |
| RIVERS, SPRINGS                                    | 5, 11, 13, 14<br>21, 22, 25 | -16.3 to -10.2                              | 61 to 94                                | -12.8 $\pm$ 0.9                     | 75 $\pm$ 3                    |
| MINE WATERS  | 15, 16, 17, 24              | -16.3 to -10.2                              | 38.7 to 55.2                            |                                     | 44 $\pm$ 5                    |
| GEOHERMAL<br>SPRINGS                               | 8, 35, (9)                  | -7.8 to -3.1                                | 10.4 to 26.9 (75.5)                     |                                     | 19 $\pm$ 3                    |
| GEOHERMAL SPRING<br>BOREHOLES<br>(depth 50-1100 m) | 1-12, 26                    | -6.6 to 0.3*<br>-0.9 to -0.4**              | 1.3 to 6.9                              | -2.9 $\pm$ 0.7                      | 4.5 $\pm$ 0.5                 |
| CO <sub>2</sub> gas                                | 3                           | -4.5  |   |                                     |                               |
| BOREHOLE ROCKS<br>depth 200-1000 m                 | 10, 26, 27                  | -8.4 to -1.1*<br>0.4 to 2.7***              |   |                                     |                               |

\* Granodiorite

\*\* Granite

\*\*\* Marble from mine



in mine waters and springs collected above 1,300 m asl are lower than 80 mg/l and 15 mg/l, respectively. Going down the aquifer, their contents increase and, in geothermal waters, reach values of 0.5 g/l  $\text{HCO}_3^-$ , (in Bujanovac even 1.4 g/l for carbonates and 200 mg/l for  $\text{CO}_2$  dissolved). Thermal waters show a sodium (calcium) bicarbonate (sulphated) character, slightly alkaline ( $\text{pH} = 6.5-7.5$ , Figure 4). They are mineralized (1.1-1.3 g/l) with fluoride (5-7 mg/l) and silica (10-90 mg/l). Maximal ion concentrations of Na, K, Ca, and  $\text{SO}_4$  are 500, 10, 65, and 500 mg/l for the Vranjska Spa and 1,000, 60, 65, and under 200 mg/l for Bujanovac, respectively.

#### Relation $\delta\text{D}$ - $\delta^{18}\text{O}$

The precipitation data lie on a least squared line (Figure 5):

$$\delta\text{D} = (7.1 \pm 0.2) \delta^{18}\text{O} + (4 \pm 2) \quad (1)$$

with  $n = 32$ , a correlation coefficient of  $r = 0.99$ , and with a standard error of  $\sigma = -3.7\text{‰}$ . For rivers, a value of 8 for both parameters was calculated, but their dispersion is much larger (Figure 6). In the case of springs, the parameters and their limits are lower,  $4 \pm 1$  for the slope and  $-27 \pm 11\text{‰}$  for the intercept (Figure 7). Nevertheless, mean values for rivers, springs, and geothermal waters cluster under the cited local meteoric water line (Equation 1), although with the same lower limit of maximal error (Figure 8).

#### Altitude Effect

The gradients for the altitude effect calculated from the relation:

$$\delta^{18}\text{O} (\delta\text{D}) = f(\text{altitude, m asl})$$

are, for precipitation:

$$-0.2 \pm 0.02\text{‰} (\delta^{18}\text{O})/100 \text{ m and } -1.5 \pm 0.01\text{‰} (\delta\text{D})/100 \text{ m}$$

According to the  $\delta^{18}\text{O}$  precipitation gradient, compared to the mean isotopic composition of geothermal waters:

$$[\delta^{18}\text{O} = -11.0 \pm 0.4\text{‰} \text{ and } \delta\text{D} = -8.17 \pm 4.2\text{‰}]$$

the recharge area lies above 1,000 m asl. Including the limits of error, this area extends to altitudes above 800 m. Deuterium data move the recharge area in the direction of higher elevations (within the limits 1,200-1,800 m asl). The lower limits obtained from the  $^{18}\text{O}$  altitude effect are more probable, although higher  $^{18}\text{O}$  content might originate in interaction between rocks and waters at high temperatures ( $^{18}\text{O}$  shift).

#### Source of Groundwater

Thus far, both geological and isotopic investigations indicate that the source of water in the aquifer is meteoric. Waters that infiltrated higher parts of the system penetrate along faults into its depth, forming many "subaquifers" with different residence times. According to the concentrations of  $^3\text{H}$ ,  $^{14}\text{C}$ ,  $^{13}\text{C}$ , and

chemical composition of geothermal waters, especially changes of carbonates in the system, the investigated geothermal waters can be classified into approximately three groups.

The first group is characterized by fast-water exchange, higher  $^3\text{H}$ , and  $^{14}\text{C}$  contents in a range of 17-69 TU and 61-94% modern. These are springs located above or on a contact of the open aquifer with an insulator (Figure 2).

The older waters found in the mine galleries, boreholes, and springs at 500-1,300 m elevations also contain tritium (13-58 TU). Their  $^{14}\text{C}$  values from 39 to 55% modern correspond to the age of 3,000 to 6,000 years (for  $A_0 = 85\%$ ). They indicate that practically a whole flowpath is through granodiorite. The fact that mine waters are older than those in natural springs at the same or rather lower elevations (400 and 910 m asl) shows that the aquifer is vertically divided by slightly impermeable barriers.

The third zone is distinguished by tritium-free waters with very low  $^{14}\text{C}$  content (1.3-6.9% modern). They appear at the locations in the Vranjska and Bujanovac Spa. The low content of  $^{14}\text{C}$  and the absence of tritium are a clear mark of the existence of groundwater older than 10,000 years. Because the initial activity of infiltrated waters has not yet been determined, the age of these waters cannot be calculated exactly. For  $A_0 = 85\%$ , DIC = 6.6 to 0.3‰ indicate dilution by "dead" carbon (magmatic or marine origin), so that the age of waters may be less.

#### Estimation of Geothermal Water Temperatures

Geothermal water temperatures have been estimated from various quartz and cation-ratio geothermometers (Figure 9). The highest silica concentration of 90 mg/l from boreholes suggests the base temperature of 130°C (maximum measured is 126°C) for Vranjska Spa thermal waters. It seems that this value is in agreement with prediction of Na/K/Ca corrected geothermometer (117-125°C). They are considerably lower than temperatures predicted by Na/K ratio (125-192°C). This means that the likely maximum water temperature, which is expected at depth, is probably around 130°C in granodiorite. Temperatures predicted by cation geothermometers should be considered as the upper limit of base temperature. For the Bujanovac Spa location, the quartz geothermometer and the Na/K/Ca corrected thermometer predict temperatures of 100°C which are much higher than the measured ones (42°C). This is in good agreement with geologic data which predict that here it is dealing with the secondary aquifer, whereas the place of the primary with higher temperatures is unknown.

#### Conclusions

Up-to-date investigations show that the Surdulica aquifer is a complex system with groundwaters of different ages and temperatures. Isotopic and chemical compositions of examined waters have been formed under the influence of mediterranean and continental climates, and geochemical characteristics, and the structure of the granodiorite aquifer. These influences produce variations in the parameters of the meteoric water lines for precipitation, rivers, and springs. Changes of  $\text{HCO}_3^-$ , isotopic composition of carbon, and D,  $^{18}\text{O}$  and  $^3\text{H}$  contents in waters from the top down to the bottom of the aquifer indicate that the genesis of geothermal waters is from precipitation. Three types of groundwaters are identified: modern

from natural springs (61-94% of modern  $^{14}\text{C}$ , 5-69 TU), older from the middle and higher elevations (38-55% of modern  $^{14}\text{C}$ , 3-65 TU), and very old from Vranje depression. Based on  $^{14}\text{C}$  content, the age of the last is estimated between 10,000 and 28,000 years.

#### Acknowledgment

Partial financial support of this study by the IAEA (Research Contract No. 4852/R1/RB) is gratefully acknowledged.

#### LIST OF REFERENCES

- Anderson, E., 1985, Review of Vranjska Banja Geothermal Prospect, Scientific and Engineering Aspects: Wellington, New Zealand, GENZ-Geothermal Energy, New Zealand.
- Babovic, M., M. Vukanovic, V. Krajacic, M. Rakic, and M. Dimitrijevic, 1970, Basic Geological Map, Chart Vranje, Geozavod, Fed. Geol. Inst., Beograd.
- Henley, R.W., et al., 1985, Fluid-Mineral Equilibria in Hydrothermal Systems, *Reviews in Economic Geology*, Vol. 1, pp. 31-43.
- Milovanovic, B., S. Stankovic, M. Komatina, M. Hadzisehovic, M. Zupancic, N. Miljevic, R. Stepic, and B. Obelic, 1989, *Radiocarbon*, Vol. 31 (in press).
- Zujovic, J.M., 1893, Thermal springs of Vranjska Banja, in *Geology of Serbia: Serbian Royal Academy, Belgrade*, Vol. II-Granite, pp. 54-73.

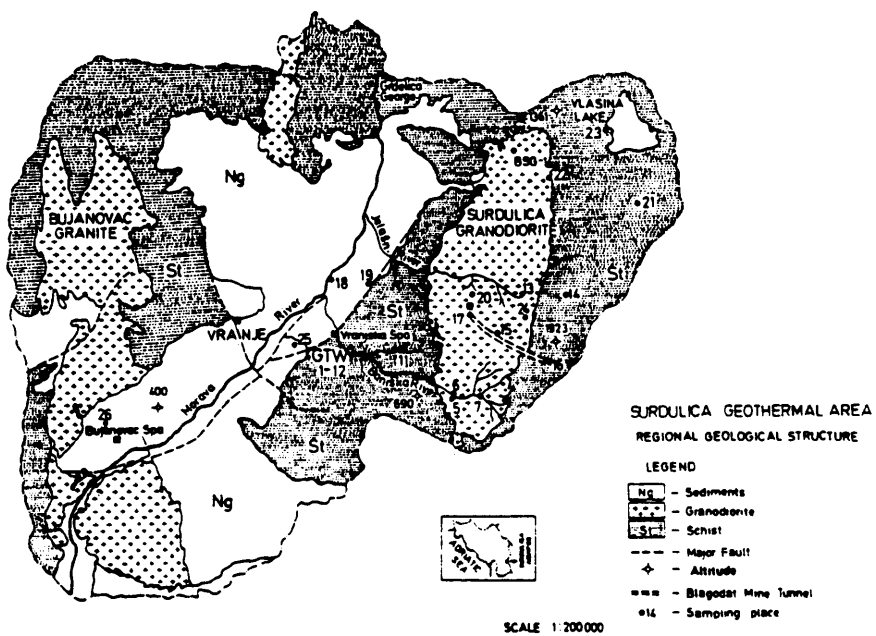
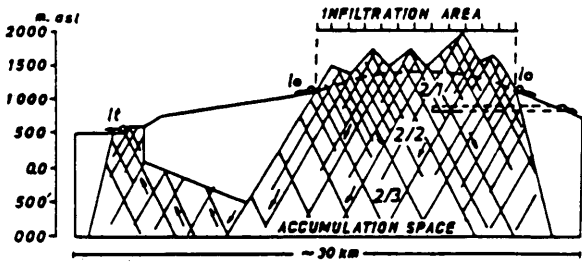


Figure 1. Geological map of area under investigation with location of sampling points.

# MODEL OF THE SURDULICA GEOTHERMAL SYSTEM

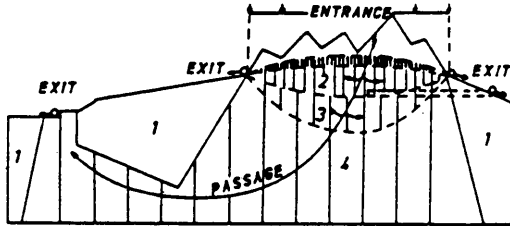
## a. MODEL OF THE HYDROGEOLOGICAL FUNCTION



### LEGEND:

- a. 1 Hydrogeological insulator
- 2 Hydrogeological collector
- 2/1 High
- 2/2 Medium
- 2/3 Low
- 1 Springs
- 1a Spring water
- 1r Mine water
- 1t Thermal water
- 1m Mine

## b. MODEL OF THE HYDRODYNAMICS



- b. Relative speed of the water exchange
- 1 Seasonal
- 2 Many years
- 3 Hundred years
- 4 Thousand years
- Passage scheme

Figure 2. Model of the Surdulica geothermal system.

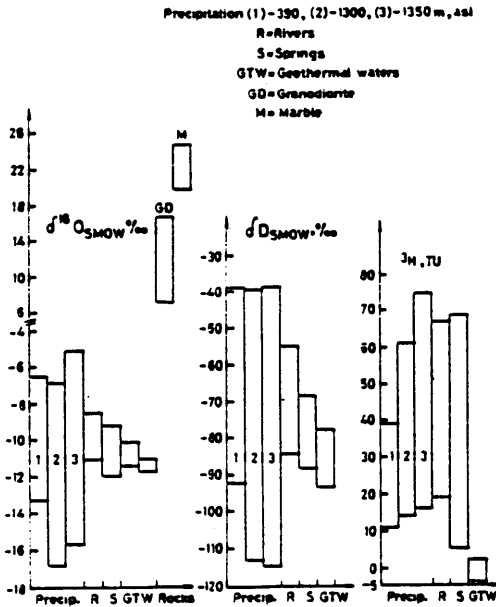


Figure 3. Data on  $^{18}\text{O}$ , D, and  $^3\text{H}$  in investigated area during 1986-89.

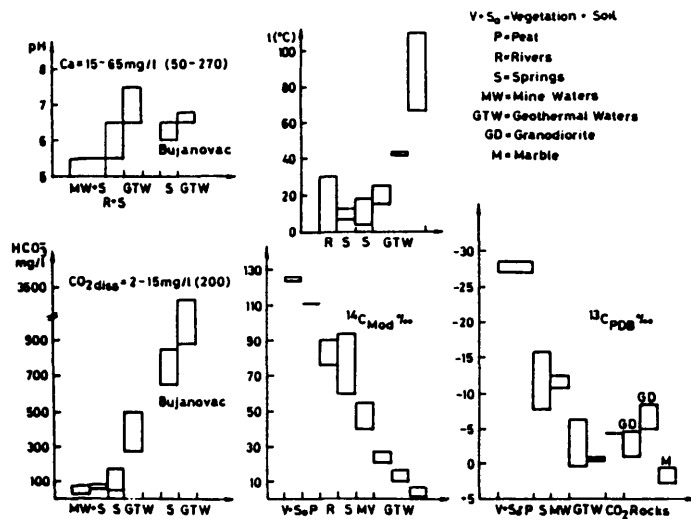


Figure 4. Isotopic variations of  $^{13}\text{C}$  and  $^{14}\text{C}$  in carbonate species of collected samples.

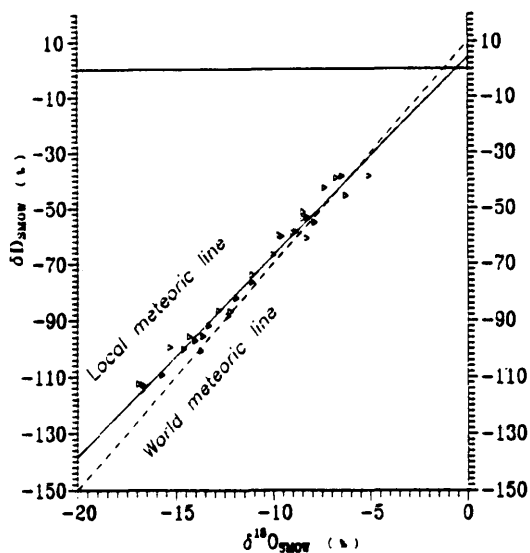


Figure 5. Local meteoric line for three stations (390-1350 m asl).

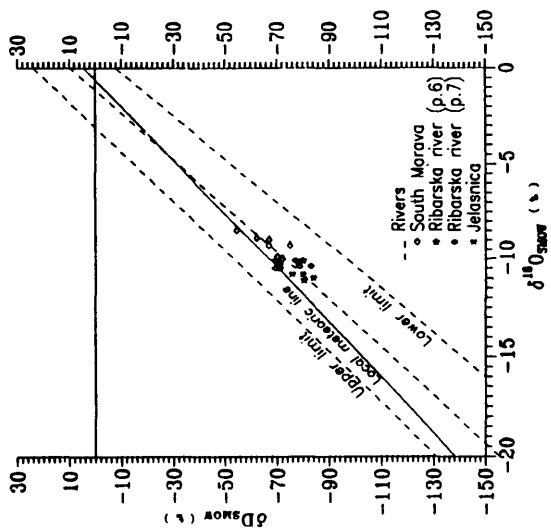


Figure 6. Position of river  $\delta D - \delta^{18}O$  relation and local meteoric line.

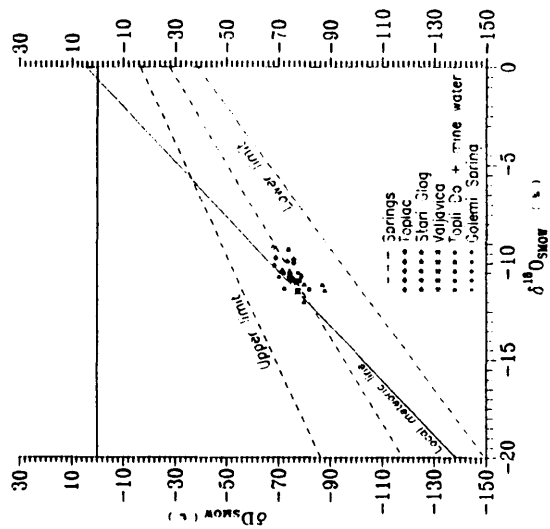


Figure 7. Position of spring  $\delta D - \delta^{18}O$  relation and local meteoric line.

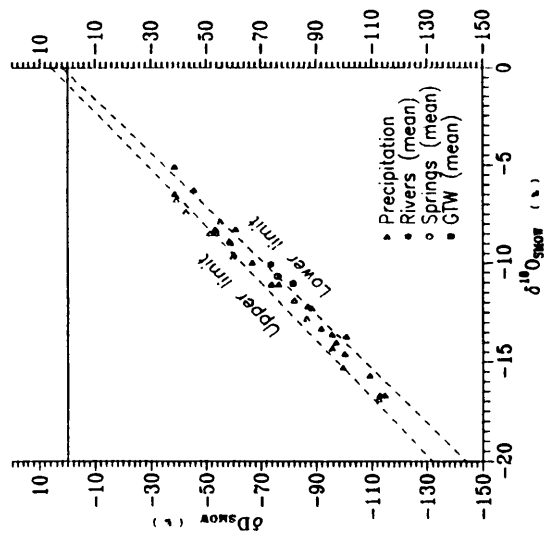


Figure 8. Range of local meteoric line with indicated mean values for rivers, springs, and geothermal waters.

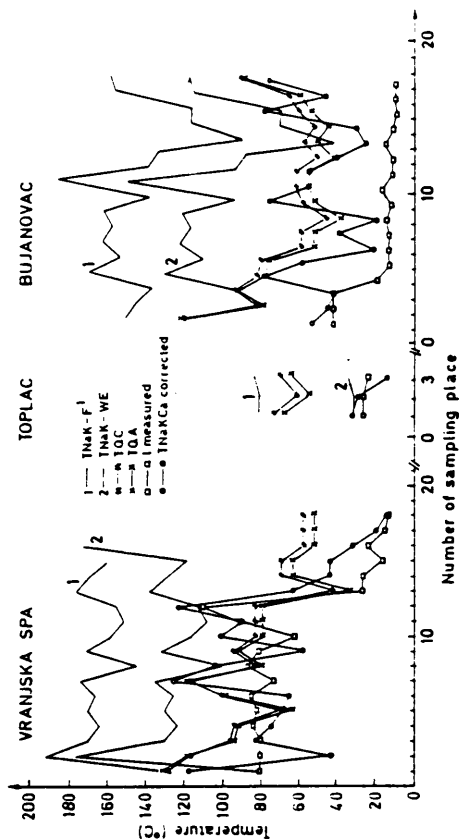


Figure 9. Groundwater temperatures evaluated by silica and cation ratio geothermometers (TNaK-F: Fournier; TNaK-We: Truesdell; TQC: Quartzz-no steam loss; TQA: Quartzz-maximum steam loss; 1: (Henley, 1985).



# COUPLED GEOCHEMICAL SPECIATION AND GROUNDWATER TRANSPORT MODELING IN SEDIMENTARY BASINS

Anne COUDRAIN-RIBSTEIN<sup>\*</sup>, Ghislain de MARSILY<sup>\*</sup> and Patrick GOBLET<sup>\*\*</sup>

<sup>\*</sup> Laboratoire de Géologie Appliquée, Université Pierre et Marie Curie, Centre National de la Recherche Scientifique, 4 place Jussieu, 75 252 Paris Cedex 05, France

<sup>\*\*</sup> Centre d'Informatique Géologique, Ecole Nationale Supérieure des Mines de Paris, 35 rue Saint Honoré, 77 305 Fontainebleau, France

**ABSTRACT** - Mass transport of solutes coupled with natural fluid convection in sedimentary basins is examined with the help of numerical experiments. The mathematical model is the result of the coupling of a fluid flow and mass transport code with a geochemical speciation code ; it thus represents the migration of reactive chemical elements as well as fluid and heat flow. The computation of precipitation and dissolution mechanisms includes the thermodynamic speciation of the solution as well as first order kinetic reactions. A theoretical example illustrates how, in a thermal convective cell, the mass transport depends on the velocity of the reactions and on the evolution of the temperature field.

## Introduction

Observations of samples from deeply buried sediments often show minerals that have been transformed by diagenetic processes. Dissolution features, crystal overgrowths and compaction effects provide evidence of processes that occur during diagenetic evolution. The modifications are due to the physical transformation of crystal grains and to chemical reactions between the mineral and liquid phases present in the pore space. But observed mineral transformations cannot be explained simply as chemical reactions between the minerals of the rock and the adjacent interstitial solution because its volume is not sufficient to supply the requested chemical elements. One therefore has to assume that the system is open to the displacement of the solution (see for example Fritz et al., 1984).

Because of the solubility dependence on temperature, movement of a fluid through a medium with variable temperature may induce dissolution and precipitation, and, fluid flow may exist in most of the geologic bodies of the crust.

The sediments are in general permeable from the time they are deposited until the pore space is completely filled by mineral precipitates or closed by compaction. Where communication with surface water is possible, forced fluid convection associated with topographic effects is certainly dominant in many sedimentary systems. Where communication with the surface water is not possible, fluid movement may be provided by thermal convection. If a horizontal density gradient exists, due for example to a gradient of temperature, the configuration is unstable. Because lithologic boundaries are never strictly planar and because of the variability of the heat transfer parameters, horizontal variability of the density must be the general case. Moreover, even if isotherms were parallel to the geopotential surfaces everywhere, it can be shown (e.g. Wood and Hewett, 1984) that, when porous fluid-saturated bodies are of great extension (e.g. greater than one kilometre), and when they are

subjected to the normal geothermal gradient, large-scale eddy currents will spontaneously arise and persist within them. The velocity of these currents is on the order of one meter per year and, taken over a period of several million years, the mass flux accompanying such fluid flow is very large.

An approximate analysis of the flow through the temperature gradients at the boundaries of a convection loop has been given by Wood and Hewett (1984). They presented a model which considers a one-dimensional flow along a streamline, assumes local equilibrium, takes into account one species subject to dissolution or precipitation (silica, calcite, feldspar or hydrocarbon). Assuming that porosity, pressure, velocity and density of the fluid are constant in space and time, an analytical solution exists. The use of such analytical solutions (see also Coudrain-Ribstein, 1988) is interesting because their formulation itself may illustrate the dependence of the results on the parameters. However, the computed results are limited due to the tight set of assumptions.

Another example of a quantitative model for convection related to diagenesis was developed for a specific configuration from a North Sea oil reservoir (Rabinowicz et al., 1985). The evolution of temperature and pressure, linked to the buoyancy movements and to the burial depth of the layer were computed. Then, assuming local equilibrium, quantities of dissolved or precipitated calcite and amorphous silica were independently computed as functions of temperature and pressure changes but neglecting the transport phenomena of the chemical elements.

Our purpose is to present a general model allowing us to take into account transport of elements in solution and geochemical reactions arising from convective flow in a variable temperature field. Numerical experiments are presented that give insights into factors controlling the distribution of the reactions such as temperature field and reaction velocities.

## 1 - MATHEMATICAL MODELLING

The model presented here takes into account the movement of fluid, and the transfer of heat and chemical elements in a porous medium. The partial differential mass-balance equations are solved by the finite element method.

### 1.1 - Modelling of fluid and heat transfer in METIS

The model used to simulate the transfer of fluid and heat is METIS (Goblet, 1981), where fluid and heat transfers are coupled by the temperature dependence of the dynamic viscosity ( $\mu$ ), using Bingham equation, and the mass per unit volume of the fluid ( $\rho$ ), using a linear expression. Balance equations of fluid and heat are solved alternately. At each time step, the hydraulic regime is assumed to establish itself very quickly, and the resulting mass balance equation is :

$$\text{div}(\rho \vec{V}) = 0 \quad (1)$$

with  $\rho$  : mass per unit volume of fluid ( $\text{kg.m}^{-3}$ ) ;  $\vec{V}$  : Darcy velocity ( $\text{m.s}^{-1}$ ) of which the expression is :

$$\vec{V} = -\frac{k}{\mu} (\overline{\text{grad}} P + \rho g \overline{\text{grad}} z) \quad (2)$$

with  $k$  : intrinsic permeability coefficient ( $\text{m}^2$ ) ;  $\mu$  : fluid viscosity ( $\text{kg.m}^{-1}.\text{s}^{-1}$ ) ;  $P$  : pressure ( $\text{kg.m}^{-1}.\text{s}^{-2}$ ) ;  $g$  :  $9.81 \text{ (m.s}^{-2}\text{)}$  ;  $z$  : vertical distance oriented upwards (m).

The unsteady temperature distribution is described by the following equation where conduction, thermal dispersion and convection are taken into account :

$$\text{div} (\lambda^* \overline{\text{grad} T} - \gamma_f \overline{V} T) = \gamma^* \frac{\partial T}{\partial t} \quad (3)$$

with  $\lambda^*$  : equivalent thermal conductivity of fluid-filled medium ( $\text{W.m}^{-1}.\text{K}^{-1}$ ) ;  $\gamma_f$  : heat capacity of the fluid ( $\text{J.m}^{-3}.\text{K}^{-1}$ ) ;  $\gamma^*$  : heat capacity of fluid-filled medium ( $\text{J.m}^{-3}.\text{K}^{-1}$ ) ;  $t$  : time.

## 1.2 - Brief overview of the modelling of reactive chemical element transport

The first question that arises is to decide whether it is necessary or not to study simultaneously the transport processes and the chemical reactions. As a first approximation, it becomes interesting to study both processes simultaneously when at least one of the following phenomena acts on the same scale as the one of interest : the kinetics of the reactions, the mixing of different solutions, the adsorption processes, or the evolution of equilibrium conditions (i.e. temperature, mineralogy, organic content).

The second question concerns the way to model the coupled processes of transport and geochemical reactions. Because the solubility depends on the activities of the species, the speciation (distribution of the chemical elements among the species) has to be computed while dissolution and precipitation are being studied.

### 1.2.1 - Uncoupled approach

In this case, the geochemical reactions (per unit space and time) and transport processes are solved independently. The balance of geochemical reactions for the space and time under consideration is estimated in proportion to the flux of water. Examples are given by Back and al. (1983) and Garven and Freeze (1984).

### 1.2.2 - Coupling equations in a one-step procedure

The two types of processes are described by a set of equations which is solved globally. Two methods are used to build such models. One is to extend geochemical path models (e.g. Helgeson, 1968) which handle mineral dissolution and precipitation, to open systems by adding a source transport term (Michard and Fouillac, 1974 ; Lichtner et al., 1986). Even with one-dimensional model, and a limited description of transport processes, these authors noticed that with this implicit formulation, one has to deal with very large sparse matrices.

The second method is an extension of the classical transport models which describe retention on the solid phase by a global partition function (the well-known  $K_d$  approach, e.g. Goblet, 1981). Thus, the extension consists in replacing this function by taking into account the interactions between several species. However, the authors dealt with a limited number of species even for a one-dimensional configuration (Rubin and James, 1973 ; Kirkner et al., 1985).

A complete description of transport and geochemical processes exists in the one-dimensional CHEMTREN model presented by Miller and Benson (1983). For realistic problems the size of the system to be solved becomes extremely large.

### 1.2.3 - Coupling equations in a two-step procedure

The two types of processes are established in two sets of equations which are solved alternatively. The first one corresponds to the aqueous speciation and yields explicit geochemical source terms. The second one corresponds to the total mass balance equations, where the chemical source terms are known.

Di Toro (1976), studying biochemical processes along vertical profiles, has demonstrated the interest of using the components and choosing them to establish the equations, and shown that the two-step procedure is more economical than the one-step one. Several authors (Cederberg, 1985 ; Sanford and Konikow, 1989) have used this two-step procedure.

To generalize the modelling to any number of species and to any precise description of transport processes, the two-step procedure is more convenient. One treats successively each set of equations of the same type. Numerical problems can be more easily handled, and matrix sizes are similar to those used when geochemical and transport codes are solved separately.

### 1.3 - Modelling of chemical transport in STELE

The first point of our approach is to emphasise the interest of defining an active geochemical system, i.e. to define which set of species, reactions and reaction rates have to be taken into account to describe the processes in the configuration under study. This definition is carried out on the basis of available chemical data, and with the help of geochemical codes. Then, this reduced system, instead of the whole data base set, is handled by the coupled code.

The second point concerns the general method that we developed to clearly pose the chemical constraints and the equations of speciation and transport. It is based on the use of chemical components as presented by Morel (1983) : each chemical species is expressed as a linear combination of components. The set of components is a mathematical basis of the vectorial set of chemical species. The advantages of this method become more apparent when the components are chosen for a specific geochemical system.

A coupled model STELE, built according to this method, and a two-step procedure, was developed on the basis of the existing transport code METIS and a geochemical speciation code CHIMERE (Coudrain-Ribstein and Jamet, 1989). For computing the speciation, a set of non-linear mass balance equations has to be solved :

$$\text{TOT}(E_i) = \sum_j \alpha_{ij} C_j \quad (4)$$

with  $\text{TOT}(E_i)$  : total concentration in the aqueous phase of the  $E_i$  component ;  $j$  : index on aqueous species ;  $\alpha_{ij}$  : stoichiometric coefficient of the  $E_i$  component in the  $E_j$  species ;  $C_j$  : concentration of the species  $E_j$ .

On the one hand, the use of this notion of components allows us to reduce the number of unknowns, when computing the speciation. It is reduced at least from  $N_s$ , the number of species of the active geochemical system, to  $N_c$ , the number of components. On the other hand, it allows us to reduce the number of unknowns when computing the transport. Assuming that each aqueous species has access to the same porosity and has the same dispersion coefficient, one only has to solve the transport equations for the total concentrations of components when they vary in space. Taking into account convection, dispersion and chemical reactions, the total mass balance equation is :

$$\text{div}\{D \overline{\text{grad}} \text{TOT}(E_i) - \overline{V} \text{TOT}(E_i)\} + \omega \phi = \omega \frac{\partial \text{TOT}(E_i)}{\partial t} \quad (5)$$

with  $D = \omega d + \alpha V$  : coefficient of dispersion ( $\text{m}^2 \cdot \text{s}^{-1}$ ) ;  $d$  : diffusion coefficient in a porous medium ( $\text{m}^2 \cdot \text{s}^{-1}$ ) ;  $\alpha$  : intrinsic dispersion coefficient (m) ;  $\omega$  : porosity ;  $\phi$  : geochemical flux ( $\text{mol} \cdot \text{l}^{-1} \cdot \text{s}^{-1}$ ), which corresponds to the transfer of this component between the solution and the mineral phase. At this stage, this term is approximately computed by the convenient kinetic relation :

$$\phi = \frac{1}{dt^*} \{ \text{TOT}(E_i)^* - \text{TOT}(E_i) \} \quad (6)$$

with  $dt^*$  : kinetic coefficient (s) ;  $\text{TOT}(E_i)^*$  : total concentration at equilibrium with mineral phases. The range of the time necessary to achieve equilibrium, without flow, is about three times  $dt^*$ . When only one reaction is taken into account between a mineral and an aqueous species, this expression is equivalent to the classical relation :

$$\phi = \pm k_c \left\{ 1 - \frac{Q}{K} \right\} \quad (7)$$

where the sign depends on how  $Q$  and  $K$  are expressed ;  $k_c$  is a kinetic coefficient ;  $Q$  and  $K$  are respectively the activity product and the thermodynamic constant of the reaction. Moreover, numerical simulations of the silica system in our temperature range showed that equations (6) and (7) are equivalent even when several aqueous species are involved. Whatever the difference is between these two formulations of the reaction rate, the conclusions derived from the results, presented later, about the range of the dissolved and precipitated quantities, and about the location of the maxima would not be changed. However, it is clear that it would be better to exchange equation (6) for an equation with dependence on the temperature, pH and mineral surface (e.g. Knauss and Wolery, 1988). In addition, the problem is how best to handle a non-linear problem. We have to transport several chemical entities which are bound by their geochemical fluxes. For both extremes, we know how to solve the problem.

The first extreme is when we are far from equilibrium with respect to the mineral phases. The problem becomes quasi-linear : geochemical fluxes may be determined before the solution of the mass balance equations. Their estimation after the solution is almost the same as before. Simulations presented below, assuming slow rates of geochemical reactions, belong to this first case.

The second extreme, is, on the contrary, when local equilibrium is assumed. The total concentrations of the components affected by equilibrium condition with respect to mineral phases are completely determined by the local temperature, and by the total concentrations of the components which are dependant on the equilibrium conditions. In equation 5, established for these components, the only unknown term is the geochemical flux. It can be expressed as an explicit form of the total concentrations of the preceding time step and the total concentrations at equilibrium.

In intermediate cases, when the time steps are too large to compute a good estimate of the geochemical fluxes at the beginning of the time step, the problem is non-linear and requires another development with iterations.

Another point to be noticed is that, when solving the mass balance equation (5), one assumes that the dispersivity of the medium is rather small. Because the geochemical flux term is a non-linear function of the concentrations, the simulation of the evolution of the mean concentration would be different from the evolution of the mean of the concentrations (Villermaux, 1985). For an accurate description of the coupled phenomena, when the dispersion of the transport processes is strong, we would suggest the use of a stochastic transport model.

## 2 - SIMULATION

A case study illustrates this coupled model and how it may be used for numerical experiments. It has a very simple, closed configuration where fluid motion is only due to thermal eddy currents. As a fluid particle moves, it encounters successively regions of high and low temperatures. For a

material such as quartz with a water solubility which increases with temperature, material will be leached from regions where the fluid is being heated and precipitated where it is cooled. For minerals such as calcite which show retrograde solubility, the precipitation and dissolution pattern will be reversed. Such geochemical structures are presented for the sandstone reservoirs of the Gabon Basin (Tardy and Cassan, 1981) and the North Sea chalk oil reservoir (Rabinowicz et al., 1985).

## 2.1 - Fluid and heat transfer

We considered a porous homogeneous layer whose horizontal extent is large compared to its 1 000 m thickness. The phenomena are simulated in a vertical cross section using the following parameters :

$\alpha_g = 5 \times 10^{-4} \text{ K}^{-1}$  ;  $k = 3.3 \times 10^{-13} \text{ m}^2$  ;  $\lambda^* = 1.96 \text{ W.m}^{-1}.\text{K}^{-1}$  ;  $\gamma_f = 4.18 \times 10^6 \text{ J.m}^{-3}.\text{K}^{-1}$  ;  $\gamma^* = 2.44 \times 10^6 \text{ J.m}^{-3}.\text{K}^{-1}$  ;  $d = 10^{-9} \text{ m}^2.\text{s}^{-1}$  ;  $\omega = 0.2$  ; dispersivity  $\alpha = 50 \text{ m}$

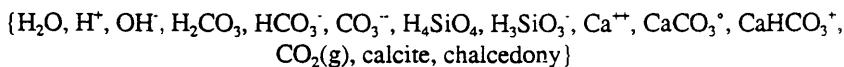
A preliminary simulation provides the evolution of the associated temperature and fluid velocity fields. According to a mean geothermal gradient, the initial temperature field, called  $T^*$ , shows temperatures increasing linearly with depth. They are prescribed on the upper ( $15^\circ\text{C}$ ) and lower ( $45^\circ\text{C}$ ) horizontal boundaries. In such a theoretical configuration, movement will occur if the Rayleigh number is greater than  $4\pi^2$  (Combarnous, 1970). But, if there is a departure of the isotherms from the horizontal, the fluid is unconditionally unstable and flow will occur regardless of the value of the Rayleigh number. In our simulated configuration, fluid motion appears ( $Ra^* \approx 150$ ) with square convection cells. Because of symmetry, we can reduce the simulation to one convective cell whose boundaries are closed to fluid and chemical elements. The simulation was done through 100 000 years, steady state is reached in approximately 10 000 years.

Simulations showed that the velocity field is almost achieved after 6000 years. A usual result is that, the maxima of velocity are in the middle of the edges (Fig. 1.a). Starting from the initial temperature distribution, the temperature is increased in the ascending flow path, and decreased in the descending flow path by a maximum of  $10^\circ\text{C}$  (Fig. 1.b). At 10 000 years, the temperature gradient with respect to space is maximum at the edge of the ascending and descending flow paths.

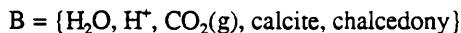
## 2.2 - Transport of chemical reactants

At the initial stage, the solution corresponds to a solution at equilibrium with respect to silica, calcite and a partial pressure of  $\text{CO}_2(\text{g})$  of  $10^{-2} \text{ atm}$  which is brought to equilibrium with respect to these two minerals at the temperature defined locally and in a system closed to carbon dioxide gas. A value of  $10^{-2} \text{ atm}$  for the  $\text{CO}_2(\text{g})$  partial pressure is consistent with measured ones in most groundwaters. With such conditions and using the thermodynamic data collected by Fritz (1981), the silica concentration increases with depth from  $1.26 \times 10^{-4} \text{ mol.l}^{-1}$  in the upper part to  $3.66 \times 10^{-4} \text{ mol.l}^{-1}$  at the bottom, when the calcium concentration decreases from  $1.54 \times 10^{-3} \text{ mol.l}^{-1}$  to  $1.37 \times 10^{-3} \text{ mol.l}^{-1}$ . When depth increases, the pH decreases from 7.36 to 7.04, when the partial pressure of  $\text{CO}_2$  increases from  $6.55 \times 10^{-3}$  at  $15^\circ\text{C}$  to  $2.12 \times 10^{-2}$  at  $45^\circ\text{C}$ .

Then, chemical transport simulations are carried out with a steady velocity field equal to the final one (Fig. 1). After the beginning of the circulation, we assume that the configuration remains closed to  $\text{CO}_2(\text{g})$ , and that dissolution and precipitation of calcite and chalcedony occur with a kinetic parameter  $dt^*$  equal to 1, 10 or 50 years (equation 6). At each time step, the geochemical reactions are computed for the prevailing temperature field. The species taken into account are :



The basis of components used is :



Assuming that the  $H_2O$  activity is constant and equal to 1, to compute the equilibrium speciation, two mass balance equations have to be solved :

$$TOT(H^+) = 0 \quad \text{and} \quad TOT(CO_2) = TOT^*(CO_2)$$

where \* designates the initial value. In our example, assuming that dissolution-precipitation of calcite and chalcedony may occur, the transport equations (5) in  $TOT(\text{calcite})$  and  $TOT(\text{chalcedony})$  must be solved. The other total concentrations of components remain constant.

### 2.2.1 - Temperature field influence

Field of precipitated and dissolved quantities of chalcedony after 1 000 years are given in figure 2. Along the descending path, silica is dissolved and calcite precipitates. On the contrary, along the ascending path, silica precipitates and calcite is dissolved. The maxima are respectively for chalcedony and calcite in the range of 0.075 and 0.05 mole per cubic meter of fluid-filled medium. This difference is in agreement with the smaller absolute value, with our assumptions, of the co-ordinate gradient of calcium concentration with regard to the silica one. After 1 million years, this quantity could reach 50 moles per cubic meter ; the porosity would then be reduced by about 1% which is in agreement with the value computed by an analytical solution by Wood and Hewett (1984).

It is interesting to note the location of the maxima of dissolved and precipitated quantities. It appears that the maximum of dissolution and precipitation are a function of the water flux and of the temperature gradient along the flow path. Because Wood and Hewett (1984) considered only the final temperature field, their discussion led to the conclusion that the maximum is to be expected at the edge of the vertical flow path where the temperature field is the strongest. When the temperature field is assumed to be constant and equal to the final one, our computed results are in agreement with such a conclusion (Fig. 2.b and Fig. 3.a). But, when the temperature field changes from  $T^*$  to the steady state one, two maxima coexist. One is located in the middle of the vertical flow path (Fig 2.a and Fig. 3.a, asterisk and black star symbol curves) where the flow crosses the isotherms and the velocity is maximum. The other one is located as the previous one, at the edge of the vertical flow path.

We also observe that, at the very beginning, the quantities are larger with the steady temperature field. This corresponds to the fact that the evolution of temperature with time crosses the influence of the evolution of temperature with depth. At one point of the ascending flow path, temperature increases with time (Fig. 1.b). This could induce dissolution of chalcedony. On the contrary, at this same point, the flow comes from the hot zone to the colder one, and this may induce precipitation. As a matter of fact, this competition causes the quantities precipitated before 100 years to be dissolved between 100 years and 500 years (Fig. 3.b, black triangle symbol curve to black star symbol curve). After this time, the consequence of the evolution of temperature with time is hidden by the precipitation linked to the transport process.

## 2.2.2 - Kinetic influence

The figure 3.b shows the influence of the kinetic parameter. After one hundred years and with a constant temperature field  $T^*$ , the greater the reaction velocity, the greater the precipitated quantity. When  $dt^*$  increases from 1 to 50 years, the maximum after one hundred years passes from  $8 \times 10^{-3}$  to  $5 \times 10^{-3}$  mol per cubic meter of porous medium. At one hundred years, the temperature field ( $T=f(t)$ ) almost equals the initial one. For same kinetic coefficient ( $dt^*=50$  years), the precipitated quantities for these two temperature fields are equal (empty rhombus and black triangle symbol curves).

After 500 years, one may compare how big is the difference between the two profiles computed on the one hand with a kinetic coefficient of 10 years and a constant linear temperature field  $T^*$  (white star symbol curve), and on the other hand, with a variable temperature field ( $T=f(t)$ ) and a kinetic coefficient of 50 years (black star symbol curve). The black star symbol curve presents smaller precipitated quantities than the black star symbol one, because of a difference in the kinetic coefficients, but also because the evolution with time of the temperature field ( $T=f(t)$ ) is taken into account (black triangle symbol profile progresses to the black star one).

## DISCUSSION AND CONCLUSION

In a large basin, fluid movements are to be expected in nearly all porous formations, either in an open system (topographic effects) or in a closed one (thermal eddy currents). Along a flow path, the chemical composition of the fluid changes as the chemical and physical conditions (composition of rocks or gases, pressure, temperature) vary. Thus, the movement of the fluid allows transport of chemical elements from one place (dissolution) to another (precipitation).

Little is known about the microscopic mechanisms or basin-wide systematics of reaction and transport in subsurface media. The study of the sedimentary environment is complicated by the wide range of the reaction rates of the different processes. Furthermore, direct observations can be made only at an instant in geologic time and laboratory experiments are difficult to extrapolate to natural scales of time and distance.

At present, the coupled mathematical models allow us to simulate the associated phenomena in a rigorous manner with respect to heat and mass balance. They provide tools for numerical experiments allowing us to evaluate the influence of each parameter or assumption on the evolution of the geochemical phenomena. The main difficulty when studying a real case is how to determine to the initial and boundary conditions of the configuration. At the modelling stage, the main difficulties are to take into account the space heterogeneity of the porous medium (Matheron and Marsily, 1980) and to compute the evolution of the permeability as a function of the dissolution-precipitation phenomena.

For our purpose, one has to account for transport processes (diffusion, dispersion, convection) and geochemical reactions linked to the evolution of chemical and physical parameters. On the one hand, transport codes solve linear differential equations and deal with one chemical species and hundreds to thousands of nodes ; on the other hand, geochemical codes solve algebraic non linear equations and deal with only one elementary space but with hundreds of species. Thus, the complexity of the full integration of geochemical calculations into a transport code could provide impractical tools consuming too much time and storage, and produce results too complex to be clearly interpreted. To minimize computing time and storage and to clearly write the balance equation, it is very important



to define the active geochemical system (which reactions and which reaction rates should be taken into account), to carefully choose the chemical components of the mathematical basis of each specific geochemical system and to use a two-step procedure.

The model built according to these rules is illustrated here by a theoretical example of a confined layer where the free convective movements are prompted by the normal geothermal gradient. The numbers derived from this simulation should be used with some caution considering the approximate nature of the calculations. For instance, we did not simulate the compaction phenomena, nor the evolution of porosity, nor the complex evolution of permeability. Computer analysis is presented here for its ability to sort out the competing processes, maintain natural scales of time and distance, and give integrated pictures.

The simulations show that even in quite unfavourable configurations silica and calcium carbonate transport and precipitation can be significant, and that a measurable alteration of the porosity by this mechanism can occur on time scales of millions of years. By unfavourable configuration, we mean, that the system is confined and the flow is limited to buoyancy movements, and that the value of the parameters (hydraulic and chemical) are smoothly distributed. Simulations also show how the evolution of the temperature field may influence the pattern of the quantities of dissolved and precipitated minerals.

To support such simulations, ore and oil prospecting ought to provide sufficient data (field studies, rock sample analyses) to identify the geochemical transfer and to localize the different convective movements.

**ACKNOWLEDGEMENTS** - The development of the model presented was supported by the "Agence Française pour la Maîtrise de l'Energie" and the "Centre National de la Recherche Scientifique", Paris, France.

#### References

- Back, J.W., Hanshaw, B.B., Plummer, L.N., Rahn, P.H., Rightmire, C.T. and Rubin M., 1983, Process and rate of dedolomitisation : mass transfer and  $^{14}\text{C}$  in a regional carbonate aquifer. *Geol. Soc. Am. Bull.*, Boulder, **94**, p. 1415-1429, 13 fig., 9 tab.
- Cederberg, G.A., 1985, TRANQL : A ground water mass-transport and equilibrium chemistry model for multicomponent systems. Ph. D., Stanford Univ., 117 p.
- Combarnous, M.A., 1970, Convection naturelle et convection mixte en milieu poreux. Th. Doctorat ès Sc. Phys., Univ. Paris, Ed. Technip.
- Coudrain-Ribstein, A., 1988, Transport d'éléments et réactions géochimiques dans les aquifères. Th. ès Sc. Univ. Strasbourg, 381 p.
- Coudrain-Ribstein, A. et Jamet, Ph., 1989, Choix des composantes et spéciation d'une solution. *C. R. Acad. Sc. Paris*, II, note bilingue, **309**, p.239-244.
- Di Toro, D.M., 1976, Combining chemical equilibrium and phytoplankton models - a general methodology. in Canale ed., *Modelling biochemical processes in aquatic ecosystems*, Arbor Sc. Pub. Inc., Michigan, p. 233-255.
- Fritz, B., 1981, Etude thermodynamique et modélisation des réactions hydrothermales et diagénétiques. Th. ès Sc. Univ. Strasbourg, *Sc. Géol. Mém.*, Strasbourg, **65**, 197 p.

- Fritz, B., Cassan, J.P., Clauer, N. and Tardy, Y., 1984, Interstitial fluid circulations and diagenetic mineral transformations in sedimentary basins : a geochemical modelling approach. in "Thermal phenomena in sedimentary basins", ed. Durand B., Technip, Paris, p. 293-300.
- Garven, G. and Freeze, R.A., 1984, Theoretical analysis of the role of ground water flow in the genesis of stratabound ore deposits. 1- Mathematical and numerical model. 2- Quantitative results. *Am. J. Sci.*, New Haven, 284, p. 1125-1174.
- Goblet, P., 1981, Modélisation des transferts de masse et d'énergie en aquifère. Th. D. I., Ec. Nat. Sup. Mines Paris, 225 p.
- Helgeson, H.C., 1968, Evaluation of reversible reactions in geochemical processes involving minerals and aqueous solutions. I- Thermodynamic relations. *Geochim. Cosmochim. Acta*, 32, p. 853-877.
- Knauss, K.G. and Wolery Th.J., 1988, The dissolution kinetics of quartz as a function of pH and time et 70°C. *Geochim. Cosmo. Acta*, 52, p. 43-53.
- Kirkner, D.J., Jennings, A.A. and Theis, T.L., 1985, Multisolute mass transport with chemical interaction kinetics. *J. of Hydrology*, 76, p. 107-117.
- Lichtner, P.C., Oelkers, E.H. and Helgeson, H.C., 1986, Interdiffusion with multiple precipitation-/dissolution reactions : transient model and the steady state limit. *Geochim. Cosmochim. Acta*, 50, p. 1951-1966.
- Matheron, G. and Marsily, G. de, 1980, Is transportation in porous media always diffusive ? A counter example. *Water Resour. Res.*, 16(5), p. 901-917.
- Michard, G. and Fouillac, Ch., 1974, Evaluation des transferts d'éléments au cours des processus d'altération des minéraux par des fluides. *C.R. Acad. Sc. Paris*, 278, série D, p. 2727-2729.
- Miller, C.W. and Benson, L.V., 1983, Simulation of solute transport in a chemically reactive heterogeneous system : model development and application. *Water Resour. Res.*, 19(2), p. 381-391.
- Morel, F.M.M., 1983, Principles of aquatic chemistry. Wiley & Sons, London, 446 p.
- Rabinowicz, M., Dandurand, J.L., Jakubowski, M., Schott, J. and Cassan, J.P., 1985, Convection in a North Sea oil reservoir : inferences on diagenesis and hydrocarbon migration. *Earth Planet. Sci. Lett.*, Amsterdam, 74, p. 387-404.
- Rubin, J. and James, R.V., 1973, Dispersion-affected transport of reacting solutes in saturated porous media : Galerkin method applied to equilibrium-controlled exchange in unidirectional steady water flow. *Water Resour. Res.*, 9(5), p. 1332-1356.
- Sanford, W.E. and Konikow, L.F., 1989, Simulation of calcite dissolution and porosity changes in saltwater mixing zones in coastal aquifers. *Water Resour. Res.*, 25(4), p. 655-667.
- Tardy, Y. and Cassan, J.P., 1981, Hypothèse sur la circulation convective des fluides de la diagenèse. Minéralogie et pétrologie des réservoirs gréseux de l'Infrasalifère du Gabon. *C. R. Acad. Sc. Paris*, 293, II, p. 587-592.
- Villiermaux, J., 1985, Génie de la réaction chimique. Conception et fonctionnement des réacteurs. Technique et Documentation, Lavoisier, 2<sup>e</sup> éd., 401 p.
- Wood, J.R. and Hewett, T.A., 1984, Reservoir diagenesis and convective fluid flow. Clastic diagenesis, AAPG, mem. 37, McDonald D.A. and Surdam R.C., eds, p. 99-110.

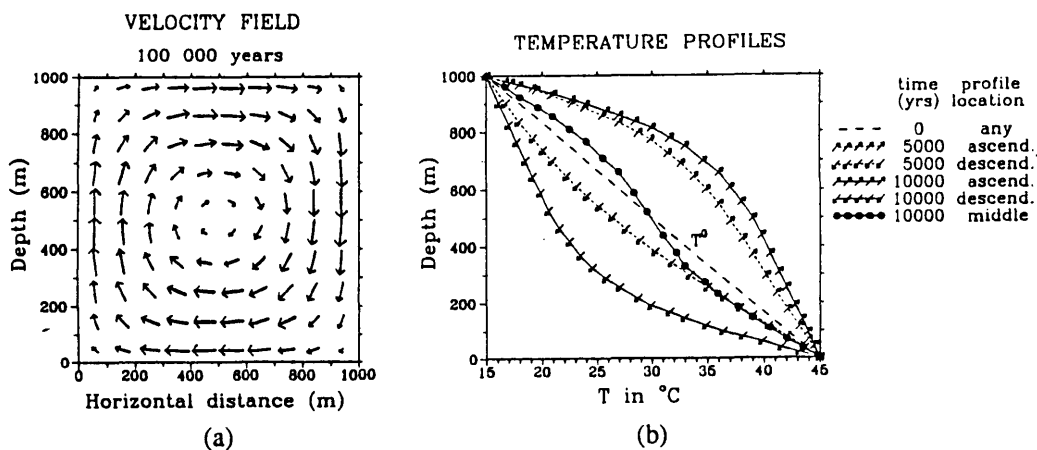


Figure 1- Computed Darcy velocities and temperature profiles.

- (a) velocities in a vertical cross-section. This steady state is achieved after 6000 years. Velocity values are proportional to arrow length, maximum equals  $1.26 \times 10^{-7} \text{ m.s}^{-1}$  ( $\approx 0.4 \text{ m.y}^{-1}$ ).
- (b) temperature. ascend.: profile in the ascending flow path ; descend.: profile in the descending flow path ; middle: profile in the central zone. The dashed line with no symbol corresponds to the initial field called  $T^*$ .

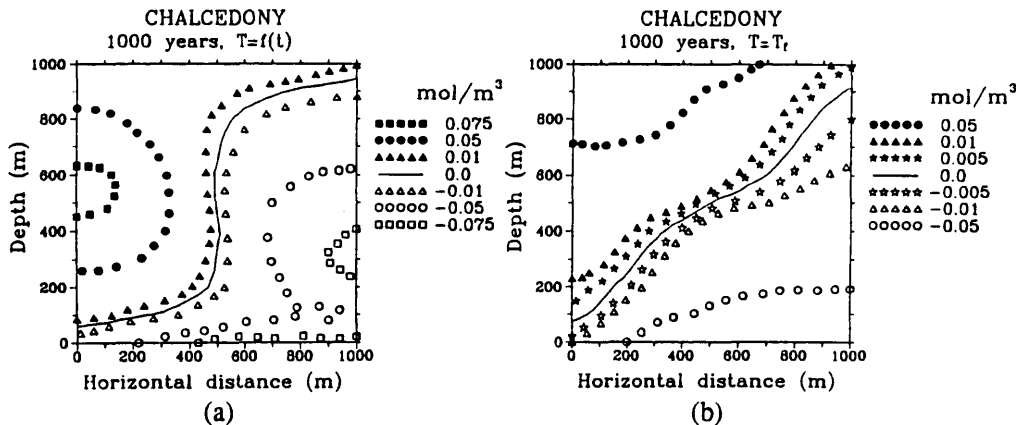


Figure 2 - Computed quantities (mol per cubic meter of fluid filled porous medium) of dissolved and precipitated chalcedony in a vertical cross-section.

- (a) evolution with time of the temperature field ( $T=f(t)$ ) is taken into account.
- (b) temperature field is assumed to be constant and equal to final one.

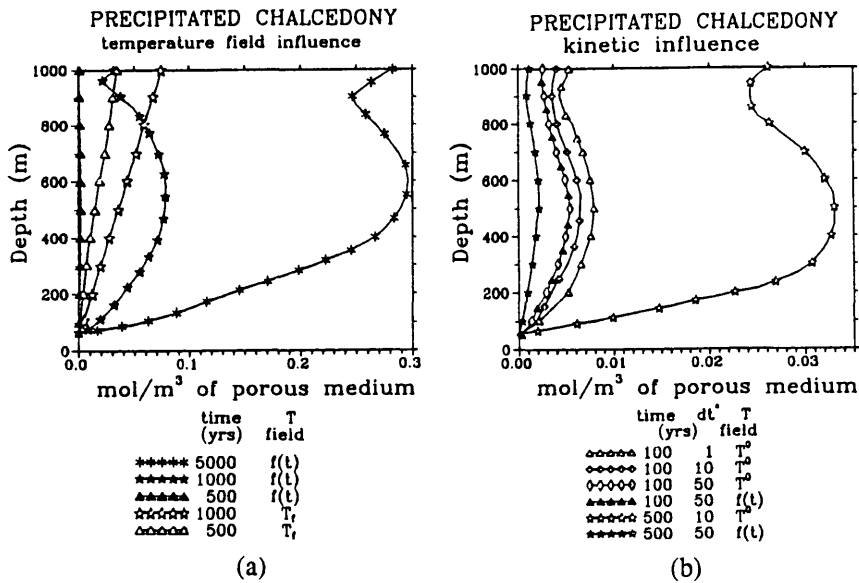


Figure 3 - Computed quantities of precipitated chalcedony along ascending flow path.

- (a) when the temperature field vary with time ( $T=f(t)$ ), the profiles at 5000 yrs and 1000 yrs present a pattern with two maxima at depth  $\approx 0$ m and  $\approx 500$ m. When the temperature field is assumed to equal the final one, the quantities are decreasing linearly with depth from 1000 m.
- (b) when the kinetic coefficient  $dt^*$  increases, the precipitated quantities decrease (compare empty symbol curves at 100 yrs and compare star symbol curves at 500 yrs).

# GROUND-WATER GEOCHEMISTRY AND INFORMATION TRANSFER IN ALLUVIAL BASINS IN ARIZONA

By

Frederick N. Robertson  
U.S. Geological Survey  
FB-44, Federal Building  
300 West Congress Street  
Tucson, Arizona 85701

---

## Abstract

Chemical and isotope analyses of ground water from 28 basins in the Basin and Range Province of Arizona and parts of adjacent States were used to evaluate ground-water quality, determine processes that control ground-water chemistry, and develop information transfer. Major processes controlling ground-water chemistry in individual basin aquifers as defined by geochemical modeling are the weathering of plagioclase, potassium feldspar, and ferromagnesian minerals; formation of montmorillonite; precipitation of calcite and probably of silica; and, in some basins, ion exchange.

The basins can be divided geochemically into two categories—closed systems that evolve under closed hydrologic conditions and open systems that are open to CO<sub>2</sub> and other constituents along the flow path. Through the categorization of the basins and the use of the geochemical models, climatic and geologic data, and analytical data of the basin-fill sediments, information transfer was developed for prediction of water quality and geochemistry throughout most of the area.

## Introduction

The U.S. Geological Survey initiated the Regional Aquifer-System Analysis Program in the late 1970's to study and define the Nation's most important aquifer systems. The Southwest alluvial-basins regional study was implemented in 1978 to evaluate the ground-water resources in the alluvial basins of the Basin and Range Province of Arizona and adjacent parts of California, Nevada, and New Mexico (Anderson, 1980). Large quantities of recoverable ground water are stored in the alluvial deposits of the intermontane basins. The water in storage is the result of accumulation over thousands of years. Recharge to the ground-water system is limited in most basins, and, in some basins, ground-water withdrawal greatly exceeds recharge. The purposes of the geochemical aspects of the investigation were to evaluate overall quality of the ground water, quantify geochemical processes that control ground-water chemistry, and provide transfer of information from intensively studied basins to other basins.

Information transfer was developed by defining the geochemistry and water quality in basins where sufficient data were acquired and projecting this knowledge to basins in which data are inadequate or geochemical histories are complex. This transfer of information is achieved primarily through the categorization of basins into closed and open systems. Under closed conditions, discrete reactions can be defined and transferred within and among basins. Reactions in open systems cannot be defined to the extent of those in closed systems but in some cases can be sufficiently defined for predicability purposes. In this paper, three basins are discussed that illustrate the transferability of geochemical information from one basin to another.

### Regional Geologic and Hydrologic Setting

The study area encompasses about 82,000 mi<sup>2</sup> of the Basin and Range Physiographic Province (Fenneman, 1931) in Arizona and adjacent small parts of California, Nevada, and New Mexico (fig. 1). The mountains and basins were formed by large-scale faulting during the Basin and Range disturbance. The faulting created a series of north-trending upthrown and downthrown blocks that were transformed by erosion and basin deposition into the present topography of alternating mountains and valleys.

The study area was divided into 72 basins or individual alluvial aquifers on the basis of ground-water divides or zones of minimal hydrologic basin interconnection. The basin-fill deposits that form the aquifers consist of clastic sediments, evaporites, interbedded volcanic rocks, stream alluvium, and flood-plain deposits and can occur as beds of sand and gravel or as poorly sorted interbedded silt, sand, and gravel. Deposits near the basin margins typically are alluvial-fan deposits or fluvial sand and gravel that grade laterally into silt, clay, and evaporites near the center of the basin. The sand and gravel deposits form the major aquifers, which are quantitatively the most important water resource in the region. Recharge to the basin aquifers occurs as infiltration of precipitation and runoff along mountain fronts and major streams. Ground-water discharge occurs through evapotranspiration and ground-water withdrawal.

### Geochemical Modeling

Chemical and isotope data were collected from 28 basins for development of geochemical models to define reactions and mass transfer that were compatible with observed changes in water chemistry and with rock minerals. The mass transfer is the amount of all pertinent minerals or gases that dissolve or precipitate in the course of these reactions. The modeling exercise relates the chemistry and mineralogy of the basin fill and the rocks of the mountains to the chemical evolution of the ground water within each individual basin.

The program BALANCE (Parkhurst and others, 1982) was used for derivation of the mass transfer similarly to that described by Plummer and others (1983). Model requirements are mineral phases and compositions and a complete chemical analysis of two points along the flow path. The mineral phases used in the modeling (table 1) were selected through known mineralogy of mountains and basin fill and through X-ray diffraction (XRD)

analyses of basin-fill material done during the study. The XRD analyses showed that plagioclase, quartz, and calcite were the most common minerals in the bulk fraction. Smectite, later determined to be montmorillonite, was the dominant mineral in the clay fraction. Some samples contained trace to small amounts of kaolinite.

Discrete reactions were defined during recharge and along general flow paths downgradient after recharge. Major reactions defined during recharge are dissolution of calcite and dolomite; weathering of plagioclase, ferromagnesian minerals, and potassium feldspar; and formation of montmorillonite. Reactions during recharge are similar for all basins and were derived using water compositions near mountain fronts. Major reactions downgradient after recharge are weathering of plagioclase and ferromagnesian

Table 1.--Phases used for derivation of mass transfer

| Reactant phases                 | Stoichiometry  |
|---------------------------------|--|
| Calcite                         | $\text{CaCO}_3$  |
| Dolomite                        | $\text{CaMg}(\text{CO}_3)_2$   |
| Oligoclase                      | $\text{Ca}_{0.25}\text{Na}_{0.75}\text{Al}_{1.25}\text{Si}_{2.75}\text{O}_8$   |
| Andesine                        | $\text{Ca}_{0.45}\text{Na}_{0.55}\text{Al}_{1.45}\text{Si}_{2.55}\text{O}_8$   |
| Potassium feldspar              | $\text{KAlSi}_3\text{O}_8$   |
| Augite                          | $\text{Ca}_{0.4}\text{Mg}_{0.8}\text{Fe}_{0.7}\text{Al}_{0.2}\text{Si}_{1.9}\text{O}_6$  |
| Hornblende                      | $\text{CaMgFeAlSi}_{3.5}\text{O}_{11}\text{OH}$  |
| Biotite                         | $\text{KMg}_{1.5}\text{Fe}_{1.5}\text{AlSi}_3\text{O}_{10}(\text{OH})_2$   |
| Silica (volcanic glass, quartz) | $\text{SiO}_2$   |
| Halite                          | $\text{NaCl}$  |
| Gypsum (anhydrite)              | $\text{CaSO}_4$  |
| Fluorite                        | $\text{CaF}_2$   |
| Aqueous phase                   | $\text{H}_2\text{O}, \text{CO}_2, \text{O}_2$  |
| Product phases                  | Stoichiometry  |
| Calcite                         | $\text{CaCO}_3$  |
| Montmorillonite                 | $\text{Ca}_{0.13}\text{K}_{0.07}\text{Mg}_{0.40}\text{Fe}_{0.10}\text{Al}_{1.99}\text{Si}_{3.65}\text{O}_{10}(\text{OH})_2$  |
|                                 | $\text{Ca}_{0.10}\text{K}_{0.13}\text{Mg}_{0.40}\text{Fe}_{0.10}\text{Al}_{1.99}\text{Si}_{3.65}\text{O}_{10}(\text{OH})_2$  |
| Goethite                        | $\text{FeOOH}$   |
| Silica (chalcedony)             | $\text{SiO}_2$   |
| Aqueous phase                   | $\text{Ca}^{+2}, \text{Mg}^{+2}, \text{Na}^+, \text{K}^+, \text{Al}^{+3}, \text{Fe}^{+3}, \text{Cl}^-, \text{SO}_4^{-2}, \text{F}^-, \text{HCO}_3^-, \text{H}_4\text{SiO}_4$ |

minerals, precipitation of calcite, and formation of montmorillonite. All reactions downgradient are not invariably similar, but they clearly indicate whether the ground water evolves under closed or open conditions.

On the basis of the geochemical modeling, the basins were divided hydrologically into two types—closed systems and open systems. Closed systems are those that do not receive additional water or gases along the flow path after initial recharge. Open systems are those in which additional water or gases enter the system after initial recharge. The aqueous geochemistry in closed systems is determined solely by the reactions of the initial recharge water in contact with the various minerals as the water moves downgradient. In these systems virtually all recharge occurs near the mountain front at the alluvium contact.

### Basins Studied

Three of the basins selected for modeling will be discussed to illustrate the evolution of ground-water chemistry under closed and open conditions (figs. 2A, B, C). Vekol Valley was selected for study because it is pristine, contains several deep wells that fully penetrate the aquifer, and is representative of many other basins. Ranegras Plain in arid western Arizona contains ground water with considerably larger concentrations of dissolved solids and trace elements than most other basins. Willcox basin is typical of the large oval-type basins in southeastern Arizona where much of the annual recharge may occur along the valley floor.

### Vekol Valley

The major aquifer in Vekol Valley is situated in the oval basin that lies to the south of the ground-water divide (fig. 2A). The basin is about 14 miles long and 13 miles wide and is typical in shape, geology, and water quality of many basins in arid south-central Arizona. The basin is bounded on the east by schist, granite, and andesite of the Table Top and Vekol Mountains and on the west by andesite, basalt, and schist of the Sand Tank Mountains (Wilson and others, 1969). Lithologic and geophysical logs of several wells throughout the basin show that the alluvial aquifer consists of several hundred feet of sand and gravel overlain throughout much of the basin by a thick silt-clay unit. The depth to water in the central part is between 400 and 450 feet below the land surface. The major recharge area of the basin is adjacent to the Sand Tank Mountains, which are the dominant mountains of the area and receive the highest precipitation. Ground-water flow is eastward toward the center of the basin and eventually southward out of the basin. Reactions were modeled along a general flow path from the recharge area about 2 miles downgradient to Vek 1 (Vekol 1) and 7 miles downgradient to Vek 2 in the basin center. Vek 2 is nearly 2,000 feet deep and fully penetrates the aquifer, which consists of about 1,000 feet of silt, sand and gravel. XRD analyses of the bulk-rock fraction of basin fill from a test well near Vek 2 indicated that labradorite, bytownite, andesine, and potassium feldspar are present throughout the column with albite and oligoclase between 1,400 and 1,900 ft. Andesine, augite, and potassium feldspar were selected as the primary reactant minerals.



The chemical composition of the ground water in the recharge area is typically a calcium bicarbonate type (table 2). Downgradient, the water evolves into sodium mixed anion type (fig. 3A). The phases and derived mass transfer associated with the evolution of the water are shown in table 3. Hydrolysis of augite and andesine and precipitation of calcite are the dominant reactions occurring along the flow path. Calcium decreases along the flow path primarily because of calcite precipitation and also partly due to montmorillonite formation. The soluble constituents of sodium, sulfate, and chloride increase substantially between Vek 1 and Vek 2. Ion exchange of calcium replacing sodium on the substrate, the most likely exchange reaction for the dilute waters, accounts for a small amount of the calcium and sodium concentrations. Alkaline earths are almost completely depleted downgradient, and bicarbonate decreases to about one-third of that of the recharge water. Potassium and fluoride concentrations increase slightly downgradient.

These observed trends in ground-water chemistry are typical in basins with water containing low to moderate dissolved-solids content that evolve under closed conditions. Depending on the individual basin and its geologic history, the waters may evolve into other types. As salinity increases, a sodium chloride, a sodium calcium sulfate, or a sodium calcium sulfate chloride type, as in Ranegras Plain, may evolve. Dissolved-solids concentrations of about 400 mg/L (milligrams per liter) in the recharge area may decrease to less than 200 mg/L downgradient owing to precipitation of calcite and montmorillonite or increase to several thousand milligrams per liter primarily as a result of dissolution of halite and gypsum.

Table 2.--Analytical data for selected wells in recharge areas, Vekol Valley, Ranegras Plain, and the Willcox basin

[Values are in millimoles per liter unless otherwise indicated; well names keyed to text]

| Phases                        | Recharge area       |                     |                     |                     |                     |                     |
|-------------------------------|---------------------|---------------------|---------------------|---------------------|---------------------|---------------------|
|                               | (13 wells)          | Vek 1               | Vek 2               | Ran 1               | Wil 1               | Wil 2               |
| pH (units)                    | 7.2                 | 7.4                 | 8.0                 | 7.7                 | 8.1                 | 7.8                 |
| Temperature (°C)              | 25.8                | 36.5                | 37.0                | 28.0                | 22.0                | 26.5                |
| Ca <sup>+2</sup>              | 1.95                | .75                 | .33                 | 3.24                | .38                 | .72                 |
| Mg <sup>+2</sup>              | .59                 | .58                 | .07                 | .20                 | .07                 | .05                 |
| Na <sup>+</sup>               | .97                 | 2.44                | 5.22                | 17.40               | 1.87                | 2.22                |
| K <sup>+</sup>                | .05                 | .04                 | .08                 | .12                 | .03                 | .08                 |
| Cl <sup>-</sup>               | .57                 | .59                 | 1.92                | 9.31                | .22                 | .45                 |
| SO <sub>4</sub> <sup>-2</sup> | .22                 | .27                 | .75                 | 7.08                | .14                 | .50                 |
| Alkalinity (meq/L)            | 4.81                | 3.56                | 1.92                | 1.32                | 1.99                | 2.49                |
| F <sup>-</sup>                | .01                 | .04                 | .03                 | .22                 | .23                 | .07                 |
| SiO <sub>2</sub>              | .72                 | .80                 | .70                 | .35                 | .57                 | .67                 |
| TDS (mg/L)                    | 495                 | 324                 | 421                 | 1,520               | 183                 | 259                 |
| PCO <sub>2</sub>              | 10 <sup>-1.70</sup> | 10 <sup>-1.98</sup> | 10 <sup>-2.80</sup> | 10 <sup>-3.01</sup> | 10 <sup>-3.48</sup> | 10 <sup>-2.61</sup> |

Table 3.--Summary of mass transfer for Vekol Valley, Ranegras Plain,  
and the Willcox basin

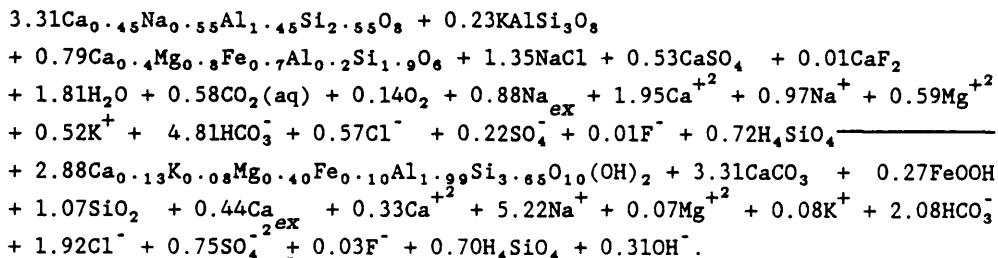
[Values\* of  $\alpha_p$  in millimoles per kilogram  $H_2O$ ; well  
names keyed to text]

| Phases                         | Flow path            |                   |                      |                      |                      |                      |
|--------------------------------|----------------------|-------------------|----------------------|----------------------|----------------------|----------------------|
|                                | Recharge<br>to Vek 1 | Vek 1 to<br>Vek 2 | Recharge<br>to Vek 2 | Recharge<br>to Ran 1 | Recharge<br>to Wil 1 | Wil 1 to<br>to Wil 2 |
| O <sub>2</sub>                 | 0.09                 | 0.05              | 0.14                 | 0.13                 | 0.18                 | -----                |
| CO <sub>2</sub>                | .33                  | .25               | .58                  | .58                  | .58                  | -0.06                |
| Calcite                        | -1.58                | -1.73             | -3.31                | -4.09                | -3.39                | .55                  |
| Oligoclase (An <sub>25</sub> ) | -----                | -----             | -----                | -----                | 4.37                 | -.78                 |
| Andesine (An <sub>45</sub> )   | 1.33                 | 2.33              | 3.66                 | 3.40                 | -----                | -----                |
| Potassium feldspar             | .06                  | .17               | .23                  | .10                  | .39                  | -.02                 |
| Augite                         | .51                  | .28               | .79                  | .73                  | -----                | -----                |
| Hornblende                     | -----                | -----             | -----                | -----                | -----                | -----                |
| Biotite                        | -----                | -----             | -----                | -----                | .50                  | -.17                 |
| Silica                         | -.83                 | -.44              | -1.07                | -1.22                | -3.19                | .67                  |
| Halite                         | .02                  | 1.33              | 1.35                 | 8.74                 | .00                  | .23                  |
| Gypsum                         | .05                  | .48               | .53                  | 8.86                 | .00                  | .36                  |
| Fluorite                       | .01                  | .00               | .01                  | .10                  | .11                  | -.02                 |
| Montmorillonite<br>(felsic)    | -----                | -----             | -----                | -----                | -3.19                | .58                  |
| Montmorillonite<br>(mafic)     | -1.06                | -1.82             | -2.88                | -2.60                | -----                | -----                |
| Goethite                       | -.25                 | -.02              | -.27                 | -.25                 | -.43                 | .19                  |
| Ion exchange**                 | .35                  | .09               | .44                  | 3.06                 | -1.02                | .35                  |

\*Reactants are positive and products are negative.

\*\*Calcium replacing sodium on the substrate.

Regardless of increases or decreases in dissolved-solids content of the water, the mass transfer of the primary silicate minerals was found to be nearly identical and provided the basis for transferability of reactions within and among basins. An example of mass transfer typical of most of the basins throughout the area is illustrated by the following equation showing reactions from the recharge along the flow path to Vek 2 written to the predominant dissolved species under observed pH and Eh conditions:



## Transferability of Reactions

The transferability of reactions determined in Vekol Valley were tested in Ranegras Plain and the Willcox basin. Chemical models were developed along general flow paths using water compositions observed in the recharge areas and downgradient along the flow paths (table 2). Reactant minerals used in the models were selected to be consistent with the respective basin geology or available XRD data. Compositions of reactant and product phases were idealized and used consistently within and among basins to confirm the presence or absence of similar reactions. Reactions also were used consistently although a particular reaction, for example, ion exchange, might not occur in all basins.

### *Ranegras Plain*

Ranegras Plain is a moderately large basin 50 miles long and 15 miles wide in arid western Arizona that contains ground water of relatively high salinity (fig. 2B). The basin is bounded on the east by basalt and granite of the Little Harquahala Mountains and granite of the Granite Wash Mountains; on the south by basalt and andesite of the Little Horn, Eagle Tail, and Kofa Mountains; and on the west and north by andesite of the Plomosa and New Water Mountains and andesite and granite of the Bouse Hills (Wilson and others, 1969). The aquifer throughout most of the basin consists of sand and gravel that are overlain by an areally extensive fine-grained unit. Depth to the water table in the center of the basin is about 120 ft.

The major recharge area is adjacent to the Little Harquahala and Granite Wash Mountains owing to the higher precipitation in these mountains relative to that occurring in adjacent mountains. The Plomosa and New Water Mountains to the west, although smaller in area and lower in altitude, probably contribute some recharge. The Kofa Mountains to the southwest may not contribute significant recharge to the basin because much of the area drains to the south. Water-level data show that ground water is moving from the mountains toward the center of the basin northward to Bouse and out of the basin. In the southern part of the basin the direction of ground-water movement is poorly defined because of the flatness of the potentiometric surface and paucity of water-level data. The ground water contains dissolved-solids concentrations greater than 3,000 mg/L and large concentrations of trace elements. Arsenic, boron, chromium, fluoride, and selenium occur naturally and commonly exceed State or Federal maximum contaminant levels for these constituents.

Reactions were modeled along a flow path between the Little Harquahala and Granite Wash Mountains to Ran 1, a well near the depositional center of the basin. The phases used in Vekol Valley also were used in Ranegras Plain because of the similarity in geology of the mountains bounding the two basins. The change in solute composition along the flow path, however, is markedly different from the changes observed along the flow path in Vekol Valley (fig. 3B). The ground water is higher in calcium, sodium, sulfate, and chloride and lower in bicarbonate. In view of the large areal

extent and diversity of physiography within the region, differences in chemistry may be caused by variables such as additional reactions, similar reactions but with different minerals or mineral compositions, differences in the mass transfer of the silicates, or differences in the mass transfer of halite or gypsum.

Assuming similarity in geology, the reactions and mass transfer of the primary silicate phases along the flow path from the recharge area to Ran 1 are indeed almost identical to those in Vekol Valley, despite the considerable differences in water chemistry. The differences in chemistry can be explained by dissolution of gypsum and halite and the modification by an additional reaction, ion exchange. Calcium exchanging for sodium apparently is a highly significant reaction in controlling the sodium and calcium concentrations of the ground water.

The close similarity of the mass transfer of the aluminosilicates between Vekol Valley and Ranegras Plain in spite of the different dissolved content is significant because it provides a decisive factor for the validity of transferability of reactions. The validity is based on an assumption that the kinetics of the primary silicates are invariant in ground water under similar hydrologic and temperature conditions and mineral environments. Thus, the mass transfer would indicate that the major reactions have been identified and that the reactions are indeed transferable within and among basins. Although the differences in the concentrations of most major dissolved species are extremely large, the two compositions can be related by similar reactions and primary silicate mass transfer. The models have defined the nearly identical mass transfer for these silicate phases, the differing mass transfer for gypsum and halite, and an ion exchange of calcium for sodium.

#### *Willcox Basin*

The Willcox basin is typical of several large, broad basins in semiarid southeastern Arizona (fig 2C). The basin is the highest in altitude of the basin lowlands, about 4,100 ft above sea level and is surrounded by mountains with altitudes greater than 10,000 ft. At these altitudes, the mountains that bound the basin receive relatively large amounts of precipitation; for example, annual precipitation in the Chiricahua Mountains exceeds 35 in. The Chiricahua and Winchester Mountains are predominantly silicic volcanic rocks and the Dos Cabezas and Dagoon Mountains are predominantly granitic and volcanic rocks. The Pinaleno Mountains consist chiefly of granite and granitic gneiss. The permeable sand and gravel deposits of the upper part of the basin fill, which range from a few hundred feet to more than 1,000 ft thick, constitute the most important aquifer of the basin. Depths to water are considerably shallower relative to most basins and range from about 200 to 400 ft at the mountain front, in the case of the Chiricahua Mountains, to less than 20 ft near the playa. The major recharge area of the basin is adjacent to the Chiricahua Mountains that bound the southeastern part. The estimated annual recharge to the basin is 54,000 to 75,000 acre-ft (Brown and Schumann, 1969), of which one-half originates near these mountains and flows toward the playa in the center of the basin. The ground-water

chemistry is characterized by a calcium sodium bicarbonate or sodium calcium bicarbonate type, generally of less than 300 mg/L dissolved solids.

Reactions were modeled along a flow path of about 30 mi from the origin of Turkey Creek, the major drainage area of the Chiricahua Mountains, along the area near Turkey Creek to the playa. Oligoclase  $An_{25}$ , potassium feldspar, and biotite were selected as the probable silicate reactant phases on the basis of the geology of the Chiricahua Mountains. Quartz, feldspar, and mica are the chief minerals in the granite, gneiss, and acidic lavas found in the Dos Cabezas and Chiricahua Mountains (Meinzer and Kelton, 1913). In contrast to the definite water-chemistry patterns observed along the flow path of dilute waters in other basins, trends in the Willcox basin are less clear (fig. 3C). The difference in water chemistry is accompanied by differing mass transfer that is inconsistent with that of other basins. The mass transfer derived from recharge to Wil 1 shows an improbable ion exchange of 2.04 mmoles of sodium replacing calcium. It is highly unlikely that monovalent sodium ions would replace divalent calcium ions on the substrate in these dilute waters owing to the greater selectivity of calcium. Between Wil 1 and Wil 2 near the playa, phases are derived that do not agree with those determined for the previously discussed basins. The mass transfer of the silicate phases is reversed; potassium feldspar, plagioclase, and biotite are precipitating out of solution and montmorillonite, goethite, and silica are dissolving. The derived reactant and product phases also do not agree with the thermodynamic saturation state of the ground water. The ground water is undersaturated with respect to plagioclase (albite), potassium feldspar (adularia), the ferromagnesian minerals (diopside and clinostatite), and with the exception of the recharge waters, to dolomite. Ground water is near saturation with respect to calcite and chalcedony and is supersaturated with respect to montmorillonite, kaolinite, and iron oxyhydroxides (Ball and others, 1980). Thus, plagioclase, potassium feldspar, and biotite should not be precipitating out of solution, nor should montmorillonite or goethite be dissolving. Modeling results for the Willcox basin contradict the field mineralogical data, consistent model results for other basins, and thermodynamic constraints.

The difference between the mass transfer determined for the Willcox basin and for basins previously modeled may be explained by the mixing of additional recharge water with underflow owing to the shallow water table and permeable deposits. The overlying coarse-grained deposits and relatively large amount of precipitation and runoff apparently allow significant recharge through the overlying deposits to depths as great as 120 ft, the predevelopment depth to water near Wil 1. As depths to water decrease downgradient, the increased leakage and mixing result in the reversed trends in chemistry and mass transfer. Leakage is indicated by the high calcium to sodium ratios, reflected in the unrealistic ion exchange between recharge and Wil 1, which is indicative of recharge waters. Indeed, the larger calcium and magnesium concentrations of the ground water throughout the basin clearly suggest additional input of a recharge-type water. The system apparently is open to  $CO_2$  as observed by a decrease of pH and increase of  $PCO_2$  downgradient. Thus, reactions cannot be defined for evolution of the ground water in the Willcox basin because the system is open to  $CO_2$  and additional recharge. The reactions cannot be

defined owing to the incompatibility of the simultaneous occurrence of recharge and downgradient reactions.

### Information Transfer

Subsequent geochemical modeling in basins has shown that most of the basins evolve under closed conditions and that mountain-front recharge is quantitatively the most important mode of recharge. Central and western basins and eastern basins that contain confined aquifers evolve under closed conditions. Eastern basins that contain unconfined aquifers and flood-plain aquifers along major streams evolve under open conditions. Factors that determine open or closed systems are the amount and seasonal distribution of annual precipitation and the presence or absence of fine-grained confining units (Robertson, in press).

As reactions can be defined for most basins, geochemical information can be transferred or projected to basins that have few data or are undeveloped. Accurate estimates of the major element chemistry and the presence of some trace elements can be predicted. If the sulfate and chloride contents of the water are known, the major element chemistry can be estimated with a high degree of accuracy through the use of a simple equation using these constituents (Robertson, 1989a). For the most dilute waters containing little sulfate and chloride, the concentrations of major ions will be close to those of Vekol Valley. If the ground water contains larger dissolved-solids concentrations, the composition will have additional sulfate and chloride concentrations plus sodium and calcium, corrected for ion exchange, proportional to the dissolution of halite and gypsum. Using these corrective techniques, surprisingly close estimates of the ground-water chemistry can be determined. In an area where a water sample is not available, the chemical composition of the ground water can nonetheless be estimated if basin-fill material is available. Concentrations of chloride and sulfate in well-cuttings leachate closely predicts the concentrations of these ions in the ground water from the completed wells. Thus, water compositions can be estimated by analyses of samples from small-diameter drill core or of material that is already stored in repositories (Robertson, 1989a). This predictability also could be applied to open systems if large dissolved-solids concentrations are anticipated, even though reactions regarding these systems were not unequivocally defined. Some predictability is possible because salinity increases are related primarily to dissolution of halite and gypsum and their mediation of other ions.

Information transfer may also suggest the presence of several trace elements in ground water. Closed hydrologic systems favor the occurrence of trace elements, fluoride, hexavalent chromium, arsenic, molybdenum, selenium, and vanadium. Hydrolysis (weathering) of silicate minerals increases the pH of the water, which can affect ion exchange or under equilibrium conditions can oxidize elements to their soluble oxyanion state, mobilizing trace metals in the basin fill. The basin fill contains an abundance of trace elements. Closed systems also may remove interfering redox potentials or dissolved scavenger trace metals such as iron or manganese, which may reduce other metals to insoluble forms. In

particular, occurrences of fluoride, hexavalent chromium, and arsenic may be anticipated in specific areas in basins or specific basins in the area (Robertson, 1986; 1989b).

The transfer of modeling and geologic information is a potentially powerful tool for the assessment of water quality and geochemistry in undeveloped areas in basins in the Southwest.

### Summary

Geochemical models were used to identify the major reactions and associated mass transfer responsible for the evolution of ground water in several basins throughout the region. The mass transfer defined was found to be consistent within and among basins, allowing a transfer of information. Through categorization of basins into closed and open hydrologic systems, as defined by the geochemical models, information transfer was developed for much of the region. Ground-water compositions can be estimated and the occurrence of some trace elements can be predicted. The predictive technique should be highly useful in the evaluation of water quality and geochemistry throughout the region.

### References

- Anderson, T.W., 1980, Study plan for the regional aquifer-system analysis of alluvial basins in south-central Arizona and adjacent States: U.S. Geological Survey Open-File Report 80-1197, 22 p.
- Ball, J.W., Nordstrom, D.K., and Jenne, E.A., 1980, Additional and revised thermochemical data and computer code for WATEQ2—A computerized chemical model for trace and major element speciation and mineral equilibria of natural waters: U.S. Geological Survey Water-Resources Investigations 78-116, 109 p.
- Brown, S.G., and Schumann, H.H., 1969, Geohydrology and water utilization in the Willcox basin, Graham and Cochise Counties, Arizona: U.S. Geological Survey Water-Supply Paper 1959-F, 32 p.
- Fenneman, N.M., 1931, Physiography of the Western United States: New York, McGraw-Hill, 534 p.
- Hem, J.D., 1985, Study and interpretation of the chemical characteristics of natural water (3d ed.): U.S. Geological Survey Water-Supply Paper 2254, 263 p.
- Mason, Brian, 1966, Principles of geochemistry: New York, John Wiley, 329 p.
- Meinzer, O.E., and Kelton, F.C., 1913, Geology and water resources of Sulphur Spring Valley, Arizona, with a section on Agriculture, by R.H. Forbes: U.S. Geological Survey Water-Supply Paper 320, 231 p.

- Parkhurst, D.L., Plummer, L.N., and Thorstenson, D.C., 1982, BALANCE—A computer program for calculating mass transfer for geochemical reactions in ground water: U.S. Geological Survey Water-Resources Investigations 82-14, 29 p.
- Plummer, L.N., Parkhurst, D.L., and Thorstenson, D.C., 1983, Development of reaction models for ground-water systems: *Geochimica et Cosmochimica Acta*, v. 47, p. 665-686.
- Robertson, F.N., 1986, Occurrence and solubility controls of trace elements in ground water in alluvial basins of Arizona, in Anderson, T.W., and Johnson, A.I., eds., *Regional aquifer systems of the United States, Southwest alluvial basins of Arizona*: American Water Resources Association Monograph Series 7, p. 69-80.
- \_\_\_\_\_, 1989a, Prediction of water quality through geochemical modeling in undeveloped areas in the desert southwest, in U.S. Geological Survey Second National Symposium on Water Quality—Abstracts of the Technical Sessions, Orlando, Florida, November 12-17, 1989: U.S. Geological Survey Open-File Report 89-409, p. 77.
- \_\_\_\_\_, 1989b, Arsenic in ground water under oxidizing conditions, southwest United States: *Environmental Geochemistry and Health*, v. 11, no 3/4, p. 171-184.
- \_\_\_\_\_, in press, Geochemistry of ground water in alluvial basins of Arizona and adjacent parts of Nevada, New Mexico, and California: U.S. Geologic Survey Professional Paper 1406-C.
- U.S. Environmental Protection Agency, 1977, National interim primary drinking water regulations: U.S. Environmental Protection Agency Report EPA-570/9-76-003, 159 p.
- Wilson, E.D., Moore, R.T., and Cooper, J.R., 1969, Geologic map of Arizona: Arizona Bureau of Mines map, scale 1:500,000.



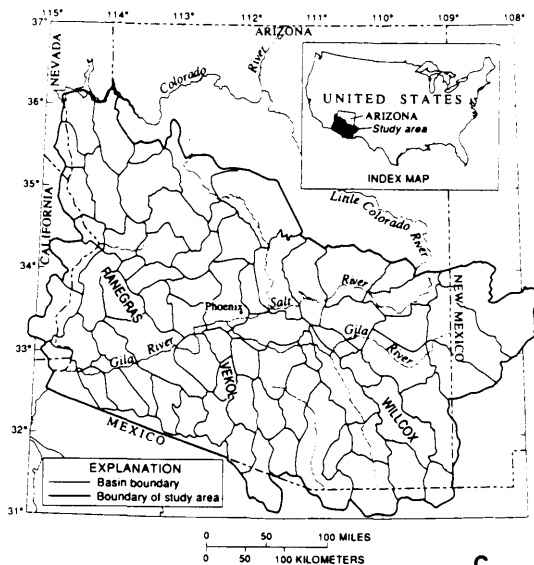
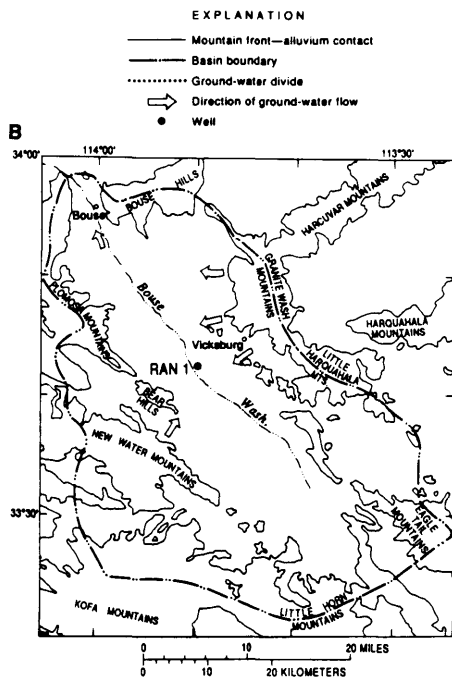


Figure 1.—Study area divided into 72 basins.



C

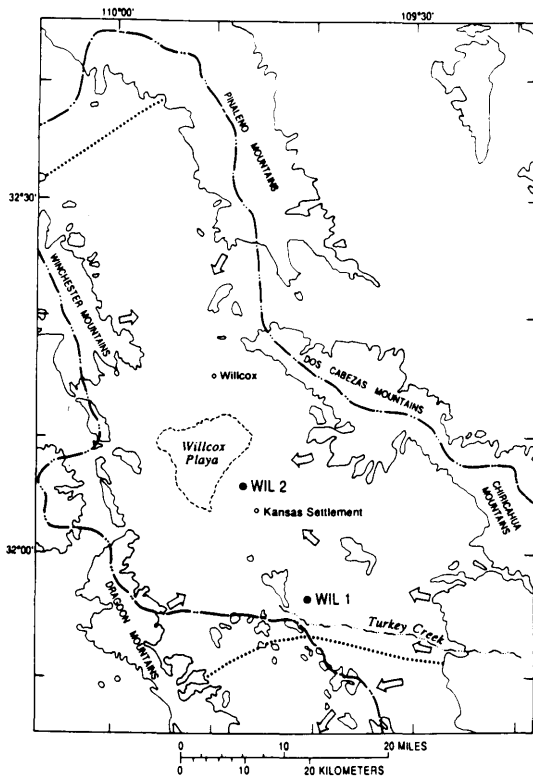


Figure 2.—Location of wells and direction of ground-water movement in basin modeled. A, Vekol Valley. B, Ranegras Plain. C, Willcox basin.

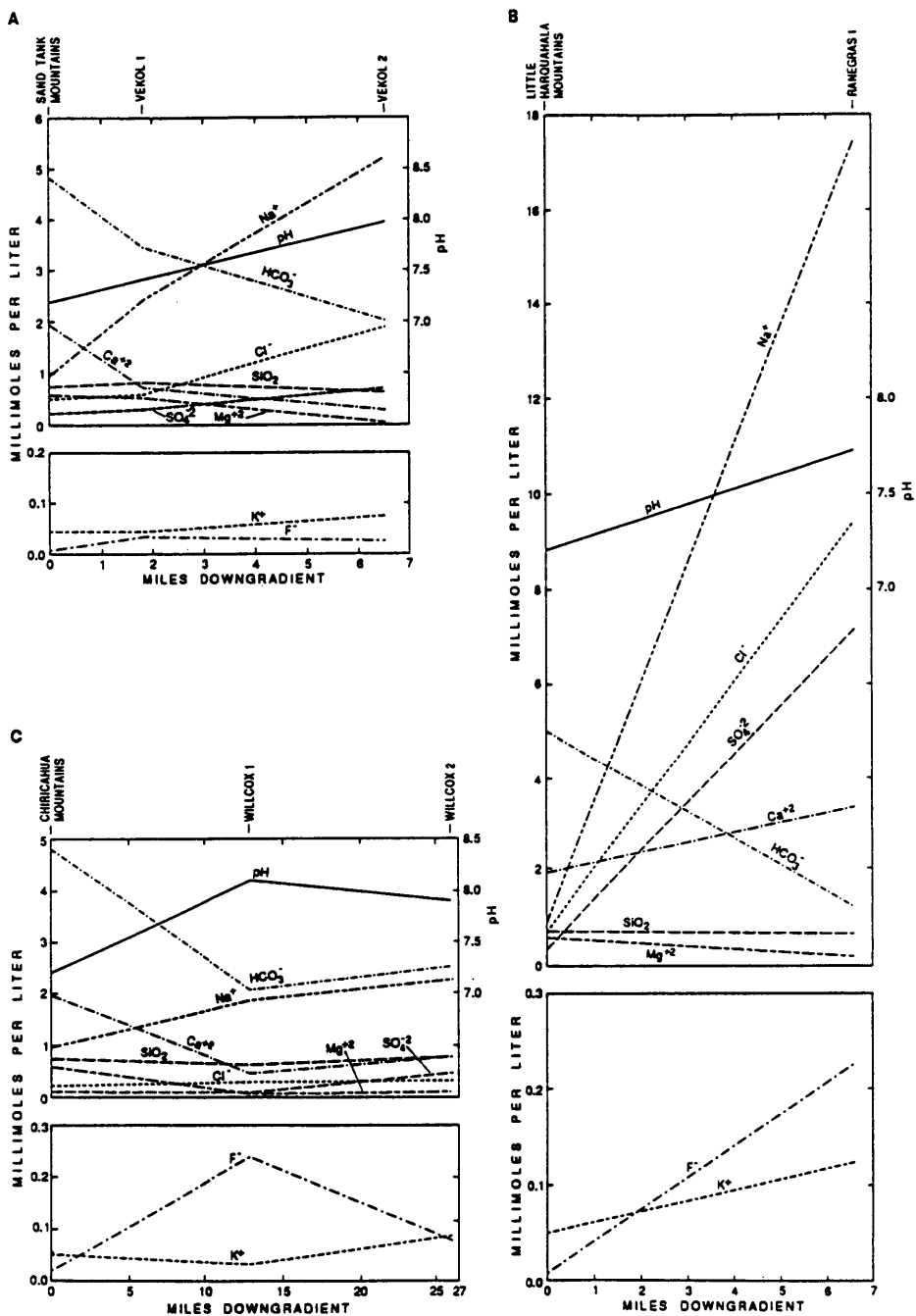


Figure 3.—Changes in concentration of dissolved chemical constituents in basins modeled. A, Vekol Valley. B, Ranegras Plain. C, Willcox basin.

SECTION 4: WETLANDS



# HYDROLOGIC AND WATER-QUALITY CHARACTERISTICS OF A WETLAND RECEIVING WASTEWATER EFFLUENT IN ST. JOSEPH, MINNESOTA

Rob G. Brown<sup>1</sup> and James R. Stark<sup>2</sup>

<sup>1</sup>U.S. Geological Survey, Ithaca, New York 14850

<sup>2</sup>U.S. Geological Survey, St. Paul, Minnesota 55101

**ABSTRACT**--Hydrologic and water-quality characteristics were determined for a wetland being used for tertiary treatment of wastewater in St. Joseph, Minnesota. The wetland consists of spruce-tamarack fen, and a cattail marsh with the wastewater being discharged into the bog, and the bog drains into the marsh. The wetland is underlain by flat-lying glacial outwash that ranges from 0 to greater than 20 m in thickness. Horizontal ground-water movement in the outwash aquifer is toward the wetland from the south, east, and west. There is a strong upward vertical hydraulic gradient (about 0.1) in the ground-water flow system beneath and around the wetland. Regionally, the glacial-outwash aquifer is unconfined, but it is confined or partly confined locally by peat deposits under the wetland. Analysis of the hydrologic balance of the bog from October 1985 through September 1986 indicates that the inflow was 44 percent ground water, 38 percent wastewater, 11 percent runoff (storm sewer), and 7 percent precipitation. The bog outflow was 93 percent surface water and 7 percent evapotranspiration. Inflow to the marsh was 74 percent surface water, 21 percent ground water, and 5 percent precipitation. Outflow from the marsh was 94 percent surface water and 6 percent evapotranspiration. Wastewater contributed 74, 96, and 81 percent of the total suspended solids, total phosphorus, and total ammonia plus organic nitrogen in the bog, respectively.

Other chemical inputs were from the storm sewer, ground water, and atmospheric deposition. The bog was found to retain 34, 14, and 14 percent of the suspended solids, total phosphorus, and total ammonia plus organic nitrogen, respectively. The marsh retained 44, 18, and 22 percent of these three constituents, respectively.

**Key Words;** wetlands, interdisciplinary, hydrology, water chemistry, ground water.

## INTRODUCTION

Small rural communities are using wetlands as a cost-effective alternative for tertiary treatment of wastewater effluent. Chemical constituents in secondarily treated effluent are assumed to be partially retained in the wetland through physical or biological action so that chemical concentrations in outflow from the wetland are within regulatory limits.

The U.S. Environmental Protection Agency, during a 1980 survey, identified 28 municipalities in Minnesota that discharge secondarily treated wastewater to wetlands for treatment (WAPORA 1983). Of those 28 municipalities, the U.S. Environmental Protection Agency identified the St. Joseph wetland in central Minnesota (Figure 1) as a research site for evaluating the effects of wastewater discharge on a wetland. The municipality of St. Joseph has been discharging secondarily treated wastewater into the wetland since 1962. The average wastewater discharge from 1962-86 was approximately 900 m<sup>3</sup> per day. The municipal sewage-treatment plant, located north of the city (Figure 1), serves a population of 3,000 permanent residents and 1,700 college students.

As part of the overall research at the St. Joseph site, the U.S. Geological Survey began a multiphase study in cooperation with the U.S. Environmental Protection Agency study to determine (1) hydrologic and water-quality characteristics of the wetland, (2) ground-water and surface-water interactions within the wetland, and (3) vegetational changes since wastewater discharges began. This paper presents the results of the first phase of the study; therefore, the results are preliminary and subject to change as additional field data collection, data analysis, and model simulation is planned in the next phases of the research.

## PHYSICAL AND HYDROLOGIC SETTING

The St. Joseph wetland is located northwest of the sewage-treatment plant and covers an area of approximately 0.186 km<sup>2</sup> (Figure 2). It consists of a 0.088 km<sup>2</sup> tamarack bog adjacent to a 0.098 km<sup>2</sup> cattail marsh (Figure 2). Grassland and isolated stands of hardwood forest surround the wetland. The surface-water drainage basin of the bog and marsh is 0.98 km<sup>2</sup>, of which 0.94 km<sup>2</sup> is drained by a storm sewer that collects runoff from the developed part of St. Joseph. Discharge from the sewage-treatment plant, overland runoff, and discharge through the storm sewer are the major surface-water sources of water to the wetland. The wetland discharges through a small channel to the South Fork Watab River approximately 400 m to the northwest.

The wetland is located on a glacial-outwash plain. Surficial geologic materials in the area consist of outwash, scattered areas of clay-rich till surrounded by outwash, alluvium associated with river valleys, and wetland deposits (Figure 1). The outwash on which the wetland is developed extends over an area of approximately 250 km<sup>2</sup>. The outwash ranges from 0 to 20 m in thickness; it is thickest in the immediate vicinity of the wetland. The aquifer consists primarily of medium to coarse, well-sorted sand. The outwash aquifer is underlain by clay-rich till that is as thick as 30 m in some areas. The till is, in turn, underlain by silty sandstone that overlays granite bedrock of Precambrian age (Kanivetsky 1978).

## GROUND-WATER FLOW

### Methods and Approach

A conceptual, three-dimensional finite-difference, ground-water-flow model was constructed from geologic and hydrologic information gathered at the site. The model was used to aid in understanding ground-water hydrology and ground- and surface-water interactions between the wetland and the aquifer. Data were not sufficient, at that time, to construct a predictive model. The model code was developed by McDonald and Harbaugh (1984). By varying model parameters, the model was used to estimate hydraulic properties of aquifer units and to aid in the design of field activities at the site.

Construction of the model required a finite-difference grid with 1,170 cells per layer and eight layers. The layers represent the outwash, till, and the underlying sandstone. These units represent a geologic section about 50 m thick. The variability spaced grid was designed with smaller cells at the edges of the wetland area (33 m along a side) and larger cells toward the margins of the modeled area. Approximately 160 water-well and test-hole logs were used to map the geometry of the geologic units and the distribution of hydraulic head. The area modeled includes 16.7 km<sup>2</sup>, which extends to the drainage divides of the South Fork Watab River in the vicinity of the wetland.

Boundary conditions at the edges of the model (drainage divides) were represented as no-flow boundaries. Sources of discharge from the model were represented as head-dependent cells and as evapotranspiration. Local recharge from precipitation and leakage from the streams and wetlands were the only sources of recharge to the model.

### Model Simulation Results

Initial numerical simulations of ground-water flow were made to determine sensitivity and recharge. Model results suggest that the initial model was sensitive to changes in vertical hydraulic conductivity, thickness of the organic deposits separating the wetland from the aquifer, and leakance of streambed sediments in the channel of the South Fork Watab River. Although additional data need to be collected to estimate the hydraulic conductivity of the organic material and head gradients in the vicinity of and underlying the wetland, model results suggest that ground-water discharge to the wetland is an important water-budget component. Borings made in the wetland show that the organic material consists of about 3 m of peat that grades vertically downward from fibrous to decomposed and compacted peat that, in turn, overlays organic-rich marl and silt. These materials (peat) form a confining bed that retards vertical movement of water between the wetland and the aquifer. The hydraulic head in wells completed in the aquifer in the open-water area of the wetland is generally about one meter greater than open water in the wetland.

Preliminary results from model simulations conducted as the study began suggested that ground-water flow is from the area of the South Fork Watab River toward the marsh. Additional drilling and observation-well installation (Figure 3) confirmed that ground-water flow is toward the central portion of the marsh. In the area between the river and the south part of the marsh, a ground-water divide separates the marsh from the river. Base-flow measurements show that the river loses discharge through the reach along the marsh.

### Hydraulic Head

The water-table elevations of the outwash aquifer measured at the observation wells indicate that ground water moves toward the wetland from the east, south, and west and that the wetland is an area of ground-water discharge. Horizontal ground-water gradients average about 0.002. In areas of the wetland, the ground-water-flow system has a strongly (approaching 0.1) upward vertical gradient. The aquifer becomes confined or partially confined beneath the wetland by organic materials. The hydraulic head in wells completed in the aquifer in areas of the wetland is generally about two to three feet greater than the elevation of open water in the wetland. Estimates of ground-water inflow to the system were calculated as a residual from a hydrologic balance of the wetland. These calculations were made because ground-water outflow from the system was shown to be negligible and because horizontal and vertical ground-water gradients were toward the wetland. Outflow from the wetland was greater than inflow, indicating net ground-water inflow to the wetland.

## HYDROLOGIC BALANCE

### Methods and Approach

Data were collected from October 1985 through September 1986 to determine the hydrologic and chemical balances of the bog and to improve quantification of ground-water and surface-water interactions within the bog and marsh.

The annual hydrologic balances for the bog and marsh were calculated using the following equations:

$$\text{Bog equation:} \quad (P + \text{SSI} + \text{WWI} + \text{GWI}) - (\text{ET} + \text{SWO}) = S \quad (1)$$

$$\text{Marsh equation:} \quad (P + \text{SWI} + \text{GWI}) - (\text{ET} + \text{SWO}) = S \quad (2)$$

where

#### Inflow Components

P = incident precipitation to the bog or marsh in cubic meters;

SSI = storm-sewer inflow to the bog in cubic meters;

WWI = wastewater inflow to the bog in cubic meters;

GWI = ground-water inflow to the bog or marsh in cubic meters;

SWI = surface-water inflow to the marsh in cubic meters (which is the same as the surface-water outflow from the bog);

#### Outflow Components

ET = evapotranspiration from the bog or marsh in cubic meters;

SWO = surface-water outflow from the bog or marsh in cubic meters; and

#### Storage Component

S = change in surface-water storage in the bog or marsh in cubic meters.

All components of the hydrologic balance, except for ground-water flow, were estimated from measurements made in the field. Ground-water inflow was estimated as the residual in the balance equations. Ground-water outflow was assumed to be insignificant because field data suggested that the entire wetland area is a zone of ground-water discharge. Surface-water inflow from the part of the surface-water drainage basin that is not storm-sewered (Figure 1) is assumed to be insignificant because the drainage area is small ( $0.04 \text{ km}^2$ ) and surface runoff would be minimal because of permeable soils and low land-surface slopes.

Precipitation was measured with a tipping-bucket rain and snow gage located 60 m southeast of the bog (Figure 2). The amount of incident precipitation in the form of snow that entered the bog and marsh was calculated from weekly density and thickness measurements of the accumulation and depletion of the snowpack on top of the bog and marsh. The two-axis method (Bethlahmy 1976) was used to extrapolate point values of precipitation to the entire bog and marsh areas. Daily values of precipitation were summed to obtain monthly values.

Evapotranspiration was estimated from daily total solar radiation, daily maximum and minimum air temperatures, and daily average air-humidity data. These data were collected at the same location as the precipitation gage (Figure 2). Monthly total evapotranspiration in the wetland was estimated using methods described by Jensen and Haise (1963) and Jensen et al (1969). In this study, evapotranspiration is equal to potential evapotranspiration because of continuously saturated conditions.



Wastewater discharge was measured using a Parshall flume and stage data recorded every 15 minutes (Figure 2). Storm-sewer inflow, bog outflow (which is also the marsh inflow), and marsh outflow were calculated from stream-stage measurements using a relationship between stage and measured discharge (Kennedy 1984).

The locations of surface-water data-collection sites are shown in Figure 2. Average discharge for all inflows and outflows of bog and marsh were calculated by summing the 15-minute discharge data and dividing by 96 times the number the days in the month.

Changes in storage within the bog and marsh were measured using data from a topographic map and water-level data collected at the bog and marsh outflows, respectively. The monthly increase or decrease in water level was multiplied by the area of the bog or marsh determined from the topographic map to obtain the change in storage.

Errors associated with calculation of the hydrologic-balance components were estimated using methods described by Winter (1981). The errors, calculated as the standard error of measurement, are expressed as the average percent error in measurement of the component as follows: (a) 8-percent error in precipitation, (b) 28-percent error in evapotranspiration, (c) 9-percent error in surface-water inflow from the storm sewer and wastewater, (d) 14-percent error in surface-water outflow (including marsh inflow), (3) 41-percent error (error of the residual) in the ground-water inflow and (f) 11-percent error in change in storage. These estimates of errors in measurement of each component represent a quantification of measurement error based on error associated with the method of data collection. The error associated with the residual (ground-water inflow) is large, as it is the accumulation of error from the other components.

#### Distribution of Components

The distribution of hydrologic-balance components for the bog and marsh for the year is given in Table 1.

Both the bog and marsh are ground-water-slope wetlands, defined as wetlands located in the headwaters of surface-water drainage basins, which receive a significant part of inflow from the ground-water system and in which surface water is the dominant outflow (Novitzki 1978). Ground-water and wastewater inflows were the dominant inflow to the bog. Inflow to the marsh was predominantly surface-water outflow from the bog and ground-water inflow. The dominant outflow from the bog was surface water to the marsh as was the dominant outflow from the marsh is surface-water flow discharge to the receiving South Fork Watab River. Precipitation and evapotranspiration were minor components in the annual hydrologic balance of both the bog and marsh. The surface-water inflow to the bog (storm-sewer flow) was minor as the flow primarily represented snowmelt runoff during early spring and major storm runoff during summer months. Discharge of wastewater into the bog affects the hydrology of both the bog and marsh. If wastewater was not discharged into the bog, ground-water inflow would be a still more significant portion of inflow to the bog and marsh.

Table 1. Distribution of components in hydrologic balance for the bog and marsh during 1986 [values are percentages of total annual input or output]

| Hydrologic-balance component | Bog | Marsh |
|------------------------------|-----|-------|
| Inflow                       |     |       |
| Wastewater                   | 38  | NA    |
| Surface water                | 12  | 74    |
| Precipitation                | 8   | 4     |
| Ground water                 | 42  | 22    |
| Outflow                      |     |       |
| Surface water                | 92  | 92    |
| Evapotranspiration           | 6   | 6     |
| Storage                      | 2   | 2     |

## Estimates of Ground-Water Inflow

An estimate of ground-water inflow to the wetland was made with flow-net analysis using Darcy's law and dividing marsh and bog shoreline areas into separate segments. Flows to the bog and marsh were calculated from hydraulic-head data (Figure 3) and transmissivity values based on the saturated thickness of the aquifer and by assuming a hydraulic conductivity of 30.5 m/d for the outwash aquifer (Helgesen et al. 1975). A net ground-water flux was calculated for each shoreline segment. These data suggest that flow to the wetland, calculated by flow-net analysis, is about 80 percent of ground-water inflow rates calculated as a residual value from the budget estimates and that approximately 60 percent of this inflow discharge to the bog.

These data are reasonable and in general agreement with ground-water inflow to the bog and marsh calculated as a residual from the hydrologic balance. The greatest ground-water flux to the bog can be explained by the larger volume of the aquifer contributing ground water to the bog. The general distribution of ground-water inflow to the wetland, calculated from separate methods, shown in Table 2.

## CHEMICAL BALANCE

### Methods and Approach

The annual chemical balances for the bog and marsh were calculated using the following equations:

$$\text{Bog equation:} \quad (A + \text{SSI} + \text{WWI} + \text{GWI}) - (\text{SWO}) = S$$

$$\text{Marsh equation:} \quad (A + \text{SWI} + \text{GWI}) - (\text{SWO}) = \pm S$$

where

### Input Components

A = atmospheric deposition to the bog or marsh in kilograms (kg);

SSI = storm-sewer input to the bog in kilograms;

WWI = wastewater input to the bog in kilograms.

GWI = ground-water input to the bog or marsh in kilograms;

SWI = surface-water input to the marsh in kilograms (which is the same as the surface-water output from the bog);

### Output Component

SWO = surface-water output from the bog or marsh in kilograms; and

### Storage Component

S = change in storage within the bog or marsh in kilograms.

Table 2. Estimates of ground-water inflow using the hydrologic balance residual, numerical simulation, and flow-net analysis [values are percentages of the total annual inflow]

| Method of calculation for<br>ground-water contribution | Ground-water inflow |       |
|--|---------------------|-------|
|  | Bog                 | Marsh |
| Hydrologic balance<br>residual                         | 42                  | 22    |
| Numerical simulation                                   | 22                  | 12    |
| Flow-net analysis                                      | 34                  | 18    |

Annual chemical balances in the bog and marsh were calculated for total suspended solids, total phosphorus, and total ammonia plus organic nitrogen by multiplying the flow volumes by the concentration in water samples collected in the field for each component except storage. Storage was calculated as the residual. Concentration data were obtained by analyzing samples for each constituent using methods described by Fishman and Friedman (1985). The ground-water input to total suspended solids was assumed to be small; therefore, ground water is not part of the equation used to compute the balance of total suspended solids. Surface-water input from the nonstorm-sewered part of the surface-water drainage basin of the wetland area is assumed to be insignificant for reasons discussed for the hydrologic balance.

Atmospheric deposition was estimated by multiplying monthly total precipitation by the constituent concentration in monthly samples of atmospheric deposition (wetfall and dryfall). The atmospheric deposition samples consisted of material collected during a month in the atmospheric sampler mounted near the precipitation gage (Figure 2). Atmospheric deposition in the bog or marsh was calculated by extrapolating surface area of the sampler to the surface area of the bog or marsh. The annual deposition was the summation of the monthly totals.

Wastewater inflow, bog outflow (also marsh inflow), and marsh outflow were sampled biweekly at the data-collection sites (Figure 2) for analysis of each constituent. The storm-sewer inflow was sampled during five storms using flow-weighted composite samples of each storm using the method described by Nelson and Brown (1983). The annual input or output was calculated from concentration and discharge data associated with each biweekly or storm sample using methods described by Nelson and Brown (1983).

Ground-water input was estimated by multiplying the bimonthly total ground-water inflow by the concentration of the bimonthly samples taken from three observation wells located in observation-well nests (Figure 2). The sampled wells were screened in the outwash aquifer underlying the peat in the bog and marsh. It was assumed that quality of water in the outwash represents the quality of ground water flowing into the bog or marsh.

The storage value is the difference between the input and output of a constituent during the year. A positive storage value indicates that there is a net retention of the constituent in the wetland during the year, while a negative value indicates that there is a net release (output greater than input).

Errors associated with calculation of each chemical-balance component were estimated using methods described by Winter (1981). The errors, as discussed for the hydrologic balance, represent the error of measurement, in percent, of the component as follows: (a) 32-percent error in atmospheric deposition (b) 14-percent error in surface-water inputs from the storm sewer and wastewater (c) 22-percent error in surface-water outputs (including marsh input) (d) 58-percent error in the ground-water input and (3) 69-percent error (error of the residual) in change of storage. These estimates of errors in measurement of each component represent only a qualitative comparison of accuracy and are not a quantification of measurement error.

### Distribution of Components

The distribution of components in the chemical balance for the bog and marsh during the year is shown in Table 3.

Table 3. Distribution of components in chemical balance for the bog and marsh during 1986 [SS, total suspended solids; P, total phosphorus;  $\text{NH}_4$ , ammonia nitrogen; N, organic nitrogen; values are percentages of total annual input or output]

| Chemical-balance component | Bog |    |                        | Marsh |    |                        |
|----------------------------|-----|----|------------------------|-------|----|------------------------|
|                            | SS  | P  | $\text{NH}_4+\text{N}$ | SS    | P  | $\text{NH}_4+\text{N}$ |
| Inflow                     |     |    |                        |       |    |                        |
| Wastewater                 | 74  | 96 | 82                     | NA    | NA | NA                     |
| Surface water              | 22  | 2  | 16                     | 96    | 98 | 84                     |
| Precipitation              | 42  | 2  | 2                      | 4     | 2  | 14                     |
| Ground water               | >1  | >1 | >1                     | >1    | >1 | >1                     |
| Outflow                    |     |    |                        |       |    |                        |
| Surface water              | 66  | 86 | 86                     | 56    | 82 | 78                     |
| Storage                    | 34  | 14 | 14                     | 44    | 18 | 22                     |

## Retention of Components

### Suspended solids

Retention of suspended solids in wetlands is directly related to flow characteristics of the particular wetland. As flow velocity decreases in a wetland, sedimentation increases (Boto and Patrick 1978). The velocity decrease, along with the presence of vegetation, promotes settling of suspended solids. Annual retention of suspended solids is 34 percent of the input in the bog and 44 percent of the input in the marsh. The capability of retaining suspended solids in the marsh is greater than that of the bog because of the dense stand of cattails in the marsh. The retention time of water in the bog and marsh is approximately 1.8 and 3.1 days, respectively. The more dense vegetational composition and longer retention time of water in the marsh promotes the settling of suspended solids at a greater rate than the less dense, open-water characteristics of the bog. The bog retains suspended solids primarily by decreasing velocity through ponding, while suspended solids are retained in the marsh by a decrease in velocity through ponding and by the "filtering" action of the cattails.

### Total phosphorus

Particulate or undissolved phosphorus is removed from the water column through the same processes discussed for suspended solids (Boto and Patrick 1978). Major mechanisms that remove dissolved phosphorus from the water column in a wetland have been postulated in previous studies as precipitation or sorption of phosphorus on organic matter (Spangler et al. 1977) and (2) assimilation of phosphorus by flora fauna (Kitchens et al. 1975). Removal of phosphorus from the water column is highly dependent on the hydrologic regime of the wetland. A low velocity of flow through a wetland is essential for net accumulation of particulate phosphorus in the litter and assimilation of dissolved phosphorus by plants (van der Valk et al. 1978). Removal or retention of dissolved phosphorus depends on a long residence time of water in the wetland, which is required for biological processes to occur (Klopatek 1975).

Retention of total phosphorus or removal of the constituent from the water as it passes through the bog and marsh is probably through sedimentation, as the residence time of water in the bog or marsh generally is too short for removal of dissolved phosphorus. The part of total phosphorus that is retained probably is the part associated with suspended solids that are retained in the bog and marsh. Several paired analyses of total versus dissolved phosphorus indicated that about 80 to 90 percent of the incoming and outflowing phosphorus is particulate or undissolved phosphorus. Annual retention of total phosphorus is 14 percent of the input in the bog and 18 percent of the input in the marsh. The retention capability of the marsh is greater than that of the bog because of the dense stand of cattails in the particulate phosphorus, similar to suspended solids, at a greater rate than the less dense, open-water characteristics of the bog.

## Nitrogen

Particulate or undissolved nitrogen is removed from the water column in a wetland through the same processes discussed for suspended solids (Boto and Patrick 1978). The major mechanism of removing dissolved nitrogen in a wetland is through denitrification (Klopatek 1975 et al. 1975). The removal of nitrogen, similar to phosphorus, from the water column is highly dependent on the hydrologic regime of the wetland. A low velocity of flow through a wetland is essential for net accumulation of particulate nitrogen in plant litter and assimilation of dissolved nitrogen by the wetland flora and fauna (van der Valk et al. 1978). Removal or retention of dissolved nitrogen depends on a long residence time of water in the wetland, which is required for biological processes to occur (Klopatek 1975).

Retention of total ammonia plus organic nitrogen or removal of the constituent from the water as it passes through the bog and marsh probably is through sedimentation, as the residence time of water in the bog or marsh generally is too short (1 to 3 days) for removal of dissolved nitrogen. Periodic paired analyses of dissolved and total ammonia plus organic nitrogen during the study indicated that 75 to 90 percent of the nitrogen is undissolved or particulate matter. Therefore, the part of total ammonia plus organic nitrogen that is retained probably is the particulate organic nitrogen associated with suspended solids that are retained in the bog and marsh. Annual retention of total ammonia plus organic nitrogen is 14 percent of the input in the bog and 22 percent of the input in the marsh. It should be noted, however, that the retention of ammonia plus organic nitrogen may not be actually a retention but may be in part a conversion of both organic and ammonia nitrogen to nitrate from nitrogen through denitrification. Since the nitrogen budget is not complete without the analysis of nitrate, it cannot be stated that ammonia and organic nitrogen is actually being retained in the wetland or being converted to another form. However, since the ammonia plus organic nitrogen entering the wetland is primarily particulate matter and the retention time of water flowing through the wetland is short, it is assumed that the denitrification process is limited. The retention capability of the marsh is greater than that of the bog because of the dense stand of cattails in the marsh. The more dense vegetational composition of the marsh promotes settling of particulate nitrogen, similar to suspended solids, at a greater rate than the less dense, open-water characteristics of the bog.



## CHANGES IN VEGETATIONAL COMPOSITION

The hydrologic and chemical balances of the bog and marsh are affected greatly by the wastewater discharge. The most obvious effect of the wastewater discharge on the bog and marsh is the documented change in vegetational composition since discharge began in 1962. Historical records indicate that spruce and tamarack have dominated the vegetation of the present-day marsh and the bog since the 1800s (written communication, Starns County Historical Society, St. Cloud, Mn, 1986). A detailed vegetational inventory of the bog and marsh was completed in 1985 by Williams (1985) using historical and recent aerial photography followed by field verification. The inventory included a detailed analysis of the change in vegetation from 1958 to 1986 (four years prior to the start of wastewater discharge). The vegetational composition in 1958 was 30 percent spruce, 30 percent tamarack, and 40 percent wetland grass in the bog, and about 30 percent tamarack and 70 percent wetland grass in the marsh (Williams 1985). Vegetational composition in 1986 was 5 percent spruce, 45 percent tamarack, 15 percent sedge grass, 20 percent duckweed, and 15 percent cattail in the bog and 25 percent tamarack and 75 percent cattail in the marsh. The change in vegetational composition between 1958 and 1986 likely was the result of changes in both the hydrologic and chemical balances of the bog and marsh as a result of the wastewater discharge. Introduction of cattails into both the bog and marsh is an indication of how the ecosystem has been altered between 1958 and 1986. Cattails have been shown to thrive in situations where wastewater is introduced. The eventual outcome is a monoculture of cattails in wetlands that receive wastewater (Godfrey et al. 1985).

## LITERATURE CITED

- Bethlahmy, N. 1976. The two-axis method: A new method to calculate average precipitation over a basin. *Hydrologic Sciences Bulletin* 21:379-385.
- Boelter, Donald H. 1975. Methods for analyzing the hydrological characteristics of organic soils in marsh-ridden areas. p. 161-182. *In* Hydrology of marsh-ridden areas. UNESCO Press, Paris, France.
- Boto, K. G., and W. H. Patrick, Jr. 1978. Role of wetlands in the removal of suspended sediments. p. 479-489. *In* P. E. Greeson, J. R. Clark, and J. E. Clark (eds.) Wetland functions and values: The state of our understanding. American Water Resources Association, Minneapolis, MN, USA.
- Fishman, M. J., and L. C. Friedman (eds.) 1985. Methods for determination of inorganic substances in water and fluvial sediments. U.S. Geological Survey Open File Report 85-495.
- Godfrey, P. J., E. R. Kaynor, S. Pelczarski, and J. Benforado (eds.) 1985. Ecological considerations in wetland treatment of municipal wastewaters, Van Nostrand Reinhold, New York, NY, USA.
- Helgesen, J. O., D. W. Ericson, and G. F. Lindhold, 1975. Water resources of the Mississippi and Sauk Rivers watersheds, Central Minnesota: U.S. Geological Survey Hydrologic Investigations Atlas HA-534
- Jensen, M. E. and H. R. Hasie. 1963. Estimating evapotranspiration from solar radiation. *Journal on Irrigation and Drainage* 89:15-41.
- Jensen, M. E., D. C. Rob, and C. E. Franzoy, 1969. Scheduling irrigations using climate-crop-soil data. National Conference on Water Resources Engineering, New Orleans, LA, USA.
- Kanivetsky, R. 1978. Hydrogeologic Map of Minnesota, Bedrock Hydrogeology. Minnesota Geological Survey, State Map Series S-2.
- Kennedy, E. J. 1984. Discharge ratings at gaging stations. U.S. Geological Survey Techniques of Water-Resources Investigations.
- Kitchens, W. M., Jr., J. M. Dean, L. H. Stevenson, and S. M. Cooper. 1975. The Santee Swamp as a nutrient sink. p. 349-366. *In* F. G. Howell, J. R. Gentry, and M. B. Smith (eds.) U.S. Energy and Research Development Administration Symposium CONF-740513.
- Klopateck, J. M. 1975. The role of emergent macrophytes in mineral cycling in a freshwater marsh. p. 367-393. *In* F. G. Howell, J. R. Gentry, and M. B. Smith (eds.) U.S. Energy and Research Development Administration Symposium CONF-740513.
- Lee, G. F., E. Bentley, and R. Amundson. 1975. Effects of marshes on water quality. p. 105-127. *In* A. D. Hasler (ed.) Coupling of land and water systems. Springer-Verlag.
- McDonald, M. G., and A. W. Harbaugh, 1984, A modular three-dimensional finite-difference ground-water-flow model. U.S. Geological Survey Open File Report 83-875.
- Nelson, L., and R. G. Brown, 1983. Streamflow and water-quality data for lake and wetland inflows and outflows in the Twin Cities Metropolitan Area, Minnesota. U.S. Geological Survey Open File Report 83-543.

#### LITERATURE CITED (continued)

- Novitzki, R. P. 1978. Hydrologic characteristics of Wisconsin's wetlands and their influence on floods, stream flow, and sediment. p. 377-388. In P. E. Greeson, J. R. Clark, and J. E. Clark (eds.) Wetland functions and values: The state of our understanding. American Water Resources Association, Minneapolis, MN, USA.
- Spangler, F. L., C. W. Fetter, Jr., and W. E. Sloey, 1977. Phosphorus accumulation-discharge cycles on marshes. *Water Resources Bulletin* 13(4):1191-1201.
- Van der Valk, A. G., C. B. Davis, J. L. Baker, and C. E. Beer. 1978. Natural freshwater wetlands as nitrogen and phosphorus traps for land runoff. p. 475-467. In P. E. Greeson, J. R. Clark, and J. E. Clark (eds.) Wetland functions and values: The state of our understanding. American Water Resources Association, Minneapolis, MN, USA.
- WAPQRA Inc. 1983. The effects of wastewater treatment facilities on wetlands in the Midwest. U.S. Environmental Protection Agency Report EPA-905/3-83-002.
- Williams, R. J. 1986. Aerial photographic analysis of wastewater treatment plant impacts on wetlands, Wisconsin, Minnesota Michigan, and Illinois. U.S. Environmental Protection Agency Report EPA-TS-AMD-83122/8353.
- Winter, T. C. 1981. Uncertainties in estimating the water balance of lakes. *Water Resources Bulletin* 17(1):82-114.

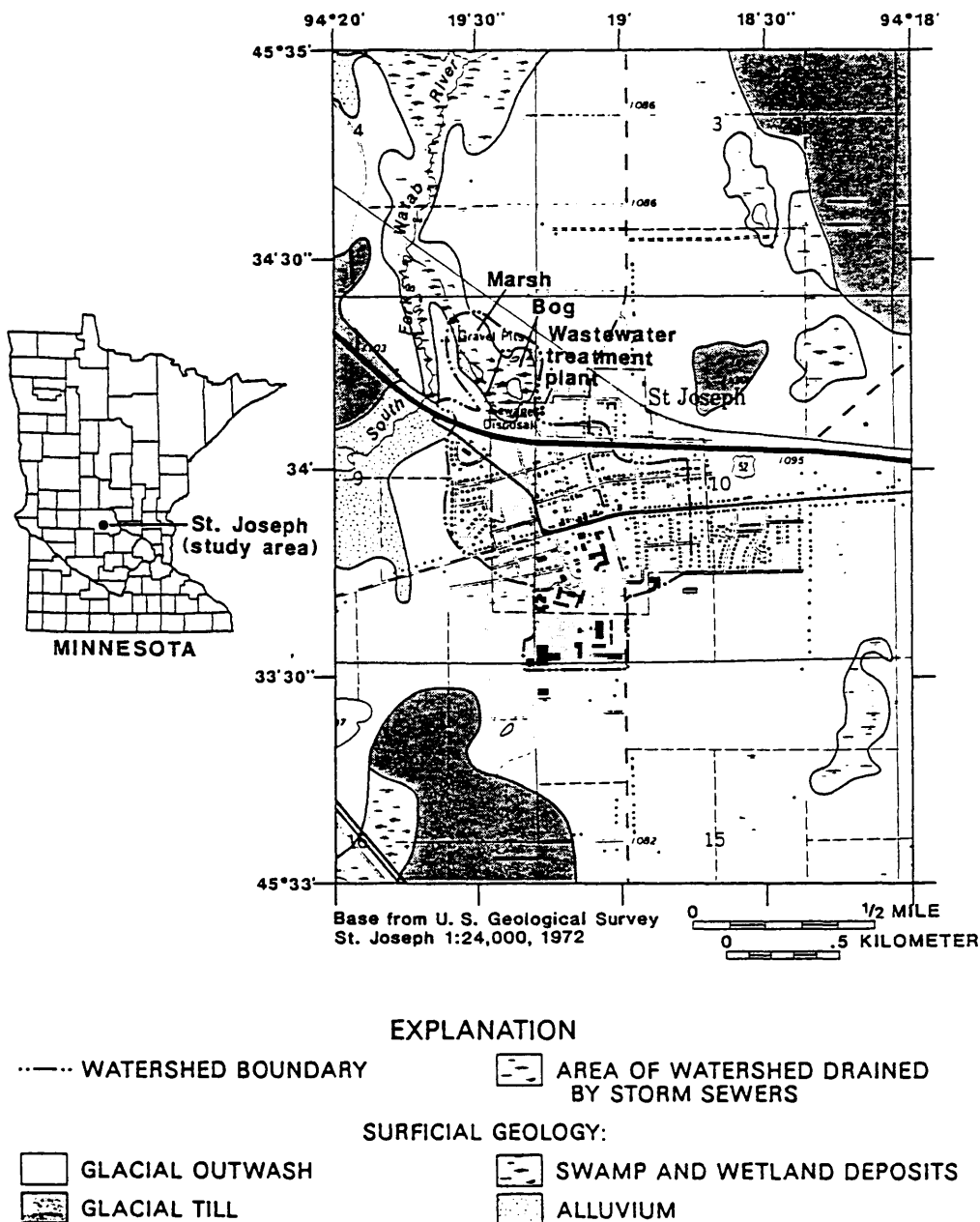
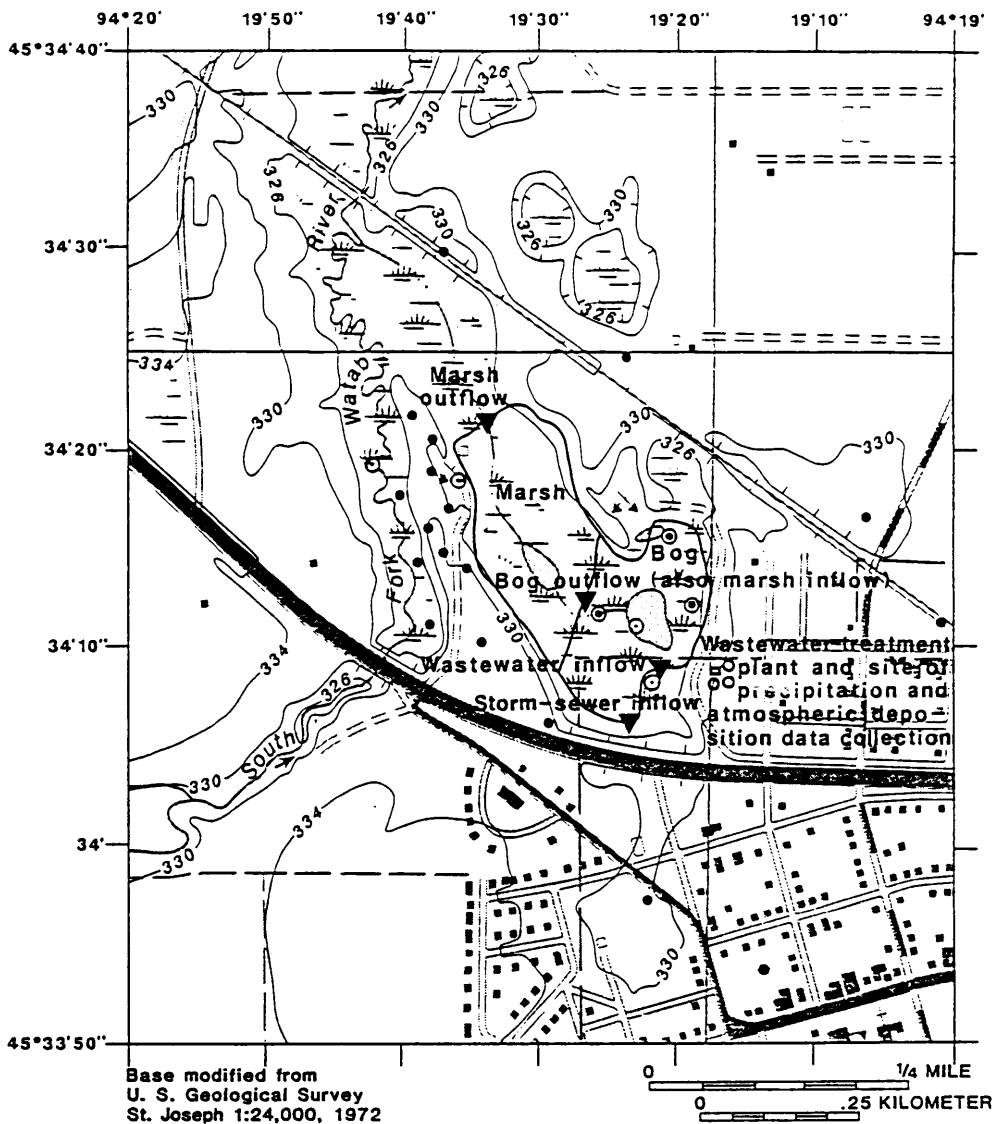


Figure 1.--Location and physical features of study area



### EXPLANATION

—330— TOPOGRAPHIC CONTOUR LINE  
Interval 4 meters. Datum is  
mean sea level

▼ SURFACE-WATER DATA-  
COLLECTION SITE

### WELL SITES:

• OBSERVATION WELL

⊙ NEST OF OBSERVATION WELLS  
IN WHICH A WELL WAS SAM-  
PLED FOR WATER-QUALITY  
ANALYSIS

○ NEST OF OBSERVATION WELLS

Figure 2.--Location of wetland areas and data-collection sites



# GROUNDWATER SYSTEMS ANALYSIS OF THE NAARDERMEER WETLAND, THE NETHERLANDS

P.P. Schot

Department of Environmental Studies, University of Utrecht  
P.O. Box 80.115, 3508TC Utrecht, The Netherlands

## Abstract

A large number of wetland nature reserves are present on the Vecht river plain in the Central Netherlands. Mesotrophic plant communities in these wetlands are threatened due to a.o. groundwater extraction in the adjacent recharge area and drainage in the river plain.

A groundwater systems analysis was carried out in order to formulate measures towards preservation and restoration of the wetland ecosystems. Use was made of:

1. a computer model to calculate groundwater flow lines
2. data on groundwater composition to determine groundwater origin and the spatial distribution of solutes
3. environmental isotopes to determine groundwater origin and groundwater age

This paper presents a case-study of the Naardermeer wetland. Five groundwater systems are distinguished which make clear the relation between quantity and quality of groundwater. Moreover, they enable evaluation of the effects of hydrological changes on the wetland and provide a basis for impact assesment of groundwater pollution.

## Introduction

The Vecht river plain is located in the Central Netherlands between Amsterdam and Utrecht. It contains a large number of wetlands of which several have been designated as nature reserves (fig. 1). An essential part of the flow of water and matter in the wetlands occurs through inflow and outflow of groundwater. Most groundwater is recharged in the sandy ridge east of the river plain.

Over the last few decades the supply of groundwater has decreased as a result of groundwater extraction from the ridge for industrial and drinking water supply (Witmer, 1986). Besides, human activities in urban areas on the ridge pose a threat to groundwater quality (Janssen & Verkroost, 1989). Artificial drainage of the river plain for agricultural purposes constitutes an additional problem.

Decreased seepage along with drainage in the river plain result in water deficits in the wetlands during dry summer periods. These deficits are compensated by suppletion of surface water from the Vecht river. This polluted, eutrophic water has negative effects on the occurrence of mesotrophic plant species in the wetlands (Barendregt et al., 1985). Mesotrophic water is provided primarily by seepage flow of groundwater. Management directed towards preservation and restoration of mesotrophic wetland ecosystems must therefore take into account the role of

groundwater. A hydrological framework is needed to formulate adequate measures. For this purpose a regional groundwater systems analysis was carried out (Schot, 1989). It describes the flow of groundwater and solutes to and from the mesotrophic wetland ecosystems in the river plain. In this paper a case-study of the Naardermeer wetland is presented.

### Methods

The following methods were employed in the regional groundwater systems analysis to describe the transport of groundwater and solutes:

- 1) Two-dimensional computer simulation of groundwater flow lines.  
The groundwater model FLOWNET was used to calculate and plot flow lines for a vertical inhomogeneous anisotropic section of the subsoil. The vertical groundwater flow pattern is of particular importance as it shows the connection between recharge areas and discharge areas. Input consists of hydraulic head data along upper, lower, left and right boundaries and allocation of horizontal and vertical permeabilities to each cell. Details of FLOWNET are given by Van Elburg & Engelen (1986).
- 2) Chemical analysis of groundwater and surface water.  
Chemical analysis of groundwater is necessary to determine the spatial distribution of solutes in groundwater. Changes in solute concentrations in the direction of flow may reflect hydrochemical processes. In addition, the chemical composition of groundwater was used as a tracer of recharge areas.
- 3) Isotope analysis of groundwater and surface water.  
Oxygen-18 and deuterium were used to trace infiltration of surface water and mixing of waters of different origin. Tritium and carbon-14 were used to determine groundwater age. Finally, carbon-13 provided information concerning hydrochemical processes.

Each method has its own specific use in the determination of solute transport by groundwater flow. However, each in itself does not contribute the comprehensive information necessary to fully describe this complex process. The best results are obtained from an integrated approach (e.g. Hendry et al., 1983) in which the results of the separate methods are combined into an integral understanding of the problem. During recent years this integrated approach has been given a theoretical and systematic basis in the concept of groundwater systems analysis (Engelen and Jones, 1986). A groundwater system may be defined as a coherent unit of groundwater and earth materials in space and time, natural or influenced by man. Groundwater systems connect recharge areas with discharge areas.

The specific use of each of the methods in the analysis of flow systems is illustrated through cross-sections of the wetland Naardermeer which show a number of the variables mentioned above. The results are integrated to delineate groundwater systems which are used to evaluate the effects of hydrological changes and groundwater pollution.



## Results

### Description of the Naardermeer area

The Naardermeer is located 15 km southeast of the city of Amsterdam (fig.1). It consists mainly of lakes, ditches and marshes fringed by woodland. In 1906 the Naardermeer became the first nature reserve in the Netherlands. It is famous as a bird sanctuary but it is also of botanical importance and has been put on the list of international important wetlands (Ramsar Convention).

The 7 km<sup>2</sup> wetland is topographically flat with an elevation of about -0.8 m above mean sea level (a.m.s.l.). To the east the Naardermeer is bordered by the region of Het Gooi ranging in elevation from 0 to 30 m a.m.s.l. This ice-pushed ridge consists mainly of unconsolidated Pleistocene fluvial sands and gravel which form an unconfined aquifer of 150-200 m thickness. In the Naardermeer area west of the ridge this aquifer is covered by Pleistocene coarse fluvioglacial sands with a maximum thickness of 15 m and fine eolian sands of about 4 m. On top, a semi-confining layer of Holocene peat and clay deposits is found, increasing in thickness from 0 m in the east to about 2-3 m in the west of the Naardermeer. The Naardermeer and surrounding agricultural areas are polders with artificially controlled surface water levels.

### Groundwater flow

Fig. 2 shows a groundwater level contour map for the Pleistocene sand aquifer. Groundwater flow is from the topographic high recharge area Het Gooi in the east to the Vecht river in the west. Seepage and infiltration areas can be derived from differences between phreatic (or surface) water level and piezometric groundwater level. In the Naardermeer seepage occurs in the eastern part, infiltration in the western part. In the central lakes-area surface water and piezometric water levels are more or less equal (Schot et al., 1988).

Fig. 3 shows the results of the groundwater model along cross section A-B for September 1985 (average summer conditions). In the eastern part of the ridge infiltration water is transported towards the wells of the Huizen groundwater extraction. Somewhat to the west a low topographic elevation causes upward groundwater flow under the town of Naarden. Vertical groundwater flow in the river plain is clearly determined by the artificially controlled surface water levels in the polders. Groundwater from the ridge flows upward in the eastern part of the Naardermeer. In the western part of the wetland infiltration occurs as a result of the lower surface water level downstream. This is also reflected in fig. 2 by horizontal groundwater flow directions within the Naardermeer towards the adjacent polders. The high surface water level of the Vecht river also results in infiltration.

The overall pattern of seepage and infiltration at the surface as calculated by the groundwater model compares well to that on existing maps which were compiled from differences in piezometric groundwater level and surface water level.

### Groundwater quality

Chloride is considered nonreactive in most hydrogeological environments and may therefore be used as a tracer for various groundwater sources. Fig. 4 shows chloride concentrations along cross-section A-B. Note that depth in fig. 4 is only 70 m contrary to 250 m in fig. 3.

The ridge contains fresh groundwater which is discharged into the eastern part of the Naardermeer. The deep groundwater in the northern Vecht river plain is brackish as a result of Holocene marine transgressions with intrusions of salt water from the surface into the underlying fresh groundwater through density flow (Engelen, 1981). In the Naardermeer brackish water is found at the western edge of the seepage area where deep flow lines reach the surface. Chloride concentrations under the Karnemelksloot canal, under the lakes and ditches in the western Naardermeer and under the Vecht river reflect infiltration of surface water.

The observed trend in chloride concentrations can be used as a rough check on the vertical groundwater flow pattern in Fig. 3. The occurrence of low chloride concentrations in the eastern part of the Naardermeer is in agreement with the flow lines in the model, which indicate precipitation on the ridge as source of this groundwater. Chloride concentrations and flow lines also show corresponding infiltration depth of surface water from the Vecht which is in the order of 50-60 m. However, the flow lines in the western part of the Naardermeer show infiltration to depths of over 150 m, while chloride concentrations indicate infiltration depth at present is in the order of 20 m. This indicates that the boundary between the Naardermeer infiltration water and the brackish groundwater is still moving downward and a stationary situation has not yet been reached.

Apart from the use as a tracer of groundwater flow, chloride may also indicate groundwater pollution. Concentrations in groundwater recharge by precipitation are below 20 mg/l (Leeftang, 1938; KNMI/RIVM, 1987). Higher concentrations in groundwater in the ridge (fig. 4) indicate pollution by human activities, mainly in urban areas (through cesspools, leaky sewerage, etc.). Pollution is also reflected by nitrate concentrations (fig. 5). Groundwater from the ridge shows concentrations clearly in excess of natural values which are below 10 mg/l. A considerable amount of samples show concentrations which even exceed drinking water standards (50 mg/l  $\text{NO}_3^-$ ).

### Groundwater isotopes

In geohydrology stable isotopes, especially oxygen-18, are used to study problems related to the origin of waters. In general oxygen-18 values of groundwater reflect those of precipitation in the recharge area. Deviating values may originate from mixing with water of different isotopic composition or from evaporation. Evaporation tends to concentrate the heavier water molecules, containing oxygen-18, in the remaining water. Evaporation occurs mainly from surface water present in lakes, pools and ditches in the river plain.

Radioactive isotopes like tritium are used to study groundwater age. Tritium concentrations of groundwater decrease in time due to radioactive

decay. This makes it possible to use tritium for (relative) age determination. Generally a distinction is possible between relatively old groundwater and groundwater which has a component of precipitation which infiltrated during the last 30 years.

In fig. 6 oxygen-18 concentrations along cross-section A-B are shown. In the ridge  $\delta^{18}\text{O}$  values vary from -7.7 to -7.2 ‰, which correspond to average values in precipitation in the study area (Mook, 1984). These values are also found in the area with seepage of fresh groundwater in the eastern part of the Naardermeer. Under the Karnemelksloot canal and in the central and western part of the Naardermeer  $\delta^{18}\text{O}$  values reflect infiltration of surface water which has been subject to evaporation ( $\delta^{18}\text{O} > -5.5$  ‰). Seepage of Naardermeer infiltration water in the adjacent polder is reflected by the  $\delta^{18}\text{O}$  value in the shallow well directly west of the Naardermeer. Groundwater under the Vecht river shows values comparable to those in the ridge and in precipitation. However, the groundwater model and the chloride concentrations indicate infiltration of surface water from the Vecht river. The major source of Vecht water is the Rhine river with a  $\delta^{18}\text{O}$  value of -9.0 ‰ (Mook, 1984). The oxygen-18 concentrations under the Vecht river must therefore be interpreted as Rhine water enriched by evaporation. Oxygen-18 values in the brackish water have been corrected for mixing with seawater ( $\delta^{18}\text{O} = 0$  ‰) on basis of chloride content. The corrected values range from -6.7 to -6.1 ‰ indicating that the fresh groundwater component at the time had been subject to evaporation before infiltration.

The tritium concentrations of groundwater along cross-section A-B (fig. 7) are subdivided in three groups:

- tritium values below 3 T.U. indicate relatively old groundwater which infiltrated at least 30 years ago (1 Tritium Unit equals 1 tritium atom in  $10^{18}$  atoms)
- tritium values between 3 and 10 T.U. indicate mixing of old and young groundwater or groundwater of approximately 30 years
- tritium values above 10 T.U. indicate relatively young groundwater recharged during the last 30 years

Brackish groundwater shows the lowest tritium values in accordance with its middle Holocene origin. Water from the ridge shows increasing age on its way to the seepage area of the Naardermeer. Values in the shallow filters in the seepage area indicate mixing with recent, locally infiltrated precipitation. Tritium values under the Karnemelksloot canal, the central and western Naardermeer and Vecht river confirm recent infiltration of surface water.

#### Groundwater systems

Combination of the information from the foregoing sections makes it possible to delineate groundwater systems in the Naardermeer area (fig. 8). The main groundwater systems and their characteristics are as follows.

1. The groundwater extraction system. Extraction from the ridge for drinking water supply is the driving force of this completely man-made system. In the east the system is bordered by the main regional groundwater divide, in the west it has created its own artificial groundwater divide.

2. The ridge system. This natural groundwater system originated from the topographic difference between the ridge and the low lying polderland. Infiltration water from the ridge is transported to the eastern part of the Naardermeer. The seepage water is of the calcium-bicarbonate type due to calcite dissolution in the groundwater on its way from the ridge to the wetland. On several places in the ridge the groundwater shows moderate to strong pollution. In the most western part of the seepage area in the Naardermeer the flow lines from the ridge system force old brackish groundwater to the surface.
3. The Karnemelksloot canal system. This small local groundwater system is induced by the hydraulic head difference between the surface water of the Karnemelksloot canal and the underlying groundwater of system 2. Water from the canal infiltrates and seeps up in the most eastern part of the Naardermeer. As the canal is partly supplied by effluent from a sewage purification plant, the groundwater from this system pollutes the wetland.
4. The Naardermeer infiltration system. Seepage water from the east of the Naardermeer is transported further into the wetland by way of ditches. The difference in surface water level between the Naardermeer and the surrounding polders created a system of infiltration from the Naardermeer in the west of the wetland with subsequent seepage in the adjacent polders. Groundwater quality in this system is a mixture of local precipitation with seepage water from systems 2 and 3. The infiltration water from the Naardermeer replaces old brackish groundwater under the river plain. Part of this brackish groundwater is discharged in the polder west of the Naardermeer.
5. The Vecht river system. Water from the Vecht river infiltrates to a depth of about 60 m. This is the result of a large hydraulic head difference (about 1.5 m) between the river and the adjacent polder areas. Although chloride content of the Vecht river is about 200 mg/l, it is relatively low compared to chloride concentrations in the brackish groundwater system from which it is therefore easily distinguished.

### Discussion

The applied methods partly confirm each other by showing the same trends and partly they are supplemental. The numerical model provides information on groundwater flow systems in the Naardermeer area. The simulation results make clear the connection between recharge areas and discharge areas of groundwater. Contents of chloride, oxygen-18 and tritium in groundwater can be used as a rough check on the simulated groundwater flow patterns, but also provide additional information. Chloride concentrations confirm infiltration on the ridge and subsequent seepage of water from the ridge in the eastern part of the Naardermeer. Furthermore, the front between fresh and brackish groundwater in the Naardermeer infiltration system indicates that this system is relatively young, as fresh water has not yet fully replaced the old brackish groundwater. Oxygen-18 values confirm infiltration of surface water from the Karnemelksloot, the Naardermeer and the Vecht river. Trends in tritium values agree with those displayed by the other methods. Moreover, they give an impression of groundwater age and indirectly of system scale. The groundwater flow systems

and water quality types in fig. 8 present an overall view on the available information.

The groundwater systems analysis enables evaluation of the effects of hydrological changes. The original volume of the ridge system has decreased by the size of the groundwater extraction system. The effect of extraction is a reduced discharge of the ridge system into the Naardermeer. This effect is intensified by a decreased input to the ridge system through increased construction of sewerage in the urban areas upstream of the wetland (Janssen & Verkroost, 1989). As a result of decreased discharge the western boundary of the ridge system shifted eastward. This was compensated by the flow of brackish water up to ground surface at the western edge of the seepage area in the Naardermeer. Thus the groundwater systems enable an explanation of the seepage of brackish groundwater in the eastern part of the wetland. Chemical analyses of the brackish seepage water in the eastern part of the wetland confirm the foregoing hypothesis. High calcium and relatively low sodium contents point to cation-exchange reactions, where sodium from the brackish groundwater replaced calcium from the adsorption complex of the soil (Schot, 1988). This indicates salination of a former fresh water aquifer (Geirnaert, 1973). Moreover, analyses of lake water near the seepage area show an increase in chloride content over the last decades (ZAG, 1986). This may be accounted for by the recent discharge of brackish groundwater in the eastern part of the Naardermeer. The effect of the low surface water levels in the polders adjacent to the Naardermeer is reflected in the development of the Naardermeer infiltration system.

The groundwater systems provide a tool for impact assesment of groundwater pollution in the ridge. Groundwater pollution is evident from chloride and nitrate concentrations (fig. 4 and 5) and from other parameters (PWS, 1985). Depending on their position in the hierarchy of flow systems, the pollutants will either discharge through the wells of the drinking water supply (system 1) or in the wetland (system 2). To determine the eventual concentrations in the discharge area of a groundwater system, the physical and chemical processes along the flow path need to be considered. Changes in solute concentrations especially are to be expected in organic layers, e.g. during seepage through organic debris on the bottom of lakes and ditches. Determination of hydrochemical processes which affect water quality in the wetlands on the river plain, is still in progress.

The hydrological changes discussed above affect the ecosystems of the Naardermeer. Changes in vegetation composition during the last hundred years were studied by Barendregt et al. (in prep.). Forty years ago plant species characteristic for mesotrophic wetland ecosystems were abundantly present in the seepage area of the Naardermeer (Meyer and de Wit, 1945). Recent vegetation releves in the seepage area show that at present most of these species are absent in places with brackish groundwater and occur exclusively in areas with seepage of calcium bicarbonate groundwater (Wassen et al., 1989). It appears that the shift in groundwater systems is followed by changes in vegetations in the wetland Naardermeer.

Management which aims at the conservation and developement of mesotrophic wetland ecosystems must focus primarily on the ridge groundwater system. In this respect the Groundwater Management Plan of the Province of

Noord-Holland (1986) provides a step in the right direction. It comprises a reduction of the extraction of groundwater from the ridge by 50%. This will restore the flow of groundwater from the ridge system which is favourable to the species of mesotrophic wetland ecosystems. Furthermore the boundary of the ridge system in the Naardermeer will move to the west forcing the brackish groundwater system downward, out of reach of the plant roots. In addition measures may be recommended towards decreasing the volume of water lost through the Naardermeer infiltration system. The owner of the Naardermeer nature reserve has purchased land in the adjacent polders which opens possibilities to increase surface water levels surrounding the Naardermeer. Groundwater model calculations show that a reduction of water loss of 18 % in summer is possible with the proposed increases in polder water levels (Timmermans, 1988). Both increase in seepage water and decrease of infiltration from the Naardermeer will reduce the need for supply of external polluted surface water during dry summer periods.

#### References

- Barendregt, A., J.T. de Smidt & M.J. Wassen, 1985, Relaties tussen milieu-factoren en water- en moerasplanten in de Vechtstreek en de omgeving van Groet, Rapport Vakgroep Milieukunde, R.U. Utrecht.
- Elburg, H. van & G.B. Engelen, 1986, Two-dimensional finite difference modelling of groundwater flow systems on micro and personal computers. In: G.B. Engelen & G.P. Jones (Eds.), Developments in the analysis of groundwater flow systems. IAHS Publication No. 163.
- Engelen, G.B., The quarternary sequence of water systems in the western part of the Netherlands, in: Moderne Rekenmethoden (zoet-zout grondwater), Stichting Postakademiale Vorming Gezondheidstechniek, Delft, 1981.
- Engelen, G.B. & G.P. Jones, 1986, Developments in the analysis of groundwater flow systems. IAHS Publication no. 163.
- Geirnaert, W., 1973, The hydrogeology and geochemistry of the lower Rhine fluvial plain. Leidse Geologische Meded. 49.
- Hendry, M.J., R.W. Gillham & J.A. Cherry, 1983, An integrated approach to hydrogeologic investigations - a case history, Journal of Hydrology, 63.
- Janssen, H.M.A. & A.W.M. Verkroost, 1989, Risicodragende activiteiten en grondwaterkwaliteit in Het Gooi. Rapport Vakgroep Milieukunde R.U. Utrecht.
- KNMI/RIVM, 1987, Chemische samenstelling van de neerslag over Nederland, jaarrapport 1986.
- Leeftang, K.W.H., 1938. De chemische samenstelling van de neerslag in Nederland, Chemisch Weekblad 35.
- Mook, W.G., 1984, Principles of isotope hydrology, V.U. Amsterdam.

PWS Noord-Holland, 1985, Notitie Diffuse grondwaterverontreiniging en risicodragende activiteiten gemeente Hilversum.

PWS Noord-Holland, 1986, Provinciaal Grondwaterplan van Noord-Holland, Plan en Toelichting.

Schot, P.P., A. Barendregt & M.J. Wassen, 1988, Hydrology of the wetland Naardermeer: Influence of the surrounding area and impact on vegetation. Agricultural Water Management (14).

Schot, P.P. 1989, Grondwatersytemen en grondwaterkwaliteit in Het Gooi en randgebieden. Interfacultaire Vakgroep Milieukunde R.U. Utrecht.

Timmermans, J.S., 1988, Kwel en wegzijging in het Naardermeer, simulatie van de grondwaterstroming in het Naardermeergebied m.b.v. een quasi drie dimensionaal model.

Wassen, M.J., A. Barendregt, M.C. Bootsma & P.P. Schot, 1989, Groundwater chemistry and vegetation in gradients from rich fen to poor fen in the Naardermeer, the Netherlands. Vegetatio 79.

Witmer, M.C.H., 1986, Management of groundwater and surface water resources in the infiltration area "Het Gooi" and adjacent wetlands, IAHS Publ. no. 156.

ZAG, 1986, De waterkwaliteit van de Noordhollandse ondiepe Vechtplassen 1978-1984.

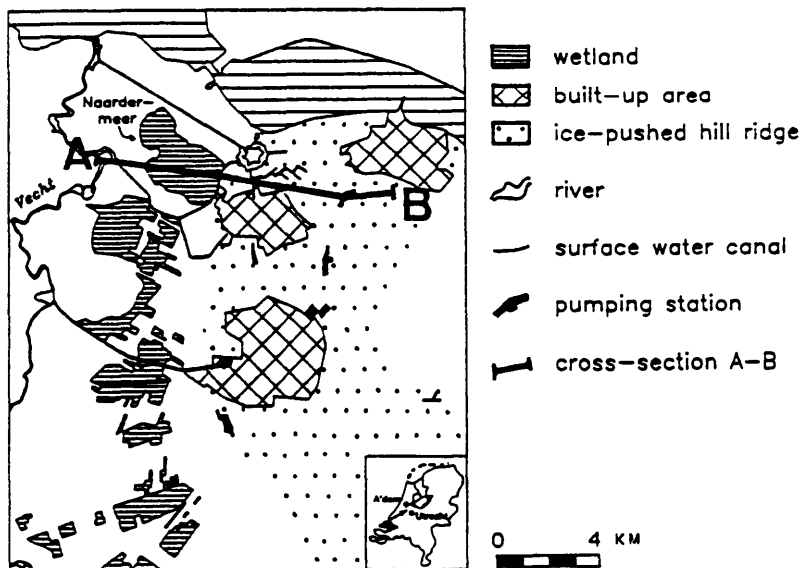


Fig. 1. Location of wetlands in the Vecht river plain.

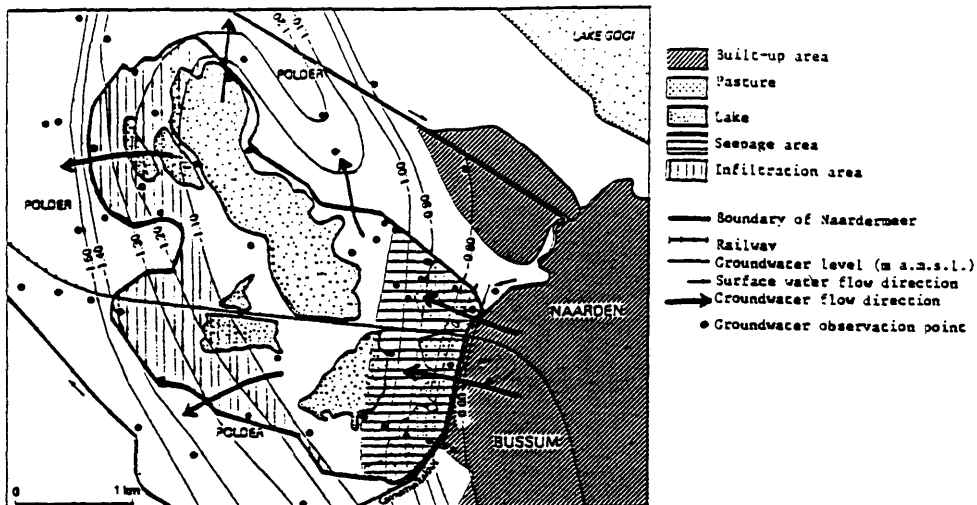


Fig. 2. Groundwater level contour map for the Pleistocene aquifer (average levels Oct.'85-Oct.'86).

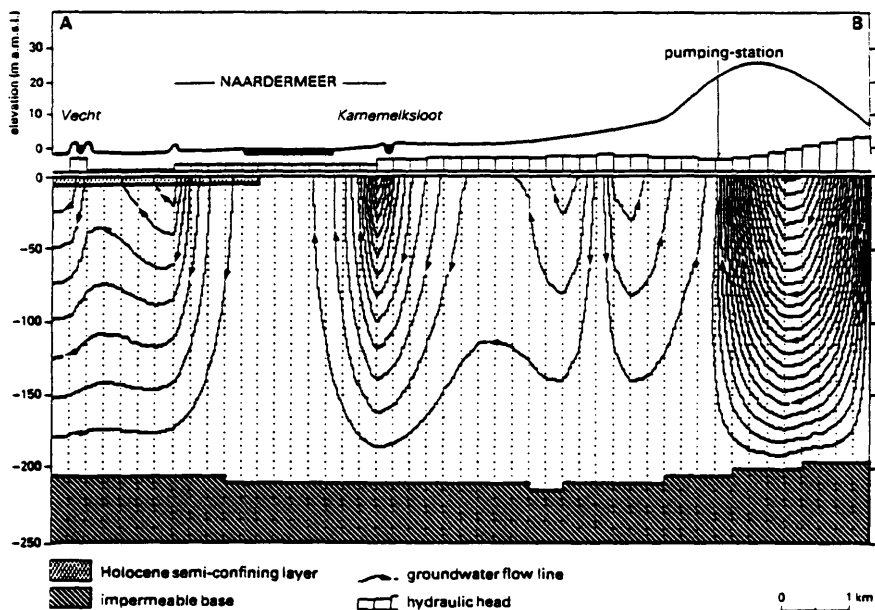


Fig. 3. Vertical groundwater flow pattern along cross-section A-B calculated by the program FLOWNET (average summer conditions).



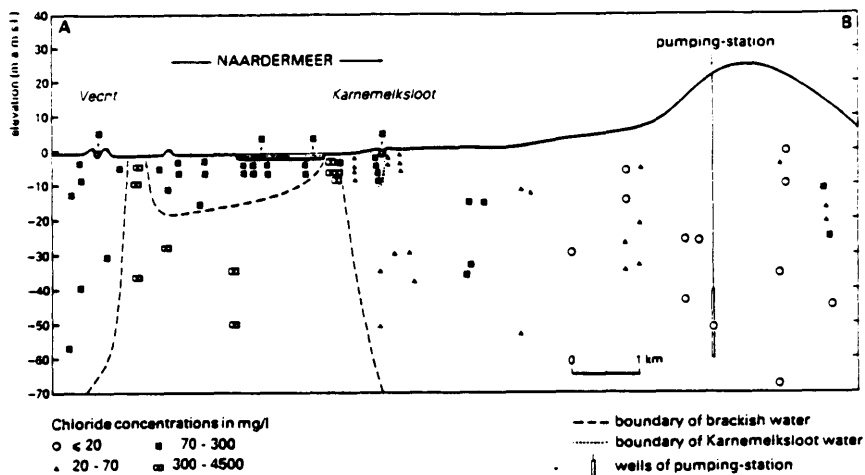


Fig. 4. Chloride concentrations along cross-section A-B.

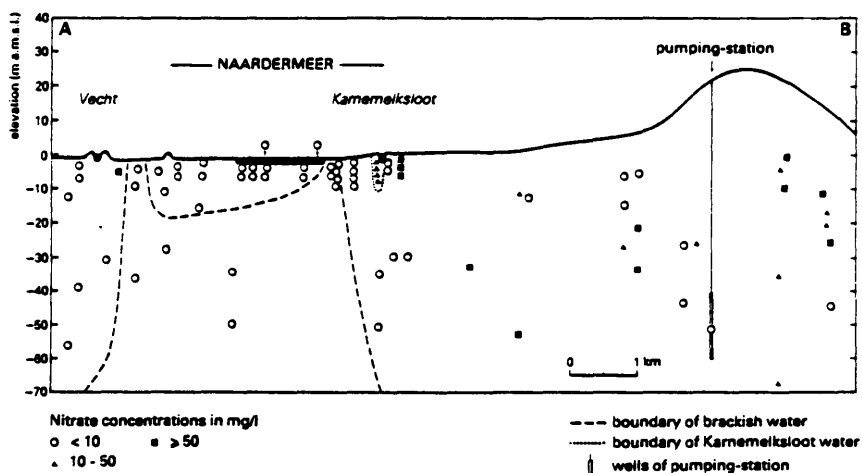


Fig. 5. Nitrate concentrations along cross-section A-B.

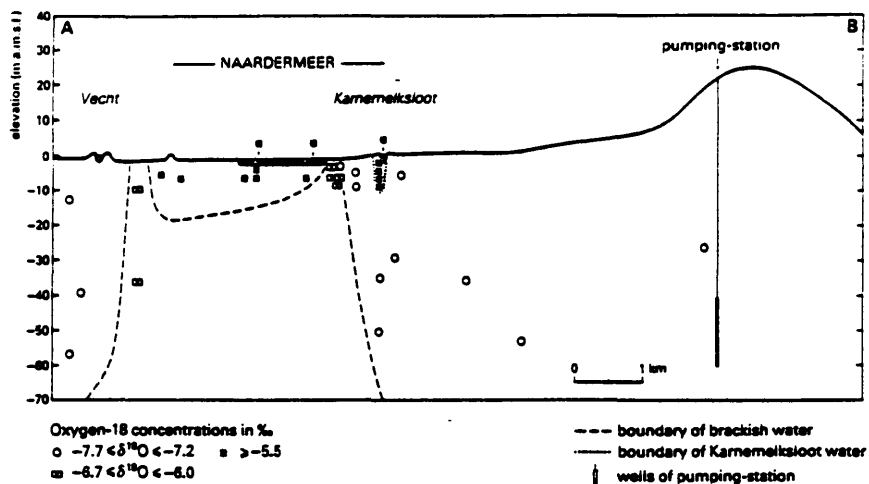


Fig. 6. Oxygen-18 concentrations along cross-section A-B. Concentrations are expressed as the deviation ( $\delta$ ) in parts per thousand from Standard Mean Ocean Water.

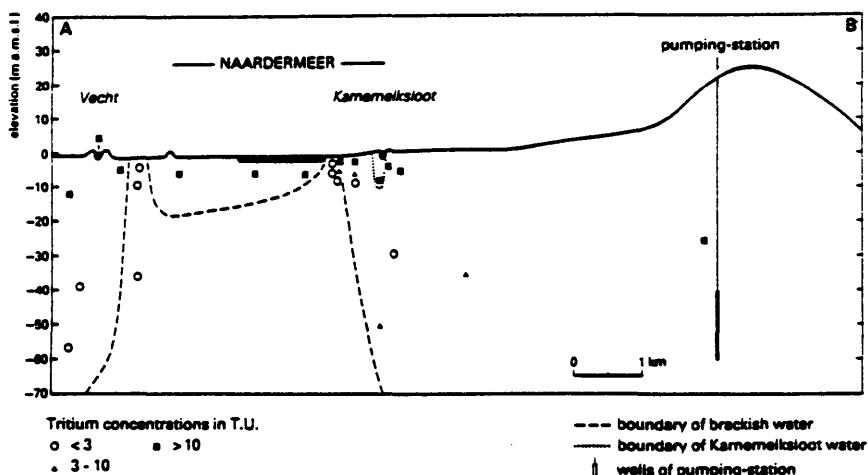


Fig. 7. Tritium concentrations along cross-section A-B. One Tritium Unit equals one tritium atom in  $10^{18}$  atoms.

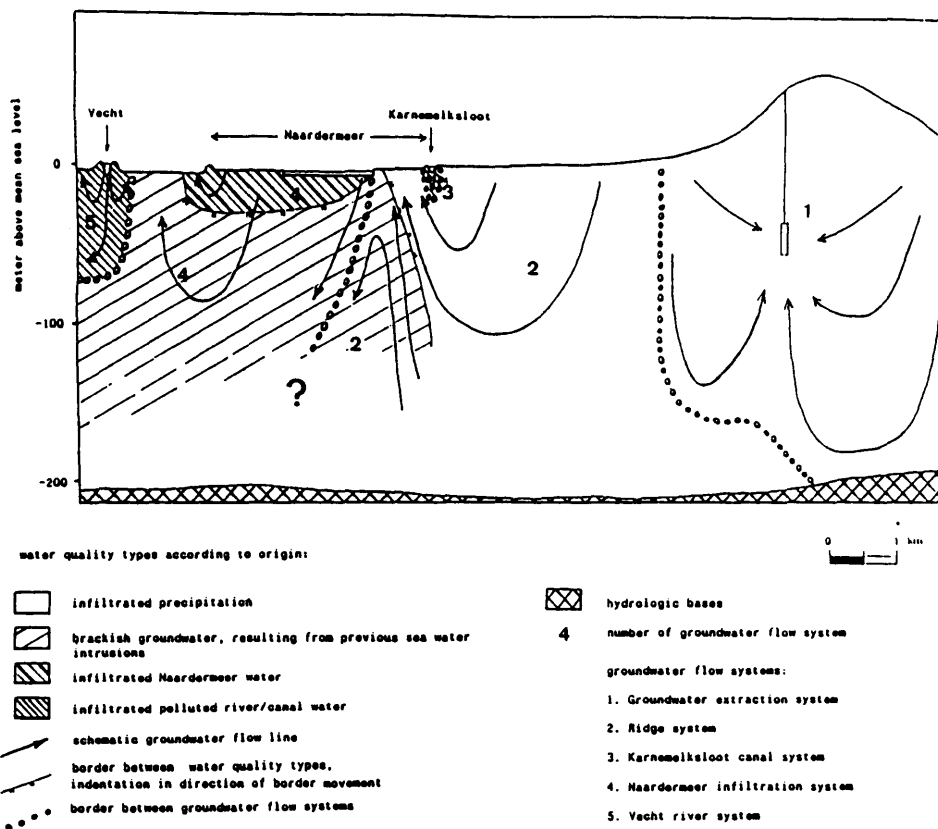


Fig. 8. Groundwater flow systems and water quality types along cross-section A-B.



WETLAND HYDROLOGIC SYSTEMS WITH SPECIAL REFERENCE  
TO THE GURINAI WETLAND WITHIN THE GOBI DESERT

Gu Weizu

Nanjing Research Institute of Hydrology and Water  
Resources, The Ministry of Water Resources, China

Abstract: About 33% of China's land is arid. In a world context, the dry lands of China are located in higher latitudes and stand at higher altitudes than many other arid regions of the world. The western Inner Mongolia is a typical arid area of this country; it is within the great arid system of the world, from north Africa through middle Asia to Mongolia. The Gurinai Wetland is within this arid region with boundaries about 100°45' to 101°30'E and 40°30' to 41°20'N, with total area about 3000 km<sup>2</sup> surrounded by Badajilin Desert about 47100 km<sup>2</sup> in area (Figure 1).

This wetland is the remnant of an ancient lake within the alluvial plain formed from the Black River (Ruohui River). Geomorphologically, it is an undulating ground with altitudes mostly between 1000 m to 1050 m above sea level. It had been an oasis for nomadic people; however, more serious degeneration was developed caused by anthropogenic impacts within recharge areas far from this wetland. Thick herbage became thin, dense sarsaoul was replaced by short bush, and groundwater quality steadily worsened. Unfortunately, many other wetlands in arid zones of this country met similar processes as in Gurinai.

The Wetland Hydrologic System

From our field experimental work, the wetland hydrologic system may be viewed as an open system within a relative narrow depth below the land surface with the following characteristics:

- (1) As shown in Figure 2, the upper horizontal boundary of this system may be taken as just above the plant canopy and the lower boundary at the bottom of the phreatic zone;
- (2) The components in this system are generally similar to those of ordinary hydrologic systems; however, the processes and storage of these components are quite different from most others;
- (3) The most important component of the system is the phreatic water which is in control of the system conditions;
- (4) Water entering the system takes mostly underground paths;
- (5) The major input is the groundwater recharge, and the major output is the evaporation and evapotranspiration from groundwater;
- (6) Surface water is mostly lost from the system near where it enters. In general, surface water input and output may be ignored;
- (7) The groundwater system is a complex of different sources of recharge;

- (8) Anthropogenic activities, even though far outside the wetland, sometimes have significant impact on the system components;
- (9) Within the system, redistribution of vadose water sometimes may be significant and serves an important role to desert plants.

### Components of the Gurinai Hydrologic System

Precipitation: The annual precipitation is about 50 mm with annual maximum and minimum of 88.3 and 9.5 mm, respectively. From gauging stations A to I (Figure 1) within the desert or located near its borders, it is found that there is an altitude-related spatial distribution of precipitation from two profiles, A to F and G to F, as shown in Figure 3. Annual precipitation decreases at a rate of about 8.3 mm/100m to 14.5 mm/100m for the F to I profile, and at a maximum decreasing rate of about 16.5 mm/100m from F to E.

Dew and water vapor: Two components of dew were examined. The dew evaporated from the land surface and condensed on the canopy is useless for plant life because it will evaporate again. However, dew deposition on the land surface from the atmosphere and infiltrating into the soil is useful. We estimate the annual input of dewfall on the wetland to be about 20 mm. This may be of importance where water is extremely scarce.

The large diurnal temperature extremes provide the driving force for water vapor flow. Figure 4 compares the diurnal soil temperature variations of bare and plant-covered soil over a year. The monthly surface soil temperature varies more than 20°C, but the variation is smaller for covered surfaces. Diurnal changes of volumetric water content near the surface have been observed as shown in Figure 5. The increments of water content every day illustrated in this figure cannot be the result of water condensation from air nor from the dewfall because the vapor pressure deficit of the atmosphere was not suitable. However, these increments have synchronous changes with differences of temperature in the corresponding soil layer. According to Cary (1965), and with some simplification, we use:

$$J_v = -D_v (dt/dz)$$

to describe vapor flow, where  $D_v$  is the thermal vapor soil water diffusivity and is nearly constant over a wide range of soil moisture conditions. It means that water flow due to thermal gradients can be reasonably calculated from temperature gradients of the soil layer. We combined this relationship with the results of lysimeter experiments conducted in this arid region, and by field observations. When the depth of the groundwater table does not exceed 4 m, we obtained:

$$J_v = 52 K^{0.6}$$

where  $J_v$  is the total annual recharge estimate of water vapor flow within the surface layer in mm for about 1 m depth. A considerable portion of  $J_v$  is concentrated in the periods of May to September.  $K$  is defined as the ratio of annual precipitation to annual potential evaporation. The areal averages after making evaporation pan corrections, are  $K \approx 0.025$  and  $J_v \approx 6$  mm. This small amount has little importance in humid regions; however, in this wetland, it is about 10% of annual precipitation.  $J_v$  also depends on soil porosity. When porosity increases,  $J_v$  does, too.

Storm rainfall in a desert system: Although storms of long duration are rare in the area, it is possible for local water vapor to be collected and concentrated locally; local storms with very short duration may be formed due to great diurnal air temperature difference, strong convection, unstable stratification, fast-moving weather systems, and frequent invasion of cold air masses from Siberia. These short-duration storms usually have very small coverage with high intensities compared with the storm records in the humid region of southern China. Figure 6 shows a typical spatial variation of these local storms which generally have spot-like distributions with multicenters of different rainfall amounts. Figure 7 shows again the general distribution characteristics of these storms. The spatial distribution may be simulated by a circle with its radius  $R$  equal to  $A/\pi$ , where  $A$  is the area of coverage.

Although the frequency of these storms is rare, on a macroscale, they, and others with smaller rainfall, occur here and there in vast desert space. In addition, in the Gobi Desert, strata of Tertiary period Q3 are widely distributed. Typical profiles show that gravel 10 to 50 mm in diameter occupy the upper layers with depths of several meters to scores of meters, overlaying coarse to fine sands. It means that storm rainfall percolates quickly until a clay layer is reached. This process is a sometimes overlooked recharge source and explains the occurrence of many small ponds with good water quality in the Badajilin Desert. It also may explain the formation of barchan springs (small lakes or springs behind the barchans) with fresh water. Ancient nomadic people called these springs "Celestial Water".

Evaporation and evapotranspiration: Annual potential evaporation averaged over 24 years from records of pan evaporation (pan area of 3000 cm<sup>2</sup>) is 2578 mm with an annual maximum of 3700 mm.

Evaporation rate,  $E_t$  (mm/day), from grassland surfaces depends on the potential evaporation rate,  $E_o$  (mm/day), and soil moisture content,  $\theta$ . From our experiments, a model of  $E_t/E_o$  versus  $\theta$  was developed as follows:

$$\begin{array}{ll} \theta > \theta_f & E_t/E_o = 1 \\ \theta_f \geq \theta \geq \theta_b & E_t/E_o = 1 - 0.96 (\theta_f - \theta) / (\theta_f - \theta_b) \\ \theta_b \geq \theta \geq \theta_w & E_t/E_o = 0.04 (\theta - \theta_w) / (\theta_b - \theta_w) \end{array}$$

where  $\theta_f$  is the field capacity,  $\theta_b$  is the moisture content of capillary bond distribution, and  $\theta_w$  is the wilting point. All the  $\theta$ s are in volumetric percentages. In our case,  $\theta_f$  ranges from 5% to 14%, and  $\theta_b$  ranges from 10% to 24%.

Evapotranspiration rates were calculated by the energy budget method at two sites having the same depth to groundwater but with different vegetation: dense meadow and sparse Siberian thorn bush. It was shown that: 1. For all months (Figure 8),  $E_t$  varied quickly in the daytime with a narrow peak at about 12:00 to 15:00 p.m. (Beijing time); 2. The duration of daytime evapotranspiration,  $T_{ev}$ , varies from month to month. Figure 9 illustrates that  $T_{ev}$  reaches a maximum of about 14 hours/day in the summer, and a minimum of about 5 hours/day in the winter; 3. Some negative net radiation occurs every month; and 4.  $E_t$  at the site with dense vegetation is greater than at the site with sparse vegetation (Figure 10).

### General View of Hydrological Conditions

Geomorphologic and lithologic features influence the formation and distribution of groundwater in this arid inland basin. In general, there are four systems of groundwater as follows:

- (1) Phreatic groundwater in Quarternary strata is distributed mainly in a vast alluvial plain where the water table is about 0.2 to 5 m below the land surface. This aquifer consists of fine sand, medium sand, and fine silt with a total depth of about 30 to 70 meters.
- (2) Confined groundwater in Quarternary strata occurs in most areas of this wetland. Aquifers consist of medium to fine sand, and silt with gravel. The top of these aquifers is about 40 to 70 meters below the land surface with its piezometric surface about 1.3 to 5 meters below land surface. In some places, the piezometric surface is above land surface.
- (3) Groundwater in fractures of Tertiary strata occurs in limited areas near the mounts, at more than 200 m below land surface in shale and sandstone. Hydraulic continuity exists between this water and groundwater recharge in the wetland.
- (4) Phreatic water occurs below the desert surface and in dunes. As mentioned above, it may be the result of accumulation from rainfall that occurs sporadically in vast areas of the Gobi Desert. It is a recharge source with good water quality.

Recharge of groundwater: Figure 1 indicates flow direction of the main inflow to the basin. Phreatic water is shown by black arrows, and confined water is shown by blank arrows. Inflow to the basin is from southeast and southwest. Outflow of groundwater is to the north. Two profiles of the ground surface with its groundwater table are taken across the wetland (Figures 11 and 1): profile I-I' from the south to north and profile II-II' from west to east. Both profiles originate and end in the Gobi Desert outside the wetland.

Profile II-II' (Figure 11b) indicates that the river is the main recharge source of the basin. It is found that the major amount of percolation water from the river usually takes a curtain-grouting pattern under the river bed to a depth of several meters to scores of meters, then begins to diffuse as indicated by the dashed line (a) in Figure 12. This form is different from the usual concept of the shape of the wetting zone as indicated by the solid line (b). Monitoring river discharge showed that infiltration loss was about 20% to 40% of the runoff within the monitored reach. The hydraulic gradient from the river to the wetland was about .0007.

To the north of the mountains, about 150 km south of the wetland (Figure 1), there occur many small lakes that are nearly parallel to the mountains, and nearly perpendicular to the dunes in that area. The lakes are a minor source of recharge because mean annual precipitation is only about 100 mm. The gradient is about 0.0006 to 0.0008 toward the wetland (Figure 12a). The dashed lines on both profiles in Figure 12 indicate inputs to the wetland from groundwater in the hilly and mountainous areas.



### Relation Between Recharge and Regional Water Quality

Four types of water quality were identified (Figure 13). These are:

- (1)  $\text{SO}_4^{2-}$  -  $\text{Cl}^-$  -  $\text{Na}^+$ , with total dissolved solids (TDS) less than 3,000 mg/l, occurs in the western part of the wetland (Figure 13a). This water is believed to be related to recharge from the river to the west. The river water type is  $\text{SO}_4^{2-}$  -  $\text{HCO}_3^-$  -  $\text{Na}^+$  -  $\text{Mg}^{++}$  -  $\text{Ca}^{++}$ , and TDS is less than 1,000 mg/l. The change between river and the aquifer occurs because evaporation causes precipitation of  $\text{Ca}(\text{HCO}_3)_2$ , and clay particles high in  $\text{Na}^+$  exchanges for  $\text{Mg}^{++}$  and  $\text{Ca}^{++}$ .
- (2)  $\text{Cl}^-$  -  $\text{HCO}_3^-$  -  $\text{SO}_4^{2-}$  -  $\text{Na}^+$ , with TDS less than 1,000 mg/l, occurs in the southeastern portion of the wetland. This water is believed to be related to recharge from local precipitation and occupies only a small portion of the basin.
- (3)  $\text{Cl}^-$  -  $\text{Na}^+$ , with TDS typically between 30,000 to 50,000 mg/l, but with maximum above 100,000 mg/l, occurs in the center of the basin. The long axis of this high TDS region coincides with the long axis of the wetland, i.e., the lowest portion of the wetland, where groundwater is subject to a high rate of evaporation. A groundwater sample from this area, analyzed by M.A. Geyh in 1988, showed the following: As, 126 ppb; Mg, 20,000 ppb; Se, 225 ppb; Al, 150 ppb; Ba, 10 ppb; Cd, 2 ppb; Co, 1 ppb; Cr, 13 ppb; Cu, 150 ppb; Fe, 180 ppb; Li, 40 ppb; Mn, 5 ppb; Pb, 1 ppb; Rb, 74 ppb; Sr, 66 ppb; and Zn, 5 ppb.
- (4)  $\text{Cl}^-$  -  $\text{SO}_4^{2-}$  -  $\text{Na}^+$ , with TDS ranging from 3,000 to 30,000 mg/l, occurs on both sides of and parallel with the high TDS region, and seems to be a transition zone between recharge from west and east, and discharge along the axis of the wetland.

### Groundwater Evaporation

The following equation is based on field experiments:

$$E_g = E_o (1 - D/10)^5$$

where:

$E_g$  = groundwater evaporation, mm/day

$E_o$  = potential evaporation, mm/day

$D$  = depth of groundwater table below the land surface, m.

It was noted that  $E_g$  is greater at night than in the daytime. Averaged over a year, for  $D = 0.5$  m, nighttime  $E_g$  is 3.1 mm, and daytime  $E_g$  is 2.6 mm. At a given value of  $D$ ,  $E_g$  is different for different soils. For example, where  $D = 1.0$  m, the monthly ratios of  $E_g$  in wetland, fine sand, and sand-gravel are about 3:0.9:1.0. Where  $D = 4.0$  m, the ratios are 0.9:0.8:1.0.

### Acknowledgment

The author gratefully acknowledges the help of Prof. Dr. Mebus A. Geyh. Special thanks are due to Dr. Thomas C. Winter and Dr. E.S. Simpson for their encouragement.

### Reference Cited

1. Cary, J.W., 1965, Water flux in moist soil, Soil Sci. 100.

### References Consulted

1. Bull, W.S., et al., 1979, Impact of climate change on an arid watershed, Quaternary Res., 11.
2. Evans, D.D., and J.L. Thames, 1983, Water in Desert Ecosystems, US/IBP Synthesis Series 11.
3. Fogel, M.M., 1969, The effect of storm rainfall variability on runoff from small semi-arid watersheds, Trans. Am. Soc. Agric. Eng. 12.
4. Gay, L.W., 1973, Energy exchange studies at the Earth's surface: I. Energy budgets of desert, meadow, forest, and marsh sites. Technical Report 73-1, Oregon State University, Corvallis, Oregon.
5. Gaylon, S., and G.A.H. Campbell, 1981, Modeling soil-water-plant-atmosphere systems of deserts, Chapter 5 of Water in Desert Ecosystems, US/IBP Synthesis Series 11.
6. Jackson, R.D., 1965, Water vapour movement in relatively dry soil, Soil Sci. Soc. Am. Proc. 28, 29.
7. Packard, F.A., 1974, The hydraulic geometry of a discontinuous ephemeral stream on a Bajada near Tucson, Arizona, University of Arizona, Tucson, Arizona.
8. Simpson, E.S., et al., 1982, Digital mixing-cell models for the study of groundwater quality changes, IAH International Symposium, Prague, Czechoslovakia, V. 16, Part 3.
9. Yair, A., et al., 1973, The influence of surface properties on flow and erosion processes on debris-covered slopes in an arid area, Catena, 1.

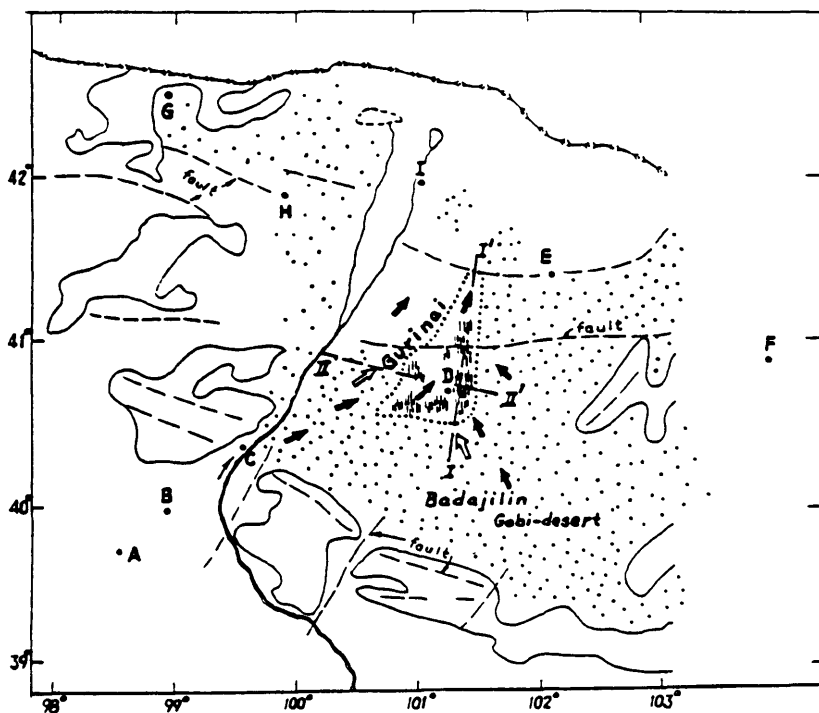


Figure 1. Location of Gurinai Wetland and its neighbors.

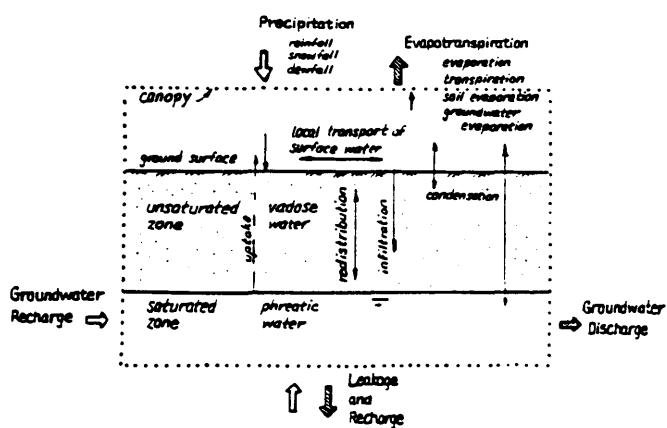


Figure 2. Components of wetland hydrologic system.

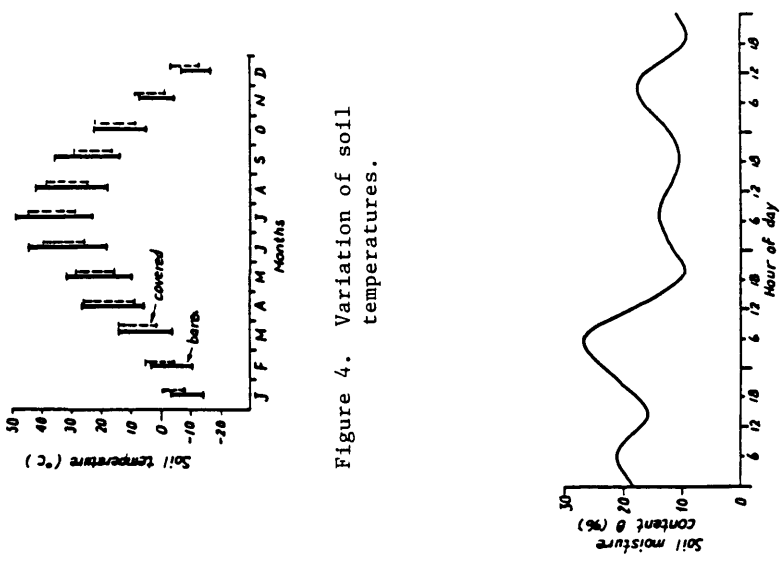


Figure 4. Variation of soil temperatures.

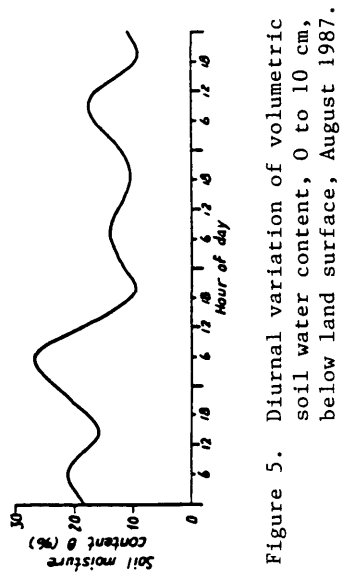


Figure 5. Diurnal variation of volumetric soil water content, 0 to 10 cm, below land surface, August 1987.

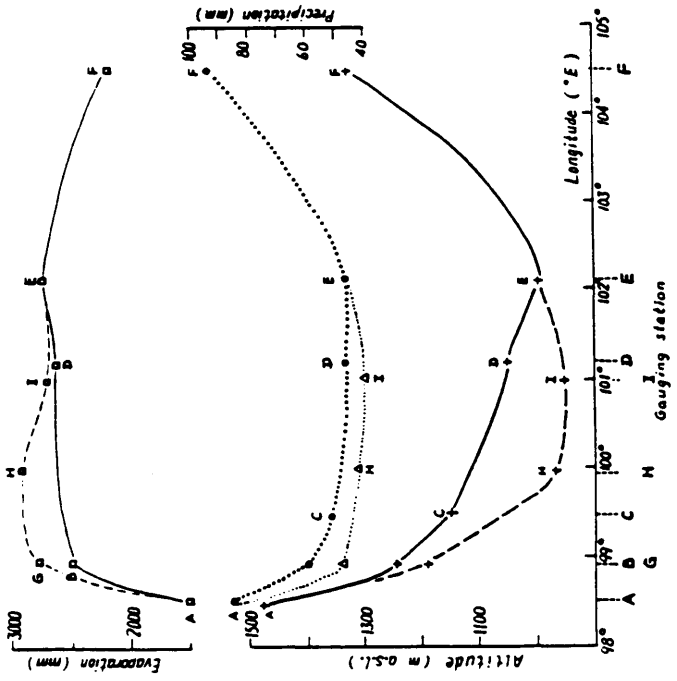


Figure 3. Altitude related annual precipitation and annual evaporation (see Fig. 1 for location of gauging stations).

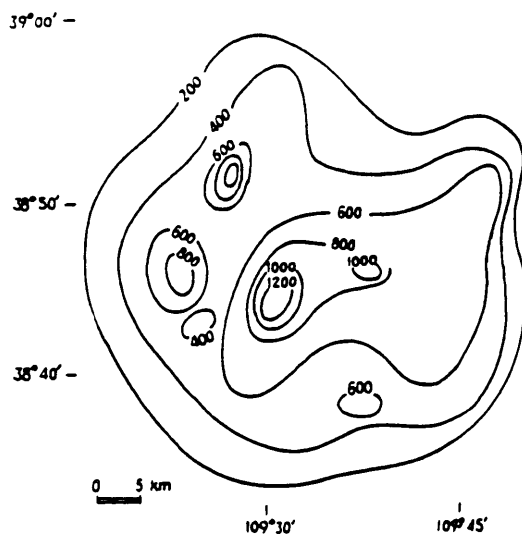


Figure 6. Isohyet (in mm) of a storm event in Inner Mongolia, August 7, 1977.

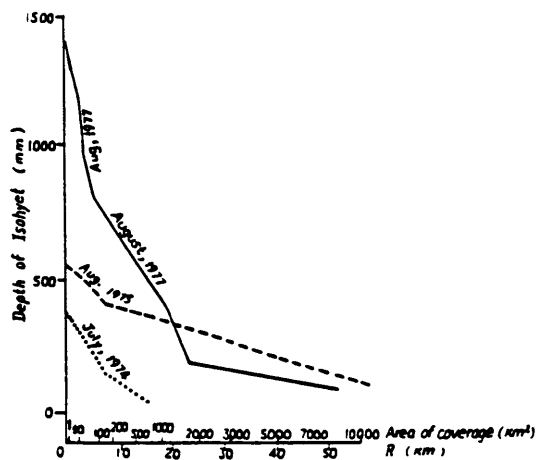


Figure 7. Depth-area curve of storms in Inner Mongolia.

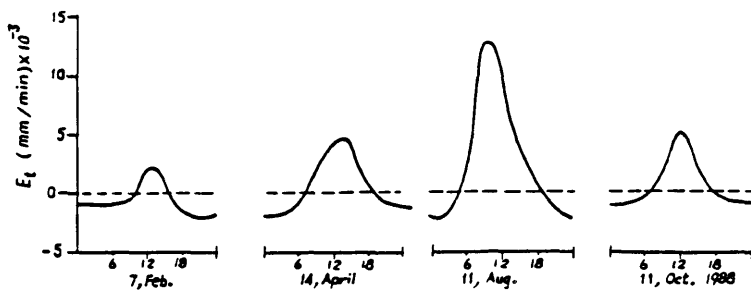


Figure 8. Calculation of evapotranspiration rates by energy budget.

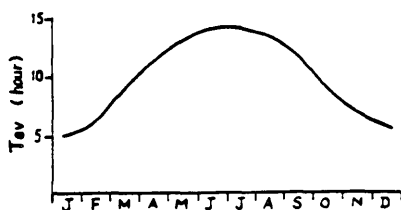


Figure 9. Variation of  $T_{ev}$ .

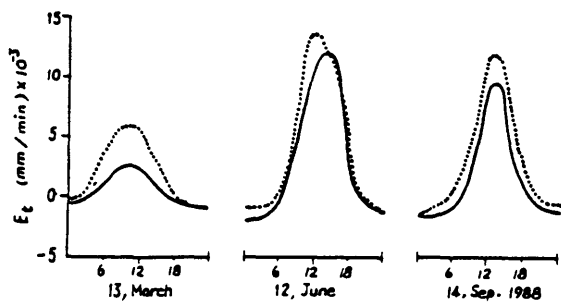


Figure 10. Comparison of diurnal variation of evapotranspiration rates for various months.

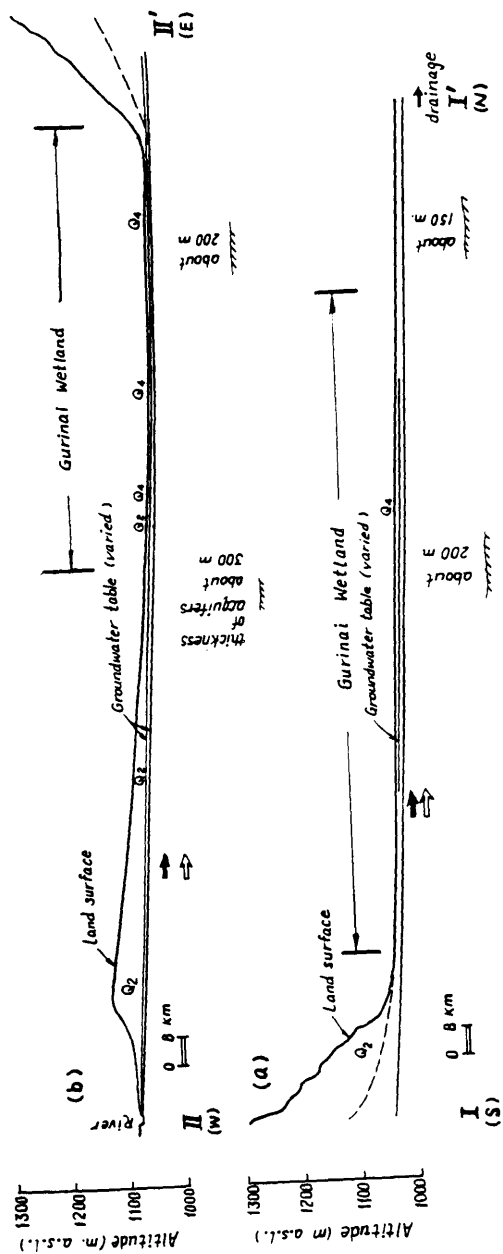


Figure 11. Profiles across Gurinai Wetland (see Fig. 1 for locations).

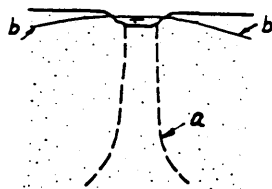


Figure 12. Percolation patterns of a desert river (see text for explanation).

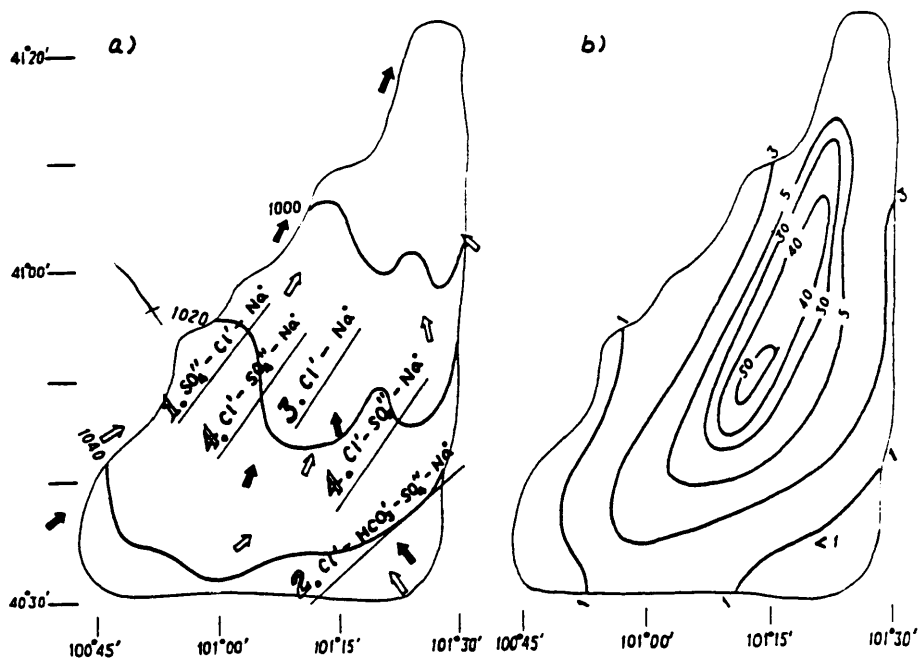


Figure 13. Gurinai Wetland: (a) regional distribution of water quality; (b) isohaline map.



NUMERICAL MODELLING OF THE GROUNDWATER CONTRIBUTION  
TO THE HYDROLOGICAL BUDGET OF LAKES

A.S. Crowe

National Water Research Institute,  
Canada Centre for Inland Waters,  
867 Lakeshore Road, P.O. Box 5050,  
Burlington, Ontario, L7R 4A6,  
Canada.

**ABSTRACT:** Groundwater typically has been given little significance in the water budget of lakes because groundwater inflow to or outflow from a lake can not be accurately measured. A lumped-parameter, watershed model has been developed specifically to quantify the role of groundwater in the water balance of lakes. This model extends conventional water balance methods because hydrostratigraphic units are represented by a series of storage elements, temporal variability is considered by routing water through hydrological components of the model, and solute transport through the various components of the watershed provides a test for values assigned to the model parameters. The model simulated measured lake surface-elevations and salinity for two lakes in a Canadian prairie setting. Groundwater outflow is the dominant factor maintaining a low salinity for Wabamun Lake even though the lake is highly evaporitic. Groundwater inflow to and outflow from Baptiste Lake influences this lake to a lesser degree.

**RÉSUMÉ:** Les eaux souterraines typiquement ont reçu peu d'attention dans le bilan d'eau des lacs puisque leurs débits d'entrée et de sortie ne peuvent être mesurés avec précision. Un modèle mathématique du bassin hydrographique se basant sur la conception d'un paramètre global, a été élaboré spécifiquement pour quantifier l'importance des eaux souterraines dans le bilan d'eau des lacs. Ce modèle est une amélioration des techniques conventionnelles de bilans des eaux parce que les unités hydrostratigraphiques ont été représentées par une série d'éléments emmagasineurs; la variabilité temporelle a été prise en considération par le passage d'eau entre les composantes hydrologiques du modèle et le transport des solutés entre les différentes composantes du bassin hydrographique permet d'essayer des valeurs assignées aux paramètres du modèle. Le modèle a simulé les élévations mesurées du niveau du lac et la salinité des lacs pour deux lacs dans les prairies du Canada: La sortie des eaux souterraines est le facteur dominant dans le maintien d'une salinité basse pour le lac Wabamun même si ce lac est très évaporitique. L'entrée et la sortie des eaux souterraines à au lac Baptiste influencent ce lac faiblement.

Introduction

Freshwater lakes are a valuable resource for domestic and industrial water supply, recreation and wildlife management. However, there are many cases where the quality of the water has been impaired by the introduction of contaminants or nutrients. While stream flow, surface runoff and precipitation are generally studied as sources of contaminants or nutrients entering a lake, the effects of groundwater

flow into or from a lake are seldom considered. Several field-oriented studies have shown that groundwater may represent a large portion of recharge to or discharge from a lake, and therefore, the groundwater component of the hydrological balance of lakes can not be ignored.

Techniques that can be used to quantify groundwater flow into and from a lake include: (1) a field-oriented approach, (2) numerical simulations and (3) hydrological balance of the lake-watershed. Each has its advantages and disadvantages depending upon the specific goals of the study.

Two field-oriented approaches are the installation of shallow piezometers in the vicinity of a lake and the use of seepage meters placed on the bottom of the lake. Piezometer nests can be used to demonstrate potential pathways for groundwater flow into or from a lake (Jaquet, 1976; Karnauskas and Anderson, 1978; Rhinaldo-Lee and Anderson, 1980; Winter, 1986). Measurements of hydraulic head obtained from piezometer nests combined with the Darcy Equation have been used to quantify groundwater flux (Loeb and Goldman, 1979; Rhinaldo-Lee and Anderson, 1980). However, the estimates generally are not accurate because of spatial variability of permeability, and the structure and hydraulic gradient (including temporal fluctuations) of the aquifer. Also, the detailed hydrogeological data suitable for this method requires extensive instrumentation which is very expensive. The use of seepage meters placed on the bottom of a lake will supply accurate data on groundwater and solute flux (Belanger and Mikutel, 1985; Brock et al., 1982; Lee, 1976; Lee et al., 1980; Lock and John, 1978), but only on a localized scale. Considerable variability in the hydraulic gradients, permeability and heterogeneity of sediments and the placement of the seepage meters will lead to errors when extrapolating point specific measurements to an entire lake (Brock et al., 1982; Cherkauer and Nader, 1989), especially if the lake is large (Cherkauer and McBride, 1988; Cherkauer and Nader, 1989). To adequately estimate groundwater flux, both the piezometer and seepage meter approach require considerable instrumentation in order to characterize groundwater flux from all the hydrostratigraphic units and to ensure that important discharge zones are not missed.

Computer-oriented studies are very useful for understanding the controlling parameters and processes affecting groundwater flow patterns in the vicinity of lakes and groundwater flux at a lake. However, these models are typically limited to hypothetical scenarios (McBride and Pfannkuch, 1975; Pfannkuch and Winter, 1984; Winter, 1978a, 1978b, 1981, 1983; Winter and Pfannkuch, 1985) because detailed field data as discussed above are required to construct an accurate model which represents the natural conditions. Computer models of actual lake-watershed have been developed and used to quickly assess groundwater flux under a variety of hydrological conditions (Anderson and Munter, 1981; Munter and Anderson, 1981; Rhinaldo-Lee and Anderson, 1980).

The most common method of assessing the sources and volume of water and nutrients entering and leaving a lake is the hydrological balance or budget technique. Although balance techniques ignore the spatial variability of natural systems that lead to errors associated with the

previous field methods, they are subject to the accuracy in estimates hydrological components affecting lakes. However, if the purpose of a study is to determine the net contribution of groundwater to the hydrological balance of a lake, and not to determine flow pathways or point sources and concentrations of solutes, then a balance approach has advantages over the field methods. Hydrological studies of lake-watershed systems are typically based on quantifying the water balance among precipitation, evaporation, surface runoff, lake discharge and groundwater inflow to and outflow from the lake. Because all the components effect the volume of water in the lake, this relationship can be expressed as:

$$\Delta S_{\text{lake}} = P + SW_{\text{in}} + GW_{\text{in}} + SRO - E - SW_{\text{out}} - GW_{\text{out}} \pm \text{others} \quad (1)$$

where:  $\Delta S_{\text{lake}}$  = change in volume of water in the lake,  
 $P$  = precipitation falling directly on the lake,  
 $SW_{\text{in}}$  = surface water inflow to lake (eg. rivers, streams),  
 $GW_{\text{in}}$  = groundwater discharge to the lake,  
 $SRO$  = surface runoff directly to the lake,  
 $E$  = evaporation directly from the surface of the lake,  
 $SW_{\text{out}}$  = surface discharge from the lake (eg. river, stream),  
 $GW_{\text{out}}$  = discharge from the lake via groundwater,  
 $\text{other}$  = other factors affecting lake storage,  
 (eg. irrigation, industrial withdrawal).

Contributions to the volume of water within a lake from the hydrological components other than groundwater are measurable, or in the case of evaporation, calculated by standard formulae (Gray et al., 1970). However, the quantities of groundwater flow into or from a lake can not be measured accurately due to the geological complexity of the subsurface and the detailed field methodology required to adequately characterize the hydrostratigraphy. Therefore, for convenience, typical studies assume that groundwater has little significance in the water budget or have ignored the groundwater component completely. Thus, under these assumptions, the balance equation which is typically solved is:

$$\Delta S_{\text{lake}} = P + SW_{\text{in}} + SRO - E - SW_{\text{out}} \pm \text{others} \quad (2)$$

The hydrological balance (equation (1)) can not be used to uniquely assess the role of groundwater inflow and outflow in the water budget of a lake, or its associated contaminant or nutrient input. All values other than groundwater inflow and outflow in equation (1) can be measured, and the substitution of these known values into equation (1) will produce one equation with two unknowns ( $GW_{\text{in}}$  and  $GW_{\text{out}}$ ) which is typically included in the balance equation as groundwater flux to the lake ( $\Delta GW_{\text{lake}}$ ):

$$\Delta GW_{\text{lake}} = GW_{\text{in}} - GW_{\text{out}} \quad (3)$$

Thus, there is not a unique solution to estimating groundwater inflow to or outflow from a lake. At best, only the net groundwater flux to the lake ( $\Delta GW_{\text{lake}}$ ) can be estimated, or one of the two terms in equation (3) is set to zero to allow the other to be estimated (Cole and Fisher,

1979; Cook et al., 1977; Enell, 1982; Karnauskas and Anderson, 1978; Rhinaldo Lee and Anderson, 1980; Steenbergen and Verdouw, 1982).

The objectives of this paper is (1) to present an improved hydrological balance model assessing the contribution of groundwater to the hydrological budget of a lake, and specifically, to develop a technique which can arrive at a good estimate using readily available field data, and (2) to use the model to determine the groundwater inflow to and outflow from lakes in a Canadian prairie setting.

#### Description of the Model

A lumped-parameter model has been developed to study the water balance of lakes, and specifically to quantify the role of groundwater inflow to and outflow from a lake. The major hydrological components characterizing the watershed, such as the groundwater zone, unsaturated soil zone, and processes affecting the lake, such as precipitation, surface discharge from the lake, river or stream discharge to the lake, etc., are represented by lumped-parameter elements. The model is designed to simulate hydrological conditions within a watershed in a Canadian prairie environment. Thus, it must take into account climatic considerations such as the accumulation of snow, ice formation at the lake surface, spring runoff, etc. that affect both the volume of water and chemistry of the lake. All the major hydrological components and processes affecting the lake considered in the model are illustrated by Figure 1. This model extends conventional water balance techniques in three ways.

First, the main problem with applying a simple water balance expression, such as equation (1), to a natural watershed is that this expression only considers the storage of water at a fixed moment in time. Routing calculations allows temporal variability of the watershed parameters to be considered as a simulation moves forward in time. Thus, by simulating both storage within all the hydrological components and the routing of water among the components at a number of time steps, a series of dependent equations of the following form results:

$$\Delta S_{\text{lake}}(t_1) = P(t_1) + SW_{\text{in}}(t_1) + GW_{\text{in}}(t_1) + SRO(t_1) - E(t_1) - SW_{\text{out}}(t_1) - GW_{\text{out}}(t_1) \pm \text{others}(t_1) \quad (4)$$

where:  $t_1$  = time step at which a balance is calculated.

Because this technique calculates a series of daily, weekly or monthly water balances, it is more accurate than a conventional long-term average. As the number of time steps increase and the size of the time step decreases, the accuracy of the estimate of groundwater inflow and outflow will increase because the number of dependent balance equations in the form of equation (1) that must be solved simultaneously increases.

The structure of this watershed model (Figure 1) is similar to other lumped-parameter watershed models (for example, Crawford and Linsley, 1966; Croley, 1983). However unlike the existing watershed models, the new model is focused towards the hydrological characteristics of lakes rather than runoff hydrographs, and requires only basic climatic and hydrological data which are commonly available

from field studies. Most existing watershed models are quite complex and require a variety of input parameters, many of which are not routinely measured (eg. slope of ground surface, solar radiation, wind speed, interception of precipitation by tree species, etc).

Secondly, because the focus of this model is towards estimating both groundwater inflow to and outflow from a lake, the groundwater flow system is represented in more detail than typical balance models. The major hydrostratigraphic units within the watershed are represented as a series of groundwater storage elements. The model uses four types of groundwater storage elements; (1) a shallow storage element with an overlying unsaturated soil zone, (2) a shallow storage element without an overlying unsaturated zone, (3) a deep storage element underlying the shallow storage elements and (4) a composite storage element which has the properties of a shallow element until storage is depleted by evaporation to a minimum limit after which it has the characteristics of a deep element. Recharge to these elements may occur from precipitation, the unsaturated zone, the lake, other storage elements or from out of the watershed. Discharge occurs through evaporation, to rivers, to the lake, to other elements or out of the watershed. Groundwater discharge from a storage element is a function of recharge and discharge from the present and previous time step. These are related through a series of routing coefficients defined by a storage delay time and time for recharge to an element as defined by Dooge (1960):

$$Q_t = c_0 R_t + c_1 R_{t-1} + c_2 Q_{t-1}, \quad (5)$$

where:  $Q_t$  = groundwater discharge during the present time step,  
 $Q_{t-1}$  = groundwater discharge during the previous time step,  
 $R_t$  = groundwater recharge during the present time step,  
 $R_{t-1}$  = groundwater recharge during the previous time step,  
 $c_0, c_1, c_2$  = routing coefficients.

The third improvement incorporated into the model is that dissolved mass, in the form of ions, is also routed through the various components of the watershed. Although using a model based on equations (4) and (5) will provide a better estimate of the groundwater inflow to and outflow from a lake, it is still possible to arrive at a non-unique balance. The problem of a non-unique solution is resolved by adding a second balance equation which is based on the chemistry of the hydrological components of the watershed. Thus, the long-term chemical character of the lake is simulated as a mixture of all waters entering the lake modified by processes such as evaporation and ice formation as follows:

$$\begin{aligned} \Delta C[S_{lake}(t_1)] &= C[P(t_1)] + C[SW_{in}(t_1)] + C[GW_{in}(t_1)] + C[SRO(t_1)] \\ &\quad - C[E(t_1)] - C[SW_{out}(t_1)] - C[GW_{out}(t_1)] \\ &\quad - C[ice(t_1)] \pm C[others(t_1)] \end{aligned} \quad (6)$$

where:  $C[...]$  = concentration of the given hydrological component.

As illustrated by Figure 1, water entering or leaving the lake may either decrease the salinity of the water in the lake (surface discharge, precipitation, melting of ice), increase its salinity (groundwater inflow, formation of ice, evaporation), or simply remove

salts without a net change in the salinity of the lake water (discharge as stream flow or groundwater flow). The ability of the model to route mass provides an independent test of the uniqueness of the values assigned model variables. The solute transport and balance portion of the model is simplified by not incorporating chemical reactions into the code. Non-reactive solutes such as  $\text{Cl}^-$ ,  $\text{Na}^+$ , or total salinity of the waters are cycled through this model. Because they are highly soluble and are not taken up by organisms, their concentrations are controlled by physical processes and not chemical or biological processes.

Where possible, values of the climatic, hydrological and watershed parameters required for a simulation should be obtained from field data. These data include temperature, precipitation, potential evaporation, lake surface elevations, lake chemistries, and the chemistries of water in the various watershed components. The values of other parameters, such as unsaturated zone moisture capacity, storage delay time and routing paths among the groundwater elements are initially inferred from field observations, but require a trial and error procedure of matching measured lake levels and chemistry to determine acceptable values. The reader is referred to Crowe and Schwartz (1981a) for a detailed discussion of the model and its input parameters.

#### Application of the Model

The model has been applied to two lakes in Alberta, Canada, with the objective of quantifying the role of groundwater in the water balance of these lakes. The major difference between the two lakes is that Wabamun Lake occupies a relatively large portion of its watershed, while Baptiste Lake occupies only a small portion of its watershed. Figure 2 shows the location and size of the two lakes relative to their respective watersheds.

##### Wabamun Lake

Wabamun Lake occupies 78 km<sup>2</sup> of its 418 km<sup>2</sup> watershed. The watershed is mainly forested, being within an aspen parkland natural vegetation region, or is cleared for agriculture. Development consists of summer cottages along the shore of Wabamun Lake, two large coal strip mines and two major thermal electric generating stations are located on the shore of the lake. The topography of the watershed is rolling to hilly. With the exception of spring runoff, there is essentially no continuous stream flow into the lake and discharge through the single outlet creek is intermittent. Other hydrological information for Wabamun Lake, its watershed and climate is listed in Table 1.

One important characteristic of Wabamun Lake is that it is highly evaporitic. However, the salinity of the lake is very low even though the total annual evaporation from the lake exceeds total annual precipitation, and there is essentially no stream inflow which would replenish the lake with freshwater, nor stream discharge from the lake which would flush the saline water from the lake. Based upon the similarity between the chemical character of the lake water and local groundwaters, it has been proposed that the lake is strongly influenced by groundwater discharge to the lake and that the low salinity of

Wabamun Lake is due to discharge from the lake as groundwater (Nursall et al., 1972; Fritz and Krouse, 1973; Schwartz and Gallup, 1978).

Table 1. Characteristics of Wabamun Lake and its watershed.

---

|                                    |   |  |
|------------------------------------|---|--|
| 488 mm                             | : | mean total annual precipitation            |
| 534 mm                             | : | mean total annual potential evaporation    |
| -15.3°C                            | : | mean minimum monthly temperature           |
| 16.6°C                             | : | mean maximum monthly temperature           |
| 418.2 km <sup>2</sup>              | : | area of the watershed (including the lake) |
| 724.7 m amsl                       | : | mean lake surface elevation                |
| 77.7 km <sup>2</sup>               | : | surface area of Wabamun Lake               |
| 11.0 m                             | : | maximum depth of Wabamun Lake              |
| 6.5 m                              | : | mean depth of Wabamun Lake                 |
| 503x10 <sup>6</sup> m <sup>3</sup> | : | lake volume                                |
| 400µS/cm                           | : | average specific conductance of the lake   |

---

Groundwater recharge to the lake occurs through the coal, sandstone and shale units north and west of Wabamun Lake (Fritz and Krouse, 1973; Schwartz and Gallup, 1978). Groundwater discharge from the lake is thought to occur only through the deep bedrock units south of the lake (coal and sandstone/shale below the coal) or an alluvial deposit at the east end of the lake (Fritz and Krouse, 1973).

Table 2. Groundwater storage elements for the Wabamun Lake watershed.

---

| hydrostratigraphic unit                | mean specific<br>conductance (µS/cm) | storage<br>elements |
|--|--------------------------------------|---------------------|
| till                                   | 883                                  | 1                   |
| alluvium                               | 800                                  | 1                   |
| sandstone above coal (N of lake)       | 635                                  | 1                   |
| sandstone above coal (S of lake)       | 1121                                 | 1                   |
| coal (N and S of lake)                 | 1076                                 | 1                   |
| sandstone/shale below coal (N of lake) | 1372                                 | 1                   |
| sandstone/shale below coal (S of lake) | 1372                                 | 1                   |

---

The choice of values assigned to the parameters for the model are based upon Crowe and Schwartz (1985) but have been modified for the present simulations. Groundwater storage elements represent surficial sand and till, and the shallow and deep bedrock units within the Wabamun Lake watershed (Table 2). In addition to the parameters characterizing the watershed, lake-functions specific to Wabamun Lake are required. These lake functions include stage-area and a stage-volume curves for the lake and stage-discharge curves for the outlet stream. Numerous trials were undertaken with the model in which the parameters, such as the routing coefficients, were adjusted in order to simulate the lake surface elevations and the lake chemistry. The values of these variables

which are adjusted or inferred during the calibration of the model are typical of conditions in a Canadian prairie setting.

The resulting agreement between the simulated and measured lake levels and chemistry (Figure 3 and 4, respectively) is good considering that the model requires only basic climatic data for a simulation. The results of the simulation indicates that the important components in the water balance for Wabamun Lake are precipitation, surface inflow, evaporation and discharge from the lake as groundwater. Inflow to and outflow from Wabamun Lake for all the hydrological components were calculated on a monthly basis. The yearly proportion of inflow to and outflow from Wabamun Lake attributed to groundwater varied from 1-10% and 30-38%, respectively during the last 20 years (Figure 5). The box and whisker plot on Figure 5 shows that over 20 years, the median annual percentage of inflow to the lake via precipitation directly on the lake, surface water inflow and groundwater discharge to the lake was 55.3%, 39.3% and 5.7%, respectively. Also, there is little variance from the median, as illustrated by the interquartile ranges (Figure 5). For example, the ranges of groundwater inflow and outflow are the smallest, being 4.3% and 2.8%, respectively. The greatest interquartile range is displayed by precipitation (10.2%) and surface water outflow (10.0%). The median annual discharge from the lake as evaporation, surface discharge and groundwater flow was 59.6%, 4.3% and 36.2%, respectively. The points plotted outside of the outer hinge points of box and whisker plots on figure 5 also shows that the percentage of groundwater outflow and evaporation were abnormally low compared to the other 19 years, and that surface inflow and outflow were unusually high during 1974 because precipitation was much greater than normal that year.

This simulation shows that although the lake is dominantly evaporitic, the low salinity of Wabamun Lake is due to two factors. First, most recharge enters the lake as precipitation falling directly on the lake, or as surface runoff or stream flow during the spring. The quantity of groundwater entering the lake, which is a principle source of dissolved mass, is very low. Thus, groundwater inflow has a negligible contribution to the salinity of Wabamun Lake. Secondly, the solutes which accumulate in the lake water due to evaporation are flushed from the lake via groundwater.

To illustrate the importance of groundwater in the hydrological budget of Wabamun Lake, and the importance of supplementing the water balance with a chemical balance, the hydrological balance of the lake-watershed was again simulated but without a groundwater component. Previous recharge to the lake as groundwater now enters as surface water inflow. Previous groundwater outflow from the lake now leaves as evaporation from the lake surface because the calculations for evaporation are much less accurate than surface water discharge which is closely monitored and cannot be increased above the measured discharge rates. Simulations conducted without the groundwater component reproduce the observed lake levels as well as the previous simulations which include a groundwater component (Figure 3). However, the salinity of Wabamun Lake has dramatically increased without the flushing of dissolved mass from the lake via groundwater (Figure 4).



### Baptiste Lake

Baptiste Lake has a surface area of approximately 9 km<sup>2</sup> and unlike Wabamun Lake, it occupies only a small portion of its 318 km<sup>2</sup> watershed. The watershed is comprised primarily of forest and swamps, with a small portion being used for agriculture. The natural vegetation within the region is classified as boreal forest. The topography of the watershed is rolling to hilly. Numerous creeks flow into the lake and one stream drains Baptiste Lake. Information characterizing Baptiste Lake and its watershed is listed in Table 3.

Table 3. Characteristics of Baptiste Lake and its watershed.

|                                     |   |  |
|-------------------------------------|---|--|
| 493 mm                              | : | mean annual total precipitation            |
| 546 mm                              | : | mean annual total potential evaporation    |
| -17.9°C                             | : | mean minimum monthly temperature           |
| 16.2°C                              | : | mean maximum monthly temperature           |
| 319.1 km <sup>2</sup>               | : | area of the watershed (including the lake) |
| 578.1 m amsl                        | : | mean lake surface elevation                |
| 9.2 km <sup>2</sup>                 | : | surface area of Baptiste Lake              |
| 27.5 m                              | : | maximum depth of Baptiste Lake             |
| 9.3 m                               | : | mean depth of Baptiste Lake                |
| 86.5x10 <sup>6</sup> m <sup>3</sup> | : | lake volume                                |
| 325µS/cm                            | : | average specific conductance of the lake   |

With the exception of a detailed study by Trew et al. (1980), very little information about the hydrology of the Baptiste Lake watershed exists, and even less is known about the groundwater flow system. Borneuf (1973) indicated that Baptiste Lake is situated in a bedrock depression at the confluence of two buried preglacial valleys. Drilling (Crowe, 1978) confirmed the existence of sands and gravels at the base of the valleys which probably intersect the lake. Because the primary surficial deposit is till and the underlying bedrock is shale, these deposits would be an important source for groundwater inflow to and from the lake.

Table 4. Groundwater storage elements for the Baptiste Lake watershed.

| hydrostratigraphic unit                   | mean specific conductance (µS/cm) | storage elements |
|---|-----------------------------------|------------------|
| shallow till (with & without unsat. zone) | 1000                              | 2                |
| alluvium (with & without unsat. zone)     | 1025                              | 2                |
| aeolian                                   | 255                               | 1                |
| deep till                                 | 1250                              | 1                |
| deep sand (N buried valley)               | 1120                              | 1                |
| deep sand (S buried valley)               | 760                               | 1                |

The values assigned to the input parameters for the lake-watershed model are discussed in Crowe and Schwartz (1981b). The groundwater

elements representing the Baptiste Lake watershed correspond to till and sand at the surface, with and without an overlying unsaturated zone, and deeper till and sand (Table 4). Groundwater may flow into or from the lake via either of the deep units. Again, model calibration was used to simulate the measured lake surface elevations and lake salinity.

Although the record of lake levels and lake chemistry is much shorter than that for Wabamun Lake, sufficient data are available for simulating watershed responses. Good agreement was obtained between the observed and predicted lake levels and salinity for Baptiste Lake (Figures 6 and 7). Groundwater does not exhibit as dominant a role on the water balance of Baptiste Lake as it does for Wabamun Lake. Groundwater inflow to and outflow from the lake varied from 7% to 23% and 7% to 15%, respectively, during the seven years of records (Figure 8). The major hydrological components controlling surface elevation of Baptiste Lake and its salinity are surface water inflow and outflow. The median annual contribution of precipitation falling directly on the lake, surface water inflow and groundwater inflow to Baptiste Lake, as shown by the box and whisker plot (Figure 8) were 13.6%, 73.3% and 13.1%, respectively. The median annual losses from the lake as evaporation from the lake surface, surface outflow and groundwater outflow were 13.5%, 74.6% and 11.9%, respectively. The interquartile range of groundwater inflow and outflow is 9.0% and 2.5%, respectively.

Simulations undertaken without a groundwater component can produce an acceptable reproduction of the observed lake levels (Figure 6). However, the specific conductance of Baptiste Lake is a groundwater component in the water balance is only a third of that as when a groundwater component is included in the model.

### Conclusions

A lumped-parameter, lake-watershed model has been developed specifically for assessing the groundwater contribution to the water budget of lakes. The model successfully simulated measured lake surface elevations over a period of 26 and 6 years, and lake water salinity for 2 years each, for two lakes in a Canadian prairie setting. Groundwater outflow is the dominant factor maintaining a relatively low salinity for Wabamun Lake even though approximately 60% of water loss from the lake is by evaporation. Groundwater inflow and outflow to Baptiste Lake, (13% and 11%, respectively) influences the salinity of this lake to a lesser degree. Although good agreement was obtained between the predicted and measured surface elevations of the lakes when the groundwater component was not considered, the simulated salinity of the lakes differed dramatically from that measured. By simulating the routing of both water and solutes through all components in the watershed, a good agreement between the measured lake levels and salinity was obtained, thus quantifying the role of groundwater in the hydrological budget of these lakes. These simulations show that a hydrological balance model should route solutes through the system as an additional balance for verifying the model parameters and quantify the balance among the hydrological components as a function of time. Also, it need only use basic data which are typically available, to simulate lake levels and chemistry, and thus estimate groundwater inflow to and outflow from a lake.

## References

- Anderson, M.P. and J.A. Munter, 1981, Seasonal reversals of groundwater flow around lakes and the relevance to stagnation points and lake budgets, *Water Resour. Res.*, 17:1139-1150.
- Belanger, T.V. and D.F. Mikutel, 1985, On the use of seepage meters to estimate groundwater nutrient loading to lakes, *Water Resour. Bull.*, 21:265-272.
- Borneuf, D., 1973, Hydrogeology of the Tawatinaw area, Alberta, NTS 83I, Alberta Res. Counc. Rep. 72-11, Edmonton, Alberta.
- Brock, T.D., D.R. Lee, D. Janes and D. Winek, 1982, Groundwater seepage as a nutrient source to a drainage lake; Lake Mendota, Wisconsin, *Water Res.*, 16:1255-1263.
- Cherkauer, D.A. and J.M. McBride, 1988, A remotely operated seepage meter for use in large lakes and rivers, *Ground Water*, 26:165-171.
- Cherkauer, D.S. and D.C. Nader, 1989, Distribution of groundwater seepage to large surface-water bodies: the effect of hydraulic heterogeneities, *J. Hydrol.*, 109:151-165.
- Cole, J.J. and S.G. Fisher, 1979, Nutrient budgets of a temporary pond ecosystem, *Hydrobiol.*, 63:213-222.
- Cook, G.D., M.R. McComas, D.W. Waller and R.H. Kennedy, 1977, The occurrence of internal phosphorus loading in two small, eutrophic, glacial lakes in northeastern Ohio, *Hydrobiol.*, 56:129-136.
- Crawford, N.H. and R.K. Linsley, 1966, Digital simulation in hydrology: Stanford Watershed Model IV, Dept. Civ. Eng. Technol. Rep. 39, Stanford Univ., Stanford, Calif.
- Croley II, T.E., 1983, Great Lake basins (U.S.A.-Canada) runoff modeling, *J. Hydrol.*, 64:135-158.
- Crowe, A.S., 1978, Baptiste Lake groundwater investigation: preliminary report, Earth Sci. Div., Alberta Environ., Edmonton, Alberta.
- Crowe, A.S. and F.W. Schwartz, 1981a, Simulation of lake-watershed systems: 1. Description and sensitivity analysis of the model, *J. Hydrol.*, 52:71-105.
- Crowe, A.S. and F.W. Schwartz, 1981b, Simulation of lake-watershed systems: 2. Application to Baptiste Lake, Alberta, Canada, *J. Hydrol.*, 52:107-125.
- Crowe, A.S. and F.W. Schwartz, 1985, Application of a lake-watershed model for the determination of water balance, *J. Hydrol.*, 81:1-26.
- Dooce, J.C.I., 1960, The routing of groundwater recharge through typical elements of linear storage, *Int. Assoc. Sci. Hydrol. Gen. Assem.*, Helsinki, Int. Union Geod. Geophys., Publ. No. 52, pp. 286-300.
- Enell, M., 1982, The phosphorus economy of a hypertrophic seepage lake in Scania, south Sweden, *Hydrobiol.*, 86:153-158.
- Fritz, P. and H.R. Krouse, 1973, Wabamun Lake past and present, an isotopic study of the water budget, *in* Proc. Sympos. on the Lakes of Western Canada, ed. E.R. Reinelt, A.H. Laycock and W.M. Schultz, Univ. Alberta Water Resour. Cent. Publ. 2, Edmonton, Alberta, pp. 244-259.
- Gray, D.M., G.A. McKay and J.M. Wigham, 1970, Energy, evaporation and evapotranspiration, *In*: D.M. Gray, (editor-in-chief), *Handbook on the Principles of Hydrology*, Sect. III, Water Inform. Cent., Port Washington, N.Y.
- Jaquet, N.G., 1976, Ground-water and surface-water relationships in the glacial province of northern Wisconsin - Snake Lake, *Ground Water*, 14:194-199.

- Karnauskas, R.J. and M.P. Anderson, 1978, Ground-water lake relationships and ground-water quality in the sand plain province of Wisconsin - Nepco Lake, *Ground Water*, 16:273-281.
- Lee, D.R., 1976, The role of groundwater in eutrophication of a lake in glacial outwash terrain, *Int. J. Speleol.*, 8:117-126.
- Lee, D.R., J.A. Cherry and J.A. Pickens, 1980, Groundwater transport of a salt tracer through a sandy lakebed, *Limnol. Oceanogr.*, 25:45-61.
- Lee, D.R., 1980, Groundwater - solute influx, *Limnol. Oceanogr.*, 25:183-186.
- Lock, M.A. and P.H. John, 1978, The measurement of groundwater discharge into a lake by a direct method, *Int. Revue ges. Hydrobiol.*, 63:271-275.
- Loeb, S.L. and C.R. Goldman, 1979, Water and nutrient transport via groundwater from Ward Valley into Lake Tahoe, *Limnol. Oceanogr.*, 24:1146-1154.
- McBride, M.S. and H.O. Pfannkuch, 1975, The distribution of seepage within lakebeds, *J. Res. U.S.G.S.*, 3:505-512.
- Munter, J.A. and M.P. Anderson, 1981, The use of ground-water flow models for estimating lake seepage rates, *Ground Water*, 19:608-616.
- Nursall, J.R., J.B. Nuttall and P. Fritz, 1972, The effect of thermal effluent in Lake Wabamun, Alberta, *Verh. Internat. Verein. Limnol.*, 18:269-277.
- Pfannkuch, H.O. and T.C. Winter, 1984, Effect of anisotropy and groundwater system geometry on seepage through lakebeds; 1. Dimensional and analog analysis, *J. Hydrol.*, 75:213-237.
- Rhinaldo-Lee, M.B. and M.P. Anderson, 1980, High water levels in ground-water dominated lakes - a case study from northwestern Wisconsin, *Ground Water*, 18:334-339.
- Schwartz, F.W. and D.N. Gallup, 1978, Some factors controlling the major ion chemistry of small lakes: examples from the prairie parkland of Canada, *Hydrobiol.*, 58:65-81.
- Steenbergen, C.L.M. and H. Verdouw, 1982, Lake Vechten: aspects of its morphometry, climate, hydrology and physico-chemical characteristics, *Hydrobiol.*, 95:11-23.
- Trew, D.O., D.J. Beliveau and E.I. Yonge, 1980, The Baptiste Lake study technical report, *Water Qual. Control Branch, Pollut. Control Div.*, Alberta Environ., Edmonton, Alberta.
- Winter, T.C., 1978, Ground-water component of lake water and nutrient budgets, *Verh. Internat. Verein. Limnol.*, 20:438-444.
- Winter, T.C., 1978, Numerical simulation steady state three-dimensional groundwater flow near lakes, *Water Resour. Res.*, 14:245-254.
- Winter, T.C., 1981, Effects of water-table configuration on seepage through lakebeds, *Limnol. Oceanogr.*, 26:925-934.
- Winter, T.C. and H.O. Pfannkuch, 1984, Effect of anisotropy and groundwater system geometry on seepage through lakebeds: 2. Numerical simulation analysis, *J. Hydrol.*, 75:239-253.
- Winter, T.C., 1986, Effect of ground-water recharge on the configuration of the water table beneath sand dunes and on seepage in lakes in the Sandhills of Nebraska, U.S.A., *J. Hydrol.*, 86:221-237.

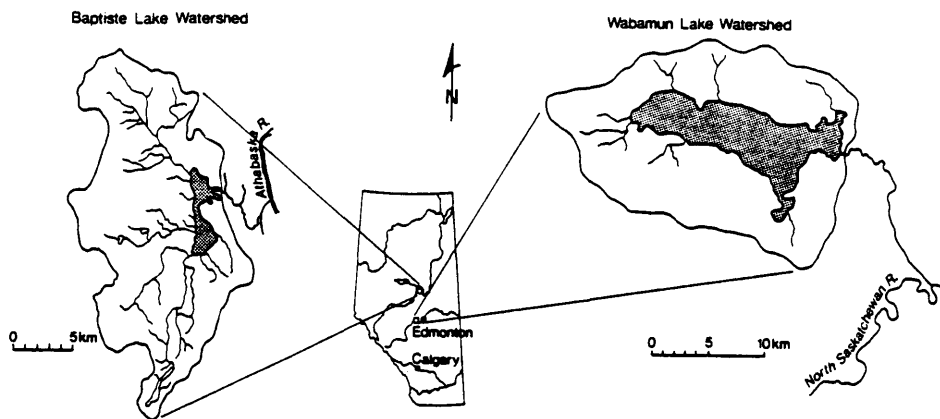


Figure 1 Location of the Wabamun Lake and Baptiste Lake watersheds.

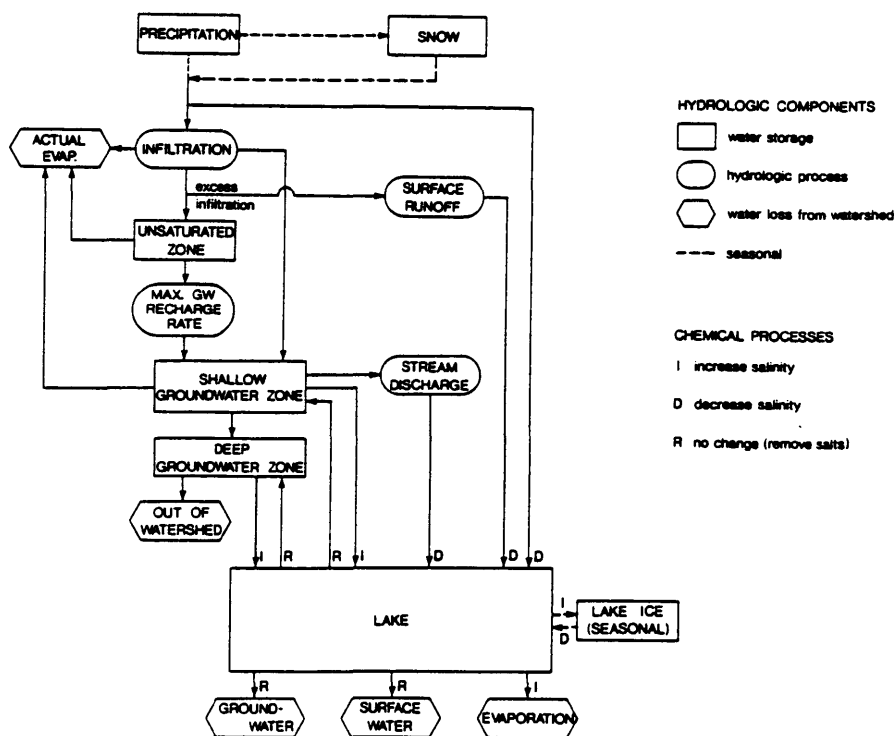


Figure 2 Schematic illustration of the components and processes in the lake-watershed model.

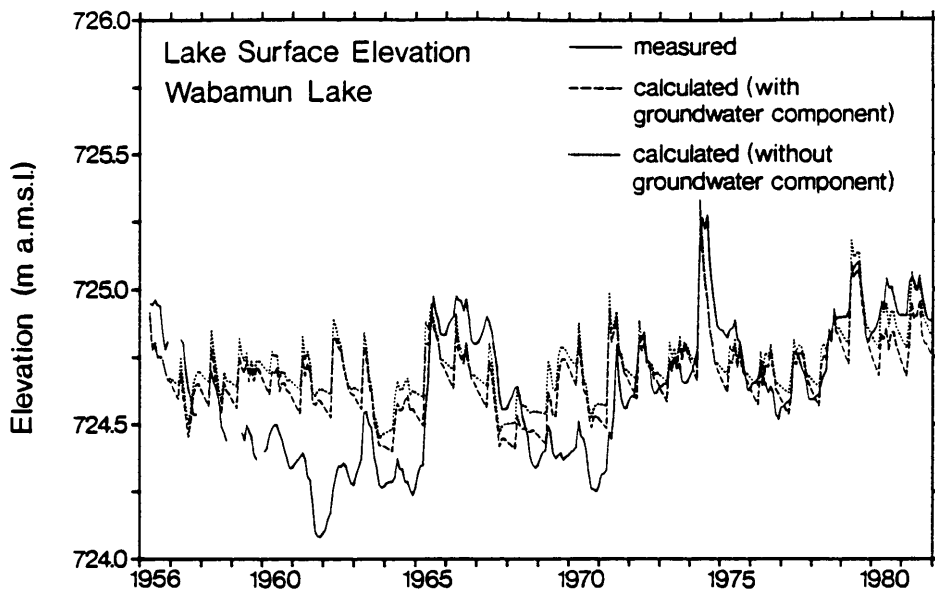


Figure 3 Simulation of the elevation of the surface of Wabamun Lake.

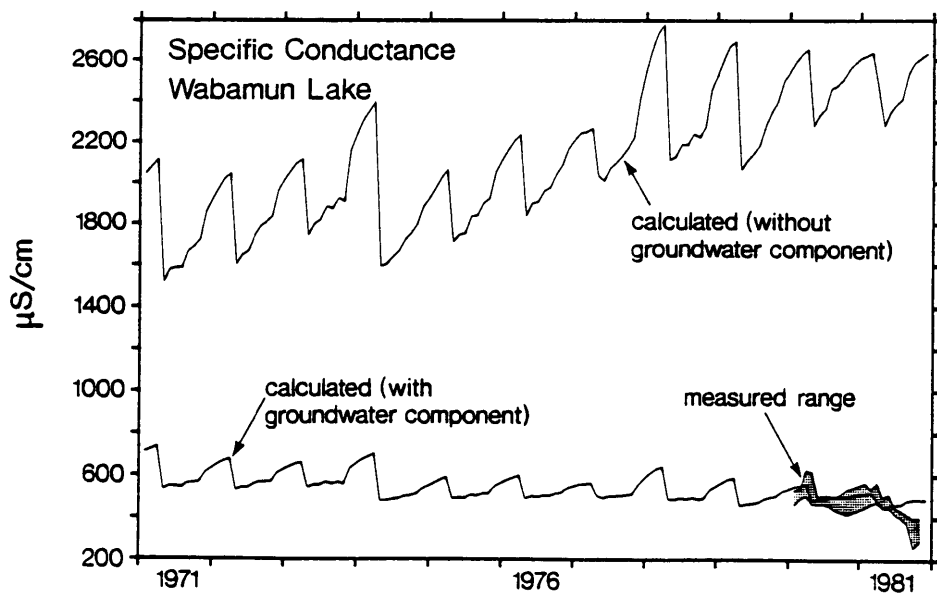


Figure 4 Simulation of the specific conductance of Wabamun Lake.

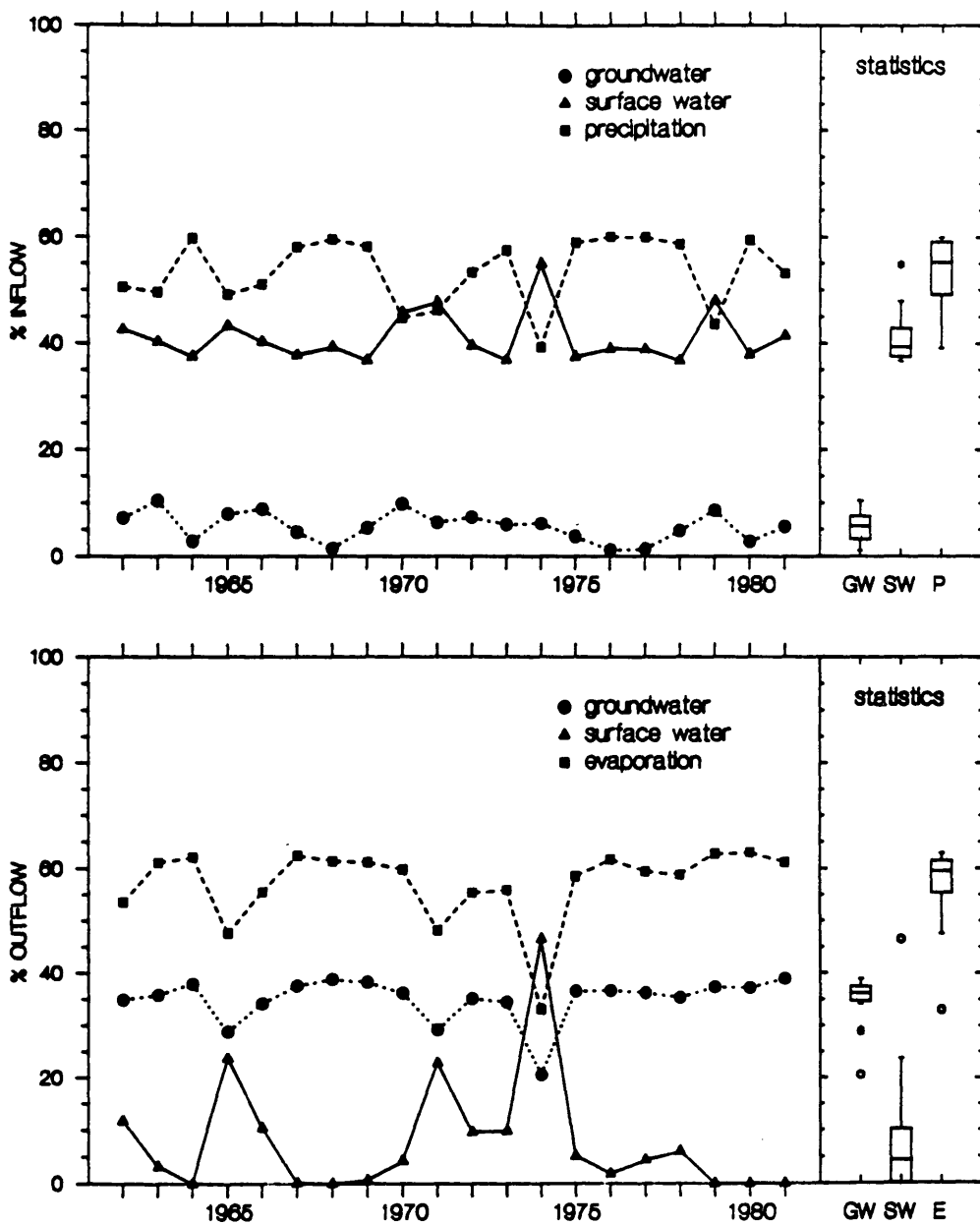


Figure 5. Inflow to and outflow from Wabamun Lake as annual and median percentages.

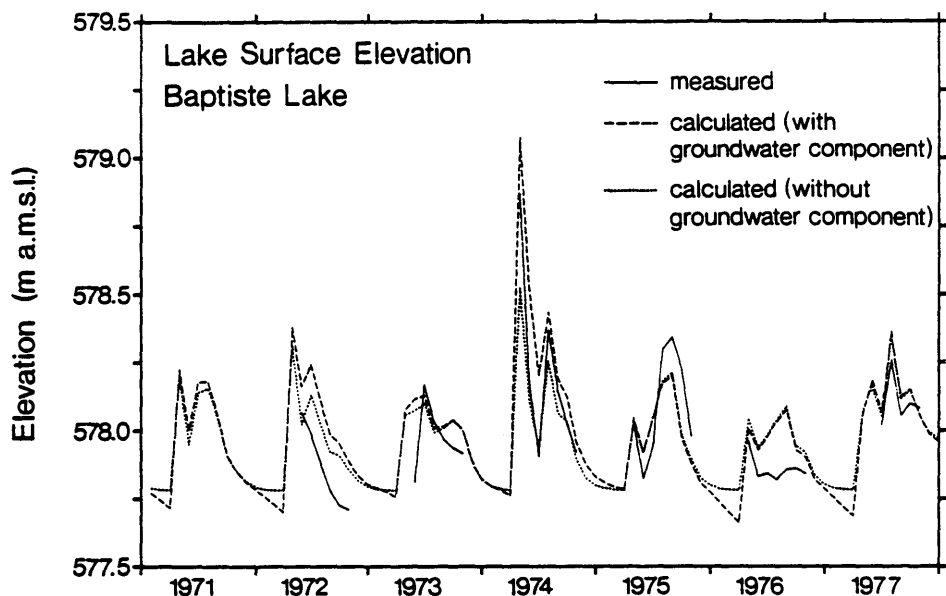


Figure 6 Simulation of the elevation of the surface of Baptiste Lake.

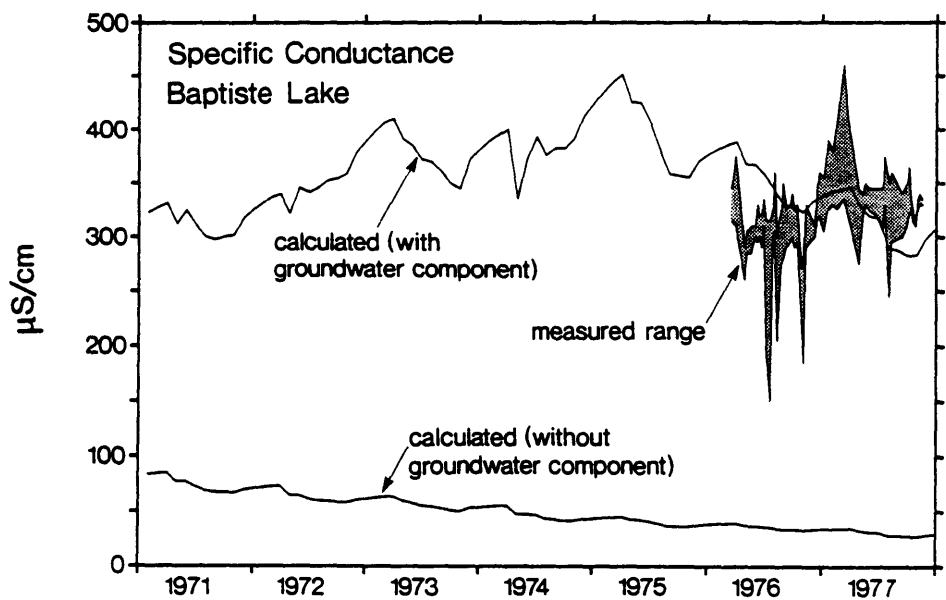


Figure 7 Simulation of the specific conductance of Baptiste Lake.



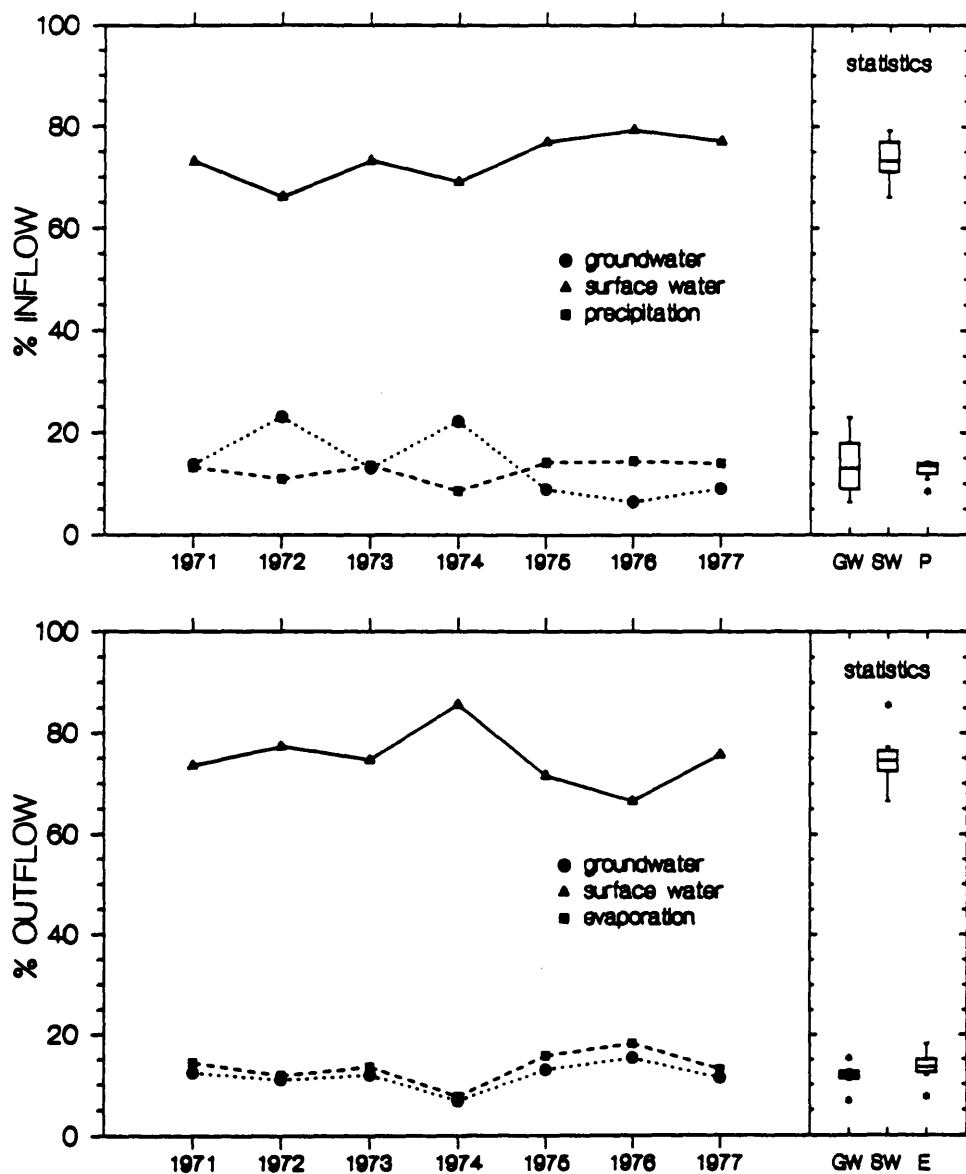


Figure 8. Inflow to and outflow from Baptiste Lake as annual and median percentages.



## GROUNDWATER INDICATOR PLANTS IN THE TERTIARY

### AQUIFERS OF CENTRAL SPAIN

F.G. Bernaldez, J.M. Rey Benayas, B. Peco, and C. Levassor

Departamento Interuniversitario de Ecología  
Universidad Complutense and Universidad Autonoma  
28049 Madrid

**ABSTRACT:** Groundwater flow to the soil surface is often associated with wetlands systems: wet meadows, sedge meadows, riverine forests, and water bodies. Certain plant species in these communities can be used as indicators of groundwater characteristics such as flow path length, piezometric levels, pH, electrical conductivity, and some major ions as shown by statistical relationships. Three main ecological groups can be distinguished: glycophytes, halophytes, and alcalinophytes, which correspond to different types of groundwater flow systems and different degrees of water dynamics in the aquifer.

### Introduction

In the Tertiary detrital aquifers of central Spain, groundwater produces different types of wetlands: riverine thickets, sedge meadows, and water bodies (Bernaldez et al., 1988a), the majority of which have been transformed by human activities. Jointly with their value as grazing areas, the main importance of these wetlands lies in their positive effect on biological diversity and landscape variety (Bernaldez et al., 1989a). This paper is part of a wider research project including aspects of landscape ecology (Gonzalez Bernaldez et al., 1987; Bernaldez et al., 1989a), toponymy and environmental perception (Gonzalez Bernaldez et al., 1989b), vegetation (Herrera, 1987; Herrera et al., 1987a,b; Bernaldez et al., 1988a; Bernaldez et al., 1988b), and resource management (Gonzalez Bernaldez, 1988; Rey Benayas, 1989).

### Study Area

The study is centered on two representative areas of the Spanish Central Plateau, located on both sides of the Central Ranges, covering an area of 85,000 km<sup>2</sup> each (Figure 1), consisting of detrital deposits, mainly miocene arkoses, although river terraces, aeolic sands, and pliocene outwash deposits cover smaller surfaces. The climate is semi-arid Mediterranean; the total precipitation and average August temperature are 453 mm and 22°C (data from Tordesillas in the northern part of the sampling area).

The study of the groundwater-vegetation relationships in the area is greatly facilitated by (a) the sharp contrasts between discharge wetlands and the surrounding land, and (b) the relatively homogeneous lithology of the detrital material forming the aquifer. Most of the observed relationships are thus transposable to similar areas in the world (Toth, 1966; Rey Benayas, 1989).

## Material and Methods

Vegetation sampling was carried out by means of 383 sampling plots, 10x10 m, located in 176 groundwater discharge habitats. The abundance-dominance values (Braun-Blanquet, 1950) of 250 perennial plant species were recorded. The sampling plots were distributed among the major representative discharge environments, each discharge type receiving the same number of plots regardless of their area (Godron, 1974). Due to the large numerical fluctuation of annual plants for climatic reasons (Peco et al., 1987) and the difficulty of identification during the unfavorable season, which impedes their use as indicators (Herrera et al., 1987a), only perennial species were considered.

Groundwater samples were collected from 550 wells and sources distributed across the study area. These samples were analyzed for pH, electrical conductivity, and major ions ( $\text{Na}^+$ ,  $\text{K}^+$ ,  $\text{Ca}^{++}$ ,  $\text{Mg}^{++}$ ,  $\text{SO}_4^{--}$ ,  $\text{Cl}^-$ ,  $\text{CO}_3^{--}$ , and  $\text{CO}_3\text{H}^-$ ). Water levels in wells were also recorded.

### Photointerpretation

Aerial panchromatic stereopairs 1:18000 were used to identify groundwater discharge areas and for their mapping at 1:50000 (Rey Benayas et al., 1989).

## Data Processing

Correspondence factor analysis (Benzecri, 1973), a multivariate nonparametric ordination method specially suited for semiquantitative data such as Braun-Blanquet's abundance scale, was applied to the vegetation data. The analysis allows the representation of both observations and variables on the same factor space defined by the correspondence axes (independent variation trends, Legendre and Legendre, 1979).

Shepard's algorithm (Shepard, 1968) consisting in a bidimensional point interpolation for irregularly-spaced data was used to attribute groundwater data to neighboring vegetation plots.

Corrected frequency profiles and mutual information (species-factor) parameters (Godron, 1968; Gounot, 1969) were used to test plant-groundwater relationships and plant sensitivity to the ranges of factor variation, thus facilitating the detection of indicator species. The criterion for determining the limits of factor class intervals was the maximum factor entropy obtainable, i.e., the homogeneous distribution of the sampling plots between factor classes (Rey Benayas, 1989).

## Results

### Plant Responses to Groundwater Variables

Tables 1 through 4 show the relationships between plant frequencies and groundwater piezometric levels, conductivity, pH, and  $\text{Na}^+$  as expressed by means of corrected frequency profiles and mutual information. These variables influence plant distribution more than the rest of groundwater characteristics. In this relatively flat, gently-sloping aquifer, piezometric level is correlated with

Table 1. Corrected frequency (x 100) profile for piezometric levels (m). Only species with mutual information  $\geq 0.1$  are included. Corrected frequencies  $\leq 1.2$  have been omitted.  $\pm$  means indifference for the corresponding factor class interval.

| Class Intervals                  |                 |
|----------------------------------|-----------------|
| 685-725-775-900-1100             |                 |
| <i>Aeluropus littoralis</i>      | 400             |
| <i>Artemisia coerulescens</i>    | 400             |
| <i>Suaeda vera</i>               | 400             |
| <i>Convolvulus lineatus</i>      | 240 144         |
| <i>Juncus maritimus</i>          | 240 129         |
| <i>Plantago maritima</i>         | 135 146 $\pm$   |
| <i>Puccinellia festuciformis</i> | $\pm$ 174 $\pm$ |
| <i>Trifolium repens</i>          | 161 195         |
| <i>Daucus carota</i>             | 146 195         |
| <i>Galium verum</i>              | 131 220         |
| <i>Convolvulus arvensis</i>      | 136 223         |
| <i>Alopecurus arundinaceus</i>   | 140 234         |
| <i>Agrostis castellana</i>       | 136 237         |
| <i>Lolium perenne</i>            | 133 244         |
| <i>Carex divisa</i>              | $\pm$ $\pm$ 137 |
| <i>Plantago lanceolata</i>       | 208             |
| <i>Trifolium fragiferum</i>      | $\pm$ 209       |
| <i>Hypochaeris radicata</i>      | $\pm$ 212       |
| <i>Eryngium campestre</i>        | $\pm$ 222       |
| <i>Poa pratensis</i>             | $\pm$ 226       |
| <i>Hieracium pilosella</i>       | $\pm$ 240       |
| <i>Senecio jacobea</i>           | $\pm$ 260       |
| <i>Cynosurus cristatus</i>       | $\pm$ 273       |
| <i>Poa trivialis</i>             | $\pm$ 293       |
| <i>Juncus inflexus</i>           | $\pm$ 304       |
| <i>Trifolium pratense</i>        | $\pm$ 304       |
| <i>Potentilla reptans</i>        | 312             |

Tables 2 and 3. Corrected frequency (x 100) profile for electrical conductivity,  $\mu\text{S}/\text{cm}$ , (Table 2) and pH (Table 3) of groundwater. Only species with mutual information  $\geq 0.1$  are included. Corrected frequencies  $\leq 1.2$  have been omitted.  $\pm$  means indifference for the corresponding factor class interval.

|                                  | 216-500-628-850-1750-6620 |       |       |           |
|----------------------------------|---------------------------|-------|-------|-----------|
| <i>Festuca ampla</i>             | 500                       |       |       |           |
| <i>Convolvulus arvensis</i>      | 279                       | $\pm$ |       |           |
| <i>Eryngium campestre</i>        | 243                       | $\pm$ | $\pm$ |           |
| <i>Agrostis castellana</i>       | 250                       | 142   |       |           |
| <i>Alopecurus arundinaceus</i>   | 183                       | 183   | $\pm$ |           |
| <i>Lolium perenne</i>            | 175                       | 187   |       |           |
| <i>Cynosurus cristatus</i>       | 161                       | 225   |       | $\pm$     |
| <i>Juncus inflexus</i>           | 141                       | 179   | $\pm$ | $\pm$     |
| <i>Galium verum</i>              | 212                       |       | 133   |           |
| <i>Scirpus holoschoenus</i>      | 188                       |       | 151   | $\pm$     |
| <i>Holcus lanatus</i>            | 212                       | $\pm$ |       | 121       |
| <i>Carex divisa</i>              | $\pm$                     | 131   | $\pm$ | $\pm$     |
| <i>Festuca arundinacea fenas</i> | $\pm$                     | 138   | $\pm$ | 158       |
| <i>Cynodon dactylon</i>          | $\pm$                     | $\pm$ | $\pm$ | 121       |
| <i>Juncus maritimus</i>          |                           | $\pm$ |       | $\pm$ 249 |
| <i>Convolvulus lineatus</i>      |                           |       |       | 292       |
| <i>Koeleria vallesiana</i>       |                           |       |       | 421       |
| <i>Aeluropus littoralis</i>      |                           |       |       | 515       |
| <i>Artemisa coerulescens</i>     |                           |       |       | 515       |
| <i>Suaeda vera</i>               |                           |       |       | 515       |

|                                  | 6.5-7.0-7.4-7.6-8.1-9.2 |       |       |           |
|----------------------------------|-------------------------|-------|-------|-----------|
| <i>Trifolium pratense</i>        | 645                     | $\pm$ | $\pm$ |           |
| <i>Festuca ampla</i>             | 1312                    | 125   |       |           |
| <i>Senecio jacobea</i>           | 583                     | 166   | $\pm$ |           |
| <i>Poa trivialis</i>             | 490                     | 180   | 185   |           |
| <i>Agrostis castellana</i>       | 375                     | 143   | 165   |           |
| <i>Alopecurus arundinaceus</i>   | 350                     | 167   | 172   |           |
| <i>Cynosurus cristatus</i>       | 339                     | 226   | 133   |           |
| <i>Juncus inflexus</i>           | 314                     | 154   | 224   |           |
| <i>Convolvulus arvensis</i>      | 309                     | 132   | 166   |           |
| <i>Lolium perenne</i>            | 306                     | 187   | 129   |           |
| <i>Daucus carota</i>             | 250                     | 214   | 122   |           |
| <i>Potentilla reptans</i>        | 700                     |       | 137   |           |
| <i>Mentha suaveolens</i>         | 477                     |       | 327   |           |
| <i>Cyperus longus</i>            | 437                     |       | 386   |           |
| <i>Plantago lanceolata</i>       | 266                     |       | 190   | $\pm$     |
| <i>Suaeda vera</i>               |                         |       |       | 251       |
| <i>Artemisia coerulescens</i>    |                         |       |       | 272       |
| <i>Juncus maritimus</i>          |                         |       |       | 154 165   |
| <i>Plantago maritima</i>         |                         |       |       | $\pm$ 170 |
| <i>Puccinellia festuciformis</i> |                         |       |       | $\pm$ 205 |

Table 4. Corrected frequency (x 100) profile for groundwater Na<sup>+</sup> (meg/l). Only species with mutual information 0.1 are included. Corrected frequencies  $\leq 1.2$  have been omitted.  $\pm$  means indifference for the corresponding factor class interval.

|                               | Class intervals |           |            |     |
|-------------------------------|-----------------|-----------|------------|-----|
|                               | .35-1.60        | 3.50-6.05 | 6.05-51.14 |     |
| <i>Festuca ampla</i>          | 398             |           |            |     |
| <i>Agrostis castellana</i>    | 227             | $\pm$     |            |     |
| <i>Juncus inflexus</i>        | 163             | 120       | $\pm$      |     |
| <i>Galium verum</i>           | 157             | 153       | $\pm$      |     |
| <i>Scirpus holoschoenus</i>   | 150             | 140       | $\pm$      |     |
| <i>Carex divisa</i>           | $\pm$           | 132       | $\pm$      |     |
| <i>Juncus maritimus</i>       |                 |           | $\pm$      | 236 |
| <i>Aeluropus littoralis</i>   |                 |           |            | 407 |
| <i>Artemisia coerulescens</i> |                 |           |            | 407 |
| <i>Suaeda vera</i>            |                 |           |            | 407 |

groundwater residence time in the aquifer and with flow-path length (Bernaldez et al., 1989b).

## Vegetation Ordination

Figure 2 represents the distribution of the most characteristic species on the plane defined by correspondence axes I and II. The first axis can be considered as a halophytism gradient opposing the most glycophytic species, growing on the less mineralized discharges (*Festuca ampla*, *Agrostis castellana*, *Potentilla reptans*, among others) to the most halophytic (*Limonium costae*, *Juncus subulatus*, *Suaeda vera*, etc.). Species corresponding to stages of intermediate mineralization, representing intermediate groundwater evolution phases, are displayed in the middle. These intermediate species consist of alcalinophytes (*Juncus acutus*, *Festuca arundinacea* subsp. *fenas*, and others) and tolerants (*Cynodon dactylon* and others). Axis II displays on the left the non-phreatophytic species (psammophilous plants growing on the margins of quaternary aeolian deposits and calcicolous species occurring on the elevated parts of the wetland micro-relief) unaffected by groundwater (Bernaldez et al., 1989a). Xerohalophytes (Bernaldez et al., 1989a) cluster together also. These species correspond to areas with salt accumulation in the topsoil originated by migration from relatively deep, slightly mineralized groundwater.

## Halophytism and Groundwater Evolution

Correspondence axis I, considered as a vegetation halophytism gradient, is closely correlated with variables indicating chemical evolution of groundwater along flow paths in the aquifer. Correlations with the estimated maximum length of flow path, electrical conductivity, and sodium content were  $r = 0.845$ ,  $r = 0.778$ , and  $r = 0.808$ , respectively ( $p \leq 0.01$ ). Figure 3 shows the regression of the vegetation halophytism gradient, represented by a correspondence axis on maximum possible flow length. The latter was estimated as the distance from the upper aquifer limit (the basement outcrop) to every vegetation sampling plot, measured perpendicularly to the piezometric lines. Vertical curvature was ignored. Although other factors may contribute to groundwater evolution (resulting in sodium and conductivity increase), the relatively homogeneous lithology and fairly flat topography of this gently-sloping aquifer account for the clear relationships observed (Toth, 1963; Freeze and Cherry, 1979).

Therefore, glycophytes are distributed in enclaves within recharge areas with high piezometric levels, characterized by relatively dissected landscapes dominated by local groundwater flow systems. Alcalinophytes and xerohalophytes are typical of areas dominated by subregional discharges with intermediate flow systems. Lowest piezometric levels corresponding to regional discharges and to the longest flow paths of regional flow systems are characterized by halophytes.

## Concluding Remarks

The most important conclusion is that groundwater chemical changes along the flow paths from recharge to discharge areas is the main factor controlling vegetation variation in the studied wetlands. This evolution results in an increase of electrical conductivity and in the steady replacement of bivalent cations by sodium.



Plant adaptation types correspond to groundwater chemical characteristics. Strict glycophytes (conductivity up to 628  $\mu\text{S}/\text{cm}$ ,  $\text{pH} \leq 7.5$ ,  $\text{Na}^+ \leq 3.5 \text{ meq/l}$ ) such as *Juncus effusus* and *Agrostis castellana* are related to local groundwater flow systems. Alcalinophytes (conductivity up to 1750  $\mu\text{S}/\text{cm}$ ,  $\text{pH} \leq 8$ ) such as *Juncus acutus*, *J. gerardi*, etc., and xerohalophytes: *Plantago maritima* and *Camphorosma monspelliaca* characterize subregional discharges. The lowest piezometric levels (conductivity 1750  $\mu\text{S}/\text{cm}$  and  $\text{Na}^+$  up to 51.4 meq/l) support halophytic communities with *Juncus maritimus* and *Suaeda vera*, typical of regional discharges and long flow paths.

#### Acknowledgments

This research has been supported by Grant PB 85-0229-C02 from CAICYT.

## LIST OF REFERENCES

- Alcazar, A., A. Martinez, J.M. Rey Benayas, J.P. Ruiz (in press), Toponimia y lexico relacionado con las descargas de aguas subterraneas en la cuenca del Duero, Estudios Geograficos.
- Benzecri, J.P., et al., 1973, L'analyse des donnees, 2 V., Dunod, Paris, 615-619.
- Bernaldez, F.G., C. Montes, P. Herrera, A.G. Besteiro, y A. Sastre, 1988a, Genetical typology of the Madrid aquifer wetlands, Int. Symp. on Hydrology of Wetlands in Semiarid and Arid Regions, C.S.I.C. and The Spanish Chapter of IAH, Seville (Spain), May 1988, 173-176.
- Bernaldez, F.G., P. Herrera, C. Levassor, B. Peco, y J.M. Rey Benayas, 1988b, Groundwater indicator plants in the Madrid Aquifer, Int. Symp. on Hydrology of Wetlands in Semiarid and Arid Regions, C.S.I.C. and The Spanish Chapter of IAH, Seville (Spain), May 1988, 37-39.
- Bernaldez, F.G., J.M. Rey Benayas, C. Levassor, and B. Peco, 1989a, Landscape ecology of uncultivated lowlands in Central Spain, *Landscape Ecology*, 3, 3-18.
- Bernaldez, F.G., A. Martinez, J.P. Ruiz, and J.R. Rey Benayas, 1989b, Understanding people's perception of wetlands, Inc. The people's role in wetland management, The Center for Environmental Studies, Leicester University, Leiden (The Netherlands), June.
- Bernaldez, F.G., J.M. Rey Benayas, C. Levassor, and B. Peco, 1989c, Plants as indicators of groundwater chemical quality in Central Spain, 28<sup>th</sup> Int. Geological Congress, I.U.G.S., Washington (USA), July.
- Braun-Blanquet, J., 1950, Fitosociologia, Ed. Blume, Madrid, Spain.
- Freeze, R.A., and J.A. Cherry, 1979, Groundwater, Prentice-Hall, Inc., Englewood Cliffs, New Jersey.
- Godron, M., 1968, Quelques applications de la notion de frequence en ecologie vegetale, *Oecol. Plant.*, 3, 185-212.
- Godron, M., 1974, Les achantillonnages phytoecologiques, Recueil de Methodes phytoecologiques, 2, 18 p., C.N.R.S. C.E.P.E.
- Gonzalez-Bernaldez, F., P. Herrera-Moreno, A. Sastre-Merlin, J.M. Rey Benayas, y R. Vicente Lapuente, 1987, Comparacion preliminar de los ecosistemas de descarga de aguas subterraneas de las cuencas del Duero y Tajo, IV Simposio Nacional de Hidrogeologia, Asociacion Espanola de Hidrologia subterranea, Palma de Mallorca, Octubre 1987, Hidrogeologia y Recursos Hidraulicos, XI: 89-103.
- Gonzalez-Bernaldez, F., 1988, Typology of wetlands and evaluation of the resources they represent. Int. Symp. on Hydrology of Wetlands in Semiarid and Arid Regions, C.S.I.C. and The Spanish Chapter of IAH, Seville (Spain), May, 7-36.
- Gonzalez-Bernaldez, F., J.M. Rey Benayas, y J.P. Ruiz, 1988, Terminologia vernacula y percepcion ambiental de los humedales (wetlands), Homenaje a Pedro Montserrat: 579-582, Jaca y Huesca.

- Gounot, M., 1969, Methodos d'etude quantitative de la vegetation, 303 p., Masson, Paris.
- Herrera, P., 1987, Aspectos ecologicos de las aguas subterraneas en la facies arcossica de la cuenca de Madrid, Tesis doctoral, Univ. de Alcala de Henares.
- Herrera, P., F.G. Bernaldez, C. Levassor, y B. Peco, 1987a, Plantas indicadoras de características químicas del acuífero de Madrid: aguas subterráneas, IV Simposio Nacional de Hidrogeología, Asociación Española de Hidrología Subterránea, Palma de Mallorca, Octubre, 1987, Hidrogeología y Recursos Hidráulicos, XI: 65-87.
- Herrera, P., F.G. Bernaldez, C. Levassor, y J.M. Rey Benayas, 1989b, Plantas indicadoras de características químicas del acuífero de Madrid: suelos de zonas de descarga, IV Simposio Nacional de Hidrogeología, Palma de Mallorca, Asociación Española de Hidrología Subterránea, Octubre 1987, Hidrogeología y Recursos Hidráulicos, XI: 89-103.
- Legendre, L. et P. Legendre, 1979, Ecologie numerique, 2 vols. Masson, Paris.
- Peco, B., C. Olmeda, M.A. Casado, C. Levassor et F.D. Pineda, 1988, Differentiation entre les effets des oscillations meteorologiques et le processus successional dans un paturage mediterraneen, Time Scales and Water Stress, Proc. 5<sup>th</sup> Int. Conf. on Mediterranean Ecosystems, di Castri et al. (eds.), I.U.B.S., Paris.
- Rey Benayas, J.M., 1989, Ecosistemas de descarga de acuíferos en la cuenca del Duero, Tesis doctoral, Univ. Autonoma de Madrid, Spain.
- Rey Benayas, J.M., C. Perez Perez, F. Gonzalez-Bernaldez, y M.R. Zabalet Franco (in press), Tipología y cartografía por fotointerpretación de los humedales de las cuencas del Duero y Tajo, Mediterranea.
- Shepard, D.S., 1968, A two-dimensional interpolation function for irregularly spaced data. Proceedings 23 Long. Assoc. Comput. Mach., 517-523.
- Toth, J., 1963, A theoretical analysis of groundwater flow in small drainage basins. *Journal of Geophysical Research*, 68:4795-4812.
- Toth, J., 1966, Mapping and interpretation of field phenomena for groundwater reconnaissance in a prairie environment, Alberta (Canada), *Bull. Int. Assoc. Sci. Hydrol.*, 9:20-68.



Figure 1. Location of the study area.

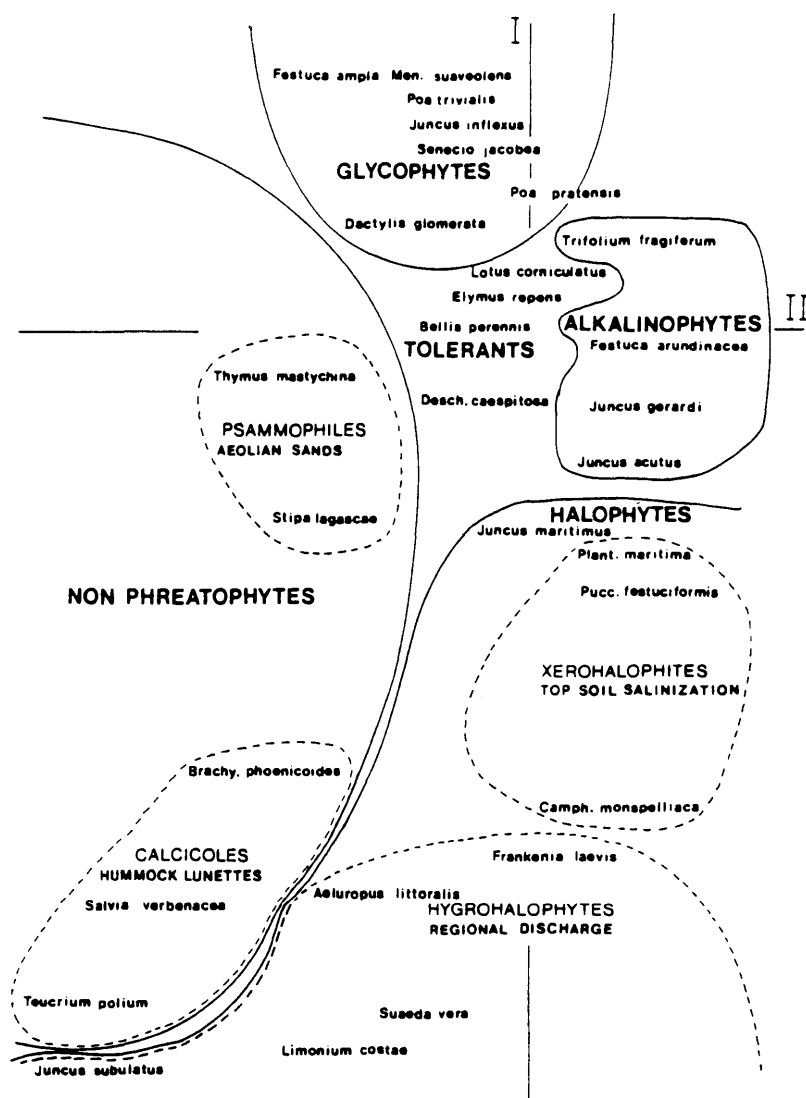


Figure 2. Correspondence analysis of discharge habitat vegetation. The first axis ordiates vegetation samples along a halophytism gradient, while the second separates the false phreatophytes (psammophilous and calciolous species growing in the most elevated parts of wetland microrelief). Only some of the most characteristic species are included.

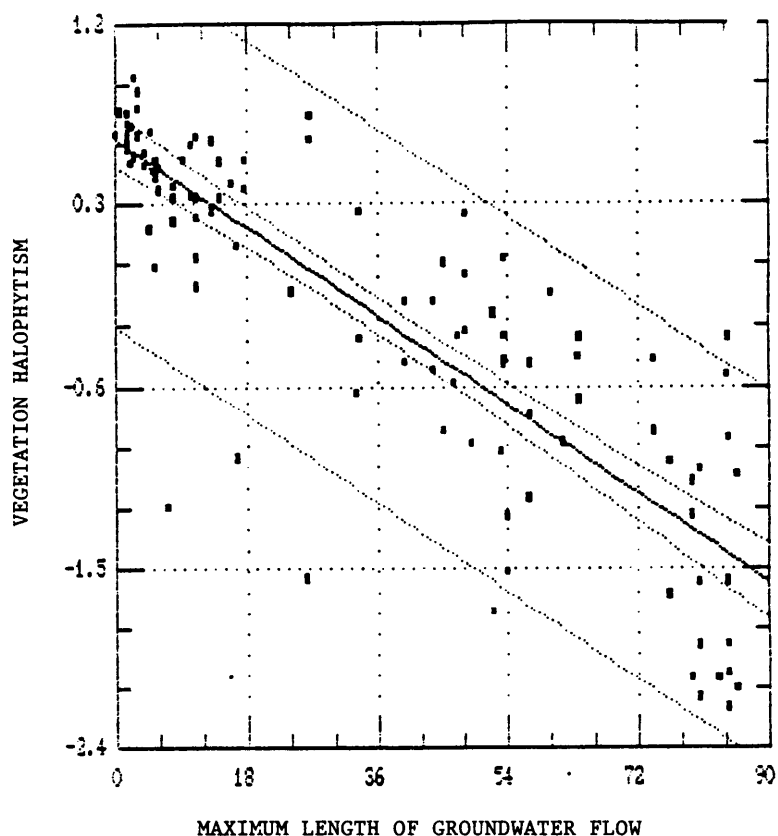


Figure 3. Relationships between maximum possible length of groundwater flow and vegetation halophytism gradient (coordinates on the 1st correspondence axis of vegetation analysis). Maximum length of groundwater flow path was estimated as the distance between the upper limit of the aquifer and every vegetation sampling plot, measured perpendicularly to piezometric lines ( $r = -0.845$ ,  $p \leq 0.01$ ).

SECTION 5: FRACTURED ROCK





## MORPHOLOGICAL ANALYSIS OF A NATURAL FRACTURE

Sylvie Gentier

BUREAU DE RECHERCHES GEOLOGIQUES ET MINIERES  
BP 6009, 45060 ORLEANS CEDEX 2 - FRANCE

**Abstract :** Understanding and modeling the hydromechanical behavior of a natural single fracture require the knowledge of its morphology under various kinds of stress. In this paper we expose methods to characterize and to quantify the morphology of a fracture and the results concerning a tension fracture in a granite. The morphology of each side of the fracture is investigated by studying profiles. Statistical, geostatistical and spectral methods are used to quantify some geometrical characteristics : height, curvature, angularity. Then the morphology of the fracture voids is investigated by casting. Image analysis is used to study the cast of the voids and we present some examples of treatments.

### Introduction

The hydromechanical behavior of a single natural fracture in any kind of rock under normal stress or shear stress depends on the morphology of the fracture. Channeling of the flow is an illustration of the role of the morphology.

Morphology of a fracture is a complex concept. We define a fracture as two sides plus the voids which remain between the two sides after matching. Consequently, the "morphology" of the voids is the resultant of the "morphology" of each side of the fracture and of the degree of match of the two sides. The "morphology" of the sides of the fracture is a function of the type rock (petrography, texture), of the nature of the fracture (tension, shear...) and of the history of the fracture. The degree of match of the two sides is a function of the stress field applied on the fracture. To attempt to define the morphology of a fracture, several studies are performed on cylindrical samples with a diameter of 12 cm and all cored perpendicular to the mean plane of the same natural tension fracture in a granite. Each sample contains a part of the fracture at middle height. The material is a slightly porphyroid medium grain granite. The path of the fracture in the rock is successively intergranular (using grain joints as guide) and intragranular (using clivages as guide). We have shown (Gentier, 1986) that the path of the fracture is not independant of the texture of the rock. The study of the hydromechanical behavior of this fracture is presented in Gentier (1990).

### Morphology of each side of the fracture

The studying of the morphology of each side of the fracture is based on profiles. On each side of the fracture, profiles are recorded with a "rugosimeter". With this method we obtain 2D data called profiles. A profile is defined as a function  $Z(x_1)$ . It represents the height of the surface relative to the mean plane of the fracture, sampled at points  $x_1$  regularly spaced by

$\Delta x$  along the course of the stylus of the rugosimeter. This method was used previously by Rengers (1970), Dight and Chiu (1981), Bandis et al (1983) Zongqi (1983) and Barton et al (1985). It is well adapted to study the morphology of each side of a fracture. A global quantitative analysis of the morphology of the fracture is extremely difficult.

The first way to characterize the morphology of each side of a fracture is to compute roughness parameters. In rock mechanics, Nuri and Halling (1975), Swan (1981) and Zongqi (1983) use the following parameters :

$$\text{CLA} = \frac{1}{N} \sum_{i=1}^N |Z(x_i)| ; \text{MSV} = \frac{1}{N} \sum_{i=1}^N Z(x_i)^2 \quad \text{or} \quad \text{RMS} = \text{MSV}^{1/2} \quad (1)$$

where  $N$  is the number of values  $Z(x_i)$  of height sampled at regular steps  $\Delta x$  along the profile. These two parameters were used previously by Myers (1962) in the field of metallurgy associated to others parameters including :

$$Z_2 = \left[ \frac{1}{N(\Delta x)^2} \sum_{i=1}^N (Z(x_{i+1}) - Z(x_i))^2 \right]^{1/2} \quad (2)$$

In metallurgy, an other parameter is used frequently : the linear roughness defined by Chermant and Coster (1978) :

$$R_L = \frac{L_e}{L} \quad (3)$$

where  $L_e$  is the ratio of the length of the profile to the length of the reference line. This parameter leads to an areal roughness parameter  $R_A$  which is a 3D parameter. It represents the ratio of the area of the surface to the area of its projection onto the mean plane. Various relationships between  $R_L$  and  $R_A$  are exposed among others in Chermant and Coster (1978), El Soudani (1978), Gentier and Riss (1987). Some results are presented in Table I.

Table I : Roughness parameters and distribution of heights ( $\bar{h}$  : mean height ;  $\sigma$  : standard deviation ;  $a_3$  : skewness coefficient ;  $a_4$  : kurtosis coefficient).

| N° sample | CLA   | RMS   | $R_L$ | $Z_2$ | $\bar{h}(\text{mm})$ | $\sigma(\text{mm})$ | $a_3$  | $a_4$ |
|-----------|-------|-------|-------|-------|----------------------|---------------------|--------|-------|
| 1         | 2.228 | 2.505 | 1.028 | 0.242 | 4.430                | 2.505               | -0.176 | 1.686 |
| 2         | 1.526 | 1.998 | 1.026 | 0.234 | 7.362                | 1.998               | -1.150 | 4.307 |
| 3         | 1.440 | 1.772 | 1.029 | 0.254 | 3.762                | 1.772               | -0.381 | 2.215 |
| 4         | 1.929 | 2.336 | 1.029 | 0.249 | 6.011                | 2.336               | -0.118 | 2.269 |
| 5         | 2.505 | 2.947 | 1.028 | 0.242 | 5.260                | 2.947               | 0.067  | 1.947 |
| 6         | 1.700 | 2.056 | 1.027 | 0.236 | 5.738                | 2.056               | -0.466 | 2.544 |
| 7         | 0.906 | 1.125 | 1.026 | 0.232 | 2.256                | 1.125               | 0.561  | 2.664 |

All these parameters require the definition of a reference line. We choose the trace of the mean plane of the fracture in the profile plane. The

influence of the choice of the reference line is discussed in Gentier (1986). The two parameters CLA and RMS are more sensible to this choice than the parameters  $R_L$  and  $Z_2$ . Other parameters are proposed by El Soudani (1978), Tse and Cruden (1979), Serra (1982), Brock (1983), and Barton et al (1985) in various fields.

Roughness parameters are easy to calculate but the information they contain is too global and it is difficult to know exactly what is the best characteristic roughness parameter regarding hydraulic or mechanical properties of the fracture. They can be used to classify rock joints.

To improve the knowledge of the morphology some specific geometric characteristics are studied.

One of these characteristics is the topography of the fracture surface. It can be studied by various methods : statistical, geostatistical and spectral analysis of height distributions. The distribution of the heights relative to the mean plane of the fracture is slightly bimodal (figure 1a). Statistical summaries are presented in Table I. The mean height is bigger than the mean size of the grain of the granite (0.500 mm). The morphology of the fracture is not governed directly by the size of the grains.

This statistical analysis is not sufficient, we need to know the spatial correlation between the points which constitute the surface. These spatial informations are obtained by geostatistics. This technique is based on the variogram which is defined by :

$$\gamma(h) = \frac{1}{2N(h)} \sum_{i=1}^{N(h)} (Z(x_i+h) - Z(x_i))^2 \quad (4)$$

where  $Z(x_i)$  are the heights along the profile sampled at the points  $x_i$  and  $x_i+h$  and  $N(h)$  is the number of couples of points a distance  $h$  apart. It is characterized by its behavior at the origin and at infinity. The range is the distance beyond which there is no longer correlation between two sampled points. The sill corresponds to the variance of the phenomenon. An example is presented on figure 2b.

If the profile presents a trend we use the generalized variogram which is defined by :

$$\Gamma_k(h) = \frac{1}{M_k} \text{Var} \left[ \sum_{q=0}^{k+1} (-1)^q C_{k+1-q} Z(x_i + (k+1-q)h) \right] \text{ with } M_k = \frac{k+1}{2k+2} \quad (5)$$

A generalized variogram of order  $k$  filters trends of  $k^{\text{th}}$  order. For  $k$  equal to zero we have the variogram defined at the equation (4). For  $k$  equal 1 we filter a linear trend. An example is presented on figure 2c.

The result of the geostatistical analysis of the profiles on all the samples is presented on figure 2d. Each side of the fracture can be described by two nested families of structures. Their ranges are respectively 4 to 6 mm and 18 to 20 mm. These two families of structures are superimposed to a third family of structures which cannot be sampled at the size of the sample. This third family is responsible for the trend we observe on some profiles.

Then the experimental variograms defined above are fitted by a combination of theoretical models of variograms (cubic, spherical, exponential, gaussian). The reconstruction of the topography of each side of

the fracture is possible by kriging, which is an interpolation function based on the theoretical variograms. Figure 3 shows such a reconstruction.

The informations we obtain by the geostatistical analysis are linked to the informations we can obtain by others methods like autocovariance function and spectral analysis.

The autocovariance function defined by :

$$\gamma_{xx}(h) = \frac{1}{N(h)} \sum_{i=1}^{N(h)} (Z(x_i) - \overline{Z(x)}) (Z(x_i+h) - \overline{Z(x)}) \quad (6)$$

gives the same information that the variogram but it is only defined for stationary phenomenon. Its use is more limited. The autocorrelation function is the autocovariance function normalized to the variance (figure 4).

The spectral analysis is frequently applied (Brock, 1973, Passoja and Amberski, 1978). Each profile is decomposed in a set of frequencies. The amplitude of each frequency is directly linked to the "participation" of this frequency in the general function. Figure 5 shows a spectral function which is defined by

$$I(f) = |\hat{Z}(f)|^2 = \int_{-\infty}^{+\infty} Z(x) e^{-i2\pi f x} dx \quad (7)$$

$\hat{Z}(f)$  is the Fourier transform of the function  $Z(x)$ .

The autocorrelation function can also be derived from the spectral analysis as the following convolution product :

$$Z(x) \otimes \overline{Z(-x)} \quad (\overline{Z(-x)} \text{ is the conjugate of } Z(-x)) \quad (8)$$

All these methods are redundant if the phenomenon is stationnary. If it is not, corrections or filters must be used. Using the generalized variogram presents the advantage that trends (linear, second order,...) can be removed without knowing their coefficients. In the case of the autocorrelation function the trend must be removed before any analysis. The knowledge of the coefficients of the trend is essential. Using spectral analysis is more complex on numerical data and requires the use of special algorithms like FFT (Fast Fourier Transforms) and various kinds of filters.

To complete the study of each side of the fracture we consider the following geometrical characteristics : curvature and angularity.

The radius of curvature is defined as the radius of the circle which fits best the profile in the neighbor of given points. It is calculated at only some points called : peaks and valleys. They are the points along the profile where the sign of the slope changes. The results are presented in the table II and on figure 1c.

For this granite the mean radius of curvature is between 4 and 7 mm. The distributions are disymmetrical and have a strong concentration around the mean value. Simultaneously, a study of the height of the peaks and valleys are realized (figure 1b). It shows that there is no correlation between the height of peaks or valleys and the radius of curvature.

Table II : radius of curvature and angularity ( $\bar{\rho}$  : mean radius of curvature ;  $\bar{\alpha}$  : mean inclination ;  $\sigma$  : standard deviation ;  $a_3$  : skewness coefficient ;  $a_4$  : kurtosis coefficient)

| N° sample | $\bar{\rho}$ (mm) | $\sigma$ (mm) | $a_3$ | $a_4$  | $\bar{\alpha}(^\circ)$ | $\sigma(^\circ)$ | $a_3$ | $a_4$ |
|-----------|-------------------|---------------|-------|--------|------------------------|------------------|-------|-------|
| 1         | 4.332             | 6.162         | 7.834 | 79.769 | -1.27                  | 6.31             | -1.63 | 2.89  |
| 2         | 6.947             | 23.581        | 9.115 | 90.345 | 3.20                   | 5.94             | -2.16 | 3.00  |
| 3         | 5.016             | 3.905         | 1.769 | 5.772  | 1.52                   | 6.02             | -1.78 | 1.31  |
| 4         | 5.685             | 7.812         | 4.692 | 29.398 | -0.94                  | 6.50             | 0.30  | 2.30  |
| 5         | 4.618             | 5.622         | 6.911 | 61.690 | 4.37                   | 6.02             | -0.55 | 0.62  |
| 6         | 3.725             | 4.705         | 8.404 | 86.470 | -1.79                  | 6.34             | -0.17 | 0.46  |
| 7         | 4.993             | 6.142         | 4.604 | 29.049 | -0.93                  | 6.28             | -0.87 | 0.55  |

The last point we study is the angular analysis. The profile is described by successive segments which form an angle  $\alpha_1$  with the mean plane of the fracture. Their projected length on the mean plane is constant and equal to  $\Delta x$ . Elements of statistical analysis of directional data are given by Mardia (1972). The results are presented table II. The distribution on figure 1d represents the absolute values of the apparent colatitudes.

The mean value of inclinations is very low. The distributions are quasi symmetrical, and are relatively concentrated around the mean value.

From the above 2D distribution (figure 1d) we get the 3D distribution by applying a model developed by Scriven and Williams (1965) (figure 1e). This model requires some hypotheses : (1) the surface has an axis of symmetry which is the normal to the mean plane, (2) the colatitudes and azimuths are independent, (3) the azimuths of facets fit to a uniform distribution between  $[0, 2\pi]$ , (4) facets have finite dimensions. Then the above 3D distribution is fitted to theoretical distributions like the Fisher or Dimroth-Watson distributions (Gentier and Riss, 1987). These models are characterized by a concentration parameter K (Mardia, 1972). To extend these distributions, and to obtain a better fitting, "generalized distributions" are proposed by Gentier and Riss (1987). They depend on two parameters : K, coefficient of concentration and  $\beta$ , exponent of  $\cos\theta$  :

$$F(\theta, K) = e^{K \cos^\beta \theta} \sin\theta / \int_0^\pi e^{K t^\beta} dt \quad (9)$$

A stationarity of likelihood method is used for the fitting. For this granite the best couple is ( $K = 7.95$ ,  $\beta = 2.36$ ). However this fitting overestimated the high values of  $\cos\theta$ .

A further study (Riss and Gentier, 1989) presents the relationships between the parameters  $R_L$ ,  $R_A$  and  $Z_2$  and the distributions of colatitudes. Another model is derived, adding to the previous method the double exigence of having adequate values for  $R_L$  and  $Z_2$  ; the model becomes :  $K = 10.35$ ,  $\beta = 1.64$  (figures 1d and 1e). For such a 3D distribution  $R_A = 1.079$ .

In conclusion of this first part, the fracture surface is constituted by :

- two populations of heights (bimodality)
- asperities (peaks) with a curvature radius between 4 to 7 mm

- surface elements with colatitudes not greater than  $40^\circ$  and the mean absolute value between 2 and  $3^\circ$ .

The first two points are partially contained in the geostatistical study. The two populations of heights are linked to the two families of structures. The mean curvature radius corresponds to the size of the first family of structures.

Finally using the two parameters  $R_L$  and  $Z_2$  is essential to fit well the angular distribution.

### Morphology of the fracture voids

If it is easy to reproduce independantly the morphology of each side of the fracture in this way, the knowledge and the simulation of the "fracture voids" requires the ability to fit together the profiles of each side. The variogram of the heights of the voids deduced from the fitting of profiles is shown on figure 7. The range is between 5 and 7 mm and corresponds to the range of the first family of structures defined above.

The operation of fitting is difficult at best. Moreover this technique is not applicable to the measurements of the fracture voids under stresses.

The first way we used to achieve informations in the plane on the fracture, and not perpendicular to it as above, under normal stresses is based on the insertion of a thin plastic film ( $< 12 \mu\text{m}$ ) between the two sides of the fracture. Then it is submitted to several normal stress levels. The film is damaged where there are contacts between the two sides, and intact otherwise. The estimation of the area of the damaged zones gives an upper bound of the contact area. Its evolution with stress is given on figure 8.

Another technique proposed by Pyrac-Nolte et al (1987) is injecting a low melting point metal in the fracture. This technique requires sophisticated experiments and the study of the cast is not easy.

The 3D characterization of the fracture voids can be directly achieved only by casting the voids between the two sides of the fracture. The laboratory casting technique developped jointly by Bureau de Recherches Géologiques et Minières and Lawrence Berkeley Laboratory (LBL) allows a direct study of these voids and their evolution under stresses. The material used for casting is a silicon polymer resin manufactured by Rhône-Poulenc. The procedure is described in Gentier et al (1989). We obtain a thin cast, which may show holes at contacts between the two sides of the fracture. Once a cast has been obtained, a pixel map is recorded using a video camera placed above the cast while it is illuminated from below by a powerful light source. For the grey-level map (figure 9) to be useful, it must be translated into a map of the thicknesses of the voids. This processing consists of two operations. Firstly, trends in the image due to the heterogeneities of the light-source must be removed. Secondly a one to one correspondence between grey-levels and thicknesses must be defined. In order to calibrate the grey level image in terms of thicknesses, a "calibration wedge" is cast using the same resin as for the fracture voids in a precision engineered mold. It is digitized and light-source-induced trends are removed in exactly the same way as for the fracture image. It is then easy to establish a correspondence between grey-levels and thicknesses and to get informations like the histo-

gram of voids thicknesses or apertures (figure 6).

The map of apertures contains a big density of informations (theoretical resolution of 200 $\mu$ m for a standard camera with 512 x 512 pixels and for a cast of 12 cm of diameter). Various treatments must be applied to extract the sufficient but not overabundant data needed to perform some specific applications. The treatments we present here concern the study of the channeling in a fracture.

The method the most immediate to simplify the grey level image is binarization. A range of grey levels (Min, Max) is isolated for which the pixels are set to 255 (white). Out of the range the pixels are set to 0 (black). This operation applied to a fracture permits the isolation of a range of apertures where flow is possible or not (figure 10b). The black areas correspond to possible channels for apertures greater than 183  $\mu$ m. The evolution of the connectivity of the channels can be studied by increasing the threshold (figure 10a). It corresponds to a 17  $\mu$ m closing of the fracture.

To concentrate ever more the informations contained in the image, we realize a skeleton of the binary image (Coster and Chermant, 1985). The aim of the operation is to extract only the essential data. It is performed by successive operations called "thinning" until a stable structure is obtained. Skeletons are presented on figures 10c and 10d.

The simplification of the image can be continued further in the case of steady state flow. The deadends and little loops are eliminated (figures 10e and 10f) by application of specific masks. They correspond for the first ones to the possible configurations of the extreme points in a square grid. The second ones are removed by operations of dilation and erosion.

Skeleton is a network of lines which can be easily introduced in models by the finite elements method. However this operation presents a disadvantage. The simplification of the image leads to the loss of the third dimension (aperture). To avoid this, during the operation of "skeletonization" we keep and cumulate the grey levels in the directions of thinning. The result of this integration is the knowledge of a grey level on each pixel of the skeleton. Each segment of the network can be subdivided in elements of given aperture.

### Conclusion

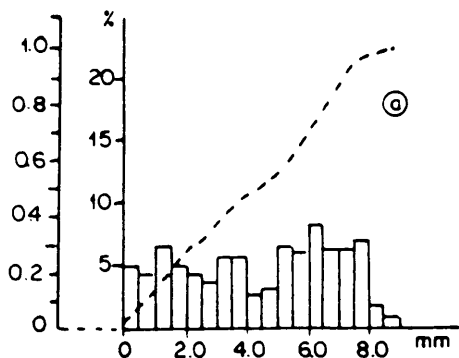
In this paper we present various ways to study and to quantify the morphology of the fracture.

The morphology of a fracture is complex and roughness parameters are not sufficient to characterize it. Various geometrical characteristics must be considered. These characteristics are important for the modeling of the mechanical behavior of the fracture. These models are based for example on the distribution of aperture, on the curvature, and on the angularity (shear behaviour). The knowledge of the fracture voids is essential for modeling flow. In order to study the coupled hydromechanical behavior a better knowledge of the relation between morphology of each side of the fracture and morphology of its voids is needed. This will be the subject of further work.

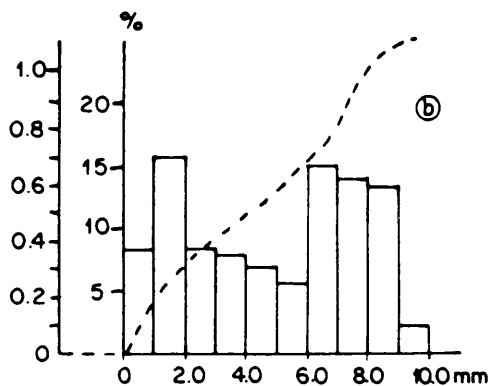
## References

- Bandis, S., A.C. Lumsden, and N. Barton, 1983, Fundamentals of rock joint deformation, *Int. J. Rock Mech. Min. Sci.*, 20, n° 6, 249-268.
- Barton, N., S. Bandis, and K. Bakhtar 1985, Strength, deformation and conductivity coupling of rock joints, *Int. J. Rock Mech. Min. Sci.*, 22, n°3, 121-140.
- Brock, M., 1983, Fourier analysis of surface roughness, *Technical Review*, 3, 3-45.
- Chermant, J.L., and M. Coster, 1978, Fractographie quantitative, *Bull. Cercle Etudes des Métaux*, XIV, 93-146.
- Coster, M., and J.L. Chermant, 1985, *Précis d'analyse d'images*, Editions du CNRS, France, 521p.
- Dight, P.M., and H.K. Chiu, 1981, Prediction of shear behaviour of joints using profiles, *Int. J. Rock Mech. Min. Sci.*, 18, n° 1, 369-386.
- El Soudani, S.M., 1978, Profilometric analysis of fractures, *Metallography*, 11, 247-336.
- Gentier S., 1986, Morphologie et comportement hydromécanique d'une fracture naturelle dans le granite sous contrainte normale, Doctoral thesis, Orléans University, France, 637p.
- Gentier, S., 1990, Hydromechanical behavior of a single natural fracture under normal stress, in these proceedings.
- Gentier, S., D. Billiaux, and L. Van Vliet, 1989, Laboratory testing of the voids of a fracture, *Rock Mechanics and Rock Engineering*, 22, 149-157.
- Gentier, S., and J. Riss, 1987, Spherical distribution of fracture surface elements from linear and/or areal roughness, *Acta Stereol.*, 6/III, 877-882.
- Mardia, K.V., 1972, *Statistics of directional data*, Academic Press, London, 357p.
- Myers, N.O., 1962, Characterization of surface roughness, *Wear*, 5, 182-189.
- Nuri, K.A., and J. Halling, 1975, The normal approach between rough flat surfaces in contact, *Wear*, 32, 81-93.
- Passoja, D.E., and Amborski, 1978, Fracture profile analysis by Fourier transform method, *Microstructural Science*, 6, 143-153.
- Pyrac-Nolte, L.J., L.R. Myer, N.G.W. Cook, and P.A. Witherspoon, 1987, Hydraulic and mechanical properties of natural fractures in low permeability rock. 6th International Congress on Rock Mechanics, Montreal, Canada, 225-231.
- Rengers, N., 1970, Influence of surface roughness on the friction properties of rock planes, 2nd International Congress on Rock Mechanics, Belgrade, 1-31.
- Riss, J., and S. Gentier, 1989, Linear and areal roughness of non planar rock surfaces of fracture, for Stereology, Freiburg, Germany, in press.
- Scriven, R.A., and H.D. Williams, 1965, The derivation of angular distribution of planes by sectioning methods, *Transactions of the metallurgical of Society AIME*, 233, 1593-1602.
- Serra, J., 1982, Flatness and roughness of non planar surfaces, N-760, Centre de Geostatistique et Morphologie Mathématique - Fontainebleau, France, 19 p.
- Swan, G., 1981, Tribology and characterization of rock joints, *Proc. 22nd U.S. Rock Mech. Symp.*, Boston, 432-437.
- Tse, R., and D.M. Cruden, 1979, Estimating joint roughness coefficients, *Int. J. Rock. Mech. Min. Sci.*, 16, 303-307.
- Zongqi, S., 1983, Fracture mechanics and tribology of rocks and rock joints, Doctoral thesis, Luleå University, Sweden, 207p.

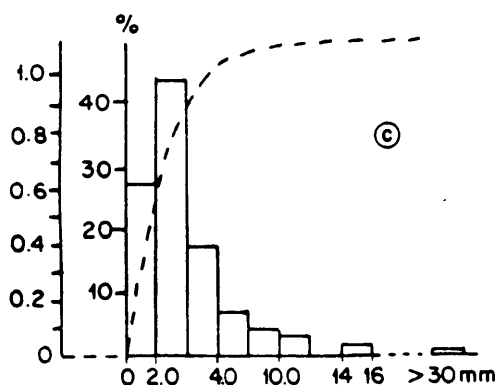




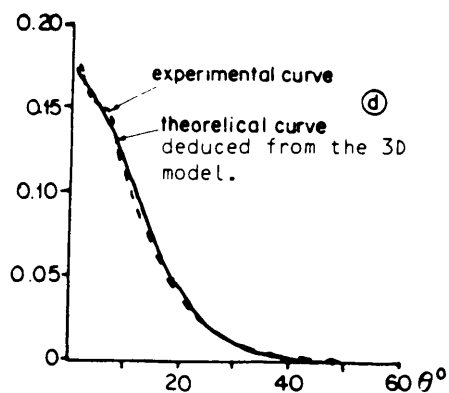
Distribution of the heights of the surface (sample 1).



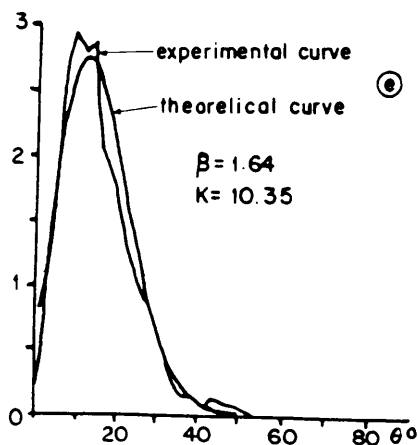
Distribution of the heights of the peaks (sample 1).



Distribution of the radii of curvature of the asperities (sample 1).



Distributions of apparent colatitudes.



Distribution of colatitudes deduced from the Scriven and Williams' model and the theoretical generalized distribution.

Figure 1 : distributions of some geometrical characteristics.

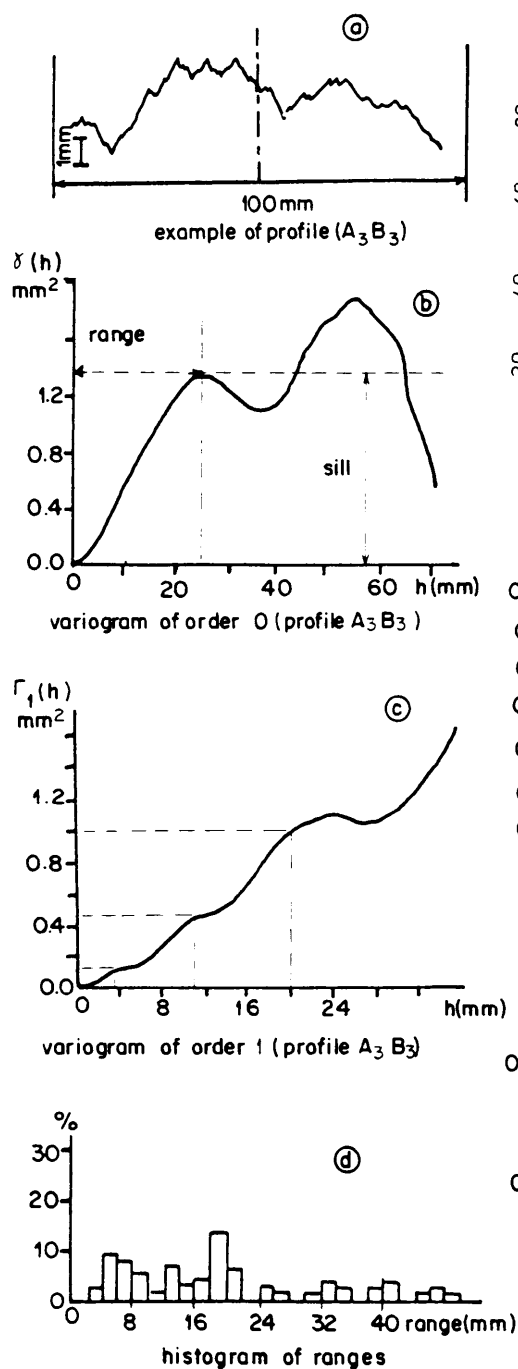


Figure 2 : geostatistical analysis.

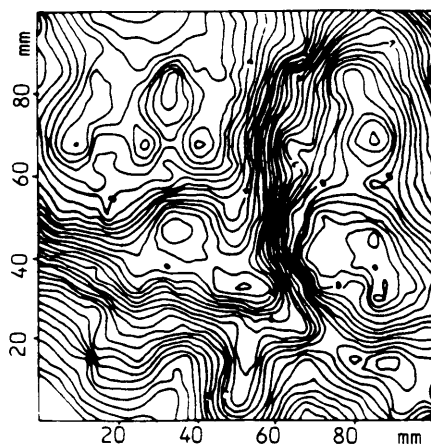


Figure 3 : example of kriging.

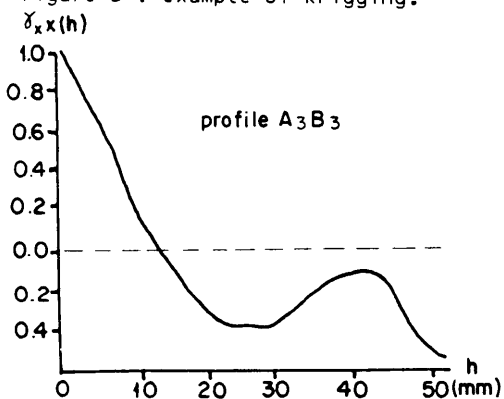


Figure 4 : autocorrelation function.

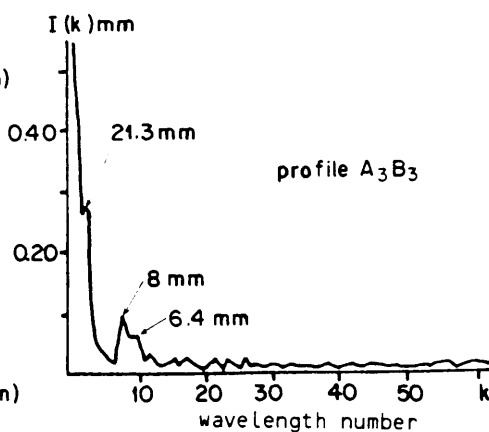


Figure 5 : spectral function.

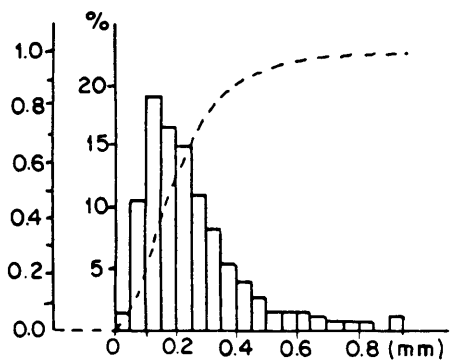


Figure 6 : experimental distribution of the voids.

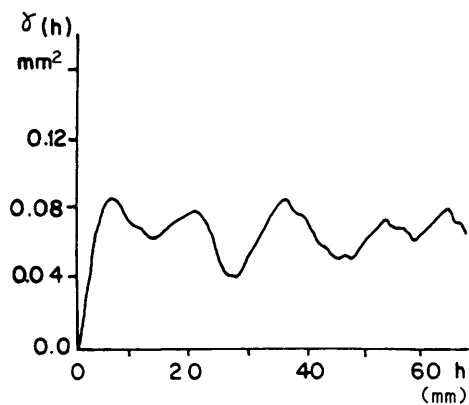


Figure 7 : experimental variogram of the voids.

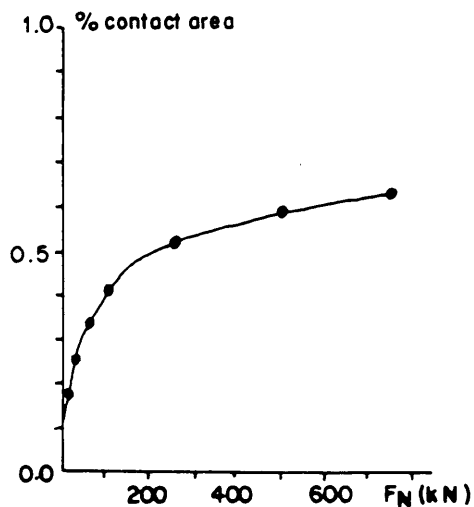


Figure 8 : evolution of the contact area with the load.

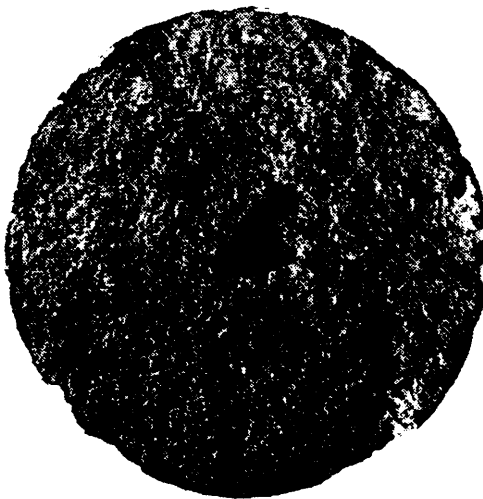


Figure 9 : grey-level image of a cast. (the thicker areas are in black).

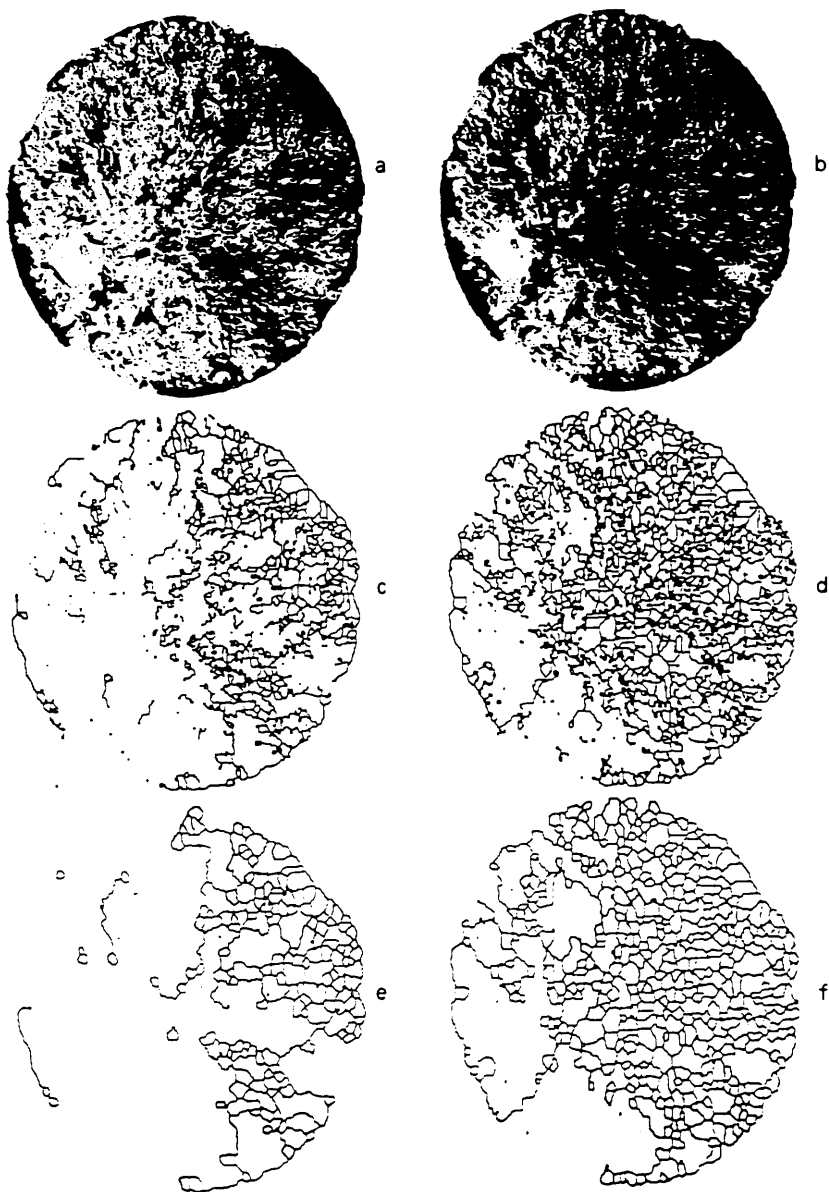


Figure 10 : example of treatments on a grey-level image.

- . a and b : binary images.
  - a : white = aperture  $< 200 \mu\text{m}$  ; black = aperture  $> 200 \mu\text{m}$  ;
  - b : white = aperture  $< 183 \mu\text{m}$  ; black = aperture  $> 183 \mu\text{m}$  ;
- . c and d : skeletons.
- . e and f : backbone of the skeletons (deadends and isolated islands removed).

# HYDROMECHANICAL BEHAVIOR OF A SINGLE NATURAL FRACTURE UNDER NORMAL STRESS

S. Gentier

BUREAU DE RECHERCHES GEOLOGIQUES ET MINIERES  
BP 6009 - 45060 ORLEANS CEDEX 2 - FRANCE

**Abstract :** The hydromechanical behavior of a single natural fracture is an important factor in underground works. To understand it, we perform mechanical and hydromechanical tests in laboratory on samples containing a natural fracture. In this paper we present experimental results and their interpretation in terms of the morphology of the fracture. Various models of mechanical behavior are tested and we propose a model which considers the confining pressure on the asperities during the loading. The classical cubic law is introduced in the mechanical behavior. We show that only at low stress levels ( $< 15$  MPa), the experimental results can be fitted by this law. At high stresses the phenomenon of channeling is too important. Then we propose some reflections on the concept of hydraulic aperture of a fracture.

## Introduction

The hydromechanical behavior of fractures is an important information for studies relative to the disposal of waste at great depth. For a long time the flow in a fracture was considered as decreasing with depth. This idea is based on the hypothesis that the stress increasing with depth, "closes" the fracture. This is now much debated and is false in many cases. Hydraulic tests in boreholes at great depth have yielded non negligible flows.

Another aspect of the problem is the choice of a conceptual model to flow. Either the fluid is located only on some areas of the fracture or it can flow every where. To understand this, we perform laboratory tests on several cylindrical samples with a diameter of 12 cm. The fracture studied in this paper is the same as the fracture used for the morphology analysis published in these proceedings (Gentier, (1990).

## Mechanical Experiments

Before studying the hydromechanical behavior by coupled hydraulic and mechanical experiments we consider only the mechanical behavior of the fracture. This first step intends to fix the conditions of the coupled tests.

Each sample contains a part of the natural fracture at middle height, the mean plane of the fracture is perpendicular to the axis of the sample. They are equipped with four LVDT gauges located opposite on two orthogonal diameters. The set is put on the loading frame. During the test we record continuously the four displacements and the force applied on the sample. The recorded displacements integrate first the displacements due to the closure of the fracture and second the displacements due to the deformation of the rock mass between the two supports of the LVDT gauge.

The first step of the test consists in checking that the two halves of the sample are well matched. It must erase the laboratory history of the sample (handling, recording profiles,...). We perform it using the following procedure (figure 1) :

- the fractured sample is submitted to a preloading ( $\sim 1,2$  MPa),
- we apply a series of increasing cycles of loading and unloading. The maximum stress for the higher cycle corresponds to the half of the compressive strength of the intact rock,
- we return to the preloading between each cycle.

At this stage we define a "closure at preloading". It corresponds for a part to the matching of the sample and for another part to the hysteresis of the behavior. It decreases when the number of cycles increases and is inversely proportionnal to the maximum load,

- then the sample is totally unloaded. At this stage we define the "final irreversible closure" in contrast with the closure mentioned above which is reversible in part.

The repetition of such a set of cycles, called an "experiment", shows a decrease of the "final irreversible closure" (until its quasi-complete cancellation at the end of the third experiment).

Beyond the third experiment we observe a complete reversibility and reproductibility of the behavior for stress levels up to 80 MPa : It seems that it is possible to correctly match the two halves of the sample to get the intrinsic behavior of the fracture. This procedure is applicable to fracture surfaces which are not damaged by the successive loadings.

The evolution of the mean displacement, as a function of the stress can be subdivided in two parts :

- a non linear behavior between 0 and 15 MPa. In this part the closure of the fracture dominates,
- a linear behavior for stress levels greater than 15 MPa. In this part the displacement due to the deformation of the rock mass dominates. The slope is very close to the elastic modulus of the intact rock.

The curve of fracture closure versus stress is obtained by removing the displacement due to the deformation of the rock.

These tests show that the maximum closure of the fracture (30 to 40 % of initial mean aperture) is reached at 15 MPa. The maximum closure varies from a sample to another between 40  $\mu\text{m}$  and 67  $\mu\text{m}$ . The shape of the curve is directly linked to the evolution of the contact area with increasing stress. Beyond a critical stress value, the contact area is quasi constant (Gentier , (1990). These results confirm the ones described by Goodman (1976), Bandis et al (1983), Barton et al (1985) and Tsang and Witherspoon (1983).

The behavior recorded by each gauge is similar in shape to the mean behavior described above, but the amplitudes are different. The variation of the closure from a gauge to another is a function of the distribution of contact areas in the plane of the fracture. Differences between the four measured maximum closures can reach 200 %. When the contact areas have a homogeneous distribution the variation from a gauge to another is small.

#### Theoretical mechanical models

Various models are proposed in literature by Shehata (1971), Goodman (1976), Detournay (1979), Bandis et al (1983), Tsang and Witherspoon (1983),

Zongqi (1983). Only some models include the morphological aspect of the fracture. Bandis et al (1983) introduce it via the roughness parameter, JRC, defined in a mechanical manner. Tsang and Witherspoon (1983) express it by a distribution of aperture.

Two models are detailed in this paper. The first model is developed by Zongqi (1983). In this model each side of the fracture is considered as a set of spheres. The basic mechanical behavior of two spheres in contact is given by Hertz.

The load is defined by :

$$P = \frac{8}{3} \pi E' \mathcal{A} \eta_1 \eta_2 (R_1 R_2 R_c)^{1/2} \int_0^{Z_m} \int_0^{Z_m - Z_1} \alpha^{3/2} h_0 \phi_1(Z_1) \phi_2(Z_2) d_{z1} d_{z2} \quad (1)$$

where :

$$E' = \frac{E}{2(1-\nu^2)} ; \text{ (E is the Young modulus and } \nu \text{ is the Poisson ratio)}$$

- .  $\mathcal{A}$  is the nominal area ;
- .  $\eta_1$  and  $\eta_2$  are the areal density of asperities on the sides of the fracture ;
- .  $R_1$  and  $R_2$  are the mean radii ( $R_c = R_1 + R_2$ ) ;
- .  $\phi_1$  and  $\phi_2$  are the distributions of the heights of asperities ;
- .  $Z_m$  is the maximum distance between an asperity on one side and an asperity on the other side of the fracture ;
- .  $h_0$  is the degree of match of the two sides of the fracture ;
- .  $\alpha$  is the displacement due to the load.

The area of contact is given by :

$$A_T = 2 \pi^2 R_1 R_2 \eta_1 \eta_2 \int_0^{Z_m} \int_0^{Z_m - Z_1} \alpha h_0 \phi_1(Z_1) \phi_2(Z_2) d_{z2} d_{z1} \quad (2)$$

The morphological data we need are the distribution of the heights of the asperities (peaks), their mean radius of curvature, and their areal density for each side of the fracture. These data are easily obtained from the morphological analysis of the fracture described in Gentier (1990)..

The degree of match being impossible to get from the morphological data, a systematic calculation is performed for several matches.

Despite a good global estimation of the fracture closure, the theoretical curves do not reproduce shape of the experimental curves (figure 2).

The contact area calculated with this model is very low (3 cm<sup>2</sup>) and represents only 2,5 % of the fracture surface. This is due to the constant radius spherical shape assumed for the asperities. Even a more complex spherical model introducing nested spheres of various radii is not able to reproduce the behavior at high stresses (Archard, 1957).

The difference between theoretical and experimental curves at high stress leads us to take into account a confining pressure on the asperities. But the spherical model is not well adapted to such an improvement.

Billiaux et al (1984) propose another model. The fracture consists of two rigid plane surfaces, one of them supporting teeth with variable heights.

We consider that the difference of height between two successive teeth is very small. Consequently each loaded tooth is always surrounded by unloaded teeth. The latter ones apply a confining pressure on most of the height of the loaded tooth. The confining pressure  $\sigma_{31}$  applied on a tooth submitted to a normal stress  $\sigma_{11}$  is a function of the ratio of the area of the loaded part to the whole area, written  $(1 - \tau(e^+))$  :

$$\sigma_{31} = \beta \sigma_{11} \quad \text{with } \beta = \frac{v}{1-v} (1 - \tau(e^+))^{1/2} \quad (3)$$

where  $e^+$  is the aperture of the fracture normalized by the maximum aperture ( $e_0$ ), and  $\tau(e^+)$  is the normalized free area of the fracture deduced from the void height distribution.

Introducing the failure criterion of Hoek and Brown (1980), we define a failure normal stress  $\sigma_L$  as a function of the confining pressure applied on the tooth for a given spacing :

$$\sigma_L = \sigma_c \frac{(m\beta + (m^2 \beta^2 + 4(1-\beta)^2 s))^{1/2}}{2(1-\beta)^2} \quad (4)$$

where  $\sigma_c$  is the uniaxial strength,  $m$  and  $s$  are the parameters of the failure criterion.

Beyond the elastic limit, various post-failure behaviors  $g(e^+)$  are proposed. The residual stress in each broken tooth is

$$\sigma_R(e^+) = \sigma_L g(e^+) \quad (5)$$

The behavior of tooth "i" of height  $h_1^+$  under no stress is :

$$\left. \begin{array}{ll} * \text{ if } h_1^+ < h_L^+ (h_L^+ : \text{limit height}) \\ \sigma_{11} = E \frac{(h_1^+ - e^+)}{\alpha h_1^+} & \text{linear elastic behavior} \\ \text{with } \alpha = 1 - 2v\beta \\ * \text{ if } h_1^+ > h_L^+ \\ \sigma_{11} = \sigma_R(e^+) & \text{post failure behavior} \end{array} \right\} \quad (6)$$

Integrating the behavior of all teeth on the surface of the fracture we get :

$$\sigma_N = \underbrace{\sigma_R(e^+) (1 - \tau(h_L^+))}_{\text{teeth with post failure behavior}} + \underbrace{\frac{1}{\alpha} \int_{e^+}^{h_L^+} E \frac{(h^+ - e^+)}{h^+} \tau(h^+) dh^+}_{\text{teeth with elastic behavior}} \quad (7)$$



where  $1-\tau(h^*_L)$  represents the fraction of the surface where the teeth have a height greater than  $h^*_L$  and  $\tau'(h^*) dh^*$  represents the fraction of the surface where the teeth have a height between  $h^*$  and  $h^*+dh^*$ .

To fit the stiffness of the experimental curves at high stresses ( $> 15$  MPa), the residual stress in each broken tooth is assumed to be at least equal to the limit stress  $\sigma_L$  (figure 3).

Globally this model fits well the experimental curves. However the behavior between 5 and 10 MPa is not perfect.

Even if introducing a confining pressure on the loaded asperities gives a better fit, no model permits to reproduce the change of behavior from fracture-dominated to matrix-dominated.

### Hydromechanical experiments

Then the same samples are used to perform hydraulic tests at several stress levels.

We core an injection hole along the axis of one of the half sample. The basis of the sample is equipped with an injection head linked to a pump. Two gauges are fixed to record the closure of the fracture during the test and to verify that the mechanical behavior with fluid injection is similar to the mechanical behavior without fluid injection. With this set-up the flow is a radial divergent flow. During the test we record continuously :

- the load ;
- the displacement ;
- the injection pressure ;
- the flow.

At each stress level the fluid is injected at constant flow and we wait for the injection pressure to stabilize. The intrinsic transmissivity is given by the relation :

$$k_{g.e} = \frac{\mu}{2\pi} \frac{Q}{P_o} \ln \frac{r_a}{r_i} \quad (8)$$

where  $\mu$  is the dynamic viscosity,  $r_i$  and  $r_a$  are respectively the inner and outer radii,  $Q$  is the flow and  $P_o$  is the stabilized injection pressure.

The mechanical procedure is the same as for the mechanical tests : the fracture is submitted to several increasing cycles of loading and unloading (figure 4).

The curves giving the transmissivity as a function of the stress show :

- a fast decrease of the intrinsic transmissivity when the stress increases for stresses lower than 10 MPa, then a stabilization ;
- a similarity with the fracture closure versus stress curves ;
- the influence of the matching of the two halves of the sample. Between the first loading cycle and the second one we observe an important decrease of the intrinsic transmissivity for a given stress level. This has been already described by Gale (1982), Feuga and Vouille (1984), Barton et al (1985), and Raven and Gale (1985).

The curves obtained for each sample are similar in shape but we find important discrepancies in the values of the intrinsic transmissivity (factor of 100 between the samples). These variations depend for a big part

on the morphology of the voids in the vicinity of the borehole.

If we consider that the fracture is equivalent to two parallel planes an equivalent hydraulic aperture  $\bar{e}_h$  can be estimated :

$$k_{\sigma}.e = \frac{\bar{e}_h^3}{12} \quad (9)$$

It corresponds to the aperture of a smooth fracture which would have the same intrinsic transmissivity as the real fracture. The results are presented in Table I and are compared to the mean aperture of the fracture modified by the closure due to the stress. We find that :

- the equivalent hydraulic aperture is very close to one half of the mean geometrical aperture of the fracture ;
- the variations of this ratio with the stress are very small.

Table I : geometrical aperture ( $\bar{e}$ ), hydraulic aperture ( $\bar{e}_h$ ) and roughness (C) versus stress

| $\sigma_N$ (MPa) | $\bar{e}$ ( $\mu\text{m}$ ) | $\bar{e}_h$ ( $\mu\text{m}$ ) | $\bar{e}_h/\bar{e}$ | $\tau/C$ | $\tau$ | C    | $k/D_h$ |
|------------------|-----------------------------|-------------------------------|---------------------|----------|--------|------|---------|
| 1.53             | 161                         | 88                            | 0.55                | 0.17     | 0.83   | 5.22 | 0.61    |
| 3.63             | 153                         | 83                            | 0.54                | 0.16     | 0.76   | 4.78 | 0.57    |
| 7.00             | 144                         | 77                            | 0.53                | 0.15     | 0.63   | 4.15 | 0.50    |
| 10.63            | 140                         | 74                            | 0.53                | 0.13     | 0.60   | 4.08 | 0.50    |
| 14.13            | 139.5                       | 71                            | 0.51                | 0.13     | 0.55   | 4.04 | 0.49    |
| 17.38            | 139                         | 71                            | 0.51                | 0.13     | 0.52   | 3.97 | 0.49    |
| 26.25            | 138.5                       | 70                            | 0.51                | 0.13     | 0.49   | 3.86 | 0.47    |
| 35.25            | 138                         | 69                            | 0.50                | 0.12     | 0.46   | 3.71 | 0.46    |

This approach does not take in account the roughness of the fracture and the existence of contact area. Louis (1967) propose the following relation :

$$k_{\sigma}.e = \frac{\tau}{C} \frac{e^3}{12} \quad (10)$$

where  $\tau$  is the normalized free flow area and C is a roughness parameter. The ratio  $\tau/C$  can be calculated using the mean geometrical aperture of the fracture at each stress level. The results are presented in Table I. The ratio  $\tau/C$  is the coefficient of correction accounting for the geometry of the fracture needed to obtain coherent intrinsic transmissivities.

If we introduce the experimental values of  $\tau$  (Gentier, 1990) in the ratio  $\tau/C$  we obtain the values of the roughness parameter C. Using the relation :  $C = 1 + 8,8 (k/D_h)^{3/2}$ , we can then deduce the relative roughness  $k/D_h$ , where k is the height of the asperities and  $D_h$  is the hydraulic diameter. The definitions of these parameters lead to a minimum theoretical value of 0.5 when the two sides of the fracture are in contact. The experimental results are presented in Table I. The values of the relative roughness are lower than 0.5 for this sample and decrease when the stress

increases : the match of the two sides is better than the best match defined by Louis (1967). This is not the case for other samples where the values are greater than 1 and increase with increasing stress (Gentier, 1986). These samples have a low permeability and an important and well distributed contact area. Moreover the relationship established by Louis (1967) between the roughness coefficient  $C$  and the relative roughness  $k/D_h$  is an empirical one deduced from tests on fractures having a maximum relative roughness of 0.5. This relationship is not well adapted to our case.

To understand the variations of the intrinsic transmissivity with the stress we inject a blue dyed water in the fracture. Then we record at each stress level the outlets around the sample. The locations of the outlets around the sample and their evolution with stress are presented in figure 5 and the evolution of the number of outlets with stress is shown figure 6.

This test can explain the results of the hydraulic tests. The fast decrease of the intrinsic transmissivity for the first stress levels corresponds to the decrease of the number of channels. Beyond the critical value of the stress (15 MPa), the number of channels is constant. Moreover the mean distance between two successive outlets is equal to 4 mm at the lower stress level and to 18 mm after stabilization. These two values correspond to the ranges of the two nested structures found by the geostatistical study (Gentier, 1990).

#### Theoretical hydromechanical behavior

Some authors propose relationships between the conductivity or the transmissivity in a fracture and the stress (Sharp and Maini, 1972, Detournay, 1979, Gale, 1982, Feuga and Vouille, 1982, Tsang and Witherspoon, 1983, Raven and Gale, 1985, Barton et al, 1985). All these models are based on the "cubic law" for each stress level.

When the fracture has no contact and when the aperture of the fracture is large relative to the height of its asperities, the cubic law is well adapted.

We have tested two relationships between the intrinsic transmissivity  $k_{f.e}$  and the normal stress  $\sigma_N$  which are :

- the relationship of Raven and Gale (1985)

$$k_{f.e} = \beta \sigma_N^\alpha \quad (11)$$

when  $\beta$  and  $\alpha$  are two coefficients representing, respectively, the transmissivity at a stress of 1 MPa and the slope of the curve in logarithmic coordinates ;

- the relationship of Feuga and Vouille (1984) :

$$k_{f.e} = A e^{-\sigma_N/B} \quad (12)$$

where  $A$  is the intrinsic transmissivity under no stress and  $B$  is a coefficient equivalent to a stress.

The experimental curves are represented in logarithmic coordinates on figure 7a and in semi-logarithmic coordinates on figure 7b. These curves are not linear. So the fitting is performed in two parts ; one for stresses lower

than 15 MPa and one for stresses greater than 15 MPa.

These relationships between stresses and intrinsic transmissivity can be used for modeling the hydromechanical behavior of a fracture under normal stress if the stresses are lower than 15 MPa. In fact, at low stresses, the flow can be considered as generalized. Channeling does not dominate, because the number of channels is great. When stresses increase channeling dominates and the flow cannot any more be considered as generalized.

We also tried to couple the cubic law with the "confined teeth" model described above. The intrinsic transmissivities we obtained are greater than the experimental transmissivities and the general shape of the curves is right only for some examples.

### Conclusion

This study shows how experimental results on the hydromechanical behavior of a natural single fracture under normal stress can be explained by the analysis of its morphology. However a quantitative modeling of this behavior using morphology is not yet achieved.

The hydromechanical behavior of a fracture can be summarized as follows :

- At low stresses, the flow in the fracture can be considered as generalized. The density of channels is high and is governed by the range of the smaller structures. The contact area is low. At these stress levels the cubic law can be used ;

- When stresses increase up to 15 MPa, the contact area increases while the fracture aperture and the intrinsic transmissivity decrease rapidly. Flow paths progressively concentrate in preferential channels, until connectivity effects become predominant ;

- Beyond 15 MPa, the contact area stays constant, as well as the fracture aperture and the transmissivity. Flow is not generalized any more, channels govern the flow. Their spacing is linked to the range of the larger structure detected on variograms.

Further studies of channeling include the deduction of the channel network from morphological analyses (Gentier, 1990). The variations of the network topology can then be compared with experimental results.

### References

- Archard, J.F., 1957, Elastic deformation and the laws of friction, *Proc. Roy. Soc., Serie A*, t. 243, 190-195.
- Bandis, S., A.C Lumsden, and N. Barton, 1983, Fundamentals of rock joint deformation, *Int. J. Rock Mech. Min. Sci.*, 20, n° 6, 249-268.
- Barton, N., S. Bandis, and K. Bakhtar, 1985, Strength, deformation and conductivity coupling of rock joints, *Int. J. Rock Mech. Min. Sci.*, 22, n° 3, 121-140.
- Billiaux, D., B. Feuga, and S. Gentier, 1984, Etude théorique et en laboratoire du comportement d'une fracture rocheuse sous contrainte normale, *Revue Française de Géotechnique*, 26, 21-29.
- Detournay, E., 1979, The interaction of deformation and hydraulic conductivity in rock fracture, Improved stress determination procedures by hydraulic fracturing : Final report , Minneapolis, University of Minnesota, 47 p.

- Feuga, B., and G. Vouille, 1984, Comportement thermo-mécanique des fractures dans le granite, Documents du BRGM n° 84, Orléans, France.
- Gale, J.E., 1982, The effects of fracture type on the stress - fracture closure - fracture permeability relationships, Proc. 23rd US Rock Mechanics Symp., Berkeley CA, 290-298.
- Gentier, S., 1986, Morphologie et comportement hydromécanique d'une fracture naturelle dans le granite sous contrainte normale, Doctoral thesis, University of Orléans, France, 637 p.
- Gentier, S., 1990, Morphological analysis of a natural fracture, in these proceedings.
- Goodman, R.E., 1976, Methods of geological engineering in discontinuous rock, New York, West., 432 p.
- Hoek, E., and E.T. Brown, 1980, Underground excavations in rock, The Institution of Mining and Metallurgy, London, 527 p.
- Louis, C., 1967, Etude des écoulements d'eau dans les roches fissurées et de leurs influences sur la stabilité des massifs rocheux, Doctoral thesis, University of Karlsruhe, Germany, 128 p.
- Raven, K.G., and J.E. Gale, 1985, Water flow in a natural rock fracture as a function of stress and sample size, Int. J. Rock Mech. Min. Sci., 22, n° 4, 251-261.
- Shehata, W.M., 1971, Geohydrology of Mount Vernon Canyon area, Ph. D. Thesis, Colorado School of Mines.
- Sharp, J.C., and J. Maini, 1972, Fundamental considerations on the hydraulic characteristics of joints in rock, Proc. Symp. Percolation through fissured rock, Stuttgart, Germany.
- Tsang Y.W., and P.A. Witherspoon, 1983, The dependence of fracture mechanical and fluid flow properties on fracture roughness and sample size, J. of Geophys. Res., 88, n° B3, 2359-2366.
- Zongqi S., 1983, Fracture mechanics and tribology of rocks and rock joints, Doctoral thesis, Lulea University, Sweden, 207 p.

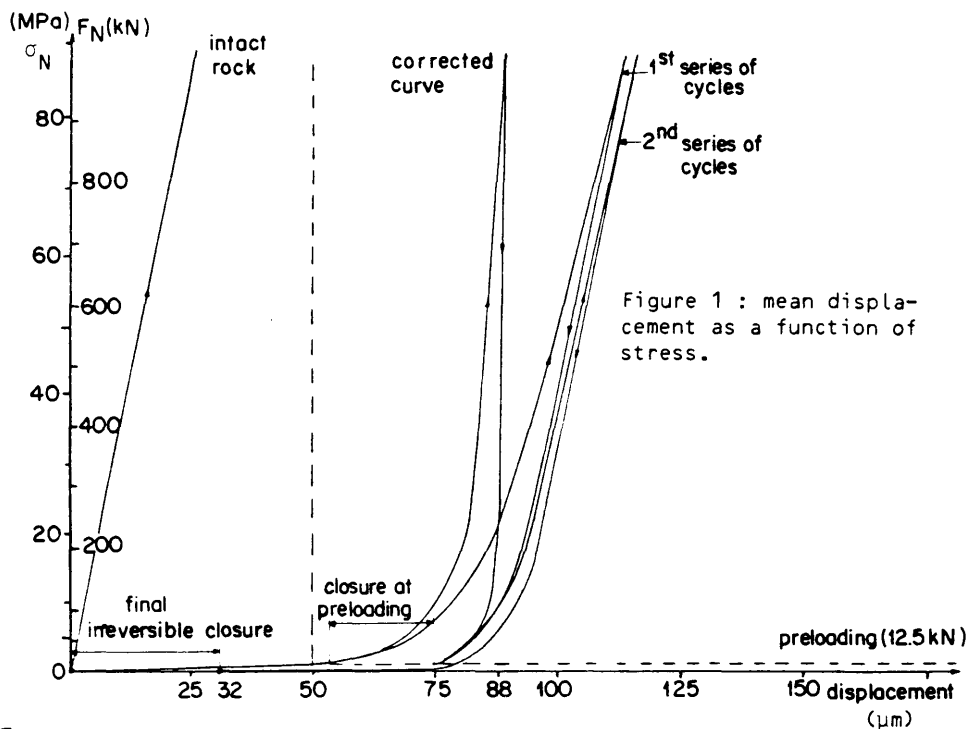


Figure 1 : mean displacement as a function of stress.

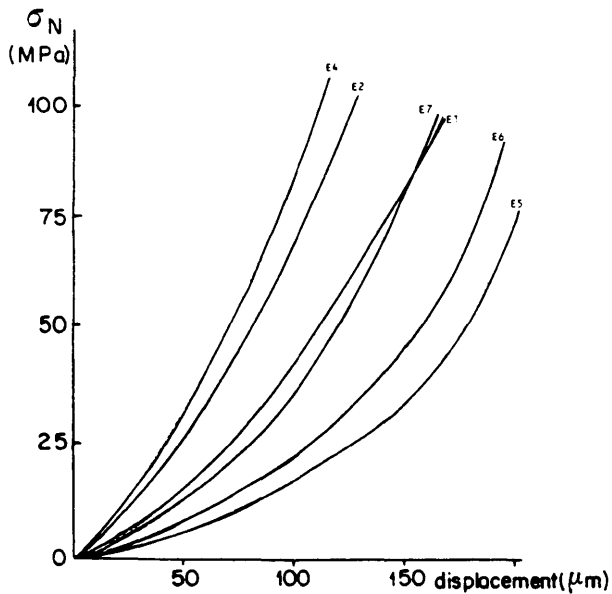


Figure 2 : theoretical curves obtained by the model of Zongqi (1983), (6 samples).

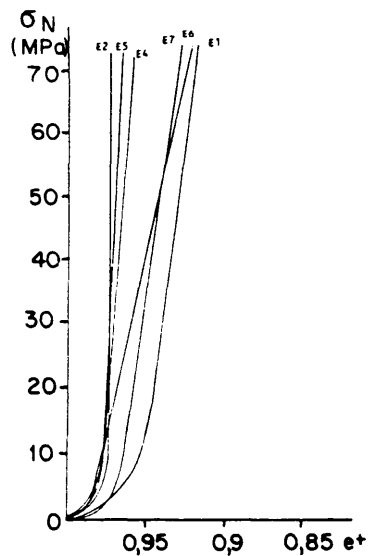


Figure 3 : theoretical curves obtained by the model of "confined teeth", (6 samples).

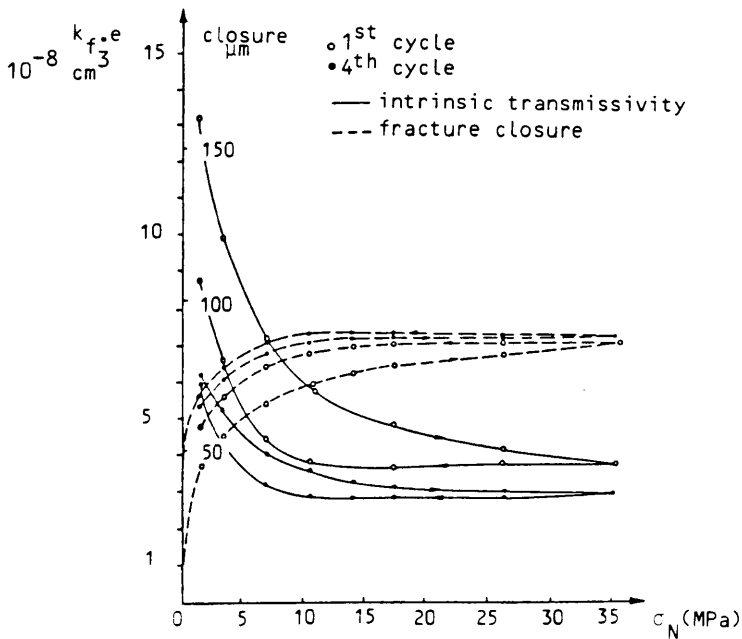


Figure 4 : intrinsic transmissivity and fracture closure versus stress.

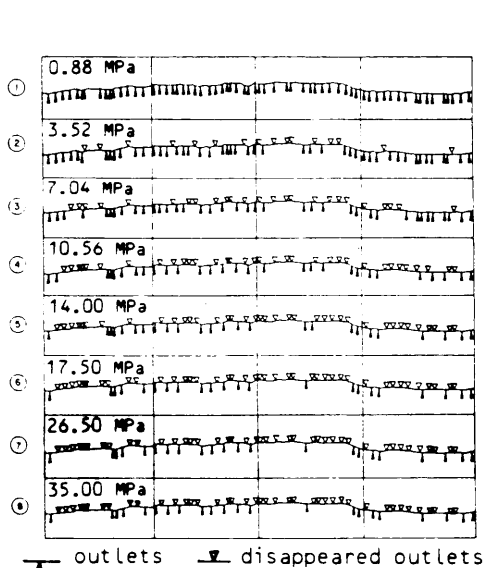


Figure 5 : evolution of the location of the outlets around the sample with the stress.

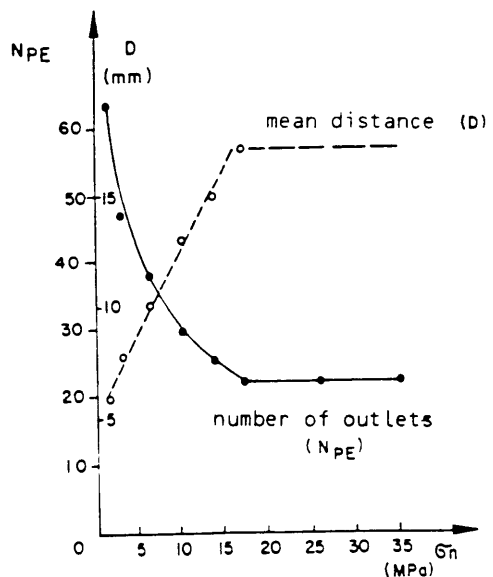
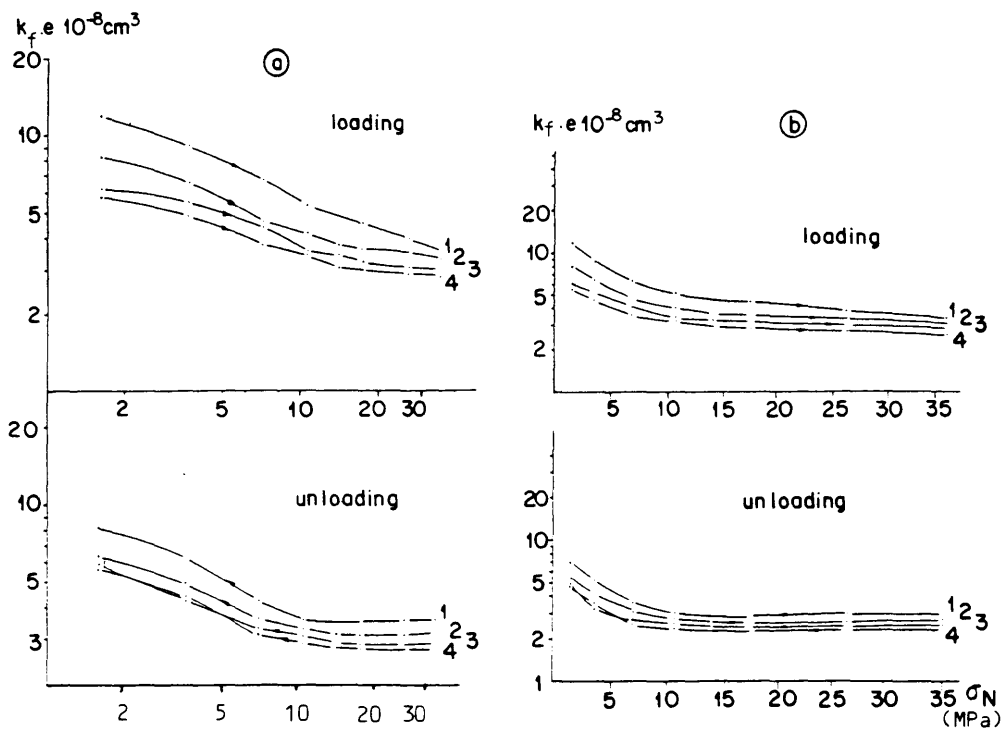


Figure 6 : variation of the number of outlets and of the mean distance with the stress.



|                                |                          | 1st cycle             |                       | 4th cycle             |                       |                          |                       | 1st cycle             |                        | 4th cycle             |           |
|--------------------------------|--------------------------|-----------------------|-----------------------|-----------------------|-----------------------|--------------------------|-----------------------|-----------------------|------------------------|-----------------------|-----------|
|                                |                          | loading               | unloading             | loading               | unloading             |                          |                       | loading               | unloading              | loading               | unloading |
| $\sigma_N \leq 15 \text{ MPa}$ | $a$                      | - 0.44                | - 0.46                | - 0.24                | - 0.40                | $A$<br>( $\text{cm}^3$ ) | $1.34 \cdot 10^{-7}$  | $8.85 \cdot 10^{-8}$  | $5.83 \cdot 10^{-8}$   | $5.76 \cdot 10^{-8}$  |           |
|                                | $B$<br>( $\text{cm}^3$ ) | $1.56 \cdot 10^{-7}$  | $1.05 \cdot 10^{-7}$  | $6.42 \cdot 10^{-8}$  | $6.74 \cdot 10^{-8}$  | $B$<br>(MPa)             | 10.97                 | 10.66                 | 21.35                  | 12.68                 |           |
|                                | residu                   | $1.67 \cdot 10^{-17}$ | $1.10 \cdot 10^{-17}$ | $6.84 \cdot 10^{-18}$ | $1.75 \cdot 10^{-18}$ | residu                   | $3.88 \cdot 10^{-17}$ | $3.07 \cdot 10^{-17}$ | $17.29 \cdot 10^{-17}$ | $2.55 \cdot 10^{-17}$ |           |
| $\sigma_N > 15 \text{ MPa}$    | $a$                      | - 0.39                | 0.002                 | - 0.13                | 0.002                 | $A$<br>( $\text{cm}^3$ ) | $5.91 \cdot 10^{-8}$  | $3.42 \cdot 10^{-8}$  | $3.27 \cdot 10^{-8}$   | $2.68 \cdot 10^{-8}$  |           |
|                                | $B$<br>( $\text{cm}^3$ ) | $1.37 \cdot 10^{-7}$  | $3.40 \cdot 10^{-8}$  | $4.25 \cdot 10^{-8}$  | $2.67 \cdot 10^{-8}$  | $B$<br>( $\text{cm}^3$ ) | 64.25                 | 26.21                 | 18.58                  | 61.68                 |           |
|                                | residu                   | $1.33 \cdot 10^{-18}$ | $1.65 \cdot 10^{-19}$ | $5.66 \cdot 10^{-20}$ | $9.45 \cdot 10^{-20}$ | residu                   | $1.61 \cdot 10^{-19}$ | $1.67 \cdot 10^{-19}$ | $1.19 \cdot 10^{-19}$  | $9.23 \cdot 10^{-20}$ |           |

Figure 7 : relationships between the intrinsic transmissivity and the normal stress ( four cycles of loading and unloading), and the goodness of fit coefficients :

$$a : k_f \cdot e = \beta \sigma_N^\alpha$$

$$b : k_f \cdot e = A e^{-\sigma_N/B}$$



## HYDRAULIC IMPEDANCE TECHNIQUE FOR UNSATURATED ROCK CHARACTERIZATION

Daniel D. Evans and Todd C. Rasmussen  
Department of Hydrology and Water Resources  
University of Arizona, Tucson AZ 85721

**ABSTRACT:** The impeding layer technique developed for measuring the unsaturated hydraulic properties of soil is extended to measure fractured rock properties. A hydraulic impedance layer is placed along a rock surface, either on the ground surface or within a borehole, and a positive pressure is applied to the outer surface of the layer. The impedance of the layer should be of sufficient magnitude so that the pressure drop across the layer is greater than the applied pressure, resulting in negative fluid pressures on the rock side of the impeding layer. After steady state flow is attained, the flow rate through the previously calibrated layer is used in conjunction with the known or computed matric suction at the rock face to determine the unsaturated hydraulic conductivity. Different applied pressures provide estimates of unsaturated hydraulic conductivities over a range of matric suctions. Blocks of slightly welded tuff with natural fractures have been studied in the laboratory using ceramic plates as impeding layers, and flexible tubular membranes have been assessed for making similar field measurements using boreholes in the same rock type. The approach shows promise for determining the magnitudes and relative importance of flow through the rock matrix and fractures under different moisture contents and matric suctions, which are particularly important to the prediction of solute transport through unsaturated fractured rock.

### Introduction

The processes of fluid flow and contaminant transport through unsaturated fractured geologic media are receiving increased interest, primarily because of the number and severity of existing and potential contaminated sites in such geologic media. A special interest in the United States is related to the possibility of locating a high-level radioactive waste repository in unsaturated fractured volcanic tuff, a few hundred meters below the land surface and above the regional water table in an arid climate. Site characterization involves predictions of water flow and radionuclide travel times and release rates from the potential repository site to a defined accessible environment. Flow and transport are considered to be through the rock matrix as well as through the fracture system with the dominant pathway determined by the geometry of the fracture and matrix pores as well as the existing matric suction. The fracture system is expected to dominate flow at low suctions when fractures with large effective apertures are filled with water while at higher suctions matrix flow will dominate. Due to the fragility of natural fractures, fracture characterization must be done in situ without disturbance to the fracture system.

Techniques for the in situ determination of fracture transmissivity as a function of matric suction are not presently available. Until adequate methodologies are developed to determine this functional relationship, a simple step function of fracture transmissivity is assumed. The critical matric suction becomes the important fracture parameter which defines the matric

suction above which a specific fracture does not significantly conduct water. A frequency distribution of this parameter for fractures intersecting the measuring surface will aid in the assessment of the relative importance of fracture and matrix flow under prevailing conditions.

Hillel and Gardner (1970) presented the impedance technique for imposing a negative pressure head along the soil surface for the purpose of estimating unsaturated hydraulic properties of soils. The technique proposed here involves use of an impeding layer to apply water under suction to an initially unsaturated segment of a borehole rock surface containing a natural fracture trace. The impeding layer is in the form of an expandable tube fitted to the diameter of the borehole. The impedance of the layer has a magnitude sufficient to apply water at the highest suction desired along the borehole test segment while still maintaining a positive water pressure within the tube. The positive pressure is required to maintain good hydraulic contact between the downhole instrument and the rock surface. The pressure within the tube is adjusted to yield variations in suction within the fracture while the outflow or inflow rate for the tube is measured.

In addition to geometric factors, the flow rate depends on the combined hydraulic conductivity of the rock matrix and the transmissivity of the fracture at the imposed suction. At high suctions, flow through the rock matrix will dominate, but as the suction is reduced, fracture saturation will increase causing a dramatic increase in measured flow for the highly conducting fractures of interest. The suction at which the flow dramatically increases is the desired parameter. A further refinement to the downhole instrument is to place a tube of higher conductivity between the impeding layer and the borehole wall to provide a relatively constant applied suction along the section of the borehole and less restrictive flow pathways to the narrow fracture inlet.

The objective of these experiments is to identify the critical capillary suction of a fracture at which the moisture status changes between drained and filled with water as a function of a threshold matric suction. An additional objective has been the development of a device which can be used to estimate the critical capillary suction for fractures under *in situ* conditions. To achieve these objectives a series of laboratory experiments have been conducted which attempt to reproduce many of the conditions expected in the field. The following sections describe the laboratory block and cylinder tests employed to characterize unsaturated fracture hydraulic properties.

#### Laboratory Block Tests

The hydraulic impedance approach was first tested in the laboratory using shaped blocks of tuffaceous rock (approximately 20 cm x 20 cm x 50 cm high), each with a single natural fracture extending from the top to the bottom of the block and located midway between two sides of the block (Figure 1). Clamps held the two sides of the block together to maintain a constant fracture aperture. The laboratory arrangement also allowed for changing the effective fracture aperture by applying a greater mechanical force normal to the fracture and measuring the fracture and matrix flow at different matric suctions. Such studies are now in progress.

Three 2-bar ceramic plates were placed in hydraulic contact with both the upper and lower block surfaces. A narrow plate covered the fracture trace on the upper surface while two wider plates covered the matrix surfaces on each side of the fracture. Each plate had a sealed water reservoir in contact with the side of the plate opposite to the rock surface for maintaining a constant applied pressure. The plates were first individually calibrated to obtain the relationships between flow rate and pressure drop across the plate. In practice, the pressure head at the rock surface is calculated from the measured flow rate and the applied pressure. A constant suction boundary condition was established at the rock surface by adjusting the water pressure in each reservoir, according to its calibration. A silica flour slurry was placed between each plate and the rock surface to improve hydraulic contact, and the block was enclosed within a canopy to minimize evaporation losses.

Pressure monitoring ports were drilled into the rock faces for matric suction measurements in the rock matrix as well as along the fracture within the matrix. To monitor the matric suction, a miniature tensiometer was constructed using a pressure transducer in conjunction with a porous ceramic cup. The ceramic cup was inserted into the port until contact was made with the rock at the end of the hole. Sufficient time was then allowed for equilibration between the rock and the fluid within the ceramic cup before a reading was taken.

The first experiment performed was a vertical infiltration study in which the previously air-dried block was subjected to a constant matric suction of 1.5 kPa (15 cm of  $H_2O$ ) at the upper boundary. Inflow rates measured during a period of 170 days are presented as Figure 2. After a relatively high initial infiltration rate, the rate dropped rapidly to a low value, and then increased to a near constant rate for the remainder of the time. Most of the fluctuations are considered to be due to the slow response associated with the adjustment of the applied pressure at the upper boundary. The applied pressure had to be adjusted as the flow rate changed in order to maintain the constant upper boundary condition. The location of the wetting front was noted periodically on a grid attached to each of the four sides.

The location of the wetting front for the fracture sides is shown in Figure 3 for selected days. The wetting front location is variable at small times due to heterogeneities of the rock sample. It is interesting to note that the wetting front location becomes smoother and more horizontal at times greater than seven days. It appears that the fracture did not contribute significantly to vertical percolation at the relatively low suction at the upper boundary. From this experiment it can be inferred that the critical suction at which the fracture ceases to be of importance to vertical fluid flow is less than 1.5 kPa. The measured matric suctions using the miniature tensiometers compared favorably with matric suctions determined from the flow rate calculations. In related studies using conservative tracers applied at suctions less than the critical suction for the fracture, it was shown that flow through the center narrow plate was mostly through the fracture while flow through the other plates was entirely through the rock matrix.

To aid in the interpretation of the laboratory results, the flow system was modeled using the Boundary Integral method (Rasmussen and Evans, 1989) to show the head distribution and the flow lines within the four flow regions: ceramic plate, fracture plate, rock matrix, and fracture. A steady-state flow

system was assumed and constant potential boundary conditions on the upper surface of the porous plates and the lower rock surface were imposed. Values of the hydraulic parameters for the plates were as measured and those for the rock matrix and the fracture were adjusted to approximate the inflow measured through the plates during the experiment discussed above. No lateral water movement was allowed along the rock-plate interfaces, i.e., there was no permeable layer inserted along that interface. The calculated streamlines are shown in Figure 4. For the conditions assumed, most of the fracture flow at depth came through the matrix near the upper boundary, indicating variable suction at the upper rock surface due to the relatively high transmissivity of the fracture. A conclusion from this analysis is that a permeable layer between the rock and plate should yield a more constant boundary at the rock surface and less interaction between the rock matrix and the fracture.

#### Laboratory Cylinder Tests

The application of the impeding layer approach within boreholes was investigated in the laboratory by cutting a cylinder of Apache Leap tuffaceous rock with an inside and outside diameter of 10 and 15 cm, respectively, and a length of 19.5 cm (Figure 5). A 10-cm, single tubular membrane was inserted into the rock cylinder and sealed at both ends. When water was added under pressure within the annulus of the synthetic borehole,  $P_o$ , the membrane expanded to make good hydraulic contact with the rock surface. The cylinder was then placed within a water reservoir to maintain a constant pressure at the outer rock surface,  $P_e$ . The rock sample was kept saturated throughout these tests. The flow rate through the membrane and rock cylinder was measured at selected applied pressures and the resulting pressure at the rock/membrane boundary,  $P_{mr}$ , was calculated. After preliminary tests of different types of membranes using small samples in a filter holder, a membrane was found which has an optimal hydraulic conductance. (The hydraulic conductance is defined as being the flow rate per unit cross-sectional area per unit head drop). The optimal value of membrane conductance was determined based on the rock hydraulic conductivity and reasonable applied pressures required to yield the desired  $P_{mr}$  range.

The hydraulic conductivity of the rock cylinder was measured using the setup of Figure 5 without a membrane. The calculated saturated hydraulic conductivity,  $K_{sat}$ , was  $2.31 \times 10^{-8} \text{ m s}^{-1}$ . Using the calculated saturated hydraulic conductivity, Figure 6 presents the calculated straight line relationship between flow and applied pressure difference,  $P_o - P_e$ , from near zero to 150 kPa. The calculation assumes that the rock hydraulic conductivity and the membrane conductance remain constant over the duration of the measurements. Figure 7 presents the observed injection rate as a function of the pressure difference across the membrane and cylinder. The membrane conductance is estimated as  $7.62 \times 10^{-8} \text{ s}^{-1}$  from these data. Figure 8 presents the calculated pressure at the membrane-rock interface,  $P_{mr}$ , as a function of the pressure difference across the membrane and the cylinder. Figure 9 presents the calculated pressure at the membrane-rock interface as a function of injection pressure,  $P_o$ , when the external pressure,  $P_e$ , is held at various values.

## Discussion

An approach for determining the unsaturated hydraulic properties of discrete fractures using in situ measurements in boreholes is under assessment. The parameter of interest in the current study is the determination of the matric suction above which fracture flow is not significant and only matrix flow needs to be considered. To obtain in situ measurements, two layers of low permeability material are placed next to the borehole wall and a positive fluid pressure is maintained within the annulus of the borehole. The impedance of the two layers and applied pressures must be matched to the expected range of permeabilities of the fractured rock and of matric suctions required. The approach can be used to obtain a distribution for the critical matric suction parameter, which is critical to the characterization of flow and transport systems in unsaturated fractured rock.

It is apparent from the analyses presented here that a negative pressure can be maintained inside the rock at the membrane surface, and large openings within the rock would desaturate if air was allowed to enter. Fractures intersecting the borehole will constitute the single largest source of large openings. The effects of flow through a fracture at various suctions is of greatest interest to this study. Experiments which incorporate a single discrete discontinuity of known aperture are ongoing.

Nine 10-cm diameter inclined boreholes have been drilled in slightly welded, fractured tuff at a 45 degree angle to facilitate the removal of oriented cores and to intersect vertical fractures. The locations of individual fractures along the boreholes were determined by core logging and confirmed using water and air injection tests. The saturated water permeability and the air permeability at existing matric suctions for three meter intervals along the boreholes range over five orders of magnitude. The lower values relate to the rock matrix permeability and the higher values relate to fracture permeabilities. To differentiate the flow through fractures from matrix flow, the dual membrane approach will be emplaced at selected intervals. Fracture flow should be distinguishable by a sharp change in the measured flow rate at the critical matric suction.

## References

- Hillel, D. and W.R. Gardner, 1970, "Measurement of unsaturated conductivity and diffusivity by infiltration through an impeding layer", *Soil Sci.*, 109:149.  
Rasmussen, T.C. and D.D. Evans, 1989, "Fluid flow and solute transport modeling through three-dimensional networks of variably saturated discrete fractures", *NUREG/CR-5239*, 193 pp.

## Acknowledgements

Funding for this research was provided by the U.S. Nuclear Regulatory Commission, Office of Nuclear Regulatory Research, Division of Engineering, FIN D1662 and G1112. The NRC project technical monitor was Thomas J. Nicholson. Several graduate students, including Jinshan Tang, William Haldeman, and Yueh Chuang, contributed substantially to this work.

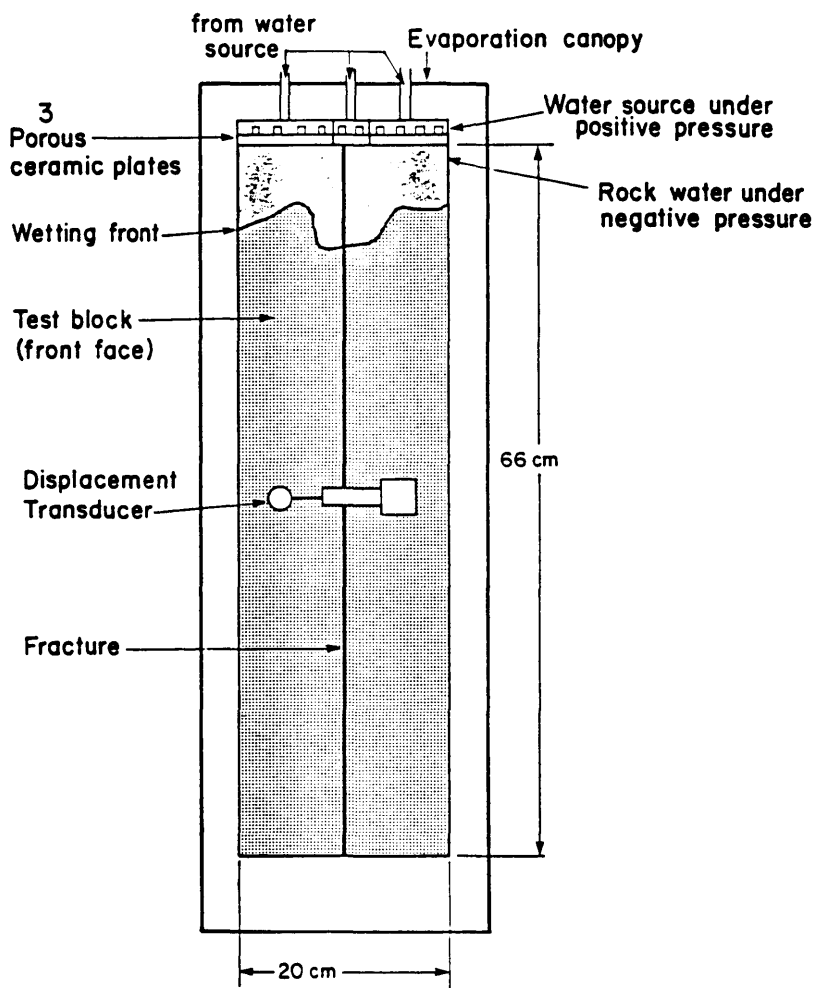


Figure 1: Laboratory setup for determining unsaturated hydraulic properties of fractured rock showing ceramic impedance plates and sketch of wetting front advance when applied matrix suction is insufficient to induce fracture flow.

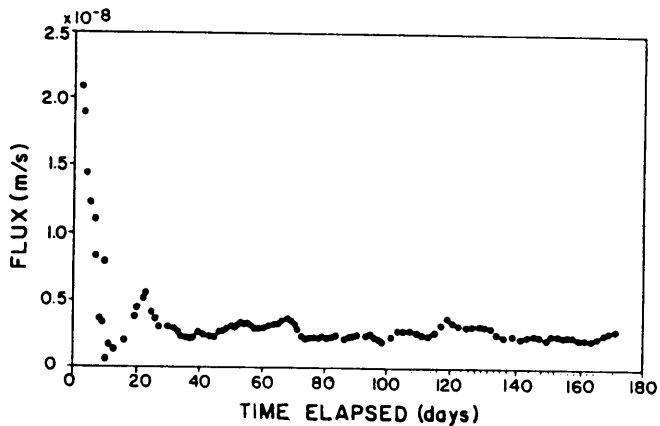


Figure 2: Water intake rate from the plate over the fracture.

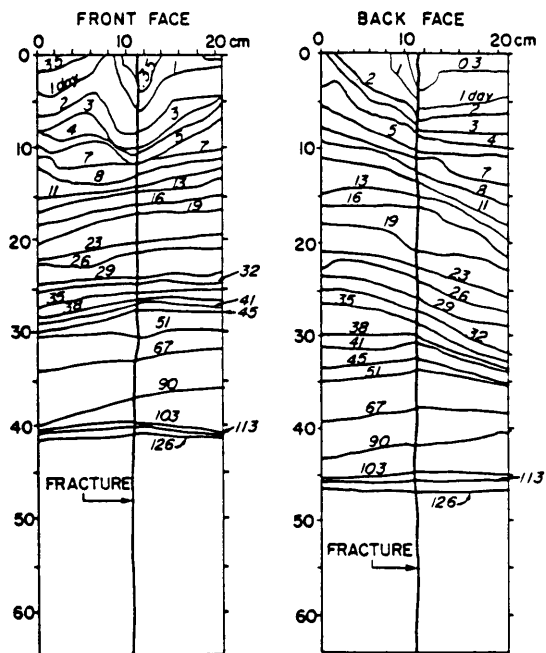


Figure 3: Wetting front vs. time (days). Matric suction at the upper boundary equals 1.5 kPa (15 cm). Note that the fracture does not significantly influence the wetting front pattern.

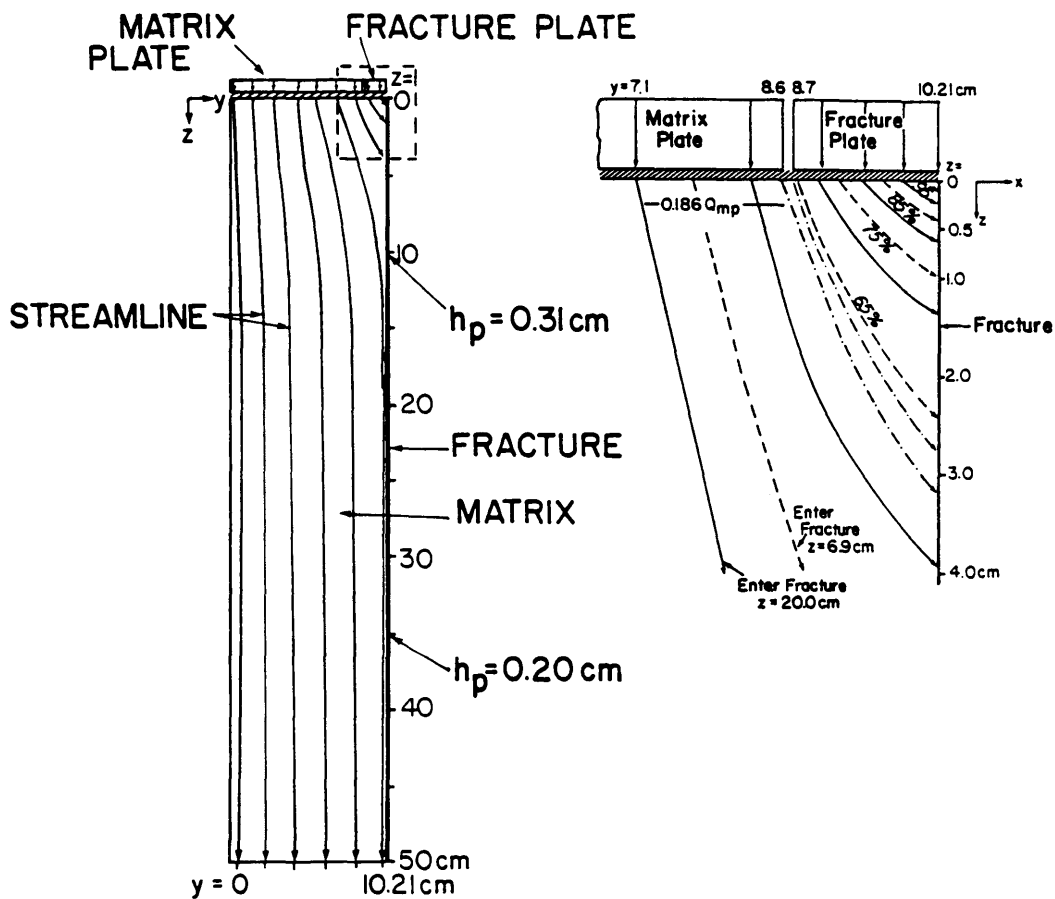


Figure 4: Streamline pattern showing fracture-matrix-plate interaction.



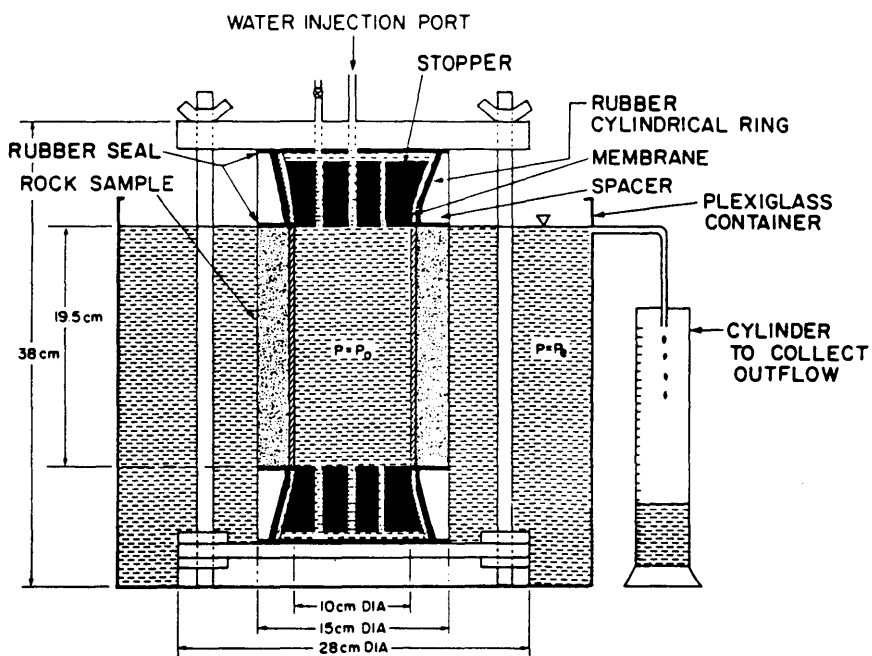


Figure 5: Experimental setup cross-section for rock cylinder hydraulic conductivity and membrane conductance.

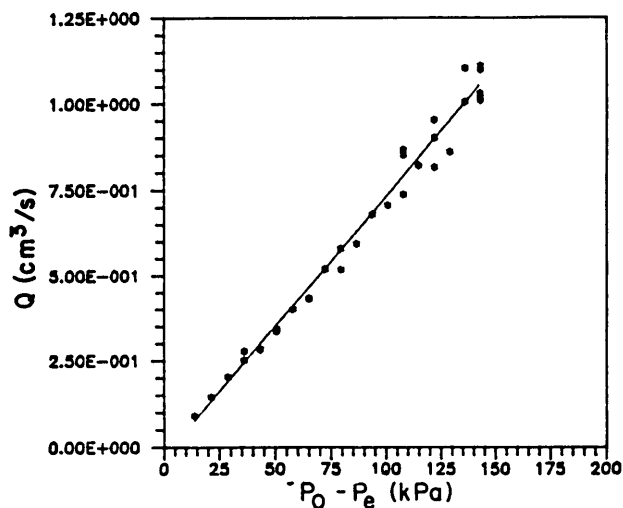


Figure 6: Injection rate ( $Q$ ) vs. injection minus external pressure ( $P_o - P_e$ ) for rock cylinder only. Calculated  $K_{int} = 2.31 \times 10^{-8} \text{ m s}^{-1}$  (approximately 2.3 millidarcys).

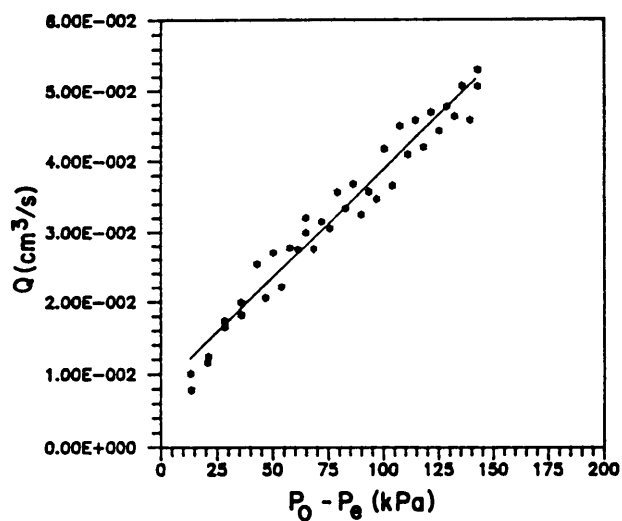


Figure 7: Injection rate ( $Q$ ) vs. injection minus external pressure ( $P_o - P_e$ ) for membrane and cylinder. Calculated membrane conductance equals  $7.62 \times 10^{-8} \text{ s}^{-1}$  (approximately 23 millidarcys).

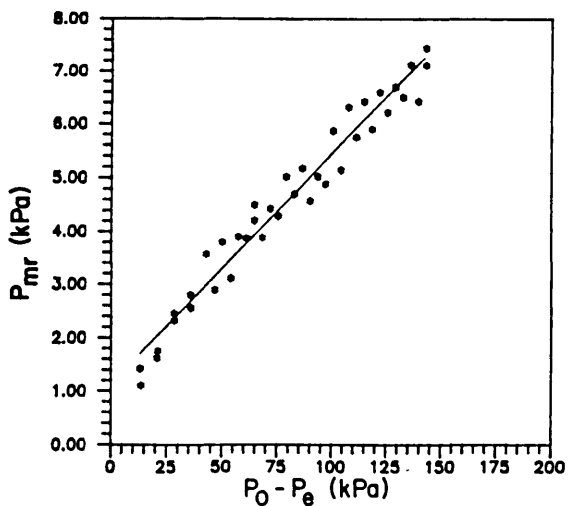


Figure 8: Calculated pressure at the membrane-rock interface ( $P_{mr}$ ) vs. injection minus external pressure ( $P_o - P_e$ ) for membrane and cylinder.

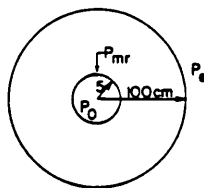
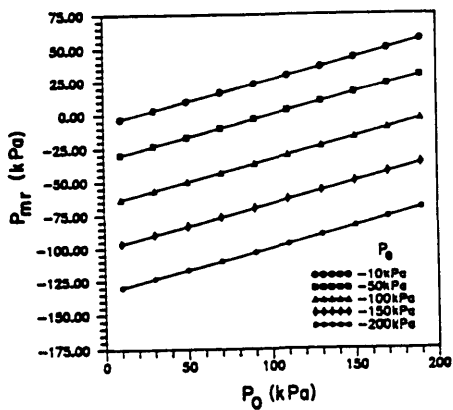


Figure 9: Calculated pressure at the membrane-rock interface ( $P_{mr}$ ) vs. injection pressure ( $P_o$ ) when the external pressure ( $P_e$ ) is held constant.



EVALUATION OF AQUIFER PARAMETERS AND WELL  
CHARACTERISTICS IN FRACTURED ROCK FORMATIONS  
IN KARNATAKA, INDIA

B.B.S. Singhal and D.C. Singhal  
University of Roorkee  
Roorkee, India

Abstract: The Karnataka State in South India suffers from occasional droughts after every two or three years. The region is comprised of a variety of hard rock formations: viz, granite-gneisses, charnockites, basalts, limestones, greywackes, and schists. Pumping tests were conducted on wells tapping different geological formations to evaluate formation characteristics. The double-porosity model suggested by Streltsova-Adams (1978) for heterogeneous confined aquifers appears to give satisfactory results. The transmissivity of the fractures ( $T_f$ ) is much higher for all types of formations as compared with that of blocks. The fracture transmissivity in gneisses, basalts, charnockites, and limestones is usually higher (105 to 250 m<sup>2</sup>/d) than in greywackes (15 to 50 m<sup>2</sup>/d). The storativity ( $S_f$ ) of fractures is smaller ( $10^{-3}$  to  $10^{-6}$ ) than that of blocks ( $S_b$ ) ( $10^{-2}$  to  $10^{-3}$ ).

Specific capacity of dug wells, tapping weathered shallow fractured horizons in basalts, granitic gneisses, and limestones is in the range of 15.5 to 523.6 l/min/m, while specific capacity index (specific capacity per unit surface area) is in the range of 0.16 l/min/m<sup>2</sup>. The specific capacity values of borewells tapping deeper fractures in basalts and limestones are higher (in the range of 15 to 1050 l/min/m) than greywackes and gneisses.

The computation of spacing for borewells has been carried out using two approaches: (1) the radius of influence approach, and (2) from recharge considerations. The former approach suggests spacing of 100-380 m, while the recharge approach indicates a range of 190 to 490 m, with density of wells varying from six to 35 wells/km<sup>2</sup>.

From the present studies, it is found that borewells are preferable to both dug wells and dug-cum-bore wells in terms of cost of groundwater.

### Introduction

The State of Karnataka in South India faces frequent droughts due to the failure of monsoons, resulting in increased water demands and drying up of shallow dug wells in many parts of the state. This has led to a greater demand of borewells, which have been drilled indiscriminately in large numbers, resulting in the over-exploitation of groundwater at some places. Therefore, it is necessary to study the aquifer characteristics to determine the feasibility of various types of wells, especially borewells, their optimal spacing, and other characteristics.

### Hydrogeology

The State of Karnataka is composed mainly of crystalline rocks of Precambrian age. The principal rock types are granites, charnockites, greywackes, schists, limestones, and basalts. The granites, gneisses, charnockites, greywackes, and schists belong to the Dharwar supergroup of Precambrian age. The limestones belong to the Bhima group of upper Precambrian age, and basalts are part

of the Deccan Trap volcanic suite of rocks of lower Tertiary age. These rocks are fractured and weathered to varying extent, imparting secondary porosity which is responsible mainly for storing and transmitting groundwater.

The depth of large diameter dug wells is usually ten to 15 m. In recent years, small diameter (seven to 15 cm) borewells of depths of 30 to 80 m have become more common and are drilled by down-the-hole hammer (DTH) rigs. The borewells are a better source of assured water supply, especially during summer season and drought periods.

#### Hydraulic Characteristics of Aquifers

Aquifer performance tests were carried out on borewells constructed in different formations in 12 well fields for determining aquifer characteristics. The drawdown and recovery data were observed both in the pumped wells and in the observation wells.

Figure 1 shows the time-drawdown plots in an observation well in Srinivas Saradgi village, tapping a basaltic aquifer. The data curve was matched with Theis' type curve for homogeneous confined aquifers, Hantush's type curve for leaky confined aquifers, Boulton's type curve for unconfined aquifers, and Streltsova's type curve for fractured aquifers. Keeping in mind the fractured nature of the aquifer and drawdown pattern as well as a better match with the Streltsova's type curves, the aquifer characteristics have been computed using the method of Streltsova-Adams (1978) (Figure 1).

In general, the transmissivity values obtained from pumped wells are lower than those obtained from observation wells. In pumped wells, the apparent transmissivity is likely to be lower, due to drawdown resulting from well losses and dewatering of fractures. Therefore, the time drawdown data from pumped wells may not give representative values of transmissivity. Accordingly, the values of transmissivity, storage coefficient, and other hydraulic parameters computed from observation well data are more representative.

The computed hydraulic parameters from different well fields are given in Table 1. The results show that the transmissivity of fractures in greywackes is lower than in basalts, gneisses, and limestones.

#### Specific Capacity

The specific capacity of wells was determined from pumping tests. The values are quite variable in different geological formations. In limestones, the specific capacity of borewells ranges from 15 to 1050 l/min/m, in basalt 475-523 l/min/m, and is low (27-98 l/min/m) in granitic gneisses and charnockites. The wide range of specific capacity in limestones may reflect the extent to which solution cavities are developed.

Angadi (1986) and Qadir (1989) computed specific capacity of large diameter wells tapping different formations in Bijapur, Belgaum, and Bangalore districts. For the sake of comparison, they also considered concepts of unit area specific capacity (Narasimhan, 1965) and specific capacity index (Singhal, 1973). The specific capacity divided by the cross-sectional area of the well gives unit area specific capacity. When two wells of different diameters are pumped at the same

Table 1. Hydraulic parameters computed from aquifer performance tests by the double-porosity model method

| Site No. | Location & Formation                    | Well a | Transmissivity of Fractures (m <sup>2</sup> /day) | Storage Coefficient  |                      | Characteristic of Fracture Block Flow (day <sup>-1</sup> ) |                      | Transmissivity in Vertical Direction (m <sup>2</sup> /day) |
|----------|---|--------|---|----------------------|----------------------|--|----------------------|--|
|          |   |        |   | S <sub>f</sub>       | S <sub>b</sub>       | 1  | T <sub>f</sub>       |  |
| 1        | Anchatgiri, Dharwar (Greywacke)         | PW     | 2.6   | ---                  | ---                  | ---  | ---                  | ---  |
|          |   | OW     | 16.5  | 6.2x10 <sup>-3</sup> | 5.6x10 <sup>-2</sup> | 3.2x10 <sup>-3</sup>                                       | 1.8x10 <sup>-4</sup> |  |
| 2        | Yanakarni, Belgaum (Basalt)             | PW     | 0.6   | ---                  | ---                  | ---  | ---                  | ---  |
|          |   | OW     | 26.1  | 2.0x10 <sup>-4</sup> | 1.8x10 <sup>-3</sup> | 7.8  | 1.4x10 <sup>-2</sup> |  |
| 3        | Ambadgatti, Belgaum (Greywacke)         | PW     | 11.8  | ---                  | ---                  | ---  | ---                  | ---  |
|          |   | OW     | 44.8  | 5.8x10 <sup>-3</sup> | 5.8x10 <sup>-3</sup> | 21.8   | 1.3x10 <sup>-4</sup> |  |
| 4        | Sirsi, Karwar (Latterite and Greywacke) | OW1    | 40.2  | 5.5x10 <sup>-2</sup> | 0.5                  | 6.4x10 <sup>-3</sup>                                       | 3.1x10 <sup>-3</sup> |  |
|          |   | OW2    | 23.8  | 9.0x10 <sup>-3</sup> | 8.1x10 <sup>-2</sup> | 2.8x10 <sup>-2</sup>                                       | 2.2x10 <sup>-3</sup> |  |
| 5        | Tonidkatti, Belgaum                     | OW1    | 117.5   | 8.2x10 <sup>-2</sup> | 0.7                  | 6.4x10 <sup>-2</sup>                                       | 4.7x10 <sup>-2</sup> |  |
|          |   | OW2    | 111.9   | 5.1x10 <sup>-2</sup> | 0.5                  | 1.9x10 <sup>-4</sup>                                       | 8.9x10 <sup>-3</sup> |  |
| 6        | Harthi Dharwar (Metabasalt)             | PW     | 1.2   | ---                  | ---                  | ---  | ---                  | ---  |
|          |   | OW     | 63.3  | 6.8x10 <sup>-3</sup> | 6.1x10 <sup>-2</sup> | 1.7x10 <sup>-2</sup>                                       | 1.0x10 <sup>-3</sup> |  |

Table 1--Continued

|    |   |                  |                         |                      |  |                      |  |     |  |     |  |
|----|---|------------------|-------------------------|----------------------|--|----------------------|--|-----|--|-----|--|
| 7  | Vadagur, Kolar<br>(granitic<br>gneiss)                | PW<br>OW         | 1.9<br>251.8            | ---                  | 2.3x10 <sup>-3</sup>                         | ---                  | 2.1x10 <sup>-2</sup>                         | --- | 26.4   | --- | 5.5x10 <sup>-1</sup>                         |
| 8  | Bylore, Mysore<br>(Charnockites)                      | PW<br>OW1<br>OW2 | 45.8<br>104.6<br>10.46  | ---                  | 2.9x10 <sup>-3</sup><br>5.8x10 <sup>-4</sup> | ---                  | 2.6x10 <sup>-2</sup><br>5.2x10 <sup>-3</sup> | --- | 8.4x10 <sup>-2</sup><br>2.1x10 <sup>-1</sup> | --- | 2.2x10 <sup>-3</sup><br>1.1x10 <sup>-3</sup> |
| 9  | Kinnikambla,<br>S. Kanara<br>(Laterite and<br>Gneiss) | PW<br>OW1<br>OW2 | 9.6<br>8.6<br>9.1       | ---                  | 4.2x10 <sup>-3</sup><br>1.2x10 <sup>-4</sup> | ---                  | 3.8x10 <sup>-4</sup><br>1.2x10 <sup>-3</sup> | --- | 352.7<br>68.7                                | --- | 2.3x10 <sup>-1</sup><br>7.9x10 <sup>-1</sup> |
| 10 | Guddathahalli<br>Bangalore<br>(Granitic<br>Gneiss)    | OW               | 210.5                   | 1.6x10 <sup>-4</sup> | 1.4x10 <sup>-3</sup>                         | 432.0                | 6.0x10 <sup>-1</sup>                         |     |  |     |  |
| 11 | Srinivas Sarad-<br>gi, Gulbarga<br>(Basalt)           | PW<br>OW1<br>OW2 | 233.0<br>738.8<br>741.5 | ---                  | 4.3x10 <sup>-4</sup><br>7.1x10 <sup>-4</sup> | ---                  | 3.8x10 <sup>-3</sup><br>6.4x10 <sup>-3</sup> | --- | 21.6<br>17.2                                 | --- | 8.2x10 <sup>-2</sup><br>0.11                 |
| 12 | Narbanda,<br>Raichur<br>(Granite)                     | OW               | 154.1                   | 9.2x10 <sup>-4</sup> | 9.1x10 <sup>-2</sup>                         | 7.9x10 <sup>-2</sup> | 7.2x10 <sup>-3</sup>                         |     |  |     |  |
| a  |   | PW:              | Pumping Well            | OW:                  | Observation Well                             |                      |  |     |  |     |  |



rate, a large diameter well would yield a greater quantity of water for a given drawdown, and thus withstand longer hours of pumping than a well of small diameter. Therefore, unit area specific capacity is a better indicator of the performance of the well. Singhal (1973) suggested that specific capacity of a well divided by the total surface area ( $2\pi rh$ ) of the aquifer tapped by the well would incorporate variations in well diameter as well as saturated thickness, and will give an improved idea of the performance of wells having different diameters and depths. The ranges of these parameters for dug wells in different formations are listed in Table 2.

### Spacing of Wells

In order to avoid the overexploitation of groundwater, it is necessary to provide certain criteria for optimum spacing of wells so that there is a balance between recharge and withdrawal within reasonable limits.

Two approaches have been used to evaluate well spacing. One uses the pumping test data to develop a graphical relationship between the duration of pumping and corresponding radii of influence in different geological terrains, using groundwater flow equations. The second approach is based on groundwater recharge to arrive at density of wells such that the total draft does not exceed the annual groundwater recharge.

The presently applicable norms of minimum spacing between adjacent borewells for the purpose of funding by government agencies are uniform for granular and fractured aquifers. In view of the different characteristics of unconsolidated and crystalline rock formations, it is necessary to evaluate the minimum spacing between wells in hard rock surfaces.

Therefore, an attempt was made to use the Theis equation to compute the stabilized drawdown which would be substituted in Thiem's formula to calculate the radius of influence of a pumped well. The aquifer characteristics (transmissivity and storativity) used in the calculation were evaluated by the double-porosity model of Streltsova-Adams (1978). In computing the radius of influence of the fractured aquifer,  $T_1$  was assumed to be the aquifer transmissivity and  $S_1$  the aquifer storage coefficient. The radius of influence was evaluated using different discharges (ranging from 200 m<sup>3</sup>/day to 2000 m<sup>3</sup>/day).

According to this method, the well spacing was computed to range from 110 to 382 m (Table 3).

In order to avoid overdevelopment in an area, the groundwater draft should not exceed the groundwater recharge to avoid lowering of water levels. This criterion was also used to determine well spacing and density of wells.

Table 3 is a summary of the well spacing and maximum density of wells using the above-mentioned two approaches. It is seen that well spacing evaluated from the recharge approach gave a range of values from 190 to 492 m, with the maximum density of wells in the range of five to 35 wells/km<sup>2</sup>.

The recharge method may be considered better in deciding the well spacing because it also accounts for groundwater recharge. The values obtained from the above two methods can, however, be used to complement each other, i.e., the radius

Table 2. Specific capacity of dug wells in different formations

| Formation | Specific Capacity<br>$C$<br>(l/min/m) | Unit Area Specific<br>Capacity - $C/\text{Area}$<br>(l/min/m/m <sup>2</sup> ) | Specific Capacity<br>Index<br>$C/2\pi rh$<br>(l/min/m/m <sup>2</sup> ) |
|-----------|---------------------------------------|---|--|
| Basalt    | 29.4-364                              | 0.35-5.04   | 0.16-3.02  |
| Limestone | 30.4-348                              | 0.53-19.83  | 0.16-14.14   |
| Shale     | 28.4-39.3                             | 0.53-1.22   | 0.26-0.37  |
| Gneiss    | 15.5-228.6                            | 0.23-10   | ---  |
| Sandstone | 54.3                                  | 0.97  | 0.60   |
| Latrite   | 582.2                                 | 12.57   | 5.10   |

Table 3. Well spacings in different formations

| Formation                          | <u>Radius of Influence Approach</u><br>Well Spacing (m) | <u>Recharge Approach</u> |  |
|------------------------------------|---|--------------------------|--|
|                                    |   | Well Spacing<br>(m)      | Well Density<br>(per km <sup>2</sup> ) |
| Greywackes                         | 110-136   | 224-448                  | 6 to 25                                |
| Basalt and related<br>rocks        | 170-256   | 370-417                  | 7 to 9                                 |
| Limestones                         | 126   | 415                      | 7                                      |
| Gneisses/Granites/<br>Charnockites | 134-382   | 191-492                  | 5 to 35                                |
| Laterites<br>(coastal areas)       | 130-275   | 190-225                  | 25 to 35                               |

of influence approach for spacing between adjoining wells and the rainfall recharge approach can be used to decide the density of wells in an area.

### Well Economics

In the present study, an attempt was also made to determine the total cost of well construction, pumping equipment, and the energy consumption for withdrawing water from different types of wells. A graph is plotted between the total cost (in Indian rupees) per m<sup>3</sup> of water versus the annual groundwater withdrawal (Figure 2). The figure shows that for groundwater discharge up to 22,000 m<sup>3</sup>/day, dug wells are generally more economical than borewells and dug-cum-borewells. However, for higher discharges, the borewells seem to be marginally more economical than dug-cum-borewells and dug wells. It should be mentioned that there is a large scatter of plots for borewells and the fitting curve is approximate. One of the reasons for the large scatter of plots for borewells may be that this type of well taps varying numbers of fractures at different depths resulting in varying discharges. However, a trend is still discernible, which indicates better economics for borewells than for dug-cum-borewells.

In most cases, dug-cum-borewells are constructed by drilling in the bottom of existing dug wells to revitalize them; therefore, they are likely to be more economical than shallow borewells, if the cost of construction of dug wells is excluded from these calculations. The dug-cum-borewell will also be a dependable source of water in drought periods when water in open dug wells is no longer available. For new groundwater structures, borewells are expected to be more economical than other types for obtaining large discharges, while dug-cum-borewells can be suitable for revitalized structures.

The above conclusions are not in agreement with the studies made by Subramanyam and Shankar (1979), who recommended dug wells and dug-cum-borewells as ideal groundwater structures for irrigation purposes, especially for marginal farmers. However, according to Radhakrishna et al. (1974), Reddy (1975), and Campbell (1981), borewells are better suited structures for irrigation purposes than dug wells. The investigations carried out by the Central Ground Water Board (CGWB), Government of India, under the Vedavati Project (CGWB, 1980) showed that dug wells and borewells cost more or less the same; however, the relative yield from borewells is approximately 6 1/2 times more than from dug wells. A comparative statement of cost benefit ratio of dug and borewells studied in the CGWB project area indicates that the average investment cost per m<sup>3</sup> of water per year is 1.46 Indian rupees for dug wells as compared to 0.36 rupees for borewells, thereby indicating that borewells are more economical than dug wells.

### Conclusions

From the above studies, it can be concluded that in the fractured aquifers of Karnataka State, India, the double-porosity model of Streltsova-Adams may be used satisfactorily for computing hydraulic characteristics.

Specific capacity of borewells and open dug wells indicates low productivities of wells in charnockites and shales in comparison to those in limestones, gneisses, and basalts.

Well spacing, computed for different geological formations by using the radius of influence approach and the rainfall recharge approach, was found to range from 110 to 380 m and from 190 to 490 m, respectively. The maximum density of wells was found to range from five to 35 wells per km<sup>2</sup>. These two methods can be used to complement each other for deciding well spacings.

These studies also indicated the economic viability of deep borewells and dug-cum-borewells over open dug wells in terms of cost of groundwater and its availability.

### References

- Angadi, K.S., 1986, Hydrogeological studies of the lower parts of Ghataprabha Basin, Belgaum and Bijapur districts of Karnataka, India, Ph.D. Thesis (unpublished), University of Roorkee, Roorkee, India, 250 p.
- Campbell, M.D., 1981, Economic consideration on groundwater exploration and development in igneous and metamorphic rocks, International Seminar on Ground Water in Hard Rocks, UNESCO Report, Coimbatore, India, p. 105.
- CGWB, 1980, Groundwater studies in the Vedavati River basin-parts of Karnataka and Andhra Pradesh, Unpublished Report, CGWB, p. 49.
- Narasimhan, T.N., 1965, On testing open wells, *Indian Geohydrology*, I, pp. 101-105.
- Qadir, A., 1989, Specific capacity of dug wells in Devanahalli Taluk, Bangalore District, Karnataka State, M.E. Special Problem (unpublished), University of Roorkee, Roorkee, India.
- Radhakrishna, B.P., et al., 1974, Groundwater development in hard rocks of Karnataka State, India, Government of Karnataka, Department of Mines and Geology, Bangalore, *Ground Water Studies*, 150, pp. 1-5.
- Reddy, B.B., 1975, A comparative study of drilled wells and dug wells, Government of Karnataka, Department of Mines and Geology, Bangalore, *Ground Water Studies*, 163, pp. 4-6.
- Singhal, B.B.S., 1973, Some observation on the occurrence, utilization, and management of groundwater in the Deccan trap areas of Central Maharashtra, India, Proceedings of International Symposium on the Development of Groundwater Resources, Madras, 3, pp. 75-81.
- Streltsova-Adams, T.D., 1978, Well hydraulics in heterogeneous aquifer formations, (in) Chow, V.T. et al., *Advances in Hydrosociences*, 11, pp. 357-423.
- Subramanyam, C.V., and B.N. Shankar, 1979, A comparative analysis of open dug wells vs. borewells for irrigation in Mandya District, Government of Karnataka, Department of Mines and Geology, Bangalore, *Ground Water Studies*, 199, p. 12.

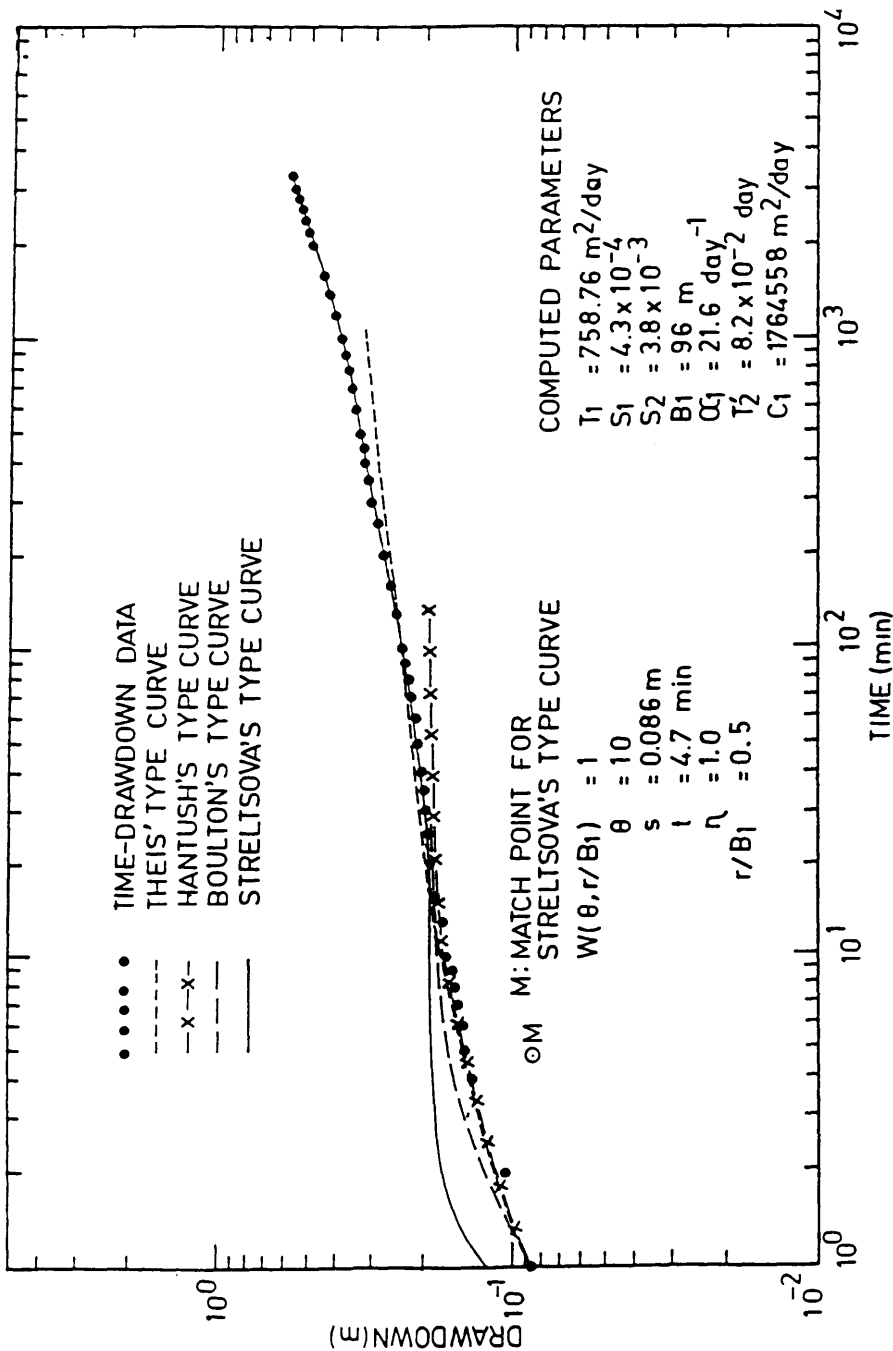


FIG.1\_ TIME DRAWDOWN CURVE FOR AN OBSERVATION WELL IN BASALTIC AQUIFER IN VILLAGE SRINIVAS SARADGI , KARNATAKA STATE , INDIA

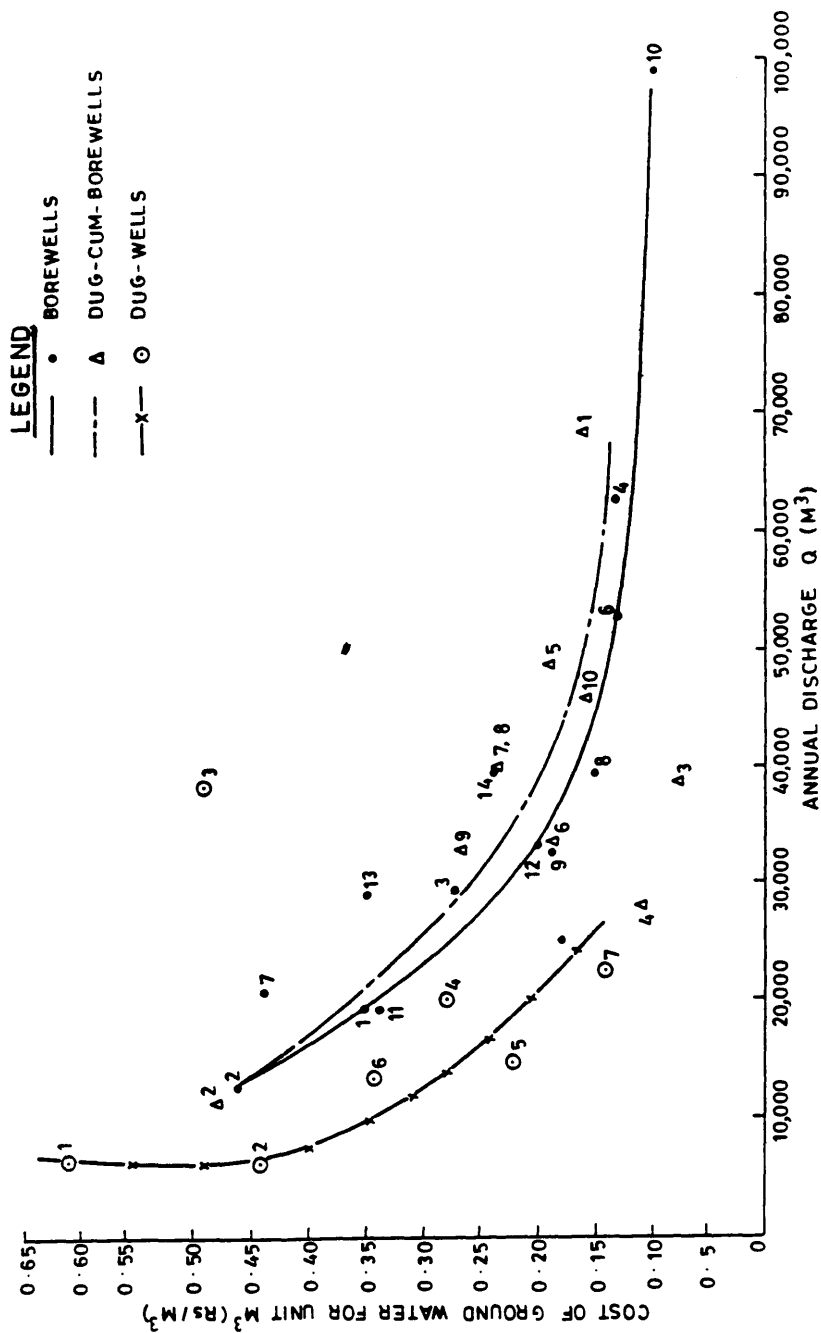


FIG. 2 PLOT OF COST PER UNIT VOLUME OF GROUNDWATER Vs ANNUAL DISCHARGE FOR DIFFERENT GROUNDWATER STRUCTURES



SECTION 6: WATER MANAGEMENT



## DYNAMIC MANAGEMENT OF SURFACE AND GROUNDWATER HYDROLOGIC SYSTEMS

Nathan Buras, Ph.D.

Department of Hydrology and Water Resources  
University of Arizona, Tucson, AZ 85721

**ABSTRACT:** Effective management of regional water resources must account for the dynamic character of hydrologic systems and formulate policies based on this attribute. When operated conjunctively, surface streams and groundwater aquifers can meet regional demands for water in a technically optimal fashion. The management model presented below features an irrigated area overlaying an aquifer, and the aquifer may function as both a source of water and as storage facility. The dynamic characteristics of the regional hydrologic system which included surface supply are captured by a dynamic programming formulation. Because the movement of groundwater is orders of magnitude slower than surface flows, I used a simulation model to estimate the response of the aquifer to pumping or to recharge, and integrated the results of the simulation into the dynamic programming framework. Writing a benefit function for each period of operation as a function of surface supplies, groundwater pumpage and recharge, I formed a Lagrangian expression that included a storage capacity constraint of the aquifer. The Lagrangian Multiplier is the value of the water stored in the aquifer during the period in question.

### Introduction

Proper water resource management requires making trade-offs between competing demands. Although the nature of the competing demands in a developing society differs from those in a more complex, established one, methodologies to resolve the conflict and maximize satisfaction are the same. In developing societies most demands result from the need for increasing economic growth through agriculture, hydropower, production, and technology. Costs of structures, policies, and institutions to provide reliable supplies of water to these societies must be evaluated in light of the economic benefits to be derived from both the additional water available and the associated increased reliability. Furthermore, the rush to develop today must be balanced by the need to insure a basis for a sustained economy tomorrow. It is therefore imperative that a successful method of managing water resources possesses the capacity to balance competing demands so that the final operating policy optimizes the net benefit of the region, as perceived by that society. The problem then is how to meet regional demands for water in an optimal fashion. An attractive and viable alternative is to develop and manage conjunctively surface supplies and groundwater aquifers.

### A Systems Approach

Empirical analysis of optimal conjunctive management has been performed using several mathematical programming techniques. Linear programming methods have been used to analyze a broad range of problems, including the operation of injection systems in the arid Southwest (Gisser 1970). Gorelick (1983) reviewed the use of systems analytical techniques, mostly linear programming, that incorporated the response of the physical system (the aquifer) in models reflecting management decisions. The advantage of linear programming formulations is that the existing software packages enable us to solve a variety of models. The disadvantages is that these formulations are mostly static and

deterministic.

Dynamic programming formulations were used by several workers (Buras 1963, 1985; Loucks et al. 1981), and these models, because of the dimensionality problem inherent in dynamic programming, restricted the specification of the ground and surface water subsystems to low-dimension representations. In order to overcome the "curse of dimensionality" of dynamic programming, optimal control models were proposed (Noel and Howitt, 1982). In these models, the linearized output of hydrologic and economic models is combined in a discrete time, linear, quadratic control formulation. They have two significant advantages. First, they represent the direct interaction between a complex hydrologic system and the demand for water. Second, the model can be solved by any one of several algorithms. A shortcoming of the model is its lack of sufficient flexibility when used to evaluate empirically alternative water policies and institutions.

#### A Dynamic Programming Framework

Dynamic programming (Bellman, 1957) was used quite extensively in water resources engineering, especially in surface hydrology (Buras, 1966). However, the integration of groundwater hydrology within a dynamic programming formulation of a surface source raises the issue of the different effects that time has on surface and groundwater components. Whereas the changes produced in a surface reservoir, due to either man's intervention or to natural events (stream-flow, for example) tend to disappear generally within one yearly cycle, man's actions - especially vigorous pumping - tend to have more persistent effects in aquifers. Thus, to represent more accurately the behavior of an aquifer, the effects of pumping and/or of recharge must be carried over a number of stages, thus increasing the dimensionality of the problem. Within relatively few stages, the computational burden becomes unwieldy. To overcome this difficulty, a somewhat modified approach is taken as shown subsequently: the groundwater component is embedded within a dynamic programming formulation of the surface component.

The overall dynamic programming framework uses the following notation.

|             |   |
|-------------|---|
| $Q_t$       | -seasonal inflow into a surface reservoir, season $t$ , $t = 1, 2, 3$ .   |
| $Q_{it}$    | -inflow magnitudes in season $t$ , $i = 1, 2, \dots$  |
| $Q_{j,t+1}$ | -inflow magnitudes in season $t + 1$ , $j = 1, 2, \dots$  |
| $P_{ij}^t$  | -conditional probabilities that inflow $j$ will occur in season $t + 1$ , given that inflow $i$ occurred in season $t$ .      |
| $S_{l,t+1}$ | -final storage in surface reservoir in season $t$ (identical with initial storage in season $t + 1$ ), $l = 1, 2, \dots$      |
| $S_{kt}$    | -initial storage in surface reservoir in season $t$ , $k = 1, 2, \dots$   |
| $R_t$       | -reservoir release in season $t$ , composed of $D_t$ , direct uses (e.g., irrigation) and $x_t$ , groundwater recharge. Thus, |

$$R_t = D_t + x_t \quad (1)$$

- $E_{klt}$  - evaporation and seepage losses from surface reservoir in season  $t$ ; a function of initial and final storage.
- $C_t$  - average natural recharge of groundwater in season  $t$ .
- $G_{mt}$  - initial groundwater availability in season  $t$  (as measured by depth to water table).
- $G_{n,t+1}$  - final groundwater availability in season  $t$  (identical with initial availability in season  $t + 1$ , as measured by depth to water table).
- $\pi_t$  - groundwater pumpage in season  $t$ .
- $L_{mnt}$  - groundwater losses, primarily to deep percolation, in season  $t$ ; a function of initial and final water table levels.

The model must reflect the following constraining elements:

- $K$  - active storage capacity of surface reservoir.
- $\Gamma$  - "active storage capacity" of aquifers.

The following continuity conditions must be satisfied:

For the surface component

$$R_{kilt} = S_{kt} + Q_{it} - E_{klt} - S_{l,t+1} \quad \forall k, i, t: l \text{ feasible} \quad (2)$$

For the groundwater component

$$\pi_{mnt} = G_{mt} + C_t + x_t - L_{mnt} - G_{n,t+1} \quad \forall m, t; n \text{ feasible} \quad (3)$$

Equation (1) links the two components in the sense that  $x_t$  volume units of water released from the surface reservoir are recharged artificially into the aquifer in season  $t$ . The decision regarding the magnitude of  $x_t$  should be based primarily on hydrologic - economic considerations. Here, however, the analysis will be limited to physical quantities - a relatively recent approach (Loucks et al., 1981; Buras, 1985).

The exclusion of economic considerations at this point necessitates the formulation of a measure of system performance in physical terms alone. To do so, one needs to define targets to be attained during the operation of the system expressed in physical quantities. The following targets are defined.

- $T_t^S$  - final surface storage in season  $t$ .
- $T_t^G$  - final water table level in season  $t$ .
- $T_t^R$  - surface water releases in season  $t$ .
- $T_t^\pi$  - groundwater pumping in season  $t$ .

The operation of the system as a multi-stage decision process will yield quantities different from targets. The measure of system performance (to be minimized, in this case) will be the sum of squares of the deviations of the actual quantities from their above targets. Denote this measure of performance as  $B_{kiltmt}$ .

Define now

$f_t^n(k, i, m)$  - total minimum expected value of system performance with  $n$  periods (seasons) remaining in its operation (including the current season  $t$ ), given that the initial surface storage is  $S_{kt}$ , the water table level is equivalent to  $G_{mt}$ , the inflow in season  $t$  is  $Q_{it}$ , and pursuing an optimal policy.

Thus, for one season remaining in the operation of the systems.

$$f_3^1(k, i, m) = \min_{\ell, n} \{B_{kiltm3}\}, \quad \forall k, m, i; \ell, n \text{ feasible for given } k, m, i. \quad (4)$$

In general,

$$f_t^n(k, i, m) = \min_{\ell, n} \{B_{kiltmt} + \sum_j p_{ij}^t \cdot f_{t+1}^{n-1}(\ell, j, n)\} \quad \forall k, m, i; \ell, n \text{ feasible};$$

$$n = 1, 2, \dots$$

$$t = 1, 2, 3. \quad (5)$$

Were the measure of system performance,  $B$ , defined in economic (rather than physical) terms and the optimization criterion were the maximization of (net) benefits, equation (5) would be re-written as

$$f_t^n(k, i, m) = \max_{\ell, n} \{B_{kiltmt} + (1 + r)^{-1} \sum_j p_{ij}^t \cdot f_{t+1}^{n-1}(\ell, j, n)\}$$

$$\forall k, m, i; \ell, n \text{ feasible};$$

$$n = 1, 2, \dots, t = 1, 2, 3. \quad (6)$$

where  $r$  is the interest rate.

#### Simulation of the Groundwater Subsystem

An important item of information for the manager of a regional water resources system is a functional relationship that links seasonal pumpage (and/or recharge) to the corresponding fluctuations of the water table (piezometric surface) averaged over the entire area of the aquifer. Thus,

$$S_t = f(Q_t) \quad (7)$$

where  $S_t$  is the average drawdown (rise) of the water table in season  $t$  due to pumpage (recharge)  $Q_t$ .

Considering the year to be divided into three seasons and looking ahead over a span of three years, equation (7) was re-written as follows, taking into

account the possible persistence of pumping (recharge) effects beyond any one season.

$$\begin{aligned}
 B_1 Q_1 &= S_1 \\
 B_1 Q_2 + B_2 Q_1 &= S_2 \\
 B_1 Q_3 + B_2 Q_2 + B_3 Q_1 &= S_3 \\
 B_1 Q_4 + B_2 Q_3 + B_3 Q_2 + B_4 Q_1 &= S_4 \\
 B_1 Q_5 + B_2 Q_4 + B_3 Q_3 + B_4 Q_2 + B_5 Q_1 &= S_5 \\
 B_1 Q_6 + B_2 Q_5 + B_3 Q_4 + B_4 Q_3 + B_5 Q_2 + B_6 Q_1 &= S_6 \\
 B_1 Q_7 + B_2 Q_6 + B_3 Q_5 + B_4 Q_4 + B_5 Q_3 + B_6 Q_2 + B_7 Q_1 &= S_7 \\
 B_1 Q_8 + B_2 Q_7 + B_3 Q_6 + B_4 Q_5 + B_5 Q_4 + B_6 Q_3 + B_7 Q_2 + B_8 Q_1 &= S_8 \\
 B_1 Q_9 + B_2 Q_8 + B_3 Q_7 + B_4 Q_6 + B_5 Q_5 + B_6 Q_4 + B_7 Q_3 + B_8 Q_2 + B_9 Q_1 &= S_9
 \end{aligned} \tag{8}$$

where  $B_t$  are coefficients that connect  $S_t$  to  $Q_t$ . They were estimated by simulating the response of the aquifer for selected pumping values over nine time periods (seasons). Some results of these simulations are presented in Table 1 below. The flowchart for groundwater simulation is shown in Figure 1.

Table 1 Aquifer response to pumpage: average drawdown, ft/season.

| Pumping rate<br>ft <sup>3</sup> /grid sq/day | 1.0 x 10 <sup>6</sup> | 1.1 x 10 <sup>6</sup> | 1.3 x 10 <sup>6</sup> | 1.5 x 10 <sup>6</sup> |
|--|-----------------------|-----------------------|-----------------------|-----------------------|
| Season                                       |                       |                       |                       |                       |
| 1  | 1.277                 | 1.575                 | 2.173                 | 2.771                 |
| 2  | 1.114                 | 1.429                 | 1.999                 | 2.568                 |
| 3  | 2.830                 | 3.102                 | 3.651                 | 4.204                 |
| 4  | 1.037                 | 1.298                 | 1.819                 | 2.349                 |
| 5  | 0.939                 | 1.190                 | 1.696                 | 2.210                 |
| 6  | 2.644                 | 2.894                 | 3.387                 | 3.896                 |
| 7  | 0.869                 | 1.110                 | 1.603                 | 2.099                 |
| 8  | 0.784                 | 1.016                 | 1.498                 | 1.983                 |
| 9  | 2.508                 | 2.737                 | 3.211                 | 3.692                 |

For each pair of values  $S_t$  and  $Q_t$ , the corresponding  $B_t$  was calculated. As it may be expected the values of  $B_t$  for different values of pumpage (and drawdown) in the same season were not constant, because aquifer response depends non-linearly on the magnitude of the stress imposed upon the aquifer. The functional relationship between the  $B_t$  and the drawdowns  $S_t$  were estimated by linear regression as follows:

$$\begin{aligned}
 B_1 &= 0.391 + 0.190S_1 \\
 B_2 &= -0.358 + 0.175S_2 \\
 B_3 &= -0.197 + 0.168S_3 \\
 B_4 &= -0.367 + 0.157S_4 \\
 B_5 &= 0.274 + 150S_5 \\
 B_6 &= -0.258 + 0.146S_6 \\
 B_7 &= 0.467 + 0.142S_7 \\
 B_8 &= -0.633 + 0.136S_8 \\
 B_9 &= 0.395 + 0.133S_9
 \end{aligned} \tag{9}$$

The values of the parameters in equations (9) will depend, of course, on the operations decisions regarding the aquifer, so that these equations, and the analysis leading up to them, represent a methodological approach to the class

of problems involving the dynamic management of complex hydrologic systems. Note that the slope of the linear relationships shown by equations (9) is monotonically decreasing indicating that following a prolonged operation of the system,  $B_t$  will tend to reach constant values regardless of the amount pumped (and its consequent drawdown) within a given range.

### Integration of Surface and Groundwater Subsystems

The integration of the two hydrological subsystems is attained by means of a dynamic programming framework within which the details of the groundwater component are worked out using a simulation algorithm (McDonald and Harbaugh, 1984). The generalized flowchart for the dynamic optimization of a complex hydrologic system consisting of both surface and groundwater elements is given in Figure 2 (Buras and Salmon, 1986).

### Dynamic Value of Aquifer Storage

The dynamic programming model developed here uses only physical quantities - deviations from storage and pumpage targets - in order to derive optimal operating policies. A more complete formulation defines the measure of performance in economic terms, as indicated in equation (6). In most cases, economic terms include benefits produced by irrigation water and costs of supplying it. Usually, water would be supplied when marginal benefits exceed marginal costs. However, it seems indicated to include in the economic analysis also the value of water stored in an aquifer, particularly considering the dynamics of the hydrologic system. An approach to this problem was proposed by Buras and Duckstein (1985).

The following model was derived:

- $i$  - surface water available at beginning of period  $t$ .
- $j$  - surface water available at beginning of period  $t + 1$ .
- $p_{ij}^t$  - probability that  $j$  surface water will be available in  $t + 1$  given that  $i$  is available in period  $t$ .
- $x_t$  - surface water supplied for irrigation in period  $t$ .
- $r_t$  - surface water stored in aquifer in period  $t$ .

$$x_t + r_t \leq i \quad (10)$$

$m$  or  $G_t$  - groundwater available at beginning of period  $t$ .

- $n$  - groundwater available at beginning of period  $t + 1$ .
- $g_t$  - groundwater supplied for irrigation in period  $t$ .
- $\alpha_t$  - groundwater seeping out of aquifer in period  $t$ .

$$G_{t+1} = (G_t - g_t + r_t)\alpha_t, \quad 0 \leq \alpha_t \leq 1. \quad (11)$$

$B_t$  - regional benefit during period  $t$ .



$a_1, a_2, a_3, b_1, b_2, b_3$  - parameters

$$B_t = (a_1 x_t - b_1 x_t^2) + (a_2 g_t - b_2 g_t^2) + (a_3 r_t - b_3 r_t^2) \quad (12)$$

$d_t$  - irrigation demand in period  $t$ .

$$d_t = x_t + g_t. \quad (13)$$

$\Gamma$  - total effective storage volume (capacity) of aquifer.

$$\max r_t = \Gamma - G_{t+1} \quad (14)$$

Combining equations (11) and (14), one obtains

$$r_t = \frac{1}{1 + \alpha_t} [\Gamma - \alpha_t (G_t - g_t)] \quad (15)$$

The dynamic programming formulation resembles equation (6).

$$f_t(i, m) = \max_n \{ B_{imnt} + \left( \frac{1}{1 + u} \right)^{t-1} \sum_j p_{ij}^t \cdot f_{t-1}(j, n) \} \quad (16)$$

$$\forall i, m; t = 1, 2, \dots, T,$$

$$f_1(i, m) = \max_n \{ B_{i1m1} \} \quad \forall i, m. \quad (17)$$

where  $u$  is periodic rate of interest.

Solution of equations (16) and (17) yields an optimal trajectory for regional groundwater levels over a time span of  $T$  periods.

We shall re-write now the criterion function (equation (12)) substituting the value of  $x_t$  from equation (13), and subjecting it to a capacity constraint of the regional groundwater sub-system:

$$B_t = a_1(d_t - g_t) - b_1(d_t - g_t)^2 + a_2 g_t - b_2 g_t^2 + a_3 r_t - b_3 r_t^2 \quad (18)$$

s.t.

$$r_t = \frac{1}{1 + \alpha_t} [\Gamma - \alpha_t (G_t - g_t)]. \quad (19)$$

Forming the Lagrangian, we obtain

$$L(g_t, r_t, \lambda_t) = B_t - \lambda_t \left\{ r_t - \frac{1}{1 + \alpha_t} [\Gamma - \alpha_t (G_t - g_t)] \right\} \quad (20)$$

Taking the first derivatives and setting them equal to zero

$$\frac{\partial L}{\partial g_t} = -a_1 + 2b_1d_t - 2b_1g_t + a_2 - 2b_2g_t + \frac{\lambda_t \alpha_t}{1 + \alpha_t} = 0, \quad (21)$$

$$\frac{\partial L}{\partial r_t} = a_3 - 2b_3r_t - \lambda_t = 0, \quad (22)$$

$$\frac{\partial L}{\partial \lambda_t} = r_t + \frac{\Gamma}{1 + \alpha_t} - \frac{\alpha_t G_t}{1 + \alpha_t} + \frac{\alpha_t g_t}{1 + \alpha_t} = 0, \quad (23)$$

we can calculate the value of the Lagrange multiplier:

$$\lambda_t = \phi_1(\alpha_t) + \phi_2(\alpha_t, \Gamma) + \phi_3(\alpha_t, G_t) + \phi_4(\alpha_t, d_t). \quad (24)$$

Equation (24) shows that the time (season) - dependent Lagrange multiplier is a sum of four polynomial functions which reflect (i) total capacity of the aquifer ( $\Gamma$ ); (ii) current availability of groundwater ( $G_t$ ); (iii) current irrigation demand ( $d_t$ ); (iv) current seepage losses from the aquifer ( $\alpha_t$ ). Related to the optimal trajectory of regional groundwater levels produced by the solution of equations (16) and (17), a trajectory of Lagrange multipliers  $\lambda_t$  can be generated. This trajectory of  $\lambda_t$  is the dynamic value of aquifer storage.

A graphical representation of two trajectories of the Lagrange multipliers  $\lambda_t$  for select values of  $a_i$ ,  $b_i$ ,  $d_t$ ,  $\Gamma$ ,  $\alpha_t$  is shown in Figure 3.

### Conclusions

A judicious combination of analytical tools - simulation and optimization models - provides an effective means for describing dynamic, complex hydrologic systems. It also forms useful guidelines for management decisions.

The formulation of the problem using an expanded simulation - optimization model allows the integration of policy factors by means of the coefficients of the benefit function. These coefficients may reflect water demand, production quotas for crops, price supports through subsidies, or taxes levied to discourage overpumping of aquifers.

The value of water stored in aquifers depends on the physical characteristics of aquifers and on the policy of exploiting them. Since this value is time-dependent, trajectories of Lagrange multipliers represent a dynamic value of aquifer storage.

### References

- Bellman, R.S., 1957, Dynamic Programming, Princeton University Press, Princeton, NJ.
- Buras, N., 1963, Conjunctive operation of dams and aquifers, Jour. of Hydraulic Division, ASCE, 89(HYG):111-131.
- Buras, N., 1966, Dynamic programming in water resources development, Advance in Hydro Science, vol. III, Academic Press, New York, pp. 375-412.

- Buras, N., 1985, An application of mathematical programming in planning surface water storage, Water Resour. Bull., 21(6):1013-1020.
- Buras, N., and L. Duckstein, 1985, Dynamic value of aquifer storage in a stream - aquifer system, presented at the annual fall meeting, American Geophysical Union, San Francisco.
- Buras, N. and R.F. Salmon, 1987, Dynamic Management of Stream-Aquifer Hydrologic Systems, Report submitted to the World Bank, 94 pp.
- Gisser, M., 1970, Linear Programming models for Estimating the Agricultural demand Function for Imported Water in the Pecos River Basin, Water Resour. Res., 6:1025-1032.
- Gorelick, S.M., A review of distributed parameter groundwater management modeling methods, WRR, 19(2):305-319, 1983.
- Loucks, D.P., J.R. Stedinger and D.A. Haith, 1981, Water Resources Systems Planning and Analysis, Prentice-Hall, Eaglewood Cliffs, NJ.
- McDonald, M.G. and A.W. Harbaugh, 1984, A Modular Three-Dimensional Finite Difference Ground-Water Flow Model, U.S. Geological Survey, Reston, Virginia.
- Noel, J.E. and R.E. Howitt, 1982, Conjunctive Multibasin Management: An Optimal Control Approach, Water Resources Research, 18:753-763.

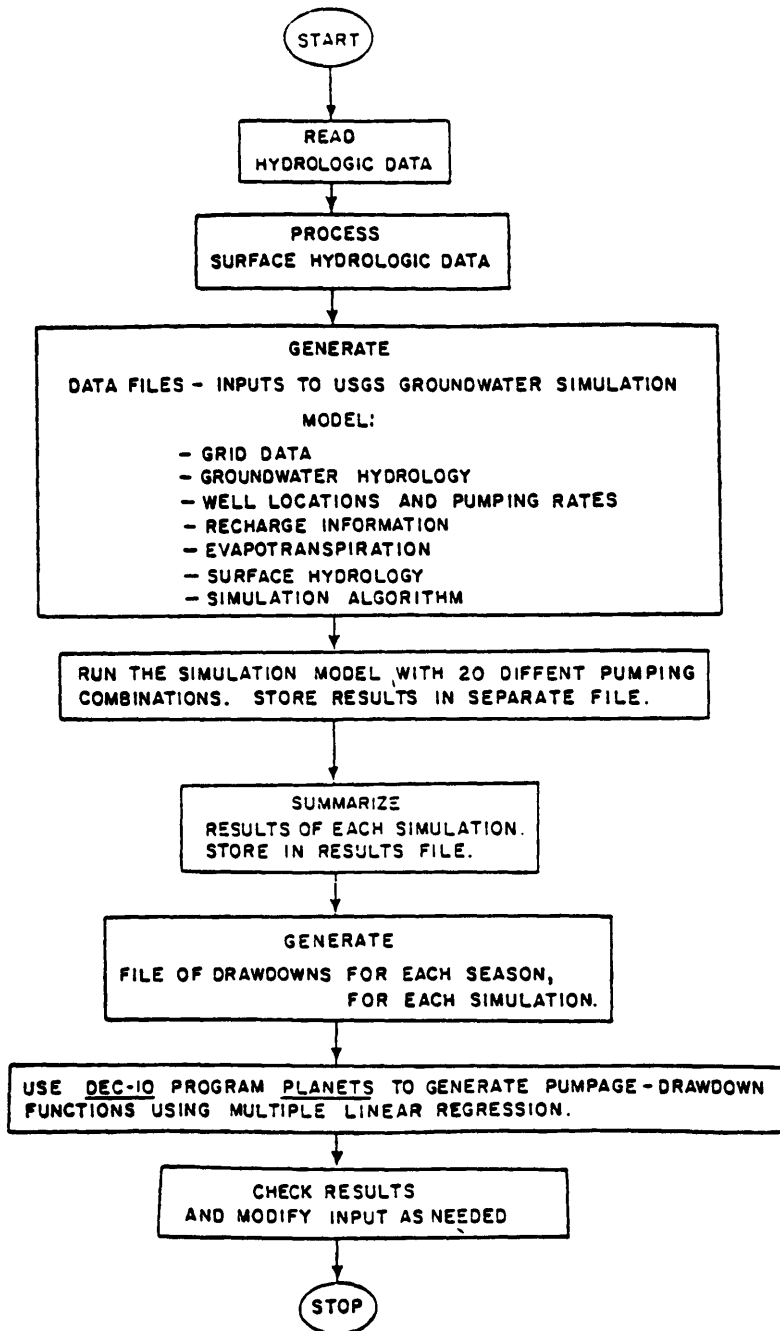


Figure 1. Flowchart for Groundwater Simulation.

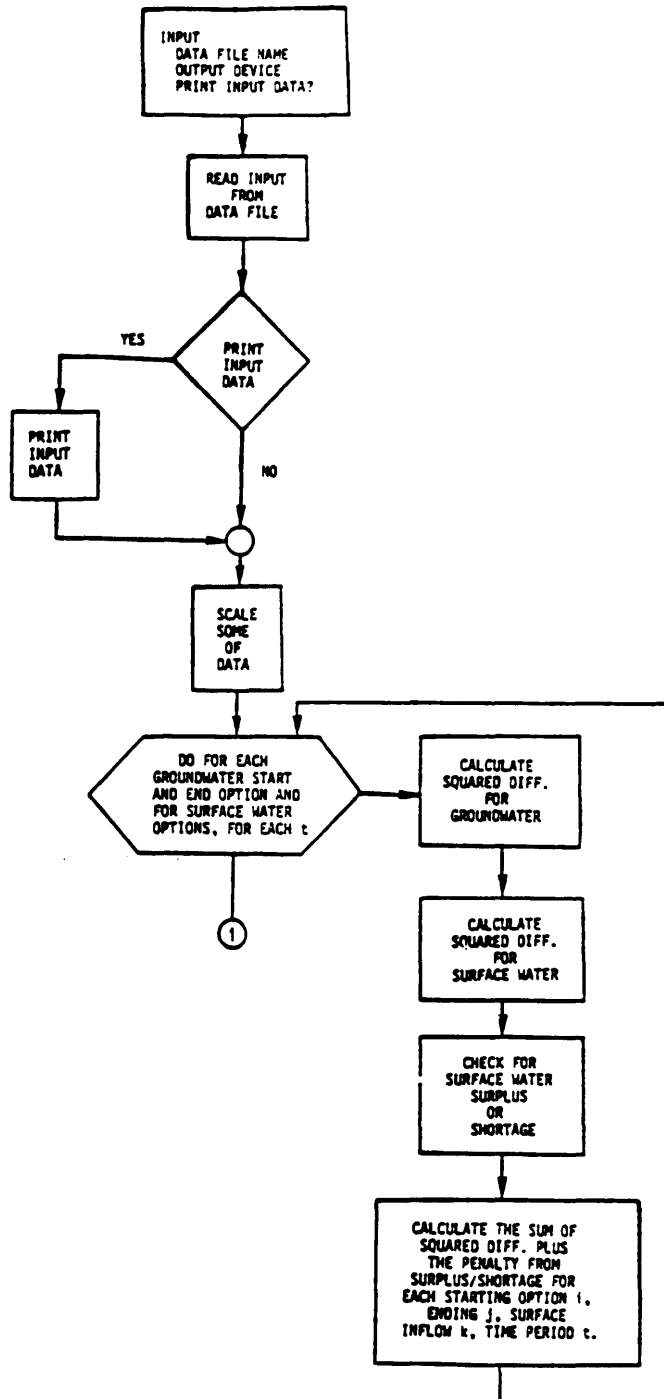


Figure 2. Flowchart of the dynamic optimization program.

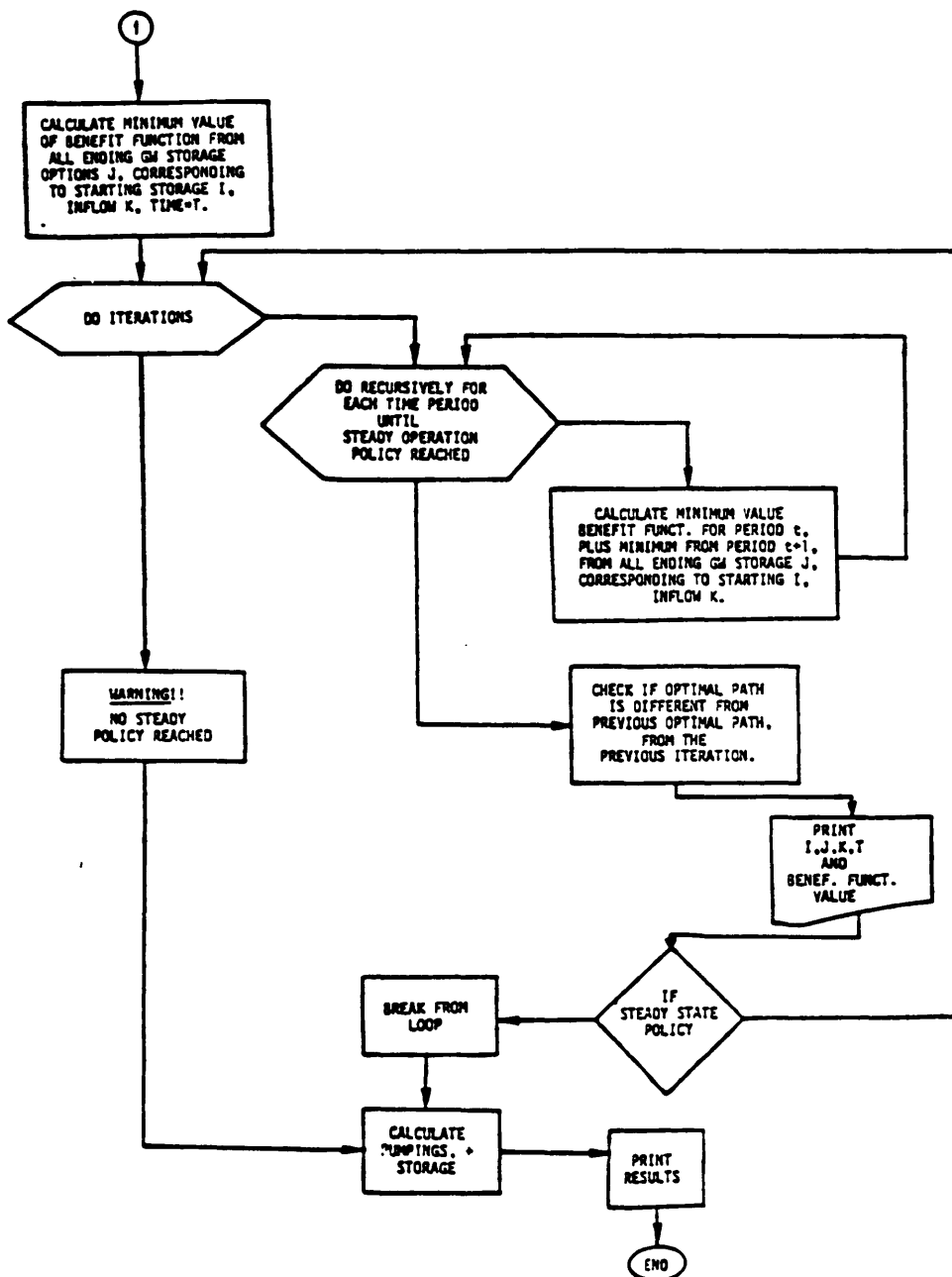


Figure 2. (continued) Flowchart of the dynamic optimization program.

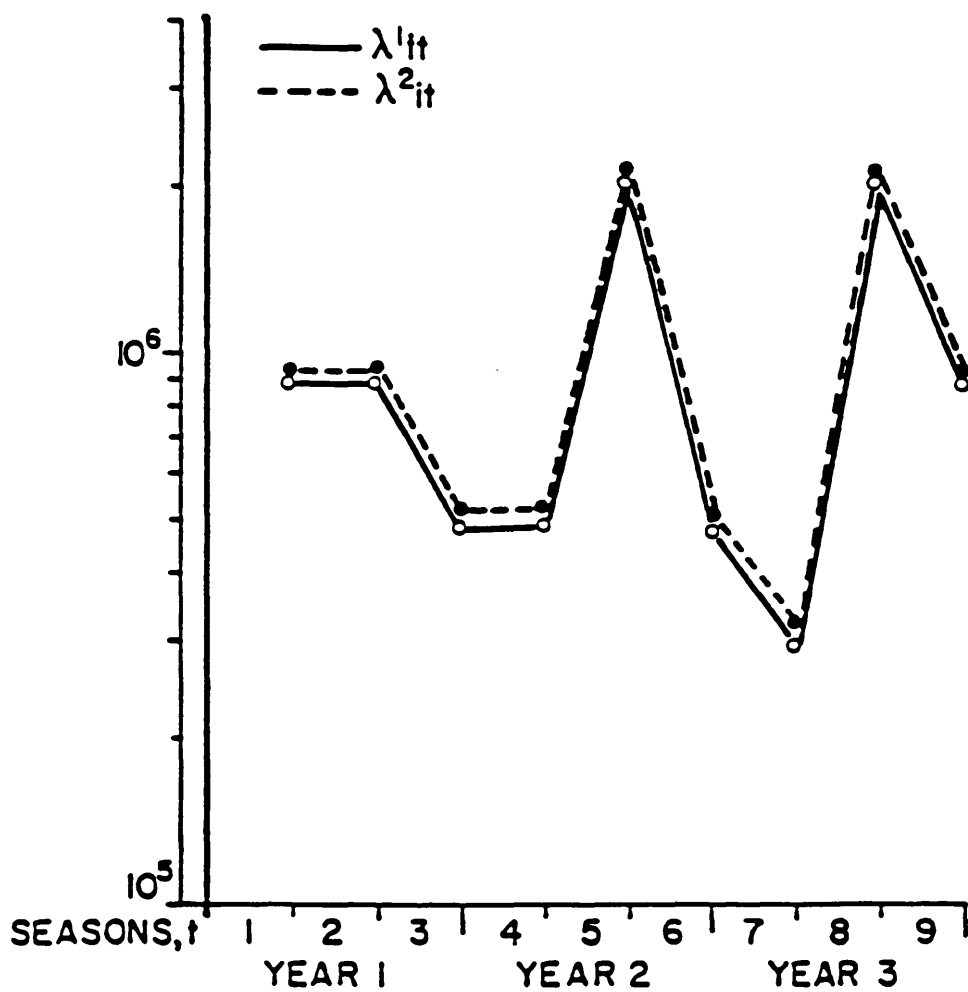


Figure 3. Dynamic Value of Aquifer Storage.





WELL HEAD PROTECTION AREAS FOR PRESERVING NATURAL  
DRINKING WATER QUALITY - EXPERIENCES AND NEW DEVELOPMENTS  
IN THE FEDERAL REPUBLIC OF GERMANY

R. Schleyer and G. Milde

Institute for Water, Soil and Air Hygiene  
of the Federal Health Office  
Corrensplatz 1  
D-1000 Berlin 33  
Federal Republic of Germany

ABSTRACT: Groundwater provides the major resource for public drinking water supplies in the Federal Republic of Germany. The most important aspect of groundwater quality protection in the drainage areas of drinking water catchment sites is the establishment of a protected area, which is divided into up to four different zones with increasing bans and limitations towards the drinking water wells. Summarizing the experiences with this time-distance integrated protection scheme it has to be noted that it is not always simple to achieve a satisfactory balance between necessary protection measures and other conflicting interests in this highly industrialized country, but altogether it served up to now relatively successful to provide drinking water of good hygienic quality. However, new findings on the behaviour of pathogens and investigations on persistence and residence time of organics, especially pesticides, and inorganics reveal that a successful protection of groundwater for drinking water purposes can only be achieved by carefully assessing all potential sources of contamination and by developing optimal protection strategies including all site specific criteria.

### Introduction

Natural groundwater taking part in the water cycle in an unimpeded way and being unaffected by anthropogenic changes will as a rule be clean, fresh, tasty, free from pollutants, microorganisms, or viruses. In most cases, its natural state will be largely in conformity with current requirements for drinking water quality. Essentially, the reasons for this good quality are protective geological barriers, the filtration effect of the subsoil and the aquifer as well as the long period over which the water remains in the subsoil, with its favourable influences on the degradation of certain substances and the retention of pathogenic microorganisms including viruses. Therefore, by tradition, groundwater provides the major resource for drinking water supplies in Central Europe. In the Federal Republic of Germany, for example, more than 70 % of the public supply of drinking water and almost all private water supply are derived from groundwater (wells, springs). However, experiences for more than 100 years have shown that the fact to occur subterraneously is not sufficient to protect the groundwater against anthropogenetic influences and illustrates the necessity of a specific groundwater quality protection, in cases where it is used for drinking water.

Therefore, in the Federal Republic of Germany a multilateral network of acts exists to guarantee an adequate protection of groundwater quality. According to §1a para. 1, for example, of the German Water Resources Policy

Act ("Wasserhaushaltsgesetz"), "water bodies .... should be managed in such a way that they serve the benefit of the community and in conformity with this objective, also the benefit of individuals, and that there is no avoidable interference" (Deutscher Bundestag 1986). The need for a specific protection of groundwater in the drainage areas of water catchment installations is expressed by §19 of the Act, where the establishment of protected areas is regulated. This is of special importance because it gives expression to a most important underlying concept: there is groundwater which particularly deserves protection because it is used as drinking water and there is groundwater which is less worthy of protection because it is not used for such purpose.

### The protection zone concept

In the Thirties a concept of time-distance integrated groundwater-protection concept has been developed in Germany for drinking water wells, which recommend a classification of protected areas for drinking water production by up to four different zones (I, II, III A and III B; Fig. 1) with bans and limitations on their use increasing towards the catchment site (Tab. 1):

Zone I: The area within a 10 m-distance from the drinking water well.

Zone II: The area within a distance which covers a tracered groundwater within 50 days.

Zone III A: The area within a 2 km-distance from the drinking water well.

Zone III B (optional): The area beyond a 2 km-distance from the drinking-water well, maximally up to the drainage area boundary.

Technical rules for the designation of protected areas in which groundwater resources are used for drinking water supply can be found in regulations of the federal states ("Länder") and in the "Manual W 101 of the Collection of DVGW Rules" ("Deutscher Verein des Gas- und Wasserfachs" = German Association for Gas and Water): "Guidelines for protected areas used for the production of drinking water, part I: protected areas for groundwater" which was published first in 1953. Revised versions were published in 1961 and 1975 (DVGW 1975). One of the basic items of this concept is the time-dependend boundary of protection zone II (50-days line). When establishing the dimensions of that zone, the most important aspect was that of the elimination of pathogenic bacteria and viruses. Since 50 days had been considered as sufficient for inactivation (Knorr 1937, 1951; Knorr and Muselmann 1940), zone II was delimited by "a line from which groundwater need appr. 50 days to reach the water well". Also for degradable and retention-prone chemicals, a 50-days groundwater passage was considered as sufficient for their elimination. The limits of the other zones do not depend on flow periods. Rather, flow distances have been fixed. Any groundwater endangering activities concerning micro-organisms or degradable substances are to be kept away from protection zone II. More persistent and mobile substances, however, have to be avoided in the total drainage area. Whereas the protection of areas closed to a well has been forged ahead, evident difficulties appeared while establishing the extended protection zones, particularly those reaching up to the boundary of the drainage area.

Designation of protected areas, together with the associated bans on and limitations to their utilization, lead to conflicting interests due to different demands for utilization. Such conflicts are often resolved by juri-

TABLE 1: Activities, processes, and installations not acceptable in well head protection areas (Federal Republic of Germany). All bans and restrictions in a zone of lower protection quality are also valid in more protected zones.

|                            |  |  |
|----------------------------|--|--|
| zone<br>I<br>(10m)         | vehicle and pedestrian traffic<br>agriculture<br>manure and pesticides   | (and all mentioned<br>bans or restrictions<br>of zone II, III A and III B) |
| zone<br>II<br>(50<br>days) | <p> constructions, plants and workshops<br/> farms, stables and sheds<br/> building sites and stock of building material<br/> roads and railways<br/> transfer points and parking lots<br/> sport facilities and camping sites<br/> tenting and bathing establishments at surface waters<br/> car washing and oil change<br/> cemeteries<br/> removal of surface layers<br/> mining and blow-ups<br/> intensive grassing<br/> allotments<br/> fuel storage and transport of water endangering substances<br/> waste water pipes<br/> fishponds </p>                                  | (and all mentioned<br>bans or restrictions<br>of zone III A and III B)     |
| zone<br>III A<br>(2km)     | <p> commercial use of water endangering substances<br/> mass livestock<br/> open storage and use of water endangering pesticides<br/> waste water treatment<br/> hospitals, sanatoriums and urbanizations<br/> storage of water endangering substances<br/> airports and associated facilities<br/> military facilities and manoeuvres<br/> waste sites<br/> sewage treatment plants<br/> injection of cooling water<br/> essential removal of surface layers<br/> new cemeteries<br/> shunting stations<br/> road construction with water endangering substances<br/> drilling </p> | (and all mentioned<br>bans or restrictions<br>of zone III B)               |
| zone<br>III B              | <p> oil refineries and smelting works<br/> chemical plants and nuclear reactors<br/> waste water injections<br/> deposition and underground storage of water endangering substances<br/> pipelines for water endangering substances </p>   |  |

dical means and/or compensation payments. This occurs particularly often in urban agglomerations where competing demands for utilization of land increase with the population density. If all 26,000 well head protection areas which are needed in the Federal Republic of Germany would have been designated as such, this would mean bans and limitations to utilization of areas in the interest of groundwater protection for appr. 11 % (without zone III B) of the territory. Thus, it is not surprising that so far, only part of the necessary protected areas have been designated as such with legal effect, with proportions greatly varying among the federal states: from 70 % in Baden-Württemberg to 1 % in Schleswig-Holstein.

Summarizing the experiences with the outlined groundwater protection schemes, it has guaranteed for decades a safe drinking water supply from the hygienic point of view. However, some new scientific investigations show gaps especially in regard to the importance of the 50-days line, the boundary of zone II. It has been revealed, for example, that the elimination of pathogenic bacteria and viruses depends on flow distances rather than flow periods and that many environmental chemicals may persist in groundwater for more than 50 days.

#### Microorganisms

Extensive laboratory investigations of pathogeneus bacteria and viruses under conditions comparable to the groundwater environment resulted in elimination times partly well over 50 days (Fig. 2) (DVGW 1983; Mattheß et al. 1985a; Filip et al. 1986). A decrease of 7 magnitudes of order (from  $10^{6-7}/l$  to  $10^{0-1}/l$ ) took 300 days for *Yersinia enterocolitica*, *Chlostridium perfringens* and *Bacillus cereus*, 290 days for *Salmonella typhimurium*, 225 days for *Escherichia coli* and 20 days for *Staphylococcus aureus*. The inactivation constants of the pathogeneus viruses Coxsackie A9, Coxsackie B1, Polio-1 and ECHO-7 varied depending on virus and conditions between 0.008 and 0.04.

In addition, transport studies were carried out in the laboratory as well as in field experiments. Essentially, they explain the good elimination of bacteria and viruses in sandy aquifers by adsorption/desorption and filtration processes. From the epidemiological angle, this means that all well filtrating aquifers are sufficiently protected by the 50-days line. This is, however, not true in aquifers without such good sorption capability, e.g. karst aquifers or rocks with wide open space structures. Here, the 50-days line is not a sufficient protection of drinking water against epidemics.

#### Environmental pollutants

In the past the behaviour of many substances in the groundwater environment (mobility, capability of accumulation and persistency) has been estimated inadequately referring to their groundwater hazard. Above all in the Federal Republic of Germany this is true for the non-point source impact of contaminants by agriculture (some fertilizers, especially nitrogen fertilizers, and pesticides) as well as for the point source impact by contaminated sites (plants, waste disposal sites), which adversely have affected the groundwater quality in many cases.

## NON-POINT SOURCES OF POLLUTANTS FROM AGRICULTURE:

**NITRATE:** In regions with extensive agricultural activity and cattle-breeding groundwaters have shown rising levels of nitrate (0.5 - 3 mg/l'a) (DVGW 1985). As a consequence of the nitrate limit value for drinking water of 50 mg/l, this has caused considerable problems of drinking water supply in a number of cases. While, depending on the federal state involved, the proportion of wells used by public supply systems which have exhibited nitrate values above the limit varies between 0 and 8 %, this proportion is up to 50 % for private supply systems (LAWA 1986). The reason for this is well known: excess fertilization and a resulting leaching of nutrients at rates above the average.

A reduction of manure and fertilizers only within areas closed to the drinking water well is not a sufficient protection of groundwaters. Therefore, requirements have been recommended to be adhered to by agriculture (Mehlhorn 1987):

- Limitation of soil nitrogen to 45 kg N/ha late in October;
- Adjustment of fertilization to site-specific nitrogen requirements; a ban on nitrogen fertilization during the non-vegetation period or even a general ban on nitrogen fertilization;
- Avoidance of the ploughing of permanent grassland or even reconversion of fields to grassland;
- Bans on certain crops or crop rotations requiring much fertilization.

**PESTICIDES:** Most of the pesticide application in the Federal Republic of Germany is for agricultural purposes. 30,000 metric tons of active substance applied each year correspond to a mean application of 2.5 kg/ha, with extreme values ranging from 1 to 100 kg/ha. It becomes evident from the distribution of the 280 approved organic substances by classes of active ingredients that herbicides, insecticides and fungicides account for 80 % of the individual compounds used. To cope with such amounts, the degradation potential of a soil should be one of 99.99 %, to warrant groundwater levels below the limit value for drinking water of 0.1 µg/l (single substance) or 0.5 µg/l (cumulative), assuming an annual groundwater recharge of appr. 200 mm of leachate (Müller-Wegener and Milde 1988).

Such degradation potential is not reached for certain soils and certain pesticides, so that in the respective cases there is a hazard for groundwater. In particular, areas with well permeable soils low in humus must be considered as most vulnerable against pesticides. In fact, pesticide concentrations which are clearly above the limit value for drinking water have been demonstrated in inadequately protected groundwaters. Peak concentrations were e.g. reached for atrazine (up to 17.5 µg/l), aldicarb (up to 130 µg/l) and 1,3-dichloropropene (up to 8620 µg/l). Estimates for orientation purposes based on the published results of inquiries suggest that at present about 50 % of the drinking water distributed in the Federal Republic of Germany has been influenced by pesticides (Müller-Wegener and Milde 1989).

Extensive studies about the occurrence and the genesis of such contaminations clearly show that the use of pesticides with a high groundwater mobility should be avoided above vulnerable aquifers irrespective of groundwater protection zones. In an unprotected karst drainage area, for example, atra-

zine was applied on 1 % of the total area. This results in concentrations of 0.5 µg/l (mean: 0.12 µg/l) in the drinking water support (Gießl and Hurle 1984). Another study in a vulnerable pleistocene sandy aquifer resulted in recommendations to restrict the cultivation of maize to less than 15 - 20 % of the drainage area in order to keep a concentration of <0.1 µg/l atrazine in the drinking water well (Milde and Friesel 1987).

Simazine is classed into a group of pesticides with an intermediate groundwater endangering potential (former "W2"). Therefore, its application was permitted beyond zone II. However, studies in an artificial sandy aquifer with a groundwater flow velocity of 0.56 m/d have shown that 50 days are not sufficient for its total elimination (Herklotz and Pestemer 1987). Thus a prohibition of its application in the total drainage area has to be taken into consideration.

Not only field investigations, but also numerical computer simulations using substance specific and aquifer specific data can help to assess the groundwater endangering potential of substances and the groundwater protection measures to be taken into account. In fig. 3 the half-life times of some pesticides are plotted versus their retardation factors under the specific aquifer conditions of 0.1 % org. C and 1 m/d groundwater flow velocity. It is demonstrated, for example, that a solution of triazine (Fig. 3, No. 8) with a realistic concentration of 0.1 - 1 mg/l has to be injected more than 3 km far from a drinking water catchment site to guarantee a concentration of less than 0.1 µg/l in the delivered drinking water (Mattheß et al. 1985b). Consequently, the application of triazine should be limited under these specific aquifer conditions in areas beyond a 3 km distance from a catchment site, which means in zone III B or the total drainage area.

Several suggestions have been made for a better protection of groundwaters against impacts of pesticides from agriculture. With regard to drainage areas of drinking water catchment sites the following two measures seem to be the most successful ones:

- limitations and bans on the application of defined pesticides and
- application of pesticides only by special operators.

#### POINT SOURCES OF GROUNDWATER POLLUTION:

CONTAMINATED SITES: Waste deposits and other contaminated sites such as gas works, coke plants etc. are of eminent importance as sources of pollutants affecting groundwater quality because of their high number, the complexity of the substance matrix of many leachates contaminating groundwaters and the large volume of leachates in most cases resulting in high pollutant concentrations in the immediate downstream groundwater and extensive pollutant plumes.

According to data collected by the federal states, some 50,000 sites have been recorded at present (Henkel 1988). If distributing these uniformly over the territory of the Federal Republic of Germany (248,708 km<sup>2</sup>), each square of 2.2 km edge length would include a site, i.e. a site with potential groundwater pollution.

With regard to drainage areas of water catchment installations, a clear distinction must be made between existing sites and sites which can still be avoided. As far as possible, new activities and sites which are likely to influence groundwater should not take place in drainage areas of water catchment. If they are unavoidable, construction should be subjected to stringent requirements to prevent the penetration of substances into groundwater, to permit an immediate recognition and rehabilitation of leaks in emergency situations. Such requirements include construction measures to seal the subsoil, groundwater observation pipes which are regularly checked, preventive construction measures for sanitation purposes which become immediately effective in accident situations and the permanent availability of a numeric transport model to simulate different accident situations and corresponding rehabilitation measures.

Regrettably, cases of groundwater pollution from existing or abandoned contaminated sites are still detected mostly accidentally, e.g. by looking for the possible causes of a sudden occurrence of pollutants in delivery wells at a catchment site for drinking water, and not by systematic sampling and analysis of all groundwaters downstream of suspect sites (Kerndorff et al. 1985). Therefore, not only a systematic recording of their location, history and inventory of substances involved but also a systematic recording and regular monitoring of effects on groundwater should be demanded. Furthermore, the possible pollutant load must be estimated by numeric transport modelling, taking into account the capacity of the drinking water well and the hydrogeological conditions. There should be a uniform evaluation of possible hazards with the aid of a standardized procedure. If a hazard is present, measures to ensure safety and rehabilitation must be taken immediately.

While at contaminated industrial sites, there are often known production-specific substances (target substances) which may pollute groundwater, those involved at waste deposits are generally not known and only the water-soluble ones may penetrate into groundwater. Systematic evaluation of a great number of analyses of groundwater sampled downstream of waste deposits has shown that 'merely' judging by their order of magnitude, the detection frequency of 100 substances was  $>0.1\%$  (main contaminants) (Plumb Jr. 1985). Within the group of substances with a detection frequency of  $>10\%$ , the volatiles were predominant (Schleyer et al. 1988). This group of substances has a high water solubility and penetrability into groundwater. In single cases, migration over distances of up to 20 km could be observed in oxygenated aquifers with low content of organic detritus (MELUF BW 1987). The initially present substances will not always show persistency. Rather, under anaerobic conditions with sufficient organic matter, they may be subject to a reductive dehalogenation finally producing even vinyl chloride which poses particular problems with regard to environmental hygiene (Milde et al. 1987).

Problems are posed by the evaluation of contaminants found in groundwater. There are no legal limit values for groundwater, so limit values for drinking water are often used as a substitute. While this may be a preliminary tool for the range of inorganic substances, another problem arises with regard to the organic ones: such limit values exist only for a few of the 100 substances whose presence has been demonstrated with a certain frequency. There is considerable need for research activities in this field, especially what concerns the determination of toxicity, penetrability into groundwater and persistence of these substances. It must be added that, although limit

values for drinking water may be used as a yardstick in the evaluation of endangered drinking water catchment but not where other objects deserving protection such as surface waters or parts of construction having contact with groundwater are involved.

Restoration of groundwater contaminations involves high costs. It is not an infrequent occurrence that costs reach 10 million DM and more, with figures depending on the level of restoration to be achieved. There should be research into the development of meaningful objectives of restoration, as well as control and systematic checking of the effectiveness of restoration measures already performed. When establishing restoration targets, the individual characteristics of sites, i.e. the specific development of the contamination and the specific use situation are to be taken into account. There should be no efforts to develop general limit values for groundwater or even emission limits for sources of contamination because such a rigid tool would not meet the specific hydrogeological conditions and the different distances between the sites of the groundwater use and the source of contamination.

**LEAKS IN SEWER NETWORKS:** Contamination of groundwater from leaks in sewer networks have only recently become a public issue. The size of the problem become obvious when one imagines that there are some 285,000 km of public and some 600,000 km of private underground sewers in the Federal Republic of Germany (Gilles 1987) (other sources mention a length of more than 1 million km) (Buysch 1988), of which 10 - 15 % are estimated to have surpassed their calculated life (Stein 1988). Thus, an evaluation of a TV inspection of 70 km of sewers in Düsseldorf which do not permit inspection by personnel has revealed damage in 50 % of these sewers (Wille 1988). In discussions, a total volume of between 50 and 120 billion DM to cover rehabilitation costs in the Federal Republic of Germany has been mentioned (Lühr 1988). So far, little knowledge has been gained on the extent of pollution, the range of pollutants and their concentrations in groundwater.

**ATMOSPHERIC POLLUTANTS:** Well head protection areas do not preserve groundwater quality against atmospheric pollutants. Therefore, this new field has to be investigated intensively.

**ACID RAIN:** The emission of sulphur dioxide on the territory of the Federal Republic of Germany which had been ca. 200,000 t/a in 1850 rose considerably after World War II and reached a maximum of ca. 3.7 million t/a in the midseventies. Owing to the use of low-sulphur oil from the North Sea and as a consequence of the Regulations on large furnaces ('Großfeuerungsanlagen-Verordnung'), SO<sub>2</sub> emission dropped to a present 3 million t/a; a further reduction to about 1.3 million t/a by the year 2000 is expected. Contrary to the emission of sulphur dioxide, that of nitrogen oxides has shown a continued rise, with a present level of ca. 3.5 million t/a in the Federal Republic of Germany. The pH value of precipitation dropped from appr. 5.6 (before 1850) to present values of appr. 4.3 - 4.1 (no forest situations) and 3.3 (spruce forests) (Krieter 1988).

This corresponds to a mean deposit from precipitation per ha and year in non-forest outdoor situations of 0.52 kg protons, 9.02 kg ammonium (as N), 6.67 kg nitrate (as N), 0.36 kg phosphate (as P), 18.3 kg sulphate (as S) and 16.21 kg chloride (Führer et al. 1988).



Soils rich in carbonate have a high neutralization and buffer capacity in relation to acids manifesting itself in an increase of calcium, magnesium and potassium ions as well as of nitrate ions in groundwater. This is of relatively low hygienic importance. In contrast, especially groundwaters below soils poor in limestone are endangered by acid rain if the buffer capacity becomes exhausted since in such a case, above a defined pH value, silicates will be destroyed quite suddenly (first feldspars, then clay minerals) while setting free ions of aluminium, iron, manganese and heavy metals. The soil will lose its important property of cation storage and thus its filter function. Today, the limit values stipulated in the Drinking Water Regulations for the last mentioned ions are surpassed in springs of some regions of the low mountain ranges in the Federal Republic of Germany (e.g. aluminium: limit value 0.2 mg/l; measured values up to 5 mg/l).

**ORGANIC POLLUTANTS IN PRECIPITATION:** The effects of deposits of organic atmospheric pollutants on groundwater have been relatively little studied. As part of a current research project, atmospheric waters, leachate and groundwater of four forest areas in Hesse which are not influenced by industry and agriculture are examined for their content of organic substances. In soil leachate, concentrations of up to 60 µg/l AOX (adsorbable organic halogen) have been measured. From the bulk of 140 peaks in chromatograms, 31 substances could be identified, which were present mostly in concentration in the 10 ng/l range. In particular, these were chlorinated hydrocarbons, benzene, toluene, xylenes, naphthalin, chlorobenzenes and phthalates (Renner and Mühlhausen 1989).

The degradation products of chlorinated hydrocarbons would seem to be of particular interest with regard to groundwater quality. At present, ca. 250,000 t/a of these volatiles are used as solvents in the Federal Republic of Germany and a major part of these is emitted into the atmosphere. It appears that in the atmosphere, they are oxidized to form chlorinated organic acids, in particular trichloroacetic acid (up to 3 µg/l in atmospheric waters), which are then decarboxylated into trichlormethane in the soil. In springs of a drainage area completely free from agricultural and industrial influences, concentrations of up to 2.5 µg/l trichlormethane have been demonstrated (Renner and Mühlhausen 1989).

Absolute new territory, scientifically, means the protection of groundwater and drinking water catchment sites against the diffuse pollution by precipitations loaded with contaminants. The most vulnerable aquifers are characterized by a small groundwater quantity and a high portion of new formed groundwater as well as a high permeable filter zone with a low thickness and a low content of carbonate. From a long-term point of view many other aquifers are also endangered by atmospheric influences. Because site specific measures like the establishment of well head protection areas are inefficient against those influences, a consequent reduction of emissions into the atmosphere is the only way to protect groundwaters against atmospheric diffuse impacts.

### Conclusions

The groundwater protection scheme in Germany based on a four-zoned protected drainage area of a drinking water catchment site served up to now suc-

cessfully to provide drinking water of good hygienic quality. However, it could be optimized due to experiences in the past and new scientific results.

Groundwater resources which are used as drinking water are given top priority with regard to protection. Generally, it should be demanded that preferentially all drainage areas with water catchment for public as well as private use should be systematically recorded and delimited up to their drainage divides. The concept of protected areas should be applied. Based on the varying hydrogeological conditions (vulnerability), the drainage areas must be divided into zones with different degrees of protection. When this task has been accomplished, work could concentrate on a categorization of groundwater resources which do not yet serve water supply so that this domain of possible future use could be given protection, if necessary, on an extended basis.

Within the entire drainage area of a water well agriculture must adhere to the classification by zones with a varying degree of protection and the associated requirements which in turn depend on the specific hydrogeological conditions and the vulnerability or degree of protection of the aquifer.

The prevention of a projected use of groundwater-endangering substances in a drinking water catchment area is relatively easy. However, the maximum possible impact of a resident plant must be simulated with the aid of numerical computer transport models. Additionally, groundwater observation wells have to be installed directly downgradient to possible point sources of pollution and to be monitored regularly in order to an early detection of a contamination. This concept of a sufficient scientific assessment on the one hand and regular controls on the other is also true for the evaluation of a possible remedial action necessity for waste disposal sites and other groundwater-endangering sites in drinking water catchment areas.

It is a prerequisite for the functioning of a groundwater protection system that groundwater resources, their volumes, their drainage areas and in particular, their vulnerability are completely mapped ("groundwater vulnerability maps"). Such work will result in an increasing differentiation in the structure of protected areas. The concept of protected areas will be effective only if all affected parties are most intensively informed in detail about the zoning and its importance with regard to bans, obligations not to perform certain activities and precautionary measures.

Beyond this, there should be monitoring of groundwater quality and its regional development with time (groundwater quality monitoring network) which covers the entire territory of the Federal Republic of Germany. Thus, e.g. changes affecting large areas and long-term changes like those caused by atmospheric pollutants can be recognized in time.

A concept of groundwater protection policy should take into consideration, if necessary, the ratio of the amounts of groundwater which are used at present, those which will be used in the future and the total amount of groundwater within the water cycle. All protective measures which are difficult to enforce should be applied first to the benefit of the groundwater which is being used as drinking water, then to that of the groundwater for future use and finally to that of the "total" groundwater. Furthermore, in groundwater protection, a clear distinction must be made between preventive

and curative measures. While for prevention very high requirements can be put up for groundwater quality, such requirements have to be clearly reduced where damage which has already occurred is to be remedied because it is impossible to restore conditions existing prior to the contamination event even at the highest expenditure on technology.

### References

- Buysch, H.-P., 1988, Rechtliche Konsequenzen aus Kanalisationsschadensfällen, IWS-Schriftenreihe, 5, 289-295.
- Deutscher Bundestag, 1986, Gesetz zur Ordnung des Wasserhaushalts (Wasserhaushaltsgesetz - WHG) in der Fassung vom 23. Sept. 1986, Bundesgesetzblatt, Teil I, 1529-1654.
- DVGW (Deutscher Verein des Gas- und Wasserfachs) (ed.), 1975, Richtlinien für Trinkwasserschutzgebiete, I. Teil: Schutzgebiete für Grundwasser, DVGW Regelwerk Arbeitsblatt W101, ZfGW-Verlag, Frankfurt.
- DVGW (Deutscher Verein des Gas- und Wasserfachs) (ed.), 1983, Proc. Forum Mikroorganismen und Viren in Grundwasserleitern, DVGW-Schriftenreihe Wasser, 35.
- DVGW (Deutscher Verein des Gas- und Wasserfachs) (ed.), 1985, Zu hohe Nitratkonzentrationen im Trinkwasser - Gesundheitliche Relevanz und Maßnahmen zur Verringerung, DVGW-Schriftenreihe Wasser, 46.
- Filip, Z., H. Dizer, D. Kaddu-Mulindwa, M. Kiper, J. M. Lopez-Pila, G. Milde, A. Nasser, and K. Seidel, 1986, Untersuchungen über das Verhalten pathogener und anderer Mikroorganismen und Viren im Grundwasser im Hinblick auf die Bemessung von Wasserschutzzonen, WaBoLu-Hefte, 3/1986.
- Führer, H.-W., H.-M. Brechtel, H. Ernstberger, and C. Erpenbeck, 1988, Ergebnisse von neuen Depositionsmessungen in der Bundesrepublik Deutschland und im benachbarten Ausland, DVWK-Mitteilungen, 14.
- Gießl, H., and K. Hürle, 1984, Pflanzenschutzmittel und Grundwasser, Agrar- und Umweltforschung in Baden-Württemberg, 8, Verlag Eugen Ulmer, Stuttgart.
- Gilles, J., 1987, Öffentliche Abwasserbeseitigung im Spiegel der Statistik, Korrespondenz Abwasser, 34, 414-437.
- Henkel, M. J., 1988, Altlasten in der Bundesrepublik Deutschland - Eine Zwischenbilanz, in: Brandt, E. (ed.), Altlasten - Untersuchung, Sanierung, Finanzierung, Eberhard Blottner Verlag, Taunusstein, 25-35.
- Herklotz, K., and W. Pestemer, 1987, Modelluntersuchungen zur Charakterisierung des Mobilitätsverhaltens von Pflanzenschutzmitteln, Schriftenreihe des Vereins für Wasser-, Boden- und Lufthygiene, 68, 191-202.
- Kerndorff, H., V. Brill, R. Schleyer, P. Friesel, and G. Milde, 1985, Erfassung grundwassergefährdender Altablagerungen - Ergebnisse hydrogeochemischer Untersuchungen, WaBoLu-Hefte, 5/1985.
- Knorr, M., 1937, Die Schutzzonenfrage in der Trinkwasserhygiene, GWF, 80, 330-334 and 350-355.
- Knorr, M., 1951, Zur hygienischen Beurteilung der Ergänzung und des Schutzes großer Grundwasservorkommen, GWF, 92, 104-110 and 151-155.
- Knorr, M., and R. Muselmann, 1940, Lotrechte Infiltration und Filtration in ihrer Bedeutung für die Schutzzonenfrage, Arch. Hyg. Bakt., 23, 493-502.
- Krieter, M., 1988, Gefährdung der Trinkwasserversorgung in der Bundesrepublik Deutschland durch "Saure Niederschläge", DVGW-Schriftenreihe Wasser, 57.
- LAWA (Länderarbeitsgemeinschaft Wasser) (ed.), 1987, LAWA-Wasserversorgungsbericht 1986, Erich Schmidt Verlag, Berlin.

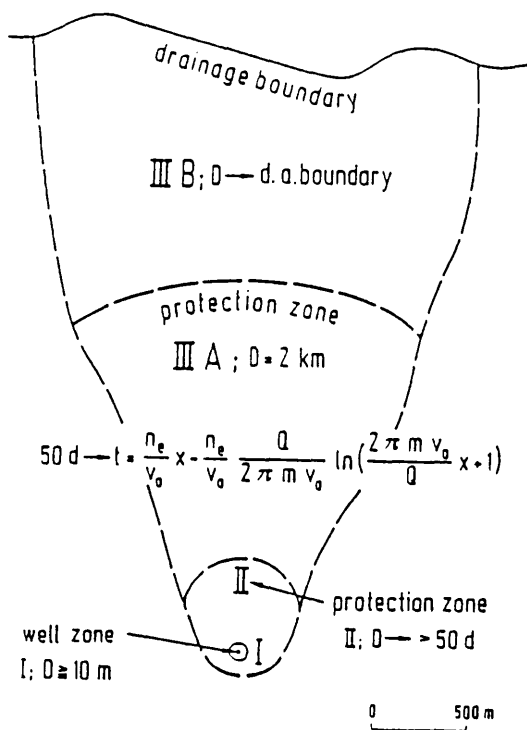
- Lühr, H.-P., 1988, Die Bewertung von Boden- und Grundwasserbelastungen, IWS-Schriftenreihe, 5, 179-192.
- Mattheß, G., I. Alexander, H. Althaus, H. Dizer, Z. Filip, G. Havemeister, P. Hirsch, K. D. Jung, D. Kaddu-Mulindwa, W. Käss, J. Lopez, G. Milde, A. Nasser, A. Pekdeger, E. Rades-Rohkohl, R. Riemer, R. Ritter, C. Sacré, J. Schröter, K. Seidel, and K.-P. Seiler, 1985a, Lebensdauer von Bakterien und Viren in Grundwasserleitern, Materialien des Umweltbundesamtes, 2/1985, Erich Schmidt Verlag, Berlin.
- Mattheß, G., M. Isenbeck, A. Pekdeger, D. Schenk, and J. Schröter, 1985b, Der Stofftransport im Grundwasser und die Wasserschutzgebietsrichtlinie W 101 - Statusbericht und Problemanalyse, UBA-Berichte, 7/1985, Erich Schmidt Verlag, Berlin.
- Mehlhorn, H., 1987, 75 Jahre Grundwassergewinnung im Donauried durch die Landeswasserversorgung, Wasserwirtschaft, 77, 598-607.
- Milde, G., 1987, Trinkwasserschutzgebiete - Einrichtungen zur Sicherstellung von Grundwässern mit Trinkwasserqualität, in: Aurand, K., U. Hässelbarth, G. von Niding, W. Schumacher, and W. Steuer (eds.), Die Trinkwasserverordnung, 2nd ed., Erich Schmidt Verlag, Berlin, 362-388.
- Milde, G., and P. Friesel (eds.), 1987, Grundwasserbeeinflussung durch Pflanzenschutzmittel, Schriftenreihe des Vereins für Wasser-, Boden- und Lufthygiene, 68.
- Milde, G., and P. Friesel, 1987, Grundwasserqualitätsbeeinflussungen durch Pflanzenschutzmittel, Schriftenreihe des Vereins für Wasser-, Boden- und Lufthygiene, 68, 11-43.
- Milde, G., and U. Müller-Wegener (eds.): Pflanzenschutzmittel und Grundwasser - Bestandsaufnahme, Verhinderungs- und Sanierungsstrategien, Schriftenreihe des Vereins für Wasser-, Boden- und Lufthygiene, 79.
- MELUF BW (Ministerium für Ernährung, Landwirtschaft, Umwelt und Forsten Baden-Württemberg) (ed.), 1987, Grundwassergefährdungen durch Altablagerungen am Beispiel Eppelheim, Landesanstalt für Umweltschutz Baden-Württemberg, Karlsruhe.
- Milde, G., M. Nerger, and R. Mergler, 1987, Biological Degradation of Volatile Chlorinated Hydrocarbons in Groundwater, Proceedings of an International Symposium on Groundwater Microbiology - Problems and Biological Treatment, Aug. 4-6 1987, Kuopio, Finland.
- Müller-Wegener, U., and G. Milde, 1988, Grundwasserkontaminationen durch Anwendung von Pflanzenschutzmitteln, DVGW-Schriftenreihe Wasser, 58, 269-284.
- Müller-Wegener, U., and G. Milde, 1989, Pflanzenschutzmittelanwendung und Grundwasserschutz - Eine Einführung zu aktuellen Fragen, Schriftenreihe des Vereins für Wasser-, Boden- und Lufthygiene, 79, 9-24.
- Plumb Jr., R. H., 1985, Disposal Site Monitoring Data: Observations and Strategy Implications, in: Hitchon, B., and M. Trudell (eds.), Hazardous Wastes in Groundwater: A Soluble Dilemma, Proceedings of the Second Canadian/American Conference on Hydrogeology, Banff, Alberta, Canada, June 25-29 1985, 66-77.
- Renner, I., and D. Mühlhausen, 1989, Immissionsbelastungen - Konsequenzen für die Grundwasserqualität, VDI-Bericht, 745, in print.
- Schleyer, R., J.-D. Arneth, H. Kerndorff, and G. Milde, 1988, Main Contaminants and Priority Pollutants from Waste Sites: Criteria for Selection with the Aim of Assessment on the Groundwater Path, in: Wolf, K., W. J. van den Brink, and F. J. Colon (eds.), Contaminated Soil '88, Proceedings of the Second International TNO/BMFT Conference, April 11-15 1988,

Hamburg, Germany, Kluwer Academic Publishers, Dordrecht, Boston, London, 247-251.

Stein, D., 1988, Stand der Zustandserfassung und Zustandsbewertung von Kanalisationen, IWS-Schriftenreihe, 5, 121-134.

Wille, B., 1988, Bestandsaufnahme von Schäden an Kanalisationen am Beispiel Düsseldorf, IWS-Schriftenreihe, 5, 121-134.

### Figures



### Legend:

50 d : 50 days; distance which a traced groundwater covers within this time

t : residence time of groundwater

$n_e$  : effective porosity

$v_0$  : flow velocity of undisturbed groundwater

x : distance covered by groundwater

Q : quantity of groundwater withdrawn

m : thickness of aquifer

FIGURE 1: Schematic scetch illustrating a well head protection area with its classification into up to four zones (I, II, III A, III B) in a drainage area of a drinking water catchment site

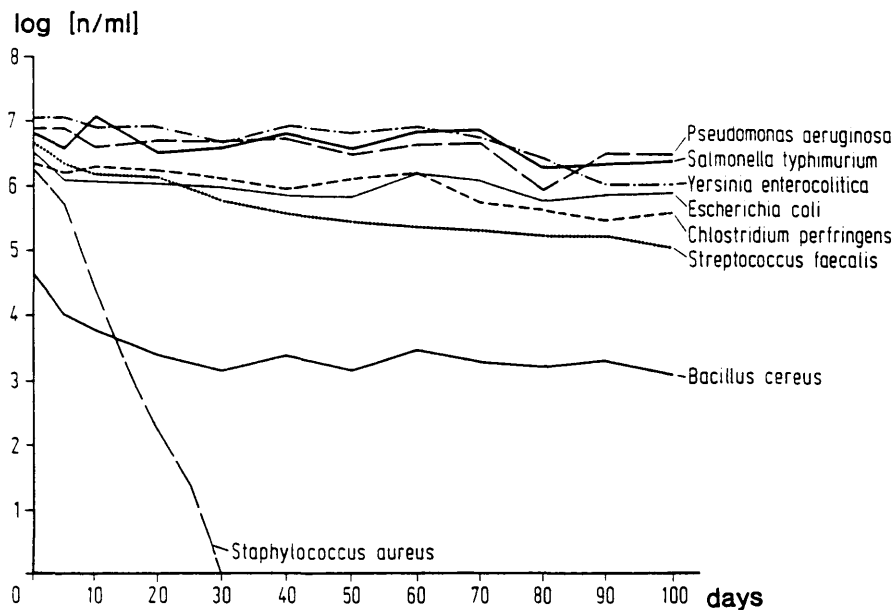


FIGURE 2: Elimination of pathogenous bacteria in aquifer environment models (Mattheß et al. 1985a)

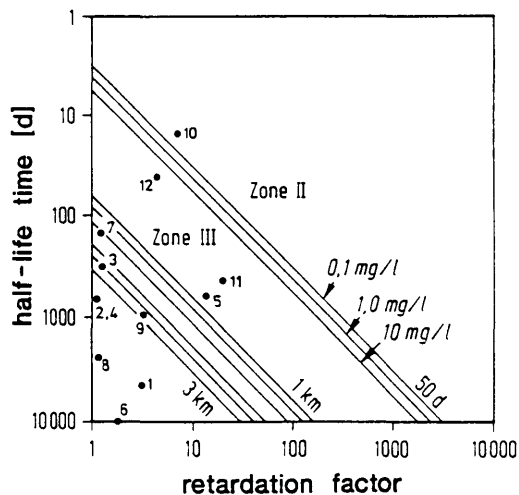


FIGURE 3: Half-life times versus retardation factors of 12 pesticide groups under the specific aquifer conditions of 0.1 % org. C and 1 m/d groundwater flow velocity. 1: halogenated hydrocarbons; 2: carbamates; 3: aniline and amides; 4: carbamide derivatives; 5: organophosphates; 6: diphthiridiles; 7: uraziles; 8: triazines; 9: phenoxy aliphatic acids; 10: nitrophenols; 11: dichlobenile; 12: methylisothiocyanate (Mattheß et al. 1985b)

# A VARIABLE SCALE APPROACH FOR THE DELINEATION OF GROUNDWATER PROTECTION ZONES USING FIELD AND NUMERICAL MODELLING TECHNIQUES

Georg Teutsch

Institut für Wasserbau, Universität Stuttgart  
Pfaffenwaldring 61, 7000 Stuttgart 80, F.R.G.

## Abstract

The general approach in wellhead protection implies the delineation of protection zones surrounding the point of abstraction. These zones are usually defined based on simple traveltime calculations employing pumpingtest data. Increasing groundwater pollution problems originating from agricultural and industrial activities indicate that in some cases a more sophisticated approach is required. Appropriate field investigation and numerical modelling techniques have to be carefully selected in order to meet the project requirements in terms of scale, dimensionality and reliability. Results from an ongoing field and model case study in the Rhine valley are presented to further emphasize the importance of a variable scale approach towards groundwater protection zones.

## Introduction

Groundwater protection in densely-populated and highly-industrialised areas is a very complex technical and economical matter, which requires interdisciplinary solutions. This paper restricts itself to the presentation of a new technical approach, which extends the already generally accepted concept of wellhead protection areas. The main focus concerns the scale problems encountered in the investigations for the delineation of wellhead protection areas.

In many European countries, the general approach towards groundwater protection employs some type of zoning system, either based on traveltime or distance-to-source contours, or a combination of both.

Below, the protection zone system as applied in the Federal Republic of Germany is briefly described. It is based on a number of federal regulations and recommendations, the first of which was already published back in 1953. Protection zone systems employing similar criteria have been adopted in some other European countries (Waegeningh, 1985).

The system comprises four protection zones characterized by varying degrees of restrictions on activities potentially threatening the groundwater quality.

ZONE I covers the immediate wellhead area with a radius of at least 10 m. The area is usually fenced in and therefore protected against unauthorized access.

ZONE II comprises the area within the 50 days traveltime contour. This zone was originally introduced to ensure hygienic standards.

ZONE IIIA extends up to 2 km from the abstraction point. This zone is thought to protect the well from low biodegradability contaminants. Petrol stations, deep excavations and all types of waste disposal sites are prohibited within ZONE IIIa.

ZONE IIIb covers the entire catchment area. It is meant to protect the groundwater from all non-degradable or radioactive contaminants. Construction or operation of uncontrolled waste disposal sites, wastewater infiltration facilities, and pipelines carrying chemicals of high pollution potential are prohibited within ZONE IIIb.

It is accepted that this well established protection zone system has some limitations. Intensive agricultural activities outside ZONE II have caused major groundwater quality problems, due to the missapplication and/or unexpected low degradability of some of the agrochemicals in use. Furthermore, accidental spills and undetected leaks of low biodegradable organic pollutants like chlorinated hydrocarbons have caused groundwater pollution problems in many industrialized areas.

Some of the described problems may be overcome by using more appropriate soil and groundwater investigation methods for the delineation of the protection zones. The selection of the most applicable method for field investigation and modelling has to be based on the project objectives, the specific aquifer conditions, and the general properties of the method itself.

#### Variable Scale Approach

A prerequisite for field and modelling investigations for the delineation and operation of groundwater protection zones concerns the question: At what scale and at what level of detail do we have to carry out our investigations ?.

In order to answer this question it is helpful to introduce some of the concepts developed in the field of stochastic modelling of groundwater flow and transport as presented by Dagan (1986).

In general, three length scales are defined. Firstly, the laboratory scale with a typical length of about  $10^0$  m, secondly the local scale with a typical range between  $10^1$  and  $10^2$  m, and thirdly the regional scale with a typical range between  $10^3$  and  $10^5$  m. Time-scale relationships, equally important for the protection zone concept, are beyond the scope of this paper.

The first type of length-scale L characterizes the extent of the flow or transport domain. The second type of length-scale I characterizes the extent of the heterogeneities in the system. The third type of length-scale D characterizes the space averaging of the variable of interest. D depends on the available measurement device and/or the measurement objective. For a thorough description of the scale concept, including the mathematical framework in the context of groundwater flow and transport through porous media, the reader is referred to Dagan (1986).

Protection zone systems as described above, imply different scale hierarchies of L and I. It is therefore essential to understand the dimensionality and scale of the groundwater investigation methods employed in a protection zone study. Table 1 summarizes some of the common investigation methods indicating their type, dimensionality and scale.

The methods are classified as direct or indirect field- or laboratory-methods. A method is called direct if the parameter investigated results directly from the measurement, e.g. hydraulic conductivity from permeameter measurements. An in-



**Table 1: Common groundwater investigation methods, their type, dimensionality and scale**

| Variable of Interest           | Method               | Type | Dim. | Scale |
|--------------------------------|----------------------|------|------|-------|
| geometry, lithology            | drilling             | f/d  | 1    | D1-D2 |
|                                | surface resistivity  | f/i  | 2-3  | D2-D3 |
|                                | seismics             | f/i  | 2-3  | D2-D3 |
|                                | borehole geophysics  | f/i  | 1    | D1-D2 |
| water balance                  | precipitation, temp. |      |      |       |
|                                | discharge, etc...    | f/i  | 2    | D3    |
| hydraulic conductivity         | pumping test         | f/d  | 2    | D2-D3 |
|                                | slug test            | f/d  | 1    | D1-D2 |
|                                | packer tests         | f/d  | 2-3  | D1-D2 |
|                                | pumping+flowmeter    | f/d  | 2-3  | D1-D2 |
|                                | surface resistivity  | f/i  | 2-3  | D2-D3 |
|                                | seismics             | f/i  | 2-3  | D2-D3 |
|                                | borehole geophysics  | f/i  | 1    | D1-D2 |
|                                | permeameter          | l/d  | 1    | D1    |
| flow direction                 | sieve analysis       | l/i  | 0    | D1    |
|                                |                      |      |      |       |
| flow direction                 | water level meas.    | f/i  | 0-1  | D2    |
|                                | single-hole flowm.   | f/d  | 0-1  | D1-D2 |
| groundwater quality            | integral sampling    | f/d  | 0    | D1-D2 |
|                                | multilevel sampling  | f/d  | 1    | D1-D2 |
| dispersion, effective porosity | forced gradient      |      |      |       |
|                                | tracer test          | f/d  | 2-3  | D2    |
|                                | natural gradient     |      |      |       |
|                                | tracer test          | f/d  | 2-3  | D2-D3 |
| adsorption, decay              | column experiments   | l/d  | 1    | D1    |
|                                | batch and column     |      |      |       |
|                                | experiments          | l/d  | 0    | D1    |
|                                | C-org. content       | l/i  | 0    | D1    |

(f=field method, l=laboratory method, d=direct method, i=indirect method, Scales: 1=laboratory ,2=local ,3=regional)

direct method provides parameters by means of a prior transformation, e.g. lithological information obtained from geoelectrical measurements. In general, the reliability of results obtained by direct methods is higher than those from indirect methods.

Data interpretation problems arise whenever the scale or dimensionality of the domain of interest differs considerably from that of the investigation method. For protection zone investigations one would typically expect a scale hierarchy such as  $D \leq L \Leftrightarrow I$  within ZONE II, and  $D \ll L \Rightarrow I$  within ZONE IIIa and ZONE IIIb.

Moreover, the type of pollutant source has to be considered. Groundwater pollution can originate from either point- or areal-sources. A point-source extends over a much smaller area than the length-scale of the transport-domain  $L$ . An example for a point-source would be a leak in a storage tank. A typical areal-source would be the input of agrochemicals over extended areas within the catchment.

Table 2 presents a simplified classification of the general ability to predict the underground transport of a conservative pollutant originating from a point- or areal-source located at various distances from the abstraction point. It is based on the assumption of an average conductivity porous formation in an area lacking extreme heterogeneities.

Table 2: Predictability of pollutant transport in groundwater protection zones

|                               | point-sources   | areal-sources   |
|-------------------------------|---|---|
| ZONE II (local scale $L_2$ )  | unpredictable spatial moments, concentr. or breakthrough time | predictable <u>average</u> conc. (2D or 3D investig.)               |
| ZONE IIIa (reg. scale $L_3$ ) | predictable spatial moments (2D or 3D investig.)              | predictable <u>average</u> conc. and <u>variance</u> (2D investig.) |
| ZONE IIIb (reg. scale $L_3$ ) | predictable conc. and breakthrough time (2D investig.)        | predictable <u>average</u> conc. and <u>variance</u> (2D investig.) |

Another important feature of groundwater protection zones is the generally converging groundwater flow pattern, caused either by an abstraction well or by the natural outflow at a spring. Consequently the quantity and quality of the abstracted water is the result of near- and far-distance processes of different duration and intensity. It is important to keep this in mind when trying to correlate singular local scale phenomena with the observed abstraction water quality.

#### Case Study

During a groundwater protection zone project which started in 1987 special emphasis was given to the aspects of scale-dependance of the field and modelling methods employed.

The investigation presented refers to a planned wellfield in the Rhine valley near the city of Karlsruhe. The objective of the project is to predict the local and regional groundwater level decline and to delineate the 50 days traveltime contour (ZONE II) for the anticipated abstraction.

The aquifer consists of approximately 35 m of sand and gravel with some interbedded silt layers. Due to several non-hydrogeological constraints (e.g. available open land, distance to the city, distance to the Rhine floodplains etc.) the location of the future pump wells was fixed a priori (Fig.1).

Based on the already available field data a horizontal, two-dimensional finite-element model was developed to simulate the present regional ground water flow in the whole catchment area. A fine mesh with a 100 m spacing was used in an area somewhat greater than the expected 50 days traveltime contour in order to facilitate subsequent small scale investigations (see Fig. 1 and 3). The regional model was carefully calibrated on a monthly base over a period of 5 years. It was used to describe as accurately as possible the flow conditions prior to the construction of the planned waterworks. The model was also used to calculate the expected regional drawdowns assuming different pumping scenarios.

A sensitivity analysis could show that the remaining uncertainty with respect to the available aquifer parameter data was acceptable at the regional scale but not at the local scale. Based on the available hydrogeological information a reliable local scale prediction of the water level decline and the 50 days traveltime contour could not be achieved.

Therefore, further local scale investigations were undertaken, including the drilling of 11 additional monitoring wells, the analysis of core samples, and the recording of geophysical borehole logs. A 45 day pumpingtest was carried out in order to obtain reliable aquifer parameters in the area of the anticipated waterworks. The groundwater flow to the abstraction well was monitored using 5 different tracers which were introduced in the monitoring boreholes. The tracers were sampled in 8 sampling tubes located in the gravel pack of the abstraction well. Integrated samples were obtained from the abstraction water. The 2" sampling tubes were arranged as such to provide directional information about the groundwater flow at different depths. Figure 2 shows the pumpingtest and tracertest setup, including the sampling tubes installed in the gravel pack of the abstraction well.

For the numerical simulation of the pumpingtest and tracertest a local and a sub-local three-dimensional unsteady-state groundwater flow and transport model were developed. These models were coupled to the regional finite-element flow model using a nested structure as described in Figure 3.

During the 45 day pumpingtest, the boundary condition between the regional and the local model was assumed to be steady-state. Between the local and the sub-local model unsteady-state conditions were assumed, due to the cone of depression extending beyond the boundary of the sub-local model.

The time-step in the local-model and in the sub-local model was varied between 1 min at the beginning and 1 day at the end of the simulation period.

Contemporaneously with the pumpingtest the above mentioned tracertest was carried out within the area of the sub-local model (forced-gradient test). The tracer

transport was simulated using a recently developed three-dimensional random-walk program (Pressmar, 1987).

Even though the pumpingtest results indicate very homogeneous conditions with transmissivities between 3.5 and  $4.0 \times 10^{-2} \text{ m}^2/\text{d}$ , the measured tracer breakthrough curves display a high variability in the data obtained from different directions and sampling depths. Figure 4 shows two of the breakthrough curves obtained from the sampling tube P4S and P2S (compare Fig. 2) together with the breakthrough curve sampled in the abstraction well. The presented data clearly indicates that the 50 days traveltime contour based on the tracertest results would considerably differ from that calculated using the pumpingtest data. A more quantitative comparison of the model predictions based on the hydraulic and the tracertest data is presented elsewhere (Teutsch and Hofmann, 1990).

The presented case study should demonstrate how regional scale field and modelling investigations can be used for the delineation of protection ZONES IIIA and IIIB in combination with local scale field and modelling investigations for the delineation of ZONE II.

The entire process of delineation and operation of new protection zones can be summarized as follows:

1. Regional hydrogeological investigation
2. Regional groundwater flow modelling
3. Local field investigations
4. Local flow- and transport modelling
5. Regional model recalibration
6. Construction of waterworks
7. Follow-up field investigations
8. Operation and update of model tools (regional+local)

Out of the eight phases the presented case study covered only the phases two, three and four. The next step will be the recalibration of the regional model. Finally, after the waterworks construction, the nested model tools developed during this study can be used for the management of the protection zones, for risk analysis, and for the design of monitoring networks.

### Summary and Conclusions

A new, variable scale approach towards the delineation of groundwater protection zones is presented. This approach emphasizes the selection of field and modelling methods for groundwater protection investigations on the bases of method properties such as the scale and dimensionality of the measurement. A practical application of the variable scale approach is presented for a case study where a new waterworks is planned in the Rhine valley. Moreover, the case study investigations could show that a large discrepancy is to be expected between the results obtained by common hydraulic tests and those by tracertests.

### References

- Dagan, G., 1986, Statistical Theory of Groundwater Flow and Transport: Pore to Laboratory, Laboratory to Formation, and Formation to Regional Scale, *Water Resour. Res.*, 22, 120S-134S.
- Pressmar, R., 1987, Unvollständige Brunnen zur Grundwassersanierung - Numerische Modellierung für geschichtete Grundwasserleiter, Master Thesis [program documentation] at the Institut für Wasserbau, University of Stuttgart, 77 p.
- Teutsch, G., B. Hofmann, 1990, The Delineation of Groundwater Protection Zones using Forced-Gradient Tracer Tests - A Model Validation Case Study, [to be presented at the] International Conference on Calibration and Reliability in Groundwater Modelling, The Hague, Sept. 3-6.
- Waegeningh van, H.G., 1985, Overview of the Protection of Groundwater Quality, in Matthess, G. et al. (eds.), *Theoretical Background, Hydrogeology and Practice of Groundwater Protection Zones*, IAH, Vol. 6, 159-166.

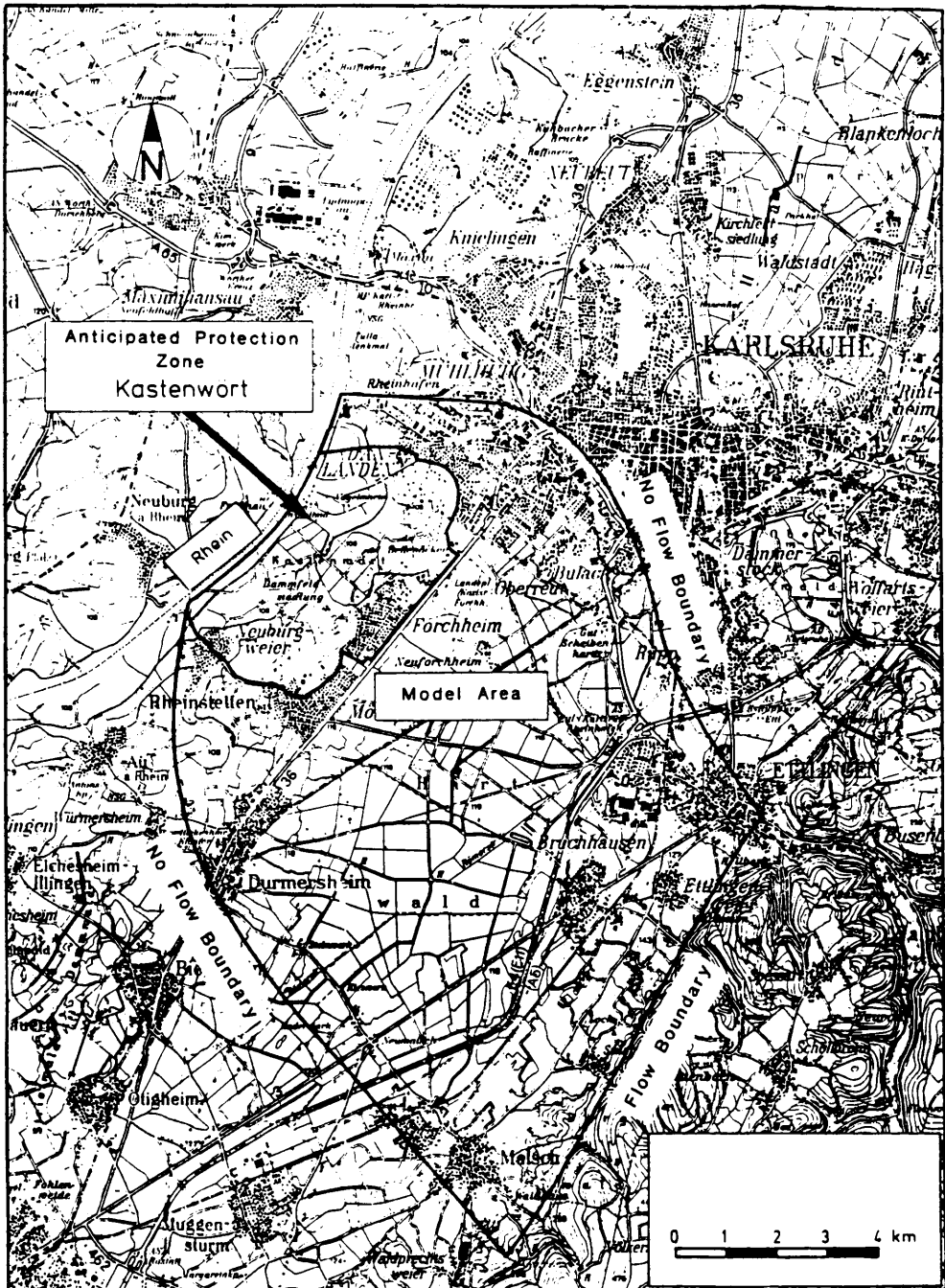


Fig. 1: Project area with model boundaries

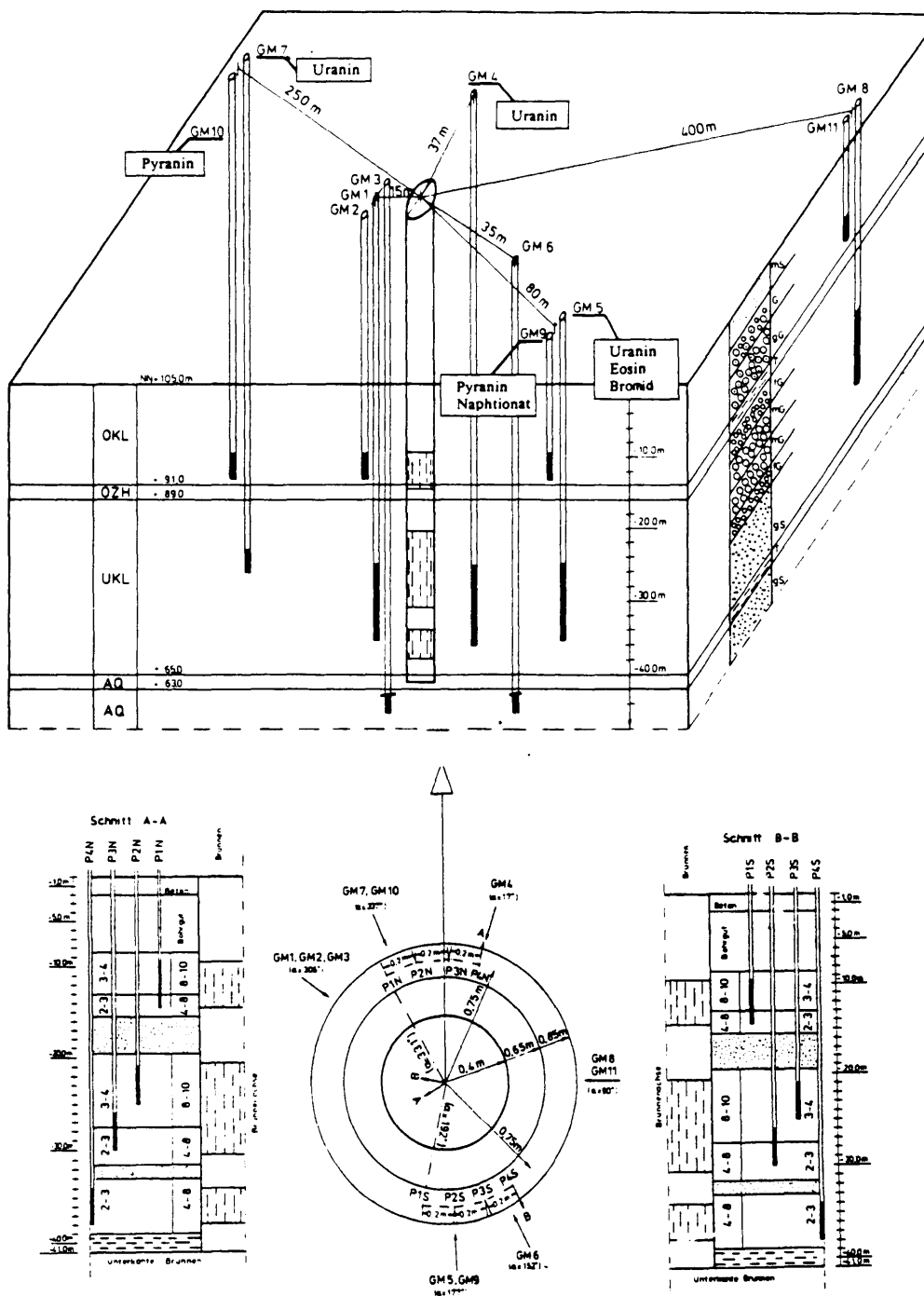


Fig. 2: Pumpingtest and tracer test setup with sampling tubes in the gravel pack

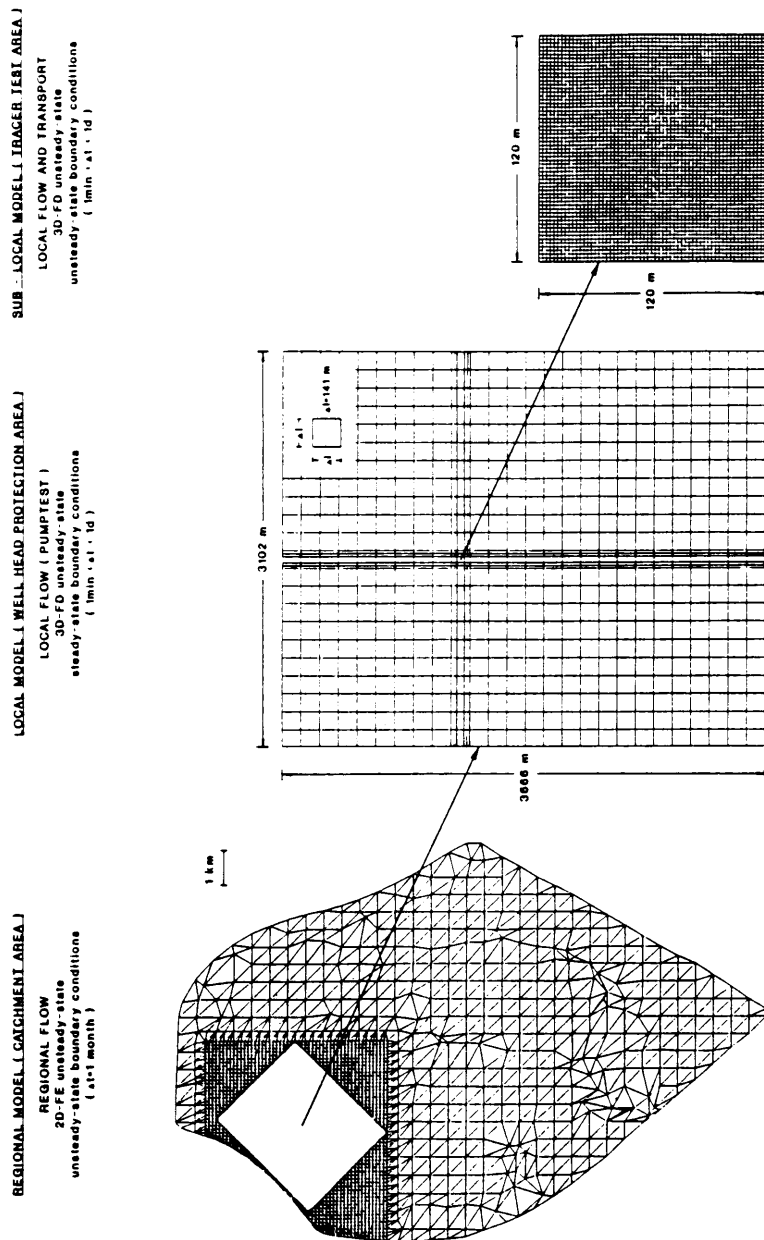


Fig. 3: Regional, local and sub-local models (nested structure)



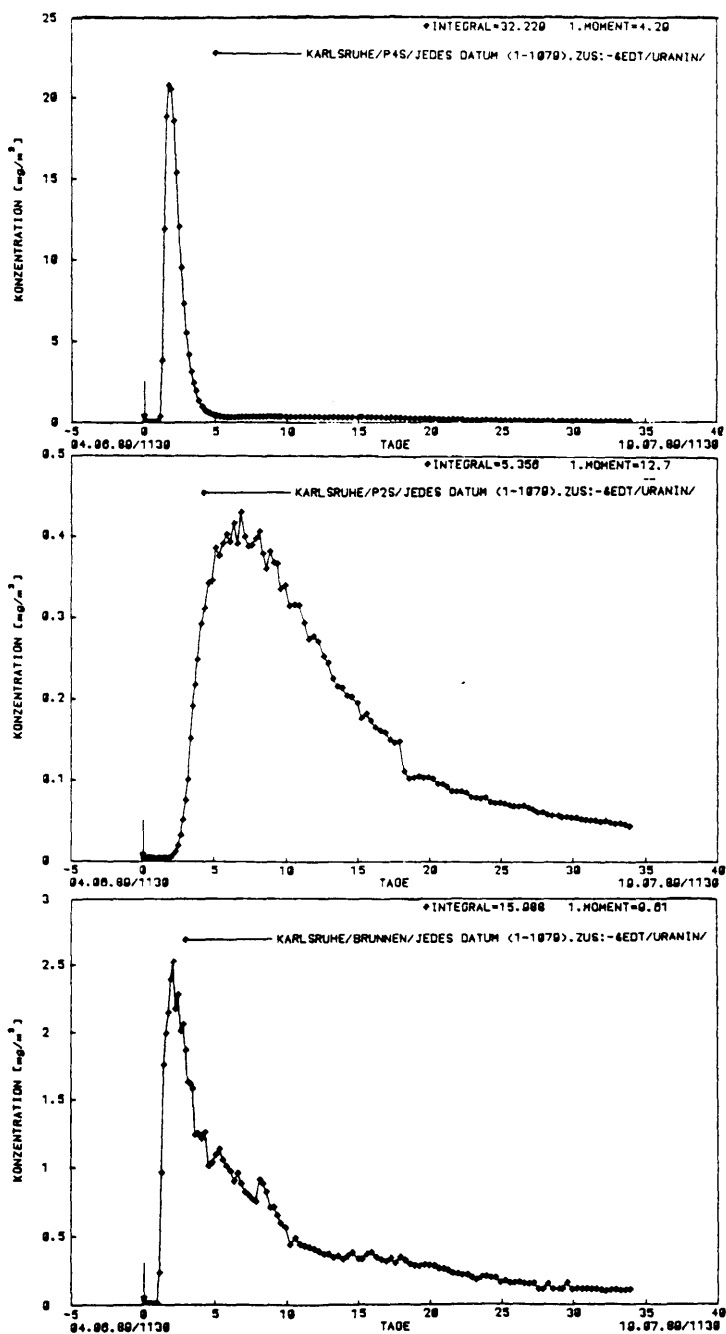


Fig. 4: Tracer breakthrough curves measured at P4S, P2S and in the well



# WELLHEAD PROTECTION: ASSESSING THE POTENTIAL FOR MICROBIAL CONTAMINATION OF DRINKING WATER

Marylynn V. Yates  
Department of Soil & Environmental Sciences  
University of California  
Riverside, California 92521

**ABSTRACT:** Septic tanks are the most frequently reported causes of contamination in ground-water disease outbreaks associated with the consumption of untreated ground water in the United States. The placement of septic tanks is generally controlled by county-wide or state-wide regulations, with little consideration given to the local hydrogeologic, climatic, and land use conditions. Using local values for virus inactivation rate, hydraulic gradient, and transmissivity, the travel time necessary to achieve a 7-order-of-magnitude reduction in virus number was calculated. A wide range of septic tank setback distances (from less than 15 m to greater than 300 m) was calculated for a 200-km<sup>2</sup> area of the Tucson Basin. This study makes use of disjunctive kriging to calculate the conditional probabilities associated with the setback distance estimates. The results are presented in two different ways: first, given a setback distance, the probabilities that the level of viruses will be within acceptable limits are calculated; and second, the desired probability level is specified, and the setback distances required to achieve that level of confidence that the water will be free of virus contamination are calculated. The methods have potential for use by local government officials for the establishment of wellhead protection zones.

## Introduction

In 1980, it was estimated that there were 22 million septic tanks in the United States, serving approximately one-third of the population (U.S. EPA, 1986). Septic tanks contribute more than one trillion gallons of waste to the subsurface every year (OTA, 1984); this waste is the most frequently reported cause of ground-water contamination (U.S. EPA, 1977). In addition, the overflow or seepage of sewage, primarily from septic tanks and cesspools, was responsible for 38% of the outbreaks and 58% of the cases of illness caused by the use of contaminated, untreated well water from 1971 to 1980 (Craun, 1986).

Septic tank effluent may contain a variety of potentially infectious microorganisms, including bacteria, parasites, and viruses. Pathogenic microorganisms which have been found in domestic waste water include Salmonella, Shigella, Entamoeba, Giardia, hepatitis A virus, rotavirus, and poliovirus.

An association between microorganisms in septic tank effluent and waterborne disease outbreaks has been demonstrated several times using dye tracers studies. These studies have shown that the dye traveled from the septic tank to the well in question, thus it was postulated that microorganisms could have done so as well (Craun, 1979). There have also been studies that directly examined the movement of viruses from a septic tank to

a ground-water well (Hain and O'Brien, 1979; Stramer, 1984; and Vaughn et al., 1983). These studies showed that viruses could move as far as 65 m from the septic tank (Vaughn et al., 1983) and persist for up to 131 days in the ground water (Stramer, 1984). Yates (1985) reviewed the ground-waterborne disease outbreaks caused by microorganisms present in septic tank effluent.

Numerous studies have shown that microorganisms can travel considerable distances in the subsurface; these have been reviewed by Yates and Yates (1988). Viruses, in particular, due to their small size (20 to 200 nm) and long survival times, can migrate very large distances in soil and ground water; as much as 1600 m has been reported for certain viruses in karst terrain (Gerba, 1984a) and up to 400 m in sandy soil (Keswick and Gerba, 1980).

In the past, most government agencies have regulated septic tank placement by requiring minimum setback distances between septic tanks and drinking water wells (Perkins, 1984). Setback distances range from 15 to 91 meters, with typical values averaging 15 to 30 m (Plews, 1977). These setback distances are generally imposed over at least a county-wide area, with little consideration given to the local geology, hydrology, and meteorology. Based on the results of the above-mentioned studies, it becomes clear that a setback distance of 15 to 30 m may not be adequate to prevent viral contamination of ground water, and possibly waterborne disease outbreaks, under certain environmental conditions.

In the present study, the variability in septic tank setback distances over city-wide area that resulted when hydrogeologic variables and virus inactivation rates at each well were used in the setback calculations is shown. In addition to calculating the septic tank setback distances, the probabilities that these setback distances are adequate to protect ground water from viral contamination were calculated using disjunctive kriging, a nonlinear estimation technique. Two situations were considered: 1) Given a setback distance (e.g., specified by regulation), what is the probability that this would be adequate to protect the ground water from viral contamination at different locations in the city? and 2) Given a desired probability level, what setback distance would be necessary to be that confident that the ground water would be protected from contamination by viruses?

### Methods

#### Determination of Virus Inactivation Rates

Water samples were collected from 71 continuously pumping municipal drinking water wells located in the Tucson basin (Figure 1). Fifty-ml aliquots of each water sample were placed in sterile, polypropylene containers, and approximately  $10^5$  infective units of virus per ml were added. Each container was incubated at the measured in situ ground-water temperature. On days 0, 1, 2, 3, 5, 7, 10, and 20; 1-ml subsamples were withdrawn from each container and assayed to determine the number of infective units of virus remaining. The inactivation rate of the virus in each water sample was determined by calculating the slope of the line resulting from a plot of the number of virus particles remaining vs. time.

## Calculation of Setback Distances

Setback distances between septic tanks and drinking water wells were calculated using the simplest model available, a modified form of Darcy's law (Freeze and Cherry, 1979):

$$D = (tKi)/n_e \quad [1]$$

where D is the setback distance (m), t is the travel time (d), K is the hydraulic conductivity ( $m\ d^{-1}$ ), i is the hydraulic gradient ( $m\ m^{-1}$ ), and  $n_e$  is the effective porosity of the aquifer.

Travel times were calculated for each sample location using the virus inactivation rates and are based on the amount of time required to achieve a 7-order-of-magnitude reduction in virus numbers. The 7-order-of-magnitude reduction in virus numbers was chosen for the following reason: the World Health Organization (WHO) has recommended that there be no viruses detectable in 1000 liters of water (Gerba, 1984b). If we assume that 10 viruses per ml ( $10^4$  per liter) septic tank effluent travel through the soil and reach ground water, then a decrease of 7 orders of magnitude in virus numbers would be required to approach the WHO's recommendation of zero viruses per 1000 liters (there would actually be one virus per 1000 liters if a 7-order-of-magnitude reduction occurred).

Hydraulic conductivity values were calculated for each sample location based on transmissivity values at each location provided by the State of Arizona Department of Water Resources (the aquifer thickness was assumed to be constant). Hydraulic gradients at each sample site were calculated from a water table elevation map obtained from the City of Tucson.

## Geostatistical Analyses

The techniques used to estimate the setback distances and conditional probabilities are referred to as geostatistical methods. This field of statistics, unlike classical statistics, assumes that the samples are not independent of one another, and that the value of a variable at one sample location is related to its value at another location. Kriging is a geostatistical technique which allows one to estimate the value of a variable at an unsampled location using known values at nearby locations, based on a linear weighted averaging. A complete discussion of geostatistical techniques can be found in Journel and Huijbregts (1978). Disjunctive kriging, which is a nonlinear technique, also allows one to calculate a value at an unsampled location using surrounding known values. In addition, the conditional probability that the estimated value is greater than a prescribed cutoff level is calculated. All geostatistical analyses were performed using the software package GEOPACK (U.S. Environmental Protection Agency, R.S. Kerr Environmental Research Laboratory, Ada, Oklahoma).

## Results and Discussion

A contour map of the septic tank setback distances estimated by disjunctive kriging of the calculated setback distances at each well is shown in Figure 2. The values range from less than 15 m to over 75 m, with the higher setbacks generally located in the north central area of the map. The location

of the higher setback distances corresponds to an area of high transmissivity, where the wells are adjacent to an intermittent stream. The virus inactivation rates in these wells are low due to the relatively cool temperature (19 °C) of the ground water in this area. (Ground water temperature has a significant negative correlation with virus inactivation rates [Yates et al., 1985]). The combination of low virus inactivation rates (which makes  $t$ , the time for 7 orders of magnitude reduction in virus number, large) and high transmissivity (which, owing to the fairly uniform thickness of the aquifer, makes the hydraulic conductivity large) results in the calculation of large distances to minimize the possibility of viruses being present in drinking water.

#### Case-1: Probabilities Associated with Specified Setback Distances.

Probability maps were calculated for two setback distances for comparative purposes. The probabilities estimated for a specified setback of 15 m are shown in Figure 3a. Comparing the 15-m contours in Figure 2 with the corresponding contours in Figure 3a, one can see that these contours have a probability of 0.70. In other words, if a 15-m cutoff level is specified, there is a 70% probability that 15 m would be adequate to prevent virus contamination of ground water at the 15-m contours.

Figure 3b shows the probability contour map calculated using a 30-m cutoff level. Looking at the 15-m contours on Figure 2 once again, and comparing them with the corresponding contours on Figure 3b, the contours now have a 0.85 probability. This is because, at this location, we had estimated that 15 m would be adequate to protect the ground water from contamination. Now we have imposed a 30-m setback at this location. It follows that the probability that 30 m would be adequate is higher (85%) as compared with the probability estimated for 15 m (70%).

#### Case 2: Setback Distances Associated with Specified Probabilities

In this case, rather than specifying a setback distance and calculating the associated probabilities, the desired probability level is specified and the associated setback distances are calculated. In the first example, a probability level of 0.9 was specified. In other words, what setback distance is necessary to be 90% certain that the actual setback distance is less than or equal to that distance? Comparing the 15-m contours of Figure 2 with those roughly corresponding on Figure 4a, it can be seen that a 40-m setback distance would be required to be 90% certain that the ground water would be adequately protected from virus contamination. If one wanted to be 99% certain that the setback was adequate to prevent viral contamination, an 80-m setback distance would be required in those locations where 15-m distances were calculated (Figure 4b).

These methods of calculating septic tank setback distances have potential for use as management decision-making aids in regulating septic tank placement in a community. Although a very simple model was used here for illustrative purposes, it is expected that if the proposed techniques were to be used by a municipality, a more comprehensive ground-water travel time model would be used to calculate setback distances. Vertical transport through the unsaturated zone and the presence of pumping wells are among the factors which would have to be considered.

To demonstrate the effect of adding pumping wells to the regional ground-water flow in the travel time calculations, a simple one-well case was used. The well chosen is pumped at a rate of  $9.46 \times 10^{-3} \text{ m}^3 \text{ sec}^{-1}$  (150 gpm). In the disjunctive kriging calculation, in which only regional ground-water flow was used in the setback distance calculation, this well was located on a 60-m contour (Figure 2). When the  $9.46 \times 10^{-3} \text{ m}^3 \text{ sec}^{-1}$  pumping rate is added to the travel time calculation, a setback distance of 156 m is required to achieve a 7-order-of-magnitude reduction in virus number (Figure 5). The actual calculations would be more complicated than described here, as the effects of all of the wells' pumping would have to be included to get an accurate picture of the flow field in the Basin. This simple example does show, however, that pumping has a large impact on the travel time, and thus setback distance, calculations and must be considered if the method is to be used for municipal planning purposes.

With the appropriate modifications to model the specific situation of interest, the methods could be used for community planning purposes. The first case described, namely calculating the conditional probabilities given a specified cutoff level, would be useful in a situation where the minimum setback distance was specified by regulation. For example, a certain community has a regulation stating that 30 m is the minimum separation between a well and a septic tank. Disjunctive kriging could be used to generate a conditional probability contour map. A decision to allow a septic tank to be placed in a certain location could then be based on the calculated probabilities. For example, it might be decided that if the probability was 75% or greater, a septic tank would be permitted on any lot, provided that soil percolation test requirements were met. If the probability was between 50% and 75%, soil percolation test requirements could be made more stringent or the minimum lot size could be increased in order for a septic tank permit to be issued. If the probability was less than 50%, it might be decided that septic tanks would not be allowed at all.

The approach described in the second case could also be used for community planning purposes, in that a desired probability level could be specified (e.g., in a regulation), and the setback distances necessary to achieve that level would be calculated. One advantage of using this method is that the implicit assumption that the hydrogeologic characteristics of the area are constant would be avoided. The regulations would only have to specify a probability level to be met in order to allow a septic tank permit.

Models of this type will become more important in the future, especially in light of the proposed maximum contaminant level goal (MCLG) for viruses in ground water. In November, 1985, the U.S. Environmental Protection Agency proposed an MCLG of 0 viruses in drinking water. Rather than require monitoring of all drinking water for the presence of viruses (as is done for coliform bacteria), it was proposed that all ground waters must be disinfected prior to distribution. It was anticipated that variances from the mandatory disinfection requirement might be granted if it could be shown that it is unlikely that viruses could contaminate the drinking water. It has been suggested that if it could be shown, using a model, that the travel time of domestic waste from the source to the well will result in an 8 to 10 order-of-magnitude reduction in virus numbers, a variance could be granted (Gerba, 1984a). In this model, the setback distance was calculated based on a 7-

order-of-magnitude reduction in virus numbers, although this could easily be modified for any amount of virus inactivation.

### References

Craun, G.F., 1979, Waterborne disease - a status report emphasizing outbreaks in ground-water systems, Ground Water 17, 83-191.

Craun, G.F., 1986, Statistics of waterborne outbreaks in the U.S. (1920-1980), In: Waterborne Diseases in the United States. G.F. Craun, ed. CRC Press, Boca Raton, Florida. chap. 5, pp. 73-159.

Freeze, R.A. and J.A. Cherry, 1979, Groundwater. Prentice-Hall, Inc., Englewood Cliffs, N.J.

Gerba, C.P., 1984a, Microorganisms as groundwater tracers, In: Groundwater Pollution Microbiology. G. Bitton and C.P. Gerba, eds. John Wiley & Sons, New York. pp. 225-234.

Gerba, C.P., 1984b, Strategies for the Control of Viruses in Drinking Water. American Association for the Advancement of Science, Washington, D.C.

Hain, K.E. and R.T. O'Brien, 1979, The survival of enteric viruses in septic tanks and septic tank drainfields. WRRI report no. 108, Las Cruces, New Mexico.

Journel, A.G. and C.J. Huijbregts, 1978, Mining Geostatistics. Academic Press, Inc., New York.

Keswick, B.H. and C.P. Gerba, 1980, Viruses in groundwater, Environ. Sci. Technol., 14, 1290-1297.

Office of Technology Assessment, 1984, Protecting the Nation's Groundwater from Contamination. U.S. Congress, Washington, D.C. rept. no. OTA-O-233.

Perkins, R.J., 1984, Septic tanks, lot size and pollution of water table aquifers. J. Environ. Hlth. v. 46, pp. 298-304.

Plews, G., 1977, Management guidelines for conventional and alternative onsite sewage systems-Washington state. In: Individual Onsite Wastewater Systems, Proceedings of the Third National Conference, 1976. N.I. McClelland, ed. Ann Arbor Science, Ann Arbor, Michigan.

Stramer, S.L., 1984, Fates of poliovirus and enteric indicator bacteria during treatment in a septic tank including septage disinfection. Ph.D. dissertation, University of Wisconsin, Madison.

United States Environmental Protection Agency, 1977, The Report to Congress- Waste Disposal Practices and Their Effects on Ground Water. U.S.EPA, Washington, D.C.

United States Environmental Protection Agency, 1986, Septic Systems and Ground-Water Protection: An Executive's Guide. Office of Ground-Water Protection, Washington, D.C.



Vaughn, J.M., E.F. Landry, and M.Z. Thomas, 1983, The lateral movement of indigenous enteroviruses in a sandy sole-source aquifer. In: Microbial Health Considerations of Soil Disposal of Domestic Wastewater. U.S.EPA publication no. EPA-600/9-83-017.

Yates, M.V., 1985, Septic tank density and ground-water contamination, Ground Water, 23, 586-591.

Yates, M.V., C.P. Gerba, and L.M. Kelley, 1985, Virus persistence in groundwater. Appl. Environ. Microbiol., 49, 778-781.

Yates, M.V. and S.R. Yates, 1988, Modeling microbial fate in the subsurface environment, CRC Crit. Rev. Environ. Control, 17, 307-344.

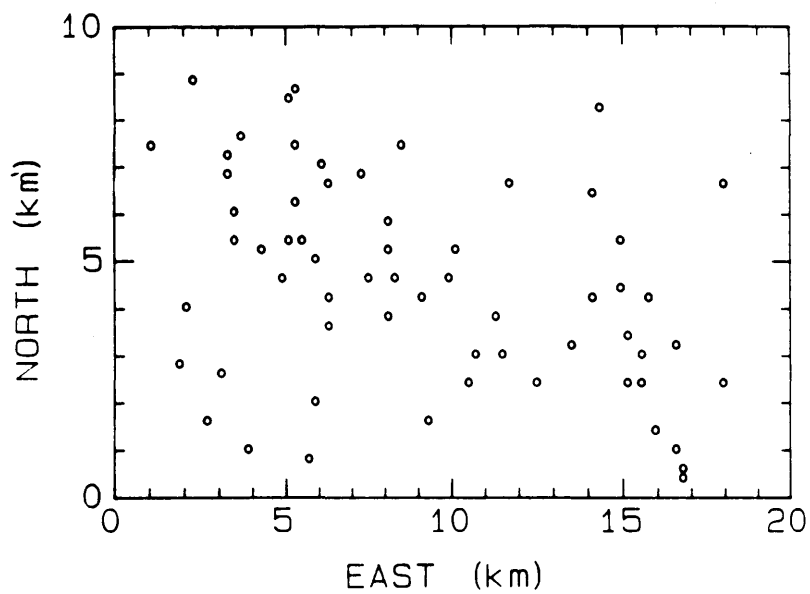


Figure 1. Sample collection sites. Origin is Arizona quadrant D, township 14S, range 14E, section 19, CCC.

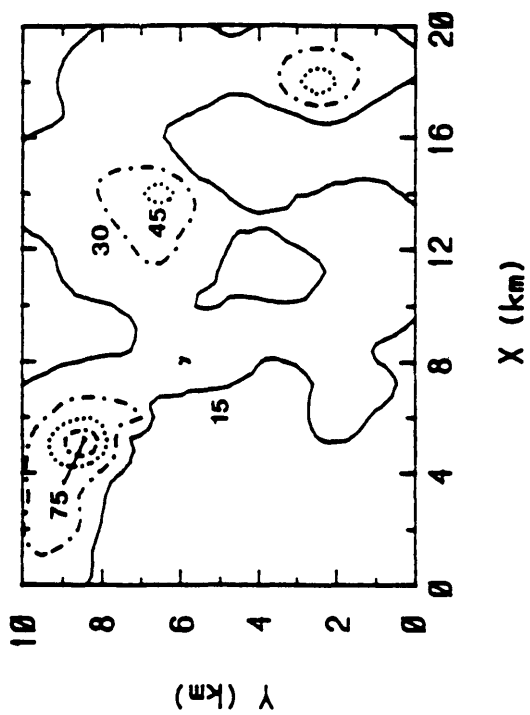


Figure 2. Septic tank setback distances (m) estimated by disjunctive kriging. Legend: 15 m (—), 30 m (---), 45 m (...), 60 m (---), and 75 m (-.-).

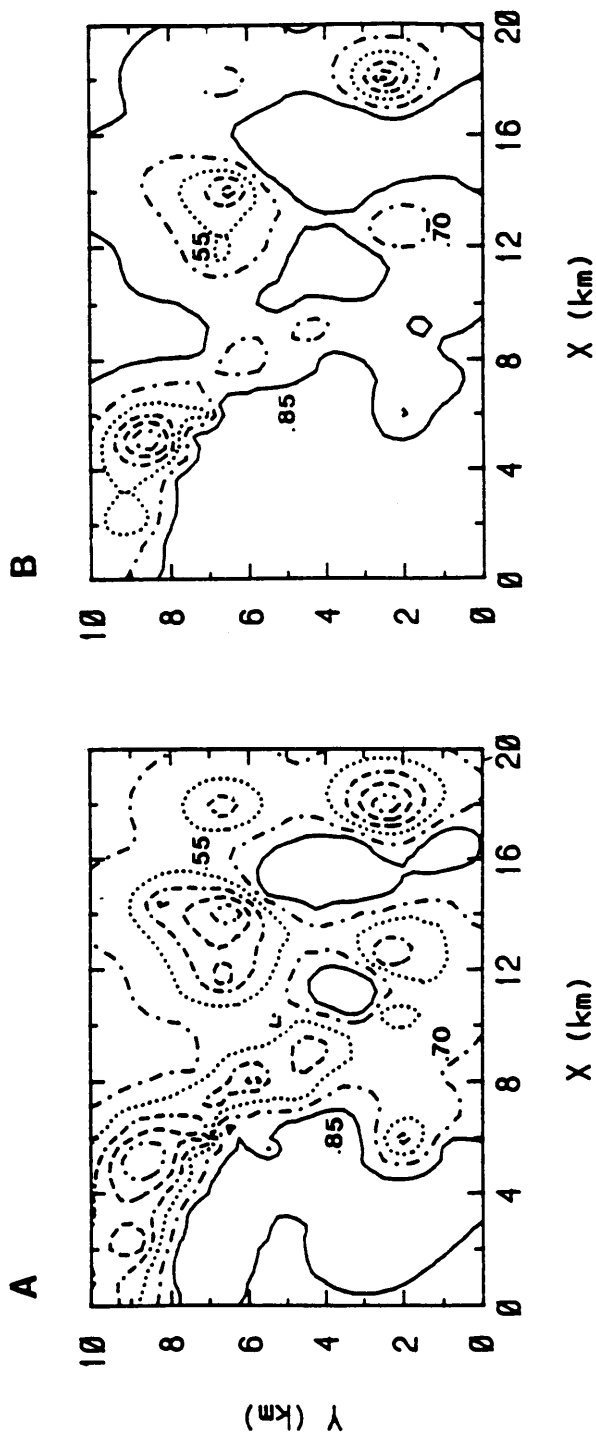


Figure 3. Contour diagrams for the conditional probabilities that the set - back distances are greater than A) 15 m and B) 30 m. Legend: 0.85 (—), 0.70 (---), 0.55 (...), 0.40 (-.-), 0.25 (-.-.-), and 0.10 (-.-.-).

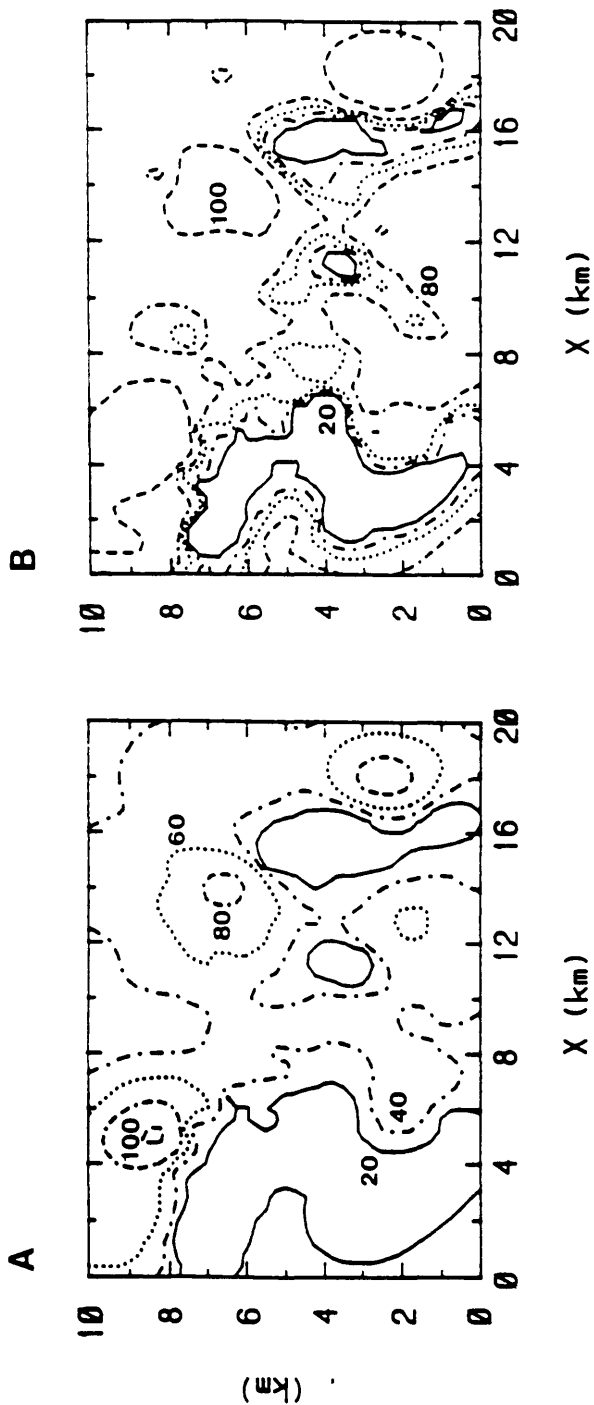


Figure 4. Contour diagrams for the setback distances (m) given a conditional probability of A) 0.10 and B) 0.01. Legend: 20 m (—), 40 m (---), 60 m (.), 80 m (-.-), and 100 m (- - -)

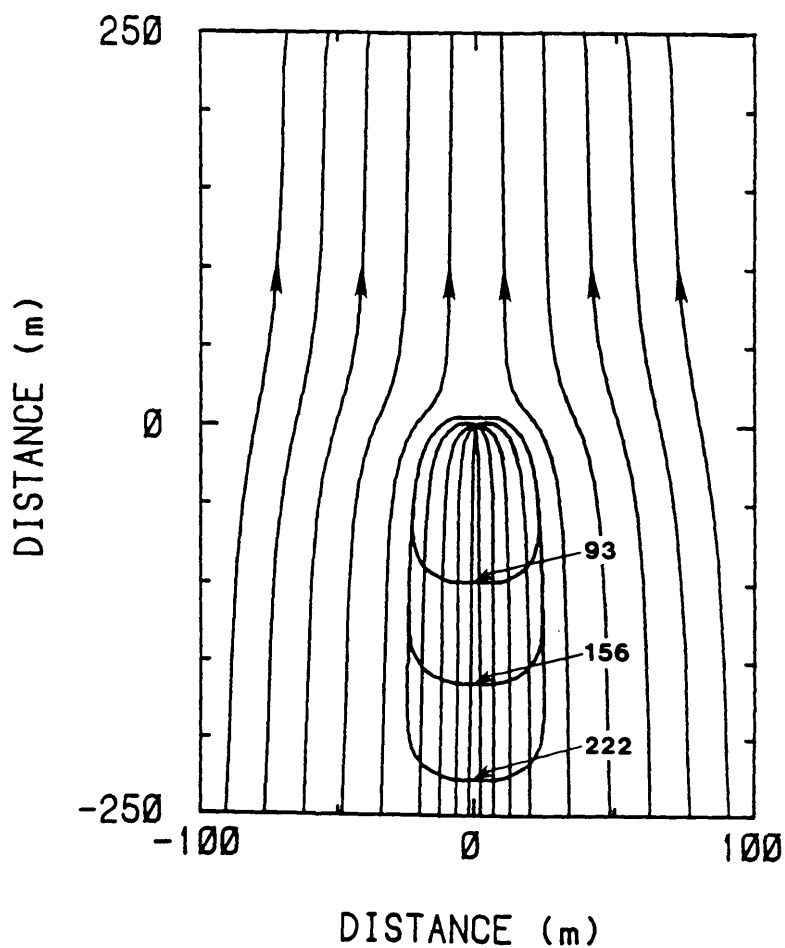


Figure 5. Setback distances (m) calculated for a pumping well in a regional flow field for 4, 7, and 10 orders-of-magnitude reduction in virus number.

# COMPACT EXPERT SYSTEM FOR WATER RESOURCES ASSESSMENT IN AFRICA

PATRICE POYET\* and MICHEL DETAY\*\*

(\*) CSTB, B.P. 141, 06561 Valbonne, France.

(\*\*) CEFIGRE, B.P. 113, 06561 Valbonne Cedex, France.

## Abstract

For more than twenty years African states have devoted themselves to the improvement of water supply to the rural population. The problem of water prospecting became crucial and in 1989 the most optimistic statistics show that drinking water is still not available to more than 80% of the rural population in developing countries. The various estimations carried out within the scope of the Drinking Water and Sanitation Deceny (1980-1990) show that the water demand in countries of Western and Central Africa is considerable. As far as the village water supply is concerned, extrapolating the 1976 estimations leads to 100.000 water points to be carried out by 1990. To meet the water demand in developing countries, thousands of water points remain to be created within the scope of programs for village water supply.

Since 1973, we devoted ourselves to extending the water resources of developing countries and we reflected upon the mechanisms governing the hydrodynamic characteristics of aquifers. Since 1985, we have modelled this approach thanks to computer tools based on the expert system technology. We have developed an expert system dedicated to optimize the location of drilling sites.

This paper is an overview of hydrogeological studies in the field of village water supply programs. Its primary interest lies in the way it identifies decisive hydrogeological parameters and in its use of artificial intelligence techniques in this domain. We first present the main features of African hydrogeology, then we summarize the methods generally used by experts for well-location studies. We explain our methodology to identify decisive hydrogeological parameters and present original data showing connections between data collected during the location studies and the hydrodynamic parameters registered during the drillings.

The primary importance of a drinkable water-supply, the existence of a large amount of statistical data that could be applied to the location criteria, the repetitive nature of the steps to be carried out for a hydrogeological search and the African technicians' training needs, all led us to develop an expert system. We explain the possibility of modelling the process used by a hydrogeologist to successfully carry out drilling sites studies using computer assisted functions. We then detail the expert system HYDROLAB architecture, the rules of the software, its principal functions, its model of control and its system for recognizing solutions.

## 1. Main Features of African Hydrogeology

In Africa the geological context is divided into three large groups:

- The *Precambrian crystalline bedrock*, corresponding to the basement complex. It represents the oldest formations of the African Shield (granites, gneiss, quartzites, schist, etc.) ;

- *Old formations*, tabular, Infracambrian and Primary, associated with the deep-seated complex ;
- *Sedimentary formations*, both post-primary and recent deposits.

From those three geological context, two major types of aquifer systems can be determined: sedimentary and igneous/metamorphic.

The sedimentary formations and recent deposits are permeable formations and generally enclose continuous aquifer. These often meet in great sedimentary basins, mainly situated in the Sahel latitude: the Senegalo-Mauritanian basin, the central delta of the Niger river, the Taoudeni basin, the Nigerian basin, and the Chadian basin. They represent 85% of the surface area of Senegal, 65% of Mauritania, 75% of Nigeria, 64% of Mali, 65% of the Congo, 52% of Chad, and also form a narrow coastal band occupying a small portion of the Ivory Coast, Togo, Benin, Gabon, the Togo and Cameroon.

The precambrian crystalline bedrock and the old formations characteristically have a discontinuous aquifer. They occupy the main part of the Ivory Coast (97% of the country's superficial area), Burkina Faso (95%), Togo (94%), Benin (83%), Cameroon (89%), and Gabon (80%), and correspond to zones of high population density.

## 2. Classical Investigation and Assessment Techniques Used by Experts

Ideally groundwater development should be preceded by proper investigation and assessment. In this chapter we propose a comprehensive evaluation of the decisional parameters used by groundwater specialists to realize well-location. The four major techniques of groundwater exploration are discussed from the viewpoint of a professional consultant :

- *Basic studies* : localization of villages on maps, study of the background data available concerning the zone and a first approach to its geology, climatology, hydrogeology, geomorphology ;
- *Aerial photographs* make excellent base maps. Stereopairs can be used for three-dimensional study of hydrologic features in order to distinguish rock and soil types, identify pattern of fractures, detect springs and marshes and facilitate classification of a region into areas of good, fair and poor groundwater prospects ;
- *Field studies* allows on site recognition of relevant geological features. At this stage an inventory of water resources can be realized. A discussion with the village authorities will allow the socio-economic demands of the village to be taken into account.
- *Geophysical exploration methods* are used to obtain information on the character of formations. The electrical resistivity method is a major geophysical tool used in groundwater exploration efforts.

The expertise required to utilize these different methods varies widely. All of the methods discussed in this chapter tend to complement one other, interpretation of data is an intricate process.



### 3. Search for Decisive hydrogeological Parameters

The research that we have undertaken in this field since 1973 covers fifteen or so countries in Africa and benefits from various studies where we applied artificial intelligence techniques to engineering problems (Detay, 1985), (Detay *et al.*, 1986, 1988, 1989), (Bernardi *et al.*, 1975, 1989), (Poyet, 1986), (Poyet *et al.*, 1988, 1989).

Few tasks in hydrogeology are more difficult than locating drilling sites for water in igneous and metamorphic rocks nevertheless they are at or near the surface in more than 20 % of the land surface of the world, that is about 80% in Africa and 50% of the wells in some areas are classed as failures. Extreme variations of lithology and structure coupled with highly localized water-producing zones make geological and geophysical exploration difficult. Soil and vegetation commonly cover outcrops and make the necessary detailed geological observations impossible.

#### 3.1. The Cognitive Aspect

In this chapter we describe in ten points what we believe to be the major decisive hydrogeological parameters taking as an example the crystalline aquifer environment. As we will see in the next chapters expert systems use expertise rules (i.e. the decisional process of the experts) and interpretative models (i.e. statistic decisional models). To permit a better understanding of the expert system approach, we describe for each point some of the rules of expertise (referred as *Re.*) and the connected interpretative models (referred as *Im.*).

*The geomorphological environment* : The first stage in photo interpretation and in the field study is a phase of observation. Topography has been found to be an important indication of well yield in certain regions. Wells on flat uplands and in valleys tend to yield larger amount of water than wells on valley sides and sharp hill tops. Rules of thumb can be deduced such as *Re. 1*: "in hard rocks move away from crystalline domes, mountain crests and sides which are non-water bearing".

The lack of water on or near the steeper slopes can be explained by the fact that erosion has removed much of the weathered and more permeable rocks. Water levels are also further below the surface because groundwater drains to points of discharge in adjacent lowlands.

*The drainage pattern* : The size of the stream, its declivity, its profile, the shape of the bed and the morphology, are elements that permit an evaluation of groundwater recharge and discharge together with varying associated water levels, water quality and pollution.

*The position of the piezometric level* : This parameter is a decisive element. The piezometric level can be situated either in a porous zone (weathered zone), in the fissured zone or in the fractured zone. In North Cameroon, we observed that the distribution of the piezometric level obtained from 527 observations shows that in 90% of the cases in a crystalline environment, the piezometric level is located in the weathered zone. In terms of rules of expertise, the position of the piezometric level in the weathered rocks, that can be observed thanks to the pre-existing traditional wells, is a very favorable element in the search for groundwater : and conversely its absence introduces a high percentage of risk.

*The sheet-type joint system* : It can be studied from aerial photographs. There is often a correlation between fracturing and the drainage pattern which indicates

the potential water-bearing fracture system. Rules of expertise can be based, in hard rocks, on the evaluation of the density and extent of the system of cracks and fractures. Schematic searches can be made in the catchment area for major multikilometric fractures where the maximum volume of saprolite reservoir can be drained.

*The rock type* : The water-bearing characteristics of most crystalline rocks are primarily controlled by weathering and structure. Rock type alone is commonly of secondary importance. Differences in well yields tend to reflect differences in degree of weathering or fracturing rather than inherent differences of mineralogy or fabric within the rocks.

*Extent and thickness of the weathered layer* : The in situ weathered overburden thickness and the connections existing with the hydrodynamic characteristics of the aquifer, have been quantified (Detay, 1987). Probabilistic functions have been deduced showing the connections between the size of the weathered zone, the hydrodynamic characteristics of the aquifer (yield, specific yield), and the percentage of chances of obtaining the infra-yield.

*The depth of borings: is there an optimal depth ?* : To attempt to answer this question we worked on the depths of penetration into the crystalline basement itself (i.e. the total depth of the boring minus the size of the weathered zone). With 427 borings as a starting point, we calculated the depth of penetration into the crystalline basement by five meter segments of increasing depth, and we calculated the average yield in cubic meters per hour (m<sup>3</sup>/h) per segment. An interpretative model as been deduced, showing the relationship between well yield per unit length of well penetration in the aquifer. It shows from 5 to 50 meters of drilling into the crystalline basement a negative relationship between the increase in depth and the increase in yield and from 50 to 60 meters a positive relationship.

The water production per meter of well decreases rapidly with an increase in well depth. The optimum depth of water wells in crystalline rocks is determined largely by economic factors unless the geological structure is known in detail.

*The climatological data: efficient rainfall, evapotranspiration, etc.* : The efficient rainfall linked to the geophysical, geomorphological and climatological data permit to deduce the effective infiltration and to estimate the infiltration capacity. This is calculated according to the size of the catchment basin, the relative development of the reservoirs, the morphological position of the village, etc. For example, in the basement complex, the study of the efficient rainfall linked with the hydrodynamic characteristics permit to identify three domains where a minimum size of catchment basin is needed to get a positive drilling. These are respectively 8km<sup>2</sup>, 5km<sup>2</sup> and 3km<sup>2</sup> for the domains of efficient rainfall of below 125 mm/year, between 125 and 500 mm/year, and above 500 mm/year, respectively.

*Geoelectrical investigation (longitudinal conductance)* : The research work carried out by our team since 1975 (Bernardi *et al.*, 1975, 1980, 1989) shows a relationship between the registered longitudinal conductances, the percentage of failure in the drillings and the hydrodynamic characteristics of the aquifer (Table. 1).

| Conductance (mho) | Villages | Success rate (%) | Yield(m <sup>3</sup> /h) |
|-------------------|----------|------------------|--------------------------|
| inf. to 0.1       | 48       | 6 %              | 0.6                      |
| 0.1 to 0.2        | 61       | 40 %             | 0.9                      |
| 0.2 to 0.5        | 88       | 84 %             | 3.6                      |
| 0.5 to 2.5        | 76       | 92 %             | 3.8                      |

Table. 1. : Relationship between yield, success rate and longitudinal conductance.

Table. 1., established after 273 drillings, carried out in Togo, Benin, Central African Republic, Cameroon and Burkina Faso, statistically indicates that relatively high yields correspond to the high values of the total longitudinal conductance and inversely, low yields correspond to the low values of longitudinal conductance. Rules of expertise and interpretative models can be deduced. For more detailed informations refer to (Bernardi *et al.*, 1989).

*Influence of the thickness of the saturated weathered zone* : Thanks to kriging, we have been able to represent geometrically (Detay, 1989) the relation between the thickness of the saprolite reservoir, the importance of the saturated weathered zone and the yield.

The thickness of the saturated weathered zone may be negative when the piezometric level is situated in the bedrock. The yield appears to be directly linked to the thickness of the saturated zone. This relation reflects the mechanism of the aquifer system.

### 3.2. Decision-making parameters

Proper well location, however, is but one of a number of problems facing the prospective well owner. Poor water quality, biological contamination, future lowering of water levels in wells, and improper completion methods are some of the many problems dealt with frequently by hydrogeologists. To make relevant recommendations, the hydrogeologist uses decision-making process. In order to make the expert system operational we undertook the task of quantify decision-making parameters (*Dmp.*).

We defined:

- *First order parameters*, which help in the decision to establish well location studies. Figure 1. indicates the probabilist evolutionary tendencies of the hydrodynamic characteristics according to the thickness of the saprolite reservoir. The utilization of these graphs enable to do the following:

- \* *Dmp. 1.a* : evaluate the percentage of obtaining the infra-yield (boring risk) ;
- \* *Dmp. 1.b* : evaluate the average potential yield limit of the future wells ;
- \* *Dmp. 1.c* : evaluate the average potential specific yield limit of the future wells.

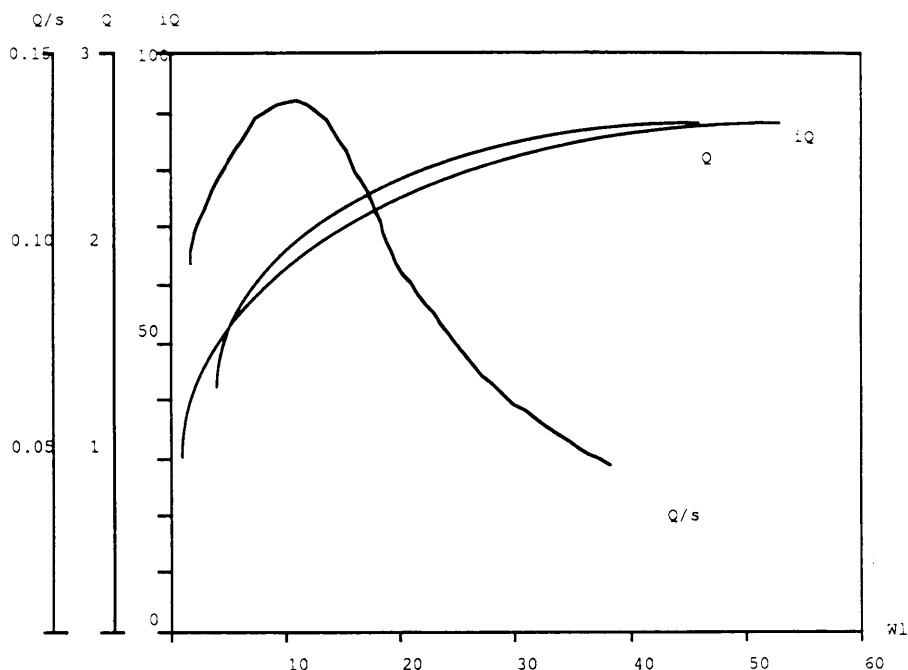


Figure 1 : Hydrodynamic characteristics and success rate according to the thickness of the saprolite layer ( $Wl$  stands for thickness of the weathered layer,  $iQ$  for the succes rate,  $Q$  for the yield, and  $Q/s$  for the specific yield).

- *Second order parameters*, which help in the decision-making when carrying out the drilling. Depth and cost are second order decision-making parameters. They intervene not only from an economic point of view, but are also decisive in the potential failure or success in the drilling. We could assess the following second order parameters:
  - \* *Dmp. 2.a* : evaluate the chances of obtaining the infra-yield (boring risk) ;
  - \* *Dmp. 2.b* : decide to what extent it would be opportune to continue the boring or whether it would be better to stop drilling, taking into account the finance available for the project ;
  - \* *Dmp. 2.c* : evaluate at each moment by scales of boring depth the average yield and the average specific yield and their evolutionary tendencies.
- *Third order parameters*, which help in the decision-making to design the well equipment and use properly completion methods..

following the project requirement and the water needs, these decision-making parameters help the user to take the right decision. In HYDROLAB the rules coming from the Dmp. appears as recommendations at the end of the experts system cycle.

## 4. The Expert System Approach

### 4.1. Introduction

Expert systems come from applied research in artificial intelligence. Computer aided softwares aim to help in the decision-making process, they are designed to solve complex problems while trying to imitate human reasoning. Unlike mathematical or stochastic models, which operate on precise numerical data, expert systems use a symbolic representation of the problem, known as a knowledge base and an associated chain of reasoning called strategy of inference.

The software had to run on microcomputers, in order to be widely available and useful to geologists who are faced with the real problems of developing countries. For this reason, HYDROLAB was written in TURBO-PROLOG™, a high-level language that includes some of the main characteristics of PROLOG as defined by (Colmerauer, 1977), (Colmerauer, 1983) (Clocksin *et al.*, 1986), but that also allows a very efficient compilation on microcomputers. Some of the original PROLOG interpretative mechanisms have been suppressed in this dialect because they were very resource consuming. The global performance and the compactness of the generated code are then very impressive. For more details on PROLOG efficiency, refer to (Warren, 1977) and (Borland, 1986).

As far as the user is concerned, the system acts at the dialog level as a diagnostic-like expert system, asking questions, analysing user answers, and building plans in order to schedule the appropriate set of actions enabling an intelligent data gathering. Interaction with the software is achieved through a natural language module and a windowing system displaying the current state of the program. A control panel is associated with the inference engine, in order to display the internal activity of the system at a high symbolic level. The user is informed in this way of the current goal and subgoal pursued by the system, the current position and the depth in the search tree, the current rule fired from the conflict set and the number of solutions encountered so far during the run. Moreover, we developed a wide set of self-explanation functionalities in order to use this system in computer aided learning, mainly for African technicians, in the water-supply domain.

The aim of the system is to build a model of the user's problem and to try to match it initially, using a fuzzy logic, with a set of drilling case studies corresponding to typical well patterns stored by HYDROLAB in a data-base-like structure. When this reasoning step fails, the system builds a new plan to gather relevant data that could be lacking, then tries to rematch the currently-described situation with real solutions (i.e. case studies) and finally with generic ones. The typology of generic solutions is based on the favorability of two major concepts such as the amount of water intake and the properties of the water bearing level.

For all cases, the system is able to make a diagnosis about the user's situation based on the hydrogeological parameters described in section 3.1, to give advice in order to increase the user's average success, and to evaluate the hydrodynamic characteristics of the future well, according to the decision making parameters previously highlighted in section 3.2.

### 4.2. Description and start-up

The system is composed of several hierarchical levels of data collection. These data are analysed and correlated at each stage and generate more and more accurate intermediate hypotheses until a relevant estimation of local hydrogeological resources is obtained. The start-up and the use of the system is

extremely simple. The user is encouraged to volunteer in natural language with HYDROLAB in order to provide various parameters that correspond to the data acquired relating to the given environment.

The system evaluates the nature of the risk using the *Im.* and offers various solutions. Depending on the significance of the risk it may even reconsider its approach and ask for additional information on some point or other it considers important.

Thanks to an interactive window, it is possible for the user to follow the objectives of the system at any time, and to inquire about the implications of questions that have been asked to the user. In this way it confers functions of computer-assisted learning (CAL) on the HYDROLAB system.

Finally, the system identifies the hydrogeological context. HYDROLAB directs itself towards two types of solutions: firstly the *analogical* one related to case studies that appeared to account for very representative hydrogeological local contexts, and secondly the *generic* solution of a given problem, based on abstract concepts such as the water intake or the water bearing structure. These two models of solutions are closely related to the control strategy implemented for the HYDROLAB system, the first set being derived during the first control phase and the second after that a new plan could be triggered when complementary data appeared to be useful. This mechanism was referred as the double pass model of control, described in the next section.

#### 4.3. A double pass model of control

The main part of HYDROLAB is a planner that schedules tasks. Each task stores partial results in the PROLOG main memory database ignoring the work accomplished by other modules, in a blackboard-like manner (Hayes-Roth, 1985 ; Nii, 1986 ; Poyet, 1988). The user is asked a set of very discriminating questions in the initial phase, so that a primary plan can be drawn up. HYDROLAB is then able to make suppositions on various contexts, according to specific databases, and to initialize a primary plan, focusing on decisive topics according to the presupposed context.

The list of tasks to be undertaken is thus built up in a dynamic manner and may be modified in a reflexive way by the system as reasoning goes on. The questions asked by the system represent the visible part of the activated tasks. They tend to be focused on a subpart of the overall problem as they correspond to subgoals previously identified and pushed on to the task list by the planner. When the initial plan comes to an end, the system activates the inference module and tries to match, using fuzzy logic, the user data stored in the blackboard with known solutions stored in disk database and loaded in main memory with a consult system call.

If this step fails in the well-site database, the system switches back to the control module. HYDROLAB then tries to identify the missing data which could have guided it towards a real solution, as well as data which might be useful for the elaboration of a generic solution. The associated tasks are identified and pushed by the planner on to the task list, and the control passes again to the scheduler.

At the end of this cycle, the blackboard is supposed to be completed, all relevant information to be available and the user to be no longer in a position to help elaborate a solution. The control, therefore, is transferred definitively to the inference module. A solution can then be obtained by establishing a relationship between the list of current objects and their observed states, and a situation of analogical reference. It can also be built entirely by HYDROLAB starting from a conceptual model of a high symbolic level, with the help of basic information supplied by the user.

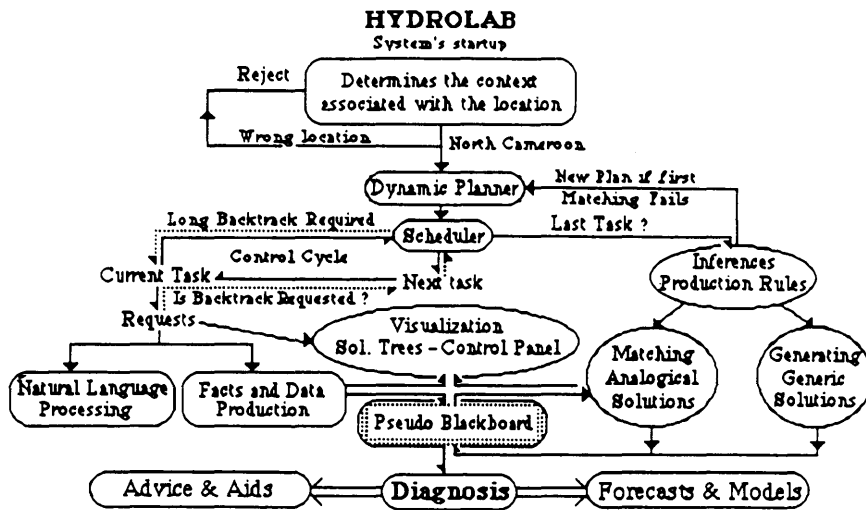


Figure 2. Simplified HYDROLAB system flowchart.

A few systems have developed this ability to react to and to reflect on failure to this degree. We have applied this ability in the way we have designed the control structure of HYDROLAB. We call this kind of model the double pass model of control (Figure 2).

#### 4.4. Knowledge representation

A very interesting property of HYDROLAB is its ability to reason on a set of static databases which can be updated with a simple text editor. No modification need to be made to the expert system code in order to take into account the new information stored in the database. The inference mechanisms are able to deal in a generic way with an arbitrary number of dug well or drilling descriptions. As a first approach the aim is to match, using a fuzzy logic, the user data with at least one of the known well patterns stored in the database. If this step fails, the system activates a new plan and draws inferences for the generic solutions.

A large part of the knowledge embedded in the system relies on a static description of the geological, geomorphological, hydrogeological, geophysical, etc., characteristics of a huge amount of well-site studies in Africa. This knowledge describes for each record of the database the well's hydrodynamical properties. An important objective followed during the conception of the architecture of HYDROLAB was to mix in an efficient manner an object-oriented representation of the declarative knowledge stored in the databases, with a powerful control structure based on tasks scheduling.

#### 4.5. Solution recognition

When the first phase of the task scheduling process ends, facts relevant to the user situation are all asserted and stored in the blackboard. The inference module then tries to match the user data for each parameter with solutions stored in the analogical database. For each reference and for each significant parameter, the system calculates the distance between the user's data and the analogical reference database. The matching is done for each parameter with specialized predicates that

give a measure, according to a context dependant metric, of the distance between the user given value and the recorded values for the supposed solution.

When this processing is done for each attribute, the system is then able to deduce a matching level which is a measure of similarity between the plausible solution and the user data ; the system also computes a consistency measure which takes into account the number of channels used during the matching process to compute the previous similarity.

The specialized predicates which calculate, attribute by attribute, the distances depend on the context and should be invoked with the fuzzy pattern matching, in a manner which takes into account the diversity of the metrics encountered.

4.6. An advanced interactive system

A working session with HYDROLAB is attractive for the users because of its ability to explain its own reasoning, to understand the questions asked in natural language, to explain its approach at any given time and to undergo changes and acquire new data.

Moreover, its range of analogical solutions is provided in a database which can be updated as the drilling campaign is in progress. In this way, the system acquires a considerable analogical knowledge, with a wide range of solution. Diagnosis carried out will be more relevant and precise as its analogical range of solution is larger (figure 3).

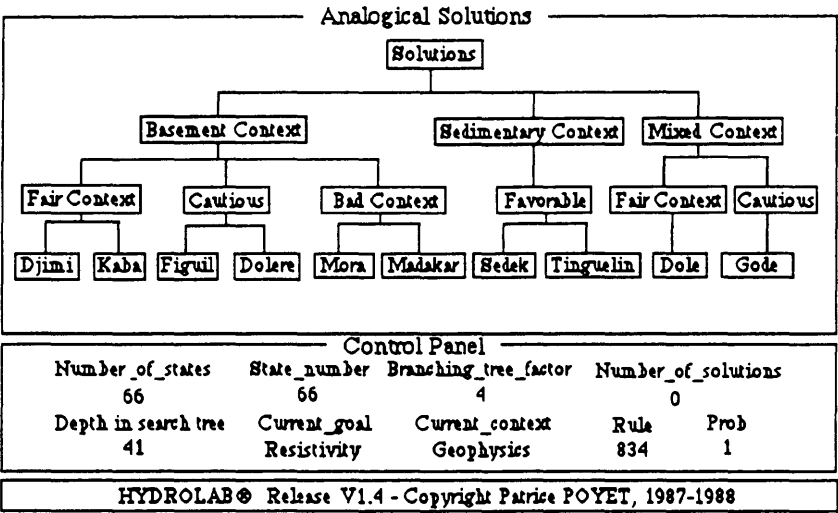


Figure 3. HYDROLAB interface showing the windowing system.

5. An Example of a Hydrolab Utilization Sequence

To show the pertinence of the system, we shall briefly describe the sequences used by HYDROLAB to evaluate the thickness of the saprolite reservoir and then to control this evaluation.



As we have seen, the thickness of the weathering zone is a first order decision-taking element. An evaluation of this parameter is therefore justified. In order to do so, the system calls for several levels of estimation :

- from the drainage pattern, described from aerial photographs.
- from the inventory of the water resources (realized on the spot). The system ask a group of questions relating to the currently known available water resources. At the end of this enquiry it knows the thickness of the saprolite reservoir. It can, if there are several wells, determine an average thickness of the reservoir, and be able to know if there is some local variation of this layer.
- with the data obtained from geoelectric prospection. Following the described situation, HYDROLAB can be led to ask for a reconnaissance by electrical sounding.

Parallel to this and following the identified contexts, the inference strategy will lead the system to evaluate the proximity of a groundwater intake, to test the possibility of the existence of an underflow aquifer, to calculate the thickness of the saturated weathered zone, and to look for the difference in level between the center of the village and the groundwater intake axes.

At the same time, a number of filters are activated : these filters aim at controlling the homogeneity of the data (types of lithological formation, position of the piezometric level, control dug well cuttings, morphological position, efficient rainfall domain, etc.).

Thus the elements used are numerous and complementary. They enable the statistical hydrogeological characteristics to be controlled : the lithotype can be identified, the piezometric level studied, the hydrogeological context analyzed, and the structure context determined, etc.

## 6. Conclusions

We summarized the main features of African hydrogeology and the methods used by experts for well-location studies. We went through the identification of decisive hydrogeological parameters and we described the expert system approach to model the process used by a hydrogeologist to successfully carry out drilling sites studies.

In 1989 the world population and specially africans have to face the desertification problems (20% of the world surface, i.e. 200.000 km<sup>2</sup> are lost every year). Desertification hazards directly affect about one-third of the land surface and one-sixth of the world's population. According to FAO's publications, 1250 million people, of which 700 million children, seriously lack of water ; clean water is accessible to only 38% of the third world.

Those reasons were very serious motivations when developing the HYDROLAB expert system. We hope that in the near future the growth of this technology will play a significant role in solving the water problem in the Africa.

## REFERENCES

- Albert, P., 1985, Prolog et les objets: Proc. Fifth international workshop on Expert Systems and their Applications, Avignon, 1985, France, p. 332-350.
- Arrivet, L., 1987, Introduction du flou dans un système expert: Mémoire d'Ingénieur de l'Ecole Supérieure d'Informatique d'Electronique et d'Automatique, Paris France, 44p.
- Bernardi, A., Detay, M., 1988, Corrélations entre les paramètres géoélectriques et les caractéristiques hydrodynamiques des forages en zone de socle, to be published in *Revue du BRGM*, 15 p.
- Borland International, 1986, Turbo Prolog Owner's Handbook: Borland Eds., 221 p.
- Clayton, B., 1985, ART<sup>TM</sup> reference manual: Inference Corporation eds., Los Angeles, California, Vol 1, 138 p., Vol 2, 158 p., Vol 3, 102 p.
- Colmerauer, A., 1977, Programmation en Logique du premier ordre: Actes des journées La compréhension, I.R.I.A, France, p. 124-132.
- Colmerauer, A., 1983, Prolog in Ten Figures: Proc. of Eighth International Joint Conference on Artificial Intelligence, p. 487-499.
- Clocksin, W.F., and Mellish, C.S., 1984, Programming in PROLOG: Springer-Verlag, Berlin, 304 p.
- Detay, M., Poyet, P., 1989f. La Place de l'Informatique dans les Géosciences. Géologues, Sciences de la Terre et Techniques Modernes, *Revue Officielle de l'Union Française des Géologues*, ISSN 0016-7916, numéro 89/2, 1989, 8pp.
- Detay, M., Poyet, P., 1989e. Introduction aux Méthodes Modernes de Maîtrise de l'Eau. *Revue Hydrogéologie*, 1989, 22 pp.
- Detay, M., Poyet, P., 1989d. HYDROFORM le Système Expert hydrogéologue du CEFIGRE, L'Eau, L'Industrie, les Nuisances, n° 130, Septembre 1989, ISSN 0755-5016, p. 56-58.
- Detay, M., Poyet, P., 1989c. Development and Evaluation of a Field Prototype Expert System for Village Water Supply Programs, International Symposium on Groundwater Managment: Quantity and Quality, International Association of Hydrogeologists, Benidorm, Spain, October 2-5, 1989.
- Detay, M., Poyet, P., Emsellem, Y., Bernardi, A., Aubrac, G., 1989b. Influence du développement du réservoir capacitif d'altérites et de son état de saturation sur les caractéristiques hydrodynamiques des forages en zone de socle cristallin. *Comptes Rendus de l'Académie des Sciences de Paris*, ISSN 0249-6313, t. 309, Série II, 1989, p. 429-436.
- Detay, M., Poyet, P., 1989a. Design and Implementation of a Field Expert System for Village Water Supply programs. *Bulletin of Engineering Geology*, Published by the International Association of Engineering Geology, Laboratoire Central des Ponts et Chaussées, 1989.
- Detay, M., Poyet, P., 1988c. Environnement et Géologie: Application de l'Intelligence Artificielle en Hydrogéologie, *Géologues, Sciences de la Terre et Techniques Modernes*, *Revue Officielle de l'Union Française des Géologues*, ISSN 0016-7916, numéro 85-86, 1988.2/3, p. 41-47.
- Detay, M., Poyet, P., 1988b. HYDROLAB: le système expert de l'hydraulique villageoise, *Bulletin de liaison du Comité Interafricain d'Etudes Hydrauliques*, n°76, Avril 1989, p.25-41.
- Detay, M., Poyet, P., 1988a. HYDROEXPERT®: Un système expert en hydrogéologie de terrain. HYDROPLAN International Exhibition of Agricultural, Rural, Urban, and Industrial hydraulic Engineering, May 1988, *Actes des Communications Scientifiques*, p. 191-195.

- Detay, M., 1987, Identification analytique et probabiliste des paramètres numériques et non-numériques et modélisation de la connaissance en hydrogéologie sub-saharienne: Thèse de Doctorat d'Etat Sciences, Université de Nice - France, 456 p.
- Detay, M., Goulnik, Y., Casanova, R., Ballestracci, R., Emsellem, Y., 1986b, HYDROLAB an Expert System for groundwater Exploration in Africa: in Bull. IWRA - International Conference on Water Resources Needs and Planning in drought prone areas - Khartoum Soudan, 6 p.
- Detay, M., Goulnik, Y., Casanova, R., Ballestracci, R., 1986a, HYDROLAB un Système Expert pour la recherche des eaux souterraines en Afrique: Actes du deuxième colloque Int. Eau Gestion des données et aide à la Décision, Montpellier - France, p. 94-99.
- Forgey, C. L., 1982, A fast Algorithm for the Many Pattern - Many Object Pattern Match problem: A.I. journal n° 19, 1982, p. 17-37.
- Haren, P., Neveu, B., Corby, O., Montalban, M., 1985, MEGAR: Un moteur d'inférences pour la conception en ingénierie: 5 ème Congrès Reconnaissance des Formes et Intelligence Artificielle, Grenoble 27, 29 Novembre 1985 - France, p. 1273-1280.
- Haren, P., Neveu, B., Giacometti, J.P., Montalban, M., Corby, O., 1985, SMECI: Cooperating Expert Systems for Civil Engineering Design: SIGART Newsletter, (April 1985), n° 92, p. 67-69.
- Hayes-Roth, B., 1984, BB1: An architecture for blackboard systems that control, explain and learn about their own behavior: Heuristic Programming Project, Report n° HPP-84-16, Stanford University, 22 p.
- Konolidge, K., 1979, An inference net compiler for the PROSPECTOR rule based consultation system: Proc. of Sixth International Joint Conference on Artificial Intelligence, p. 487-489.
- Nii, P., 1986, Blackboard systems: the blackboard model of problem solving and the evolution of blackboard architectures. A.I. magazine, July 1986, p. 38-53.
- Nii, P., 1986, Blackboard system, blackboard application system, blackboard systems from a knowledge engineering perspective. A.I. magazine, August 1986, p. 82-106
- Poyet, P., Delcambre, B., 1989g. NOE: Expert System on Technical Inspection of Waterproofing on Flat Roofs, Expert Systems in Civil Engineering, Published by the International Association for Bridge and Structural Engineering, ISBN 3-85748-058-0, Vol 58, 1989, p. 175-187.
- Poyet, P., De La cruz, P., Miléo, T., Loiseau, J.N., 1989f. Récentes Etudes en Matière de Simulations Tactiques Intelligentes, Conférence Intelligence Artificielle et Défense, Neuvièmes Journées Internationales sur les Systèmes Experts et leurs Applications, ISBN 2-906899-24-0, 1989, p.149-181.
- Poyet, P., Haren, P., 1989e. A.I. Modelling of Complex Systems, in: Modelling Techniques and Tools for Computer Evaluation, R. Puigjaner and D. Potier Editors, Plenum Publishing Company, London, (Reprinted from local citation [Poyet et al., 1988c]) 22 pp.
- Poyet, P., Detay, M., 1989d. HYDROLAB: A New Generation of Compact Expert Systems. Computers and Geosciences - An International Journal, Pergamon Press, ISSN 0098-3004, Vol. 15, No. 3, 1989, p. 255-267.
- Poyet, P., Detay, M., 1989c. HYDROLAB: Un Système Expert de Poche en Hydraulique Villageoise. Technique et Science Informatiques, ISSN 0752-4072, TSI, Vol. 8, n° 2, 1989, p. 157-167.
- Poyet, P., Detay, M., 1989b. HYDROEXPERT™ Version V1.4, Un Système Expert d'Aide à l'Implantation de Forages en Hydraulique Villageoise, Manuel d'introduction et de référence, Rapport de Recherche de l'Institut National de Recherche en Informatique et en Automatique, Numéro 936, Déc. 1988, ISSN 0249-6399, 43pp.

- Poyet, P., Detay, M., 1989a. Enjeux Sociaux et Industriels de l'Intelligence Artificielle en Hydraulique Villageoise. Convention I.A. 1989, Première Conférence et Exposition Européenne sur les Techniques et les Applications de l'Intelligence Artificielle en milieu Industriel, Editions Scientifiques et Techniques Hermes, ISBN 2-86601-171-6, Vol. 2, 1989, p. 621-652.
- Poyet, P., Detay, M., 1988d. L'Avènement d'une Génération de Systèmes Experts de Terrain, Proceedings of the Sahel Forum on the State-of-the-Art of Hydrology and Hydrogeology in the Arid and Semi Arid Areas of Africa, Ouagadougou, Burkina Faso, Edited by Misganaw Demissie and Glenn E. Stout, International Water Resources Association, Illinois, p. 567-577.
- Poyet, P., Haren, P., 1988c. A.I. Modelling of Complex Systems, Invited Paper to the ACM and IFIP 4th International Conference on Modelling Techniques and Tools for Computer Performance Evaluation, Sept. 1988, Palma de Majorque, 34 pp.
- Poyet, P., De La Cruz, P., 1988b. Une Nouvelle Classe de Simulateurs Destinée aux Aides tactiques et aux Systèmes d'Armes. Conférences Spécialisées Science et Défense, Huitièmes Journées Internationales sur les Systèmes Experts et leurs Applications, ISBN 2-906899-07-0, Vol. Specialized Conferences, 1988, p. 89-99.
- Poyet, P., Detay, M., 1988a. HYDROEXPERT®: Aide à l'Implantation d'Ouvrages d'Hydraulique Villageoise. Huitièmes Journées Internationales sur les Systèmes Experts et leurs Applications, ISBN 2-906899-07-0, Vol. 2, 1988, p. 397-410.
- Poyet, P., 1987d. La Conception de Systèmes Intelligents: Exemples d'Applications dans les Géosciences. Cours de Maîtrise des Sciences et Techniques, Laboratoire de Géologie et Géochimie, Université de Nice, Parc Valrose, 06034 Nice Cédex, 72 pp.
- Poyet, P., 1987c. La structure de contrôle dans les systèmes experts de simulation., 6ème Congrès Reconnaissance des Formes et Intelligence Artificielle de l'Association Française de Cybernétique Economique et Technique, Dunod Eds., ISBN 2-04-013480-8, Vol. 2, 1987, p.723-738.
- Poyet, P., Haren, P., De la Cruz, P., 1987b. Un système expert de simulation navale. 6ème Congrès Reconnaissance des Formes et Intelligence Artificielle de l'Association Française de Cybernétique Economique et Technique, Dunod Informatique Eds., ISBN 2-04-013475-1, Vol. 1, 1987, p. 587-592.
- Poyet, P., De La Cruz, P., 1987a. Simulation Navale en Environnement Hostile. Actes de l'Ecole d'Automne d'Intelligence Artificielle. Article invité par l'Institut d'Expertise et de Prospective de l'Ecole Normale Supérieure de la rue d'Ulm, Campus Thomson, Jouy en Josas, Oct. 1987, 10 pp.
- Poyet, P., 1986b. Un logiciel convivial de traitement et d'intégration des données géochimiques sur micro ordinateur IBM AT, Rapport INRIA MC 14868, 1986, 52 pp.
- Poyet, P., 1986a. Un système d'aide à la décision en prospection uranifère: Méthodes de discrimination des anomalies géochimiques multiélémentaires significatives. Thèse de Doctorat d'Etat ès Sciences, Université de Nice - INRIA, 436 pp. + annexes.
- SMECI, 1988, Le manuel SMECI V1.3: ILOG S.A. eds., France, 112p.
- Stefik, M., Bobrow, D. G., Mittal, S., Conway, L., 1983, "Knowledge programming in LOOPS". A.I. Magazine (Fall 1983) p. 3-13.
- Stefik, M. J., Bobrow, D. G., Kahn, K. M. , 1986, "Integrating Access Oriented Programming into a Multiparadigm Environment". IEEE Software, January 1986, p 10-18.
- Warren, 1977, Implementing PROLOG, D.A.I Research Rep. Vol 1 et 2, University of Edinburgh.

SECTION 7: MISCELLANEOUS



ASSESSMENT OF PREDICTIVE ACCURACY OF A MODEL OF  
ARTIFICIAL RECHARGE EFFECTS IN THE UPPER COACHELLA  
VALLEY, CALIFORNIA

Leonard F. Konikow  
U.S. Geological Survey  
431 National Center  
Reston, VA 22092

and

Lindsay A. Swain  
U.S. Geological Survey  
3600 West Broad Street, Room 606  
Richmond, VA 23230

**ABSTRACT:** Two-dimensional, finite-element, ground-water flow and solute-transport models were applied to the upper Coachella Valley, California, to help predict the effects of artificial recharge on ground-water levels and dissolved-solids concentration from 1974-80. The flow model (calibrated with data from 1936-73) predicted that water levels would rise by more than 60 ft near the artificial-recharge site but decline in more than two-thirds of the rest of the valley. A comparison of observed and predicted water-level changes indicates that model calibration to nearly 40 years of observed water-level fluctuations was not sufficient to predict accurately and precisely the water-level changes that would occur in the next 7 years. The errors have a mean of -8.8 ft and range from about -96 to +15 ft. The greatest errors are in areas where tributary canyons enter the main valley. Recharge from creeks discharging from tributary valleys during 1974-80 was significantly greater than the long-term average; this difference is a major source of predictive error. The solute-transport model indicated that the dissolved-solids plume from the artificial recharge site would migrate about 1.1 mi. The actual concentrations in 1981 were within 20 percent of the predicted values in four nearby observation wells. Predicted ground-water velocities were about 2 ft/d; the actual velocity of the centroid of the plume is about 2.4 ft/d. Although the transport-model predictions appear to be accurate, the short travel time and very limited number of observation wells may not permit a rigorous test of its predictive accuracy. In general, it is desirable for model predictions to include an assessment of their reliability that is based on the uncertainty in model parameters, including assumed future stresses.

### Introduction

Deterministic ground-water flow and transport models are being used with increasing frequency to predict future changes in ground-water systems. Applications include assessments of toxic waste sites or other types of ground-water contamination problems (for example, Robertson, 1974; Kipp *et al.*, 1986; Mercer *et al.*, 1983), design of clean-up schemes for contaminated aquifers (for example, Andersen *et al.*, 1984; Gorelick *et al.*, 1984; Ward *et al.*, 1987), and prediction of saltwater intrusion in response to withdrawals from water-supply wells or other

factors (for example, Andersen *et al.*, 1988; Merritt, 1986). Perhaps the most extreme example in which ground-water models are being used for prediction are cases involving the performance assessment and approval of high-level radioactive waste repositories, for which regulators in the United States are requiring predictions of ground-water transport for 10,000 years into the future, so as to comply with the Nuclear Waste Policy Act of 1982.

In light of the economic importance of these types of assessments, it may be asked whether there is any evidence in the record that such models can indeed accurately predict the future state of a ground-water system. One way to assess the predictive accuracy of ground-water models is through postaudits of the areas that were modeled (for examples, see Konikow and Person, 1985; Konikow, 1986; Alley and Emery, 1986; Lewis and Goldstein, 1982; and Hanson, 1989). However, the predictive accuracy of ground-water models are rarely assessed after the fact. This paper analyzes and documents the predictive accuracy of ground-water models that had been applied previously to one particular area, so that the record upon which to base our faith (or lack of faith) in model predictions can be strengthened.

The authors wish to thank John Freckleton and Mark Person for their assistance in data compilation and analysis.

### Description of Study Area

The upper Coachella Valley (Figure 1) is a 300-mi<sup>2</sup> area in Riverside County, California. Ground-water withdrawals in the valley were small prior to the late 1930's (less than 5,000 acre-ft/yr), but have increased significantly since then. The average pumping rate during 1968-73 was about 49,200 acre-ft/yr (60.7 hm<sup>3</sup>/yr) (Swain, 1978). Artificial recharge to the ground-water basin of the upper Coachella Valley was started in 1973 in an effort to counteract declining ground-water levels of more than 100 ft from 1936-73 that had been measured in some parts of the area. Water was available for artificial recharge from the Colorado River Aqueduct. Since 1973, this imported water has been recharged to the ground-water basin through the Whitewater River channel into the spreading basin where the permeable channel is diked to form ponds (Figure 1) (Swain, 1978).

The surficial aquifer consists of unconsolidated valley-fill sediments. Shallow ground water has a dissolved-solids concentration of less than 300 mg/L in most of the upper valley. Because the imported water being recharged has a higher dissolved-solids concentration (600 to 750 mg/L) than the native ground water, there was a need to evaluate and predict changes in water-level and water-quality conditions brought about by the recharge. Swain (1978) applied two-dimensional, finite-element, ground-water flow and solute-transport models to the area to provide a basis for predicting the effects of the artificial recharge on water levels and water quality.

### Description of Models

#### Governing Equations

The model is based on a finite-element solution (using isoparametric quadrilateral elements) of the equation governing transient, two-dimensional,



areal, ground-water flow in an isotropic heterogeneous aquifer, which can be written--

$$S \frac{\partial h}{\partial t} = \frac{\partial}{\partial x} \left( T \frac{\partial h}{\partial x} \right) + \frac{\partial}{\partial y} \left( T \frac{\partial h}{\partial y} \right) - W, \quad (1)$$

where  $S$  is the aquifer storativity or storage coefficient [dimensionless],  $h$  is hydraulic head [L],  $t$  is time [T],  $x$  and  $y$  are the Cartesian coordinates in the horizontal plane [L],  $T$  is transmissivity [ $L^2 T^{-1}$ ], and  $W$  is the volumetric discharge (+) or recharge (-) rate per unit area [ $LT^{-1}$ ]. For transient flow, the initial head is specified at all locations. Possible boundary conditions for (1) include specified head and specified flux.

A conventional form of the advection-dispersion equation governing nonreactive solute transport in two dimensions is (after Konikow and Grove, 1977)--

$$\epsilon b \frac{\partial C}{\partial t} = \frac{\partial}{\partial x_i} \left( \epsilon b D_{ij} \frac{\partial C}{\partial x_j} \right) - \epsilon b V_i \frac{\partial C}{\partial x_i} + W(C - C'), \quad (2)$$

where  $C$  is the volumetric concentration of the solute [ $ML^{-3}$ ],  $\epsilon$  is porosity [ $L^3 L^{-3}$ ],  $b$  is the saturated thickness [L],  $D_{ij}$  is the dispersion tensor [ $L^2 T^{-1}$ ],  $V_i$  is the fluid seepage velocity vector [ $LT^{-1}$ ], and  $C'$  is the concentration in the source fluid ( $W < 0$ ) [ $ML^{-3}$ ]. For a two-dimensional system, the subscripts  $i$  and  $j$  range from 1 to 2, so that in  $x$ - $y$  Cartesian coordinates  $x_1 = x$ ,  $x_2 = y$ ,  $V_1 = V_x$ , and  $V_2 = V_y$ . For hydraulic sinks ( $W > 0$ ),  $C' = C$ .

Assuming that changes in concentration are small enough that they do not affect fluid properties, then the flow and transport equations are linked by the velocity term. Velocity can be determined from the solution of the flow equation (1) through Darcy's law and the relation of velocity to flux--

$$\epsilon b V_i = -T \frac{\partial h}{\partial x_i}. \quad (3)$$

We follow the conventions of neglecting molecular diffusion as a separate process and characterizing dispersion by the longitudinal ( $\alpha_L$ ) and transverse ( $\alpha_T$ ) dispersivities [L] [e.g., Bear, 1979]--

$$D_{ij} = \alpha_T |V| \delta_{ij} + (\alpha_L - \alpha_T) \frac{V_i V_j}{|V|}, \quad (4)$$

where  $\delta_{ij} = 1$  for  $i = j$ , and  $\delta_{ij} = 0$  otherwise, and  $|V|$  is the magnitude of seepage velocity--

$$|V| = [(V_x)^2 + (V_y)^2]^{1/2}. \quad (5)$$

The computer program used by Swain (1978) in the analysis of ground-water flow and solute transport in the upper Coachella Valley was developed by G. F. Pinder (Princeton University, written commun., 1974). Additional details on the numerical methods are presented by Swain (1978) and Swain and Pinder (1978).

## Model Application

A flow model for the upper Coachella Valley was developed for only the Garnet Hill and Whitewater River subbasins because an earlier study using an analog model (Tyley, 1974) showed that artificial recharge in the Whitewater River subbasin would have no effect north of the Banning fault (Swain, 1978). Steady-state and transient simulations of ground-water flow were applied and calibrated prior to the transport model. The flow model covered an area of about 125 mi<sup>2</sup>, which was discretized into a variably-spaced grid consisting of 209 quadrilateral elements and 262 nodes (Figure 2). The model had specified-flux boundaries everywhere except the southeast boundary, where a constant-head boundary condition was imposed because water levels in that area had been relatively unchanged since 1936.

A steady-state flow model was calibrated first to key in on the hydrogeologic factors responsible for water levels before any significant man-induced stresses occurred. As determined by Tyley (1974), 1936 is a period that best represents a natural equilibrium condition for the aquifer and for which sufficient hydrologic data were available to permit reasonable simulation and calibration. Swain (1978) estimated steady-state recharge, discharge, underflow, and areal distribution of transmissivity based on this calibration. Calculated water levels were within 4 ft of measured 1936 water levels throughout the model area (Swain, 1978).

Next, the transient-flow model was calibrated for the period 1936-68 on the basis of measured annual net pumpage, estimated average annual recharge, and initial water levels and transmissivity values estimated from the calibrated steady-state flow model. Areal distribution of storage coefficient values were based on field measurements and adjustments during calibration of the transient flow model that yielded the best fit of calculated to observed transient water-level changes. From 1936-68, observed water-level declines exceeded 50 ft in more than two-thirds of the study area. The difference between the measured and model-generated water-level declines was less than 10 ft in more than 90 percent of the area and less than 5 ft in more than two-thirds of the area. Figure 3 shows a comparison of measured water-level declines in selected wells with declines determined by the calibrated model at nodes near the selected well. Swain (1978) states that the similarity in the shape of the hydrographs during the transient calibration period (1936-68) indicates that the model closely represents the hydrologic response of the ground-water system.

The accuracy of the calibrated flow model was next tested by running the model for the period 1968-74 using annual pumpage for that time. Agreement between observed and calculated water levels during this "verification" period were reasonably close (as shown in Figure 3), and Swain (1978, p. 15) concluded that "...parameters chosen were reasonable and that the model was capable of duplicating the response of the aquifer, it is now possible to use the model to predict water levels from projected pumpage and (or) projected artificial recharge."

Ground-water pumping rates for the modeled area were projected by extrapolation for the period 1974-80. The extrapolations indicated that pumping rates would increase throughout the valley during 1974-80, with the increases in the Whitewater River subbasin ranging from 10 percent in the Thousand Palms subarea to 45 percent in the Palm Springs subarea. On the basis of these new stresses, the model was used to predict the change in water level under the

imposition of artificial recharge (see Figure 4). The model predicted that in 1980 the water level would rise by more than 60 ft close to the artificial recharge site, while declining in more than two-thirds of the rest of the valley. Predicted declines at the end of 1980 exceed 20 ft in part of the area about 13 miles downgradient from the recharge site.

The solute-transport model was used to analyze dissolved-solids concentration in the aquifer and was applied only to a smaller subarea of the flow model--an area of about 20 mi<sup>2</sup> near and downgradient from the artificial recharge site (as shown in Figure 2). This smaller scale model used a grid consisting of 360 nodes and 312 elements. The areas of the elements in the transport model grid ranged from 0.015 to 0.2 mi<sup>2</sup> (compared to the coarser grid of the flow model, in which element size ranged from about 0.14 to 3.6 mi<sup>2</sup>).

It was assumed that the dissolved-solids concentration in the aquifer would change because of mixing with the artificially recharged water, which had a significantly higher dissolved-solids concentration, and that the dissolved-solids concentration would not be affected by chemical reactions. Additional parameters required by the solute-transport model, beyond those calibrated for the flow model, include porosity, saturated thickness, dispersivity, and initial dissolved-solids concentration. On the basis of recharge studies by Tyley (1973) and data from drillers' logs, a porosity of 25 percent was used in the model (Swain, 1978). Saturated thickness ranged from 750 to 1,000 ft. The longitudinal and transverse dispersivities used in the model (100 and 33 ft, respectively) were based on values used in other model studies at similar scales and with similar aquifer material (Robson, 1974; Konikow and Bredehoeft, 1974; and Bredehoeft and Pinder, 1973). Sensitivity tests of the model showed that the results were relatively unaffected by uncertainty in the chosen values of dispersivity. Finally, a uniform initial dissolved-solids concentration of 210 mg/L was specified. Swain (1978) notes that because no significant water-quality changes had been observed in the area at the time the model study was conducted, the transport model was, in effect, uncalibrated at the time the predictions were made.

Because the model is two-dimensional in the areal plane, it implicitly assumes complete mixing throughout the saturated thickness of the aquifer. If the effective boundary of the plume is defined as a dissolved-solids concentration greater than 300 mg/L, the model prediction indicates that, by 1981, the dissolved-solids plume from the artificial recharge site would extend 1.1 miles downgradient and would have a maximum width of about 1 mile (compared to the nearly 0.5 mi width of the simulated source area).

#### Assessment of Predictive Accuracy

The study area includes 98 wells at which water-level measurements were made in both January 1974 and in December 1980. So as not to give undue weight to any local area, six wells were eliminated from further analysis because they were located very close to another of the wells (that is, within the same 40-acre subdivision of a section, the area of which equals 1 mi<sup>2</sup>). The remaining 92 wells provide the basis for assessing the predictive accuracy of the ground-water flow model.

A comparison of observed and predicted water-level changes during 1974-80 is presented in the scattergram shown in Figure 5. The diagonal solid line represents a theoretical line of perfect fit between observed and predicted change. The requisite data were available for only three wells in or near the artificial recharge area. These three data points are clustered together in the upper-right quadrant indicating that water-level rises were both predicted and observed. However, all three points fall on one side of the diagonal line--the side indicating that observed water-level rises were greater than predicted. For most of the valley where there are observation wells, water-level declines were predicted. Declines actually occurred in most of the valley, but declines were generally less than predicted. The data on observed and predicted changes used to plot Figure 5 have a correlation coefficient of 0.75.

Figure 6 presents a frequency distribution (or histogram) of the errors (defined as predicted water-level change minus observed water-level change). The frequency distribution is skewed primarily by the data from wells in the artificial recharge area and in or near the tributary valleys. The errors for all 92 wells have a mean of -8.8 ft, a median of -5.6 ft, a standard deviation of 17.7 ft, and range from about -96 to +15 ft. (For comparison, the observed water-level changes have a mean of -5.3 ft, a median of -12.8 ft, a standard deviation of 25.0 ft, and range from -30 to 92 ft.) The mean error indicates a bias towards overpredicting the magnitude of water-level declines and the wide range in errors indicates some lack of precision. The frequency distribution of the errors in the 80 wells located in the main part of the valley more closely approximates a normal distribution. These errors have a mean of -3.8 ft and a standard deviation of 7.2 ft.

A map of the spatial distribution of errors (Figure 7) illustrates that the greatest errors are in and near the areas where tributary canyons enter the main valley. Flow and recharge from creeks discharging from these tributary valleys during 1974-80 turned out to be significantly greater than the long-term average, which had been imposed on the model as an assumed stress (see Table 1). The annual discharge during 1978-80 was much above average. Also, the annual discharge from these tributary valleys is highly variable. For example, during 1974-80, the annual discharge in Palm Canyon Creek ranged from only 15 acre-ft in

Table 1.--Average annual discharge and ground-water recharge from selected tributaries

|                   | Annual flow (acre-feet per year)                 |                                    |  |
|-------------------|--|------------------------------------|--|
|                   | Long-term average<br>discharge<br>(through 1973) | Assumed<br>recharge<br>(1974-1980) | Actual average<br>discharge<br>(1974-1980) |
| Tahquitz Creek    | 2,770  | 2,300                              | 7,430                                      |
| Palm Canyon Creek | 2,410  | 2,000                              | 8,520                                      |
| Deep Creek        | 375  | 2,000                              | 2,970                                      |

1975 to 34,920 acre-ft in 1980. The data plotted in Figure 5 show the distinctly separate clustering of those points representing wells in or near the canyon areas of the three tributary valleys. Thus, a dominant source of the predictive error in this model is attributable to imprecise assumptions about future stresses (specifically, the underestimation of recharge). From a different perspective, it might be postulated that the predictive period was simply too short to assess the predictive accuracy of the model, at least for those parts of the valley sensitive to natural recharge from tributary creeks. If the predictive period had been long enough to include several cycles of wet and dry years, the magnitude of long-term trends might not have been overwhelmed by responses to short-term deviations from average stresses. Alternatively, if the last 3 years of the same 1974-80 predictive period had instead experienced approximately average recharge, and extreme high- or low-flow conditions occurred during the first few years, then, by the end of 1980, recovery from earlier years of extreme flow conditions might have been completed and the prediction might have appeared to be highly accurate.

At the time the prediction was made, the uncertainty in future stresses as a source of error could have been recognized by presenting the model predictions with confidence limits, which could have been derived from a sensitivity analysis based on the expected variability in future stresses. For recharge from tributary valleys, a statistical description of flow frequency (or variability) could have been incorporated into the model analysis, perhaps through a Monte Carlo approach.

As can be seen from Figures 5-7, the magnitude of the error in much of the area is less than 10 ft. It should be noted that where more than one well occurs within the area of one element of the model grid, the range in measured water levels at one time is generally about  $\pm 5$  ft from the mean. Thus, better agreement between measured and predicted water-level changes for individual wells of less than  $\pm 5$  ft should not be expected. There is no evidence that deficiencies or errors in the estimation of the hydraulic properties of the aquifer contributed significantly to the predictive errors, or that the predictive accuracy would have been improved by a better definition of aquifer properties.

Only a few observation wells are sufficiently close to the recharge site to compare observed and predicted water-quality changes. Measurements of water samples from these few wells indicate that actual concentrations are within less than 20 percent of predicted values. As shown in Figure 8, the actual plume (as estimated from the limited number of observation wells) is similar to the predicted one. The measured plume extended longitudinally down the valley approximately 750 ft farther than the 1.1 mi predicted for the 1981 plume, a difference of about 13 percent. This discrepancy may be partly the result of the dispersivities that were chosen for the model analysis being uncalibrated and incorrect, but may also be partly caused by other factors, such as incomplete vertical mixing.

Ground-water velocity predicted by Swain (1978) is approximately 2 ft/d. Measurement of the displacement of the centroid of the observed plume (extent of the 450 mg/L line of the equal concentration) indicates a velocity of about 2.4 ft/d. This close match of the predicted versus measured values indicates a lack of major flaws in the model and reflects a good understanding of the hydrogeologic system and its boundaries. However, the match perhaps is fortuitous to some extent considering that the travel distances are relatively short and that the solute-transport model was uncalibrated and unverified, as no differences in water quality had been historically available previously.

Field measurements of the water quality at greater depths within the aquifer indicate that the plume has remained somewhat stratified, in that lower concentrations still exist at depth below the recharged water. Thus, the assumption of complete mixing within the entire aquifer thickness, which was made in order to approximate this system using a two-dimensional model, may have been in error.

### Conclusions

Overall, the accuracy of the upper Coachella Valley ground-water flow and solute-transport models is considered reasonable. The models constituted a useful management tool that provided a quantitative basis for estimating the consequences of imposing a new hydrologic stress on the area, and thereby provided the basis for monitoring these effects. However, model calibration to nearly 40 years of observed water-level fluctuations, in itself, was not sufficient to predict accurately and precisely the water-level changes that would occur in the next 7 years. This limitation appears to be caused primarily by an inability to predict future recharge.

The transport-model predictions appear to be relatively accurate, although this assessment is constrained by the very limited number of observation wells in the area where transport is affecting concentrations. Because changes in hydraulic head propagate more rapidly through an aquifer than does the actual transport of solutes, it is typical to apply a transport model to a much smaller area than a flow model, as was done by Swain (1978). For the same reason, the predictive accuracy of a flow model can be assessed sooner than a transport model over the same size area. A corollary is that, for a given elapsed predictive period, such as the 7-year period evaluated in the upper Coachella Valley case, there is a stronger basis for assessing a flow model than there is for a transport model.

In general, model predictions should be accompanied by an assessment of their reliability that is based on the uncertainty in all model parameters. If a ground-water system is sensitive to seasonal or annual variations in recharge or streamflow, then predictions (or a range of predictions) should be based on the distribution of flows in the streams, as derived from the historical record or estimated from climatic records. The accuracy of predicted responses can certainly be no better than the accuracy of assumed future stresses.

A postaudit of a model prediction is a valuable exercise. It demonstrates the predictive accuracy of the model, which in turn reflects the degree of understanding of the properties, boundaries, and stresses of the field area. The evaluation of the nature, magnitude, and distribution of predictive errors should itself lead to an improved understanding of the modeled system and of the value of and confidence in a subsequently revised model.

### References

- Alley, W.M., and P.A. Emery, 1986, Groundwater model of the Blue River basin, Nebraska--Twenty years later, *J. Hydrol.*, 85, 225-249.
- Andersen, P.F., C.R. Faust, and J.W. Mercer, 1984, Analysis of conceptual designs for remedial measures at Lipari Landfill, New Jersey, *Ground Water*, 22, 176-190.

- Andersen, P.F., J.W. Mercer, and H.O. White, 1988, Numerical modeling of salt-water intrusion at Hallandale, Florida, *Ground Water*, 26, 619-630.
- Bear, J., 1979, *Hydraulics of groundwater*, McGraw-Hill, New York, 567 p.
- Bredehoeft, J.D., and G.F. Pinder, 1973, Mass transport in flowing ground water, *Water Resour. Res.*, 9, 194-210.
- Gorelick, S.M., C.I. Voss, P.E. Gill, W. Murray, M.A. Saunders, and M.H. Wright, 1984, Aquifer reclamation design: The use of contaminant transport simulation combined with nonlinear programming, *Water Resour. Res.*, 20, 415-427.
- Hanson, R.T., 1989, Postaudit analyses of ground-water models of an alluvial aquifer system, Avra Valley, Arizona, *in* Abstracts, 28th International Geological Congress, Washington, D.C., July 9-19, 1989, 2, 27.
- Kipp, K.L., Jr., K.G. Stollenwerk, and D.B. Grove, 1986, Groundwater transport of strontium 90 in a glacial outwash environment, *Water Resour. Res.*, 22, 519-530.
- Konikow, L.F., 1986, Predictive accuracy of a ground-water model--Lessons from a postaudit, *Ground Water*, 24, 173-184.
- Konikow, L.F., and J.D. Bredehoeft, 1974, Modeling flow and chemical quality changes in an irrigated stream-aquifer system, *Water Resour. Res.*, 10, 546-562.
- Konikow, L.F., and D.B. Grove, 1977, Derivation of equations describing solute transport in ground water, *U.S. Geol. Survey Water-Resour. Inv.* 77-19, 30 p.
- Konikow, L.F., and M.A. Person, 1985, Assessment of long-term salinity changes in an irrigated stream-aquifer system, *Water Resour. Res.*, 21, 1611-1624.
- Lewis, B.D., and F.J. Goldstein, 1982, Evaluation of a predictive ground-water solute-transport model at the Idaho National Engineering Laboratory, Idaho, *U.S. Geol. Survey Water-Resour. Inv.* 82-25, 71 p.
- Mercer, J.W., L.R. Silka, and C.R. Faust, 1983, Modeling ground-water flow at Love Canal, New York, *J. Envir. Eng., ASCE*, 109, 924-942.
- Merritt, M.L., 1986, Recovering fresh water stored in saline limestone aquifers *Ground Water*, 24, 516-529.
- Robertson, J.B., 1974, Digital modeling of radioactive and chemical waste transport in the Snake River Plain aquifer at the National Reactor Testing Station, Idaho, *U.S. Geol. Survey Open-File Rept. IDO-22054*, 41 p.
- Robson, S.G., 1974, Feasibility of digital water-quality modeling illustrated by application at Barstow, California, *U.S. Geol. Survey Water-Resour. Inv.* 46-73, 66 p.
- Swain, L.A., 1978, Predicted water-level and water-quality effects of artificial recharge in the upper Coachella Valley, California, using a finite-element digital model, *U.S. Geol. Survey Water-Resour. Inv.* 77-29, 54 p.
- Swain, L.A., and G.F. Pinder, 1978, A Galerkin-finite element simulation of the effects of artificial recharge on flow and chemical quality in an alluvial aquifer,

*in* Applied Numerical Modelling--Proceedings of the 1st International Conference on Numerical Modelling, University of Southampton, 11-15th July, 1977, C.A. Brebbia [ed.], Pentech Press, London, 297-308.

Tyley, S.J., 1973, Artificial recharge in the Whitewater River area, Palm Springs, California, U.S. Geol. Survey Open-File Rept., 51 p.

Tyley, S.J., 1974, Analog model study of the ground-water basin of the upper Coachella Valley, California, U.S. Geol. Survey Water-Supply Paper 2027, 77 p.

Ward, D.S., D.R. Buss, J.W. Mercer, and S.S. Hughes, 1987, Evaluation of a groundwater corrective action at the Chem-Dyne Hazardous waste site using a telescopic mesh refinement modeling approach, Water Resour. Res., 23, 602-617.



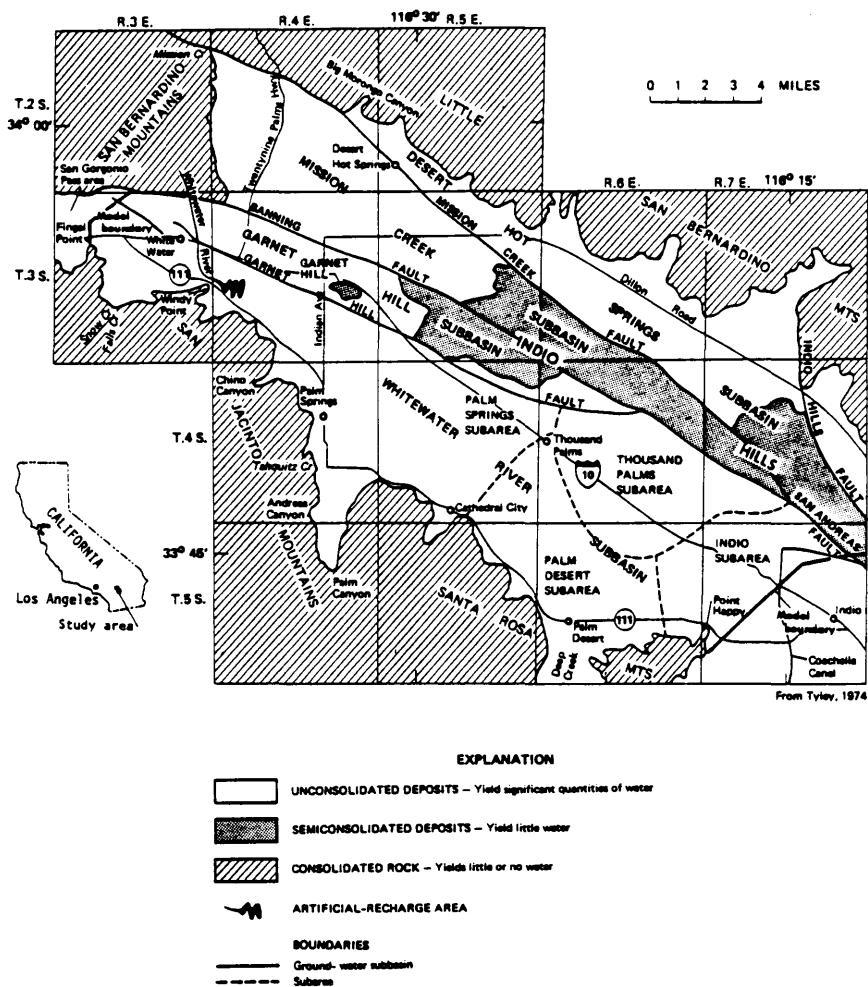


Figure 1.--Ground-water subbasins and generalized geology of the upper Coachella Valley, California (from Swain, 1978).

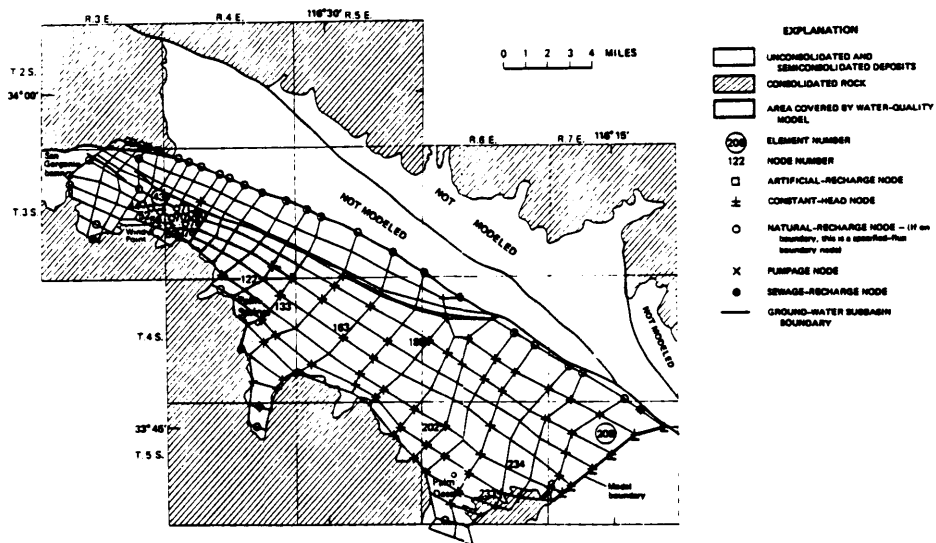


Figure 2.--Grid layout for finite-element flow model (from Swain, 1978).

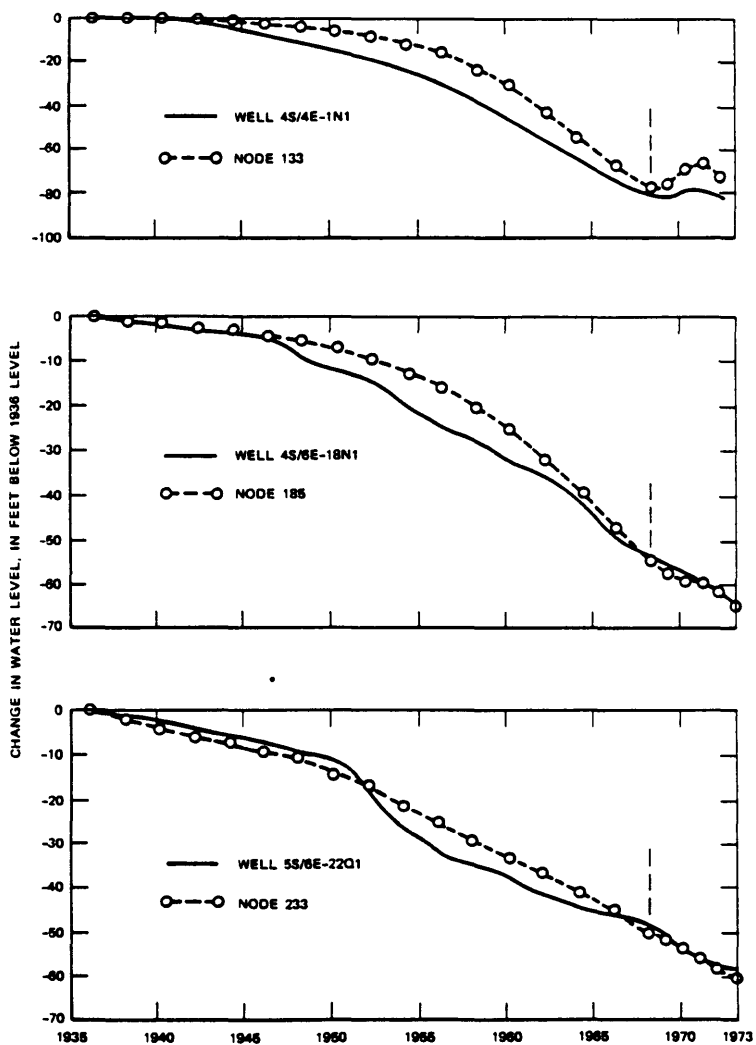


Figure 3.--Comparisons of hydrographs generated by the flow model (dashed lines) versus historical measured water levels (solid lines) (from Swain, 1978). Locations of nodes shown in Figure 2. Vertical dashed lines indicate start of verification phase of calibration period (1968-73).

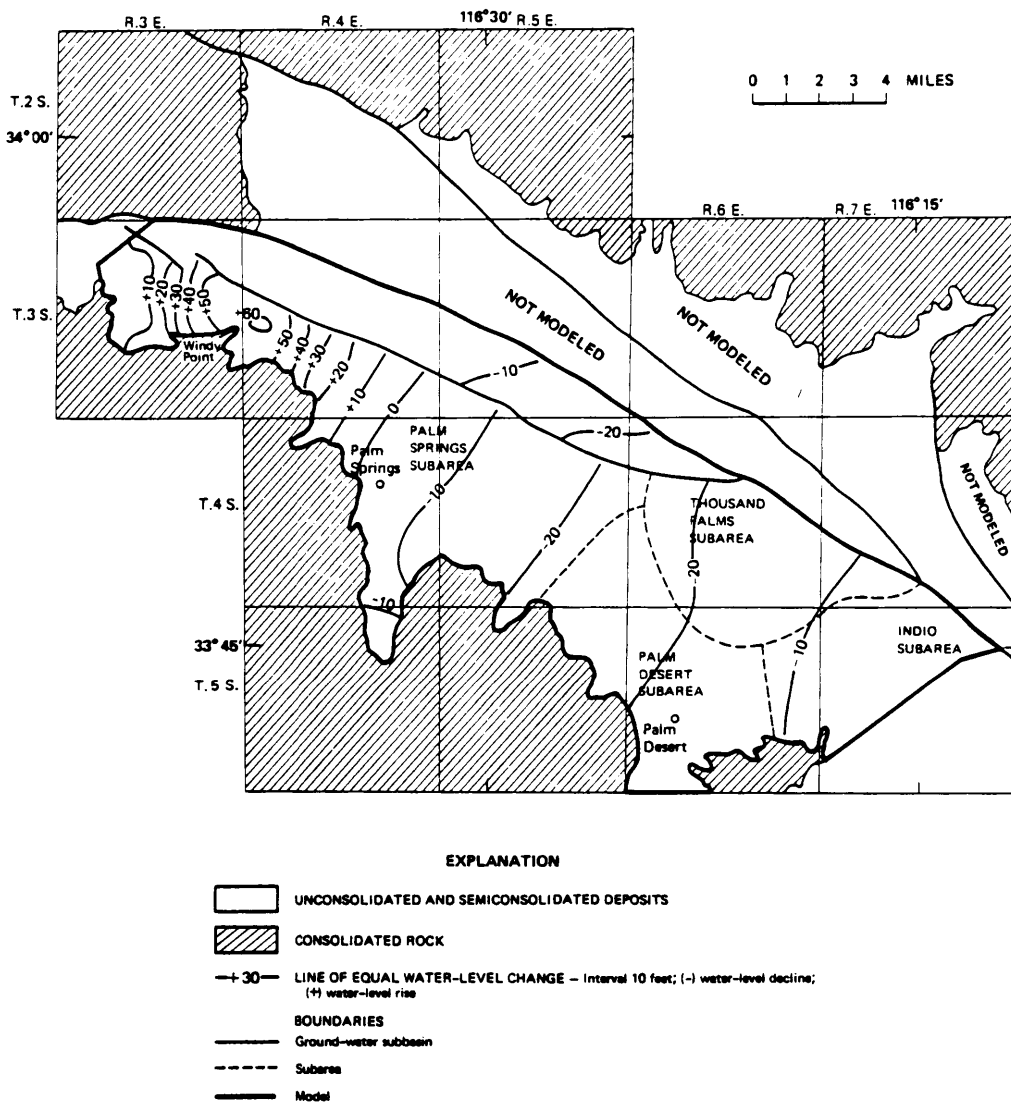


Figure 4.--Predicted water-level change, 1974-80, with artificial recharge and projected pumpage (from Swain, 1978).

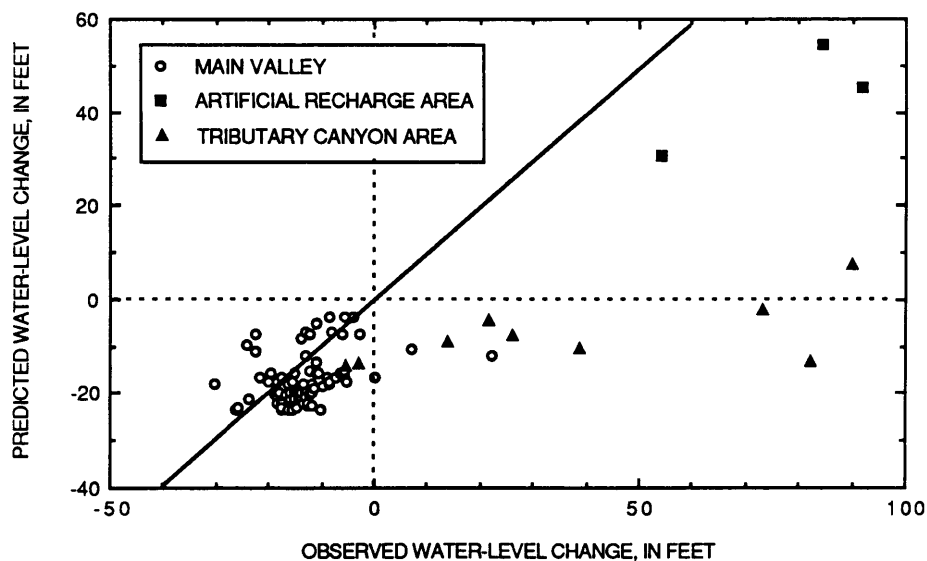


Figure 5.--Relation between predicted and observed water-level changes in the upper Coachella Valley, California, 1974-80. Solid diagonal line shows where predicted equals observed values.

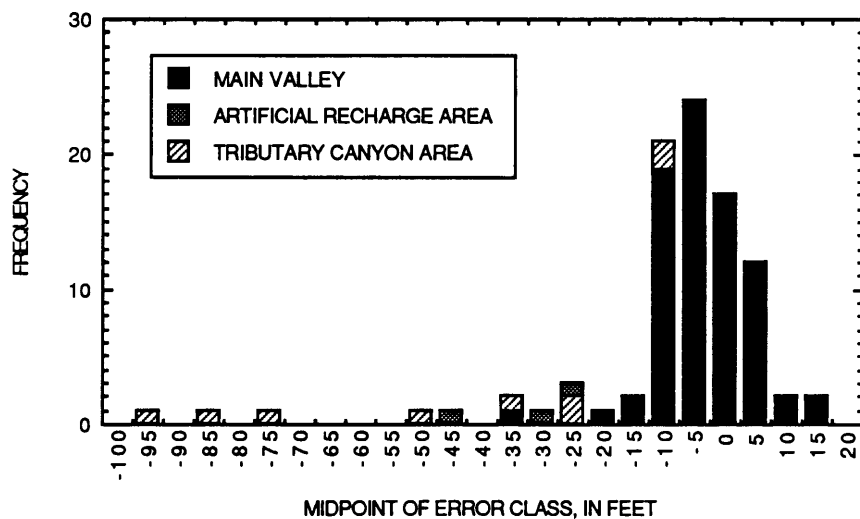


Figure 6.--Histogram showing frequency distribution of errors in water-level prediction for the ground-water flow model of the upper Coachella Valley, California, 1974-80.

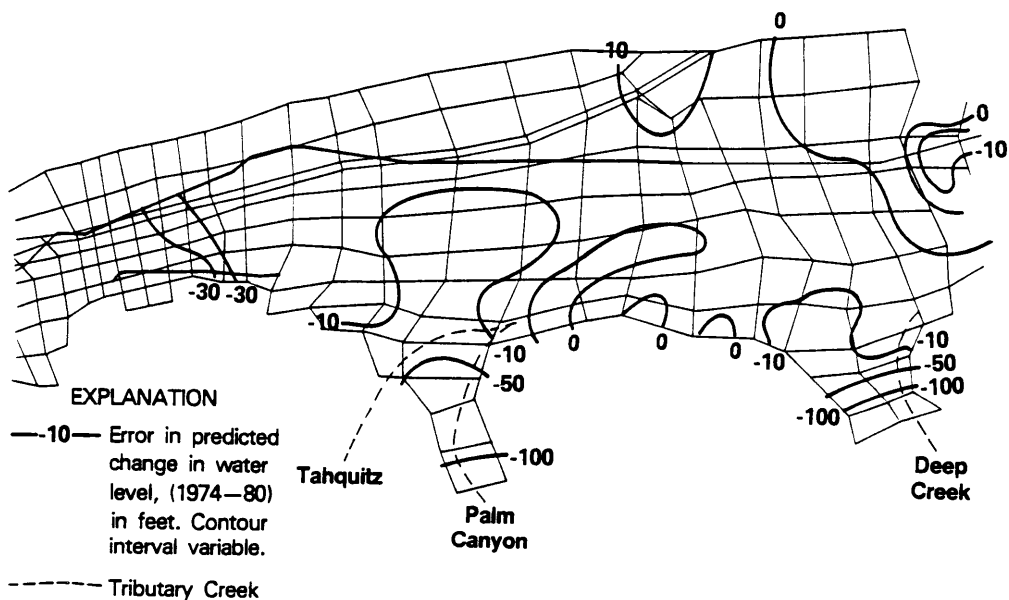


Figure 7.--Map showing the spatial distribution of errors in predicted water-level change, 1974-80, in the upper Coachella Valley, California.

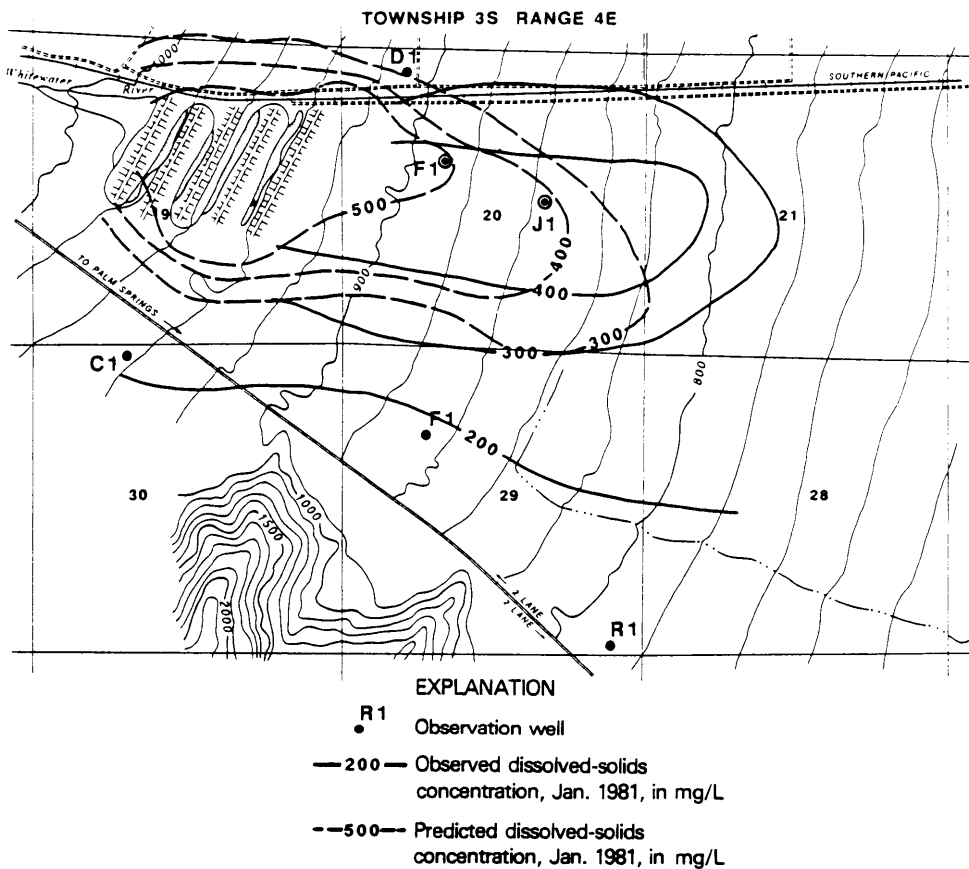


Figure 8.--Map showing observed and predicted dissolved-solids concentration, January 1981, near artificial recharge area.





## OVERFLOW THERMAL SPRINGS, CENTRAL ITALY

R. Celati, S. Grassi, C. Calore

International Institute for Geothermal Research-CNR  
Piazza Solferino 2, Pisa, Italy

and

Rakotoarimanga

Universite de Madagascar, Antananarivo, Madagascar

**ABSTRACT:** We consider a particular type of thermal spring that is very common in central Italy. This type of spring always emerges from the point of lowest elevation of the outcrops of the main regional aquifers. Based on field observations, we assume that these fractured formations can be simulated on a large scale to porous media, and we ascribe the springs emerging from their outcrops to the overflow type. The springs may be fed by water that infiltrates the same outcrop from which it discharges, or by water from the regional circulation, or by a mixture of the two.

Two-dimensional mathematical models confirm the plausibility of the conceptual model adopted and indicate that a large variety of situations may occur, depending on variations in the geohydrologic parameters involved.

### The Geothermal System

In recent years, the authors have dealt with a particular class of low-temperature geothermal systems, very widespread in central Italy, that posed a series of problems from the hydrogeological point of view.

These systems are found in regions (Tuscany and northern Latium) characterized by a hydrogeological setting that can be simply schematized as (Figure 1):

- \* a cover complex that, on the whole, can be considered impermeable because of abundant clays, shales, and marls;
- \* a carbonate-evaporitic complex forming the main regional thermal aquifer, overlying a metamorphic terrigenous complex that has a much lower permeability.

The outcrops of the carbonate-evaporitic formations represent potential recharge or discharge areas for the regional aquifer. The majority of the thermal springs of Tuscany and northern Latium are located on the boundaries of these outcrops, along the surface contact with the cover.

The outcrops of the aquifer formations can, therefore, act simultaneously as recharge and discharge areas; outcrops with this dual role are found both at low and at high elevations in the region, as shown in the schematic cross-section in Figure 2, and as can be deduced from Figure 3. The latter shows the outcrops of the aquifer formation and the springs emerging from their boundaries in Tuscany, along with the potentiometric surface of the main regional aquifer. This map also

provides information on the elevations of the thermal springs, because they coincide with the potentiometric surface at the spring emergence points, as will be discussed later.

Although the geothermal systems we are considering have been the subject of several geochemical studies (Francalanci, 1959; Bencini et al., 1977; Panichi et al., 1977; D'Amore et al., 1979; Fanelli et al., 1982), the related hydrodynamic problems have not received much attention.

All of the conceptual models presented explain the emergence of warm water by its flow through faults, joints, major fractures, or other discontinuities connecting deep permeable horizons to the surface. Such a hypothesis is also the basis of most of the quantitative models developed for various kinds of thermal springs (Sorey, 1975; Chapman et al., 1978; Nathenson et al., 1979).

In our case, however, the thermal springs generally occur in the points of lowest elevation of the contact between the permeable outcrop and the cover formations; the springs generally have no well-defined areal distribution, and a dense fracturation is observed in the outcropping formations. Based on these observations, we presume that these fractured formations act on a large scale as porous media, and we consider the springs on the borders of permeable outcrops as overflow springs.

The ratio between infiltration and spring flow rate can vary widely in the different outcrops, as infiltration in some cases will be far higher than discharge and vice versa.

There are cases where we are led to think that the springs are supplied only by the water that infiltrated the permeable outcrop from which they emerge. This happens, for example, when the permeable outcrop corresponds to a regional maximum of the potentiometric surface (main recharge area).

In other cases, the permeable outcrop is small, and the water discharged is far more than can infiltrate locally, so that the springs are primarily fed by the regional circulation (discharge area).

In general, however, both the regional and the local circulation contribute to spring supply. In all cases, as the springs are of the overflow type, their presence and flow rates are strongly influenced by surface morphology. The springs are always found in places where the permeable outcrop ground surface intersects the potentiometric surface. Other conditions being equal, the lower the emergence point, the higher the spring flow rate.

### Mathematical Modelling

Two-dimensional idealized mathematical models representing planar, vertical cross-sections were used to investigate some general features of groundwater circulation and heat transfer in the geothermal system. Given the simplifications adopted, particularly in the geometry, we expect from our models a better understanding of the large-scale phenomenology rather than quantitative matches of real systems. In all cases, we assumed steady-state conditions and homogeneous, isotropic media.

The computer code described by Rakotoarimanga et al. (1987) was generally used. This code deals only with steady-state conditions and water in liquid state.

For fluid flow, the equation assumed in the model is:

$$[k / \mu] (-p + g) = Q \quad (1)$$

and for heat transfer, the equation is:

$$v (CT) - (K_T T) = Q_c + CQ(T_w - T) \quad (2)$$

Fluid properties  $C(p,T)$ ,  $(p,T)$ , and  $\mu(p,T)$  are computed according to the formulae by VDI Wasserdampftafeln (Schmidt, 1963).

The method for solving Equations (1) and (2) is schematized in Figure 4. Each of the two equations are solved by finite difference (LSOR method).

Applied boundary conditions for pressure are:

- \* Hydrostatic pressure on the right boundary, with imposed pressure at the topmost point. Hydrostatic pressure means horizontal flow across the boundary.

where:

- C - specific heat of water
- g - gravity acceleration
- k - permeability
- $K_T$  - thermal conductivity
- p - pressure
- q - conductive heat flux
- Q - flow rate per unit volume of mass sources
- $Q_c$  - power per unit volume of heat sources
- T - temperature
- $T_w$  - fluid temperature of mass sources
- v - Darcy velocity
- $\mu$  - viscosity
- density

- \* Either no flow or hydrostatic pressure (with imposed value at the top) on the left boundary, according to the different cases.
- \* Impermeable lower boundary.
- \* Pressure or vertical pressure gradient assigned on the top.

Boundary conditions for temperature are:

- \* Zero horizontal gradient (horizontal isotherms) on left and right boundaries.
- \* Assigned temperature (20°C) at the top.

\* Assigned vertical heat flow at the bottom.

Unless otherwise specified, the intrinsic permeability is  $10^{-14} \text{ m}^2$  in the aquifer and  $10^{-30} \text{ m}^2$  in the cover; the thermal conductivity is  $2.5 \text{ W}/(\text{m}^\circ\text{C})$  everywhere.

The results of several significant cases were compared with those obtained by means of the geothermal simulator SHAFT 79 (Pruess and Schroeder, 1980).

Our results are shown by isotherms and streamlines. The stream function is based on the mass flux vector  $\mathbf{v}$  rather than on velocity  $\mathbf{v}$  in order to allow simulations with significant density changes (Norton and Knight, 1977).

### Two-Dimensional Half System

A first series of simulations deals with main recharge areas and considers only the right part of the permeable outcrop and the part of the system to its right (Figures 5 and 6). The left boundary is assumed to be a water divide and, therefore, impermeable. Pressure is assigned on the upper boundary, with a straight-line or broken-line distribution.

Some of the models also consider isothermal systems (temperature  $20^\circ\text{C}$ ), in order to isolate phenomena that occur independently of buoyancy forces.

The most interesting results obtained from these isothermal cases concern the effects of variations capable of changing the flow in the aquifer toward the right boundary, such as variations in the right boundary pressure or in the aquifer thickness. Reducing such a flow entrains a larger spring discharge; modelling shows that the increase in the discharge/infiltration ratio is accompanied by a deeper circulation of the water infiltrated. Figure 5 gives an example of how the flow pattern is modified by an increase in pressure at the right boundary.

We observed a curious effect of the change in flow resistance through the aquifer when we applied a constant heat flux of  $150 \text{ mW}/\text{m}^2$  at the base of the system to the cases run in isothermal conditions. In several cases, we observed that the spring disappeared, and infiltration occurred throughout the permeable outcrop. The viscosity reduction induced by the higher temperature had reduced the flow resistance in the aquifer to the point that all the water infiltrated flowed towards the right boundary.

In the non-isothermal cases examined in this series, forced convection appears to be the dominant phenomenon, except in cases of very low applied pressure gradients, where natural convection becomes important, as in the case shown in Figure 6. In this case, a straight-line pressure profile of very weak slope is applied to the upper boundary.

### Complete Two-Dimensional System

The complete two-dimensional system includes the entire permeable outcrop and the aquifer on its left and right sides (Figures 7, 8 and 9). This system permits us to simulate both the regional flow (assigning suitable pressure conditions to the lateral boundaries) and the local circulation, assigning infiltration and discharge in the outcrop. The conditions imposed at the lateral

boundaries are of hydrostatic pressure with assigned values at the top points, while at the top boundary, the vertical pressure gradient is imposed. Other boundary conditions remain unchanged with respect to the previous cases. The pressure imposed at the top of the lateral boundaries is indicated in the figures.

Various circulation patterns are obtained by varying the discharge/infiltration ratio in the permeable outcrop, the relative importance of the local and regional circulation, and their directions.

In Figure 7, infiltration is strong and the permeable outcrop acts as a main recharge area. The water discharged is a fraction of that locally infiltrated, which has circulated long and deep enough to reach the observed temperature (and salinity). Flow in the aquifer occurs away from the permeable outcrop on both sides.

In Figure 8, the discharge/infiltration ratio is increased with respect to the previous case. Both the local and the regional circulation contribute to spring discharge and the rise of the regional water is partly responsible, in the spring zone, for temperatures higher than in the case of the main recharge area.

Interesting results were also obtained in the cases of low infiltration and discharge. When the local and regional circulations occur in the same direction, the former may remain perched above the latter so that the spring is fed by local circulation only.

The result shown in Figure 9 is obtained by placing infiltration on the right side and discharge on the left side of the permeable outcrop. A complete separation occurs between the water infiltrated and that discharged. The local infiltration water flows entirely towards the right, while the spring is supplied by the regional circulation only.

# LIST OF REFERENCES

- Bencini, A., V. Duchi, and M. Martini, 1977. Geochemistry of thermal springs of Tuscany (Italy), *Chemical Geology*, 19, 229-252.
- Chapman, D.S., K.T. Kilty, and C.W. Mase, 1978. Temperatures and their dependence on groundwater flow in shallow geothermal systems, *Geothermal Resources Council Transactions*, 2, 79-82.
- D'Amore, F., P. Squarci, and C. Panichi, 1979. Indagine geochimica delle sorgenti termali italiane, valutazione dei serbatoi geotermici e ricostruzione geoidrologica di alcune aree preferenziali (Toscana Sud-Occidentale e Lazio Centro-Settentrionale), Report for the Commission of European Communities, Eur 6743 IT.
- Fanelli, M., L. Bellucci, and F. Nachira, 1982. Manifestazioni Idrotermali Italiane, CNR-PFE, Geothermal Energy Subproject RF13, Appendix.
- Francalanci, G.P., 1959. Contributo per la conoscenza delle manifestazioni idrotermali della Toscana, Atti Soc. Toscana Sc. Nat., Serie A, Fax. II, LXV, 373-432.
- Nathenson, M., T.C. Urban, and W.H. Diment, 1979. Approximate solution for the temperature distribution caused by flow up a fault and its application to temperature measured in a drillhole at Raft River geothermal area, Cassia County, Idaho, *Geothermal Resources Council Transactions*, 3, 477-480.
- Norton, D., and J. Knight, 1977. Transport phenomena in hydrothermal systems, cooling plutons, *American Journal of Science*, 277, 937-981.
- Panichi, C., R. Fancelli, P. Noto, and S. Nuti, 1977. Geochemical survey of the Siena province. Seminar on Geothermal Energy: First Results of Projects Funded by the European Communities, Brussels, EUR 5920, 2, 481-503.
- Pruess, K., and R.C. Schroeder, 1980. SHAFT 79 User's Manual, Lawrence Berkeley Laboratory Report No. 10861, Berkeley, California.
- Rakotoarimanga, R. Celati, L. Taffi, P. Squarci, and C. Calore, 1987. Surface heat flow and deep temperatures in the Bradano Trough (southern Italy). Possible effects of groundwater circulation, *Geothermics*, 16, 473-485.
- Schmidt, E., 1963, VDI Wasserdampfatafeln, Springer-Verlag, Berlin.
- Sorey, M.L., 1975. Numerical modelling of liquid geothermal systems, U.S. Geological Survey Open File Report 75-613, Menlo Park, California, 66 p.

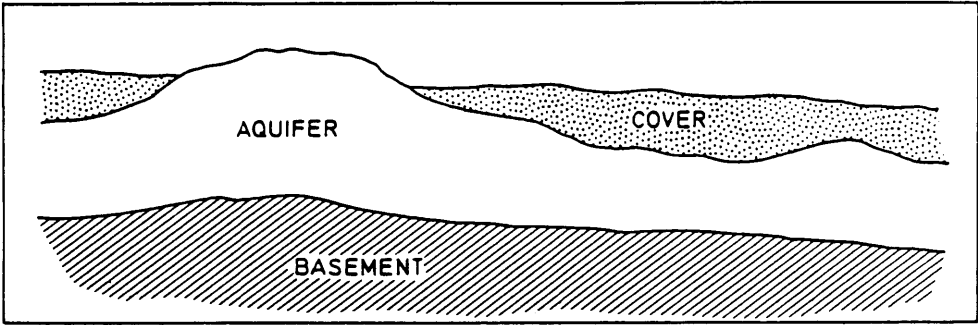


Figure 1. Schematic representation of the hydrogeological setting.

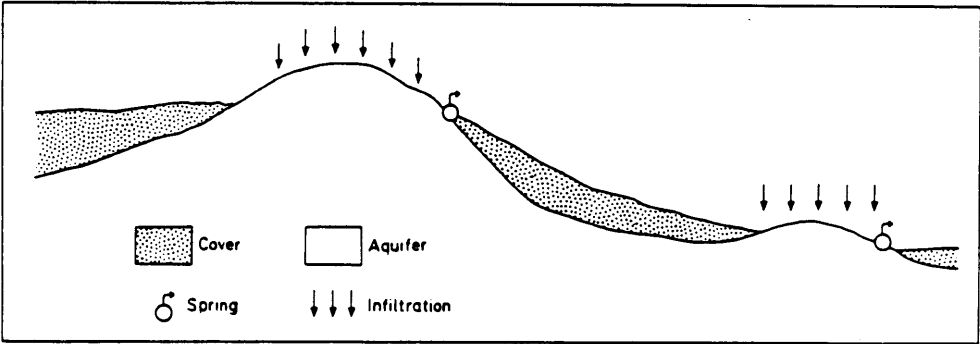


Figure 2. Outcrops acting simultaneously as recharge and discharge areas are found at very different elevations.

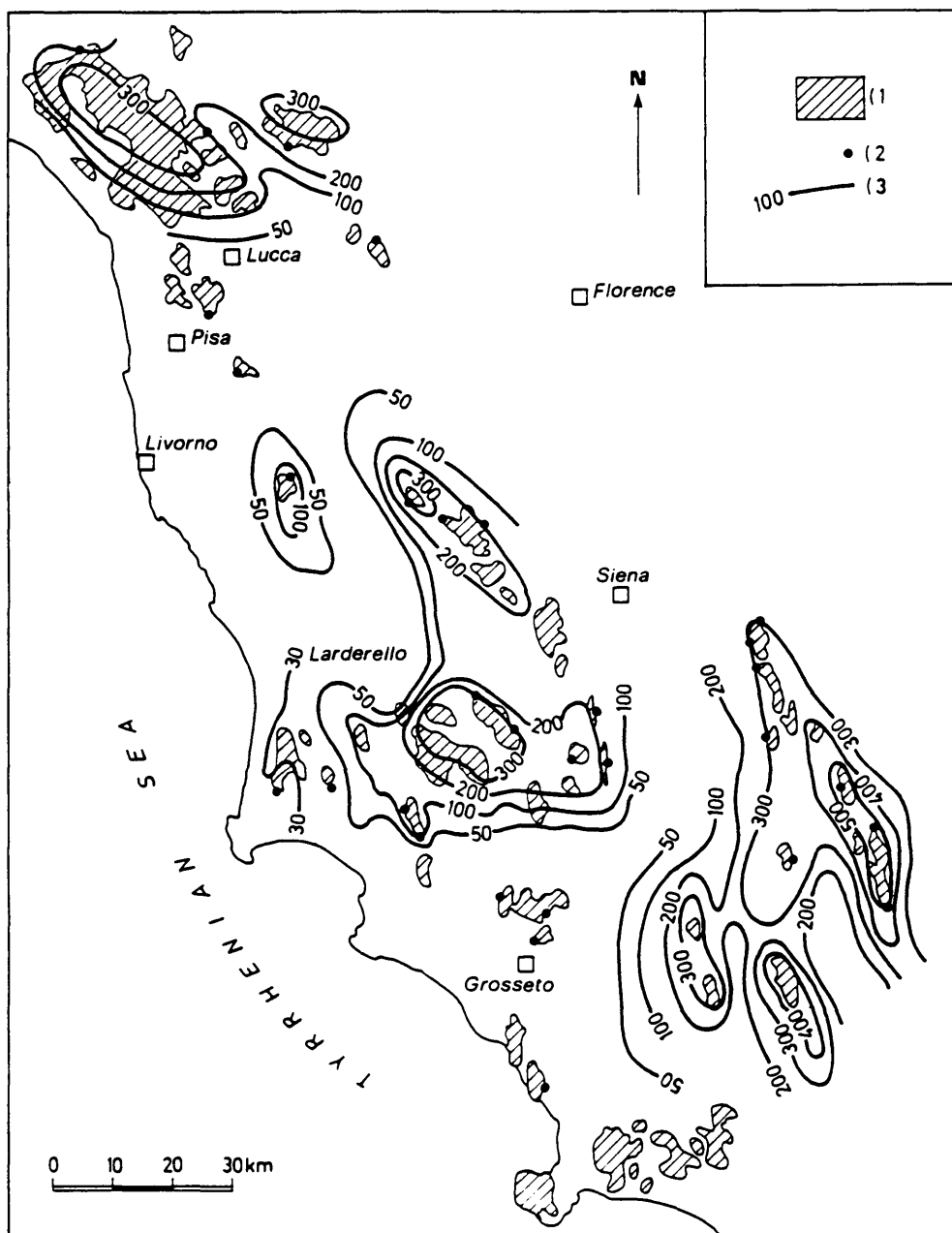


Figure 3. Schematic hydrogeological map of Tuscany. (1) Aquifer formation, (2) Thermal springs, (3) Isopiestic curve (m a.s.l.).



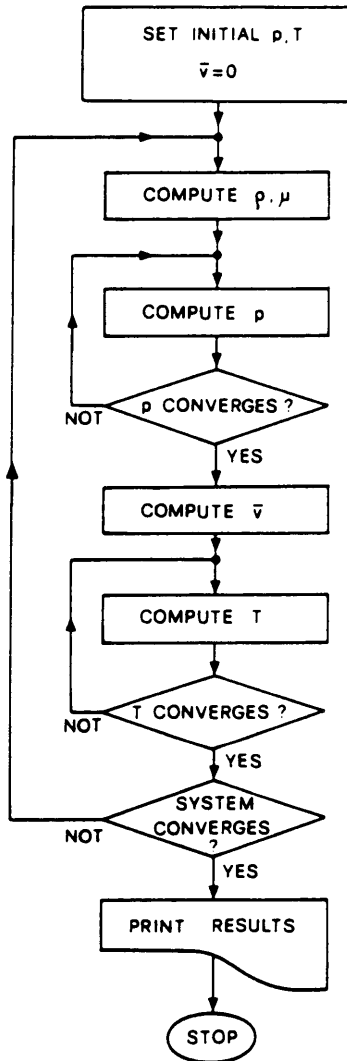


Figure 4. Iterative procedure adopted in the computer code.

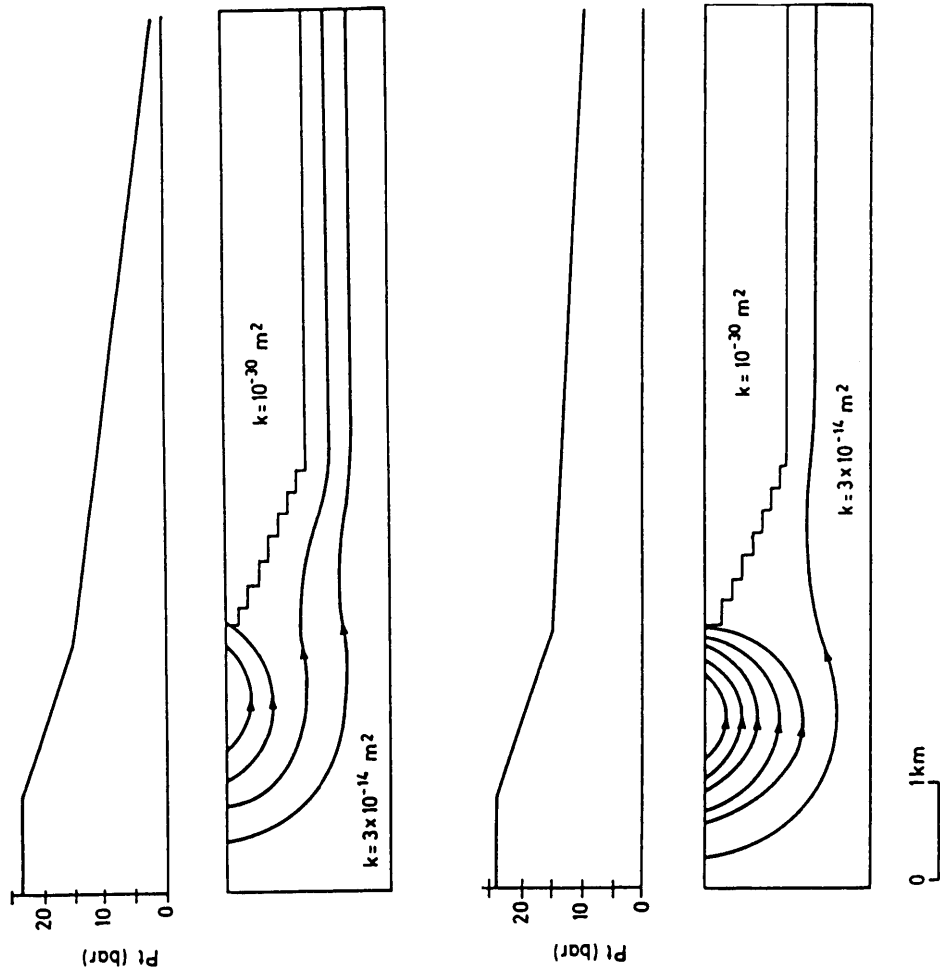


Figure 5. Main recharge area: the effect of an increase in the right boundary pressure. Streamline spacing  $3 \times 10^{-3} \text{ kg/(ms)}$ .  $P_t$  = assigned pressure at the upper boundary.

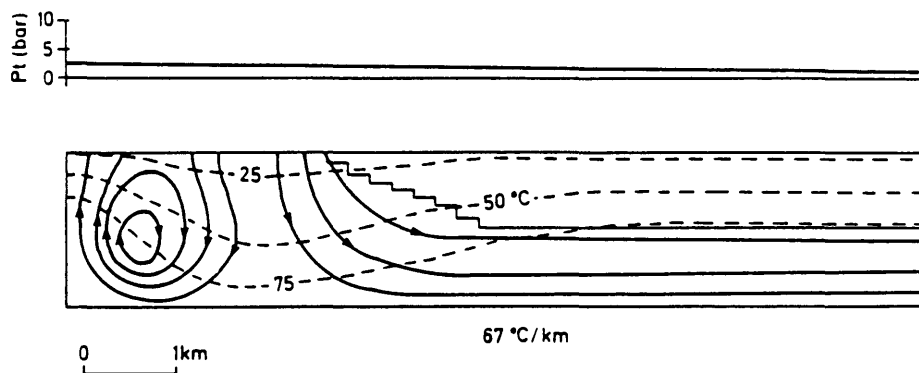


Figure 6. A case obtained from the same geometry as in Figure 5 applying a very weak pressure gradient at the top. The circulation appears to be controlled by natural convection. Streamline spacing  $3 \times 10^{-4}$  kg(ms).  $P_t$  = assigned pressure at the upper boundary.

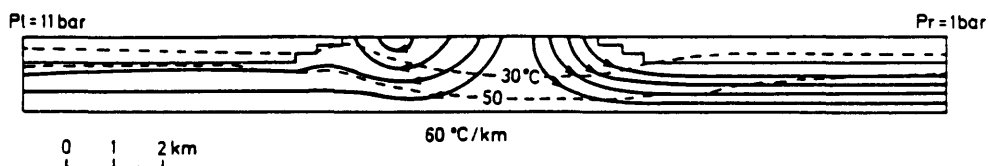


Figure 7. Model of a main recharge area. Streamline spacing  $10^{-3}$  kg/(ms).

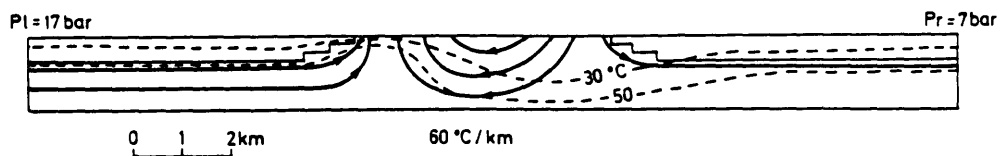


Figure 8. Example of mixed spring supply. Streamline spacing  $2 \times 10^{-3} \text{ kg}/(\text{ms})$ .

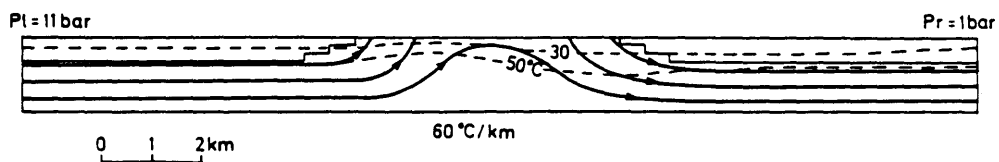


Figure 9. Separation of regional and local circulation. Streamline spacing  $5 \times 10^{-4} \text{ kg}/(\text{ms})$ .

INFLUENCE OF THE DEVELOPMENT OF THE SAPROLITE  
RESERVOIR AND ITS STATE OF SATURATION  
ON THE HYDRODYNAMIC CHARACTERISTICS OF  
DRILLINGS IN THE CRYSTALLINE BASEMENT

Michael Detay, D.Sc. and Patrice Poyet, D.Sc.

Abstract: Earlier studies led the authors to presuppose the existence of a significant influence of the weathered zone and its state of saturation on the hydrodynamic characteristics of the crystalline aquifer. After the analysis of 1,012 drillings carried out in the central African Basement Complex, they bring out arguments outlining this relation. The role of the saprolite reservoir has been quantified in order to determine the statistical hydrogeological characteristics of the drillings in the crystalline basement.

The Problem

The role played by the weathered zone of the crystalline basement was sensed by the hydrogeologists, but quantifying it remained purely empirical. Relying on numeric analyses [1, 2] performed on a sample of 1,012 drillings carried out in the Central African Basement Complex (Cameroon, Gabon, Central African Republic) [3, 4, 5], we have been able to outline the statistical hydrodynamic characteristics of the aquifer. Thanks to a probabilist approach, the influence of the thickness of the saprolite reservoir on the yield, the specific yield, and the probability of finding a minimum yield (infra-yield) has been determined. Finally, we point out the relation among the thickness of the saprolite reservoir, the thickness of the saturated zone, and the yield.

The Conceptual Model of Crystalline Aquifer and the Probabilistic Approach

In the crystalline aquifer, the cone of depression can be considered having a ramified shape [6]. The groundwater flow affects variously large areas, laterally and vertically, individualizing many subunits, some being already under the pumping effect influence, some not. In order to understand the crystalline aquifer hydrodynamics, we use a conceptual model.

The conceptual model of a crystalline aquifer: In a crystalline environment, the storage and drainage functions coexist in each aquifer level, the weathered zone being essentially a storage layer and the bedrock being a drainage system. The conceptual model of a crystalline aquifer, which is generally accepted, includes a semi-confining overburden (saprolite reservoir). This is mainly a storage reservoir supplied from the surface overlying a fissured and faulted confined aquifer (bedrock), draining the overburden and essentially having a drainage function [7, 8].

Although not exhaustive, the aim of this scheme is to facilitate analysis. In the present case, it is considered that the aquifer system in the crystalline environment presents the structure of a two-layered (Figure 1b,c,d) or even a multi-layered groundwater reservoir (Figure 1a,f). However, single-layered aquifers of saprolite, fissures, or faults (Figure 1e) may exist separately [9, 10].

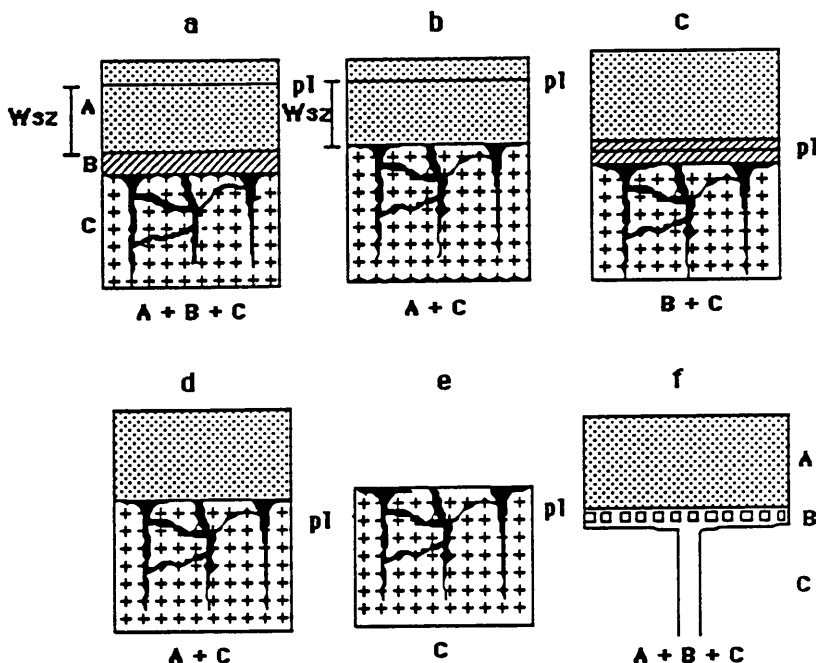


Figure 1. Conceptual model of aquifer systems in a crystalline environment.

- (A) Weathered zone ( $E_s$ )-storage function-saprolite reservoir
- (B) Fissured zone-drainage function-bedrock aquifer
- (C) Fault zone-drainage function-bedrock aquifer
- (F) Equivalent model of the A aquifer

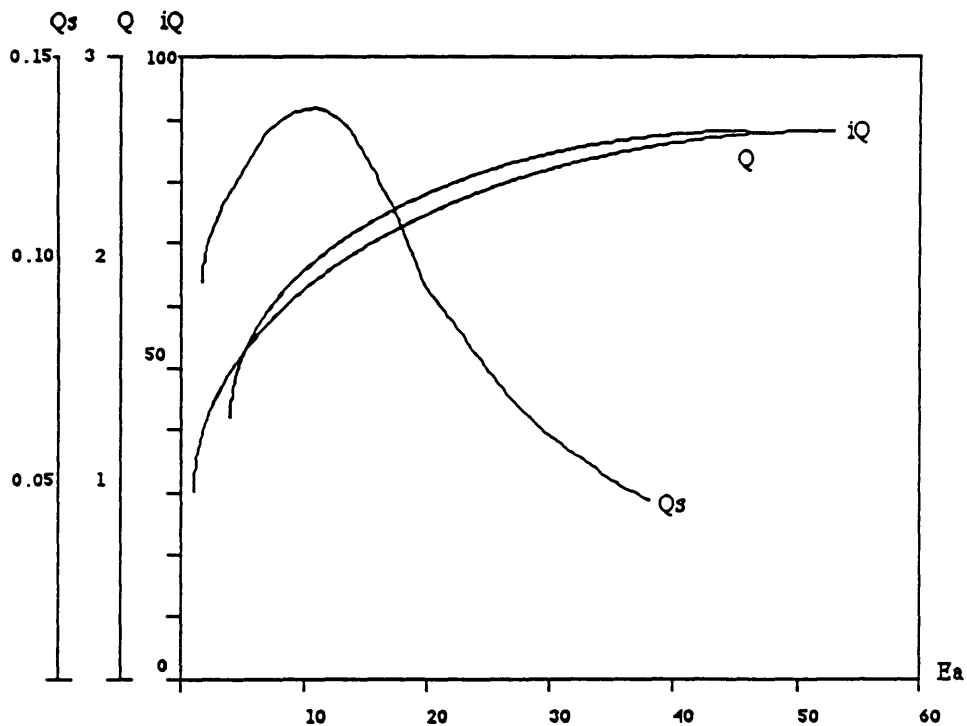
The probabilistic approach: Our analysis has a statistical significance, trying to point out the global stress of the aquifer during a pumping test. Our statistical classes have been fixed according to the sampling nature. The data have been restricted according to the objectives set by the village water supply programs: yield < 10 m<sup>3</sup>/h, specific yield < 1 m<sup>3</sup>/h/m, and thickness of the weathered zone < 60 meters.

### The Results

Our approach is based on the results of earlier analyses [1, 11, 12] which led us to think of the role played by the thickness of the saprolite reservoir and the thickness of the saturated zone.

# Influence of the Thickness of the Saprolite Reservoir ( $E_s$ )

A thorough study enables us to study the influence of  $E_s$  on the yield ( $Q$ ), the specific yield ( $Q_s$ ), and the probability of obtaining the infra-yield ( $iQ$ ) (Figure 2).



Specific yield ( $Q_s$ ) in  $m^3/h/m$ ; yield ( $Q$ ) in  $m^3/h$ ;  
infra-yield ( $iQ$  of  $0,8 m^3/h$ ) in percentage

Figure 2. Influence of the Thickness of the Saprolite Reservoir

### Influence of $E_a$ on the Yield

The yield expressed in  $m^3/h$  has been studied from pumping tests carried out on 540 operating drillings. The curve  $Q(E_a)$  shows the positive relation between the increase of  $E_a$  and the yield. The curve  $Q(E_a)$  is interpolated by the irregular rational function:

$$Q(E_a) = \frac{1.07E_a + 0.2}{0.325E_a + 1.3}$$

### Influence of $E_a$ on the Specific Yield

The curve  $Q_s(E_a)$ , determined from 176 measurements, shows a linear increase in the first 13 meters before dropping (critical threshold) to tend to reach values less than  $1 \times 10^{-1} m^3/h/m$  beyond 35 meters in the saprolite zone.

$Q_s(E_a)$  is interpolated by the regular rational function:

$$Q_s(E_a) = \frac{0.76E_a + 0.34}{0.0075E_a^3 - 0.145E_a^2 + 2.68E_a + 2.34}$$

### Influence of $E_a$ on the Infra-Yield

The probability, expressed in percentage, to obtain a minimum yield (fixed here at  $0.5 m^3/h$ ) has been determined from a series of 715 drillings.

The curve  $iQ(E_a)$  is interpolated by the regular rational function:

$$iQ(E_a) = \frac{0.7E_a + 0.9}{0.07E_a + 0.055}$$

The functions  $Q(E_a)$ ,  $Q_s(E_a)$ , and  $iQ(E_a)$  apply for values of  $E_a$  equal to or less than 60 m (limit of sampling).

### Influence of the Thickness of the Weathered-Saturated-Zone (WSZ)

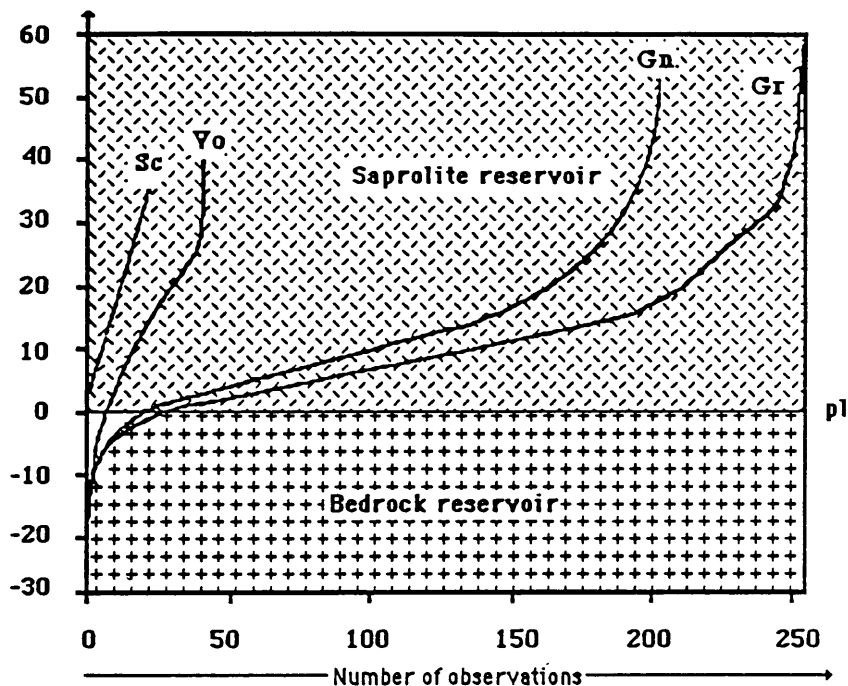
The thickness of the WSZ has been determined from the piezometric level in one or the other reservoirs (Figure 1), and the results are shown through two complementary approaches.

Influence of the position of the piezometric level: Figure 3 shows the position of the piezometric level (pl) in the various reservoirs. It has been drawn from 527 observations in bedrock formations: gneiss, granite, schist, and volcanic formations (basalt, dolerite). In 88.6% of the cases studied, the static water level is located in the saprolite reservoir. There is a strong positive correlation between the presence of a saturated saprolite environment and the yield values obtained in the water catchment facilities.



Influence of the thickness of the saturated weathered zone: Thanks to kriging [13, 14], we have been able to represent geometrically (Figure 4) the relation between the thickness of the saprolite reservoir, the importance of the saturated weathered zone, and the yield. The WSZ may be negative when the piezometric level is situated in the bedrock.

#### Thickness of the Wsz



Gn = gneiss (205 observations); Gr = granite (256 observations);  
Vo = volcanic (43 observations); Sc = schists (23 observations)

Figure 3. Position of the piezometric level in the different reservoirs.

#### Interpretations

Our results can fit into the state-of-the-art as follows:

##### Influence of the Thickness of the Saprolite Reservoir

The flows in a fractured zone are directed by the fissuring, they generally remain laminar, and comply with Darcy's law [15]. The yield coefficient being proportional to the cube of the fissure width [16], the progressive blocking of the fissures in relation to the overburden increase (mainly clayey) results in a stabilization of the yield and the exponential decrease of the specific yield when

$E_s$  increases. The probabilistic curves proposed clearly show the critical thresholds: 30 m for  $Q(E_s)$ , 13 m for  $Q_s(E_s)$ .

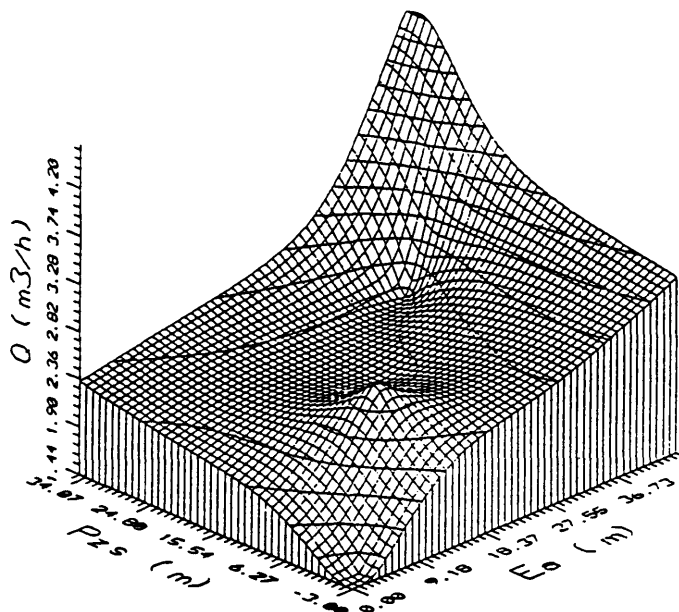


Figure 4. Influence of the Thickness of the Saturated Weathered Zone

#### Influence of the Thickness of the Saturated Zone

The yield appears to be directly linked to the thickness of the saturated zone. This relation reflects the mechanism of the aquifer system: when pumping from the fractured levels, the drainage function of the system applies [17, 18].

According to the structure of the crystalline aquifer, the storage function of the overlying saprolite plays a significant role only after a certain time of pumping. Our work is to be considered as a first approach of these phenomena which had never been previously demonstrated [19].

Studies under way concern, at another scale, the stress time of the different reservoirs during long pumping tests.

#### Conclusions

This first phase of analysis enabled us to quantify the role of the saprolite reservoir and its state of saturation, while determining the statistical hydrodynamic characteristics of drillings in the crystalline basement. Probabilistic equations have been submitted, too.

The primary importance of a drinkable water supply in the developing countries led us to integrate this expertise in a field expert system: HYDROLAB®<sup>1</sup> [20, 21, 22]. The role played by the saprolite reservoir in quantifying the hydrodynamic characteristics is an example of the expertise integrated in the expert system to help the decision-making process in the field of water-supply projects. HYDROLAB® also embodies the major techniques used by experts in the field and draws on a considerable wealth of practical knowledge gained from numerous drilling campaigns that we carried out in Africa. For more information, please refer to authors' publications.

---

<sup>1</sup> HYDROLAB® is the result of a close partnership between P. Poyet, who developed and implemented the program architecture and M. Detay, who brought the hydrogeological expertise on the project.

### References

1. Detay, M., 1987, Analytical and probabilistic identification of numeric and non-numeric parameters and knowledge representation in the sub-sahelian hydrogeological domain--application to the north Cameroon, D. Sc Thesis (These de Doctorat es Sciences), Nice University, 456 p., 5 annexes, 64 tabl., 131 fig.
2. Poyet, R., 1986, Discrimination des anomalies geochimiques multi-elementaires significatives. D. Sc Thesis (These de Doctorat es Sciences), Nice University, 436 p.
3. Arlab-Geolab, 1984, 1985, 1986, 1987, Final reports of a village water supply program in north Cameroon, Agriculture Ministry, Yaounde, 19 tomes.
4. Arlab-Geolab, 1985, 1986, Final reports of a village water supply program in north Cameroon, Mines Ministry, Yaounde, 7 tomes.
5. Arlab, 1981, 1982, 1983, and 1984, Final reports of a village water supply program in Gabon in the Nyanga, Ngounie, and l'Ogooue Maritime Provinces, Mines Ministry, 6 tomes.
6. Detay, M., P. Poyet, Y. Emsellem, A. Bernardi, and G. Aubrac, 1989, Development of the saprolite reservoir and its state of saturation, C.R. Acad. Sci. Paris, t. 309, Serie II, pp. 429-436.
7. Engalenc, M., 1978, Groundwater in the crystalline basement, CIEH.
8. Margat, J., 1982, Les milieux discontinus en hydrogeologie. Theme 3: les applications. Jubile Castany.
9. Bernardi, A., M. Detay, and D. Gaujous, 1987, Primi risultati di studi e perforazioni eseguita nel camerun settentrionale. Proceedings of the XX A.I.H. Symposium, Roma, Italy, 14 p., 4 fig.
10. Bernardi, A., M. Detay, and H. De Gramont, 1988, Groundwater research in the crystalline basement. Correlation between the geophysical parameters and the hydrodynamic characteristics of the aquifer. In *Hydrogeologie*, n°4, pp. 245-253, 7 fig.
11. Detay, M., and C. Doutambaye, 1989, Statistical hydrogeology synthesis of the Central Africa basement: main results of the village water supply in the cotton area. *Bull. du CIEH*, no76, pp. 13-24.
12. Detay, M., 1985, Statistical analysis of the first drilling campaign in the southwest Gabon. In *Bull. of the CIEH*, n°60, pp. 2-21.
13. Poyet, P., and M. Detay, 1989, HYDROLAB®: a pocket expert system for village water supply. Invited paper in "Revue Techniques et Sciences Informatiques", Special Issue on Expert Systems. TSI, Vol. 8, n°2, pp. 157-167.
14. Emsellem, Y., and J-P Bordet, 1981, Models for Water Quality Management, McGraw-Hill, pp. 222-272.
15. Louis, C., 1972, *Bull. BRGM*, Section III, n°1, Orleans, pp. 3-11.

16. Louis, C., 1974, *Bull. BRGM*, Section III, n°4, Orleans, pp. 283-356.
17. Poyet, P., and M. Detay, 1988b, Aide a l'implantation d'ouvrages d'hydraulique villageoise: Proc. Eighth International Workshop in Expert Systems and Their Applications, Avignon, France, pp. 397-410.
18. Poyet, P., and M. Detay, 1989, HYDROEXPERT®: an example of a new generation of compact expert systems. *Computers and Geosciences*, Pergamon Press, An International Journal, Vol. 15, n°3, pp. 255-267.
19. Poyet, P., and M. Detay, 1988, An expert system to help in decision making in the field of village water supply programs--introduction and reference manual. Research Report of the National Institut for Research in Computer Science and Automation (INRIA), n°936, Decembre, 38 p.
20. Detay, M., and P. Poyet, 1989, Design and implementation of a field expert system for village water supply programs. *Bull. Int. of Engineering Geology*, submitted.
21. Poyet, P., and M. Detay, 1989, HYDROEXPERT®: l'avenement d'une generation de systems experts de terrain. Proceedings of the Sahel forum on the state-of-the-art of hydrology and hydrogeology in the arid and semi-arid areas of Africa. UNESCO, CIEH, AIRE, pp. 567-577.
22. Detay, M., and P. Poyet, 1989, Development and evaluation of a field prototype expert system for village water supply programs. International Symposium on Groundwater Management: Quality and Quantity, Benidorm, Spain, October.



CONVENTIONAL METHOD AND DIGITALLY ENHANCED LANDSAT IMAGERY FOR GROUNDWATER  
EXPLORATION IN THE MAIN RIFT VALLEY OF ETHIOPIA

Tilahun Aberra\* and Heikki Wihuri\*\*

\* Department of Geology, University of Helsinki  
P.O.Box 115, SF 00170 Helsinki, Finland.

\*\* Finnish International Development Agency, Mannerheimintie 15 A  
SF 00260 Helsinki, Finland.

**Abstract:** The study area is part of the Main Rift Valley of Ethiopia. The failure of deep wells to reach an aquifer in the Eteya High Plain initiated this study. Conventional hydrogeological study coupled with satellite imagery were employed as tools of exploration. Initial study of the imagery helped identify the recharge and discharge area and later to carry out the conventional study. The area is covered by volcanic rocks. Several NNE-SSW trending faults have created a horst and graben topography. One intermittent, two perennial and three ephemeral streams drain the northern flank of Mt. Chilalo. Much of the rain that falls on the northern flank of Mt. Chilalo feeds the underlying aquifers in the discharge zone and does not generate dryweather flow to some of the streams. The groundwater from these aquifers sustains the flow of three large and several minor springs in the discharge area. Groundwater does not flow laterally from the discharge area to the adjacent Eteya plain as several faults act as barriers. The Eteya High Plain is covered by a thick mantle of expansive clay loam. The overburden inhibits direct rainfall to replenish the aquifers under the Eteya High Plain. Thus much of the subsurface water remains close to Mt. Chilalo forming the regional aquifer. In the northeastern part of the imagery, shallow groundwater extending over a large area that maintains the flow of the Wabi Shebelle River was monitored on the satellite imagery.

### Introduction

The study area is located on the eastern plateau of the rift system in central Ethiopia and forms the northern part of the Chilalo district. The water supply of the region has been very grim for decades. Water was hauled by a truck 2-3 times per day and rationed to the inhabitants of Eteya township. Efforts were made to supply the township with a dependable water source. Preliminary study of the area by Wihuri and Aberra (1970) in the absence of a base map and hydrogeological data, employed aerial photographs in a reconnaissance study of the area and their study resulted in a preliminary hydrogeological report. Wenner (1970, 1973) undertook a regional water resources inventory of the Chilalo district including the Eteya High Plain area. Critical reappraisals of Wihuri et al. and Wenner's studies were made by Aberra (1981). A Detailed survey of the area was undertaken by Aberra in 1986; this paper summarizes the findings of this survey.

As a result of Wenner's study, well drilling operations were started in Eteya High Plains and environs. Several wells were dry in the Eteya area, some of which are shown in Figure 3; well drilling was discontinued. As a short term solution, Fursa I and Fursa II springs were developed and Eteya township was hooked to a gravity pipeline system which runs from the Fursa escarpment. A more permanent solution to provide a reliable water supply

requires development of groundwater resources that will provide reticulated water throughout the Eteya High Plain to meet future water needs. The objective of this research is to refine concepts of groundwater occurrences in the Eteya High plain. Two basic approaches were employed in the study-conventional and satellite imageries. The conventional method includes geological and hydrogeological studies. The use of the satellite images entailed digital enhancement and interpretation of the enhanced images and alphanumeric products. The combined approach was found useful in revealing the hydrogeological setting of the region.

### Geologic Setting

The Eteya High Plains area is geologically complex. It is a northward extension of the Asela Plateau belt. The region is within a Tertiary volcanic province in which extrusive rocks, locally more than 4000 m thick were erupted from fissures and volcanic centers. Volcanic rocks related to the Eteya High Plain and environs are generally divisible into three groups, older plateau ignimbrites and trachybasalts of Pliocene-Eocene age; younger rhyolitic pumice flows, basalts and rift valley ignimbrites of Pliocene age and Quaternary to Recent lacustrine deposits and detrital sequences, largely alluvium that fill most of the low-lying areas on the plateau and lacustrine sediments in the rift valley (Di Paola, 1971). Beginning with the Miocene volcanism and continuing through the Quaternary, large-scale normal block faulting has disrupted the volcanic rocks. The normal faulting caused the development of miniature graben and horst topography. Figure 1 shows the general geology and structure of the region. The area close to the foothills of Chilalo and Badda Mountains is covered by a mantle of permeable lateritic soil which attains an average thickness of 3 m. Much of the Eteya High Plain is covered by a black cotton expansive clay loam. The thickness of the expansive soil is highly varied, ranging from 40 m north of Eteya to 2 m near Gonde. Over much of the Eteya High Plain, the average thickness reaches 20 m.

### Surface Hydrology

The average annual rainfall ranges from 1400 mm near Asela to about 870 mm 11 km away at Kulumsa. Generally 70 percent of the rainfall occurs in the months of June to September. The dry period lasts from October to February. A short period of light rains from March to April intervenes between the dry and rainy seasons.

Two perennial, one intermittent and three seasonal streams drain the northern watershed of Mt. Chilalo and part of Mt. Badda. The Wadecha stream with a watershed area of about 160 km<sup>2</sup> is the largest and drains the upper summits of Mount Chilalo. Downstream it joins the Galata River and flows to the Awash River in the northern part of the rift valley. The Wadecha stream is strongly fault controlled. The Gonde and Simba streams drain the northern part of Mount Chilalo. The upper reaches of the Simba stream starts inside the 6 km diameter caldera at the top of Mount Chilalo. The Gonde stream drains the upper part of Mount Chilalo and does not have access to the caldera. The two streams flow due west, cascading over the rift escarpments and joining the Katar River which discharge its water into Lake Zwai.

Between the Wadecha and Gonde streams, there are three seasonal streams. The Boru stream, which also begins on the summit of Mount Chilalo is a tributary stream to the Awash River for part of the year. Two unnamed streams with



poorly developed drainage system flow due NW and come to a dead end after forming minor gorges through a northwest-facing normal fault close to the base of Mt.Chilalo. The three seasonal streams respond only to large storms and are dry most of the year. The drainage network is shown in Figure 2A.

River networks which drain the Mt.Chilalo watershed respond to rainfall in different ways. Most of the streams which drain the western flank of the watershed have consistent flow throughout the year and areal differences in flow are relatively small. These streams have relatively higher base flows than streams which drain the northern flank of the watershed. Figure 2B shows the hydrographs of the Wadecha, Gonde and Simba streams for the 1968-1969 water years. These streams were gaged on an experimental basis for only two years. It is evident from the hydrographs of the streams that the Wadecha stream did not generate surface runoff in the 1968 water year. It is possible that the stream level fell below the zero reading on the staff gage. However in the 1969 water year, even though the amount of rainfall is lower than the 1968 water year by 20 percent as recorded at the Kulumsa weather station, the Wadecha stream started generating surface runoff in response to the small rains and continued to produce surface runoff until the rainy season came to an end in September.

Gonde stream had an intermittent flow throughout 1968. In the months of May, August, September and October the stream level fell below the zero reading on the staff gage. In the 1969 water year, the stream was producing runoff with some low flows following the rainy season. It continued to maintain the stream flow by base flow.

The Simba stream differs from the two streams in its runoff producing mechanism. In 1968, the stream often had normal flow and continued to flow through 1969, and appears to have had runoff and base flow components with a normal recession curve like other streams draining Mt.Chilalo on the western flank. The numerous discrete peaks of the Wadecha stream hydrograph confirm that the response of the catchment is mainly due to the onset of seasonal rainfall and occasional storms. Individual storms with low rainfall produce little or no runoff. The stream flow was not sustained by base flow during the dry months. Figure 3 shows the hydrographs of the three streams.

#### Hydrogeological Setting

The permeability of the volcanic rocks that make up Mt.Chilalo varies from one location to another. The area between Gonde and Keleta streams seems to have a particularly high permeability as the stream density is very low when compared with the western, eastern and southern flanks of the watershed. The northern flanks of the Mt.Chilalo and part of the Mt.Badda drainage systems appear in general to reflect less runoff to the streams and greater infiltration to the aquifers. The slopes of Mt. Chilalo are deeply affected by erosion on all sides. Variations of river channel entrenchment in the watershed from place to place is quite evident. Particularly, the drainage channels of the three seasonal streams are not deeply entrenched in the volcanic rocks. It was found that these streams do not have access to the underlying groundwater in their respective drainage basins.

The groundwater which was not tapped by the streams is released by gravity flow to the low-lying slopes to the northeast and southwest and sustains the dry weather flow of perennial streams like Gonde and Keleta and several

springs located astride the foothills of Mt.Chilalo and Mt.Badda. In the northeast, the movement of the groundwater is obstructed by the NNE-SSW facing Fursa fault that releases the water to Fursa 1 and Fursa 2 Springs. Part of the groundwater flow to the southwest feeds the Gonde Spring at the bank of the Gonde stream. Gonde, Fursa 1 and Fursa 2 are the largest springs in the area in terms of the volume of water they discharge. They have an average discharge of 5.8, 7 and 15 l/s, respectively. The similarity of the geochemistry of the three springs as shown in Figure 3 confirms that they tap a common groundwater reservoir.

The Eteya High Plain is floored by a black cotton soil with an average thickness of 20 m. Black cotton soil shrinks and forms deep cracks during the dry season. The maximum depth of crack is usually 2 m. When the clay is moistened, it expands and the cracks close up. This soil is a poor medium for transmitting recharge water to underlying aquifers. It is known also that black cotton soils generally cause drainage problems in some parts of Ethiopia. Rainfall which falls on the Eteya Plain seldom reaches the underlying aquifers. The salient features of the hydrogeology of the region are shown in Figure 4 A. Well logs showing the succession of rocks from the lowest exposure of basalt reached at a depth of 266 m below the surface of the ground upward through trachybasalt and overlying overburden at three localities are shown in Figure 4 B. The well logs indicate a uniform geology of the area.

There are three possible explanations for the occurrence of groundwater close to Mt.Chilalo and Mt.Badda and its absence in the Eteya area. Perhaps the simplest is the presence of perennial streams like Gonde and Keleta between the three seasonal streams. These perennial streams have relatively deeper drainage channels and have direct access to the groundwater in the basin which maintains base flow during the dry period. A second possibility is that the Gonde, Fursa I, Fursa II Springs and several small springs sustain their flow from the same groundwater reservoir that also replenishes the flow of the Gonde and Keleta Streams. Well No.7, located in the discharge area, reached a productive aquifer at a moderate depth of 120 m. Well No.10 located in the Eteya High Plain struck minor aquifers at a depth of 245 m; because of the poor yield and high pumping lift it was not utilized for municipal supply. Lastly, the failure of the deep wells in the Eteya High plain to reach a productive aquifer indicates the general paucity of ground water flow in the northern part of the study area. This is ascribed to the faults acting as barriers to the lateral flow of groundwater via the discharge area to the Eteya High Plain. Therefore it is concluded that the Eteya High Plain is virtually sealed off from direct rainfall or subterranean recharge, and remains a ground water shadow area.

#### Digital Image Enhancement

Several imageries representing different seasons of the study area were examined. Experience from Ethiopia has shown that dry season imageries are more suitable for hydrogeological studies than are wet season imageries. It was also found out that in all the dry weather imageries examined, identical anomalies were visible with a great deal of consistency. Figure 5A shows Landsat 2 black and white image scene 2367-06550 that was taken on January 24, 1976. The rationale for selection of the imagery was the fact that at this time of the year, the area is at the height of the dry season.

The imagery initially furnished valuable basic knowledge needed to probe the hydrogeology of the Eteya area and environs. Study of the imagery provided a regional view of the study area as related to other parts of the watershed. It helped to identify a number of previously unknown anomalies. Anomalies in the form of tonal gradients of the recharge discharge area appear conspicuous.

AS this area is geologically one of the most complex parts of the rift valley system, the regional hydrogeology was not easily perceived. Initially this study concentrated on the analysis of several imageries. The imagery was the key that revealed the hydrogeological framework of the region and helped greatly to carry out the conventional hydrogeological study presented herein.

As the anomalies in Figure 5A were subtle, A 600 by 448 pixel from the subscene shown in Figure 5A was scanned and digitally enhanced to improve the visibility of the subtle anomalies. The digital processing was performed by the edge enhancement function, the so-called LAPLACE METHOD which is based on the second derivative (Gonzalez et al., 1987). This program enhances the edges by adding the difference between the original pixel value and the local mean to the original pixel value. The desired enhancement is achieved by using an enhancement multiplying factor of 3. At this level of enhancement the noise is kept at a minimum. There is a functional program in the software package that filters noise. As the enhanced imagery appears natural to the eye, no effort was made to filter the noise. The enhancement technique has helped to achieve increased contrast and hence interpretability. The enhanced imagery is shown in Figure 5B and the flow chart in Figure 6 shows the enhancement procedures and system outputs.

The imagery in Figure 5B was reproduced from a digitally enhanced false color-infrared composite of MSS (Multi Spectral Scanner) 4, 5 and 7. In the study area three zones with various shades of grey tones are visible. The infrared composite was useful for discriminating vegetated areas, the darkest color and the densest vegetation (mixed forest) represents Mt. Chilalo and Mt. Badda, the recharge area. Zones of alternating light and dark tinges apparent in the Chilalo and Badda foothills represent the discharge zone which is the potential aquifer of the area. This area is sparsely vegetated with a mixture of shrubs and hay fields. The zone of light and dark tinges reflects the near surface saturated bedrock, soil moisture and vegetation relationships. The boundaries between the recharge and the discharge areas are shown with remarkable clarity, especially in the false-color image, that registers red and light red hues respectively. Much of the Eteya High Plain is covered by hay fields after the harvest season in January. It is natural that light color tones without anomalous tinges are characteristic signatures.

Image contrast of the study area appears to be highest in MSS images for MSS 5 and 7. Vegetation is dark in Channel 5 and lighter in Channel 7. Water features are more conspicuous in Channel 7 (Lakes Koka and Ziway) than in Channel 5. The ALPHANUMERIC maps in figure 7 A and B are produced from bands 5 and 7. The diagrams are produced in 8 digital number levels (grey tones). At this level, the information is compressed. The areas of interest are discriminated in accordance with the spectral reflectance of the recharge and discharge areas.

We also made observations of shallow groundwater anomaly signatures covering an extensive part of the Eastern Plateau. The fieldwork was conducted in June and December 1986. A large part of the Eastern Plateau is a treeless flat grassland. Elevations in the area range from 2650 over most of the plateau to 2850 m in mountainous areas. The plateau is cold and moist for most of the year. Over 1400 mm of rain falls annually on most of the plateau. In the northeast part of the imagery in Figure 5A and 5B, a notable phenomenon has been discovered. Near-surface groundwater that sustains the dry weather flow of the upper reaches of the Wabi Shebelle River has been monitored. On the periphery of the Eastern Plateau, the Wabi Shebelle River drainage system has eroded impressive canyons. A crescent-shaped shallow groundwater body wedging toward the upper reaches of the Wabi Shebelle canyon is a conspicuous anomaly on both imageries. We believe that the groundwater is contained in very thick alluvium and most of the water moves as underflow and maintains the river flow during the dry season. Some of the groundwater is probably lost through evapotranspiration, but available data are not conclusive. Built-up areas over much of the plateau are few in number and there are few motorable roads on the plateau. These factors, coupled with the vastness of the plateau, precluded detailed study. Therefore the area was field checked in less detail and provisional ideas concerning the presence of shallow groundwater over part of the drainage basin were confirmed. During our traverse of the area we came across several water-logged areas. Seepage of groundwater in several gullies was also observed. The presence of shallow groundwater was checked in hand-dug wells in Hetoferda, Kembolcha and Moye villages. We found that the water levels in the wells range in depth from 3 to 4 m below the land surface. The inset in Figure 8 shows the headwaters of the Many River on the rim of the plateau (a tributary of the Wabi Shebelle River) and localities where the presence of shallow groundwater was checked.

### Conclusions

From the foregoing, it is evident that the imagery furnished valuable basic data in the initial identification of the recharge and discharge areas. It also provided insight into how surface and subsurface waters are distributed in space and time in the study area. This study has established the occurrence of groundwater in the immediate region that borders the foothills of Mt. Chilalo and Mt. Badda (the discharge zone). Future municipal wells should probably be drilled in the discharge zone which contains the potential aquifers of the region. Any such development should be preceded by test drillings. This paper also shows that within limits, satellite imagery coupled with conventional hydrogeological studies can be employed to study certain types of hydrogeological problems.

### Acknowledgements

It is a pleasure to acknowledge the assistance of Kristina Laurila of the GTL Image Processing System laboratory (GIPSY) in Helsinki. We are grateful to Professor Richard Ojakangas of University of Minnesota, Duluth who

corrected the English. Ari Laukanen and Tapani Rämö helped with text editing. Maa ja Vesi tekniikan tuki r.y. paid for an air ticket and registration fee for the first author when the abstract of this paper was orally delivered at the 28<sup>th</sup> International Geological congress in Washington D.C in 1989.

### References

Aberra, T., 1981, Computer enhanced satellite imagery, water resources and rift system in central Ethiopia, University of Nairobi, Department of geology, Special Report. 35 p.

Di Paola, G.M., 1972, The Ethiopian rift valley (between 7° 00' and 8° 40' lat. North) Bulletin Volcanology, 36, P. 517-560.

Gonzalez, C., and Paul Wintz, 1987, Digital image processing, second edition, Addison Wesley, U.S.A., 503 P.

Wenner, C.G., 1970, A master plan for water resources and supplies with CADU's first project area. Publication No. 3, Swedish International Development Agency, Stockholm.

Wenner, C.G., 1973, A master plan for water resources and supplies in the Chilalo Awraja, Publication No. 89, Swedish International Development Agency, Stockholm.

Wihuri, H., and Tilahun Aberra, 1970, Hydrogeological reconnaissance of the Eteya area, Internal Report, Water Resources Department, Community Water Supply Division, Addis Ababa. 12 p.



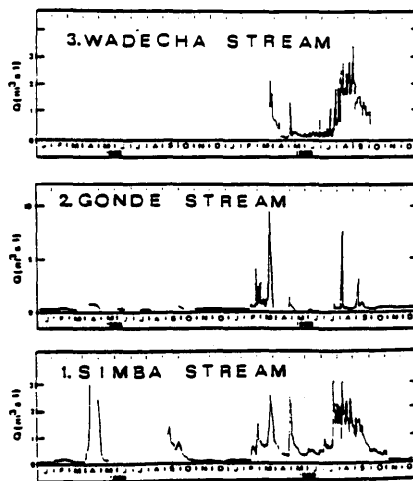
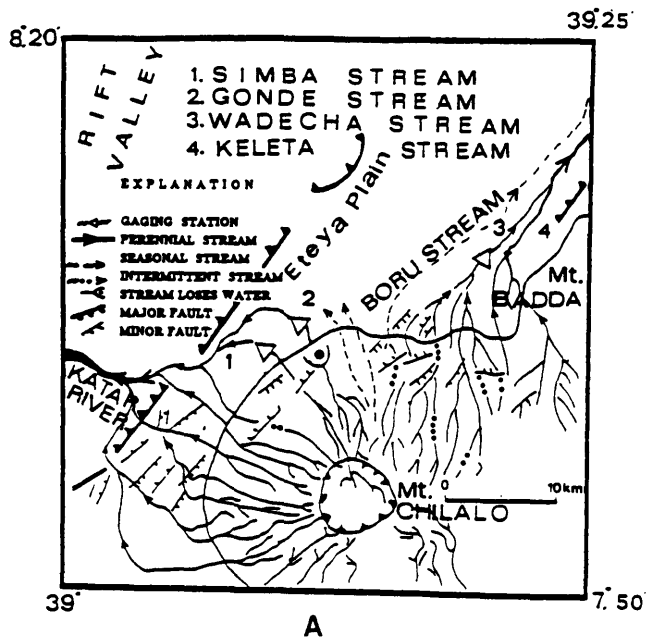


Figure 2A. Simplified drainage map of part of the Chilalo and Badda mountains watershed; 2B, hydrographs of Wadecha, Gonde and Simba streams for the 1968-1969 water years.

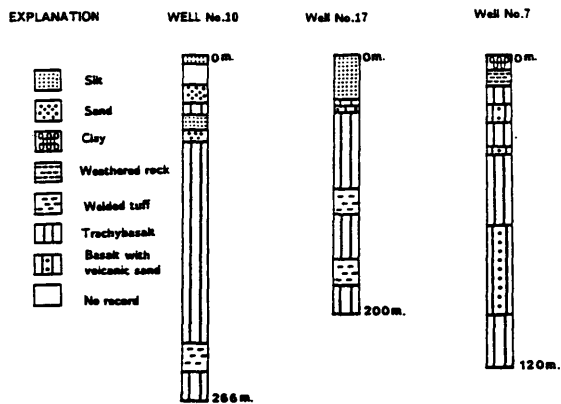
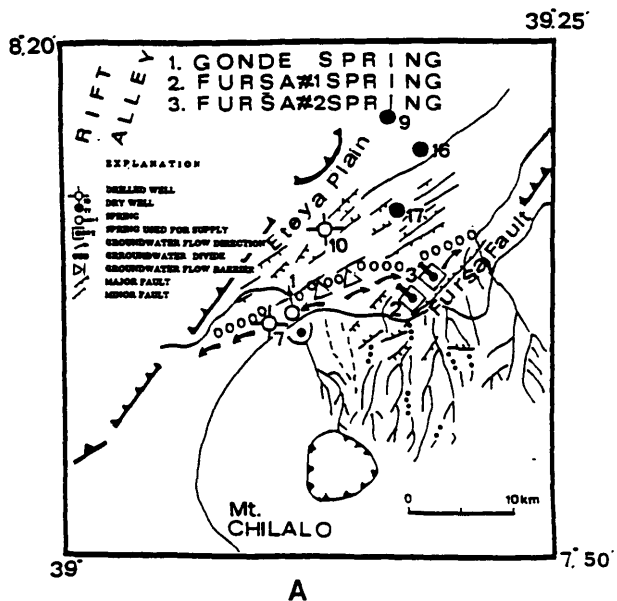
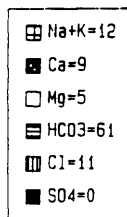
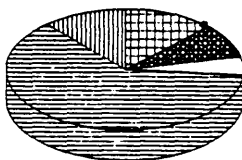


Figure 3A. Sketch map showing the hydrogeological features of the study area; 3B, Well logs.



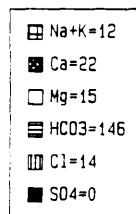
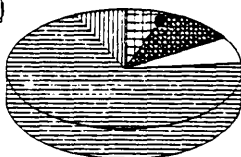
Gonde

compositions in ppm



Fursa #1 Spring

compositions in ppm



Fursa #2 Spring

compositions in ppm

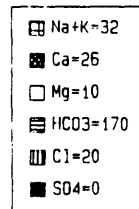
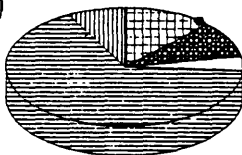


Figure 4. Pie diagram showing the geochemistry of Gonde, Fursa 1 and Fursa 2 springs.

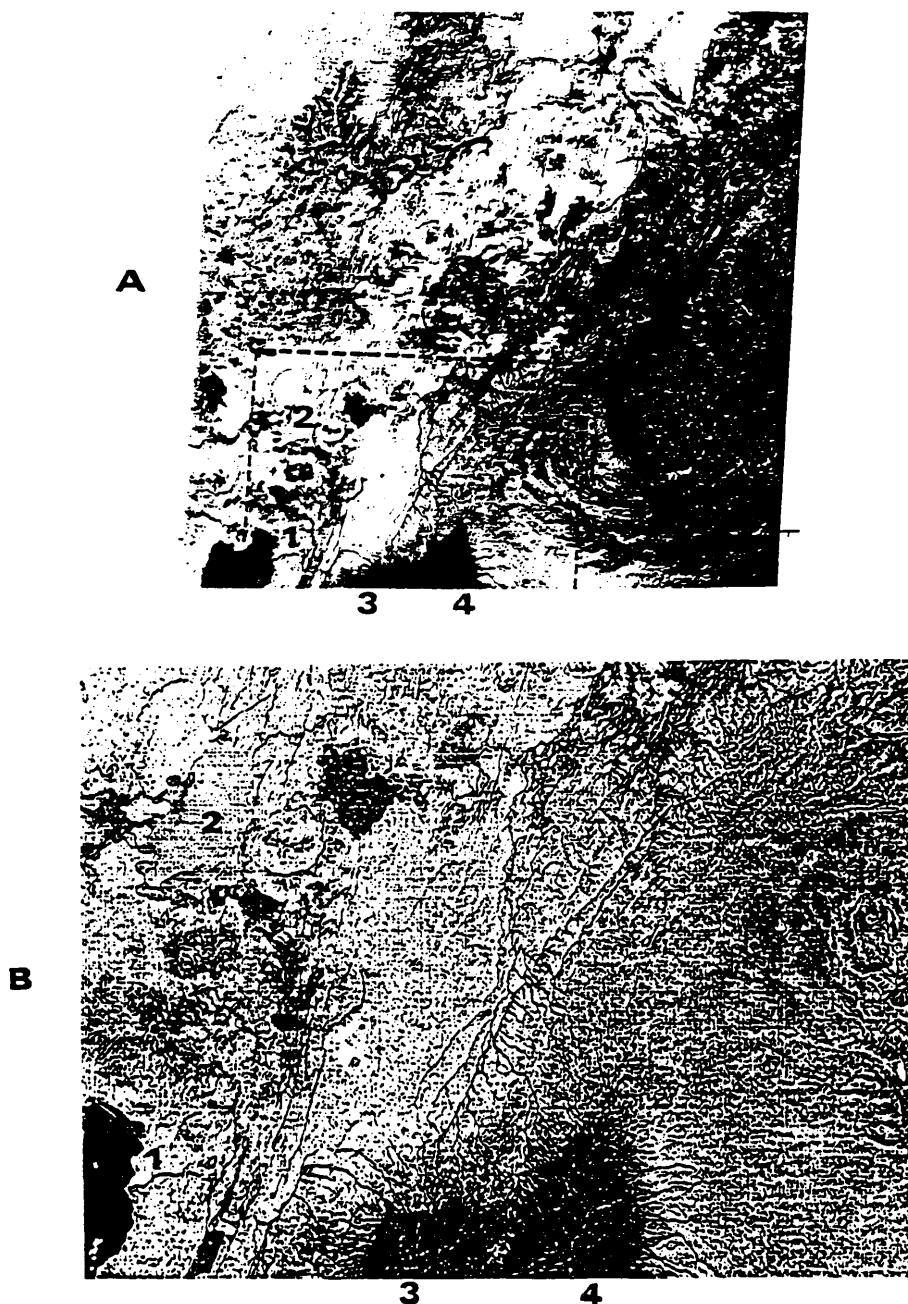


Figure 5A. Unenhanced MSS image of the study area for band 7 of Landsat scene 2367-06550, January 24, 1976. 5B. digitally enhanced image of the study area. 1-Lake Zwai; 2-Lake Koka; 3-Mount Chilalo; 4-Mount Badda.

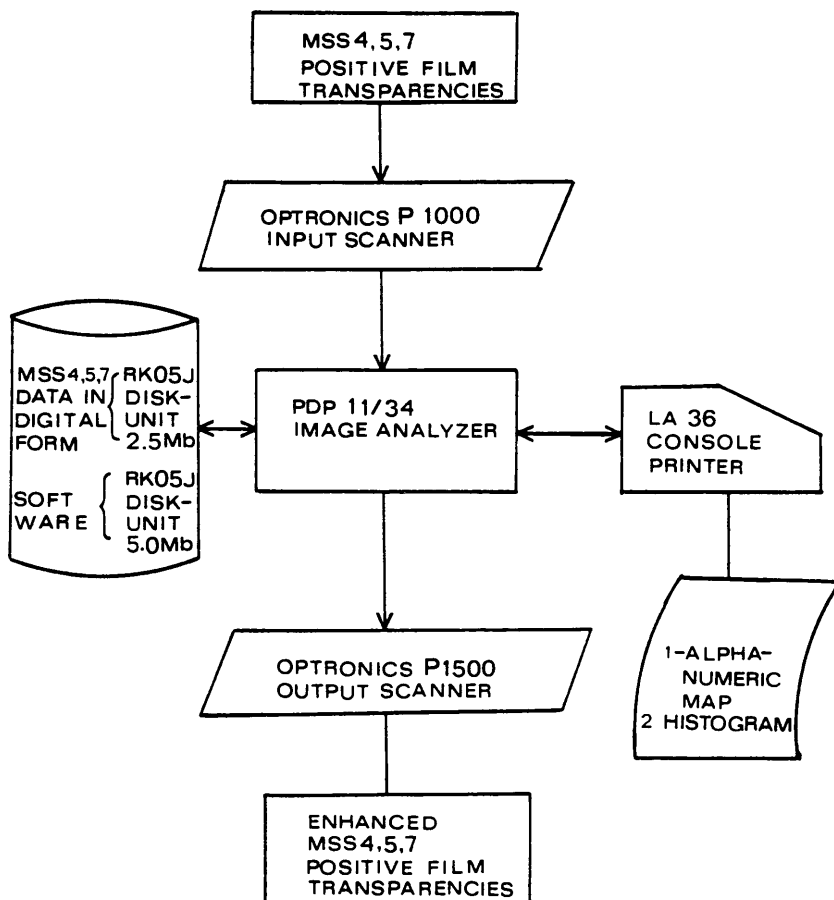
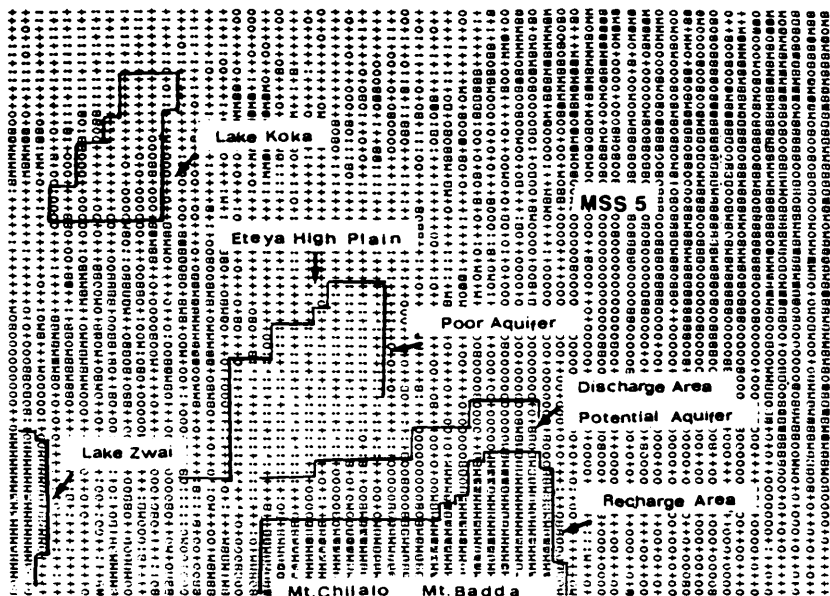
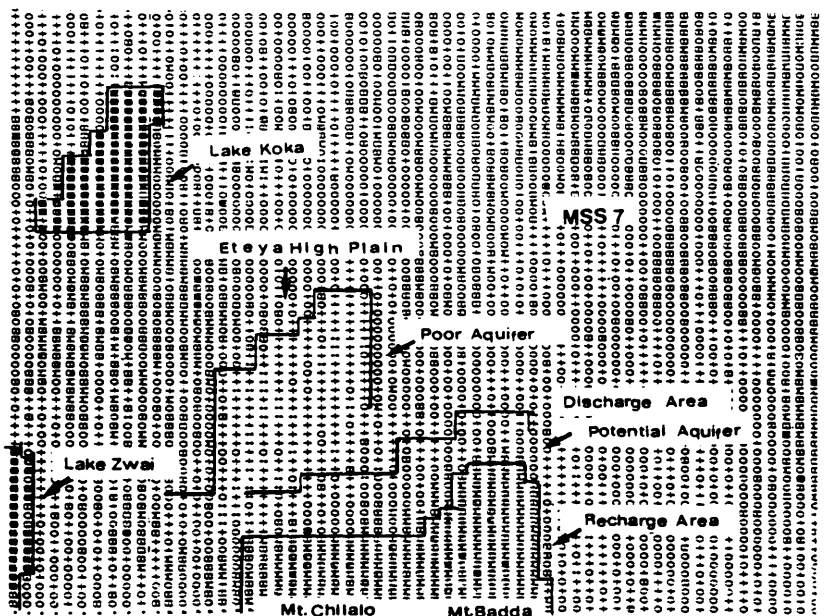


Figure 6. Flow diagram showing the sequence of steps used in processing the enhanced image and system outputs.



A



B

Figure 7. Alphanumeric maps for band 5 (A) and band 7 (B).

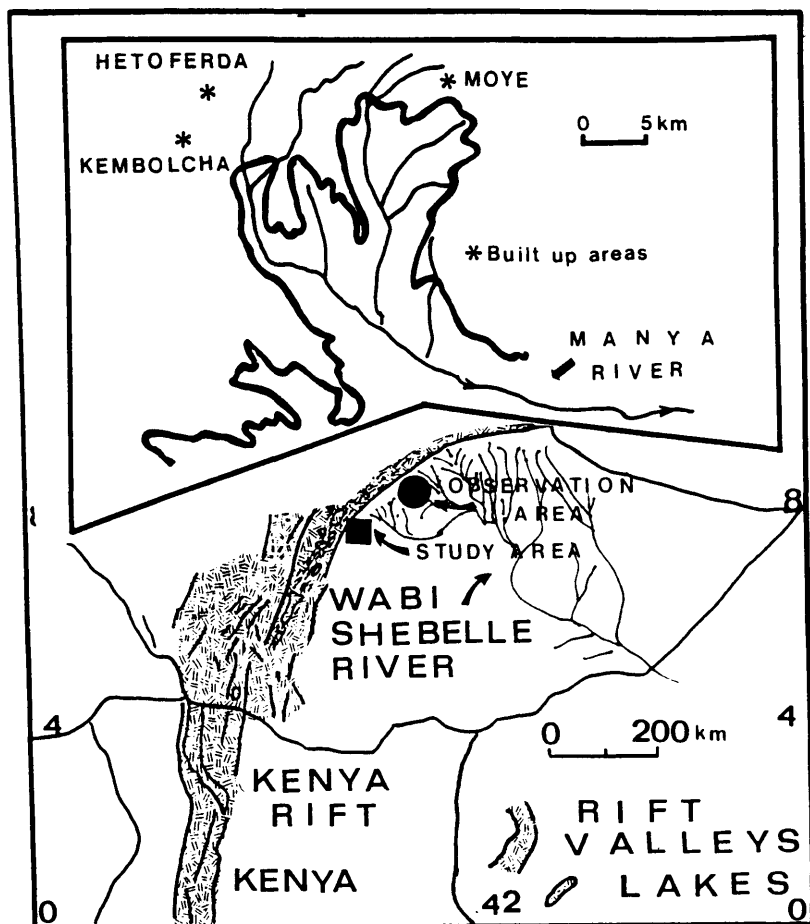


Figure 8. Sketch map showing the observation area in the Wabi Shebelle River Drainage. Inset shows the headwaters of the Manya River, tributary to the Wabi Shebelle River, and localities where groundwater level was observed in shallow wells.



WATER PROSPECTING USING SURFACE SP (SPONTANEOUS POTENTIAL):  
RECONNAISSANCE AND DETAILED STUDIES

John A. Randall-Roberts  
Apdo. Postal No. 168  
C.P. 36000  
Guanajuato, Mexico

Abstract: Water movement in both rock and gravelly aquifers is mapped by surface SP (spontaneous potential). Controlled measurements in the field make up for the smaller anomalies found as compared with work in sulphide deposits or geothermal systems. Positive anomalies are associated with discharge zones, strong lateral flow, or gravel beds. Negative readings indicate downward flow or recharge, or clayey beds. Readings in millivolts range from -30 mV to +50 mV in areas of cold to slightly warm water, with a signal from depths of 150 meters or less. Regional cartography can separate recharge from discharge zones as an aid to hydrogeological mapping. Gravel paleochannels, fractured volcanic rocks, and water-bearing fault zones can be identified. Surface SP is a good second-phase prospecting method, after hydrogeological mapping and before more costly detailed geophysics, due to its portability and rapidity. The SP dipole may be quantified using models originally derived for sulphide deposits but applicable to groundwater flow, thus providing a method for quantifying the SP curves.

### Introduction

The spontaneous potential (SP) method of geophysical prospecting has had a long, although only sporadically popular, history of more than 160 years. The basic concept of measuring electrical tension between two earthed electrodes remained difficult to accomplish in practice until the early 20<sup>th</sup> century (Kelly, 1957), due to problems in perfecting non-polarizing electrodes and in the realization that contact resistance with the Earth is, indeed, a problem. Modern studies by Ernston and Scherer (1986) and Fournier (1989) refer to the importance of using high impedance multimeters; thus, problems with electrodes and with relatively low-impedance voltmeters have caused impatience with the SP method until the present day. Many workers use electrical resistivity or induced-polarization receiving units in which the impedance is not high; still worse is the problem that there is no way to measure the mega ohms of contact resistance. This is usual in mineral exploration using these receivers, and is a debt owed by SP study to its first 140 years devoted to mining.

In the late 1960s (Ernston and Scherer, 1986), attention turned toward the use of SP in geotechnical applications, mainly in studies related to the leakage of water from reservoirs, dam site stability, and geothermal exploration. At the same time, attempts were made to understand the SP signal in reference to its origin. As opposed to many other electrical methods, SP is a passive system; no energy is injected into the Earth, and one only measures the natural tension between two electrodes. The signal provided by sulphide deposits is probably explained mostly by electrochemical half-cell potentials (Sato and Mooney, 1960); nevertheless, other sources became necessary to explain the strong anomalies measured by SP studies in the absence of redox systems. Electrokinetic, streaming, or filtration potentials have been examined by a large number of workers in the last 20 years, basing their interpretations mostly on the action of the double-layer or zeta potential in equations designed for the movement of an electrolyte

in a capillary tube. However, this application is not really quantifiable, and there are obviously other factors not yet understood involved in the voltages measured (Ernstson and Scherer, 1986). They made an important contribution (ibid, 1986) regarding the changes in absolute SP values with time and meteorological phenomena, although the form of the curves varied little. The role of water in these changes was emphasized; it is important to note that the position of the water table relative to the ground surface and to the body creating the SP signal was critical in discussions of the measured voltages (Sato and Mooney, 1960). Indeed, the recent work by Eskola and Hongisto (1989) challenged the quantitative analysis made by Ram Babu and Atchute Rao (1988) on sulphide bodies in that the latter work did not take into account the water level in their interpretation of the SP dipole in vein deposits. The SP signal from vein deposits may be heavily dependent on the saturation by slightly mineralized water in the fault zone and its interaction with the clay filling, rather than the generally low sulphide content in veins. Thus, we return to a combination of electrokinetic and electrochemical reactions whose separation may be difficult, but not necessarily in actual practice.

The recent paper by Fournier (1989) included the only good published analysis of the electrofiltration theory related to the Helmholtz equation, where he quoted Fitterman's 1978 work relating the current density to electrical conductivity multiplied by a combination of the electrical field vector plus the hydraulic gradient and the electrofiltration coupling coefficient. From this relation, it is obvious that the electrical conductivity of the water is the most important factor determining the density of current (mV of SP). He considered that in a free surface aquifer, the water table is the major source of SP. I agree with his diagnosis that SP is more effective than other electrical methods "as it is the only one depending on the groundwater flow itself." (ibid, 1989).

#### Depth of Source

Depth of source of the SP signal is a critical point in hydrogeological studies. Evidence from the present study does not necessarily relate its depth to the water table, although there are cases where very slow and probably meager infiltration to a free aquifer produces a water table anomaly. It seems certain that confined and semi-confined aquifers tend to send up the signal from the major infiltration point or horizon. This theme is also basic to the quantifiable part of this study. Since the 1940s, there have been a large number of publications relating the SP dipole to various geometrical figures; the more recent works by Bhattacharyya and Roy (1981) and Ram Babu and Atchuta Rao (1988) summarize these and propose very workable models that are used in this paper. These studies were all based on sulphide body or vein models; nevertheless, the subject of the water level always works itself into the discussion. A recent discussion by Eskola and Hongisto (1989) of the Ram Babu, Atchuta Rao (1988) based its objections on the displacement and deformation of the SP dipole (caused by the vein) by the position of the water level; indeed, according to their model, the shape of the SP curve and the resultingly calculated SP dipole is more dependent on the water table than on the mineralized body. In their reply, the original authors admit not taking the water level into account; as they mention, the usual mathematical models used did not include this factor.

These quantitative interpretation methods make use of certain parameters measured from the field curve after it is corrected for drift and, when necessary, smoothed. These are:  $V_{min}$  - the minimum SP reading in mV on a negative peak,



divided by  $V_{\max}$  = the counterpart reading on the positive peak. This is equivalent to a number used to determine the angle of the SP dipole or the "polarization angle". This is related to (1) the wavelength of the curve, or "d", or " $X_{\max} - X_{\min}$ ", depending on the author, and (2) to the average amplitude of the peak, being either negative or positive, and commonly termed  $V_1 = V_{\min} - V_{\max}$ . Therefore, the calculation base is always a function of wavelength, amplitude, and the negative/positive peak measurement. The graphical methods and nomograms give (1) "h" or the depth to the center of the body (source of the SP signal), and (2) " $X_0$ " or "O" being the displacement in plan of the point on the surface above the center of the signal source and the "cross-over" on the curve between positive and negative readings. This procedure is very much the same as that used for the interpretation of resistivity transversing or standard magnetics or electromagnetics.

Of interest to hydrologists is that, empirically, the sulphide-based models give corroborative results on both water table position (and slope) and on strong infiltration in cases of semi-confined aquifers. The water in the majority of the study areas is moderately conductive, referring to the Helmholtz equation in Fournier (1989). The aquifer in these conditions should give a good SP signal, if there is a reasonable hydraulic gradient.

Many favorable aquifers show a positive SP response, whereas the obvious infiltration zones show negative peaks. Therefore, my experience with this tends to agree with Fournier's diagnosis of negative readings in thalwegs in old basements buried by young volcanic rocks.

### Field Procedure

Work in the field with SP has tended to standardize with long radiations being the most usual system; Fournier (1989) used up to 500 meters of wire to eliminate as many base changes as possible. The single base radiation allows the most simple interpretation (Randall-Roberts, 1984), but any regional study necessarily changes bases. Certainly, a kilometer of wire is usable, but more than 600-700 meters tends to risk breakage in the bush. In hydrogeological work, where the anomalies are in the order of 30-50 mV rather than the 200-400 mV in certain near-surface massive sulphide bodies (Kelly, 1957), the short baseline "leap-frog" procedure allows for too many closure errors that would erase many low amplitude anomalies. With no scheme, is it possible to eliminate the necessarily frequent closure checks on the original point, internal checks between reference electrodes, and protection of the non-polarizing electrodes from sun and wind. I agree with Fournier (1989) that 20 cm. deep holes for the electrodes eliminate many of these problems and put the pot in contact with moist material, thus lowering the contact resistance.

### Case Histories

#### Typical Examples of SP Studies in Plan and in Section

In Figure 1, three typical cases are presented: two examples of studies in plan and one quantitative study in section. The first study in plan view is a local investigation for a well location in fractured rhyolite accomplished by two detailed radiations in about 1/4 km<sup>2</sup>, with a considerable mV range: -22 mV to +45 mV. The well location near the major positive/negative contact tested 11 l/s from

an infiltration depth of 80 m in fractured rhyolite. The northeast-trending faults shown by the geophysics are observable in the field. The well was drilled to 250 m in rhyolite. The second typical case is a multiple radiation using four bases, each tied into the previous one, over an area of about 2 kms<sup>2</sup>. The mV range is small, only -9 mV to +13 mV, but the SP pattern is very distinct, consisting of a buried stream capture zone. The well was spotted on the point of stream capture, a gravelly aquifer buried by 120 meters of dense, hard, dry rhyolite; it tested 60 l/s with very little drawdown. The weak but distinct signal came up through a thick, although poorly-conductive barrier. Both of these examples are in areas of cold water. The third example, a hydrologic and topographic profile across an influent stream, is an evaluation of the water table in an area of extremely impervious calcilutite; a well drilled here previously to a depth of 300 m in tight limey shales yielded less than 1/3 l/s. Using the Ram Babu, Atchuta Rao (1988) method, assuming a doubly-dipping sheet, the minima were calculated against the nearly symmetrical  $V_{max}$  in the scheme described previously. This system appears especially useful in studying the water table in areas of very low infiltration. Indeed, the only water in this area is close to the thalweg of the arroyo which itself is dry most of the year. The very steep dip on the water table is due to the influent recharge and very impervious rock.

#### SP Profile Across Two Aquifers in Paleochannels (near Guanajuato)

The case shown in Figure 2 is that of a typical undulatory curve in a paleochannel aquifer within an area of lake sediments, mostly impervious silt. The correction of the curve for drift is shown as well as the comparative contact resistance curve made at the same time. Note that on the far right side, the resistance curve climbs above 2 mega ohms, negating the validity of the corresponding SP curve in that part. Using the Bhattacharyya, Roy (1981) scheme, I have calculated a depth ( $X_0$ ) of 90 meters, based on the parameters  $V_{min}/V_{max} = 0.13$  (amplitude), and  $d = 70$  meters (wavelength); the very high positive peak indicates a discharge zone into the paleochannel from the underlying gravels. Here, a cylinder model is more appropriate than the sheet model used in Figure 1. The 90-meter depth is approximately correct based on the well that was recommended on the anomaly peak; the pumping test gave 18 l/s of cold water.

#### SP and Hydrology (near San Miguel de Allende, Guanajuato)

Figure 3 shows a detailed integration of SP studies in an area of about 2 km<sup>2</sup>, where information from seven water wells was also measured, including the lithology. The water table shows a strong gradient of 10 km to the southeast fed by very strong recharge from the Rio Laja, which lies about 2 km northwest of the map area. The infiltration channels are marked by strong negative peaks, up to -42 mV, ranged against a positive maximum of +24 mV. The water here is slightly thermal, 35°C, warmed by waning pleistocene volcanism, which explains this 66 mV range. The geophysically mapped infiltration channels match the known groundwater flow which is structurally controlled by faulting (NW-SE); the Rio Laja flows nearly due south here, also controlled by a fault, the youngest of the regional fracture systems. The flow system is at a depth of 150 meters on the top of a dense rhyolite.

#### High Recharge Area (near San Miguel de Allende, Guanajuato)

Figure 4, a detailed study in a small area,  $1/4 \text{ km}^2$ , shows an SP range of over 50 mV (0-55 mV) in an area of slightly thermal ( $30^\circ\text{C}$ ) groundwater. The repeated peaks showing this positive range delineate a local subterranean discharge zone, possibly from faults in the underlying rhyolite, although the pattern is quite different from that of Figure 3. Using the cylinder model of Bhattacharyya and Roy (1981), a depth of 90 meters was calculated which checks with the major aquifer depth in nearby wells. Using the Ram Babu, Atchuta Rao (1988) method, the SP dipole is nearly horizontal at a depth of 36 meters; a dug well located on the discharge zone reached the water table at 37 m, again indicating the use of the sheet model in locating the water level.

#### SP South of Leon, Guanajuato

Figure 5 shows part of a large study done in the agricultural zone south of the city of Leon, Guanajuato. The water is cold and deep; the groundwater table is at 65 m or more. The hydrological base is very close; the resistivity model given by numerous soundings shows the 10 ohm-m clay bed (pliocene lacustrine deposits) at an average depth of 100 meters. The only recently successful soundings are those which find paleochannels in the clay bed providing locally concentrated infiltration; their location has been determined often by SP studies. Note that in the plan map (upper left side of the figure), on the positive side of the SP zero line, the wells are successful, whereas on the negative side to the SE, the wells are failures: 2-3 l/s. The sharply peaked positive curve shown using the cylinder model (ibid, 1981) gives a depth calculation of 110 m correlating with data in the paleochannel explored by the 15 l/s well.

#### Regional Spontaneous Potential (south of Leon, Guanajuato)

Figure 6 shows results for an area covering nearly  $150 \text{ km}^2$  where a variety of data have been compiled in order to show the regional flow patterns, largely controlled by the NW-SE faulting prevalent in the State of Guanajuato in central Mexico. Water flow patterns from well data show the movement shifted along the geophysical contacts and somewhat altered by the largely impervious hydrological boundaries where volcanic dome complexes interrupt subsurface flow. The water is mostly cold, and the SP mV ranges are highly variable; the maximum range of -10 mV to +50 mV is considerable but probably due to the faults which act as local groundwater boundaries as well as infiltration channels, depending on whether they are filled with clay or with gravel. The flow is also affected by heavy pumping that greatly changed the pattern over the past two decades. Recharge is from the Rio de los Gomez from the northeast corner of the map, but it is no longer very effective.

#### Conclusions

I attempted to summarize a few case studies in order to illustrate the use of SP as a water prospecting method, both in a regional sense and in detailed quantitative work. The application of SP to hydrogeology borrows heavily from many workers who applied it to mineral exploration and were concerned about the groundwater effect on their curves and calculations. Without doubt, SP benefits greatly when there are resistivity (V.E.S.) soundings in the area to electrically

calibrate the stratigraphy. Above all, the geological base is necessary; without it, the numbers are without meaning. With these controls, SP has the great advantage of measuring water flow; the more mineralized and the warmer that it is, the greater SP that can be measured. Nevertheless, even cold, rather pure rain water can be traced. If the hydrogeology is reasonably well understood, the SP method used with care may be the most direct geophysical prospecting method for groundwater.

### References

Bhattacharyya, B.B., and N. Roy, 1981, A Note on the Use of a Nomogram for Self-Potential Anomalies, *Geophy. Pros.*, Vol. 29, pp. 102-107.

Ernst, K., and U. Scherer, 1986, Self-Potential Variations with Time and Their Relation to Hydrogeologic and Meteorologic Parameters, *Geophysics*, Vol. 51, No. 10, pp. 1967-1977.

Eskola, L., and H. Hongisto, 1989, Discussion on: "A Rapid Graphical Method for the Interpretation of the Self-Potential Anomaly Over a Two-Dimensional Inclined Sheet of Finite Depth Extent (Geophy. 53, pp. 1126-1128, August 1988), *Geophysics*, Vol. 54, pp. 1215-1216, and Reply by H.V. Ram Babu and D. Atchuta Rao, p. 1216.

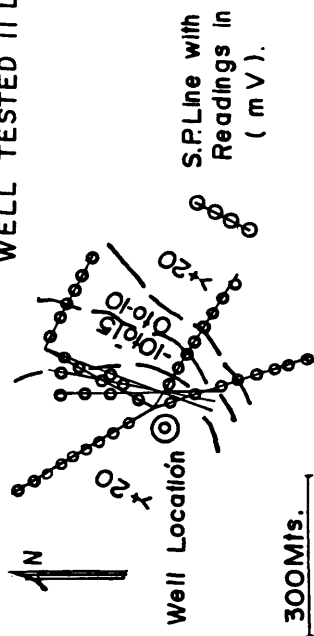
Fournier, C., 1989, Spontaneous Potentials and Resistivity Surveys Applied to Hydrogeology in a Volcanic Area: Case History of the Chaîne des Puys (Puy-de-Dôme, France), *Geophy. Pros.*, Vol. 37, pp. 647-668.

Kelly, S.F., 1957, Spontaneous Polarization, or Self-Potential Method, in "Electrical", Methods and Case Histories in Mining Geophysics, 6<sup>th</sup> Commonwealth Mining and Metallurgical Congress, United Kingdom, pp. 53-59.

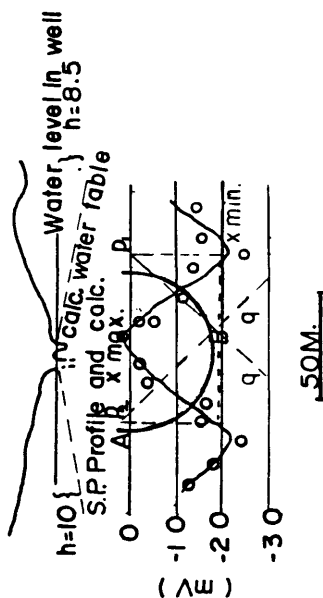
Randall-Roberts, J.A., 1984, Potencial Natural (SP) en la Búsqueda de Agua, Univ. de Guanajuato, Mexico, Fac. de Minas, Metalurgia y Geología, 43 p.

Sato, M., and H.M. Mooney, 1960, The Electrochemical Mechanism of Sulfide Self-Potentials, *Geophysics*, Vol. 25, pp. 226-249.

## TYPICAL EXAMPLES OF S.P. STUDIES IN PLAN AND IN SECTION



## HYDROLOGIC AND TOPOGRAPHIC PROFILE ACROSS AN INFLUENT STREAM.



S.P STUDIES OVER GRAVEL ACUIFER CAPPED  
BY 120M. OF DENSE DRY RHYOLITE WELL  
TESTED 60 L.P.S.

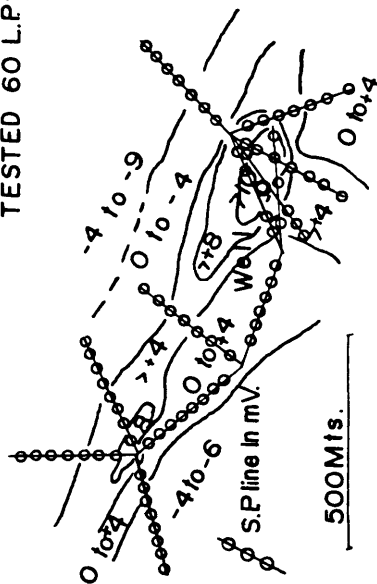
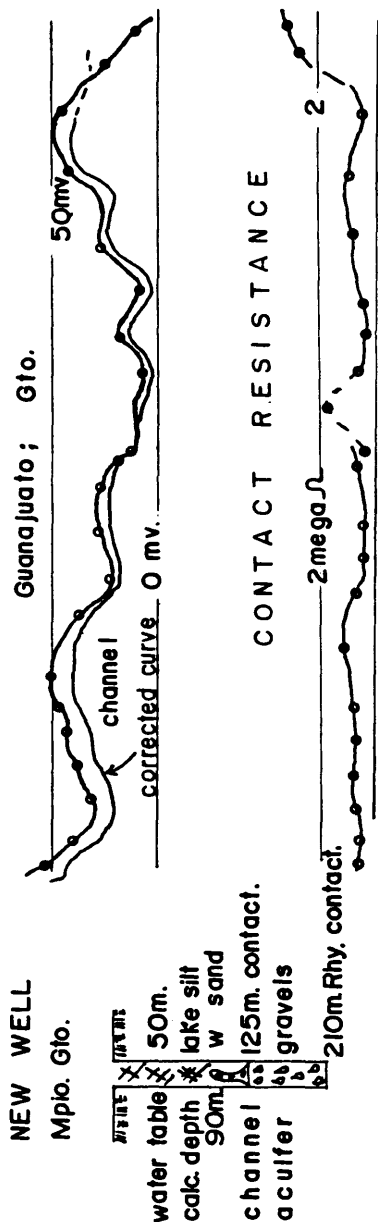
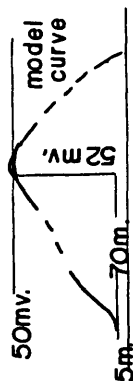


**Fig. 1**

# S.P PROFILE ACROSS 2 AQUIFERS IN PALEO-CHANNELS.



## PALEO-CHANNEL



v min 4  
v max. 52  
d = 70m.  
= 50°  
x<sub>0</sub> = 90m.

200 M.

TYPICAL UNDULATORY CURVE IN  
PALEO-CHANNEL AQUIFER

Fig. 2

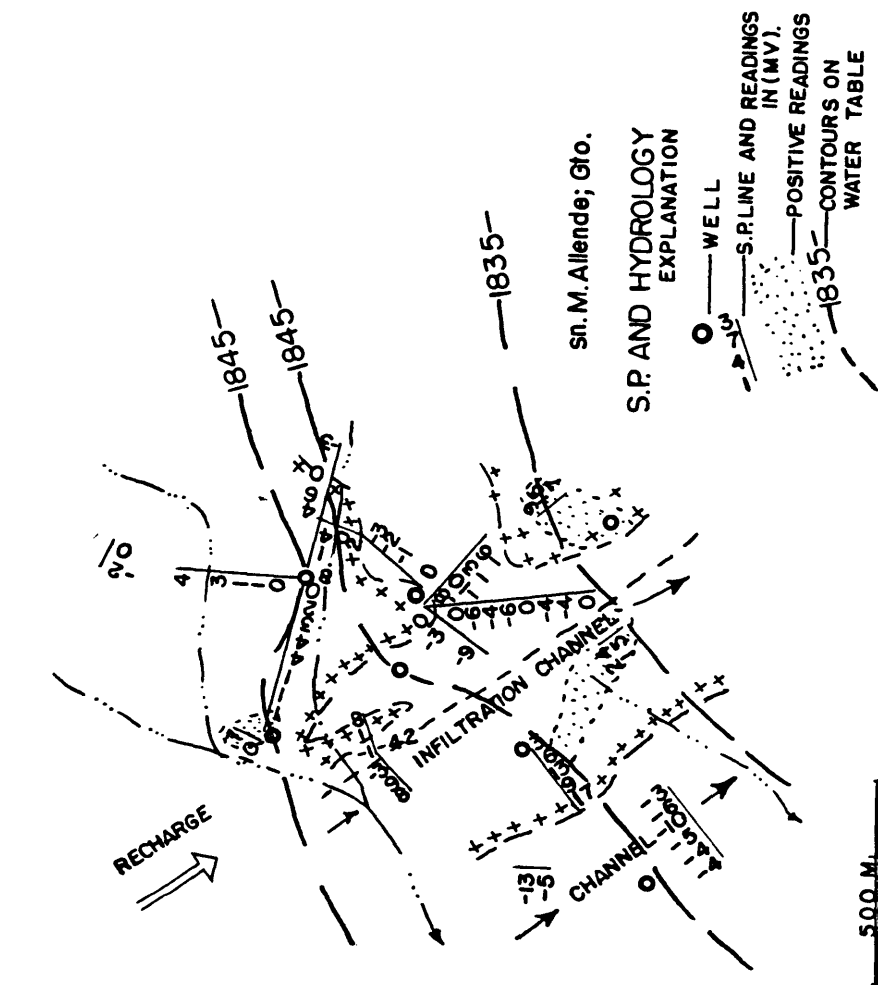
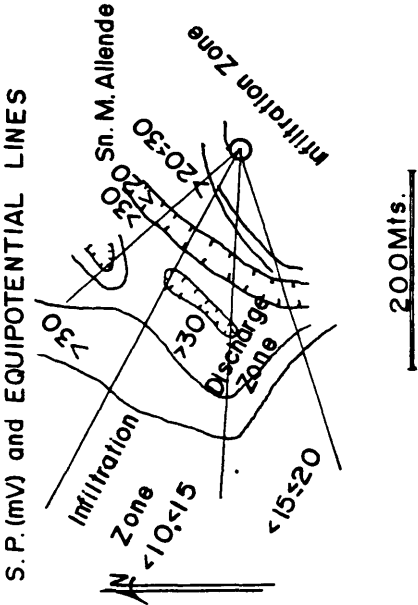


Fig. 3

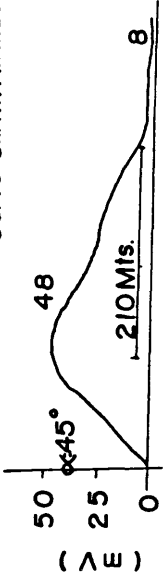
Fig. 4

HIGH RECHARGE AREA  
Sn. M.Allende , Guana juato.



CALC. METHOD OF(BHATT; ROY, 81).

Curve Sn. M. Allende



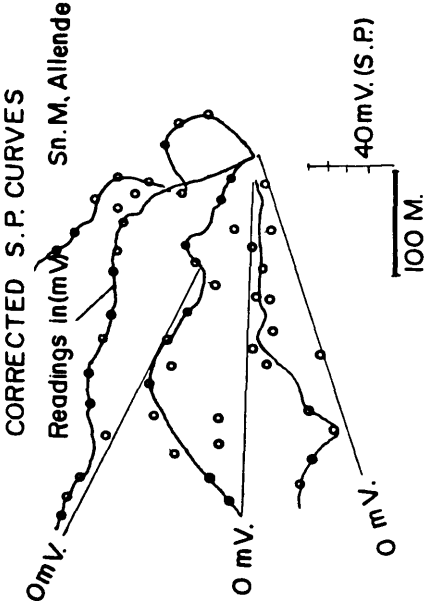
$$\frac{V_{min}}{V_{max}} = \frac{8}{48} = 0.16$$

$$d = 210 \text{ Mts.}$$

$$\alpha = 45^\circ$$

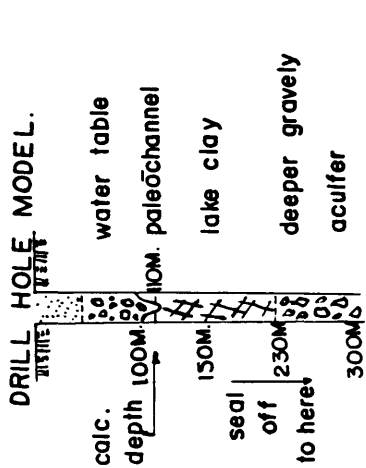
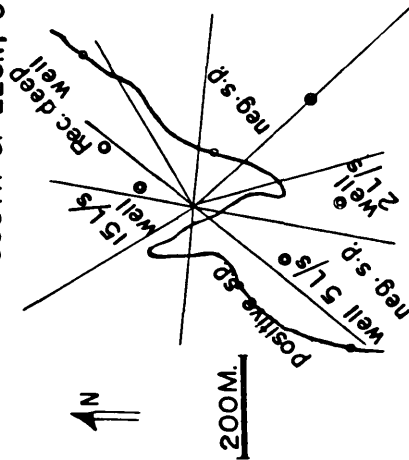
$$X_0 = 90 \text{ Mts.}$$

DEPTH OF SOURCE AQUIFER : 90M.



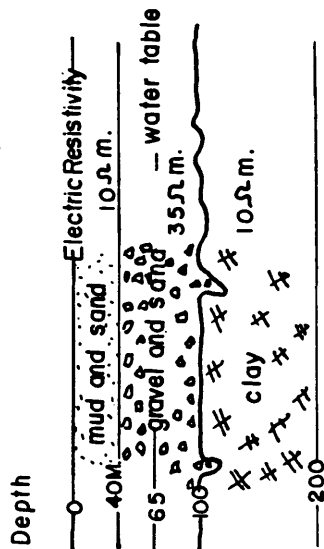


S.P.(mV) SOUTH OF LEON; GTO.

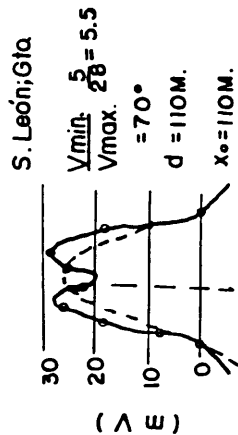


# STRATIGRAPHIC MODELS

Leon; Gto.



# PALEO-CHANNEL



sand and gravel 25Ωm.

150M.

Fig. 5

# REGIONAL SPONTANEOUS POTENTIAL

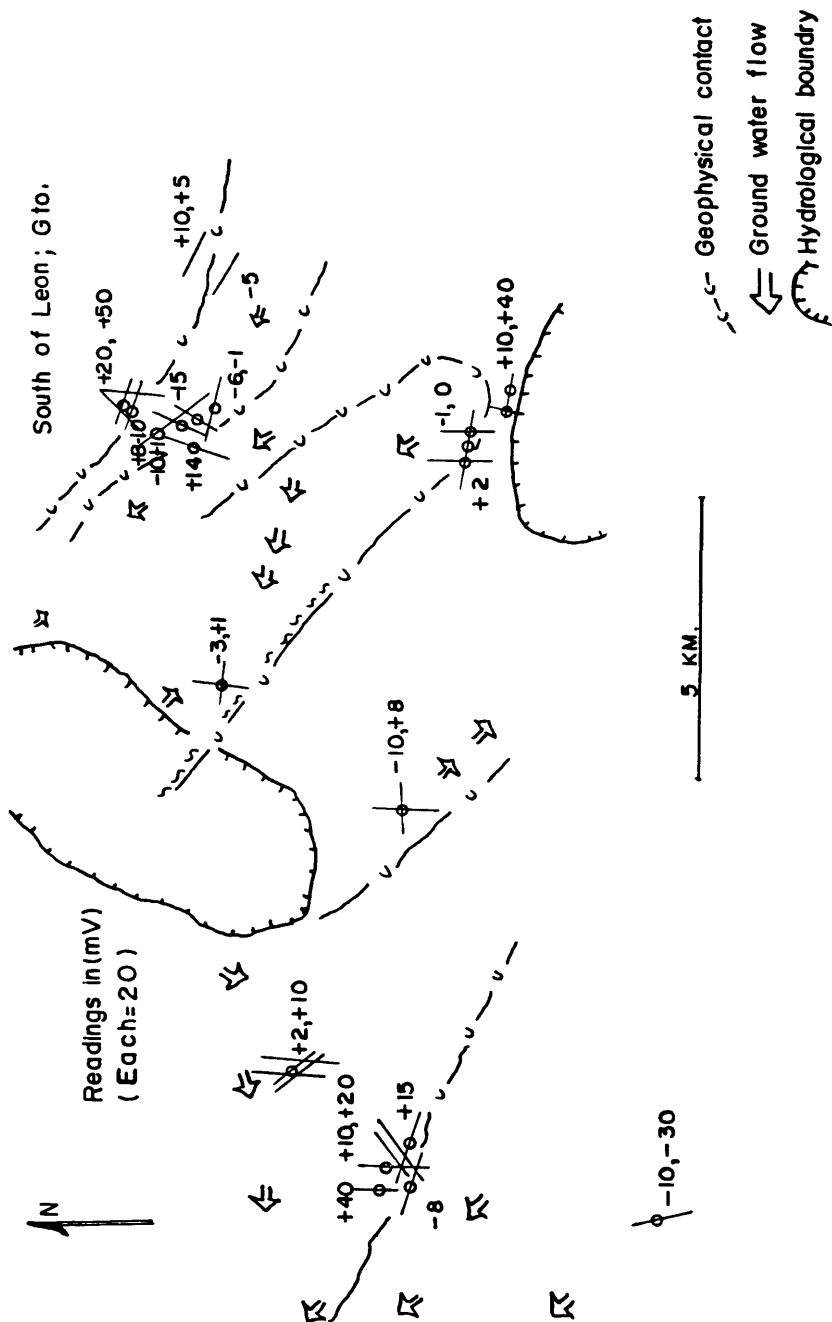


Fig. 6

## MODERN PROBLEMS OF REGIONAL HYDROGEODYNAMICS

G.S. Vartanyan and L.V. Borevsky

All-Union Research Institute for Hydrogeology  
and Engineering Geology  
142452 Zeleny-Village, Noginsk District  
Moscow Region, USSR

### ABSTRACT

Problems of regional groundwater movement have long been of scientific interest. Intensive economic development as well as greater and more rational use of natural resources, including groundwater, resulted in a relatively detailed knowledge on the regularities of formation, movement, and localization of groundwater in the zone of active water exchange of the upper hydrogeosphere. Thermodynamic and physical-chemical processes in the deeper sections of the hydrogeosphere have been studied to a much lesser extent.

The present-day ideas about the mechanism of groundwater movement in deep layers are schematic and controversial due to the lack of reliable data on hydrogeological processes that take place there. Field observations and measurements using a limited number of parameters are not enough to understand the complicated nature of the hydrogeological conditions. This explains the existence of various, sometimes incompatible, ideas about fluid dynamics in the deep layers of the subsurface.

Today, it is clear that the deep zones of the hydrogeosphere are complex thermodynamic systems where mass- and heat-transfer are affected by many factors (i.e., pressure and temperature gradients, chemical potentials of solutes, deformations, and displacements of a rock skeleton, etc.). Analysis of the modern concepts of fluid hydrodynamics in the deep lithosphere shows that the classical theory of solid media and hydraulic potentials fails to give an unambiguous interpretation of all the diverse thermodynamic phenomena and processes registered in the course of the subsurface studies.

The most complex mathematical model of mass- and heat-transfer was suggested by N.A. Ogilvi [10]. He introduced a concept of generalized thermodynamic potential of a rock, by which one should understand an open thermodynamic system where mineral skeleton and pore solutions are inseparably linked.

The equations derived by Ogilvi are similar to those used for phenomenological description of the interrelated water flows and mineral skeleton in terms of thermodynamics of irreversible processes. The major conclusion which can be drawn from the above is that groundwater movement is affected by rock migration due, for example, to neotectonic motions or rheological deformations. Even very slow movements of a rock skeleton turn out to be compatible with a flow rate in deep zones of the Earth's crust which must be taken into account while analyzing hydrodynamic fields. Practical application of the model will require a great number of phenomenological parameters which are hardly available now. Therefore, of particular importance are the new geologic-hydrogeological phenomena found over the past decade. These may also enable the establishment of regularities to help determine localization and migration of fluids in the deep sections of the lithosphere.

The discovery of global short-lived pulsating changes in the hydrogeosphere, i.e., hydrogeodeformation (HGD) [6, 7, 11] laid the foundation for understanding deep groundwater movement and major motive forces which regulate formation of hydrodynamic and hydrogeochemical situations at great depths. A close relation is established between certain parameters of the hydrogeological regime and the seismotectonic stresses, as well as seismic processes. Studies of the HGD-field within large regions contribute a new understanding of the processes that occur in the hydrogeosphere of mountain-folded areas, platforms, and crystalline shields.

In particular, the HGD-field manifests itself in a global distribution of barothermic and physical-chemical variations of the fluid-bearing environment of the lithosphere in space and time, as a result of changes in its stressed state [6, 7, 10, 11]. These changes occur continuously in time and are induced by external (including extraterrestrial) and internal factors. At the same time, changes in the hydrogeosphere do affect the stressed state of large rock masses. Here, it is necessary to touch upon some specific features of the evolution of various rocks as a water-bearing matrix that governs fluid migration and localization in the subsurface.

The present-day lithologic-petrological publications contain a considerable amount of information on the evolution of the composition of rocks under lithification and isochemical transformations of magmatic and metamorphic complexes. These are major processes affecting the subsurface accumulation and transport of various fluids because they change the rocks' storage capacity and hydraulic conductivity. For example, analysis of clay consolidation shows that porosity of marine sediments always tends to a certain limit typical of the most solid rock for the given mineralogical associations and fraction dispersivity [12, 13, 14, 15]. The above approach shows a general trend in rock formation and may be considered a rather successful approximation of the mechanisms causing sedimentation.

These ideas imply the existence of ideal sediment consolidation and treat it as a one-way process capable of hysteresis. However, a great number of natural processes, such as the well-known phenomenon of regular sediment dewatering due to multiple uplifting and sinking of the sediment basement, were neglected here. It is obvious that regular consolidation and dewatering must result in the disintegration of friable sediments, development of our new macro- and microjointing, sealing of available cavities, and so on. At the same time, the stress field and the related HGD-field of the Earth are constant and active factors which affect the storage capacity of the rocks.

Thus, from the concepts of a multi-dimensional stress field, it should be accepted that the HGD-field, at every particular moment, gives a specific "mold" to developing stresses and rock microdeformations. That is, the HGD-field reflects regional time-dependent changes (or microchanges) in physical properties of rock masses. However, as the HGD-field is recorded in almost all rocks and is characterized by time variables, it could be assumed that: (a) the consolidation curve discussed in the literature can be taken only as an idealized model of processes and is an average representation for the changes in physical properties of sediments; and (b) the hydraulic conductivity (and storage capacity, to some extent) of a rock mass will also vary in time, and the curve for the HGD-field changes can be regarded as a qualitative parameter of the above properties. Here, these variations seem to be more essential for hydraulic conductivity than for the storage capacity. In any case, dependence of hydrodynamic engineering estimates

on the accuracy of plots for regional assessments of groundwater flow deserves special attention.

As for presently accepted reconstructions of regional hydrogeodynamics, it can be said that such investigations should be complemented with the assessment of possible non-stationary hydraulic conductivities and storage capacities of rocks as a result of the HGD-field processes. In particular, short-lived microdeformations simultaneously covering huge regions cause a "wandering sieve" effect when found within some real-time intervals. Impermeable rocks (e.g., clays) can initiate sporadic upward leakages of artesian water; that is, in areas of compression, groundwater discharge stops (or is reduced), whereas, at the same time in neighboring zones with prevailing extensions, the leakage increases. Regional extensions may cover huge territories and seem to be associated with hydrodynamic, hydrogeothermic, and hydrogeochemical anomalies registered during pre-seismic periods and which degrade after seismic stress relaxation.

In direct connection with the above processes are hydrodynamic evolutions associated with neotectonics.

Despite theoretically established relations between rock-skeleton movements and geofiltration processes, many hydrogeologists believed, until recently, that the current piezometric surface cannot be affected by tectonic motions. This belief arose from the idea that vertical tectonic movements have a very slow velocity (usually a few millimeters per year) and, whatever the real coefficient of piezoconductivity may be, relaxation of the head gradients must be practically parallel to their formation. This implies the existence of an elastic filtration law, as well as a linear relation between discharges and head gradients within the whole range of their occurrence.

At the same time, deep aquifer studies revealed some factors that cannot be explained by the above-mentioned beliefs. For example, analysis of the distribution of hydrochemical and hydrodynamic fields in the Volga-Urals terrigenous water-bearing complex showed that maximum head pressures, as well as maximum mineral content of the groundwater in it, are associated with the large domes and swells, such as at Tokmovsky and Tatarian. The hydrogeological conditions of these uplifts do not seem to be favorable for groundwater recharge. In addition, a "downward" decrease in groundwater mineral content can hardly be explained in terms of classical hydrodynamics. Minimum head pressures are registered along the Volga and Kama, in the Fore-Urals marginal trough, and along the edge of the Caspian depression. In the latter case, the head pressures are below sea level. To the east of the Caspian basin, isopiestic and isomineral lines intersect almost at 90°, which also cannot be explained by the above-mentioned beliefs.

Isotopic analysis of the deep ground water indicates that it is syngenetic to the water in the water-bearing rocks. However, at the same time, hydrodynamic calculations show that the study basins had multiple water-exchange episodes. Suffice it to say such examples are in abundance.

Comparison of piezometric head gradients with neotectonic movement amplitudes for regions with low tectonic activity revealed that amplitudes of the neotectonic movement during the past one or two million years and differences in groundwater head pressures at the same points show a close match if the head-pressure gradients do not exceed  $5 \times 10^{-4}$ , and if the total movement amplitudes are not greater than 100 m. The analysis covered uplift (the Volga basin, Moldavian SSR) and subsidence (the southern part of West Siberia) regions. According to Darcy's law and the

rules of elastic filtration, relaxation of the head pressure gradients should have been completed but, as follows from the calculations, it never happened. Hence, it can be supposed that, under the considered conditions, the given gradients were too low to induce lateral filtration. In this case, partial pressure relaxation can be explained by changes in pore parameters due to variations in effective stresses, which is pronounced in lithified rocks only in terms of geological time. It should be noted that the cited studies dealt with aquifers that have a hydraulic conductivity of 0.2-0.5 m/day and indicated that fields of stratal pressure in different tectonic blocks is formed quite independently with no natural water exchange.

In areas with active tectonics, as well as in the young semilithified rocks, the response of the piezometric surface seems to be quite different; that is, water levels rise in subsiding blocks and decline in uplifting blocks. Here, a direct relation is observed between the changes in the stressed state of a rock skeleton and in stratal pressures. However, as shown in a previous case, the real relaxation of the head gradients is much slower when compared to theoretical calculations and sometimes cannot be detected by existing methods.

In deep stratified zones of the lithosphere, the above processes can result in the formation of abnormally high and abnormally low pressures. Relaxation is not gradual but impulsive, as soon as the system reaches certain critical values of the thermodynamic processes. These processes seem to contribute to the formation of the HGD-field of the Earth.

Therefore, the following conclusions can be made: (1) The latest tectonic motions can considerably affect the formation of a field of stratal pressures; (2) Factual data obtained from a number of artesian basins indicate the absence of groundwater flow, whereas the piezometric surface shows the existence of a filtration gradient; and (3) In an area with low head gradients, an evaluation of filtration rates using Darcy's law may lead to substantial errors and false conclusions concerning the water-exchange rate and even the existence or absence of groundwater flow. This should also be taken into account when solving regional filtration problems by means of mathematical modeling.

It must be admitted that today many questions concerning filtration and formation of groundwater in deep aquifers cannot be answered unambiguously. To solve them, it is necessary, first of all, to develop field methods for reliable determination of the initial filtration gradient and to identify the regularities in groundwater movement with slight piezometric slopes and with regard to rock-skeleton migration. Regime observations of the HGD-field variations at depth in representative areas may be an effective way for solving the above problem.

Among the most poorly studied problems of regional hydrodynamics is that of a lower boundary of free groundwater distribution in the Earth's crust and the related problem of global vertical water-exchange. Hypotheses which are available here are rather controversial, including possible water infiltration up to the MOHO boundary and negation of possible occurrence of free water below 5-7 km. This can be explained by the fact that a rise in temperature and pressure with depth causes dehydration and consolidation of rocks and majority of water in the zone of late katagenesis and metamorphism has undergone chemically bound modification.

According to numerous in-situ data, a gradient of stratal pressure down the profile exceeds the hydrostatic one, i.e., free groundwater filtration becomes impossible.

### References

1. Borevsky, B.V., and L.V. Borevsky, 1983, Contribution of the latest tectonic motions to formation of inhomogeneous hydrogeological fields under natural and disturbed conditions. In the book: The results of regional hydrogeological and engineering-geological processes in the sedimentary cover of young plates. Moscow, Publishing House Nauka, pp. 12-15.
2. Borevsky, L.V., G.S. Vartanyan, and G.V. Kulikov, 1984, Hydrogeological essay. In the book: Kola super-deep well. Moscow, Publishing House Nedra, pp. 240-253.
3. Borevsky, L.V., and A.A. Kremenetsky, 19 , Geological role of ground water in progressive metamorphism of open and closed systems. In the book: Ground water and evolution of lithosphere. Vol. II. Moscow, Publishing House Nauka, pp. 8-13.
4. Borevsky, L.V., and A.A. Kremenetsky, 19 , Ore-forming role of metamorphogenic hydrotherms. In the book: Ground water and evolution of lithosphere. Vol. II. Moscow, Publishing House Nauka, pp. 179-182.
5. Vartanyan, G.S., 1977, Carbonaceous water fields in mountain-folded regions. Moscow, Publishing House Nedra.
6. Vartanyan, G.S., and G.V. Kulikov, 1982, Hydrogeodeformation field of the Earth. Reports of the Academy of Sciences of the USSR, Vol. 262, No. 2, pp. 310-314.
7. Vartanyan, G.S., and G.V. Kulikov, 1983, On global hydrogeodeformation field. *Sovetskaya Geologia*, No. 5, pp. 116-125.
8. Lukyanov, A.V., Yu.M. Bykova, and V.V. Zinkov, 1987, Pressure distribution in a fluid migrating through a stratified rock mass. Modeling. In the book: Study of tectonic deformations. M: GI of the Academy of Sciences of the USSR, pp. 137-158.
9. Bondarenko, S.S., and G.S. Vartanyan [Eds.], 1986, Study methods and assessment of deep ground-water resources. Moscow, Publishing House Nedra.
10. Ogilvi, N.A., 1974, Physical and geological fields in hydrogeology. Moscow, Publishing House Nauka.
11. Vartanyan, G.S., (need names here), 1987, Developments in the Analysis of Groundwater Flow Systems. UNESCO, Wallingford, UK (in English).
12. Savarensky, F.P., 1939, Engineering Geology, 2<sup>nd</sup> Edition GONTI.
13. Savarensky, F.P., 1950, Selected publications. Publishing House of the USSR Academy of Sciences.
14. Priklonsky, V.A., 1949, Soil Science, Part 1. Gosgeoizdat.
15. Mukhin, Yu.V., 1965, Consolidation of clay sediments. Moscow, Publishing House Nedra.

At the same time, recent results of deep and super-deep drilling showed that free water occurs within the whole profile studied up to a depth of over 11 km [2] and, according to some indirect data, even to 20 km. Here, its occurrence is not local and forms rather extensive water-bearing zones of considerable thickness (to 4-5 km). The factual information available implies that the largest amount of groundwater penetrates to greater depths in the course of rock subsidence and occurs mainly in a bound state.

Solution to the problem of formation and storage of deep regional water-saturated rock masses at high temperatures and pressures lies in the discovered phenomenon of the formation of aquifers, as well as zones of hydrogenic deconsolidation of rocks in the course of their progressive transformations. Bezrodny, Borevsky, and Vartanyan are among those responsible for the discovery. Development of these zones is triggered by the change in the state and properties of water due to rock dehydration at certain thermobaric levels, which transforms chemically and physically bound water to free water. These are transition zones of matter transformations under katagenesis and metamorphosis.

In principle, this newly-formed water can migrate to the surface, thus closing the water-exchange cycle. However, the mechanism of such a discharge, the physical processes relating to it, and the problems of describing the manner in which filtration takes place are not completely studied today. Nevertheless, these problems have fundamental and applied importance. The above-mentioned phenomenon influences the origin of the physical stratification of the Earth's crust, formation of crustal pore waveguides, formation of ore-bearing hydrothermal fields (of non-intrusive character), scaly thrusting displacements, and so on. All of these items have been discussed recently in geological literature, though not in sufficient detail [2, 3, 4, 5].

Due to the condition of fluid formation, stratal pressures in the above zones must be equal to, or even exceed, lithostatic pressures, and pore formation is attributed to a volumetric reduction of the solid phase, microhydrofracturing, and dissolution. Geological events and modeling results [8] show a pulsating water discharge from these zones, which becomes more active with intensified tectonics. Here, short-lived but repeated upward superlithostatic pressures, which serve as one of the most effective mechanisms producing the Earth's HGD-field, can be observed in the overlying aquifers during fluid outbursts. Periodicity and intensity of pressure fluctuations depend on many factors, including, in particular, permeability and strength of very low permeability layers.

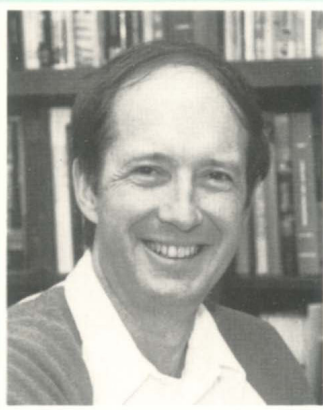
As follows from the above, modern regional hydrogeodynamics is facing such urgent problems as non-stationary filtration processes due to the evolution (sometimes spasmodic changes) of reservoirs under neotectonic activity in large regions. Therefore, joint efforts of various specialists including hydrogeologists, tectonic engineers, seismologists, and geophysicists will be required in the near future to develop a theory of fluid dynamics with regard for macro- and micro-structuring of huge rock masses.







**Eugene S. Simpson**



**John M. Sharp, Jr.**

This volume consists of 37 papers from 17 countries, selected from papers in hydrogeology presented at the 28th International Geological Congress held in Washington D. C., USA, July 9-19, 1989. The papers provide a worldwide overview of the wide spectrum of current hydrogeological research, grouped in six sections, plus the avant propos of the 1st section that sounds a warning concerning current trends in education in hydrogeology.

The 2nd section, containing ten papers devoted to carbonate systems, begins with an outline and summary of transport of chemical contaminants in karst terranes. The three following papers deal with groundwater recharge in Saudi Arabia, and with surface subsidence and sinkhole formation in the Republic of South Africa, and in Brazil. The Edwards aquifer in Texas, USA, is the focus of three papers with some diverging viewpoints, followed by papers on the effects of Hurricane Gilbert on the karst of Yucatan, Mexico; on geologic controls on the development of the Floridan aquifer system, USA; and finally on chemical reactions in a coastal aquifer in Catalonia, Spain.

Section 3 contains six papers on geochemistry and isotope geology. These discuss ultrabasic groundwater (pH 11.76) in Yugoslavia, the retention of certain heavy metals by unsaturated fractured shale in Kansas, USA; a low temperature hydrothermal system in central Italy; a study in Yugoslavia of geothermal waters in granodiorite using environmental isotopes; a numerical model that couples fluid and heat flow with the migration of reactive chemical elements; and (geochemical) information transfer in alluvial basins in Arizona, USA.

Section 4 is concerned with wetlands. Three papers describe wetland conditions in Minnesota, USA, and in the Netherlands, and in the Gobi desert of Inner Mongolia. Then follows a paper on the hydrological budget of lakes in Canada, and a paper on groundwater indicator plants in central Spain.

Section 5, on fractured rock, contains two papers analyzing the morphology and hydromechanical behavior of a single fracture; a paper describing a laboratory technique for the characterization of unsaturated rock; and a paper that evaluates well characteristics in fractured rocks in Karnataka, India.

Section 6, on water management, begins with a paper on the dynamic management of surface/groundwater systems, followed by methods for delineating wellhead and well protection zones in two regions of West Germany, and in one area of Arizona, USA. The section ends with the description of a compact expert system for water resource assessment in Africa.

Finally, section 7 consists of six miscellaneous topics: the assessment of the accuracy of a predictive digital model; thermal springs in Italy; the influence of saprolite on well production in the central African basement complex; enhanced LANDSAT Imagery for groundwater exploration in Ethiopia; surface spontaneous potential for groundwater prospecting in Mexico; and problems of regional hydrogeodynamics in USSR.

The wealth of research being pursued by the international community of hydrogeologists is demonstrated by this volume.

**ISSN 0938-6378**

**ISBN 3-922705-60-X**

**Verlag Heinz Heise GmbH & Co KG, P.O.B. 610407, D-3000 Hannover 61, FRG**